The Dissertation Committee for Tameem Mohammad Almani
certifies that this is the approved version of the following dissertation:

Efficient Algorithms for Flow Models Coupled with Geomechanics for Porous Media Applications

Committee:

Mary F. Wheeler, Supervisor

Todd Arbogast

Leszek F. Demkowicz

Mojdeh Delshad

Inderjit Dhillon

Kundan Kumar

Efficient Algorithms for Flow Models Coupled with Geomechanics for Porous Media Applications

by

Tameem Mohammad Almani, B.S., M.S., M.S.C.S.E.M.

DISSERTATION

Presented to the Faculty of the Graduate School of

The University of Texas at Austin

in Partial Fulfillment

of the Requirements

for the Degree of

DOCTOR OF PHILOSOPHY

THE UNIVERSITY OF TEXAS AT AUSTIN

December 2016

In the name of Allah, the Most Gracious, the Most Merciful.

Dedicated to my mother Hissah Mohammad Al-Zamil

Words can not express how much I owe you

Acknowledgments

First and foremost, I would like to express all my sincere thanks to my Lord, The Almighty Allah, whose blessings on me are countless.

Next, I would like to express my sincere gratitude as well to my supervisor, Prof. Mary F. Wheeler, for her support, guidance, and encouragement throughout my PhD study. Her endless enthusiasm and diligence in research inspired me to learn a lot from her. I also want to extend my gratitude to my committee members, Prof. Todd Arbogast, Prof. Leszek Demkowicz, Prof. Mojdeh Delshad, Prof. Inderjit Dhillon, and Prof. Kundan Kumar for their valuable comments, advices, and remarks on my work. I am really honored to have such a highly competent advisor and committee members.

This has been an interesting journey. It is an experience that sharpened my skills not only academically, but also in different aspects of life. I am fortunate to have had the company of many colleagues who have supported me including Dr. Kundan Kumar, Dr. Gurpreet Singh, and Dr. Gergina Pencheva. Special thanks goes to Dr. Kundan Kumar, for his continuous help, support, collaboration, and encouragement. Your help Kundan will never be forgotten. I would like to thank as well my colleagues at the Center for Subsurface Modeling for their warm support and friendship.

I am also thankful to the graduate fellowship by Saudi Aramco, and specifically to Dr. Ali Dogru for his continuous support and funding most of my conference trips. I also want to extend my gratitude to Mr. Samer AlAshgar, the current president of King Abdullah Petroleum Studies and Research Center (KAPSARC), for his great help and support with family related medical insurance issues.

Finally, and most importantly, I would like to express my countless thanks and gratitude to my mother, the true person standing behind every success I make in this life (after Allah's help and guidance). Her endless support, care, and prayers since the time I was born are just invaluable. Words just can not express how much I owe her. In fact, I cannot pay her back, even a tiny part, of what she has done to me. May Allah rewards her the best in this life and the highest paradise in the hereafter, and May Allah help me become her best servant, and her best son. My gratitude extends as well to my family including my older brother, Abdulrahman, my wonderful sisters Maali, Mawahib, and Manar for their endless love and support, and my little angel, my 4 years old daughter, Aseel, who filled my life with lots of joy and happiness. Without the support of all, after Allah's support, this work wouldn't have been completed.

Efficient Algorithms for Flow Models Coupled with Geomechanics for Porous Media Applications

Publication No. _____

Tameem Mohammad Almani, Ph.D.
The University of Texas at Austin, 2016

Supervisor: Mary F. Wheeler

The coupling between subsurface flow and reservoir geomechanics plays a critical role in obtaining accurate results for models involving reservoir deformation, surface subsidence, well stability, sand production, waste deposition, hydraulic fracturing, CO_2 sequestration, and hydrocarbon recovery. From a pure computational point of view, such a coupling can be quite a challenging and complicated task. This stems from the fact that the constitutive equations governing geomechanical deformations are different in nature from those governing porous media flow. The geomechanical effects account for the influence of deformations in the porous media caused due to the pore pressure and can be very important especially in the case of stress-sensitive and fractured reservoirs. Considering that fractures are very much prevalent in the porous media and they have strong influence on the flow profiles, it is important to study coupled geomechanics and flow problems in fractured reservoirs. In this work, we pursue three main objectives: first, to rigorously design and analyze iterative and explicit coupling algorithms for coupling flow and geomechanics in both poro-elasitc and fractured poro-elastic reservoirs. The analysis of iterative coupling schemes relies on studying the equations satisfied by the difference of iterates and using a Banach contraction argument to derive geometric convergence (Banach fixed-point contraction) results. The analysis of explicit coupling schemes result in analogous stability estimates. In this work, conformal Galerkin is used for mechanics, and a mixed formulation, including the

Multipoint Flux Mixed Finite Element method as a special case, is used for the flow model. For fractured poro-elastic media, our iteratively coupled schemes are adaptations, due to the presence of fractures, of the classical fixed stress-splitting scheme, in which fractures are treated as possibly non-planar interfaces. The second main objective in this work is to exploit the different time scales of the mechanics and flow problems. Due to its physical nature, the geomechanics problem can cope with a coarser time step compared to the flow problem. This makes the multirate coupling scheme, the one in which the flow problem takes several (finer) time steps within the same coarse mechanics time step, a natural candidate in this setting. Inspired by that, we rigorously formulate and analyze convergence properties of both multirate iterative and explicit coupling schemes in both poro-elastic and fractured poro-elastic reservoirs. In addition, our theoretically derived Banach contraction estimates are validated against numerical simulations. The third objective in this work is to optimize the solution strategy of the nonlinear flow model in coupled flow and mechanics schemes. The global inexact Newton method, combined with the line search backtracking algorithm along with heuristic forcing functions, can be efficiently employed to reduce the number of flow linear iterations, and hence, the overall CPU run time. We first validate these computational savings for challenging two-phase benchmark problems including the full SPE10 model. Motivated by the obtained results, we incorporate this strategy as a nonlinear solver framework to solve the nonlinear flow problem in multirate iteratively coupled schemes. This leads to a scheme that reduces both the number of flow and mechanics linear iterations efficiently. All our numerical implementations in this work are built on top of our in-house reservoir simulator (IPARS).

Table of Contents

List of Tables

List of Figures

Chapter 1

Introduction

1.1 Motivation

Recently, the accurate modeling of flow-structure interactions has gained more attention and importance for both environmental and petroleum engineering applications. A clear understanding of the fluid flow and the solid-phase mechanical response is needed for the accurate modeling of multiscale and multiphysics phenomena such as reservoir deformation, surface subsidence, well stability, sand production, waste deposition, pore collapse, fault activation, hydraulic fracturing, CO_2 sequestration, and hydrocarbon recovery [45], [63]. Of particular interest is the coupling between subsurface flow and reservoir geomechanics. Traditionally, the main purpose of simulating reservoirs was to obtain accurate results for reservoir flow, simplifying the influence of porous media deformations by a constant rock compressibility factor. In fact, such an influence affects pore pressure which, in turn, affects the accuracy of reservoir flow models [63]. By oversimplifying the rock compressibility coefficient with a constant rock compressibility term, the solid phase stress and strain can never be accounted for. This poses several concerns on the accuracy of flow models in stress-sensitive and naturally fractured reservoirs [63]. Therefore, it is only through the accurate coupling between subsurface flow and reservoir geomechanics that accurate and trusted results can be deduced from flow models in such types of reservoirs.

1.1.1 Examples of Subsidence Events

Due to oil extraction, especially in stress-sensitive reservoirs, rock compaction may occur inducing a subsidence event. Such subsidence events might not only affect the surrounding environment adversely, but also can result in a dramatic impact on reservoir production [85]. Below are two examples of oil fields which experienced subsidence events in the past, due

to oil extraction activities:

- Valhall Field: The Valhall field was discovered in 1975, and its development started in 1981. It started producing oil and gas in October, 1982. It is located about 180 miles offshore in the central graben of the North Sea, at a depth of 7875 ft. It consists of two oil-bearing formations: the Tor and Hod. The Tor is a soft chalk formation with a very high porosity (around 50%) and very high oil saturation (more than 90%). In mid 1986, surface subsidence was observed by satellite surveys, and infrared-wave-height measurements. After investigation, it was found that the pressure depletion of the high-porosity chalk caused plastic deformation and compaction of the reservoir which translated into the observed subsidence of surface facilities. In addition, a significant part of hydrocarbon recovery was driven by the rock compaction (lithic-drive process) [76].

- Wilmington Field: The Willmington field is located in California, near the southern edge of the Los Angeles sedimentary basin. It was producing from seven zones located at various depths (ranging from 2000 to 6000 ft), with a porosity range of 33% to 37% and a permeability range of 500 to 2000 md in the different zones. The upper zone reservoir sands are loose and unconsolidated. As a result, these sands compacted rapidly as oil was produced, resulting in decreasing its porosity by at least 3%. Consequently, the reservoir surface has subsided as much as 29 ft at its center. According to the City Civic Center, this subsidence caused millions of dollars of damage, and put the Long Beach Naval Shipyard at the threat of inundation [5].

1.2 Overview of Flow & Geomechanics Coupling Approaches

Three different coupling approaches are usually employed in modeling fluid flow coupled with reservoir geomechanics. They are known as the fully implicit, the explicit or loose coupling, and the iterative coupling methods. The fully implicit approach solves reservoir multiphase flow and mechanics equations simultaneously. It is an unconditionally stable approach [53], and considered to be the most accurate one. Typically, Newton-Raphson

method is used to linearize the coupled system [53], and the obtained solution is self-consistent. However, the main drawback of this approach is its huge computational cost compared to the other two types of coupling. In addition, it poses several numerical and computational challenges to the underlying linear solver. On the other hand, the loosely coupled approach is less accurate, but has the attractive advantage of having lower computational cost. It requires estimates of when to update the mechanical response of the system, and at best, it provides only an approximate solution to the problem. The iterative coupling approach lies in between the two extremes, and solves the two coupled subsystems iteratively by exchanging the values of the shared state variables in an iterative manner. The procedure is iterated at each time step until the solution is obtained with an acceptable tolerance [26, 53, 60, 63, 87].

1.3 Literature Review

The coupled flow and geomechanics problem has been intensively investigated in the past. The seed of this work can be tracked down to the work of Terzaghi [84] and Biot [15, 16]. Terzaghi was the first to propose an explanation of the soil consolidation process, in which he assumed that grains forming the soil are bound together by some molecular forces resulting in the formation of the porous material with elastic properties. Based on such concepts, he analyzed the settlement of a column of soil under a constant load and prevented from lateral expansions. It is the success of Terzaghi's theory in predicting the settlement of different types of soils that lead to the creation of the the science of soil mechanics [16]. More details about Terzaghi's theory of consolidation can be found in [84]. Biot then extended Terzaghi's one dimensional work to the three-dimensional case, and presented a more rigorous generalized theory of consolidation [16]. In subsequent work, Biot continued to develop the theory of elasticity and consolidation for isotropic and anisotropic porous media, including the theory of deformation of a porous viscoelastic anisotropic solid [14, 17, 18]. A treatment of thermoelasticity and the mechanics of deformation and acoustic propagation in porous media can be found in [19, 20]. Several studies and interpretations baed on Biot's consolidation theory can be found in [41,74]. To name just few, Geertsma [41] utilized Biot theory to present a united treatment of rock mechanics problems in the field

of petroleum production engineering. Rice and Cleary [74] presented applications of the Biot linearized quasi static elasticity theory of fluid-saturated porous media. Few years later, Coussy [28] presented the general theory of thermoporoelastoplasiticy for saturated materials. The work of Settari and Mourits [78] proposed robust iterative and explicit coupling schemes for coupling flow with geomechanics along with fracture propagation. A comprehensive treatment of the theory of mechanics of porous continua and poromechanics can be found in [29,30] by Coussy. Other nonlinear extensions of the theory of poroelasticity can be found in [25, 26, 35, 37, 79, 83].

Recently, the work of Mikelić and Wheeler [64] established geometric convergence (contraction with respect to appropriately chosen metrics) for different flow and geomechanics iterative coupling schemes. In addition, stability convergence analysis of similar schemes was extensively explored in the work of Kim, Tchelepi, and Juanes [51, 52]. In their work, von Neumann type of analysis was carried out to study stability of linear flow and geomechanics coupling problems, while energy methods were used to analyze nonlinear coupling problems. Moreover, techniques from matrix algebra and spectral analysis were used to derive a priori error estimates for different coupling schemes, including drained, undrained, fixed-stress, and fixed-strain splits. In the drained and undrained split methods, the pressure field and the fluid mass content are frozen during the geomechanics sub-step respectively [51]. In the fixed-stress split method, which is the method we heavily investigate in this research, the volumetric mean total stress is kept constant during the flow sub-step. This implies that the volumetric total stress is evaluated explicitly when solving for the flow problem [52,64]. On the other hand, the rate of the total strain is fixed during the solution of the flow problem in the fixed-strain split method [52]. Using von Neumann analysis and energy-based methods, the undrained split method was shown to be unconditionally stable for "backward Euler" and "midpoint rule" time discretization. On the contrary, the drained split method with the midpoint rule time discretization is unconditionally unstable. For "backward Euler" time discretization, the drained split is conditionally stable, and its stability is independent of the time step size [51]. The von Nuemann analysis also revealed that the fixed-stress split is an unconditionally stable scheme while the fixed-strain split is only a conditionally stable and oscillatory scheme [52]. It was also shown in [51, 52] that

the drained split method with a fixed number of iterative coupling iterations is not convergent, while the undrained split method is convergent for a compressible system (finite Biot modulus), and non-convergent for an incompressible system (infinite Biot modulus) with a fixed number of iterative coupling iterations [51]. It was also found that the fixed-strain split is not always convergent for a fixed number of iterative coupling iterations [52]. On the other hand, the fixed-stress split is convergent with a better accuracy than the undrained split method for a fixed number of iterative coupling iterations [52].

The existence, uniqueness, and regularity of the Biot system without fractures were investigated by a number of authors (Showalter [81], Phillips & Wheeler [70], and Girault *et al.* [44]). The interaction between fractures and the surrounding poro-elastic medium was traditionally modeled in a number of different ways. One approach, applicable to narrow fractures, treats the width of the fracture as a small parameter ϵ which tends to zero [39]. The work of Morales and Showalter [67, 68] followed this approach, in which they considered only the flow problem without coupling it with geomechanics. In their work, the fracture was modeled as a flat basis with a vertical height of the order of ϵ and the pressure was assumed to be continuous at the interfaces. Another approach treats the fracture as a thin domain in the framework of domain decomposition. Following this approach, extensive work was carried out by Jaffré, Roberts *et al.* [4,62] on Darcy flow models for thin fractures. It should be noted that the approach we will follow in this research models the fracture as a thin domain, which corresponds to a lower dimensional geometrical object. Following this approach, fractures can be considered as non-planar surfaces in three-dimensional simulations. Recently, the modeling of fracture propagation received huge attention, and is considered an active area of research. One approach to model the propagation of fractures employs a phase-field energy minimization method to track the movements and expansions of fractures [65, 66, 91].

The numerical analysis of the coupled flow and geomechanics problem in a fractured poro-elastic medium was heavily investigated by Girault *et al.* [45] in which a fully implicit approach is considered for coupling flow with mechanics. The work of Ganis *et al.* [39] considered the numerical approximation of a fracture model in a poro-elastic medium. In their work, the fracture is represented as a curve or a surface with its width being

incorporated into the fracture's flow equation. The Multipoint Flux Mixed Finite Element (MFMFE) method is used for flow discretization in the reservoir, and the Mimetic Finite Difference method is used for flow discretization in the fracture. It should be noted here that the Mimetic Finite Difference method is implemented in Python, and the MFMFE discretization scheme is implemented in IPARS. The two frameworks are coupled together through a C++ socket interface, written solely by the author of this dissertation [2]. In addition, it was primarily through this socket interface that the Python mimetic code was coupled to the IPARS compiled framework in the dissertation work of [3]. Moreover, this interface was used to couple the two frameworks to model multiphase flow with nonplanar fractures in [2]. More recently, the work of [22] used Stokes equation to model the flow in the fracture, and showed the stability of the proposed numerical scheme based on Nitsche method for Stokes-Biot model.

From such a quick survey, it is clear that the accurate modeling of reservoir flow coupled with geomechanics has received much recent attention for both environmental and petroleum engineering applications. However, the development and analysis of theoretically convergent iterative coupling algorithms in both poro-elastic and fractured poro-elastic reservoirs have received quite less attention. The main objective of this research is to bridge this gap by devising and analyzing different iterative and explicit coupling schemes for coupled flow and geomechanics problems in poro-elastic as well as fractured reservoirs.

1.4 Research Objectives

In this research, we pursue the following broad objectives:

1. To develop single rate and multirate iterative and explicit coupling schemes for solving coupled geomechanics and flow problems in poro-elastic and fractured poroelastic media. For poro-elastic meida, we will be considering two flow-mechanics splitting schemes: the fixed-stress split and the undrained split iterative coupling schemes [64]. For fractured poro-elastic media, our iterative scheme is an adaptation, due to the presence of the fractures, of the classical fixed stress-splitting scheme [43]. This is

due to the fact that the fixed-stress split scheme is the first iterative coupling scheme used to model fracture propagation in poroelastic media [65].

2. To rigorously analyze the convergence properties of the devised single rate and mulrirate coupling schemes. We will carry out a thorough mathematical analysis of the convergence properties of different variations of the "fixed stress split" iterative coupling algorithm for poro-elastic and fractured poro-elastic media. In addition, we will study convergence properties of the the undrained split coupling scheme for poro-elastic media. Most of our theoretically derived results are original, and are natural extensions of the work carried out in the literature.

3. To numerically investigate the efficiency of multirate iterative and explicit coupling schemes as natural candidate schemes for solving coupled flow and geomechanics problems as the geomechanics problem can cope with a coarser time step compared to the flow problem. Multirate schemes allow for taking larger time steps for the geomechanics problem and finer time steps for the flow problem.

4. To investigate the efficiency of the global inexact Newton method, combined with a line-search backtracking globalization technique, as a nonlinear solver framework for solving fully implicit nonlinear flow problems. When incorporated in solving the nonlinear flow problen in multirate iteratively coupled schemes, the number of flow and mechanics linear iterations are reduced efficiently, resulting in an efficient, convergent, and robust scheme.

Chapter 2

Iterative Coupling Schemes for Poroelastic Media

2.1 Introduction

In this chapter, we study single rate and multirate iterative coupling schemes for coupling flow with linear elasticity, based on two different coupling algorithms: the fixed-stress split coupling algorithm, and the undrained split coupling algorithm. Our work is inspired by the previous work of Mikelić and Wheeler [64] (see also [42]) and extends their results to cover the case of fully discrete multirate iterative coupling schemes. Convergence properties of multirate explicit coupling schemes have been heavily investigated in [80,92] for the non-stationary Stokes-Darcy model. In contrast, we consider multirate iteratively coupled flow and geomechanics problems in this work. Figures 2.1a and 2.1b illustrate the differences between single rate versus multirate iterative coupling schemes. Figure 2.1a represents a typical single rate scheme, in which the flow and mechanics problems share the exact same time step, and the coupling iteration continues until convergence. In contrast, Figure 2.1b demonstrates a typical multirate scheme, in which the flow problem takes multiple finer local time steps within one coarser mechanics time step for each iterative coupling iteration. The process is iterated until convergence. In this work, we propose different multirate iterative schemes and their analyses and deduce the contracting character of each scheme. Convergence follows immediately by applying Banach's fixed point theorem. The presence of two different time steps for different equations in such a system of PDEs introduces several complications. We define an appropriate expression of the volumetric mean stress for the multirate scheme and use the flow and mechanics estimates to derive a contraction

The theoretical work in this chapter is a collaborative work with Dr. Kundan Kumar, under the supervision of Prof. Mary Wheeler. Numerical implementations in IPARS are done primarily by Tameem Almani, with helpful discussions with Drs. Kundan Kumar and Gurpreet Singh. Dr. Ali Dogru reviewed some of the obtained results. This research work has been published in [6, 7, 11, 13].

for the difference of two successive coupling iterates. In addition, we employ mathematical induction along with a contraction argument to deduce strong convergence of the pressure and flux unknowns for flow finer time steps within a coarser mechanics time step. Our analysis also reveals the optimal values of the fixed stress split regularization term in the mass conservation equation, and the undrained split regularization term in the mechanics equation. Moreover, for the fixed-stress split method, we introduce a modified multirate iterative coupling scheme that successively corrects the fluxes in even coupling iterations so that the resulting scheme has the same convergence properties as of single rate scheme. To the best of our knowledge, this is the first analysis of multirate schemes for Biot equations.

For completeness, we note here that these iterative methods can be also used as a preconditioner for the fully implicit method. The work of Gai *et al* [36, 38] was the first to interpret the fixed stress split iterative coupling scheme (the single rate scheme) as an effective physics-based preconditioning strategy applied to a Richardson fixed point iteration. The same preconditioning operator can be applied to the fully implicit coupled system, enhancing the underlying Krylov subspace iteration as well [23, 24, 36]. We do not pursue this direction in this research as we consider the fully decoupled system. However, our theoretical work lays down a solid background for the choices of the regularization terms used in the fixed-stress split and undrained split methods. Moreover, the extensions of the proposed methods to the preconditioning of the fully coupled system will be considered in future work.

To summarize, our contributions in this chapter are as follows:

- We formulate two multirate iterative coupling schemes for the Biot system that can be viewed as the extensions of the classical fixed-stress split coupling algorithm (see [64]) to the multirate settings in which flow takes finer time steps compared to the mechanics problem.
- We establish the contracting behavior of both schemes leading to geometric speed of convergence with an explicit expression for the contracting factor.

- We derive an optimized Banach contraction result for the single rate undrained split iterative coupling scheme (compared to the result obtained in [64]), with a sharper contraction coefficient.

- We formulate multirate undrained-split iterative coupling scheme for the Biot system, and establish its contracting behavior with an explicit expression for the contracting factor.

- In terms of numerical analysis, for multirate schemes, the novelty is in combining the contraction property with an induction argument to show that the obtained solution converges to the unique solution of the original weak formulations given in Definitions 2.3.2 (for multirate fixed-stress split scheme) and 2.4.2 (for multirate undrained-split scheme).

- Moreover, the numerical examples show the sharpness of the theoretical estimates. They also reveal the CPU time savings as a result of the reduction in the number of mechanics linear iterations for the multirate scheme versus the single rate scheme, without jeopardizing the accuracy of the results.

- We establish the effect of different Young's modulus values on the contracting property of the scheme, both theoretically and numerically.

- Finally, our proof outlines a general strategy that is likely to be useful for obtaining similar estimates in other contexts.

2.1.1 Preliminaries

Let Ω be an open, connected, and bounded domain of $\mathbb{R}^d$, where the dimension $d = 2$ or 3, with a Lipschitz continuous boundary $\partial\Omega$. For the pressure unknown, we assume that the boundary is decomposed into Dirichlet boundary Γ_D, and Neumann boundary Γ_N, associated with Dirichlet and Neumann boundary conditions respectively, such that $\Gamma_D \cup \Gamma_N = \partial\Omega$. In addition, Let $\mathfrak{D}(\Omega)$ be the space of all functions that are infinitely

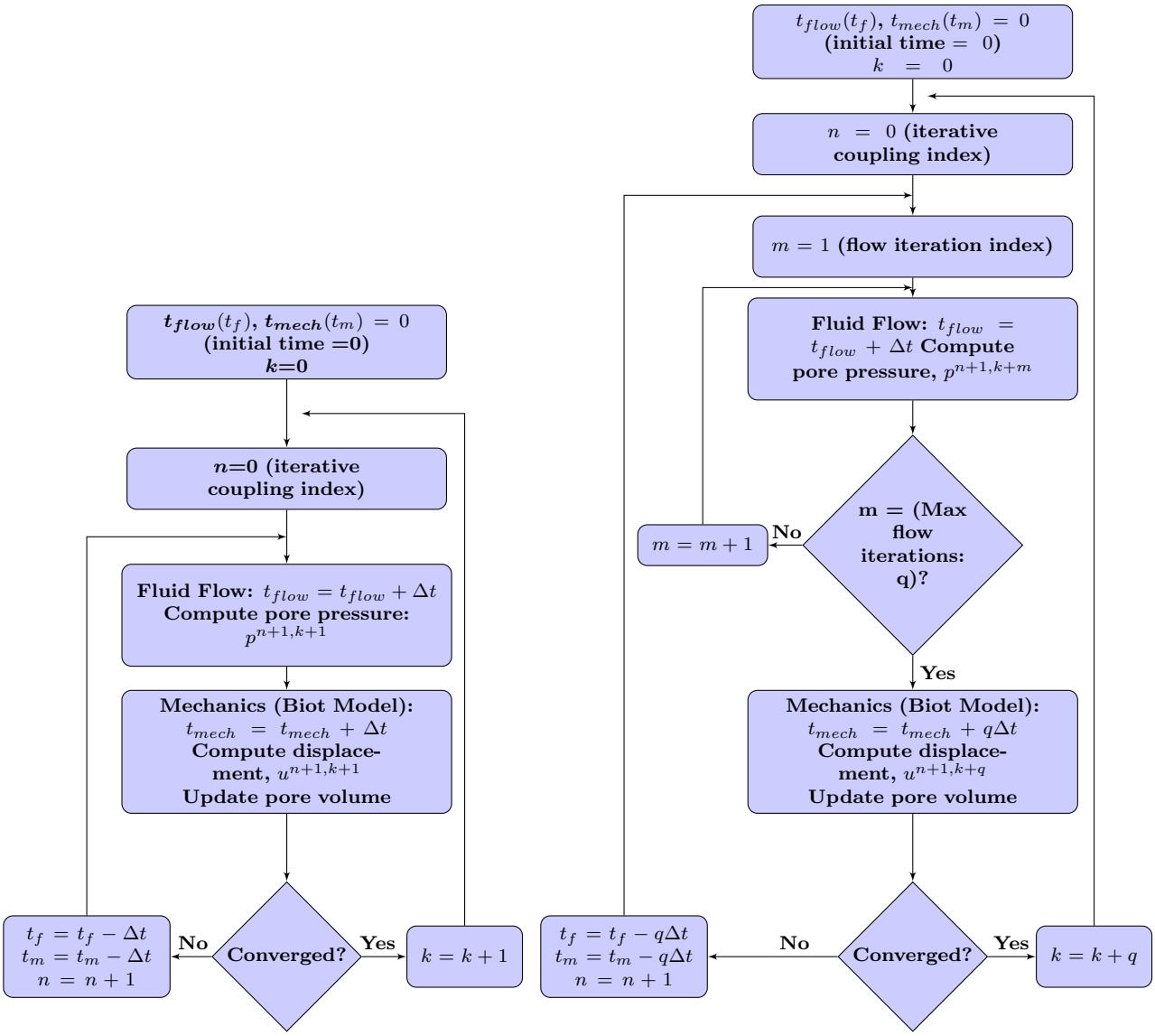

(a) Single Rate (b) Multirate

Figure 2.1: Flowchart for the iterative coupling algorithm using single rate and multirate time stepping for coupled geomechanics and flow problems

differentiable and with compact support in Ω, and let $\mathfrak{D}'(\Omega)$ be its dual space, i.e. the space of distributions in Ω. As usual, we denote by $H^1(\Omega)$ the classical Sobolev space

$$H^1(\Omega) = \{v \in L^2(\Omega)\,;\, \nabla\, v \in L^2(\Omega)^d\},$$

equipped with the semi-norm and norm:

$$|v|_{H^1(\Omega)} = \|\nabla\, v\|_{L^2(\Omega)^d} \quad , \quad \|v\|_{H^1(\Omega)} = \left(\|v\|^2_{L^2(\Omega)} + |v|^2_{H^1(\Omega)}\right)^{1/2}.$$

More generally, for $1 \leq p < \infty$, $W^{1,p}(\Omega)$ is the space

$$W^{1,p}(\Omega) = \{v \in L^p(\Omega)\,;\, \nabla\, v \in L^p(\Omega)^d\},$$

normed by

$$|v|_{W^{1,p}(\Omega)} = \|\nabla\, v\|_{L^p(\Omega)^d} \quad , \quad \|v\|_{W^{1,p}(\Omega)} = (\|v\|^p_{L^p(\Omega)} + |v|^p_{W^{1,p}(\Omega)})^{1/p},$$

with the standard modification for the case when $p = \infty$. We also define:

$$H^1_0(\Omega) = \{v \in H^1(\Omega)\,;\, v|_{\partial\Omega} = 0\},$$

and for the divergence operator, we shall use the space

$$H(\mathrm{div};\Omega)^d = \{\boldsymbol{v} \in L^2(\Omega)^d\,;\, \nabla \cdot \boldsymbol{v} \in L^2(\Omega)\},$$

equipped with the norm

$$\|\boldsymbol{v}\|_{H(\mathrm{div};\Omega)^d} = (\|\boldsymbol{v}\|^2_{L^2(\Omega)^d} + \|\nabla \cdot \boldsymbol{v}\|^2_{L^2(\Omega)})^{1/2}.$$

We recall the definition of the symmetric strain tensor: $\boldsymbol{\varepsilon}(v) = \frac{1}{2}(\nabla v + (\nabla v)^T)$, for a vector v in $I\!R^d$. For completeness, we list below two useful inequalities that will be used in this chapter:

- Poincaré's inequality in $H^1_0(\Omega)$:
  There exists a constant $\mathcal{P}_\Omega$ depending only on Ω such that

$$\forall v \in H^1_0(\Omega)\,,\ \|v\|_{L^2(\Omega)} \leq \mathcal{P}_\Omega |v|_{H^1(\Omega)}. \tag{2.1.1}$$

- Korn's first inequality in $H^1_0(\Omega)^d$:
  There exists a constant C_κ depending only on Ω such that

$$\forall \boldsymbol{v} \in H^1_0(\Omega)^d\,,\ |\boldsymbol{v}|_{H^1(\Omega)^d} \leq C_\kappa \|\boldsymbol{\varepsilon}(\boldsymbol{v})\|_{L^2(\Omega)^{d\times d}}. \tag{2.1.2}$$

2.2 Model Equations and Discretization

We assume a linear, elastic, homogeneous, and isotropic porous medium $\Omega \subset \mathbb{R}^d$, $d = 2$ or 3, in which the reservoir is saturated with a slightly compressible fluid.

2.2.1 Assumptions

We have the following assumptions on the model and data:

1. For mechanical modeling, the reservoir is assumed to be homogeneous, isotropic and saturated poro-elastic medium. The reference density of the fluid $\rho_f > 0$ is given and positive.

2. The Lamé coefficients $\lambda > 0$ and $G > 0$, the dimensionless Biot coefficient α, and the pore volume φ^* are all positive.

3. The fluid is assumed to be slightly compressible and its density is a linear function of pressure. The viscosity $\mu_f > 0$ is assumed to be constant.

4. The absolute permeability tensor, $\boldsymbol{K}$, is assumed to be symmetric, bounded, uniformly positive definite in space and constant in time.

2.2.2 Geomechanics Model

Using a quasi-static (i.e. ignoring the second order time derivative for the displacement) Biot approach to obtain the displacements (see [16]), the "geomechanics" model is as follows:

$$\boldsymbol{\sigma}^{\mathrm{por}}(\boldsymbol{u}, p) = \boldsymbol{\sigma}(\boldsymbol{u}) - \alpha\, p\, \boldsymbol{I}, \tag{2.2.3}$$

$$\boldsymbol{\sigma}(\boldsymbol{u}) = \lambda(\nabla \cdot \boldsymbol{u})\boldsymbol{I} + 2\, G\boldsymbol{\varepsilon}(\boldsymbol{u}), \tag{2.2.4}$$

$$-\operatorname{div} \boldsymbol{\sigma}^{\mathrm{por}}(\boldsymbol{u}, p) = \boldsymbol{f} \quad \text{in}\, \Omega, \tag{2.2.5}$$

where $\boldsymbol{\sigma}^{\mathrm{por}}$ is the Cauchy stress tensor, $\boldsymbol{I}$ is the identity tensor, $\boldsymbol{u}$ is the solid's displacement, p is the fluid pressure, $\alpha > 0$ is the dimensionless Biot coefficient, $\boldsymbol{\sigma}$ is the effective linear elastic stress tensor, $\lambda > 0$ and $G > 0$ are the Lamé constants, $\boldsymbol{f}$ is a body force, which is usually assumed to be a gravity loading term. The last equation represents the balance of linear momentum in the solid.

2.2.3 Single Phase Flow Model

Following a slightly different formulation compared to the one described in [45], we assume a linearized slightly compressible single-phase flow model for the fluid in the reservoir. As listed in the assumptions above, we also assume that $\boldsymbol{K}$, the absolute permeability tensor, is bounded, symmetric, and uniformly positive definite in space and constant in time (for discrete time intervals). The fluid density, ρ_f is assumed to be a linear function of pressure: $\rho_f = \rho_{f,r}(1 + c_f(p - p_r))$. The porosity, or the fluid content of the medium, denoted by φ^* is related to the "mechanical" displacement and "fluid" pressure by this relation: $\varphi^* = \varphi_0 + \alpha\nabla\cdot\boldsymbol{u} + \frac{1}{M}p$, where φ_0 is the initial porosity, and M is the Biot constant. The fluid mass balance in the reservoir, denoted by Ω, reads: $\frac{\partial}{\partial t}(\rho_f\varphi^*) + \nabla\cdot(\rho_f\boldsymbol{v}^D) = q_s$, where q_s is a mass source or sink term, and $\boldsymbol{v}^D$ is the velocity of the fluid in Ω, $\boldsymbol{v}^D = -\frac{1}{\mu_f}\boldsymbol{K}(\nabla p - \rho_f g\nabla\eta)$. Substituting the definitions of $\boldsymbol{v}^D$, ρ_f, and φ^* into the mass balance equation, we get:

$$\frac{\partial}{\partial t}\Big(\rho_{f,r}(1 + c_f(p - p_r))(\varphi_0 + \alpha\nabla\cdot\boldsymbol{u} + \frac{1}{M}p)\Big) + \nabla\cdot(\rho_{f,r}(1 + c_f(p - p_r))\boldsymbol{v}^D) = q_s.$$

which can be written as (after re-arranging terms):

$$\rho_{f,r}\Big(\frac{1}{M}(1 + c_f(p - p_r)) + c_f(\varphi_0 + \alpha\nabla\cdot\boldsymbol{u} + \frac{1}{M}p)\Big)\frac{\partial}{\partial t}p + \rho_{f,r}\alpha(1 + c_f(p - p_r))\nabla\cdot\frac{\partial}{\partial t}\boldsymbol{u}$$
$$+\nabla\cdot(\rho_{f,r}(1 + c_f(p - p_r))\boldsymbol{v}^D) = q_s.$$

For the sake of linearization, we assume that the fluid compressibility c_f is small, in the order of 10^{-5} or 10^{-6}, and the term $c_f(p - p_r)$ is also small as well (of the same order). We make the following approximations: $\frac{1}{M}(1 + c_f(p - p_r)) \approx \frac{1}{M}$, $c_f(\varphi_0 + \alpha\nabla\cdot\boldsymbol{u} + \frac{1}{M}p) \approx c_f\varphi_0$, $\rho_{f,r}(1 + c_f(p - p_r))\alpha \approx \rho_{f,r}\alpha$, $\rho_{f,r}(1 + c_f(p - p_r))\boldsymbol{v}^D \approx \rho_{f,r}\boldsymbol{v}^D$, $\rho_{f,r}(1 + c_f(p - p_r))g\nabla\eta \approx \rho_{f,r}g\nabla\eta$. With such approximations, the mass balance equation now reads:

$$\rho_{f,r}(\frac{1}{M} + c_f\varphi_0)\frac{\partial}{\partial t}p + \rho_{f,r}\alpha\nabla\cdot\frac{\partial}{\partial t}\boldsymbol{u} + \rho_{f,r}\nabla\cdot\boldsymbol{v}^D = q_s$$

which can be written as (after dividing by $\rho_{f,r}$, and submitting the expressiotn of $\boldsymbol{v}^D$):

$$\frac{\partial}{\partial t}\Big((\frac{1}{M} + c_f\varphi_0)p + \alpha\nabla\cdot\boldsymbol{u}\Big) - \nabla\cdot\Big(\frac{1}{\mu_f}\boldsymbol{K}(\nabla p - \rho_{f,r}g\nabla\eta)\Big) = \tilde{q}. \tag{2.2.6}$$

where $\tilde{q} = \frac{q_s}{\rho_{f,r}}$. This completes the derivation of the poro-elastic equations, modeling the displacement $\boldsymbol{u}$ and pressure p in Ω.

Therefore, our quasi-static Biot model, which is quite standard in literature [16, 45], reads: Find $\boldsymbol{u}$ and p satisfying the equations below for all time $t \in]0, T[$:

$$
\begin{gathered}
-\operatorname{div} \boldsymbol{\sigma}^{\mathrm{por}}(\boldsymbol{u}, p) = \boldsymbol{f} \ \text{ in } \Omega, \\
\boldsymbol{\sigma}^{\mathrm{por}}(\boldsymbol{u}, p) = \boldsymbol{\sigma}(\boldsymbol{u}) - \alpha\, p\, \boldsymbol{I} \ \text{ in } \Omega, \\
\boldsymbol{\sigma}(\boldsymbol{u}) = \lambda(\nabla \cdot \boldsymbol{u})\boldsymbol{I} + 2\, G\boldsymbol{\varepsilon}(\boldsymbol{u}) \ \text{ in } \Omega, \\
\tfrac{\partial}{\partial t}\Big((\tfrac{1}{M} + c_f\varphi_0)p + \alpha\nabla \cdot \boldsymbol{u}\Big) - \nabla \cdot \Big(\tfrac{1}{\mu_f}\boldsymbol{K}(\nabla\, p - \rho_{f,r} g \nabla\, \eta)\Big) = \tilde{q} \ \text{ in } \Omega, \\
\text{Boundary Conditions: } \boldsymbol{u} = \boldsymbol{0} \text{ on } \partial\Omega, \ \boldsymbol{K}(\nabla\, p - \rho_{f,r} g \nabla\, \eta) \cdot \boldsymbol{n} = 0 \ \text{ on } \Gamma_N, \ \ p = 0 \text{ on } \Gamma_D, \\
\text{Initial Condition } \ (t = 0): \ \Big((\tfrac{1}{M} + c_f\varphi_0)p + \alpha\nabla \cdot \boldsymbol{u}\Big)(0) = (\tfrac{1}{M} + c_f\varphi_0)p_0 + \alpha\nabla \cdot \boldsymbol{u}_0.
\end{gathered}
$$

where: g is the gravitational constant, η is the distance in the vertical direction (assumed to be constant in time), $\rho_{f,r} > 0$ is a constant reference density (relative to the reference pressure p_r), φ_0 is the initial porosity, M is the Biot constant, $\tilde{q} = \frac{q_s}{\rho_{f,r}}$ where q_s is a mass source or sink term taking into account injection into or out of the reservoir. We remark that the first three equations describe the mechanics whereas the fourth one is the flow equation. Note that the above system is linear and coupled.

2.2.4 Mixed Variational Formulation

We will use a mixed formulation for the flow and conformal Galerkin formulation for the mechanics equation. The mixed method defines flux as a separate unknown and rewrites the flow equation as a system of first order equations. Such a formulation for the flow is standard and is preferred because it is locally mass conservative and has an explicit computation for the flux. Accordingly, for the fully discrete formulation (discrete in time and space), we use a mixed finite element method for space discretization and a backward-Euler time discretization. Let $\mathfrak{T}_h$ denote a regular family of conforming triangular elements of the domain of interest, $\overline{\Omega}$. Using the lowest order Raviart-Thomas (RT) spaces , we have the following discrete spaces ($\boldsymbol{V}_h$ for discrete displacements, Q_h for discrete pressures, and

$\boldsymbol{Z}_h$ for discrete velocities (fluxes)):

$$\boldsymbol{V}_h = \{\boldsymbol{v}_h \in H^1(\Omega)^d\,;\, \forall T \in \mathfrak{T}_h, \boldsymbol{v}_{h|T} \in {\mathbb{P}_1}^d, \boldsymbol{v}_{h|\partial\Omega} = \boldsymbol{0}\} \tag{2.2.7}$$

$$Q_h = \{p_h \in L^2(\Omega)\,;\, \forall T \in \mathfrak{T}_h, p_{h|T} \in \mathbb{P}_0\} \tag{2.2.8}$$

$$\boldsymbol{Z}_h = \{\boldsymbol{q}_h \in H(\mathrm{div};\Omega)\,;\forall T \in \mathfrak{T}_h, \boldsymbol{q}_{h|T} \in {\mathbb{P}_1}^d,\ \boldsymbol{q}_h \cdot \boldsymbol{n} = 0 \ \text{ on } \Gamma_N\} \tag{2.2.9}$$

The space of displacements, $\boldsymbol{V}_h$, is equipped with the norm:

$$\|\boldsymbol{v}\|_{V_h} = \Big(\sum_{i=1}^{d} \|v_i\|^2_{H^1(\Omega)}\Big)^{1/2}.$$

We also assume that the finer time step is given by: $\Delta t_k = t_k - t_{k-1}$. In this work, we assume uniform fine flow time steps, so for simplicity, we will drop the subscript k, and denote the fine time step by Δt. If we denote the total number of timesteps by N, then the total simulation time is given by $\mathrm{T} = \Delta t$ N, and $t_i = i\Delta t$, $0 \leqslant i \leqslant N$ denote the discrete time points.

For the fully discrete scheme, we have chosen the Raviart-Thomas spaces for the mixed finite element discretization. However, the proof extends to other choices for the mixed spaces and we will state the results for Multipoint Flux Mixed Finite Element (MFMFE) spaces [87, 90] in Remark 2.3.6.

Remark 2.2.1. Notation: *Throughout this chapter, there will be two indices, one for the time step and the other for the coupling between the flow and mechanics. To avoid any confusion, let us emphasise the following notations, n denotes the coupling iteration index, k is the coarser time step iteration index (for indexing mechanics coarse time steps), m is the finer (local) time step iteration index (for indexing flow fine time steps), Δt stands for the time step, and q is the "fixed" number of local flow time steps per coarse mechanics time step. A schematic showing the relations between k, m, q, and Δt can be found in figure 2.1b.*

2.3 Fixed Stress Split Iterative Coupling

2.3.1 Standard Fixed Stress Split Algorithm

In the fixed stress split iterative coupling algorithm, we first solve the flow problem followed by the geomechanics problem. Even though we use the splitting strategy at the discrete level, it is probably easier to see this in the continuous strong form. Recalling that n denotes the coupling iteration index between the flow and mechanics problems, the steps are as follows:

Step (a): Given $\boldsymbol{u}^n$, we solve for $p^{n+1}, \boldsymbol{z}^{n+1}$

$$(\tfrac{1}{M} + c_f\varphi_0 + \tfrac{\alpha^2}{\lambda})\tfrac{\partial}{\partial t}p^{n+1} + \tfrac{1}{\mu_f}\nabla\cdot\boldsymbol{z}^{n+1} = \tfrac{\alpha^2}{\lambda}\tfrac{\partial}{\partial t}p^{n} - \alpha\nabla\cdot\tfrac{\partial}{\partial t}\boldsymbol{u}^n + \tilde{q}$$
$$\boldsymbol{z}^{n+1} = -\boldsymbol{K}(\nabla\, p^{n+1} - \rho_{f,r}g\nabla\,\eta)$$

Once the flow is computed, we update the displacement solution.

Step (b): Given $p^{n+1}, \boldsymbol{z}^{n+1}$, we solve for $\boldsymbol{u}^{n+1}$ satisfying

$$-\operatorname{div}\boldsymbol{\sigma}^{\mathrm{por}}(\boldsymbol{u}^{n+1}, p^{n+1}) = \boldsymbol{f}$$
$$\boldsymbol{\sigma}^{\mathrm{por}}(\boldsymbol{u}^{n+1}, p^{n+1}) = \boldsymbol{\sigma}(\boldsymbol{u}^{n+1}) - \alpha\, p^{n+1}$$
$$\boldsymbol{\sigma}(\boldsymbol{u}^{n+1}) = \lambda(\nabla\cdot\boldsymbol{u}^{n+1})\boldsymbol{I} + 2\,G\boldsymbol{\varepsilon}(\boldsymbol{u}^{n+1})$$

with the initial condition, independent of n,

$$\Big((\frac{1}{M} + c_f\varphi_0)p^{n+1} + \alpha\nabla\cdot\boldsymbol{u}^{n+1}\Big)(0) = (\frac{1}{M} + c_f\varphi_0)p_0 + \alpha\nabla\cdot\boldsymbol{u}_0. \tag{2.3.10}$$

Note that the flow equation has a regularization term $\alpha^2/\lambda\partial_t p^{n+1}$ added to the left hand side and a similar term added to the right hand side for consistence while the mechanics equation remains unchanged. In the case of convergence, this term vanishes retrieving the original equation. Indeed, this has been analyzed in literature and we simply state the results to elucidate our approach. Following result is obtained in Mikelić and Wheeler [64], and adapted to our model equations.

Theorem 2.3.1. *[Mikelić & Wheeler [64]] Let* $\Omega^t := \Omega\times(0,t)$, $\sigma_v := \sigma_{v,0} + \lambda\nabla\cdot\boldsymbol{u} - \alpha p$, $\sigma_v|_{t=0} = \sigma_{v,0}$ *(the initial volumetric mean total stress),* $\sigma_v^n := \sigma_{v,0} + \lambda\nabla\cdot\boldsymbol{u}^n - \alpha p^n$, *and* δ

denoting the difference of two successive iterates, the fixed stress split scheme as given in Section 2.3.1 is a contraction given by

$$\left\|\partial_t \delta\sigma_v^{n+1}\right\|_{\Omega^t}^2 + \frac{\lambda M\alpha^2}{\mu_f(M\alpha^2+\lambda(1+Mc_f\varphi_0))}\left\|K^{-1/2}\delta\nabla p^{n+1}(t)\right\|_{\Omega}^2 + 4G\lambda\|\boldsymbol{\varepsilon}(\partial_t\delta\boldsymbol{u}^{n+1})\|_{\Omega^t}^2 + \lambda^2\|\nabla\cdot\delta\boldsymbol{u}^{n+1,k}\|_{\Omega^t}^2 \leq \left(\frac{M\alpha^2}{\lambda+M\lambda c_f\varphi_0+M\alpha^2}\right)^2\left\|\partial_t\delta\sigma_v^n\right\|_{\Omega^t}^2.$$

The proof of the above results can be adapted to the fully discrete case in which a mixed formulation is used for space discretization (see section 2.3.2.2 and Theorem 2.3.2). Moreover, in the Theorem 2.3.1, the contraction is obtained on the volumetric mean stress, σ_v, involving both pressure (flow) and displacement (mechanics) unknowns. A relatively straightforward argument shows that the converged quantities solve the original coupled equations in a weak form.

Our ultimate goal in this chapter is to derive similar estimates for the case of the multirate iterative coupling scheme. Two different multirate iterative coupling algorithms will be discussed and analyzed. Even though our approach is similar to the one in [64], the fact that we solve for multiple flow finer time steps within one coarser mechanics time step leads to several complications. The adaptation of the fixed stress algorithm requires defining an appropriate mean stress quantity and the analysis introduces two adjustable parameters. Careful algebraic manipulations are required to show the contraction. Even after the contraction is achieved, the presence of the two different time scales in the coupled problem requires non-trivial arguments involving the mathematical induction to show convergence to the weak formulation (2.3.33) – (2.3.36).

We start by analyzing the single rate fixed-stress split iterative coupling scheme, adapted to our fully discrete model.

2.3.2 Single Rate Formulation and Analysis

2.3.2.1 Fully Discrete Scheme for Single Rate

As discussed above, using the mixed finite element method in space and the backward Euler finite difference method in time, the weak formulation of the single rate scheme reads as follows.

Definition 2.3.1. *Find $p_h^k \in Q_h$, and $\boldsymbol{z}_h^k \in \boldsymbol{Z}_h$ such that,*

*(***flow equation***)*

$$\forall \theta_h \in Q_h \,, \frac{1}{\Delta t}\Big((\frac{1}{M} + c_f \varphi_0)\Big(p_h^k - p_h^{k-1}\Big), \theta_h\Big) + \frac{1}{\mu_f}(\nabla \cdot \boldsymbol{z}_h^k, \theta_h) = \\ - \frac{\alpha}{\Delta t}\Big(\nabla \cdot \Big(\boldsymbol{u}_h^k - \boldsymbol{u}_h^{k-1}\Big), \theta_h\Big) + \Big(\tilde{q}_h, \theta_h\Big), \tag{2.3.11}$$

$$\forall \boldsymbol{q}_h \in \boldsymbol{Z}_h \,, \Big(\boldsymbol{K}^{-1}\boldsymbol{z}_h^k, \boldsymbol{q}_h\Big) = \Big(p_h^k, \nabla \cdot \boldsymbol{q}_h\Big) + \Big(\rho_{f,r} g \nabla \eta, \boldsymbol{q}_h\Big), \tag{2.3.12}$$

*and (***mechanics equation***)*

find $\boldsymbol{u}_h^k \in \boldsymbol{V}_h$ such that,

$$\forall \boldsymbol{v}_h \in V_h \,, 2G(\boldsymbol{\varepsilon}(\boldsymbol{u}_h^k), \boldsymbol{\varepsilon}(\boldsymbol{v}_h)) + \lambda(\nabla \cdot \boldsymbol{u}_h^k, \nabla \cdot \boldsymbol{v}_h) - \alpha(p_h^k, \nabla \cdot \boldsymbol{v}_h) = (\boldsymbol{f}, \boldsymbol{v}_h), \tag{2.3.13}$$

with the initial condition for the first discrete time step,

$$p_h^0 = p_0. \tag{2.3.14}$$

2.3.2.2 Single Rate Iterative Scheme

Here, we provide a single rate formulation of the "fixed stress split" iterative coupling algorithm and analyze its convergence properties in the next section. We begin by describing the algorithm.

Algorithm 1: Single Rate Iterative Coupling Algorithm

for $k = 0, 1, 2, 3, ..$ **do** /* Time step iteration index */

  for $n = 1, 2, ..$ **do** /* coupling iteration index */

    First Step: Flow equations

    Given $\boldsymbol{u}_h^{n,k}$ *(assuming an initial value is given for the first iteration:* $\boldsymbol{u}_h^{0,k}$*)*

    Solve for $p_h^{n+1,k}$ *and* $\boldsymbol{z}_h^{n+1,k}$ *satisfying:*

$$(\frac{1}{M} + c_f\varphi_0 + \frac{\alpha^2}{\lambda})\Big(\frac{p_h^{n+1,k} - p_h^{k-1}}{\Delta t}\Big) + \frac{1}{\mu_f}\nabla\cdot\boldsymbol{z}_h^{n+1,k} = \frac{\alpha^2}{\lambda}\Big(\frac{p_h^{n,k} - p_h^{k-1}}{\Delta t}\Big) - \alpha\nabla\cdot\Big(\frac{\boldsymbol{u}_h^{n,k} - \boldsymbol{u}_h^{k-1}}{\Delta t}\Big) + \tilde{q}_h \tag{2.3.15}$$

$$\boldsymbol{z}_h^{n+1,k} = -\boldsymbol{K}(\nabla p_h^{n+1,k} - \rho_{f,r} g \nabla \eta) \tag{2.3.16}$$

    Second Step: Mechanics equations

    Given $p_h^{n+1,k}$ *and,* $\boldsymbol{z}_h^{n+1,k}$*, solve for* $\boldsymbol{u}_h^{n+1,k}$ *satisfying:*

$$-\operatorname{div}\boldsymbol{\sigma}^{\mathrm{por}}(\boldsymbol{u}_h^{n+1,k}, p_h^{n+1,k}) = \boldsymbol{f} \tag{2.3.17}$$

$$\boldsymbol{\sigma}^{\mathrm{por}}(\boldsymbol{u}_h^{n+1,k}, p_h^{n+1,k}) = \boldsymbol{\sigma}(\boldsymbol{u}_h^{n+1,k}) - \alpha\, p_h^{n+1,k}\,\boldsymbol{I} \tag{2.3.18}$$

$$\boldsymbol{\sigma}(\boldsymbol{u}_h^{n+1,k}) = \lambda(\nabla\cdot\boldsymbol{u}_h^{n+1,k})\boldsymbol{I} + 2\,G\boldsymbol{\varepsilon}(\boldsymbol{u}_h^{n+1,k}) \tag{2.3.19}$$

The weak formulation for the flow and mechanics equations (2.3.15)-(2.3.19) (in the context of fixed stress split coupling scheme) reads:

Step (a): Find $p_h^{n+1,k} \in Q_h$, $\boldsymbol{z}_h^{n+1,k} \in \boldsymbol{Z}_h$ such that:

$$\forall\theta_h \in Q_h\,,\ \Big((\frac{1}{M} + c_f\varphi_0 + \frac{\alpha^2}{\lambda})(\frac{p_h^{n+1,k} - p_h^{k-1}}{\Delta t}), \theta_h\Big) + \frac{1}{\mu_f}(\nabla\cdot\boldsymbol{z}_h^{n+1,k}, \theta_h) = \Big(-\frac{\alpha}{\lambda}(-\alpha(\frac{p_h^{n+1,k} - p_h^{k-1}}{\Delta t}) + \lambda\nabla\cdot(\frac{\boldsymbol{u}_h^{n,k} - \boldsymbol{u}_h^{k-1}}{\Delta t})), \theta_h\Big) + (\tilde{q}_h, \theta_h) \tag{2.3.20}$$

$$\forall\boldsymbol{q}_h \in \boldsymbol{Z}_h\,,\ (\boldsymbol{K}^{-1}\boldsymbol{z}_h^{n+1,k}, \boldsymbol{q}_h) = (p_h^{n+1,k}, \nabla\cdot\boldsymbol{q}_h) + (\nabla(\rho_{f,r} g\eta), \boldsymbol{q}_h) \tag{2.3.21}$$

Step (b) Given $p_h^{n+1,k}, \boldsymbol{z}_h^{n+1,k}$, find $\boldsymbol{u}_h^{n+1,k} \in \boldsymbol{V}_h$ such that,

$$\forall\boldsymbol{v}_h \in V_h\,,\ 2G(\boldsymbol{\varepsilon}(\boldsymbol{u}_h^{n+1,k}), \boldsymbol{\varepsilon}(\boldsymbol{v}_h)) + \lambda(\nabla\cdot\boldsymbol{u}_h^{n+1,k}, \nabla\cdot\boldsymbol{v}_h) - \alpha(p_h^{n+1,k}, \nabla\cdot\boldsymbol{v}_h) = (\boldsymbol{f}, \boldsymbol{v}_h)\,, \tag{2.3.22}$$

For a given time step $t = t_k$, we define the difference between two coupling iterates as:

$$\delta\xi^{n+1,k} = \xi^{n+1,k} - \xi^{n,k},$$

where ξ may stand for $p_h, \boldsymbol{z}_h$, or $\boldsymbol{u}_h$. The volumetric mean total stress can be defined as follows:

$$\sigma_v^{n,k} = \sigma_v^{k-1} + \lambda \nabla \cdot \boldsymbol{u}_h^{n,k} - \alpha(p_h^{n,k} - p_h^{k-1}). \tag{2.3.23}$$

In terms of coupling iteration differences, this can be written as:

$$\delta\sigma_v^{n,k} = \lambda \nabla \cdot \delta\boldsymbol{u}_h^{n,k} - \alpha \delta p_h^{n,k} \tag{2.3.24}$$

Now, In terms of "coupling iteration" differences, the weak formulation reads:

$$\forall \theta_h \in Q_h\,,\ \Big(\frac{1}{\Delta t}(\frac{1}{M} + c_f\varphi_0 + \frac{\alpha^2}{\lambda})\delta p_h^{n+1,k}, \theta_h\Big) + \frac{1}{\mu_f}(\nabla \cdot \delta \boldsymbol{z}_h^{n+1,k}, \theta_h) = \Big(- \frac{\alpha}{\lambda \Delta t}\delta\sigma_v^{n,k}, \theta_h\Big) \tag{2.3.25}$$

$$\forall \boldsymbol{q}_h \in \boldsymbol{Z}_h\,,\ (\boldsymbol{K}^{-1}\delta \boldsymbol{z}_h^{n+1,k}, \boldsymbol{q}_h) = (\delta p_h^{n+1,k}, \nabla \cdot \boldsymbol{q}_h) \tag{2.3.26}$$

$$\forall \boldsymbol{v}_h \in V_h\,,\ 2G(\boldsymbol{\varepsilon}(\delta \boldsymbol{u}_h^{n+1,k}), \boldsymbol{\varepsilon}(\boldsymbol{v}_h)) + \lambda(\nabla \cdot \delta \boldsymbol{u}_h^{n+1,k}, \nabla \cdot \boldsymbol{v}_h) - \alpha(\delta p_h^{n+1,k}, \nabla \cdot \boldsymbol{v}_h) = 0 \tag{2.3.27}$$

2.3.2.3 Proof of Contraction

Let $\beta = \frac{1}{M\alpha^2} + \frac{c_f}{\alpha^2}\varphi_0 + \frac{1}{\lambda}$, which represents the coefficient in front of the first term on the left hand side of (2.3.25).

- **Step (1): Flow equations**

  Consider (2.3.25), and choose for $\theta_h = \delta p_h^{n+1,k}$,

  $$\Big(\frac{1}{\Delta t}\alpha^2\beta\delta p_h^{n+1,k}, \delta p_h^{n+1,k}\Big) + \frac{1}{\mu_f}\Big(\nabla \cdot \delta \boldsymbol{z}_h^{n+1,k}, \delta p_h^{n+1,k}\Big) = -\frac{\alpha}{\lambda \Delta t}\Big(\delta\sigma_v^{n,k}, \delta p_h^{n+1,k}\Big)$$

  $\Rightarrow$

  $$\begin{aligned}\frac{\beta}{\Delta t}\Big\|\alpha\delta p_h^{n+1,k}\Big\|^2 + \frac{1}{\mu_f}\Big(\nabla \cdot \delta \boldsymbol{z}_h^{n+1,k}, \delta p_h^{n+1,k}\Big) &= \frac{1}{\Delta t}\Big((-\alpha\varepsilon\delta p_h^{n+1,k}), (\frac{1}{\varepsilon\lambda})\sigma_v^{n,k}\Big) \\ &\le \frac{1}{\Delta t}\Big(\frac{\varepsilon^2}{2}\Big\|\alpha\delta p_h^{n+1,k}\Big\|^2 + \frac{1}{2\varepsilon^2\lambda^2}\Big\|\frac{\partial}{\partial t}\delta\sigma_v^{n,k}\Big\|^2\Big)\end{aligned}$$

  Letting $\varepsilon^2 = \beta$, we obtain

  $$\beta\Big\|\alpha\delta p_h^{n+1,k}\Big\|^2 + \frac{2\Delta t}{\mu_f}(\nabla \cdot \delta \boldsymbol{z}_h^{n+1,k}, \delta p_h^{n+1,k}) \le \frac{1}{\beta\lambda^2}\Big\|\delta\sigma_v^{n,k}\Big\|^2. \tag{2.3.28}$$

Now, consider the flux equation, (2.3.26), and choose for $\boldsymbol{q}_h = \delta \boldsymbol{z}_h^{n+1,k}$ to get

$$(\boldsymbol{K}^{-1}\delta \boldsymbol{z}_h^{n+1,k}, \delta \boldsymbol{z}_h^{n+1,k}) = (\delta p_h^{n+1,k}, \nabla \cdot \delta \boldsymbol{z}_h^{n+1,k}) \tag{2.3.29}$$

Substituting (2.3.29) into (2.3.28) and dividing by β, we obtain:

$$\left\|\alpha \delta p_h^{n+1,k}\right\|^2 + \frac{2\Delta t}{\beta \mu_f}\left\|K^{-1/2}\delta \boldsymbol{z}_h^{n+1,k}\right\|^2 \leq \frac{1}{\beta^2\lambda^2}\left\|\delta \sigma_v^{n,k}\right\|^2 \tag{2.3.30}$$

- **Step (2): Elasticity equation**

  Consider (2.3.27), choose $\boldsymbol{v}_h = \delta \boldsymbol{u}_h^{n+1,k}$, and multiply by 2λ to obtain:

$$4G\lambda\|\boldsymbol{\varepsilon}(\delta \boldsymbol{u}_h^{n+1,k})\|^2 + 2\lambda^2\|\nabla \cdot \delta \boldsymbol{u}_h^{n+1,k}\|^2 - 2\lambda\alpha(\delta p_h^{n+1,k}, \nabla \cdot \delta \boldsymbol{u}_h^{n+1,k}) = 0. \tag{2.3.31}$$

  Adding (2.3.31) with (2.3.30) and substituting the value β, we obtain:

$$\begin{aligned}
&\left\{\left\|\alpha \delta p_h^{n+1,k}\right\|^2 - 2(\alpha \delta p_h^{n+1,k}, \lambda \nabla \cdot \delta \boldsymbol{u}_h^{n+1,k}) + \|\lambda \nabla \cdot \delta \boldsymbol{u}_h^{n+1,k}\|^2\right\} \\
&+ \frac{2\Delta t \lambda M\alpha^2}{\mu_f(M\alpha^2 + \lambda(1 + Mc_f\varphi_0))}\left\|K^{-1/2}\delta \boldsymbol{z}_h^{n+1,k}\right\|^2 + 4G\lambda\|\boldsymbol{\varepsilon}(\delta \boldsymbol{u}_h^{n+1,k})\|^2 \\
&+ \lambda^2\|\nabla \cdot \delta \boldsymbol{u}_h^{n+1,k}\|^2 \leq \left(\frac{M\alpha^2}{\lambda + M\lambda c_f\varphi_0 + M\alpha^2}\right)^2\left\|\delta \sigma_v^{n,k}\right\|^2
\end{aligned}$$

  Thus we have:

$$\begin{aligned}
&\left\|\delta \sigma_v^{n+1,k}\right\|^2 + \frac{2\Delta t \lambda M\alpha^2}{\mu_f(M\alpha^2 + \lambda(1 + Mc_f\varphi_0))}\left\|K^{-1/2}\delta \boldsymbol{z}_h^{n+1,k}\right\|^2 + 4G\lambda\|\boldsymbol{\varepsilon}(\delta \boldsymbol{u}_h^{n+1,k})\|^2 \\
&+ \lambda^2\|\nabla \cdot \delta \boldsymbol{u}_h^{n+1,k}\|^2 \leq \left(\frac{M\alpha^2}{\lambda + M\lambda c_f\varphi_0 + M\alpha^2}\right)^2\left\|\delta \sigma_v^{n,k}\right\|^2
\end{aligned} \tag{2.3.32}$$

  It is clear that the contraction constant is strictly less than one as $\left(\frac{M\alpha^2}{\lambda + M\lambda c_f\varphi_0 + M\alpha^2}\right)^2 < 1$.

2.3.2.4 Convergence to The Discrete Form

From the above discussion, we obtain the following lemma.

Lemma 2.3.1. *There exist limit functions $p_h^k, \boldsymbol{u}_h^k, \boldsymbol{z}_h^k$ such that*

$$p_h^{n,k} \to p_h^k \quad \text{in } L^2(\Omega), \quad \boldsymbol{u}_h^{n,k} \to \boldsymbol{u}_h^k \quad \text{in } H^1(\Omega)^d, \quad \boldsymbol{z}_h^{n,k} \to \boldsymbol{z}_h^k \quad \text{in } H(div, \Omega)^d$$

converge strongly in the norms of the above spaces.

Proof. The contraction result in (2.3.32) implies that $\|\delta\sigma_v^{n+1,k}\|_\Omega$, $\|\nabla\cdot\delta\boldsymbol{u}_h^{n+1,k}\|_\Omega$, and $\|K^{-1/2}\delta\boldsymbol{z}_h^{n+1,k}\|_\Omega$ converge geometrically to zero. This implies that $\sigma_v^{n+1,k}$, $\nabla\cdot\boldsymbol{u}_h^{n+1,k}$, and $\boldsymbol{z}_h^{n+1,k}$ are Cauchy sequences in $L^2(\Omega)$. By the definition of $\sigma_v^{n,k}$, i.e. (2.3.23) and (2.3.24), and the fact that the addition of two Cauchy sequences is a Cauchy sequence, we obtain that $p_h^{n,k}$ also converge geometrically in $L^2(\Omega)$, and hence is a Cauchy sequence in Hilbert (complete) space and has a unique limit in $L^2(\Omega)$.

Similarly, for the displacement, (2.3.32) implies that $\boldsymbol{\varepsilon}(\delta\boldsymbol{u}_h^{n+1,k})$ converges geometrically to 0 in $L^2(\Omega)$, which implies that $\boldsymbol{u}_h^{n+1,k}$ converge geometrically in $H^1(\Omega)^d$. Thus, $\boldsymbol{u}_h^{n+1,k}$ is a Cauchy sequence in a complete Hilbert space, and hence has a unique limit in the corresponding space.

For the divergence of the flux, we note that (2.3.25) amounts to the following equality in $L^2(\Omega)$ a.e.,

$$\nabla\cdot\delta\boldsymbol{z}_h^{n+1,k}=\frac{\mu_f}{\Delta t}(\frac{1}{M}+c_f\varphi_0+\frac{\alpha^2}{\lambda})\delta p_h^{n+1,k}-\frac{\mu_f\alpha}{\lambda\Delta t}\delta\sigma_v^{n,k}$$

The convergence of $\nabla\cdot\boldsymbol{z}_h^{n+1,k}$ in $L^2(\Omega)$ follows from the convergence of $p_h^{n+1,k}$ and $\sigma_v^{n,k}$ in $L^2(\Omega)$. Therefore, we have both $\nabla\cdot\boldsymbol{z}_h^{n+1,k}$ and $\boldsymbol{z}_h^{n+1,k}$ converging geometrically to 0 in $L^2(\Omega)$, hence $\boldsymbol{z}_h^{n+1,k}$ converges in $H(div,\Omega)^d$. The existence of the limiting function in $H(div,\Omega)^d$ follows from the completeness of the space. □

It remains to pass to the limit in (2.3.20)–(2.3.22). This is straightforward since the equations are linear and all operators involved are continuous in the spaces invoked in the statement of Lemma 2.3.1. Moreover the convergences are strong. Therefore, we easily retrieve the discrete in time formulation.

The above discussions are summarized in the following main result:

Theorem 2.3.2. *The iterative scheme is a contraction given by*

$$\left\|\delta\sigma_v^{n+1,k}\right\|_\Omega^2+\frac{2\Delta t\lambda M\alpha^2}{\mu_f(M\alpha^2+\lambda(1+Mc_f\varphi_0))}\left\|K^{-1/2}\delta\boldsymbol{z}_h^{n+1,k}\right\|_\Omega^2+4G\lambda\|\boldsymbol{\varepsilon}(\delta\boldsymbol{u}_h^{n+1,k})\|_\Omega^2+\lambda^2\|\nabla\cdot\delta\boldsymbol{u}_h^{n+1,k}\|_\Omega^2$$
$$\leq\left(\frac{M\alpha^2}{\lambda+M\lambda c_f\varphi_0+M\alpha^2}\right)^2\left\|\delta\sigma_v^{n,k}\right\|_\Omega^2$$

Furthermore, the converged solution is a unique solution to the weak formulation (2.3.20) - (2.3.22).

2.3.3 Multirate Formulation and Analysis

2.3.3.1 Fully Discrete Scheme for Multirate

Using the mixed finite element method in space and the backward Euler finite difference method in time, the weak formulation of a multirate scheme reads as follows.

Definition 2.3.2. *For $1 \leq m \leq q$, find $p_h^{m+k} \in Q_h$, and $\boldsymbol{z}_h^{m+k} \in \boldsymbol{Z}_h$ such that,*

*(***flow equation***)*

$$\forall \theta_h \in Q_h \,, \frac{1}{\Delta t}\Big((\frac{1}{M} + c_f\varphi_0)\Big(p_h^{m+k} - p_h^{m-1+k}\Big), \theta_h\Big) + \frac{1}{\mu_f}(\nabla \cdot \boldsymbol{z}_h^{m+k}, \theta_h) = - \frac{\alpha}{q\Delta t}\Big(\nabla \cdot \Big(\boldsymbol{u}_h^{k+q} - \boldsymbol{u}_h^{k}\Big), \theta_h\Big) + \Big(\tilde{q}_h, \theta_h\Big), \tag{2.3.33}$$

$$\forall \boldsymbol{q}_h \in \boldsymbol{Z}_h \,, \Big(\boldsymbol{K}^{-1}\boldsymbol{z}_h^{m+k}, \boldsymbol{q}_h\Big) = \Big(p_h^{m+k}, \nabla \cdot \boldsymbol{q}_h\Big) + \Big(\rho_{f,r} g \nabla \eta, \boldsymbol{q}_h\Big), \tag{2.3.34}$$

*and (***mechanics equation***)*

find $\boldsymbol{u}_h^{k+q} \in \boldsymbol{V}_h$ such that,

$$\forall \boldsymbol{v}_h \in V_h \,, 2G(\boldsymbol{\varepsilon}(\boldsymbol{u}_h^{k+q}), \boldsymbol{\varepsilon}(\boldsymbol{v}_h)) + \lambda(\nabla \cdot \boldsymbol{u}_h^{k+q}, \nabla \cdot \boldsymbol{v}_h) - \alpha(p_h^{k+q}, \nabla \cdot \boldsymbol{v}_h) = (\boldsymbol{f}, \boldsymbol{v}_h). \tag{2.3.35}$$

with the initial condition for the first discrete time step,

$$p_h^0 = p_0. \tag{2.3.36}$$

Note that the pressure unknowns p_h and flux unknowns $\boldsymbol{z}_h$ are being solved at finer time steps $t_{k+m}, m = 0, \ldots, q$ whereas the mechanics variables $\boldsymbol{u}_h$ are being solved at $t_{iq}, i \in \mathbb{N}$. Therefore, for each mechanics time step of size $q\Delta t$, there are q flow solves justifying the nomenclature of multirate. Moreover, the above system of PDEs is linear but coupled with the coupling terms being computed at the coarse time steps. Instead of solving the problem in a coupled manner, as discussed before, we will apply a splitting algorithm to decouple the two equations and iterate between them until the solutions satisfying the above system (2.3.33) – (2.3.36) are obtained. We recall that in practice, there are 4 major splitting algorithms (drained, undrained, fixed strain and fixed stress) used for studying the Biot system depending upon whether one solves the mechanics first or flow and the physical variables which are being lagged. We will use the fixed stress splitting algorithm here because of its well established stability and excellent convergence properties as shown in Mikelić and Wheeler [64], and Mikelić et al. [63].

2.3.3.2 Original Multirate Iterative Scheme

Here, we provide the first multirate formulation of the "fixed stress split" iterative coupling algorithm and analyze its convergence properties in the next section. Recall that n denotes the coupling iteration index, k the coarser time step iteration index (for indexing mechanics time steps), m the finer (local) time step iteration index (for indexing flow finer time steps), Δt the unit time step, and q denote "fixed" number of local flow time steps within one coarse mechanics time step. We begin by describing the algorithm.

Algorithm 2: Multirate Iterative Coupling Algorithm

for $k = 0, q, 2q, 3q, ..$ **do** `/* mechanics time step iteration index */`

  for $n = 1, 2, ..$ **do** `/* coupling iteration index */`

    First Step: Flow equations

    Given $\boldsymbol{u}_h^{n,k+q}$ *(assuming an initial value is given for the first iteration:* $\boldsymbol{u}_h^{0,k+q}$*)*

    for $m = 1, 2, .., q$ **do** `/* flow finer time steps iteration index */`

      Solve for $p_h^{n+1,m+k}$ *and* $\boldsymbol{z}_h^{n+1,m+k}$ *satisfying:*

$$(\frac{1}{M} + c_f\varphi_0 + L)\Big(\frac{p_h^{n+1,m+k} - p_h^{n+1,m-1+k}}{\Delta t}\Big) + \frac{1}{\mu_f}\nabla \cdot \boldsymbol{z}_h^{n+1,m+k} = L\Big(\frac{p_h^{n,m+k} - p_h^{n,m-1+k}}{\Delta t}\Big) - \alpha\nabla \cdot \Big(\frac{\boldsymbol{u}_h^{n,k+q} - \boldsymbol{u}_h^{n,k}}{q\Delta t}\Big) + \tilde{q}_h \quad (2.3.37)$$

$$\boldsymbol{z}_h^{n+1,m+k} = -\boldsymbol{K}(\nabla p_h^{n+1,m+k} - \rho_{f,r} g \nabla \eta) \quad (2.3.38)$$

    Second Step: Mechanics equations

    Given $p_h^{n+1,k+q}$ *and,* $\boldsymbol{z}_h^{n+1,k+q}$*, solve for* $\boldsymbol{u}_h^{n+1,k+q}$ *satisfying:*

$$-\operatorname{div} \boldsymbol{\sigma}^{\mathrm{por}}(\boldsymbol{u}_h^{n+1,k+q}, p_h^{n+1,k+q}) = \boldsymbol{f} \quad (2.3.39)$$

$$\boldsymbol{\sigma}^{\mathrm{por}}(\boldsymbol{u}_h^{n+1,k+q}, p_h^{n+1,k+q}) = \boldsymbol{\sigma}(\boldsymbol{u}_h^{n+1,k+q}) - \alpha\, p_h^{n+1,k+q}\, \boldsymbol{I} \quad (2.3.40)$$

$$\boldsymbol{\sigma}(\boldsymbol{u}_h^{n+1,k+q}) = \lambda(\nabla \cdot \boldsymbol{u}_h^{n+1,k+q})\boldsymbol{I} + 2\,G\boldsymbol{\varepsilon}(\boldsymbol{u}_h^{n+1,k+q}) \quad (2.3.41)$$

The weak formulation of equations (2.3.37) - (2.3.41) reads:

For $k = iq$, $i \in \mathbb{N}$, $n = 1, 2, ..$

- Step (a) For $1 \le m \le q$, find $p_h^{n+1,m+k} \in Q_h$, and $\boldsymbol{z}_h^{n+1,m+k} \in \boldsymbol{Z}_h$ such that,

$$\forall \theta_h \in Q_h\,,\ \frac{1}{\Delta t}\Big((\frac{1}{M} + c_f\varphi_0 + L)\Big(p_h^{n+1,m+k} - p_h^{n+1,m-1+k}\Big), \theta_h\Big) + \frac{1}{\mu_f}(\nabla \cdot \boldsymbol{z}_h^{n+1,m+k}, \theta_h) = \frac{1}{\Delta t}\Big(L\Big(p_h^{n,m+k} - p_h^{n,m-1+k}\Big) - \frac{\alpha}{q}\nabla \cdot \Big(\boldsymbol{u}_h^{n,k+q} - \boldsymbol{u}_h^{n,k}\Big), \theta_h\Big) + \Big(\tilde{q}_h, \theta_h\Big), \quad (2.3.42)$$

$$\forall \boldsymbol{q}_h \in \boldsymbol{Z}_h\,,\ \Big(\boldsymbol{K}^{-1}\boldsymbol{z}_h^{n+1,m+k}, \boldsymbol{q}_h\Big) = \Big(p_h^{n+1,m+k}, \nabla \cdot \boldsymbol{q}_h\Big) + \Big(\rho_{f,r} g \nabla \eta, \boldsymbol{q}_h\Big), \quad (2.3.43)$$

with the initial condition, independent of n, for the first discrete time step,

$$p_h^{n+1,0} = p_0. \tag{2.3.44}$$

- Step (b) Given $p_h^{n+1,k+q}$ and, $\boldsymbol{z}_h^{n+1,k+q}$, find $\boldsymbol{u}_h^{n+1,k+q} \in \boldsymbol{V}_h$ such that,

$$\forall \boldsymbol{v}_h \in V_h\,,\; 2G(\boldsymbol{\varepsilon}(\boldsymbol{u}_h^{n+1,k+q}), \boldsymbol{\varepsilon}(\boldsymbol{v}_h)) + \lambda(\nabla \cdot \boldsymbol{u}_h^{n+1,k+q}, \nabla \cdot \boldsymbol{v}_h) \\ - \alpha(p_h^{n+1,k+q}, \nabla \cdot \boldsymbol{v}_h) = (\boldsymbol{f}, \boldsymbol{v}_h). \tag{2.3.45}$$

In the above scheme, L is the adjustable coefficient that will be chosen appropriately later (this choice completely determines the scheme) and q is a user-defined number of finer flow steps. Below we analyze the above weak formulation and deduce the contracting character of the iterative scheme. The proof relies on studying the difference of two successive iterates and uses Banach's fixed point theorem. The final step is to show that the converged quantities satisfy the weak formulation (2.3.33) – (2.3.36).

2.3.3.3 Proof of Contraction of the 1^{st} Scheme

Recalling that for a given time step $t = t_k$, the difference between two coupling iterates is given by:

$$\delta\xi^{n+1,k} = \xi^{n+1,k} - \xi^{n,k},$$

where ξ may stand for $p_h, \boldsymbol{z}_h$, and $\boldsymbol{u}_h$. In addition, for notational convenience, we define,

$$\beta = \frac{1}{M} + c_f\varphi_0 + L. \tag{2.3.46}$$

- **Step 1: Flow equations**

  For $n \geq 1$, by taking the difference of two successive iterates of (2.3.42), which corresponds to one local flow iteration and its corresponding local flow iteration in the previous flow and geomechanics iterative coupling iteration, testing with $\theta_h = \delta p_h^{n+1,m+k} - \delta p_h^{n+1,m-1+k}$, we obtain

$$\beta\left\|\delta p_h^{n+1,m+k} - \delta p_h^{n+1,m-1+k}\right\|^2 + \frac{\Delta t}{\mu_f}(\nabla \cdot \delta\boldsymbol{z}_h^{n+1,m+k}, \delta p_h^{n+1,m+k} - \delta p_h^{n+1,m-1+k}) = \\ \left(L(\delta p_h^{n,m+k} - \delta p_h^{n,m-1+k}) - \frac{\alpha}{q}\left(\nabla \cdot \delta\boldsymbol{u}_h^{n,k+q} - \nabla \cdot \delta\boldsymbol{u}_h^{n,k}\right), \delta p_h^{n+1,m+k} - \delta p_h^{n+1,m-1+k}\right). \tag{2.3.47}$$

Similarly, for the flux equation (2.3.43), by taking the difference of two successive iterates, followed by taking the difference at two consecutive finer time steps, $t = t_{m+k}$, and $t = t_{m-1+k}$, and testing with $\boldsymbol{q}_h = \delta \boldsymbol{z}_h^{n+1,m+k}$, we obtain

$$\Big(\boldsymbol{K}^{-1}\Big(\delta \boldsymbol{z}_h^{n+1,m+k} - \delta \boldsymbol{z}_h^{n+1,m-1+k}\Big), \delta \boldsymbol{z}_h^{n+1,m+k}\Big) \\ = \Big(\delta p_h^{n+1,m+k} - \delta p_h^{n+1,m-1+k}, \nabla \cdot \delta \boldsymbol{z}_h^{n+1,m+k}\Big). \quad (2.3.48)$$

We combine (2.3.47) with (2.3.48), apply Young's inequality and use $\nabla \cdot \delta \boldsymbol{u}_h^{n,k} = 0$ to obtain

$$\beta \Big\| \delta p_h^{n+1,m+k} - \delta p_h^{n+1,m-1+k} \Big\|^2 + \frac{\Delta t}{\mu_f}\Big(\boldsymbol{K}^{-1}\Big(\delta \boldsymbol{z}_h^{n+1,m+k} - \delta \boldsymbol{z}_h^{n+1,m-1+k}\Big), \delta \boldsymbol{z}_h^{n+1,m+k}\Big) \leq \\ \frac{1}{2\boldsymbol{\varepsilon}} \Big\| L(\delta p_h^{n,m+k} - \delta p_h^{n,m-1+k}) - \frac{\alpha}{q} \nabla \cdot \delta \boldsymbol{u}_h^{n,k+q} \Big\|^2 + \frac{\boldsymbol{\varepsilon}}{2} \Big\| \delta p_h^{n+1,m+k} - \delta p_h^{n+1,m-1+k} \Big\|^2.$$

The choice $\boldsymbol{\varepsilon} = \beta$ absorbs the pressure term on the right hand side. Together with a simple expansion of the flux product, we derive

$$\frac{\beta}{2} \Big\| \delta p_h^{n+1,m+k} - \delta p_h^{n+1,m-1+k} \Big\|^2 + \frac{\Delta t}{2\mu_f} \Big\{ \Big\| \boldsymbol{K}^{-1/2} \delta \boldsymbol{z}_h^{n+1,m+k} \Big\|^2 - \Big\| \boldsymbol{K}^{-1/2} \delta \boldsymbol{z}_h^{n+1,m-1+k} \Big\|^2 \\ + \Big\| \boldsymbol{K}^{-1/2} \big(\delta \boldsymbol{z}_h^{n+1,m+k} - \delta \boldsymbol{z}_h^{n+1,m-1+k}\big) \Big\|^2 \Big\} \\ \leq \frac{1}{2\beta} \Big\| L(\delta p_h^{n,m+k} - \delta p_h^{n,m-1+k}) - \frac{\alpha}{q} \nabla \cdot \delta \boldsymbol{u}_h^{n,k+q} \Big\|^2. \quad (2.3.49)$$

The right hand side constitutes an expression for a quantity to be contracted on. Introducing a new parameter χ, we define the volumetric mean stress for $(1 \leq m \leq q)$ as

$$\chi \delta \sigma_v^{n,m+k} = L(\delta p_h^{n,m+k} - \delta p_h^{n,m-1+k}) - \frac{\alpha}{q} \nabla \cdot \delta \boldsymbol{u}_h^{n,k+q}. \quad (2.3.50)$$

The value of χ will be chosen such that contraction can be achieved on the norm of $\sigma_v^{n,m+k}$, summed over q flow finer time steps, within one coarser mechanics time step. Multiplying (2.3.49) by $\frac{2}{\beta}$, summing up for $1 \leq m \leq q$, substituting the new definition of the volumetric mean stress (2.3.50), and noting that $\delta \boldsymbol{z}_h^{n+1,k} = 0$, we

obtain

$$\sum_{m=1}^{q}\left\|\delta p_h^{n+1,m+k}-\delta p_h^{n+1,m-1+k}\right\|^2+\frac{\Delta t}{\beta\mu_f}\left\|\boldsymbol{K}^{-1/2}\delta\boldsymbol{z}_h^{n+1,k+q}\right\|^2 + \frac{\Delta t}{\beta\mu_f}\sum_{m=1}^{q}\left\|\boldsymbol{K}^{-1/2}(\delta\boldsymbol{z}_h^{n+1,m+k}-\delta\boldsymbol{z}_h^{n+1,m-1+k})\right\|^2\leq\frac{1}{\beta^2}\sum_{m=1}^{q}\left\|\chi\delta\sigma_v^{n,m+k}\right\|^2. \tag{2.3.51}$$

- **Step 2: Elasticity equation**

  For $n\geq 1$, we take the difference of successive iterates of the mechanics equation (2.3.45), multiply by a newly introduced parameter, c_0, and test with $\boldsymbol{v}_h=\delta\boldsymbol{u}_h^{n+1,k+q}$ to get

$$2Gc_0\|\boldsymbol{\varepsilon}(\delta\boldsymbol{u}_h^{n+1,k+q})\|^2+\lambda c_0\|\nabla\cdot\delta\boldsymbol{u}_h^{n+1,k+q}\|^2-\alpha c_0(\delta p_h^{n+1,k+q},\nabla\cdot\delta\boldsymbol{u}_h^{n+1,k+q})=0. \tag{2.3.52}$$

  For the iterative scheme to be contractive, a quantity similar to the right hand side of (2.3.51), for the next iterative coupling iteration, $n+1$, has to be formed. To achieve that, we introduce a term involving a summation over all flow finer time steps in (2.3.52) by noticing that

$$\sum_{m=1}^{q}\left(\delta p_h^{n+1,m+k}-\delta p_h^{n+1,m-1+k}\right)=\delta p_h^{n+1,k+q}. \tag{2.3.53}$$

  Substituting (2.3.53) into (2.3.52) leads to

$$2Gc_0\|\boldsymbol{\varepsilon}(\delta\boldsymbol{u}_h^{n+1,k+q})\|^2+\lambda c_0\|\nabla\cdot\delta\boldsymbol{u}_h^{n+1,k+q}\|^2 - \alpha c_0(\sum_{m=1}^{q}\left(\delta p_h^{n+1,m+k}-\delta p_h^{n+1,m-1+k}\right),\nabla\cdot\delta\boldsymbol{u}_h^{n+1,k+q})=0. \tag{2.3.54}$$

- **Step 3: Combining flow and elasticity equations**

  By combining (2.3.54) with (2.3.51), and rearranging terms, we form a square term, in expanded form, summed over flow finer time steps within one coarser mechanics

time step,

$$2Gc_0\|\boldsymbol{\varepsilon}(\delta\boldsymbol{u}_h^{n+1,k+q})\|^2+\sum_{m=1}^{q}\Big\{\Big\|\delta p_h^{n+1,m+k}-\delta p_h^{n+1,m-1+k}\Big\|^2+\frac{\lambda c_0}{q}\Big\|\nabla\cdot\delta\boldsymbol{u}_h^{n+1,k+q}\Big\|^2$$
$$-\alpha c_0\Big(\delta p_h^{n+1,m+k}-\delta p_h^{n+1,m-1+k},\nabla\cdot\delta\boldsymbol{u}_h^{n+1,k+q}\Big)\Big\}+\frac{\Delta t}{\beta\mu_f}\Big\|\boldsymbol{K}^{-1/2}\delta\boldsymbol{z}_h^{n+1,k+q}\Big\|^2$$
$$+\frac{\Delta t}{\beta\mu_f}\sum_{m=1}^{q}\Big\|\boldsymbol{K}^{-1/2}(\delta\boldsymbol{z}_h^{n+1,m+k}-\delta\boldsymbol{z}_h^{n+1,m-1+k})\Big\|^2\leq\frac{\chi^2}{\beta^2}\sum_{m=1}^{q}\Big\|\delta\sigma_v^{n,m+k}\Big\|^2. \tag{2.3.55}$$

It remains to choose the values of our newly introduced parameters, χ, L, and c_0, such that the coefficients of the expanded square contributes only positive terms to the left hand side of (2.3.55). Therefore, we expand the right hand side of (2.3.55) as

$$\Big\|\delta\sigma_v^{n,m+k}\Big\|^2=\frac{L^2}{\chi^2}\Big\|\delta p_h^{n,m+k}-\delta p_h^{n,m-1+k}\Big\|^2-\frac{2\alpha L}{q\chi^2}\Big(\delta p_h^{n,m+k}-\delta p_h^{n,m-1+k},\nabla\cdot\delta\boldsymbol{u}_h^{n,k+q}\Big)$$
$$+\frac{\alpha^2}{\chi^2q^2}\Big\|\nabla\cdot\delta\boldsymbol{u}_h^{n,k+q}\Big\|^2. \tag{2.3.56}$$

Now, we match the coefficients of the expansion in (2.3.56) to the coefficients of the expanded square on the right hand side of (2.3.55). For the left hand side of (2.3.55) to remain positive, the following inequalities should be satisfied

$$1\geq\frac{L^2}{\chi^2},\qquad\frac{2\alpha L}{q\chi^2}=\alpha c_0,\qquad\frac{\lambda c_0}{q}\geq\frac{\alpha^2}{\chi^2q^2}.$$

The second inequality gives rise to $c_0=\frac{2L}{q\chi^2}$. The third inequality gives $L\geq\frac{\alpha^2}{2\lambda}$. Since the contraction factor is monotone with respect to L, its minimum is achieved when $L=\frac{\alpha^2}{2\lambda}$. The first inequality gives $\chi^2\geq L^2$. The minimum value of the contraction factor is achieved when $\chi^2=L^2$. Therefore, with

$$L=\frac{\alpha^2}{2\lambda},\qquad\chi^2=L^2,\qquad c_0=\frac{2L}{q\chi^2},$$

we group the terms of the expanded square on the left hand side of (2.3.55) to form the quantity of contraction for the next iterative coupling iteration, $n+1$, as

$$2Gc_0\|\boldsymbol{\varepsilon}(\delta\boldsymbol{u}_h^{n+1,k+q})\|^2+\sum_{m=1}^{q}\Big\|\delta\sigma_v^{n+1,m+k}\Big\|^2+\frac{\Delta t}{\beta\mu_f}\Big\|\boldsymbol{K}^{-1/2}\delta\boldsymbol{z}_h^{n+1,k+q}\Big\|^2$$
$$+\frac{\Delta t}{\beta\mu_f}\sum_{m=1}^{q}\Big\|\boldsymbol{K}^{-1/2}(\delta\boldsymbol{z}_h^{n+1,m+k}-\delta\boldsymbol{z}_h^{n+1,m-1+k})\Big\|^2\leq\Big(\frac{L}{\frac{1}{M}+c_f\varphi_0+L}\Big)^2\sum_{m=1}^{q}\Big\|\delta\sigma_v^{n,m+k}\Big\|^2. \tag{2.3.57}$$

Clearly, the contraction coefficient is strictly less than one:

$$\Big(\frac{L}{\frac{1}{M}+c_f\varphi_0+L}\Big)^2=\Big(\frac{M\alpha^2}{2\lambda+2M\lambda c_f\varphi_0+\alpha^2 M}\Big)^2<1,$$

and independent of q. This is not the case for the multirate undrained split coupling scheme, which we will consider later in this chapter. In the undrained split scheme, q appears in the denominator of the contraction coefficient.

2.3.3.4 Convergence to Discrete Multirate Formulation (1^{st} Scheme)

From the derivation above, we establish convergence of the sequences generated by the multirate fixed stress split algorithm and show that the converged quantities satisfy the weak formulation (2.3.33) – (2.3.36). The proof uses the mathematical induction for the finer flow equations combined with the contraction estimates obtained above.

Lemma 2.3.2. *For every coarser mechanics time step, $t = t_k$, there exist a limit function $\boldsymbol{u}_h^k$ such that*

$$\boldsymbol{u}_h^{n,k}\to\boldsymbol{u}_h^k \quad \textit{strongly in } H^1(\Omega)^d.$$

Proof. The contraction result in (2.3.57) implies that for a coarser time step $t = t_k$, $\|\boldsymbol{\varepsilon}(\delta\boldsymbol{u}_h^{n+1,k})\|$ converges geometrically to zero. This implies that $\boldsymbol{\varepsilon}(\boldsymbol{u}_h^{n+1,k})$ is a Cauchy sequence converging geometrically to a unique limit in $L^2(\Omega)$. It follows immediately that $\boldsymbol{u}_h^{n+1,k}$ is a Cauchy sequence converging geometrically to a unique limit in $H^1(\Omega)^d$, being a Hilbert space. □

Lemma 2.3.3. *For every two consecutive coarser mechanics time steps, $t = t_k$, and $t = t_{k+q}$, and for every $1 \le m \le q$, there exist limit functions $p_h^{m+k}, \boldsymbol{z}_h^{m+k}$ such that*

$$p_h^{n,m+k}\to p_h^{m+k} \quad \textit{in } L^2(\Omega), \quad \boldsymbol{z}_h^{n,m+k}\to\boldsymbol{z}_h^{m+k} \quad \textit{in } H(div,\Omega)^d,$$

with strong convergence in the norms of the above spaces.

Proof. The contraction result in (2.3.57) implies that the quantities $\sum_{m=1}^{q}\Big\|K^{-1/2}(\delta\boldsymbol{z}_h^{n+1,m+k}-\delta\boldsymbol{z}_h^{n+1,m-1+k})\Big\|^2$, and $\sum_{m=1}^{q}\Big\|\delta\sigma_v^{n+1,m+k}\Big\|^2$ converge geometrically to zero. It follows that for $1 \le m \le q$, $\Big\|K^{-1/2}(\delta\boldsymbol{z}_h^{n+1,m+k}-\delta\boldsymbol{z}_h^{n+1,m-1+k})\Big\|^2$,

and $\left\|\delta\sigma_v^{n+1,m+k}\right\|^2$ converge geometrically to zero. Moreover, by (2.3.38), and Poincaré inequality, $\left\|K^{1/2}\nabla(\delta p_h^{n+1,m+k} - \delta p_h^{n+1,m-1+k})\right\|^2$ and $\left\|\delta p_h^{n+1,m+k} - \delta p_h^{n+1,m-1+k}\right\|^2$ converge geometrically to zero, respectively. This implies that for every $1 \leq m \leq q$, the finer time step differences $(p_h^{n,m+k} - p_h^{n,m-1+k})$, $(\boldsymbol{z}_h^{n,m+k} - \boldsymbol{z}_h^{n,m-1+k})$, and the volumetric mean stress defined by $\sigma_v^{n,m+k}$ are Cauchy sequences in $L^2(\Omega)$.

We will show strong convergence of the pressure sequence by induction. The proof of strong convergence of the flux sequence follows in the same way. Given an initial pressure value for $t = t_0$: $p_h^{n,0} = p_0$, from the above discussion, $(p_h^{n,1} - p_0)$ is a Cauchy sequence in $L^2(\Omega)$, and, in turn, $p_h^{n,1}$ is a Cauchy sequence in the complete space $L^2(\Omega)$, and thus has a unique limit. This completes the base case for induction. For the inductive hypothesis, we assume that for any coarser mechanics time step $t = t_k$, and for any $1 \leq m \leq q$, $p_h^{n,k+m}$ is a Cauchy sequence converging to a unique limit in $L^2(\Omega)$: $p_h^{n,k+m} \to p_h^{k+m}$ in $L^2(\Omega)$. We will show that $p_h^{n,k+m+1}$ is also a Cauchy sequence converging to a unique limit in $L^2(\Omega)$. However, this follows immediately, as $(p_h^{n,k+m+1} - p_h^{n,k+m})$ is a Cauchy sequences in $L^2(\Omega)$, converging to a unique limit in $L^2(\Omega)$. This completes the inductive step. Therefore, we obtain that for all coarser mechanics time steps $t = t_k$, and for $1 \leq m \leq q$, $p_h^{n,m+k}, \boldsymbol{z}_h^{n,m+k}$ are Cauchy sequences converging geometrically to unique limits in $L^2(\Omega)$.

For the divergence of the flux, we note that (2.3.42) amounts to the following equality a.e. in $L^2(\Omega)$:

$$\nabla \cdot \delta\boldsymbol{z}_h^{n+1,m+k} = -\frac{\beta\mu_f}{\Delta t}(\delta p_h^{n+1,m+k} - \delta p_h^{n+1,m-1+k}) - \frac{\mu_f\chi}{\Delta t}\delta\sigma_v^{n,m+k}.$$

The convergence of $\nabla \cdot \boldsymbol{z}_h^{n,m+k}$ in $L^2(\Omega)$ follows from the convergence of the difference $(p_h^{n,m+k} - p_h^{n,m+k})$ and $\sigma_v^{n,m+k}$ in $L^2(\Omega)$, established above. Thus, we have both $\nabla \cdot \boldsymbol{z}_h^{n,m+k}$ and $\boldsymbol{z}_h^{n,m+k}$ converging geometrically to unique limits in $L^2(\Omega)$, and hence $\boldsymbol{z}_h^{n+1,k}$ converges to a unique limit in $H(div, \Omega)^d$. □

It remains to pass to the limit in (2.3.33)–(2.3.35), which is straightforward as the equations are linear and the operators involved are continuous in the spaces invoked in the statements of Lemmas 2.3.2 and 2.3.3. In addition, the convergences are strong.

Thus, we retrieve the fully discrete formulation.

The above discussions are summarized in the following main result:

Theorem 2.3.3. *[Multirate (1)] For $L = \frac{\alpha^2}{2\lambda}$, $\chi^2 = L^2$, and $c_0 = \frac{2L}{q\chi^2}$, the multirate iterative scheme is a contraction given by*

$$\begin{aligned}
&2Gc_0\|\boldsymbol{\varepsilon}(\delta\boldsymbol{u}_h^{n+1,k+q})\|^2 + \sum_{m=1}^{q}\left\|\delta\sigma_v^{n+1,m+k}\right\|^2 + \tfrac{\Delta t}{\beta\mu_f}\left\|\boldsymbol{K}^{-1/2}\delta\boldsymbol{z}_h^{n+1,k+q}\right\|^2 \\
&+\tfrac{\Delta t}{\beta\mu_f}\sum_{m=1}^{q}\left\|\boldsymbol{K}^{-1/2}(\delta\boldsymbol{z}_h^{n+1,m+k} - \delta\boldsymbol{z}_h^{n+1,m-1+k})\right\|^2 \\
&\qquad\qquad \leq \left(\tfrac{M\alpha^2}{2\lambda+2M\lambda c_f\varphi_0+\alpha^2 M}\right)^2 \sum_{m=1}^{q}\left\|\delta\sigma_v^{n,m+k}\right\|^2.
\end{aligned}$$

Furthermore, the sequences defined by this scheme converge to the unique solution of the weak formulation (2.3.33)–(2.3.35).

Remark 2.3.1. *The scheme presented in algorithm 2 can be modified such that the coarse mechanics time step is kept fixed as Δt, and the fine flow time step is considered as $\frac{\Delta t}{q}$, for $q \geq 1$. The proof of contraction follows in the same way except that the quantity of contraction is redefined as:*

$$\chi\delta\tilde{\sigma}_v^{n,m+k} = qL(\delta p_h^{n,m+k} - \delta p_h^{n,m-1+k}) - \alpha\nabla\cdot\delta\boldsymbol{u}_h^{n,k+q}$$

where χ is a newly introduced parameter. In this case, we have the following contraction result:

Theorem 2.3.4. *For $L = \frac{\alpha^2}{2\lambda}$, $\chi^2 = q^2L^2$, and $c_0 = \frac{2Lq}{\chi^2}$, the multirate iterative scheme is a contraction given by*

$$\begin{aligned}
&2Gc_0\|\boldsymbol{\varepsilon}(\delta\boldsymbol{u}_h^{n+1,k+q})\|^2 + \sum_{m=1}^{q}\left\|\delta\tilde{\sigma}_v^{n+1,m+k}\right\|^2 + \tfrac{\Delta t}{q\beta\mu_f}\left\|\boldsymbol{K}^{-1/2}\delta\boldsymbol{z}_h^{n+1,k+q}\right\|^2 \\
&+\tfrac{\Delta t}{q\beta\mu_f}\sum_{m=1}^{q}\left\|\boldsymbol{K}^{-1/2}(\delta\boldsymbol{z}_h^{n+1,m+k} - \delta\boldsymbol{z}_h^{n+1,m-1+k})\right\|^2 \\
&\qquad\qquad \leq \left(\tfrac{M\alpha^2}{2\lambda+2M\lambda c_f\varphi_0+\alpha^2 M}\right)^2 \sum_{m=1}^{q}\left\|\delta\tilde{\sigma}_v^{n,m+k}\right\|^2.
\end{aligned}$$

Remark 2.3.2. *We note that the contraction coefficient obtained in Theorem 2.3.4 exactly matches the contraction coefficient of the single rate optimized fixed stress split iterative method in the work of Mikelić and Wheeler [64]. In fact, in the theorem above, for $q = 1$,*

we get the same optimized single rate contraction result as the one obtained in [64] but for a fully discrete formulation (mixed formulation for flow, and CG for mechanics). Also, for the contraction results, we have assumed the compressibility term β to be positive. In case of incompressibility limits (β approaching zero), the contraction coefficient tends to 1. However, as the next remark shows we can still obtain contraction as long as the permeability remains positive. When λ approaches infinity, there is no change in the porosity in the flow equation and the contraction coefficient tends to zero.

Remark 2.3.3. *We can sharpen the contraction coefficient obtained in 2.3.4 as follows. By triangle's inequality, the quantity of contraction can be written as*

$$\left\|\delta\sigma_v^{n+1,m+k}\right\| \leq \frac{\alpha}{q\chi}\|\nabla\cdot\delta\boldsymbol{u}_h^{n+1,k+q}\|+\frac{L}{\chi}\|\delta p_h^{n+1,m+k}-\delta p_h^{n+1,m-1+k}\|.$$

The volumetric strain term can be bounded by Korn's inequality. In addition, using Poincare inequality, the pressure term can be estimated by the flux. This leads to

$$\begin{aligned}\sum_{m=1}^{q}\left\|\delta\sigma_v^{n+1,m+k}\right\|^2 &\leq C(\|\boldsymbol{\varepsilon}(\delta\boldsymbol{u}_h^{n+1,k+q})\|^2+\sum_{m=1}^{q}\left\|\boldsymbol{K}^{-1/2}\Big(\delta\boldsymbol{z}_h^{n+1,m+k}-\delta\boldsymbol{z}_h^{n+1,m-1+k}\Big)\right\|^2)\\ &\leq C\bigg(\|\boldsymbol{\varepsilon}(\delta\boldsymbol{u}_h^{n+1,k+q})\|^2+\sum_{m=1}^{q}\left\|\boldsymbol{K}^{-1/2}\Big(\delta\boldsymbol{z}_h^{n+1,m+k}-\delta\boldsymbol{z}_h^{n+1,m-1+k}\Big)\right\|^2+\left\|\boldsymbol{K}^{-1/2}\delta\boldsymbol{z}_h^{n+1,k+q}\right\|^2\bigg).\end{aligned} \tag{2.3.58}$$

for a constant $C>0$. Now, we define $\mathfrak{I}_q^{n+1,k+q}$ as:

$$\begin{aligned}\mathfrak{I}_q^{n+1,k+q} = 2Gc_0\|\boldsymbol{\varepsilon}(\delta\boldsymbol{u}_h^{n+1,k+q})\|^2+\frac{\Delta t}{\beta\mu_f}\sum_{m=1}^{q}\left\|\boldsymbol{K}^{-1/2}(\delta\boldsymbol{z}_h^{n+1,m+k}-\delta\boldsymbol{z}_h^{n+1,m-1+k}\Big)\right\|^2\\ +\frac{\Delta t}{\beta\mu_f}\left\|\boldsymbol{K}^{-1/2}\delta\boldsymbol{z}_h^{n+1,k+q}\right\|^2.\end{aligned}$$

Inequality (2.3.58) *can be written as, for a generic constant $C>0$:*

$$\sum_{m=1}^{q}\|\delta\sigma_v^{n+1,m+k}\|^2\leq C\mathfrak{I}_q^{n+1,k+q}. \tag{2.3.59}$$

The improved contraction result, based on theorem 2.3.4, can be written as:

$$\Big(\frac{1}{C}+1\Big)\sum_{m=1}^{q}\left\|\delta\sigma_v^{n+1,m+k}\right\|^2\leq\Big(\frac{M\alpha^2}{2\lambda+2M\lambda c_f\varphi_0+\alpha^2M}\Big)^2\sum_{m=1}^{q}\left\|\delta\sigma_v^{n,m+k}\right\|^2$$

which lead to the improved contraction constant,

$$\sum_{m=1}^{q} \left\|\delta\sigma_v^{n+1,m+k}\right\|^2 \leq \Big(\frac{C}{1+C}\Big)\Big(\frac{M\alpha^2}{2\lambda + 2M\lambda c_f\varphi_0 + \alpha^2 M}\Big)^2 \sum_{m=1}^{q} \left\|\delta\sigma_v^{n+1,m+k}\right\|^2. \tag{2.3.60}$$

It is difficult to estimate C in practice. However, we expect its value to increase with larger Lamé coefficients (for a fixed value of the Poisson's ratio). The derivation above implies that the contraction coefficient obtained earlier is multiplied by a factor strictly less than one: $\frac{C}{C+1} < 1$. We can conclude that the contraction estimate obtained in theorem 2.3.4 is sharper for $C \gg 1$ (as the damping factor $\frac{C}{C+1} < 1$ approaches one in this case), and looser for smaller values of C. These computations highlight the impact of the extra positive terms on the left hand side of the contraction result obtained in Theorem 2.3.4.

Remark 2.3.4. *We can theoretically derive the value of the constant C given in the previous remark. For simplicity, consider the single rate case $q = 1$. For $L = \frac{\alpha^2}{2\lambda}, \chi = L$, and by Poincare's and Korn's inequalities, we write:*

$$\begin{aligned}
\left\|\delta\sigma_v^{n+1,k}\right\| &\leq \frac{\alpha}{L}\|\nabla\cdot\delta\boldsymbol{u}_h^{n+1,k}\|_{L^2(\Omega)} + \|\delta p_h^{n+1,k}\|_{L^2(\Omega)} \\
&\leq \frac{2\lambda}{\alpha}|\delta\boldsymbol{u}_h^{n+1,k}|_{H^1(\Omega)} + \|\delta p_h^{n+1,k}\|_{L^2(\Omega)} \\
&\leq \frac{2\lambda C_\kappa}{\alpha}\|\boldsymbol{\varepsilon}(\delta\boldsymbol{u}_h^{n+1,k})\|_{L^2(\Omega)} + \mathcal{P}_\Omega\|\nabla\delta p_h^{n+1,k}\|_{L^2(\Omega)} \\
&\leq \frac{2\lambda C_\kappa}{\alpha}\|\boldsymbol{\varepsilon}(\delta\boldsymbol{u}_h^{n+1,k})\|_{L^2(\Omega)} + \mathcal{P}_\Omega\|\boldsymbol{K}^{-1}\delta\boldsymbol{z}_h^{n+1,k}\|_{L^2(\Omega)}
\end{aligned}$$

Thus, we have:

$$\begin{aligned}
\left\|\delta\sigma_v^{n+1,k}\right\|^2 &\leq \frac{4\lambda^2 {C_\kappa}^2}{\alpha^2}\|\boldsymbol{\varepsilon}(\delta\boldsymbol{u}_h^{n+1,k})\|^2_{L^2(\Omega)} + \mathcal{P}_\Omega^2\|\boldsymbol{K}^{-1}\delta\boldsymbol{z}_h^{n+1,k}\|^2_{L^2(\Omega)} \\
&\qquad + \frac{4\lambda C_\kappa\mathcal{P}_\Omega}{\alpha}\|\boldsymbol{\varepsilon}(\delta\boldsymbol{u}_h^{n+1,k})\|_{L^2(\Omega)}\|\boldsymbol{K}^{-1}\delta\boldsymbol{z}_h^{n+1,k}\|_{L^2(\Omega)} \\
&\leq \Big(\frac{4\lambda^2 {C_\kappa}^2}{\alpha^2} + \frac{2\lambda C_\kappa\mathcal{P}_\Omega\epsilon}{\alpha}\Big)\|\boldsymbol{\varepsilon}(\delta\boldsymbol{u}_h^{n+1,k})\|^2_{L^2(\Omega)} + \Big(\mathcal{P}_\Omega^2 + \frac{2\lambda C_\kappa\mathcal{P}_\Omega}{\alpha\epsilon}\Big)\|\boldsymbol{K}^{-1}\delta\boldsymbol{z}_h^{n+1,k}\|^2_{L^2(\Omega)}
\end{aligned} \tag{2.3.61}$$

For $\epsilon > 0$. Assuming that the permeability tensor $\boldsymbol{K}$ is uniformly bounded and uniformly elliptic. There exits positive constants λ_{min}, and λ_{max}, such that

$$\lambda_{min}\|\xi\|^2 \leq \xi^t\boldsymbol{K}(x)\xi \leq \lambda_{max}\|\xi\|^2. \tag{2.3.62}$$

We write:

$$\left\|\delta\sigma_v^{n+1,k}\right\|^2 \leq \left(\frac{4\lambda^2 {C_\kappa}^2}{\alpha^2} + \frac{2\lambda C_\kappa \mathcal{P}_\Omega \epsilon}{\alpha}\right)\|\boldsymbol{\varepsilon}(\delta\boldsymbol{u}_h^{n+1,k})\|^2_{L^2(\Omega)} + \frac{1}{\lambda^2_{min}}\left(\mathcal{P}^2_\Omega + \frac{2\lambda C_\kappa \mathcal{P}_\Omega}{\alpha\epsilon}\right)\|\delta\boldsymbol{z}_h^{n+1,k}\|^2_{L^2(\Omega)} \tag{2.3.63}$$

Therefore, we have:

$$\begin{aligned}&\left\|\delta\sigma_v^{n+1,k}\right\|^2 \leq \\ &\quad Max\left(\left(\frac{4\lambda^2 {C_\kappa}^2}{\alpha^2} + \frac{2\lambda C_\kappa \mathcal{P}_\Omega \epsilon}{\alpha}\right), \frac{1}{\lambda^2_{min}}\left(\mathcal{P}^2_\Omega + \frac{2\lambda C_\kappa \mathcal{P}_\Omega}{\alpha\epsilon}\right)\right)\left(\|\boldsymbol{\varepsilon}(\delta\boldsymbol{u}_h^{n+1,k})\|^2_{L^2(\Omega)} + \|\delta\boldsymbol{z}_h^{n+1,k}\|^2_{L^2(\Omega)}\right)\end{aligned} \tag{2.3.64}$$

For the single rate case (recall: $c_0 = \frac{4\lambda}{\alpha^2}$), $\mathcal{J}_q^{n+1,k}$ takes the form:

$$\begin{aligned}\mathcal{J}_q^{n+1,k} &= 2Gc_0\|\boldsymbol{\varepsilon}(\delta\boldsymbol{u}_h^{n+1,k})\|^2_{L^2(\Omega)} + \frac{2\Delta t}{\beta\mu_f}\left\|\boldsymbol{K}^{-1/2}\delta\boldsymbol{z}_h^{n+1,k}\right\|^2_{L^2(\Omega)} \\ &\geq \frac{8G\lambda}{\alpha^2}\|\boldsymbol{\varepsilon}(\delta\boldsymbol{u}_h^{n+1,k})\|^2_{L^2(\Omega)} + \frac{1}{\lambda_{max}}\frac{2\Delta t}{\beta\mu_f}\left\|\delta\boldsymbol{z}_h^{n+1,k}\right\|^2_{L^2(\Omega)} \\ &\geq Min\left(\frac{8G\lambda}{\alpha^2}, \frac{1}{\lambda_{max}}\frac{2\Delta t}{\beta\mu_f}\right)\left(\|\boldsymbol{\varepsilon}(\delta\boldsymbol{u}_h^{n+1,k})\|^2_{L^2(\Omega)} + \left\|\delta\boldsymbol{z}_h^{n+1,k}\right\|^2_{L^2(\Omega)}\right)\end{aligned} \tag{2.3.65}$$

Combining (2.3.64) *and* (2.3.65)*, we have:*

$$\left\|\delta\sigma_v^{n+1,k}\right\|^2 \leq \left(\frac{Max\left(\left(\frac{4\lambda^2 {C_\kappa}^2}{\alpha^2} + \frac{2\lambda C_\kappa \mathcal{P}_\Omega \epsilon}{\alpha}\right), \frac{1}{\lambda^2_{min}}\left(\mathcal{P}^2_\Omega + \frac{2\lambda C_\kappa \mathcal{P}_\Omega}{\alpha\epsilon}\right)\right)}{Min\left(\frac{8G\lambda}{\alpha^2}, \frac{1}{\lambda_{max}}\frac{2\Delta t}{\beta\mu_f}\right)}\right)\mathcal{J}_q^{n+1,k}$$

with the constant C given by:

$$C = \frac{Max\left(\left(\frac{4\lambda^2 {C_\kappa}^2}{\alpha^2} + \frac{2\lambda C_\kappa \mathcal{P}_\Omega \epsilon}{\alpha}\right), \frac{1}{\lambda^2_{min}}\left(\mathcal{P}^2_\Omega + \frac{2\lambda C_\kappa \mathcal{P}_\Omega}{\alpha\epsilon}\right)\right)}{Min\left(\frac{8G\lambda}{\alpha^2}, \frac{1}{\lambda_{max}}\frac{2\Delta t}{\beta\mu_f}\right)} \tag{2.3.66}$$

Clearly, C scales monotonically with the values of Lame's parameters (or more specifically, with the ratio of the Lame parameter λ to the shear modulus G). Therefore, for larger Lame parameters, the value of the constant C increases, and in turn, the damping factor $\frac{C}{1+C}$ start approaching the value of one. This results in reducing the gap between the theoretical value of the contraction coefficient $\left(\frac{M\alpha^2}{2\lambda+2M\lambda c_f\varphi_0+\alpha^2 M}\right)^2$, and the ratio of $\frac{\left\|\delta\sigma_v^{n+1,k}\right\|^2}{\left\|\delta\sigma_v^{n,k}\right\|^2}$. This is validated numerically for the Frio field model in figure 2.10.

2.3.3.5 Modified Multirate Scheme

We introduce the modified multirate iterative coupling algorithm which results in Banach contraction on the volumetric mean total stress as defined by Mikelić and Wheeler [64] for the single rate fixed stress split iterative method. The algorithm involves a slight modification in the iterative coupling algorithm, in which we employ "successive corrections" in the flow problem (the corrections cancel out in the limit). We split the iterative coupling iteration into an even and odd iterations: in odd coupling iterations, we solve exactly the same mass balance equation solved in the single rate case, in contrast, for even coupling iterations, we add flux correction terms to the left and right hand sides of the mass balance equation. The idea is to correct for the flux, as we take finer time steps within one coarser mechanics time step, so that the summation of the finer flow equations over one coarser mechanics time step retrieves the weak formation of the single rate case, hence, deduce a contraction result similar to the one obtained by Mikelić and Wheeler [64] but for a fully discrete setting.

The modified multirate scheme gives a mechanism by which the multirate iterative coupling scheme is reduced to a corresponding single rate scheme, with a coarse time step for both flow and mechanics. Flux corrections terms correct the error introduced by not solving mechanics at every flow fine time step. This reduces the scheme into a single rate scheme, and as a result, all established theoretical results for the single rate case will be applicable here as well. Another aspect is the fact that in the modified multirate scheme, the quantity of contraction is independent of q (the number of flow fine time steps within one coarse mechanics time step). This is due to the fact that the modified scheme contracts on the same volumetric mean total stress as defined in the single rate case [64]. This is not the case in the original multirate scheme, as volumetric strains are divided by q in the quantity of contraction (2.3.50). This means that as the value of q increases, volumetric strain contributions to the quantity of contraction gets reduced. This restriction is completely eliminated in the modified multirate iterative coupling scheme.

Algorithm 3: Modified Multirate Iterative Coupling Algorithm

for $k = 0, q, 2q, 3q, ..$ **do** /* mechanics time step iteration index */

  for $n = 1, 2, ..$ **do** /* coupling iteration index */

    First Step: Flow equations

    Given $\boldsymbol{u}_h^{n,k+q}$ *(assuming an initial value is given for the first iteration:* $\boldsymbol{u}_h^{0,k+q}$*)*

    For the first local flow timestep iteration, solve for $p_h^{n+1,1+k}$ *and* $\boldsymbol{z}_h^{n+1,1+k}$ *satisfying:*

$$(\frac{1}{M} + c_f\varphi_0 + \frac{\alpha^2}{\lambda})\Big(\frac{p_h^{n+1,1+k} - p_h^{n+1,k}}{\Delta t}\Big) + \frac{1}{\mu_f}\nabla\cdot\boldsymbol{z}_h^{n+1,1+k} =$$

$$\frac{\alpha^2}{\lambda}\Big(\frac{p_h^{n,1+k} - p_h^{n,k}}{\Delta t}\Big) - \alpha\nabla\cdot\Big(\frac{\boldsymbol{u}_h^{n,k+q} - \boldsymbol{u}_h^{n,k}}{q\Delta t}\Big) + \tilde{q}_h \tag{2.3.67}$$

$$\boldsymbol{z}_h^{n+1,1+k} = -\boldsymbol{K}(\nabla p_h^{n+1,1+k} - \rho_{f,r}g\nabla\eta) \tag{2.3.68}$$

    if *mod(n,2) = 1* **then** /* coupling iteration index (n) is odd */

      for $m = 2, .., q$ **do** /* flow finer time steps iteration index */

        Solve for $p_h^{n+1,m+k}$ *and* $\boldsymbol{z}_h^{n+1,m+k}$ *satisfying:*

$$(\frac{1}{M} + c_f\varphi_0 + \frac{\alpha^2}{\lambda})\Big(\frac{p_h^{n+1,m+k} - p_h^{n+1,m-1+k}}{\Delta t}\Big) + \frac{1}{\mu_f}\nabla\cdot\boldsymbol{z}_h^{n+1,m+k} =$$

$$\frac{\alpha^2}{\lambda}\Big(\frac{p_h^{n,m+k} - p_h^{n,m-1+k}}{\Delta t}\Big) - \alpha\nabla\cdot\Big(\frac{\boldsymbol{u}_h^{n,k+q} - \boldsymbol{u}_h^{n,k}}{q\Delta t}\Big) + \tilde{q}_h \tag{2.3.69}$$

$$\boldsymbol{z}_h^{n+1,m+k} = -\boldsymbol{K}(\nabla p_h^{n+1,m+k} - \rho_{f,r}g\nabla\eta) \tag{2.3.70}$$

    else /* coupling iteration index (n) is even */

      for $m = 2, .., q$ **do** /* flow finer time steps iteration index */

        Solve for $p_h^{n+1,m+k}$ *and* $\boldsymbol{z}_h^{n+1,m+k}$ *satisfying:*

$$(\frac{1}{M} + c_f\varphi_0 + \frac{\alpha^2}{\lambda})\Big(\frac{p_h^{n+1,m+k} - p_h^{n+1,m-1+k}}{\Delta t}\Big) + \frac{1}{\mu_f}\nabla\cdot\boldsymbol{z}_h^{n+1,m+k}$$

$$-\frac{1}{\mu_f}\nabla\cdot\boldsymbol{z}_h^{n+1,m-1+k} = \frac{\alpha^2}{\lambda}\Big(\frac{p_h^{n,m+k} - p_h^{n,m-1+k}}{\Delta t}\Big) \tag{2.3.71}$$

$$-\alpha\nabla\cdot\Big(\frac{\boldsymbol{u}_h^{n,k+q} - \boldsymbol{u}_h^{n,k}}{q\Delta t}\Big) + \tilde{q}_h - \frac{1}{\mu_f}\nabla\cdot\boldsymbol{z}_h^{n,m-1+k}$$

$$\boldsymbol{z}_h^{n+1,m+k} = -\boldsymbol{K}(\nabla p_h^{n+1,m+k} - \rho_{f,r}g\nabla\eta) \tag{2.3.72}$$

    Second Step: Mechanics equations

    Given $p_h^{n+1,k+q}$ *and,* $\boldsymbol{z}_h^{n+1,k+q}$*, solve for* $\boldsymbol{u}_h^{n+1,k+q}$ *satisfying:*

$$-\operatorname{div}\boldsymbol{\sigma}^{\mathrm{por}}(\boldsymbol{u}_h^{n+1,k+q}, p_h^{n+1,k+q}) = \boldsymbol{f} \tag{2.3.73}$$

Remark 2.3.5. *As indicated earlier, in contrast to the original multirate iterative coupling algorithm (Algorithm 2), in (Algorithm 3), we split the iterative coupling iterations into even and odd iterations. For the first finer flow time step, we solve exactly the same set of equations for both cases, as shown in line 5. For subsequent finer flow iterations, in the case of an even coupling iteration, we subtract flux correction terms,* $\frac{1}{\mu_f}\nabla \cdot \boldsymbol{z}_h^{n+1,m-1+k}$*, and* $\frac{1}{\mu_f}\nabla \cdot \boldsymbol{z}_h^{n,m-1+k}$*, from the left and right hand sides of the mass balance equation respectively, as shown in line 10. Upon convergence,* $\boldsymbol{z}_h^{n+1,m-1+k} = \boldsymbol{z}_h^{n,m-1+k}$ *and both terms cancel each other. In the case of an odd coupling iteration, we solve the same set of equations as in the single rate case, as shown in Line 7. With the newly introduced flux correction terms, a summation over finer time steps result in reducing the weak formulation of the multirate scheme to that of the single rate scheme. This allows us to obtain exactly the same contraction coefficient as the one obtained in the single rate case, Theorem 2.3.2. In addition, the modified scheme contracts on the volumetric mean total stress as defined in [64] for the single rate scheme.*

2.3.3.6 Proof of Contraction of the 2^{nd} Scheme

- **Step (1): Reduction to single rate weak formulation**

  Extending the work of [64] to the fully discrete formulation, we define the volumetric mean stress, constituting the quantity to be contracted on, for $n \geq 1$, as:

$$\sigma_v^{n,m+k} = \sigma_v^{n,k} + \lambda \nabla \cdot \boldsymbol{u}_h^{n,k} - \alpha(p_h^{n,m+k} - p_h^{n,k}) \qquad \text{for } 1 \leq m \leq q-1, \quad (2.3.74)$$

$$\sigma_v^{n,k+q} = \sigma_v^{n,k} + \lambda \nabla \cdot \boldsymbol{u}_h^{n,k+q} - \alpha(p_h^{n,k+q} - p_h^{n,k}) \qquad \text{for } m = q. \quad (2.3.75)$$

  In terms of the difference between two coupling iterates, we have

$$\delta\sigma_v^{n+1,m+k} = -\alpha \delta p_h^{n+1,m+k} \qquad \text{for } 1 \leq m \leq q-1, \quad (2.3.76)$$

$$\delta\sigma_v^{n+1,k+q} = \lambda \nabla \cdot \delta\boldsymbol{u}_h^{n+1,k+q} - \alpha \delta p_h^{n+1,k+q} \qquad \text{for } m = q. \quad (2.3.77)$$

  In order to obtain the single rate weak formulation, we sum up local flow iterations across one coarser mechanics time step. As we solve different mass balance equations in even versus odd coupling iterations, we need to consider each case seperately:

– **Coupling iteration index, n, is odd:**

$$(\frac{1}{M}+c_f\varphi_0+\frac{\alpha^2}{\lambda})\frac{1}{\Delta t}\sum_{m=1}^{q}\Big(p_h^{n+1,m+k}-p_h^{n+1,m-1+k}\Big)+\frac{1}{\mu_f}\nabla\cdot\sum_{m=1}^{q}\boldsymbol{z}_h^{n+1,m+k}=$$
$$\frac{\alpha^2}{\lambda\Delta t}\sum_{m=1}^{q}\Big(p_h^{n,m+k}-p_h^{n,m-1+k}\Big)-\frac{\alpha}{q\Delta t}\nabla\cdot\sum_{m=1}^{q}\Big(\boldsymbol{u}_h^{n,k+q}-\boldsymbol{u}_h^{n,k}\Big)+q\tilde{q}_h \tag{2.3.78}$$

$$\sum_{m=1}^{q}\boldsymbol{z}_h^{n+1,m+k}=-\boldsymbol{K}\nabla\Big(\sum_{m=1}^{q}p_h^{n+1,m+k}\Big)+\frac{1}{\mu_f}\boldsymbol{K}q\rho_{f,r}g\nabla\,\eta \tag{2.3.79}$$

– **Coupling iteration index, n, is even:**

Equation (2.3.79) remains unchanged. For (2.3.71), we have:

$$(\frac{1}{M}+c_f\varphi_0+\frac{\alpha^2}{\lambda})\frac{1}{\Delta t}\sum_{m=1}^{q}\Big(p_h^{n+1,m+k}-p_h^{n+1,m-1+k}\Big)+\frac{1}{\mu_f}\nabla\cdot\sum_{m=1}^{q}\boldsymbol{z}_h^{n+1,m+k}$$
$$-\frac{1}{\mu_f}\nabla\cdot\sum_{w=1}^{q-1}\boldsymbol{z}_h^{n+1,w+k}=\frac{\alpha^2}{\lambda\Delta t}\sum_{m=1}^{q}\Big(p_h^{n,m+k}-p_h^{n,m-1+k}\Big)$$
$$-\frac{\alpha}{q\Delta t}\nabla\cdot\sum_{m=1}^{q}\Big(\boldsymbol{u}_h^{n,k+q}-\boldsymbol{u}_h^{n,k}\Big)+q\tilde{q}_h-\frac{1}{\mu_f}\nabla\cdot\sum_{w=1}^{q-1}\boldsymbol{z}_h^{n,w+k} \tag{2.3.80}$$

Assuming, without loss of generality, that "$n+1$" represents an even coupling iteration, and "n" represents an odd coupling iteration, subtracting (2.3.78) from (2.3.80) to form the difference between two consecutive coupling iterates, and taking advantage of (2.3.53), we derive

$$(\frac{1}{M}+c_f\varphi_0+\frac{\alpha^2}{\lambda})\frac{1}{\Delta t}\delta p_h^{n+1,k+q}+\frac{1}{\mu_f}\nabla\cdot\delta\boldsymbol{z}_h^{n+1,q+k}=-\frac{\alpha}{\lambda\Delta t}\delta\sigma_v^{n,k+q}. \tag{2.3.81}$$

where $\delta\sigma_v^{n,k+q}=\lambda\nabla\cdot\delta\boldsymbol{u}_h^{n,k+q}-\alpha\delta p_h^{n,k+q}$ by (2.3.77). Equation (2.3.81) involves only coarser time step variables. Considering the modified multriate iterative coupling scheme as a single rate scheme, in which both the flow and mechanics problems share the coarser time step, the weak formulation in terms of the differences between

coupling iterates reads

$$\forall \theta_h \in Q_h\,,\ \Big(\frac{1}{\Delta t}(\frac{1}{M}+c_f\varphi_0+\frac{\alpha^2}{\lambda})\delta p_h^{n+1,k+q},\theta_h\Big)+\frac{1}{\mu_f}(\nabla\cdot\delta \boldsymbol{z}_h^{n+1,k+q},\theta_h) = \Big(-\frac{\alpha}{\lambda\Delta t}\delta\sigma_v^{n,k+q},\theta_h\Big), \tag{2.3.82}$$

$$\forall \boldsymbol{q}_h \in \boldsymbol{Z}_h\,,\ (\boldsymbol{K}^{-1}\delta \boldsymbol{z}_h^{n+1,k+q},\boldsymbol{q}_h)=(\delta p_h^{n+1,k+q},\nabla\cdot\boldsymbol{q}_h), \tag{2.3.83}$$

$$\forall \boldsymbol{v}_h \in V_h\,,\ 2G(\boldsymbol{\varepsilon}(\delta\boldsymbol{u}_h^{n+1,k+q}),\boldsymbol{\varepsilon}(\boldsymbol{v}_h))+\lambda(\nabla\cdot\delta\boldsymbol{u}_h^{n+1,k+q},\nabla\cdot\boldsymbol{v}_h) - \alpha(\delta p_h^{n+1,k+q},\nabla\cdot\boldsymbol{v}_h)=0. \tag{2.3.84}$$

- **Step (2): Flow equations**

  Recall $\beta=\frac{1}{M\alpha^2}+\frac{c_f}{\alpha^2}\varphi_0+\frac{1}{\lambda}$; testing (2.3.82) with $\theta_h=\delta p_h^{n+1,k+q}$ and applying Young's inequality, we obtain

$$\frac{\beta}{\Delta t}\Big\|\alpha\delta p_h^{n+1,k+q}\Big\|^2+\frac{1}{\mu_f}\Big(\nabla\cdot\delta\boldsymbol{z}_h^{n+1,k+q},\delta p_h^{n+1,k+q}\Big)=\frac{1}{\Delta t}\Big(-\alpha\varepsilon\delta p_h^{n+1,k+q},\frac{1}{\varepsilon\lambda}\sigma_v^{n,k+q}\Big) \le \frac{1}{\Delta t}\Big(\frac{\varepsilon^2}{2}\Big\|\alpha\delta p_h^{n+1,k+q}\Big\|^2+\frac{1}{2\varepsilon^2\lambda^2}\Big\|\delta\sigma_v^{n,k+q}\Big\|^2\Big).$$

  The choice $\varepsilon^2=\beta$ absorbs the pressure term on the right hand side by its corresponding term on the left hand side, leading to

$$\beta\Big\|\alpha\delta p_h^{n+1,k+q}\Big\|^2+\frac{2\Delta t}{\mu_f}(\nabla\cdot\delta\boldsymbol{z}_h^{n+1,k+q},\delta p_h^{n+1,k+q})\le\frac{1}{\beta\lambda^2}\Big\|\delta\sigma_v^{n,k+q}\Big\|^2. \tag{2.3.85}$$

  Testing (2.3.83) with $\boldsymbol{q}_h=\delta\boldsymbol{z}_h^{n+1,k}$, we obtain

$$(\boldsymbol{K}^{-1}\delta\boldsymbol{z}_h^{n+1,k},\delta\boldsymbol{z}_h^{n+1,k})=(\delta p_h^{n+1,k},\nabla\cdot\delta\boldsymbol{z}_h^{n+1,k}). \tag{2.3.86}$$

  Combining (2.3.86) with (2.3.85) leads to a sum of two positive squared norms on the right hand side of (2.3.85), in which the right hand side constitutes the quantity to be contracted on,

$$\beta\Big\|\alpha\delta p_h^{n+1,k+q}\Big\|^2+\frac{2\Delta t}{\mu_f}\Big\|K^{-1/2}\delta\boldsymbol{z}_h^{n+1,k+q}\Big\|^2\le\frac{1}{\beta\lambda^2}\Big\|\delta\sigma_v^{n,k+q}\Big\|^2. \tag{2.3.87}$$

- **Step (3): Elasticity equation**

  Testing (2.3.84) with $\boldsymbol{v}_h=\delta\boldsymbol{u}_h^{n+1,k}$, we obtain

$$2G\|\boldsymbol{\varepsilon}(\delta\boldsymbol{u}_h^{n+1,k+q})\|^2+\lambda\|\nabla\cdot\delta\boldsymbol{u}_h^{n+1,k+q}\|^2-\alpha(\delta p_h^{n+1,k+q},\nabla\cdot\delta\boldsymbol{u}_h^{n+1,k+q})=0. \tag{2.3.88}$$

Combining (2.3.87) with (2.3.88), we infer

$$\Big\{\Big\|\alpha\delta p_h^{n+1,k+q}\Big\|^2 - 2(\alpha\delta p_h^{n+1,k+q}, \lambda\nabla\cdot\delta\boldsymbol{u}_h^{n+1,k+q}) + \lambda^2\|\nabla\cdot\delta\boldsymbol{u}_h^{n+1,k+q}\|^2\Big\}$$
$$+ 4G\lambda\|\boldsymbol{\varepsilon}(\delta\boldsymbol{u}_h^{n+1,k+q})\|^2 + \frac{2\Delta t\lambda M\alpha^2}{\mu_f(M\alpha^2+\lambda(1+Mc_f\varphi_0))}\Big\|K^{-1/2}\delta\boldsymbol{z}_h^{n+1,k+q}\Big\|^2$$
$$+ \lambda^2\|\nabla\cdot\delta\boldsymbol{u}_h^{n+1,k+q}\|^2 \leq \Big(\frac{M\alpha^2}{\lambda+M\lambda c_f\varphi_0+M\alpha^2}\Big)^2\Big\|\delta\sigma_v^{n,k+q}\Big\|^2. \tag{2.3.89}$$

The first three terms form a square of the volumetric mean stress defined in (2.3.77), establishing the quantity of contraction for the next iterative coupling iteration, $n+1$, on the right hand side of (2.3.89), as

$$\Big\|\delta\sigma_v^{n+1,k+q}\Big\|^2 + \frac{2\Delta t\lambda M\alpha^2}{\mu_f(M\alpha^2+\lambda(1+Mc_f\varphi_0))}\Big\|K^{-1/2}\delta\boldsymbol{z}_h^{n+1,k+q}\Big\|^2 + 4G\lambda\|\boldsymbol{\varepsilon}(\delta\boldsymbol{u}_h^{n+1,k+q})\|^2$$
$$+ \lambda^2\|\nabla\cdot\delta\boldsymbol{u}_h^{n+1,k+q}\|^2 \leq \Big(\frac{M\alpha^2}{\lambda+M\lambda c_f\varphi_0+M\alpha^2}\Big)^2\Big\|\delta\sigma_v^{n,k+q}\Big\|^2, \tag{2.3.90}$$

with a contraction coefficient strictly less than one: $\Big(\frac{M\alpha^2}{\lambda+M\lambda c_f\varphi_0+M\alpha^2}\Big)^2 < 1$.

2.3.3.7 Convergence to The Discrete Form (2^{nd} Scheme)

In the next lemma, we establish convergence of the sequences generated by the modified multirate iterative coupling scheme for coarser mechanics time steps.

Lemma 2.3.4. *For k = 0, q, 2q, .., there exist limit functions $p_h^k, \boldsymbol{u}_h^k, \boldsymbol{z}_h^k$ such that*

$$p_h^{n,k} \to p_h^k \quad \text{in } L^2(\Omega), \quad \boldsymbol{u}_h^{n,k} \to \boldsymbol{u}_h^k \quad \text{in } H^1(\Omega)^d, \quad \boldsymbol{z}_h^{n,k} \to \boldsymbol{z}_h^k \quad \text{in } H(div,\Omega)^d,$$

with strong convergence in the norms of the above spaces.

Proof. The contraction result in (2.3.90) implies that for coarse mechanics time steps, $\|\delta\sigma_v^{n+1,k}\|_\Omega$, $\|\nabla\cdot\delta\boldsymbol{u}_h^{n+1,k}\|_\Omega$, and $\|K^{-1/2}\delta\boldsymbol{z}_h^{n+1,k}\|_\Omega$ converge geometrically to zero. This implies that $\sigma_v^{n+1,k}$, $\nabla\cdot\boldsymbol{u}_h^{n+1,k}$, and $\boldsymbol{z}_h^{n+1,k}$ are Cauchy sequences converging to unique limits in $L^2(\Omega)$. By (2.3.77), we conclude that $p_h^{n,k}$ is a Cauchy sequence converging geometrically to a unique limit in $L^2(\Omega)$, being a Hilbert space.

For the displacements, (2.3.90) implies that $\boldsymbol{\varepsilon}(\delta \boldsymbol{u}_h^{n+1,k})$ converges geometrically to 0 in $L^2(\Omega)$. It follows immediately that $\boldsymbol{u}_h^{n+1,k}$ converges geometrically to a unique limit in the Hilbert space $H^1(\Omega)^d$.

For the divergence of the flux, we note that (2.3.82) amounts to the following equality a.e. in $L^2(\Omega)$:

$$\nabla \cdot \delta \boldsymbol{z}_h^{n+1,k} = \frac{\mu_f}{\Delta t}(\frac{1}{M} + c_f \varphi_0 + \frac{\alpha^2}{\lambda})\delta p_h^{n+1,k} - \frac{\mu_f \alpha}{\lambda \Delta t}\delta \sigma_v^{n,k}.$$

The convergence of $\nabla \cdot \boldsymbol{z}_h^{n+1,k}$ in $L^2(\Omega)$ follows from the convergences of $p_h^{n+1,k}$ and $\sigma_v^{n,k}$ in $L^2(\Omega)$. Therefore, we have both $\nabla \cdot \boldsymbol{z}_h^{n+1,k}$ and $\boldsymbol{z}_h^{n+1,k}$ converging geometrically in $L^2(\Omega)$, hence $\boldsymbol{z}_h^{n+1,k}$ converges in $H(div, \Omega)^d$. The existence of the limiting function in $H(div, \Omega)^d$ follows from the completeness of the space. □

It remains to pass to the limit in the weak formulation of (2.3.67)–(2.3.73). This is straightforward in view of the linearity of equations and strong convergences obtained.

Theorem 2.3.5. *For coarser mechanics time steps, $k = 0, q, 2q, ..,$ the modified multirate iterative scheme is a contraction given by*

$$\left\|\delta \sigma_v^{n+1,k}\right\|_\Omega^2 + \frac{2\Delta t \lambda M \alpha^2}{\mu_f(M\alpha^2 + \lambda(1 + M c_f \varphi_0))}\left\|K^{-1/2}\delta \boldsymbol{z}_h^{n+1,k}\right\|_\Omega^2 + 4G\lambda \|\boldsymbol{\varepsilon}(\delta \boldsymbol{u}_h^{n+1,k})\|_\Omega^2 + \lambda^2 \|\nabla \cdot \delta \boldsymbol{u}_h^{n+1,k}\|_\Omega^2$$
$$\leq \left(\frac{M\alpha^2}{\lambda + M\lambda c_f \varphi_0 + M\alpha^2}\right)^2 \left\|\delta \sigma_v^{n,k}\right\|_\Omega^2.$$

Furthermore, the sequences defined by this scheme converge to the unique solution of the weak formulation of (2.3.67)–(2.3.73).

Remark 2.3.6. All our obtained results remain valid when the multipoint flux mixed finite element method (MFMFE) [88,90] is used for flow discretization. For clarification, consider the modified multirate scheme. Using the MFMFE method for flow discretization, (2.3.90) translate to

$$\left\|\delta \sigma_v^{n+1,k+q}\right\|^2 + \frac{2\Delta t \lambda M \alpha^2}{\mu_f(M\alpha^2 + \lambda(1 + M c_f \varphi_0))}\left(K^{-1}\delta \boldsymbol{z}_h^{n+1,k+q}, \delta \boldsymbol{z}_h^{n+1,k+q}\right)_Q + 4G\lambda \|\boldsymbol{\varepsilon}(\delta \boldsymbol{u}_h^{n+1,k+q})\|^2$$
$$+ \lambda^2 \|\nabla \cdot \delta \boldsymbol{u}_h^{n+1,k+q}\|^2 \leq \left(\frac{M\alpha^2}{\lambda + M\lambda c_f \varphi_0 + M\alpha^2}\right)^2 \left\|\delta \sigma_v^{n,k+q}\right\|^2. \tag{2.3.91}$$

where $(K^{-1}., .)_Q$ is the quadrature rule defined in [90] for the MFMFE corresponding spaces. It was shown by Wheeler and Yotov in [90], and then extended to distorted quadrilaterals

and hexahedra in [88], that for any $\boldsymbol{z}_h \in \boldsymbol{Z}_h, (K^{-1}\boldsymbol{z}_h, \boldsymbol{z}_h) \geq C\|\boldsymbol{z}_h\|^2$, for a constant $C > 0$. This immediately leads to a similar contraction result. The same argument holds for previously derived results in the first multirate scheme described earlier. Similarly, our results can be extended to other multi point flux approximation control volume method, MFPA, when used for flow discretization [54, 55]. The coercivity of the bilinear form of the fluxes has been established in [55] for quadrilaterls, and in [54] for triangular elements using the broken Raviart-Thomas, and the lowest order Brezzi-Doulas-Marini spaces respectively.

2.4 Undrained Split Iterative Coupling

In this section, we consider one of the iterative schemes often used in practice: undrained splitting and propose a multirate iterative scheme, as illustrated by Figure 2.2b. We recall that this scheme considers a finer time step for the flow model and a coarser time step for mechanics (q flow steps for each mechanics step) and then performs an iteration between the mechanics and finer flow steps. In contrast, in the single rate scheme, as illustrated by Figure 2.2a, the flow and mechanics problems share the exact same time step, and the coupling iteration continues until convergence. Both schemes are iterative in the sense that for each coarse mechanics time step, we solve for q flow finer time steps followed by a mechanics step and we further repeat the process. Details about convergence criteria can be found in [63] (also discussed in details in the numerical results section). The converged solutions solve the coupled time-discrete system consisting of q flow solves and one mechanics solve. The flow finer solve uses the mechanics at the coarse step and hence, the coupled system is fully implicit. Since the cost of mechanics is often much more than the cost of flow, fewer mechanics solves lead to considerable computational savings. This work is motivated by the recent work of Mikelić and Wheeler [63, 64] where they have considered different iterative schemes for flow and mechanics couplings and established contractive results in suitable norms, (see also [53] for studying the von Neumann stability of iterative algorithms, [80] for multirate schemes for Darcy-Stokes, and [72, 73] for the relationship of these iterative methods to the linearization procedures).

We start by analyzing the fully discrete single-rate undrained-split coupling algorithm, in

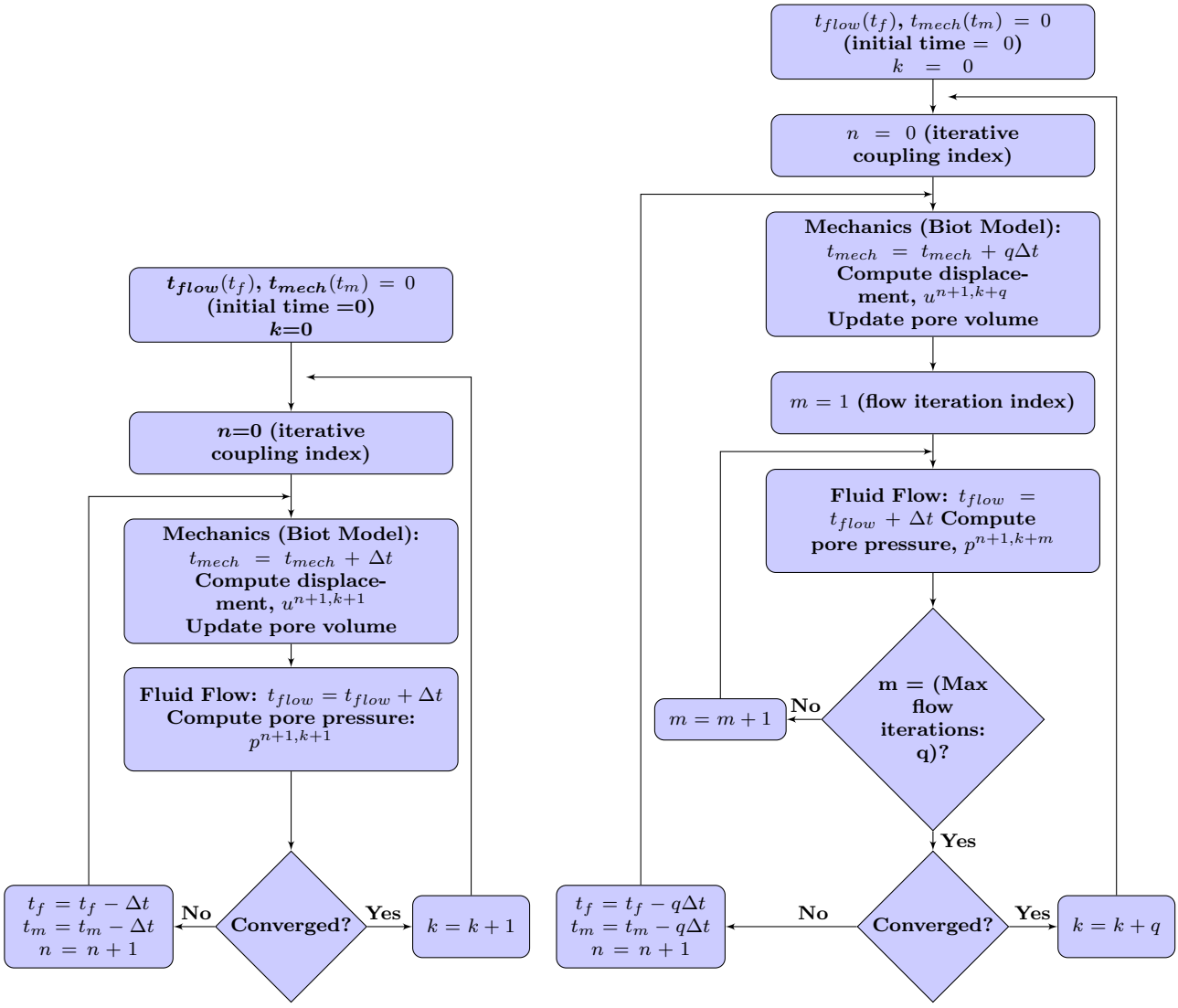

(a) Single Rate

(b) Multirate

Figure 2.2: Flowchart for the undrained split single rate and multirate iterative coupling algorithms. In the single rate scheme, both the flow and mechanics problems share the exact same time step Δt. In the multirate scheme, the flow finer time step is Δt, and the mechanics coarser time step is $q\Delta t$.

which both flow and mechanics share the exact same time step. This can be viewed as an extension of the work of Mikelić & Wheeler [64], in which conformal Galerkin is used for flow discretization (versus mixed form for the flow in this work), and the contraction coefficient obtained here is optimized. In addition, understanding the strategy of the single-rate proof

serves as a good introduction before tackling the more complicated multirate case.

2.4.1 Single Rate Formulation and Analysis

2.4.1.1 Fully Discrete Scheme for Single Rate

Using the mixed finite element method in space and the backward Euler finite difference method in time, the weak formulation of the single rate scheme reads as follows.

Definition 2.4.1. *(***mechanics equation***)*

Find $\boldsymbol{u}_h^{k+1} \in \boldsymbol{V}_h$ *such that,*

$$\forall \boldsymbol{v}_h \in V_h\,,\; 2G(\boldsymbol{\varepsilon}(\boldsymbol{u}_h^{k+1}), \boldsymbol{\varepsilon}(\boldsymbol{v}_h)) + \lambda(\nabla \cdot \boldsymbol{u}_h^{k+1}, \nabla \cdot \boldsymbol{v}_h) - \alpha(p_h^{k+1}, \nabla \cdot \boldsymbol{v}_h) = (\boldsymbol{f}, \boldsymbol{v}_h). \quad (2.4.92)$$

*and (***flow equation***) find* $p_h^{k+1} \in Q_h$*, and* $\boldsymbol{z}_h^{k+1} \in \boldsymbol{Z}_h$ *such that,*

$$\begin{aligned} \forall \theta_h \in Q_h\,, \frac{1}{\Delta t}\Big((\frac{1}{M} + c_f\varphi_0)\Big(p_h^{k+1} - p_h^{k}\Big), \theta_h\Big) + \frac{1}{\mu_f}(\nabla \cdot \boldsymbol{z}_h^{k+1}, \theta_h) = \\ - \frac{\alpha}{q\Delta t}\Big(\nabla \cdot \Big(\boldsymbol{u}_h^{k+1} - \boldsymbol{u}_h^{k}\Big), \theta_h\Big) + \Big(\tilde{q}_h, \theta_h\Big), \quad (2.4.93) \\ \forall \boldsymbol{q}_h \in \boldsymbol{Z}_h\,, \Big(\boldsymbol{K}^{-1}\boldsymbol{z}_h^{k+1}, \boldsymbol{q}_h\Big) = \Big(p_h^{k+1}, \nabla \cdot \boldsymbol{q}_h\Big) + \Big(\rho_{f,r} g \nabla \eta, \boldsymbol{q}_h\Big), \quad (2.4.94) \end{aligned}$$

with the initial conditions for the first discrete time step,

$$p_h^0 = p_0, \quad \boldsymbol{u}_h^0 = \boldsymbol{u}_0. \quad (2.4.95)$$

2.4.1.2 Single Rate Iterative Scheme

The scheme starts by solving the mechanics problem followed by the flow problem, and iterates between the two until convergence is achieved. The iteration assumes a constant fluid mass during the deformation of the structure (and can be interpreted as a regularization of mechanics equation). We start by presenting the scheme.

Algorithm 4: Undrained Split Single Rate Algorithm

for $k = 0, 1, 2, 3, ..$ **do** `/* mechanics time step iteration index */`

  for $n = 1, 2, ..$ **do** `/* coupling iteration index */`

    First Step: Mechanics equations

    Given $p_h^{n,k+1}$*, solve for* $\boldsymbol{u}_h^{n+1,k+1}$ *satisfying (assuming an initial value is given for the first iteration:* $p_h^{0,k+1}$*):*

$$-2G\nabla\cdot(\boldsymbol{\varepsilon}(\boldsymbol{u}_h^{n+1,k+1})) - (\lambda+L)\nabla\cdot((\nabla\cdot\boldsymbol{u}_h^{n+1,k+1})I) = -\alpha\nabla\cdot(p_h^{n,k+1}I) - L\nabla\cdot((\nabla\cdot\boldsymbol{u}_h^{n,k+1})I) + \boldsymbol{f} \tag{2.4.96}$$

    Second Step: Flow equations

    Given $\boldsymbol{u}_h^{n+1,k+1}$*, solve for* $p_h^{n+1,k+1}$ *and* $\boldsymbol{z}_h^{n+1,k+1}$ *satisfying:*

$$\beta\Big(\frac{p_h^{n+1,k+1}-p_h^k}{\Delta t}\Big) + \frac{1}{\mu_f}\nabla\cdot\boldsymbol{z}_h^{n+1,k+1} = -\alpha\nabla\cdot\Big(\frac{\boldsymbol{u}_h^{n+1,k+1}-\boldsymbol{u}_h^k}{\Delta t}\Big) + \tilde{q}_h \tag{2.4.97}$$

$$\boldsymbol{z}_h^{n+1,k+1} = -\boldsymbol{K}(\nabla p_h^{n+1,k+1} - \rho_{f,r}g\nabla\eta) \tag{2.4.98}$$

In the above, we have used $\beta = (\frac{1}{M} + c_f\varphi_0)$ for the notational convenience. L is a regularization parameter and the corresponding term vanishes in the case of convergence.

The convergence proof is based on studying the difference of two successive iterates and deriving the contraction of appropriate quantities in suitable norms. We recall the definition:

$$\delta\xi^{n,k} = \xi^{n+1,k} - \xi^{n,k}, \text{ where } \xi = p, \boldsymbol{u}, \text{or } \boldsymbol{z}.$$

Considering the difference between two consecutive iterative coupling iterations, the weak formulation of equations corresponding to (2.4.96), (2.4.97), and (2.4.98) can be written as follows.

Mechanics step: Given $\delta p_h^{n,k+1}$ from the previous coupling iteration, find $\delta\boldsymbol{u}_h^{n+1,k+1} \in \boldsymbol{V}_h$ such that,

$$\forall\boldsymbol{v}_h \in V_h\,,\ 2G(\boldsymbol{\varepsilon}(\delta\boldsymbol{u}_h^{n+1,k+1}),\boldsymbol{\varepsilon}(\boldsymbol{v}_h)) + (\lambda+L)(\nabla\cdot\delta\boldsymbol{u}_h^{n+1,k+1},\nabla\cdot\boldsymbol{v}_h) = \alpha(\delta p_h^{n,k+1},\nabla\cdot\boldsymbol{v}_h) + L(\nabla\cdot\delta\boldsymbol{u}_h^{n,k+1},\nabla\cdot\boldsymbol{v}_h)\,, \tag{2.4.99}$$

Flow step: Given $\delta \boldsymbol{u}_h^{n+1,k+1}$, find $\delta p_h^{n+1,k+1} \in Q_h$, $\delta \boldsymbol{z}_h^{n+1,k+1} \in \boldsymbol{Z}_h$ such that:

$$\forall \theta_h \in Q_h \,,\; \frac{\beta}{\Delta t}\Big(\delta p_h^{n+1,k+1}, \theta_h\Big) + \frac{1}{\mu_f}(\nabla \cdot \delta \boldsymbol{z}_h^{n+1,k+1}, \theta_h) = -\frac{\alpha}{\Delta t}\Big(\nabla \cdot \delta \boldsymbol{u}_h^{n+1,k+1}, \theta_h\Big) \tag{2.4.100}$$

$$\forall \boldsymbol{q}_h \in \boldsymbol{Z}_h \,,\; (\boldsymbol{K}^{-1}\delta \boldsymbol{z}_h^{n+1,k+1}, \boldsymbol{q}_h) = (\delta p_h^{n+1,k+1}, \nabla \cdot \boldsymbol{q}_h) \tag{2.4.101}$$

2.4.1.3 Proof of Contraction

The quantity to be contracted on is a composite one consisting of both pressure $p^{n,k}$ and volumetric strain terms $\nabla \cdot \boldsymbol{u}^{n,k}$. For a particular coupling iteration, $n \geq 1$, and for time step t_k, we define the quantity to be contracted on as:

$$\tilde{m}^{n,k} = \frac{L}{\gamma}\nabla \cdot \boldsymbol{u}^{n,k} + \frac{\alpha}{\gamma}p^{n,k},$$

where γ is an adjustable coefficient that will be selected carefully such that the scheme achieves contraction on $\tilde{m}$. The presence of γ does not alter the contractivity, however, it simplifies the algebra and provides a systematic technique for obtaining similar results for other problems.

- **Step (1): Elasticity equation**

  First, we analyze the mechanics equation. Testing (2.4.99) with $\boldsymbol{v}_h = \delta \boldsymbol{u}_h^{n+1,k+1}$, we get:

$$\begin{aligned} 2G\|\boldsymbol{\varepsilon}(\delta \boldsymbol{u}_h^{n+1,k+1})\|^2 + (\lambda + L)\|\nabla \cdot \delta \boldsymbol{u}_h^{n+1,k+1}\|^2 & \\ &= (\alpha \delta p_h^{n,k+1} + L\nabla \cdot \delta \boldsymbol{u}_h^{n,k+1}, \nabla \cdot \delta \boldsymbol{u}_h^{n+1,k+1}) \\ &= \Big(\gamma \delta \tilde{m}^{n,k+1}, \nabla \cdot \delta \boldsymbol{u}_h^{n+1,k+1}\Big) \\ &\leq \frac{\varepsilon}{2}\left\|\nabla \cdot \delta \boldsymbol{u}^{n+1,k+1}\right\|^2 + \frac{1}{2\varepsilon}\gamma^2\left\|\delta \tilde{m}^{n,k+1}\right\|^2 \end{aligned}$$

  by Young's inequality. For $\varepsilon = \lambda + L$, we obtain,

$$\frac{4G}{\lambda + L}\|\boldsymbol{\varepsilon}(\delta \boldsymbol{u}_h^{n+1,k+1})\|^2 + \|\nabla \cdot \delta \boldsymbol{u}_h^{n+1,k+1}\|^2 \leq \frac{\gamma^2}{(\lambda + L)^2}\left\|\delta \tilde{m}^{n,k+1}\right\|^2. \tag{2.4.102}$$

- **Step (2): Flow equations**

  Testing (2.4.100), with $\theta_h = \delta p_h^{n+1,k+1}$, and multiplying by Δt, we get: (recall $\beta =$

$\frac{1}{M} + c_f\varphi_0)$

$$\beta\left\|\delta p_h^{n+1,k+1}\right\|^2 + \frac{\Delta t}{\mu_f}(\nabla\cdot\delta\boldsymbol{z}_h^{n+1,k+1}, \delta p_h^{n+1,k+1}) = -\alpha\Big(\nabla\cdot\delta\boldsymbol{u}_h^{n+1,k+1}, \delta p_h^{n+1,k+1}\Big) \tag{2.4.103}$$

Testing (2.4.101) with $\boldsymbol{q}_h = \delta\boldsymbol{z}_h^{n+1,k+1}$, we get and taking the difference between them, we get

$$\|\boldsymbol{K}^{-1/2}\delta\boldsymbol{z}_h^{n+1,k+1}\|^2 = \Big(\delta p_h^{n+1,k+1}, \nabla\cdot\delta\boldsymbol{z}_h^{n+1,k+1}\Big). \tag{2.4.104}$$

Substituting (2.4.104) into (2.4.103), we have

$$\beta\left\|\delta p_h^{n+1,k+1}\right\|^2 + \frac{\Delta t}{\mu_f}\|\boldsymbol{K}^{-1/2}\delta\boldsymbol{z}_h^{n+1,k+1}\|^2 + \alpha\Big(\nabla\cdot\delta\boldsymbol{u}_h^{n+1,k+1}, \delta p_h^{n+1,k+1}\Big) = 0. \tag{2.4.105}$$

- **Step (3): Combining Mechanics and Flow**

  Multiplying (2.4.105) by another free parameter c^2 and adding (2.4.102), we obtain

$$\begin{aligned}&\frac{4G}{\lambda+L}\|\boldsymbol{\varepsilon}(\delta\boldsymbol{u}_h^{n+1,k+1})\|^2\\ &+\left\{c^2\beta\left\|\delta p_h^{n+1,k+1}\right\|^2 + c^2\alpha\Big(\nabla\cdot\delta\boldsymbol{u}_h^{n+1,k+1}, \delta p_h^{n+1,k+1}\Big) + \|\nabla\cdot\delta\boldsymbol{u}_h^{n+1,k+1}\|^2\right\}\\ &\qquad + \frac{c^2\Delta t}{\mu_f}\left\|\boldsymbol{K}^{-1/2}\delta\boldsymbol{z}_h^{n+1,k+1}\right\|^2 \le \frac{\gamma^2}{(\lambda+L)^2}\left\|\delta\tilde{m}^{n,k+1}\right\|^2.\end{aligned} \tag{2.4.106}$$

- **Step (4): Identifying the parameters**

  Below we provide the procedure for determining the three adjustable parameters ($c^2, \gamma,$ and L) yielding a contraction. These parameters should be chosen such that the terms on the left hand side of (2.4.106) remain positive, and the scheme achieves contraction on $\tilde{m}$. Clearly,

$$\begin{aligned}\left\|\delta\tilde{m}^{n+1,k+1}\right\|^2 &= \frac{L^2}{\gamma^2}\left\|\nabla\cdot\delta\boldsymbol{u}^{n+1,k+1}\right\|^2 + \frac{\alpha^2}{\gamma^2}\left\|\delta p^{n+1,k+1}\right\|^2\\ &\quad + \frac{2\alpha L}{\gamma^2}\left(\delta p^{n+1,k+1}, \nabla\cdot\delta\boldsymbol{u}^{n+1,k+1}\right).\end{aligned}$$

Matching coefficients by comparing with the terms in the curly brackets in (2.4.106) provides us with the following conditions:

$$\frac{L^2}{\gamma^2} = 1, \qquad \frac{\alpha^2}{\gamma^2} = c^2\beta, \qquad \frac{2\alpha L}{\gamma^2} = c^2\alpha.$$

This gives, $L = \gamma = \frac{\alpha^2}{2\beta}, \quad c^2 = \frac{2}{L}$. Substituting in (2.4.106) leads to a contraction factor of the form $\left(\frac{L}{\lambda+L}\right)^2$, which is strictly less than one.

Our main result summarises the above contraction result.

Theorem 2.4.1. *With $L = \dfrac{\alpha^2}{2\beta}$ and $c^2 = \frac{4\beta}{\alpha^2}$, the undrained single rate iterative scheme defined by* (2.4.96) - (2.4.98) *is a contraction given by*

$$\frac{4G}{\lambda+L}\|\boldsymbol{\varepsilon}(\delta\boldsymbol{u}_h^{n+1,k+1})\|^2 + \frac{c^2\Delta t}{\mu_f}\left\|\boldsymbol{K}^{-1/2}\delta\boldsymbol{z}_h^{n+1,k+1}\right\|^2 + \left\|\delta\tilde{m}^{n+1,k+1}\right\|^2 \leq \left(\frac{L}{\lambda+L}\right)^2\left\|\delta\tilde{m}^{n,k+1}\right\|^2. \tag{2.4.107}$$

Furthermore, the sequences defined by this scheme converge to the unique solution of the weak formulation (2.4.92)–(2.4.94).

Remark 2.4.1. *The above contraction result implies that the composite quantity $\tilde{m}^{n+1,k+1}$, symmetric strain $\boldsymbol{\varepsilon}(\boldsymbol{u}_h^{n+1,k+1})$, and flux $\boldsymbol{z}_h^{n+1,k+1}$ converge at a geometric rate. Relatively straightforward arguments that include standard mixed method for controlling pressure by flux, Korn's inequality to control the H^1 norm by the L^2 norm of the symmetric strain tensor, imply the unique convergence of $p_h^{n+1,k+1}, \boldsymbol{u}_h^{n+1,k+1}$ in L^2 and H^1 norms respectively.*

Remark 2.4.2. *The above remark 2.4.1 can also be used to strengthen the contraction coefficient in theorem 2.4.1. Using triangle's inequality,*

$$\left\|\delta\tilde{m}^{n,k}\right\| \leq \frac{L}{\gamma}\|\nabla\cdot\delta\boldsymbol{u}_h^{n,k}\| + \frac{\alpha}{\gamma}\|\delta p_h^{n,k}\|$$

and using standard mixed method to estimate the pressure by the flux and the Korn inequality, we obtain

$$\left\|\delta\tilde{m}^{n,k}\right\| \leq C\Big(\left\|\boldsymbol{\varepsilon}(\delta\boldsymbol{u}_h^{n,k})\right\| + \left\|\delta\boldsymbol{z}_h^{n,k}\right\|\Big). \tag{2.4.108}$$

Now consider the result in the theorem 2.4.1 and denote the first two terms on the left by $\mathcal{J}^{n+1,k+1}$*, that is,*

$$\mathcal{J}^{n+1,k+1} = \frac{4G}{\lambda+L}\|\boldsymbol{\varepsilon}(\delta\boldsymbol{u}_h^{n+1,k+1})\|^2 + \frac{c^2\Delta t}{\mu_f}\left\|\boldsymbol{K}^{-1/2}\delta\boldsymbol{z}_h^{n+1,k+1}\right\|^2.$$

The above inequality (2.4.108) *can be rewritten as using a generic* C*,*

$$\left\|\delta\tilde{m}^{n+1,k+1}\right\|^2 \leq C\mathcal{J}^{n+1,k+1}. \tag{2.4.109}$$

The inequality (2.4.107) *takes the form*

$$\left(\frac{1}{C}+1\right)\left\|\delta\tilde{m}^{n+1,k+1}\right\|^2 \leq \left(\frac{L}{\lambda+L}\right)^2\left\|\delta\tilde{m}^{n,k+1}\right\|^2$$

yielding an improved contraction constant,

$$\left\|\delta\tilde{m}^{n+1,k+1}\right\|^2 \leq \left(\frac{C}{C+1}\right)\left(\frac{L}{\lambda+L}\right)^2\left\|\delta\tilde{m}^{n,k+1}\right\|^2. \tag{2.4.110}$$

In practice, it is difficult to estimate C*, however, the above computations show the relative contributions of the extra positive terms in* (2.4.107) *affect the contraction result observed in practice. Moreover, we can theoretically derive an explicit expression of* C *in a similar way as shown in remark 2.3.4. The details are spared.*

Remark 2.4.3. *The single rate undrained split iterative coupling scheme has been rigorously analyzed by Mikelić and Wheeler [64]. In their analysis, a contraction on the fluid mass per bulk volume, defined by:* $m = m_0 + \rho_0\alpha\nabla\cdot\boldsymbol{u} + \frac{\rho_0}{M}(p-p_0)$*, has been obtained for a continuous in time and space formulation. The value of the introduced free parameter* L *has been chosen a priori to be* $L = M\alpha^2$*. Following their approach, and adapting to our fully discrete formulation (mixed form for flow, and conformal Galerkin for mechanics), we have the following result:*

Theorem 2.4.2. *[Mikelić & Wheeler [64]] Let* L *be a predetermined coefficient:* $L = M\alpha^2$*,* $\varphi_h^{*n,k} := \varphi_0 + \alpha\nabla\cdot\boldsymbol{u}_h^{n,k} + \frac{1}{M}(p_h^{n,k}-p_0)$*, and* δ *denoting the difference of two successive iterates, the undrained split scheme as given in algorithm (4) is a contraction given by*

$$\begin{aligned}\tfrac{4G\alpha^2}{\lambda+M\alpha^2}\|\boldsymbol{\varepsilon}(\delta\boldsymbol{u}_h^{n+1,k})\|^2 + \tfrac{2\Delta t}{M\mu_f}\left\|\boldsymbol{K}^{-1/2}\delta\boldsymbol{z}_h^{n+1,k}\right\|^2 \\ + \tfrac{2c_f\varphi_0}{M}\|\delta p_h^{n+1,k}\|^2 + \left\|\delta\varphi_h^{*n+1,k+1}\right\|^2 \leq \left(\tfrac{M\alpha^2}{\lambda+M\alpha^2}\right)^2\left\|\delta\varphi_h^{*n,k+1}\right\|^2.\end{aligned}$$

Furthermore, the sequences defined by this scheme converge to the unique solution of the weak formulation (2.4.92)–(2.4.94)*.*

We note that our proof is optimized in the sense that it reveals the optimal value of the parameter $L = \dfrac{\alpha^2}{2\beta}$*, which leads to a sharper contraction estimates:* $\left(\frac{L}{\lambda+L}\right)^2 = \left(\frac{\alpha^2 M}{2\lambda+2\lambda M c_f \varphi_0+\alpha^2 M}\right)^2$.

2.4.2 Multirate Formulation and Analysis

2.4.2.1 Fully Discrete Scheme for Multirate

The weak formulation of a multirate scheme reads as follows.

Definition 2.4.2. *(***mechanics equation***)*

Find $\boldsymbol{u}_h^{k+q} \in \boldsymbol{V}_h$ *such that,*

$$\forall \boldsymbol{v}_h \in V_h\,,\; 2G(\boldsymbol{\varepsilon}(\boldsymbol{u}_h^{k+q}), \boldsymbol{\varepsilon}(\boldsymbol{v}_h)) + \lambda(\nabla \cdot \boldsymbol{u}_h^{k+q}, \nabla \cdot \boldsymbol{v}_h) - \alpha(p_h^{k+q}, \nabla \cdot \boldsymbol{v}_h) = (\boldsymbol{f}, \boldsymbol{v}_h). \tag{2.4.111}$$

*and (***flow equation***) For* $1 \le m \le q$*, find* $p_h^{m+k} \in Q_h$*, and* $\boldsymbol{z}_h^{m+k} \in \boldsymbol{Z}_h$ *such that,*

$$\begin{aligned}\forall \theta_h \in Q_h\,,\; \frac{1}{\Delta t}\Big((\frac{1}{M} + c_f\varphi_0)\Big(p_h^{m+k} - p_h^{m-1+k}\Big), \theta_h\Big) + \frac{1}{\mu_f}(\nabla \cdot \boldsymbol{z}_h^{m+k}, \theta_h) = \\ - \frac{\alpha}{q\Delta t}\Big(\nabla \cdot \Big(\boldsymbol{u}_h^{k+q} - \boldsymbol{u}_h^{k}\Big), \theta_h\Big) + \Big(\tilde{q}_h, \theta_h\Big),\end{aligned} \tag{2.4.112}$$

$$\forall \boldsymbol{q}_h \in \boldsymbol{Z}_h\,,\; \Big(\boldsymbol{K}^{-1}\boldsymbol{z}_h^{m+k}, \boldsymbol{q}_h\Big) = \Big(p_h^{m+k}, \nabla \cdot \boldsymbol{q}_h\Big) + \Big(\rho_{f,r} g \nabla\, \eta, \boldsymbol{q}_h\Big), \tag{2.4.113}$$

with the initial conditions for the first discrete time step,

$$p_h^0 = p_0, \quad \boldsymbol{u}_h^0 = \boldsymbol{u}_0. \tag{2.4.114}$$

2.4.2.2 Multirate Iterative Scheme

The scheme starts by solving the mechanics problem followed by a sequence of flow problems, and iterates between the two until convergence is achieved. The iteration assumes a constant fluid mass during the deformation of the structure (and can be interpreted as a regularization of mechanics equation). We start by presenting the scheme.

Algorithm 5: Undrained Split Multirate Algorithm

e

for $k = 0, q, 2q, 3q, ..$ **do** `/* mechanics time step iteration index */`

  for $n = 1, 2, ..$ **do** `/* coupling iteration index */`

    First Step: Mechanics equations

    Given $p_h^{n,k+q}$*, solve for* $\boldsymbol{u}_h^{n+1,k+q}$ *satisfying (assuming an initial value is given for the first iteration:* $p_h^{0,k+q}$*):*

$$-2G\nabla\cdot(\boldsymbol{\varepsilon}(\boldsymbol{u}_h^{n+1,k+q})) - (\lambda+L)\nabla\cdot((\nabla\cdot\boldsymbol{u}_h^{n+1,k+q})I) = -\alpha\nabla\cdot(p_h^{n,k+q}I) - L\nabla\cdot((\nabla\cdot\boldsymbol{u}_h^{n,k+q})I) + \boldsymbol{f} \tag{2.4.115}$$

    Second Step: Flow equations

    Given $\boldsymbol{u}_h^{n+1,k+q}$

    for $m = 1, 2, .., q$ **do** `/* flow finer time steps iteration index */`

      Solve for $p_h^{n+1,m+k}$ *and* $\boldsymbol{z}_h^{n+1,m+k}$ *satisfying:*

$$\beta\Big(\frac{p_h^{n+1,m+k} - p_h^{n+1,m-1+k}}{\Delta t}\Big) + \frac{1}{\mu_f}\nabla\cdot\boldsymbol{z}_h^{n+1,m+k} = -\alpha\nabla\cdot\Big(\frac{\boldsymbol{u}_h^{n+1,k+q} - \boldsymbol{u}_h^{k}}{q\Delta t}\Big) + \tilde{q}_h \tag{2.4.116}$$

$$\boldsymbol{z}_h^{n+1,m+k} = -\boldsymbol{K}(\nabla\, p_h^{n+1,m+k} - \rho_{f,r}g\nabla\,\eta) \tag{2.4.117}$$

In the above, we have used $\beta = (\frac{1}{M} + c_f\varphi_0)$ for the notational convenience. L is a regularization parameter and the corresponding term vanishes in the case of convergence.

Following a similar approach to that of the single rate case, the convergence proof is based on studying the difference of two successive iterates and deriving the contraction of appropriate quantities in suitable norms. We recall that $\delta\xi^{n,k} = \xi^{n+1,k} - \xi^{n,k}$, where $\xi = p, \boldsymbol{u}, \text{or } \boldsymbol{z}$. It is interesting that the contracting quantity is a composite one consisting of both pressure $p^{n+1,k+m}$ and volumetric strain terms $\nabla\cdot\boldsymbol{u}^{n+1,k+q}$. For a particular coupling iteration, $n \geq 1$, and between two coarse mechanics time steps t_k and t_{k+q}, we define the quantity to be contracted on as:

$$\tilde{m}_q^{n+1,k+m} = \frac{L}{\gamma q}\nabla\cdot\boldsymbol{u}^{n+1,k+q} + \frac{\alpha}{\gamma}(p^{n+1,k+m} - p^{n+1,k+m-1}), \text{ for } 1 \leq m \leq q,$$

where γ is an adjustable coefficient that will be selected carefully such that Banach contraction holds on $\tilde{m}_q$. As in the single-rate case, the contractivity of the scheme is not altered by the presence of γ, as it only simplifies the algebra, and scales the the quantity of contraction is a way such that the contraction coefficient is most optimized.

Considering the difference between one local flow iteration and its corresponding local flow iteration in the previous coupling iteration, and the difference between two consecutive mechanics coupling iterations, the weak formulation of equations corresponding to (2.4.115), (2.4.116), and (2.4.117) can be written as follows.

Mechanics step: Given $\delta p_h^{n,k+q}$ from the previous coupling iteration, find $\delta \boldsymbol{u}_h^{n+1,k+q} \in \boldsymbol{V}_h$ such that,

$$\forall \boldsymbol{v}_h \in V_h\,,\; 2G(\boldsymbol{\varepsilon}(\delta \boldsymbol{u}_h^{n+1,k+q}), \boldsymbol{\varepsilon}(\boldsymbol{v}_h)) + (\lambda + L)(\nabla \cdot \delta \boldsymbol{u}_h^{n+1,k+q}, \nabla \cdot \boldsymbol{v}_h) = \alpha(\delta p_h^{n,k+q}, \nabla \cdot \boldsymbol{v}_h) + L(\nabla \cdot \delta \boldsymbol{u}_h^{n,k+q}, \nabla \cdot \boldsymbol{v}_h)\,, \tag{2.4.118}$$

Flow step: Given $\delta \boldsymbol{u}_h^{n+1,k+q}$, for $1 \leq m \leq q$, find $\delta p_h^{n+1,m+k} \in Q_h$, $\delta \boldsymbol{z}_h^{n+1,m+k} \in \boldsymbol{Z}_h$ such that:

$$\forall \theta_h \in Q_h\,,\; \beta\Big(\frac{\delta p_h^{n+1,m+k} - \delta p_h^{n+1,m-1+k}}{\Delta t}, \theta_h\Big) + \frac{1}{\mu_f}(\nabla \cdot \delta \boldsymbol{z}_h^{n+1,m+k}, \theta_h) = -\frac{\alpha}{q\Delta t}\Big(\nabla \cdot \delta \boldsymbol{u}_h^{n+1,k+q}, \theta_h\Big) \tag{2.4.119}$$

$$\forall \boldsymbol{q}_h \in \boldsymbol{Z}_h\,,\; (\boldsymbol{K}^{-1}\delta \boldsymbol{z}_h^{n+1,m+k}, \boldsymbol{q}_h) = (\delta p_h^{n+1,m+k}, \nabla \cdot \boldsymbol{q}_h) \tag{2.4.120}$$

2.4.2.3 Proof of Contraction

- **Step (1): Elasticity equation**

  First, we analyze the mechanics equation. Testing (2.4.118) with $\boldsymbol{v}_h = \delta \boldsymbol{u}_h^{n+1,k+q}$, we

get:

$$
\begin{aligned}
&2G\|\boldsymbol{\varepsilon}(\delta\boldsymbol{u}_h^{n+1,k+q})\|^2+(\lambda+L)\|\nabla\cdot\delta\boldsymbol{u}_h^{n+1,k+q}\|^2\\
&\quad=(\alpha\delta p_h^{n,k+q}+L\nabla\cdot\delta\boldsymbol{u}_h^{n,k+q},\nabla\cdot\delta\boldsymbol{u}_h^{n+1,k+q})\\
&\quad=\Big(\sum_{m=1}^{q}\Big(\alpha(\delta p_h^{n,m+k}-\delta p_h^{n,m-1+k})+\frac{L}{q}\nabla\cdot\delta\boldsymbol{u}_h^{n,k+q}\Big),\nabla\cdot\delta\boldsymbol{u}_h^{n+1,k+q}\Big)\\
&\quad\le\frac{\varepsilon}{2}\left\|\nabla\cdot\delta\boldsymbol{u}^{n+1,k+q}\right\|^2+\frac{1}{2\varepsilon}\gamma^2\sum_{m=1}^{q}\left\|\delta\tilde{m}_q^{n,k+m}\right\|^2
\end{aligned}
$$

by noting that $\sum_{m=1}^{q}\Big(\delta p_h^{n,m+k}-\delta p_h^{n,m-1+k}\Big)=\delta p_h^{n,k+q}$ and using Young's inequality. For $\varepsilon=\lambda+L$, we obtain after some simplifications,

$$
\frac{4G}{\lambda+L}\|\boldsymbol{\varepsilon}(\delta\boldsymbol{u}_h^{n+1,k+q})\|^2+\|\nabla\cdot\delta\boldsymbol{u}_h^{n+1,k+q}\|^2\le\frac{\gamma^2}{(\lambda+L)^2}\sum_{m=1}^{q}\left\|\delta\tilde{m}_q^{n,k+m}\right\|^2. \tag{2.4.121}
$$

- **Step (2): Flow equations**

  Testing (2.4.119), with $\theta_h=\delta p_h^{n+1,m+k}-\delta p_h^{n+1,m-1+k}$, and multiplying by Δt, we get: (recall $\beta=\frac{1}{M}+c_f\varphi_0$)

$$
\begin{aligned}
&\beta\left\|\delta p_h^{n+1,m+k}-\delta p_h^{n+1,m-1+k}\right\|^2+\frac{\Delta t}{\mu_f}(\nabla\cdot\delta\boldsymbol{z}_h^{n+1,m+k},\delta p_h^{n+1,m+k}-\delta p_h^{n+1,m-1+k})=\\
&-\frac{\alpha}{q}\Big(\nabla\cdot\delta\boldsymbol{u}_h^{n+1,k+q},\delta p_h^{n+1,m+k}-\delta p_h^{n+1,m-1+k}\Big)
\end{aligned}
\tag{2.4.122}
$$

  Now, consider (2.4.120) for two consecutive local flow finer time steps, $t=t_{m+k}$, and $t=t_{m-1+k}$, and test with $\boldsymbol{q}_h=\delta\boldsymbol{z}_h^{n+1,m+k}$ and taking the difference between them, we get

$$
\begin{aligned}
&\Big(\boldsymbol{K}^{-1}\Big(\delta\boldsymbol{z}_h^{n+1,m+k}-\delta\boldsymbol{z}_h^{n+1,m-1+k}\Big),\delta\boldsymbol{z}_h^{n+1,m+k}\Big)\\
&\qquad=\Big(\delta p_h^{n+1,m+k}-\delta p_h^{n+1,m-1+k},\nabla\cdot\delta\boldsymbol{z}_h^{n+1,m+k}\Big).
\end{aligned}
\tag{2.4.123}
$$

  Substituting (2.4.123) into (2.4.122), we have

$$
\begin{aligned}
&\beta\left\|\delta p_h^{n+1,m+k}-\delta p_h^{n+1,m-1+k}\right\|^2\\
&\qquad+\frac{\Delta t}{\mu_f}\Big(\boldsymbol{K}^{-1}\Big(\delta\boldsymbol{z}_h^{n+1,m+k}-\delta\boldsymbol{z}_h^{n+1,m-1+k}\Big),\delta\boldsymbol{z}_h^{n+1,m+k}\Big)=\\
&\qquad\qquad-\frac{\alpha}{q}\Big(\nabla\cdot\delta\boldsymbol{u}_h^{n+1,k+q},\delta p_h^{n+1,m+k}-\delta p_h^{n+1,m-1+k}\Big).
\end{aligned}
$$

By Young's inequality, with further simplifications,

$$\beta\left\|\delta p_h^{n+1,m+k}-\delta p_h^{n+1,m-1+k}\right\|^2+\frac{\alpha}{q}\Big(\nabla\cdot\delta\boldsymbol{u}_h^{n+1,k+q},\delta p_h^{n+1,m+k}-\delta p_h^{n+1,m-1+k}\Big)$$
$$\frac{\Delta t}{2\mu_f}\Big(\left\|\boldsymbol{K}^{-1/2}\delta\boldsymbol{z}_h^{n+1,m+k}\right\|^2-\left\|\boldsymbol{K}^{-1/2}\delta\boldsymbol{z}_h^{n+1,m-1+k}\right\|^2$$
$$+\left\|\boldsymbol{K}^{-1/2}(\delta\boldsymbol{z}_h^{n+1,m+k}-\delta\boldsymbol{z}_h^{n+1,m-1+k}\Big)\right\|^2\Big)=0.$$

Summing for q local flow time steps and after some simplifications (telescopic cancellations together with the fact that $\delta\boldsymbol{z}_h^{n+1,k}=0$), we get

$$\beta\sum_{m=1}^{q}\left(\left\|\delta p_h^{n+1,m+k}-\delta p_h^{n+1,m-1+k}\right\|^2+\frac{\alpha}{q}\Big(\nabla\cdot\delta\boldsymbol{u}_h^{n+1,k+q},\delta p_h^{n+1,m+k}-\delta p_h^{n+1,m-1+k}\Big)\right)$$
$$\frac{\Delta t}{2\mu_f}\left\|\boldsymbol{K}^{-1/2}\delta\boldsymbol{z}_h^{n+1,k+q}\right\|^2+\frac{\Delta t}{2\mu_f}\sum_{m=1}^{q}\left\|\boldsymbol{K}^{-1/2}\Big(\delta\boldsymbol{z}_h^{n+1,m+k}-\delta\boldsymbol{z}_h^{n+1,m-1+k}\Big)\right\|^2=0. \tag{2.4.124}$$

- **Step (3): Combining Mechanics and Flow**

  Multiplying (2.4.124) by another free parameter c^2 and adding (2.4.124), we obtain

$$\frac{4G}{\lambda+L}\|\boldsymbol{\varepsilon}(\delta\boldsymbol{u}_h^{n+1,k+q})\|^2+\sum_{m=1}^{q}\Bigg\{c^2\beta\left\|\delta p_h^{n+1,m+k}-\delta p_h^{n+1,m-1+k}\right\|^2$$
$$+\frac{c^2\alpha}{q}\Big(\nabla\cdot\delta\boldsymbol{u}_h^{n+1,k+q},\delta p_h^{n+1,m+k}-\delta p_h^{n+1,m-1+k}\Big)+\|\nabla\cdot\delta\boldsymbol{u}_h^{n+1,k+q}\|^2\Bigg\}$$
$$+\frac{c^2\Delta t}{2\mu_f}\left\|\boldsymbol{K}^{-1/2}\delta\boldsymbol{z}_h^{n+1,k+q}\right\|^2+\frac{c^2\Delta t}{2\mu_f}\sum_{m=1}^{q}\left\|\boldsymbol{K}^{-1/2}\Big(\delta\boldsymbol{z}_h^{n+1,m+k}-\delta\boldsymbol{z}_h^{n+1,m-1+k}\Big)\right\|^2$$
$$\leq\frac{\gamma^2}{(\lambda+L)^2}\sum_{m=1}^{q}\left\|\delta\tilde{m}_q^{n,k+m}\right\|^2. \tag{2.4.125}$$

- **Step (4): Identifying the parameters**

  Note that we have three free parameters: $c^2,\gamma,$ and L. Below we provide the procedure for determining these parameters yielding a contraction. These parameters should be chosen such that the terms on the left hand side of (2.4.125) remain positive, and the scheme achieves contraction on m. Clearly,

$$\left\|\delta\tilde{m}_q^{n+1,k+m}\right\|^2=\frac{L^2}{q^2\gamma^2}\left\|\nabla\cdot\delta\boldsymbol{u}^{n+1,k+q}\right\|^2+\frac{\alpha^2}{\gamma^2}\left\|(p^{n+1,k+m}-p^{n+1,k+m-1})\right\|^2$$
$$+\frac{2\alpha L}{\gamma^2 q}\left((p^{n+1,k+m}-p^{n+1,k+m-1}),\nabla\cdot\delta\boldsymbol{u}^{n+1,k+q}\right).$$

Matching coefficients by comparing with the terms in the curly brackets in (2.4.125) provides us $\frac{L^2}{q^2\gamma^2} = 1$, $\frac{\alpha^2}{\gamma^2} \leq c^2\beta$, and $\frac{2\alpha L}{\gamma^2 q} = \frac{c^2\alpha}{q}$. This gives, $L = q\gamma, \quad L \geq \frac{\alpha^2}{2\beta}$ and since the contraction factor is monotone with respect to L, its minimum is achieved when we choose,

$$L = \frac{\alpha^2}{2\beta} \text{ implying } \gamma = \frac{\alpha^2}{2q\beta} \text{ and } c^2 = \frac{4q^2\beta}{\alpha^2}.$$

Using above in (2.4.125) we note that the contraction factor is $\frac{L^2}{q^2(\lambda+L)^2}$ and is smaller when q is larger. Also, when $q = 1$, the above contraction rate reduces to that of the single rate case [64] (when the time steps for the mechanics and flow are the same).

Our main result summarizes the above contraction result.

Theorem 2.4.3. *With* $L = \dfrac{\alpha^2}{2\beta}$ *and* $c^2 = \frac{4q^2\beta}{\alpha^2}$, *the undrained multirate iterative scheme defined by* (2.4.115) - (2.4.117) *is a contraction given by*

$$\begin{aligned}
&\frac{c^2\Delta t}{2\mu_f}\left\|\boldsymbol{K}^{-1/2}\delta\boldsymbol{z}_h^{n+1,k+q}\right\|^2 + \frac{c^2\Delta t}{2\mu_f}\sum_{m=1}^{q}\left\|\boldsymbol{K}^{-1/2}\Big(\delta\boldsymbol{z}_h^{n+1,m+k} - \delta\boldsymbol{z}_h^{n+1,m-1+k}\Big)\right\|^2 \\
&+ \sum_{m=1}^{q}\left\|\delta\tilde{m}_q^{n+1,k+m}\right\|^2 + \frac{4G}{\lambda+L}\|\boldsymbol{\varepsilon}(\delta\boldsymbol{u}_h^{n+1,k+q})\|^2 \leq \frac{L^2}{q^2(\lambda+L)^2}\sum_{m=1}^{q}\left\|\delta\tilde{m}_q^{n,k+m}\right\|^2.
\end{aligned} \tag{2.4.126}$$

Furthermore, the sequences defined by this scheme converge to the unique solution of the weak formulation (2.4.111)–(2.4.113).

Remark 2.4.4. *The scheme presented in algorithm 5 can be modified such that the coarse mechanics time step is kept fixed as* Δt, *and the fine flow time step is considered as* $\frac{\Delta t}{q}$, *for* $q \geq 1$. *The proof of contraction follows in the same way except that the parameter* c *is chosen to be* $c = \sqrt{\frac{4q\beta}{\alpha^2}}$. *The same result, presented in theorem 2.4.3, hold in this case.*

2.4.2.4 Convergence to The Discrete Form

From the result obtained above, we establish convergence of the sequences generated by the multirate undrained split algorithm and show that the converged quantities satisfy the

weak formulation (2.4.111) – (2.4.114). The proof uses the mathematical induction for the finer flow equations combined with the contraction estimates obtained above.

Lemma 2.4.1. *For every coarser mechanics time step, $t = t_k$, there exist a limit function $\boldsymbol{u}_h^k$ such that*

$$\boldsymbol{u}_h^{n,k} \to \boldsymbol{u}_h^k \quad \textit{strongly in } H^1(\Omega)^d.$$

Proof. The contraction result in theorem 2.4.3 implies that for a coarser time step $t = t_k$, $\|\boldsymbol{\varepsilon}(\delta \boldsymbol{u}_h^{n+1,k})\|$ converges geometrically to zero. Using Korn's inequality, this implies that $\partial_{x_i}(\boldsymbol{u}_h^{n+1,k}), i = 1, 2, 3$ is a Cauchy sequence converging geometrically to a unique limit in $L^2(\Omega)^d$. It follows immediately that $\boldsymbol{u}_h^{n+1,k}$ is a Cauchy sequence converging geometrically to a unique limit in $H^1(\Omega)^d$, being a Hilbert space. □

Lemma 2.4.2. *For every two consecutive coarser mechanics time steps, $t = t_k$, and $t = t_{k+q}$, and for every $1 \leq m \leq q$, there exist limit functions $p_h^{m+k}, \boldsymbol{z}_h^{m+k}$ such that*

$$p_h^{n,m+k} \to p_h^{m+k} \quad \textit{in } L^2(\Omega), \quad \boldsymbol{z}_h^{n,m+k} \to \boldsymbol{z}_h^{m+k} \quad \textit{in } H(div, \Omega)^d,$$

with strong convergence in the norms of the above spaces.

Proof. The contraction result in theorem 2.4.3 implies that the quantities

$$\sum_{m=1}^{q} \left\| K^{-1/2}(\delta \boldsymbol{z}_h^{n+1,m+k} - \delta \boldsymbol{z}_h^{n+1,m-1+k}) \right\|^2 \quad \text{and} \quad \sum_{m=1}^{q} \left\| \delta \tilde{m}_q^{n+1,m+k} \right\|^2$$

converge geometrically to zero. It follows that for $1 \leq m \leq q$, $\left\| K^{-1/2}(\delta \boldsymbol{z}_h^{n+1,m+k} - \delta \boldsymbol{z}_h^{n+1,m-1+k}) \right\|^2$, and $\left\| \delta \tilde{m}_q^{n+1,m+k} \right\|^2$ converge geometrically to zero. Moreover, by (2.4.117), and Poincaré inequality, $\left\| K^{1/2} \nabla (\delta p_h^{n+1,m+k} - \delta p_h^{n+1,m-1+k}) \right\|^2$ and $\left\| \delta p_h^{n+1,m+k} - \delta p_h^{n+1,m-1+k} \right\|^2$ converge geometrically to zero, respectively. This implies that for every $1 \leq m \leq q$, the finer time step differences $(p_h^{n,m+k} - p_h^{n,m-1+k})$, $(\boldsymbol{z}_h^{n,m+k} - \boldsymbol{z}_h^{n,m-1+k})$, and the quantity defined by $\tilde{m}_q^{n,m+k}$ are Cauchy sequences in $L^2(\Omega)$.

We will show strong convergence of the pressure sequence by induction. The proof of strong convergence of the flux sequence follows in the same way. Given an initial pressure value

for $t = t_0$: $p_h^{n,0} = p_0$, from the above discussion, $(p_h^{n,1} - p_0)$ is a Cauchy sequence in $L^2(\Omega)$, and, in turn, $p_h^{n,1}$ is a Cauchy sequence in the complete space $L^2(\Omega)$, and has a unique limit. This completes the base case for induction. For the inductive hypothesis, we assume that for any coarser mechanics time step $t = t_k$, and for any $1 \leq m \leq q$, $p_h^{n,k+m}$ is a Cauchy sequence converging to a unique limit in $L^2(\Omega)$: $p_h^{n,k+m} \to p_h^{k+m}$ in $L^2(\Omega)$. We will show that $p_h^{n,k+m+1}$ is also a Cauchy sequence converging to a unique limit in $L^2(\Omega)$. However, this follows immediately, as $(p_h^{n,k+m+1} - p_h^{n,k+m})$ is a Cauchy sequences in $L^2(\Omega)$, converging to a unique limit in $L^2(\Omega)$. This completes the inductive step. Therefore, we obtain that for all coarser mechanics time steps $t = t_k$, and for $1 \leq m \leq q$, $p_h^{n,m+k}, \boldsymbol{z}_h^{n,m+k}$ are Cauchy sequences converging geometrically to unique limits in $L^2(\Omega)$.

For the divergence of the flux, we note that (2.4.119) amounts to the following equality a.e. in $L^2(\Omega)$:

$$\nabla \cdot \delta \boldsymbol{z}_h^{n+1,m+k} = -\frac{\beta \mu_f}{\Delta t}(\delta p_h^{n+1,m+k} - \delta p_h^{n+1,m-1+k}) - \frac{\alpha}{q\Delta t}\nabla \cdot \delta \boldsymbol{u}_h^{n+1,k+q}.$$

The convergence of $\nabla \cdot \boldsymbol{z}_h^{n+1,m+k}$ in $L^2(\Omega)$ follows from the convergence of the difference $(p_h^{n+1,m+k} - p_h^{n+1,m+k})$ and $\tilde{m}_q^{n+1,m+k}$ in $L^2(\Omega)$, established above (the convergence of $(p_h^{n+1,m+k} - p_h^{n+1,m+k})$ and $\tilde{m}_q^{n+1,m+k}$ implies the convergence of $\nabla \cdot \boldsymbol{u}_h^{n+1,k+q}$ by definition). Thus, we have both $\nabla \cdot \boldsymbol{z}_h^{n,m+k}$ and $\boldsymbol{z}_h^{n,m+k}$ converging geometrically to unique limits in $L^2(\Omega)$, and hence $\boldsymbol{z}_h^{n+1,k}$ converges to a unique limit in $H(div, \Omega)^d$. □

It remains to pass to the limit in (2.4.111)–(2.4.113). This is straightforward since the equations are linear and all operators involved are continuous in the spaces invoked in the statements of Lemmas 2.4.1 and 2.4.2. Moreover the convergences are strong. Therefore, we easily retrieve the fully discrete multirate formulation.

Remark 2.4.5. *As in the single rate case discussed in remark 2.4.2, in the multirate case too the contraction in theorem 2.4.3 can be improved. The above proof already provides the arguments required. Note that using triangle's inequality,*

$$\|\delta \tilde{m}_q^{n+1,k+m}\| \leq \frac{L}{\gamma q}\|\nabla \cdot \delta \boldsymbol{u}_h^{n+1,k+q}\| + \frac{\alpha}{\gamma}\|\delta p_h^{n+1,k+m} - \delta p_h^{n+1,k+m-1}\|,$$

and using standard mixed method to estimate the pressure by the flux and the Korn inequality, we obtain

$$\sum_{m=1}^{q} \left\|\delta\tilde{m}_q^{n+1,k+m}\right\|^2 \leq C(\|\boldsymbol{\varepsilon}(\delta\boldsymbol{u}_h^{n+1,k+q})\|^2 + \sum_{m=1}^{q} \left\|\boldsymbol{K}^{-1/2}\Big(\delta\boldsymbol{z}_h^{n+1,m+k} - \delta\boldsymbol{z}_h^{n+1,m-1+k}\Big)\right\|^2)$$

$$\leq C\bigg(\|\boldsymbol{\varepsilon}(\delta\boldsymbol{u}_h^{n+1,k+q})\|^2 + \sum_{m=1}^{q} \left\|\boldsymbol{K}^{-1/2}\Big(\delta\boldsymbol{z}_h^{n+1,m+k} - \delta\boldsymbol{z}_h^{n+1,m-1+k}\Big)\right\|^2$$

$$+ \left\|\boldsymbol{K}^{-1/2}\delta\boldsymbol{z}_h^{n+1,k+q}\right\|^2\bigg). \quad (2.4.127)$$

Now consider the result in the theorem 2.4.3 and denote $\mathcal{I}_q^{n+1,k+q}$

$$\mathcal{I}_q^{n+1,k+q} = \frac{4G}{\lambda+L}\|\boldsymbol{\varepsilon}(\delta\boldsymbol{u}_h^{n+1,k+q})\|^2 + \frac{c^2\Delta t}{2\mu_f}\sum_{m=1}^{q} \left\|\boldsymbol{K}^{-1/2}\Big(\delta\boldsymbol{z}_h^{n+1,m+k} - \delta\boldsymbol{z}_h^{n+1,m-1+k}\Big)\right\|^2$$

$$+ \frac{c^2\Delta t}{2\mu_f}\left\|\boldsymbol{K}^{-1/2}\delta\boldsymbol{z}_h^{n+1,k+q}\right\|^2.$$

The above inequality (2.4.127) *can be rewritten as using a generic* C*,*

$$\sum_{m=1}^{q}\|\delta\tilde{m}_q^{n+1,k+m}\|^2 \leq C\mathcal{I}_q^{n+1,k+q}. \quad (2.4.128)$$

The inequality (2.4.126) *takes the form*

$$(\frac{1}{C}+1)\sum_{m=1}^{q} \left\|\delta\tilde{m}_q^{n+1,k+m}\right\|^2 \leq \Big(\frac{L}{q(\lambda+L)}\Big)^2 \sum_{m=1}^{q} \left\|\delta\tilde{m}_q^{n,k+m}\right\|^2$$

yielding an improved contraction constant,

$$\sum_{m=1}^{q} \left\|\delta\tilde{m}_q^{n+1,k+1}\right\|^2 \leq \Big(\frac{C}{C+1}\Big)\Big(\frac{L}{q(\lambda+L)}\Big)^2 \sum_{m=1}^{q} \left\|\delta\tilde{m}_q^{n,k+1}\right\|^2. \quad (2.4.129)$$

In practice, it is difficult to estimate C*, however, the above computations show the relative contributions of the extra positive terms in* (2.4.126) *affect the contraction result observed in practice.*

2.4.3 Conclusions and Discussion

In this section, we have considered single rate and multirate iterative coupling schemes for the sequential coupling of flow with mechanics based on the undrained split iterative

coupling algorithm. For both schemes, we have proved Banach fixed-point contraction, and convergence to the weak solution of the corresponding fully discrete scheme follows immediately. The multirate is a natural extension of the single rate scheme, and contracts on a composite quantity consisting of pressure and volumetric strain terms. Contraction proofs are optimal in the sense that contraction quantities are scaled such that more terms on the left hand side are absorbed. Compared to previously obtained results [64], our derived contraction coefficients are shaper. To the best of our knowledge, this is the first time a contraction result has been rigorously obtained for the multirate undrained split iterative coupling scheme. However, It should be noted that our analysis in this chapter limits to one coarser time step and we have not considered and investigated the propagation of error due to spatial and temporal discretizations. These error estimates providing the convergence rate can be studied and analyzed, for example, in the spirit of [45] (a priori error estimates for the fixed-stress split scheme have been derived in Chapter 3. The same technique can be used to derive a priori error estimates for the undrained-split scheme). Further, the nonlinear extensions of these schemes, their mathematical analyses and computational performance are interesting questions that will be addressed in future work. Moreover, the performance of these algorithms should be investigated numerically, and appropriate convergence stopping criteria for should be devised accordingly.

2.5 Numerical Results

The first multirate iterative coupling algorithm (Algorithm 2) is implemented in the in-house reservoir simulator (The Integrated Parallel Accurate Reservoir Simulator - IPARS [57, 58]). As discussed above, the flow problem is solved using mixed method and the mechanics by conformal Galerkin (see [82,86] for more details on mechanics discretization). In the mixed method for the flow, the flux unknowns are locally eliminated and a pressure stencil is obtained. The flux is then computed by post-processing.

We consider three numerical experiments in this section as follows:

- The Mandel's problem: which is a standard benchmark problem with an analytical solution and is used to validate the accuracy of our proposed scheme. It also highlights the expected trade-off between multirate-savings and maintaining an acceptable level of accuracy of the obtained numerical solution.
- Single phase flow MFMFE model coupled with mechanics (linear elasticity): in which we will be evaluating the efficiency of of the multirate scheme (Algorithm 2) against a realistic field-scale problem, that includes a challenging reservoir geometry (the Frio model). Details about the MFMFE scheme can be found in Appendix A.
- Two phase flow MFMFE (IMPES) model coupled with mechanics (linear elasticity): for which we will be running a simple quarter wellbore model (used to study the sharpness of our derived theoretical contraction estimates against numerical observed values), and the Frio field model.

We note that except for the parallel SPE10 model considered in Chapter 8 and the Mandel's problem, all simulations considered in this dissertation were run serially on an "x86_64 Intel(R) Core(TM) i5-4590 CPU @ 3.30GHz" Linux workstation with 4 CPUs. The Mandel's problem was run serially on Bevo3, and the parallel SPE10 model, considered in Chapter 8, was run in parallel on 16 processors on Bevo3. Bevo3 is a 15 node compute cluster, with a 2 x hex core 2.93 GHz Intel Xeon X5670 processors and a total of 180 cores.

2.5.0.1 Convergence Stopping Critera

In spite of the fact that the solution of the fully implicit scheme is considered as the reference solution for iteratively coupled flow and geomechanics problems, this solution is not accessible in practice. Instead, a convergence stopping criteria should be devised in order to determine whether the iterative scheme has converged or not. Even though we implement multirate iterative coupling schemes, we still use the same convergence criteria as the one used in the single rate scheme. This is justified as follows: the multirate iterative coupling scheme can be viewed as a single rate scheme at the coarser mechanics time step level, considering the sequence of q flow solves as one coarser flow time step solve, with the last obtained pressure value being passed to the mechanics problem. We define two porosity expressions as follows:

$$\delta\varphi_{flow}^{n,k+q} = \Big(\frac{1}{M} + \frac{\alpha^2}{\lambda}\Big)\delta p_h^{n,k+q} \tag{2.5.130}$$

$$\delta\varphi_{mech}^{n,k+q} = \alpha\nabla\cdot\delta\boldsymbol{u}_h^{n,k+q} + \frac{1}{M}\delta p_h^{n,k+q} \tag{2.5.131}$$

The expression (2.5.131) is the standard definition of the fluid content of the medium [45]. The definition of $\delta\varphi_{flow}^{n,k+q}$ can be justified as follows: upon convergence, due to the contracting property of the scheme, (2.3.24) leads to

$$\delta\sigma_v^{n,k+q} = \lambda\nabla\cdot\delta\boldsymbol{u}_h^{n,k+q} - \alpha\delta p_h^{n,k+q} = 0.$$

Therefore, we have

$$\lambda\nabla\cdot\delta\boldsymbol{u}_h^{n,k+q} = \alpha\delta p_h^{n,k+q} \Rightarrow \nabla\cdot\delta\boldsymbol{u}_h^{n,k+q} = \frac{\alpha}{\lambda}\delta p_h^{n,k+q}.$$

This leads to:

$$\delta\varphi_{mech}^{n,k+q} = \alpha\nabla\cdot\delta\boldsymbol{u}_h^{n,k+q} + \frac{1}{M}\delta p_h^{n,k+q} = (\frac{1}{M} + \frac{\alpha^2}{\lambda})\delta p_h^{n,k+q} = \delta\varphi_{flow}^{n,k+q}$$

justifying the definition (2.5.130) above. Thus, upon convergence, we have $\delta\varphi_{mech}^{n,k+q} = \delta\varphi_{flow}^{n,k+q}$, or equivalently, $\alpha\nabla\cdot\delta\boldsymbol{u}_h^{n,k+q} - \frac{\alpha^2}{\lambda}\delta p_h^{n,k+q} = 0$. Accordingly, the convergence stopping criterion is defined as follows: $\left\|\frac{\varphi_{mech}^{n,k+q} - \varphi_{flow}^{n,k+q}}{\varphi_{mech}^{n,k+q}}\right\|_{L^\infty} = \left\|\frac{\alpha\nabla\cdot\boldsymbol{u}_h^{n,k+q} - \frac{\alpha^2}{\lambda}p_h^{n,k+q}}{\varphi_{mech}^{n,k+q}}\right\|_{L^\infty} < \text{TOL}$. We note that specifying the coupling iteration convergence criterion, especially in the multirate case, is still a subject of research. This is a critical subject as a "harsh" convergence stopping criteria might ruin the efficiency of the multirate scheme.

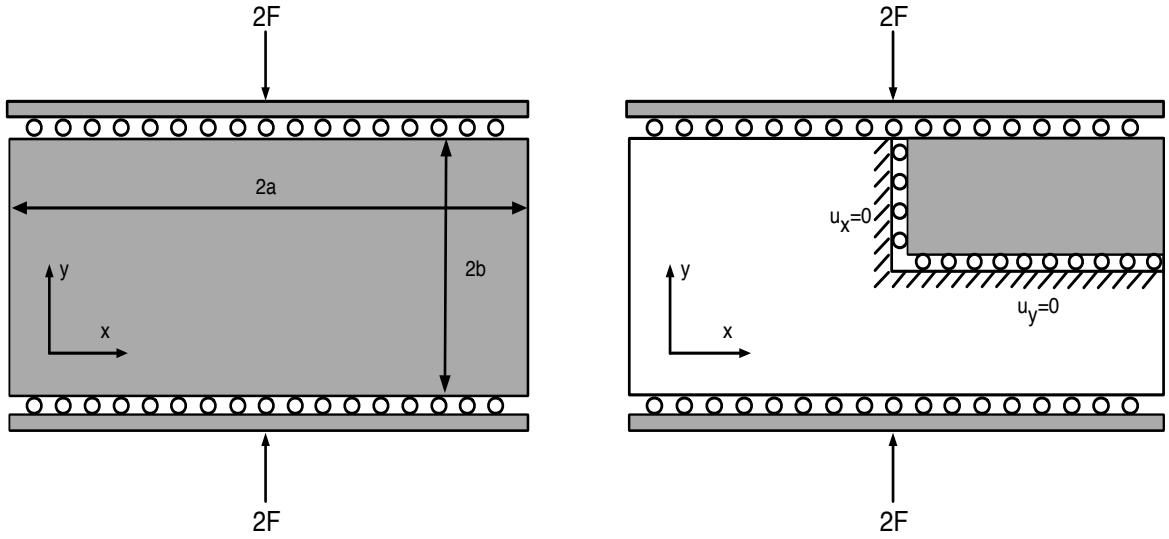

(a) Mandel's problem (original domain) (b) Mandel's problem (computational domain)

Figure 2.3: Mandel's problem original and computational domains

2.5.1 Validating the Accuracy of the Scheme - Mandel's Problem

The well-known Mandel's benchmark problem consists of a 2D saturated poroelastic slab of a rectangular shape with width $2a\ ft$ and height $2b\ ft$. The sample is loaded by a constant compressive force, of intensity $2F\ psi.ft$, applied on the rigid impervious top and bottom plates ($y = \pm b$). The slab can drain laterally, with stress-free lateral edges $x = \pm a$. The force is applied instantaneously at time $t = 0$, and gravity is neglected in this setting [86]. The original configuration of the problem is shown in figure 2.3a. The problem highlights the necessity of incorporating a poroelastic model into existing reservoir simulators, as it captures the unexpected Mandel-Cryer effect, and is a standard problem for verifying the accuracy of poroelasticity algorithms [70].

The model considered here is the linearized quasi-static Biot model [63,86]. The initial and boundary conditions are given as:

$$p|_{t=0} = 0, \quad \boldsymbol{u}|_{t=0} = 0, \quad \boldsymbol{\sigma}(\boldsymbol{u})|_{t=0} = \begin{pmatrix} 0 & 0 \\ 0 & 0 \end{pmatrix} \quad \text{in } (-a, a) \times (-b, b)$$

$$p = 0, \quad \boldsymbol{\sigma}(\boldsymbol{u})\boldsymbol{e}^1 = \boldsymbol{\sigma}_{11} = 0, \quad \text{on } x = \pm a$$

$$\boldsymbol{z}_y = 0, \quad \boldsymbol{\sigma}_{12} = 0, \quad \int_{-a}^{a} \boldsymbol{\sigma}_{22}\, dx = -2F, \quad \boldsymbol{u}_y = \text{unknown constant}, \quad \text{on } y = \pm b$$

Following a similar approach as in [63] and noting that $\boldsymbol{u}_y = \boldsymbol{u}_y(y,t)$, and $\boldsymbol{u}_x = \boldsymbol{u}_x(x,t)$, the impervious rigid plate condition (on $y = \pm b$), is replaced by:

$$\boldsymbol{z}_y = 0, \quad \boldsymbol{\sigma}_{12} = 0, \quad \boldsymbol{u}_y = U_y(\pm b, t) \quad \text{on } y = \pm b$$

where $U_y(\pm b, t)$ is the value obtained from the closed form solution of the Mandel's problem [63]. It should be noted that the problem is symmetric about the x and y axes. Therefore, only the upper-right quadrant ($(0,a) \times (0,b)$) is going to be considered for numerical simulation, as shown in figure 2.3b. This restriction should not affect the initial conditions of the problem. However, the updated boundary conditions of the computational domain are given as follows:

$$\begin{aligned}
&p = 0, \quad \boldsymbol{\sigma}(\boldsymbol{u})\boldsymbol{e}^1 = \boldsymbol{\sigma}_{11} = 0, \quad \text{on } x = a \\
&\boldsymbol{z}_x = 0, \quad \boldsymbol{u}_x = 0, \quad \boldsymbol{\sigma}_{12} = 0, \quad \text{on } x = 0 \\
&\boldsymbol{z}_y = 0, \quad \boldsymbol{\sigma}_{12} = 0, \quad \boldsymbol{u}_y = U_y(b,t) \quad \text{on } y = b \\
&\boldsymbol{z}_y = 0, \quad \boldsymbol{u}_y = 0, \quad \boldsymbol{\sigma}_{12} = 0, \quad \text{on } y = 0
\end{aligned}$$

The original analytical solution of the problem, as given by Mandel [61], specifies a closed form solution of the pore-pressure only, for the isotropic case. Later, Abousleiman et al. [1] generalized the problem to include material transverse isotropy, with compressible solid constituents and pore fluid, and they presented detailed analytical solutions for pore pressure, displacements, and stresses [1]. We refer the reader to [36, 70] for the exact expressions of the parameters involved in this problem, including the Skempton pore pressure coefficient B, the fluid diffusivity coefficient c, the undrained Poisson ration ν_u, and the analytical solutions including pore pressures p, displacements (u_x, u_y), and stresses. For our numerical tests in this paper, the input parameters are shown in Table 2.1. In addition, for the convergence stopping criterion, we set TOL = 5.E-7.

2.5.1.1 Results

Figures 2.5a, 2.5b, 2.5c, and 2.5d show numerical versus analytical results for the pressure variable at times t = 640, 1280, 5120, 10240, and 20480 seconds, for $q = 1, 2, 4,$, and 8

Total Simulation time:	50,000 seconds
Finer (Unit) time step (Δt):	80 seconds
Dimension in x (a):	328.084 ft
Dimension in y (b):	32.8084 ft
Number of grids:	1600 grids (40×40)
Grid spacing in x (Δx):	8.202 ft
Grid spacing in y (Δy):	0.8202 ft
Permeabilities: (k_{xx}, k_{yy})	100, 100 md
Initial porosity, (φ_0)	0.2
Fluid viscosity, (μ)	1.0 cp
Fluid compressibility (c_f)	2.089E-6 (1/psi)
Fluid density, ($\rho_{f,r}$):	62.4 lb_m/ft^3
Young's Modulus (E)	8.6152507E+5 psi
Possion Ratio, (ν)	0.2
Undrained Possion Ratio, (ν_u)	0.44
Biot's constant, (α)	1.0
Biot Modulus, (M)	2.3931227E+6 psi
Skempton coefficient, (B)	0.8333
Diffusivity coefficient, (c)	5.0052 ft^2/s
Introduced Fixed Stress Parameter (L)	$\frac{\alpha^2}{2\lambda}$

Table 2.1: Input Parameters for the Mandel's Problem

respectively. Results are most accurate for the single rate case $q = 1$, and accuracy degrades slightly as the value of q increases, which is expected. A similar behaviour, although at a much smaller scale, for x-displacements as shown in figures 2.6a, 2.6b, 2.6c, and 2.6d, for $q = 1, 2, 4$, and 8 respectively. CPU run times for the whole simulation run ($50,000$ seconds) are shown in figure 2.4a. For $q = 2$, we save 20.86 % in CPU runtime. For $q = 4$, and 8, we save 42.51 % and 60.09 % in CPU runtime respectively. Runtime savings can be attributed to the huge reductions in the total number of mechanics linear iterations for multirate cases. For $q = 2, 4$, and 8, the total number of mechanics linear iterations for the whole simulation run went down by 38.15 %, 65.25 %, and 82.43 % respectively. Tables 2.2 and 2.3 show the accuracy of the obtained solution against the analytical solution at two time steps during the simulation run ($t = 640$, and 20480) seconds respectively. We see that for both time steps, the accuracy of pressures degrades only slightly. Similarly, for displacements, the accuracy is only slightly affected. The numerical tests demonstrate that the multirate scheme maintains the accuracy of the solution whereas providing significant computational advantages.

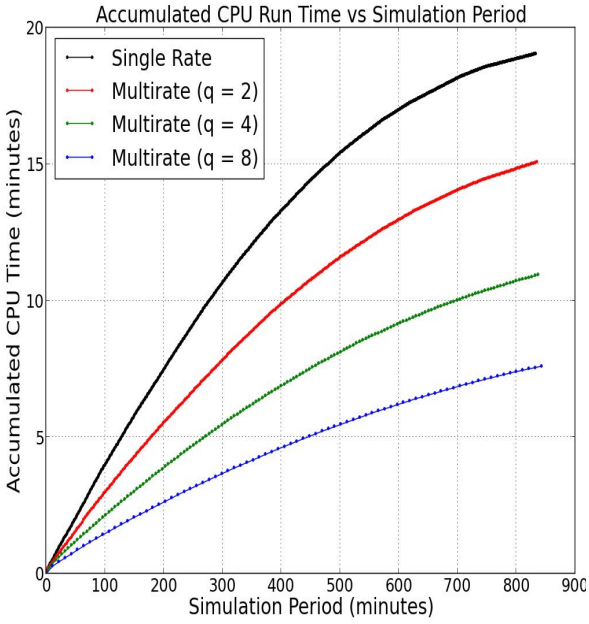

(a) CPU Run Time vs Simulation Days

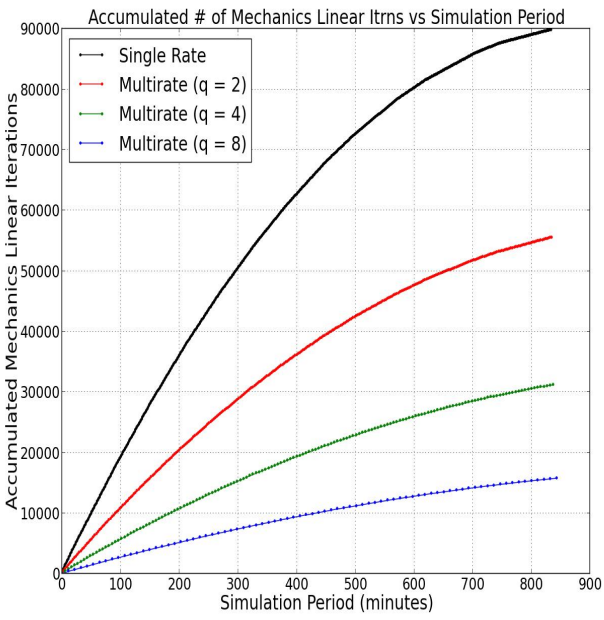

(b) Total Number of Mechanics Linear Iterations vs Simulation Days

Figure 2.4: Mandel's Problem Multirate Savings

	$q = 1$	$q = 2$	$q = 4$	$q = 8$
$\|p_h - p(t)\|^2_{\ell_2}$	1.0863e-03	1.6490e-03	3.3955e-03	7.9480e-03
$\|u_{x_h} - u_x(t)\|^2_{\ell_2}$	9.1711e-12	3.4294e-11	3.4218e-10	1.6005e-09
Reduction in CPU runtime	-	16.35%	27.90%	45.78%
Reduction in mech. linear iterations	-	42.41%	67.61%	83.46%

Table 2.2: Accuracy versus efficiency for different values of q (the number of flow finer time steps within one coarser mechanics time step) at time $t = 640$ seconds. Discrete ℓ_2 norms are computed over the top boundary of the domain ($y = b$), as x-displacements depend only on x-coordiantes. CPU time savings and reductions in the number of mechanics linear iterations are computed against the single rate case ($q = 1$).

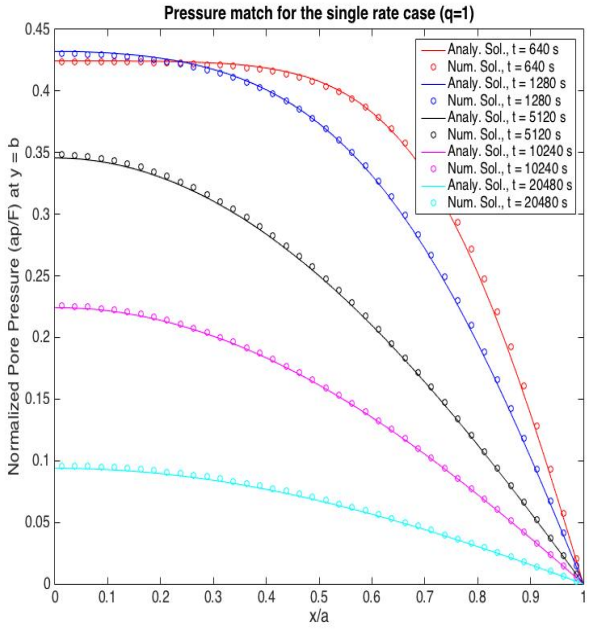

(a) Analytical vs Numerical Results ($q = 1$)

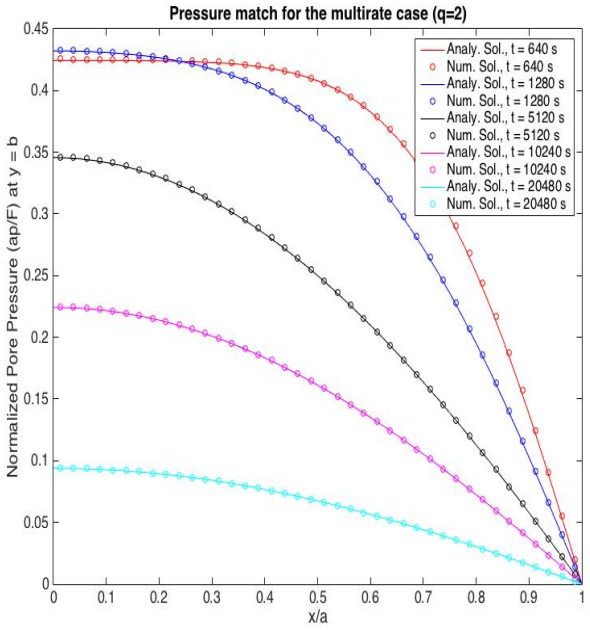

(b) Analytical vs Numerical Results ($q = 2$)

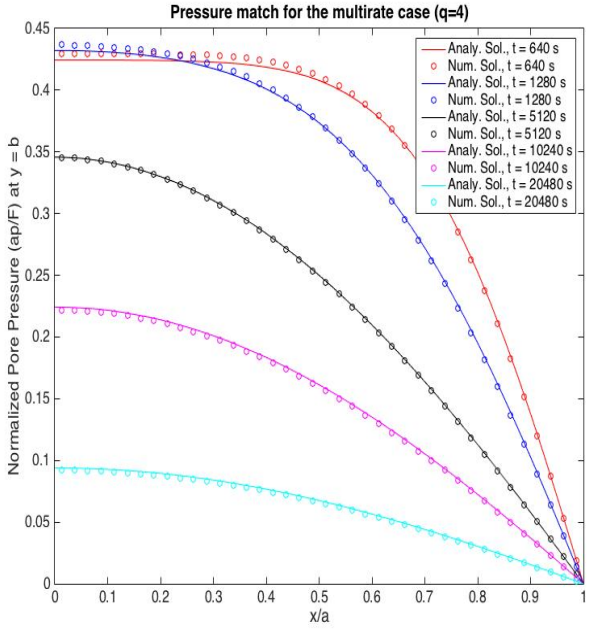

(c) Analytical vs Numerical Results ($q = 4$)

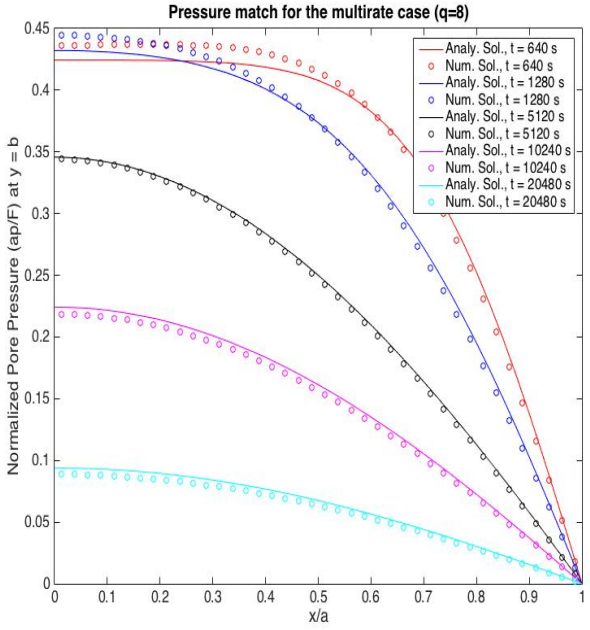

(d) Analytical vs Numerical Results ($q = 8$)

Figure 2.5: Accuracy of our Multirate Scheme on Mandel's Problem Pressure Solution

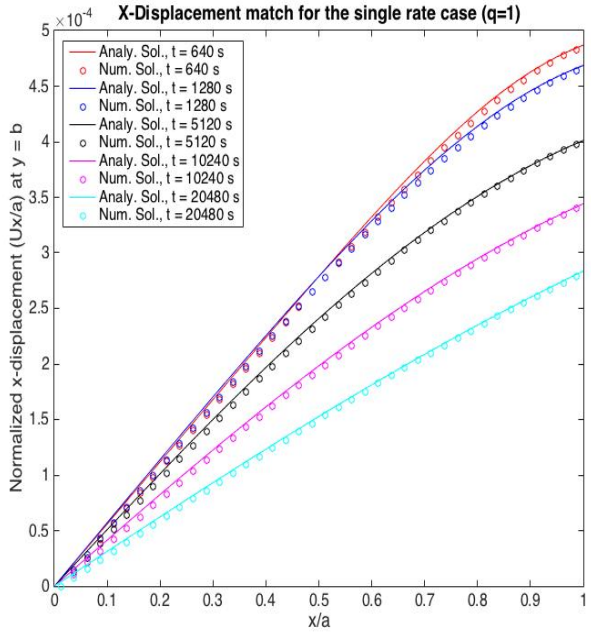

(a) Analytical vs Numerical Results ($q = 1$)

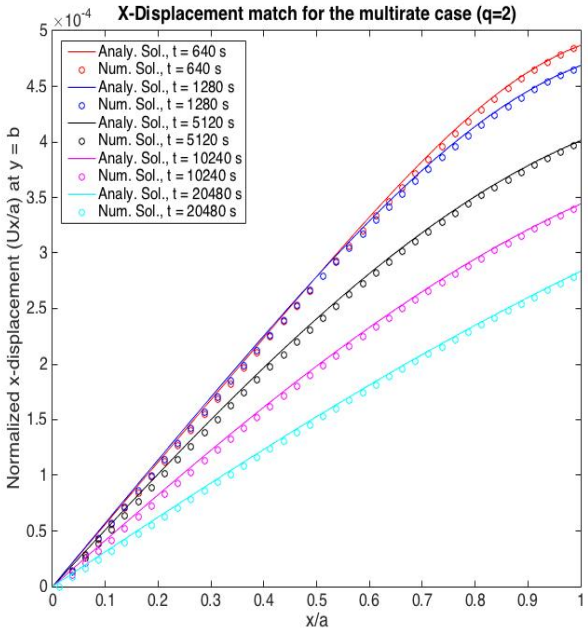

(b) Analytical vs Numerical Results ($q = 2$)

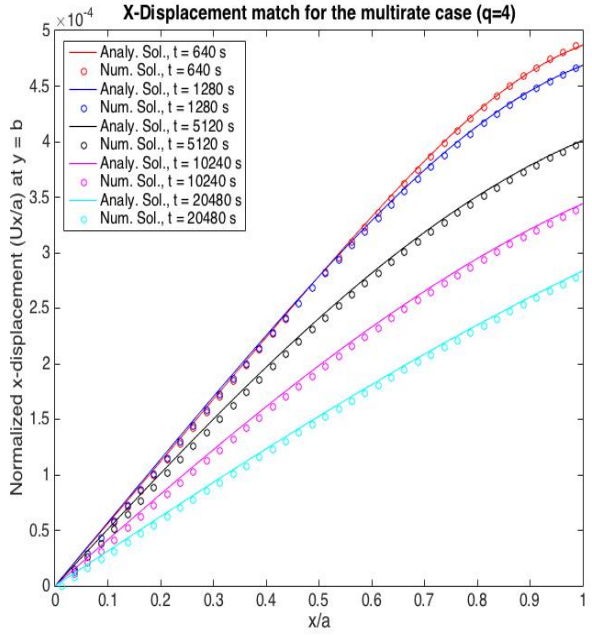

(c) Analytical vs Numerical Results ($q = 4$)

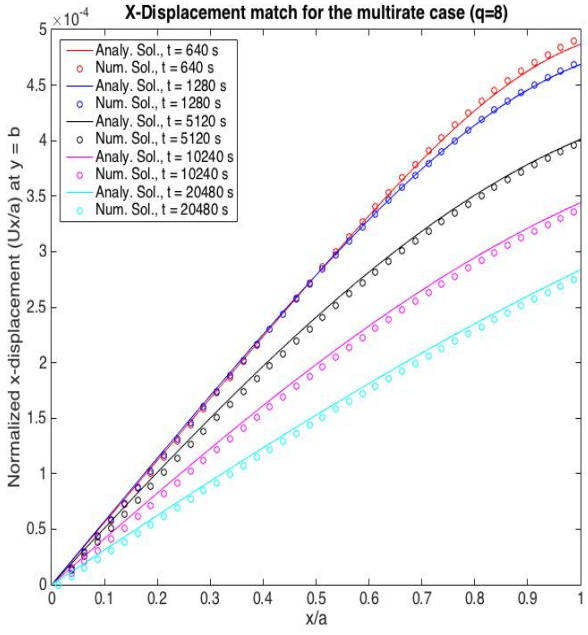

(d) Analytical vs Numerical Results ($q = 8$)

Figure 2.6: Accuracy of our Multirate Scheme on Mandel's Problem Displacement Solution

	$q=1$	$q=2$	$q=4$	$q=8$
$\|p_h - p(t)\|^2_{\ell_2}$	5.9838e-05	6.1103e-05	2.3748e-04	9.2265e-04
$\|u_{x_h} - u_x(t)\|^2_{\ell_2}$	3.1261e-11	5.1934e-13	1.6641e-11	1.4160e-10
Reduction in CPU runtime	-	26.27%	48.57%	65.51%
Reduction in mech. linear iterations	-	42.71%	69.50%	85.20%

Table 2.3: Accuracy versus efficiency for different values of q (the number of flow finer time steps within one coarser mechanics time step) at time $t = 20480$ seconds.

2.5.2 Single-phase Flow Coupled Problems

2.5.2.1 Numerical Model

The multirate iterative coupling algorithm has been implemented in the single-phase and two-phase flow models coupled with linear elasticity in IPARS. For the single-phase model, the existing implicit MFMFE formulation (details about its formulation can be found in [82]) has been modified to match the analyzed theoretical model. For a slightly compressible single phase flow model, we have:

Mass Conservation:

$$\frac{\partial(\varphi^* \rho_f)}{\partial t} + \nabla \cdot \boldsymbol{z} = q_s \qquad \text{in } \Omega \times [0,T] \tag{2.5.132}$$

Darcy Law:

$$\boldsymbol{z} = -\boldsymbol{K}\frac{\rho_f}{\mu_f}(\nabla p - \rho_f g \nabla \eta) \qquad \text{in } \Omega \times [0,T] \tag{2.5.133}$$

Constitutive Equations:

$$\varphi^* = \varphi_0 + \alpha \nabla \cdot \boldsymbol{u} + \frac{1}{M}(p - p_r) \tag{2.5.134}$$

$$\rho_f = \rho_{f,r} e^{(c_f(p-p_r))} \tag{2.5.135}$$

Boundary and Initial Conditions:

$$p = p^D \qquad \text{on } \Gamma_D \times [0,T] \tag{2.5.136}$$

$$\boldsymbol{z} \cdot \boldsymbol{n} = z^N \qquad \text{on } \Gamma_N \times [0,T] \tag{2.5.137}$$

$$p = p_0 \text{ at } t = 0 \qquad \text{in } \Omega \tag{2.5.138}$$

where $\boldsymbol{n}$ is the outward unit normal vector on $\partial\Omega, \Gamma_D \cup \Gamma_N = \partial\Omega$, φ^* is the reservoir porosity (in coupled poromechanics models [86]), ρ_f is the fluid density, μ_f is the fluid viscosity, c_f is the fluid compressibility, g is the gravitational constant, η is the distance in the vertical direction (assumed to be constant in time), $\rho_{f,r} > 0$ is a constant reference density (relative to the reference pressure p_r), φ_0 is the initial porosity, q_s is a mass source or sink term taking into account injection into or out of the reservoir.

We note that in IPARS, the single-phase MFMFE flow model is nonlinear. In contrast, our theoretical model is a simplified, and linearized single-phase flow model. Therefore, in order to better match our theoretical formulation, we carry out the following modifications. Consider the accumulation term in (2.5.132), and expand it as:

$$\begin{aligned}\frac{\partial(\varphi^*\rho_f)}{\partial t} &= \varphi^*\frac{\partial\rho_f}{\partial t} + \rho_f\frac{\partial\varphi^*}{\partial t} \\ &= \varphi^*\frac{\partial\rho_f}{\partial t} + \alpha\rho_f\frac{\partial(\nabla\cdot\boldsymbol{u})}{\partial t} + \frac{\rho_f}{M}\frac{\partial p}{\partial t}\end{aligned} \tag{2.5.139}$$

Together by (2.5.134) and the product rule. The mass balance equation (2.5.132) can then be written as:

$$\varphi^*\frac{\partial\rho_f}{\partial t} + \alpha\rho_f\frac{\partial(\nabla\cdot\boldsymbol{u})}{\partial t} + \frac{\rho_f}{M}\frac{\partial p}{\partial t} + \nabla\cdot\boldsymbol{z} = q_s \tag{2.5.140}$$

Recall that "n" denotes the coupling iteration index, and "k" denotes "coarser mechanics" time step iteration index. At this stage, we introduce the fixed-stress regularization term to the right and left hand sides of (2.5.140) as follows:

$$\begin{aligned}(\varphi^*)^{n+1}\frac{\partial\rho_f^{n+1}}{\partial t} + \Big(\frac{\rho_f^{n+1}}{M} + \frac{\alpha^2}{2\lambda}\Big)\frac{\partial p^{n+1}}{\partial t} + \nabla\cdot\boldsymbol{z}^{n+1} \\ = -\alpha\rho_f^{n+1}\frac{\partial(\nabla\cdot\boldsymbol{u}^n)}{\partial t} + \frac{\alpha^2}{2\lambda}\frac{\partial p^n}{\partial t} + q_s^{n+1}\end{aligned} \tag{2.5.141}$$

Equations (2.5.133), and (2.5.141) give the single-phase flow model in the context of the fixed-stress split coupling algorithm that we will be testing against our theoretical model.

2.5.2.2 Fully Discrete Formulation

A fully discrete formulation of the flow equations, based on the multipoint flux mixed finite element (MFMFE) space discretization, and backward Euler temporal discretization

is described in this section. A brief review of the finite element spaces and quadrature rules used in the MFMFE scheme can be found in Appendix A.

Single-phase MFMFE Coupled Model

For simplicity, we assume zero Dirichlet and no-flow boundary conditions. For a time step $t = t_{k+1}$, and for an iterative coupling iteration "$n+1$" between two consecutive time steps (t_k and t_{k+1}), the fully discrete formulation reads: Find $p_h^{n+1,k+1} \in Q_h$, and $\boldsymbol{z}_h^{n+1,k+1} \in \boldsymbol{Z}_h$ such that,

Flux Equation:

$$\forall \boldsymbol{q}_h \in \boldsymbol{Z}_h\,, \left(\frac{\mu_f}{\rho_f^{n+1,k+1}}\boldsymbol{K}^{-1}\boldsymbol{z}_h^{n+1,k+1}, \boldsymbol{q}_h\right)_{Q,E} - \left(p_h^{n+1,k+1}, \nabla\cdot\boldsymbol{q}_h\right)_E = \left(\rho_f^{n+1,k+1} g\nabla\eta, \boldsymbol{q}_h\right)_E \tag{2.5.142}$$

Mass Balance Equation:

$$\begin{aligned}\forall \theta_h \in Q_h\,, &\left((\varphi^*)^{n+1,k+1}\Big(\frac{\rho_f^{n+1,k+1}-\rho_f^k}{\Delta t}\Big), \theta_h\right)_E + \left(\Big(\frac{\rho_f^{n+1,k+1}}{M}+\frac{\alpha^2}{2\lambda}\Big)\Big(\frac{p_h^{n+1,k+1}-p_h^k}{\Delta t}\Big), \theta_h\right)_E \\ &+ \left(\nabla\cdot\boldsymbol{z}_h^{n+1,k+1}, \theta_h\right)_E = -\left(\alpha\rho_f^{n+1,k+1}\Big(\frac{\nabla\cdot\boldsymbol{u}_h^{n,k+1}-\nabla\cdot\boldsymbol{u}_h^k}{q\Delta t}\Big), \theta_h\right)_E \\ &\left(\frac{\alpha^2}{2\lambda}\Big(\frac{p_h^{n,k+1}-p_h^k}{\Delta t}\Big), \theta_h\right)_E + \left(q_s^{n+1,k+1}, \theta_h\right)_E \end{aligned} \tag{2.5.143}$$

We note that the above formulation is nonlinear. Its linearization is given in the next paragraph.

Linearization

For the linearized formulation, we introduce a third index "l" for Newton iterations. For simplicity, we "Newton" iteration lag the porosity and density coefficients in the first two terms of the mass balance equation. The linearized formulation in terms of the unknowns δp_h, and $\delta\boldsymbol{z}_h$ is as follows:

Flux Equation:

$$\left(\frac{\mu_f}{\rho_f^{l,n+1,k+1}}\boldsymbol{K}^{-1}\delta\boldsymbol{z}_h^{l,n+1,k+1},\boldsymbol{q}_h\right)_{Q,E}-\left(\delta p_h^{l,n+1,k+1},\nabla\cdot\boldsymbol{q}_h\right)_E=$$
$$-\left(\frac{\mu_f}{\rho_f^{l,n+1,k+1}}\boldsymbol{K}^{-1}\boldsymbol{z}_h^{l,n+1,k+1},\boldsymbol{q}_h\right)_{Q,E}-\left(\delta p_h^{l,n+1,k+1},\nabla\cdot\boldsymbol{q}_h\right)_E+\left(\rho_f^{n+1,k+1}g\nabla\eta,\boldsymbol{q}_h\right)_E \tag{2.5.144}$$

Mass Balance Equation:

$$\left((\varphi^*)^{l,n+1,k+1}c_f\rho_f^{l,n+1,k+1}\delta p_h^{l,n+1,k+1},\theta_h\right)_E+\left(\left(\frac{\rho_f^{l,n+1,k+1}}{M}+\frac{\alpha^2}{2\lambda}\right)\delta p_h^{l,n+1,k+1},\theta_h\right)_E$$
$$+\left(\Delta t\nabla\cdot\delta\boldsymbol{z}_h^{l,n+1,k+1},\theta_h\right)_E=-\left((\varphi^*)^{l,n+1,k+1}(\rho_f^{l,n+1,k+1}-\rho_f^k),\theta_h\right)_E$$
$$-\left(\left(\frac{\rho_f^{l,n+1,k+1}}{M}+\frac{\alpha^2}{2\lambda}\right)(p_h^{l,n+1,k+1}-p_h^k),\theta_h\right)_E-\left(\Delta t\nabla\cdot\boldsymbol{z}_h^{l,n+1,k+1},\theta_h\right)_E$$
$$-\left(\alpha\frac{\rho_f^{l,n+1,k+1}}{q}(\nabla\cdot\boldsymbol{u}_h^{n,k+1}-\nabla\cdot\boldsymbol{u}_h^k),\theta_h\right)_E+\left(\frac{\alpha^2}{2\lambda}(p_h^{n,k+1}-p_h^k),\theta_h\right)_E+\left(\Delta tq_s^{l,n+1,k+1},\theta_h\right)_E \tag{2.5.145}$$

This simplifies to

$$\left(\left((\varphi^*)^{l,n+1,k+1}c_f\rho_f^{l,n+1,k+1}+\frac{\rho_f^{l,n+1,k+1}}{M}+\frac{\alpha^2}{2\lambda}\right)\delta p_h^{l,n+1,k+1},\theta_h\right)_E$$
$$+\left(\Delta t\nabla\cdot\delta\boldsymbol{z}_h^{l,n+1,k+1},\theta_h\right)_E=-\left((\varphi^*)^{l,n+1,k+1}(\rho_f^{l,n+1,k+1}-\rho_f^k),\theta_h\right)_E$$
$$-\left(\frac{\rho_f^{l,n+1,k+1}}{M}(p_h^{l,n+1,k+1}-p_h^k),\theta_h\right)_E-\left(\Delta t\nabla\cdot\boldsymbol{z}_h^{l,n+1,k+1},\theta_h\right)_E$$
$$-\left(\left(\frac{\alpha\rho_f^{l,n+1,k+1}}{q}\right)(\nabla\cdot\boldsymbol{u}_h^{n,k+1}-\nabla\cdot\boldsymbol{u}_h^k),\theta_h\right)_E$$
$$-\left(\frac{\alpha^2}{2\lambda}(p_h^{l,n+1,k+1}-p_h^{n,k+1}),\theta_h\right)_E+\left(\Delta tq_s^{l,n+1,k+1},\theta_h\right)_E \tag{2.5.146}$$

2.5.2.3 Frio Field Model Results

This test problem consists of a realistic field-scale reservoir model, located near Dayton, Texas, at South Liberty oil field on the Gulf Coast. The field contains several geometrically challenging thin curved faults, and is curved in the depth direction [48]. In this work, we

try to consider the challenging geometry of the field along with its permeability distribution. Gravity effects are included in the model, and other input parameters are shown in Table 2.4. In addition, for the convergence stopping criterion, we set TOL = 1.E-10.

2.5.2.4 Results

Pressure profiles and displacement vector fields for the single rate scheme, and multirate schemes ($q = 4$ and 8) after 480 simulation days are shown in figures 2.7a and 2.7b respectively. For all three cases ($q = 1, 4$, and 8), results are almost identical. Accumulated CPU runtimes for the three cases are shown in figure 2.8a. Multirate schemes ($q = 4$ and 8) result in 20.43%, and 34.91% reductions in CPU run times respectively. Reductions in CPU run times come as a direct consequence of the huge reductions in the accumulative number of mechanics linear iterations for the whole simulation run. For $q = 4$, the total number of mechanics linear iterations is reduced by 58.88%, and for $q = 8$, mechanics linear iterations are reduced by 79.44%. The overhead introduced by the multirate coupling scheme over the the single rate scheme is illustrated in figures 2.8c and 2.8d. As shown in figure 2.8c, multirate schemes ($q = 4$), and ($q = 8$) result in 92.26%, and 93.40% increase in the total number of flow linear iterations for the whole simulation run. This overhead is attributed to the observed increase in the number of flow-mechanics coupling iterations for multirate schemes over the single rate scheme, as shown in figure 2.8d. It should be noted that, with respect to running times, the decrease in the number of mechanics linear iterations outperform the overhead introduced by the increase in the total number of flow linear iterations. It is this particular feature that allows the multirate scheme to outperform the single rate scheme with respect to CPU running times.

Wells:	3 production wells, 6 injection well
Injection well (1):	Pressure specified, 4000.0 psi
Injection well (2):	Pressure specified, 3300.0 psi
Injection well (3):	Pressure specified, 4000.0 psi
Injection well (4):	Pressure specified, 4400.0 psi
Injection well (5):	Pressure specified, 3700.0 psi
Injection well (6):	Pressure specified, 4400.0 psi
Production well (1):	Pressure specified, 2000.0 psi
Production well (2):	Pressure specified, 2000.0 psi
Production well (3):	Pressure specified, 2000.0 psi
Total Simulation time:	480.0 days
Finer (Unit) time step:	1.0 days
Number of grids:	1428 grids ($34 \times 14 \times 3$)
Permeabilities: k_{xx}, k_{yy}, k_{zz}	highly varying, range: (5.27E-10, 3.10E+3) md
Initial porosity, φ_0	0.2
Fluid viscosity, μ_f	2.0 cp
Initial pressure, p_0	400.0 psi
Fluid compressibility c_f:	1.E-4 (1/psi)
Rock compressibility:	1.E-6 (1/psi)
Rock density:	165.44 lb_m/ft^3
Initial fluid density, ρ_f:	56.0 lb_m/ft^3
Young's Modulus (E)	1.2E6 psi
Possion Ratio, ν	0.35
Biot's constant, α	0.9
Biot Modulus, M	1.0E8 psi
$\lambda = \frac{E\nu}{(1+\nu)(1-2\nu)}$	1.037E6 psi
L (introduced fixed stress parameter)	$\frac{\alpha^2}{2\lambda}$ (1/psi)
Flow Boundary Conditions:	no flow boundary condition on all 6 boundaries
Mechanics B.C.:	
"X+" boundary (EBCXX1())	$\sigma_{xx} = \sigma \cdot n_x = 10,000 psi$, (overburden pressure)
"X-" - boundary (EBCXXN1())	$\boldsymbol{u} = 0$, zero displacement
"Y+" - boundary (EBCYY1())	$\boldsymbol{u} = 0$, zero displacement
"Y-" - boundary (EBCYYN1())	$\sigma_{yy} = \sigma \cdot n_y = 2000 psi$
"Z+" - boundary (EBCZZ1())	$\boldsymbol{u} = 0$, zero displacement
"Z-" - boundary (EBCZZN1())	$\sigma_{zz} = \sigma \cdot n_z = 1000 psi$

Table 2.4: Input Parameters for the Frio Field Model

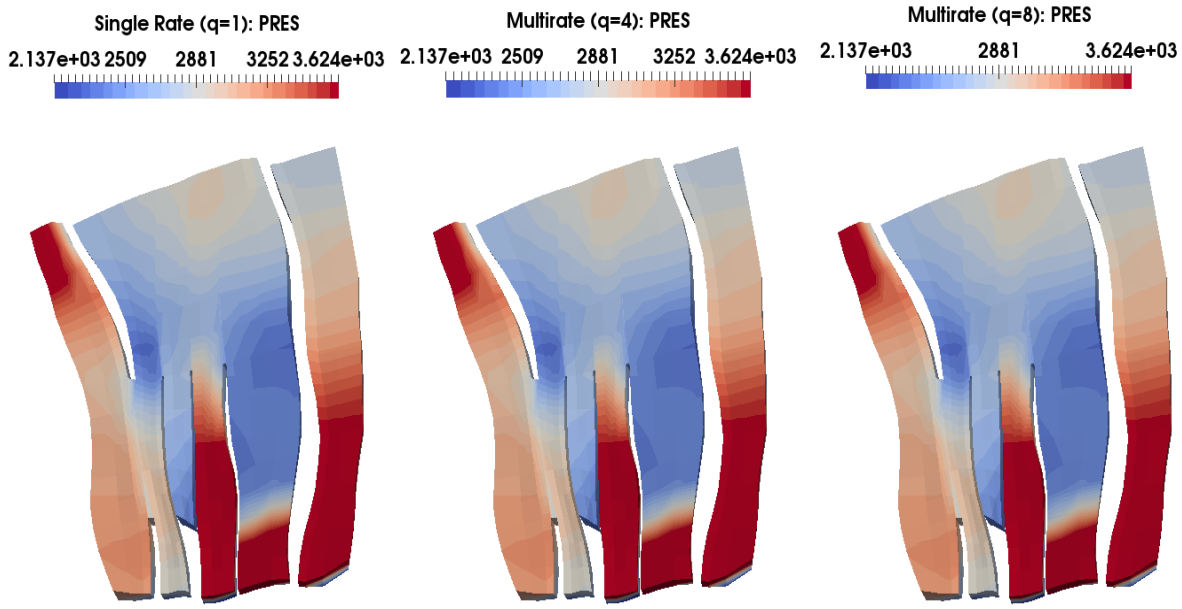

(a) Pressure Profiles after 480.0 simulation days (psi)

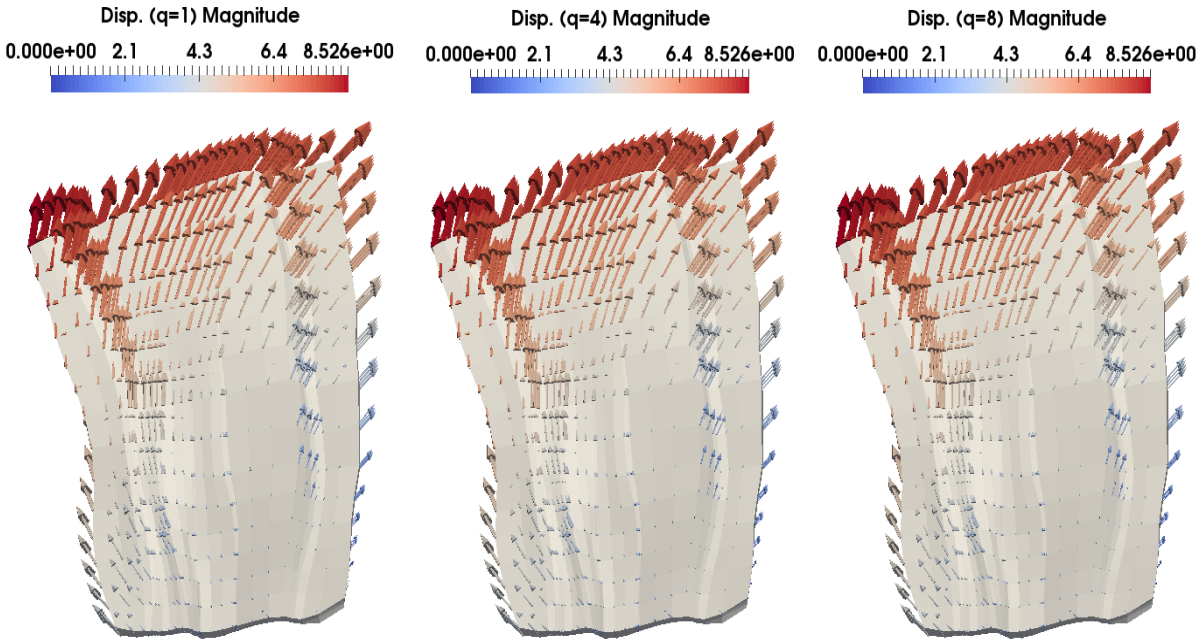

(b) Displacement Field after 480.0 simulation days (ft)

Figure 2.7: Frio Field Model Pressure and Displacement Fields at the End of the Simulation

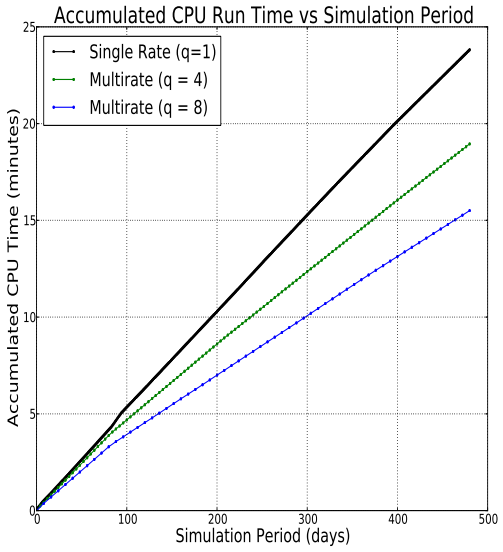

(a) CPU Run Time vs Simulation Days

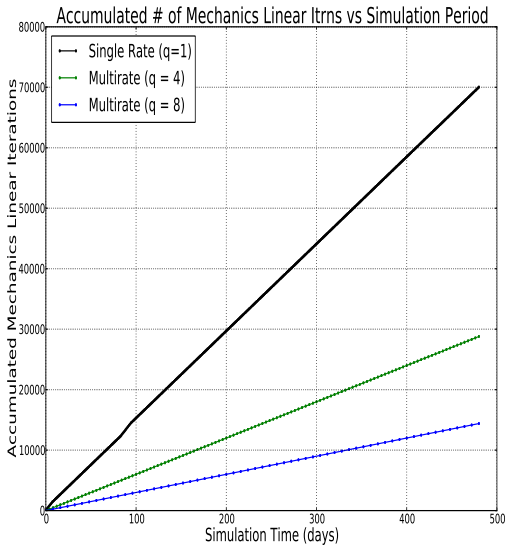

(b) Total Number of Mechanics Linear Iterations vs Simulation Days

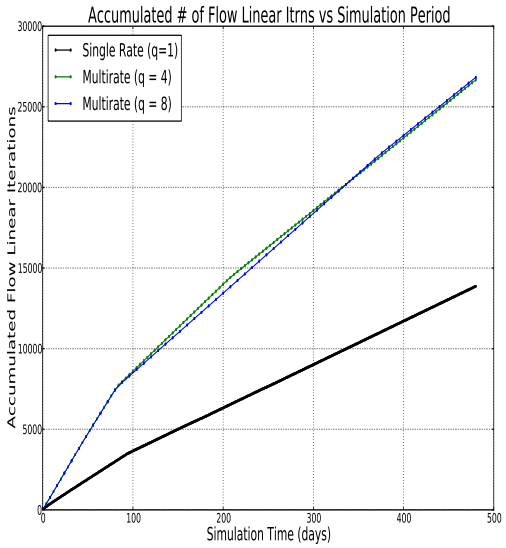

(c) Total Number of Flow Linear Iterations vs Simulation Days

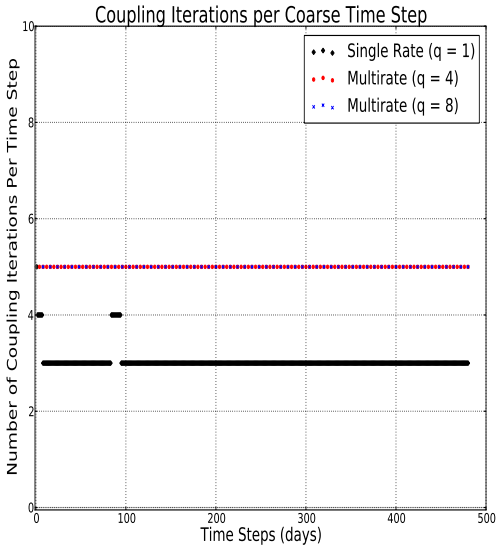

(d) Number of Iterative Coupling Iterations Per Coarser Time Step

Figure 2.8: Frio Field Model Simulation Results: CPU time savings of two multirate schemes ($q = 4$ and 8) over the single rate scheme ($q = 1$) are shown in the top left plot. The top right plot illustrates the huge reduction in the number of mechanics linear iterations for the corresponding multirate schemes over the single rate scheme. The bottom left plot illustrates the increase in the number of flow linear iterations for the multirate schemes. This is a direct consequence of the increase in the number of flow-mechanics coupling iterations observed for multirate schemes over the single rate scheme as shown in the bottom right plot.

Theoretical Vs. Numerical Contraction Coefficients

In this section, we compare theoretical contraction estimates against numerically computed values. Based on the parameters given in Table 2.4, the theoretical contraction estimate, as given in Theorem 2.3.4, is computed as: $\left(\frac{M\alpha^2}{2\lambda+2M\lambda c_f\varphi_0+M\alpha^2}\right)^2 = 0.0003665$. By computing the ratio of the quantity of contraction between two consecutive iterative coupling iterations, numerical contraction estimates can be obtained. Numerically, this is computed as follows (for $\chi^2 = L^2, \chi^2 = \frac{\alpha^4}{4\lambda^2}$, and $L = \frac{\alpha^2}{2\lambda}$):

$$
\begin{aligned}
\sum_{m=1}^{q}\|\delta\sigma_v^{n,m+k}\|_\Omega^2 &= \sum_{m=1}^{q}\|\frac{L}{\chi}(\delta p_h^{n,m+k}-\delta p_h^{n,m-1+k})-\frac{\alpha}{\chi q}\nabla\cdot\delta\boldsymbol{u}_h^{n,k+q}\|^2\\
&=\sum_{m=1}^{q}\int_\Omega\left((\delta p_h^{n,m+k}-\delta p_h^{n,m-1+k})-\frac{\alpha}{q\chi}\nabla\cdot\delta\boldsymbol{u}_h^{n,k+q}\right)^2\\
&=\frac{\alpha^2}{q^2\chi^2}\sum_{m=1}^{q}\int_\Omega\left(\nabla\cdot\delta\boldsymbol{u}_h^{n,k+q}\right)^2-\frac{2\alpha}{q\chi}\sum_{m=1}^{q}\int_\Omega\left(\nabla\cdot\delta\boldsymbol{u}_h^{n,k+q}\right)\left(\delta p_h^{n,m+k}-\delta p_h^{n,m-1+k}\right)\\
&\qquad+\sum_{m=1}^{q}\int_\Omega\left(\delta p_h^{n,m+k}-\delta p_h^{n,m-1+k}\right)^2\\
&=\frac{4\lambda^2}{q\alpha^2}\sum_{i,j,k}\left(\nabla\cdot\delta\boldsymbol{u}_h^{n,k+q}\right)^2|_{i,j,k}V(i,j,k)\\
&\qquad-\frac{4\lambda}{q\alpha}\sum_{m=1}^{q}\sum_{i,j,k}\left(\nabla\cdot\delta\boldsymbol{u}_h^{n,k+q}\right)|_{i,j,k}\left(\delta p_h^{n,m+k}-\delta p_h^{n,m-1+k}\right)|_{i,j,k}V(i,j,k)\\
&\qquad+\sum_{m=1}^{q}\sum_{i,j,k}\left(\delta p_h^{n,m+k}-\delta p_h^{n,m-1+k}\right)^2|_{i,j,k}V(i,j,k)
\end{aligned}
$$

where $V(i,j,k)$ is the bulk volume of the (i,j,k) grid block. Following this approach, the ratio of $\left(\left\|\delta\sigma_v^{n+1,k}\right\|^2/\left\|\delta\sigma_v^{n,k}\right\|^2\right)$ for the single rate scheme ($q=1$) is shown in figure 2.9. The maximum value, across all iterative coupling iterations, for each time step is plotted. Results illustrate that the theoretical estimate acts as an upper bound for numerically computed estimates. In addition, numerical contraction estimates are larger for earlier time steps. This is expected as the coupled problem has not reached the steady-state yet.

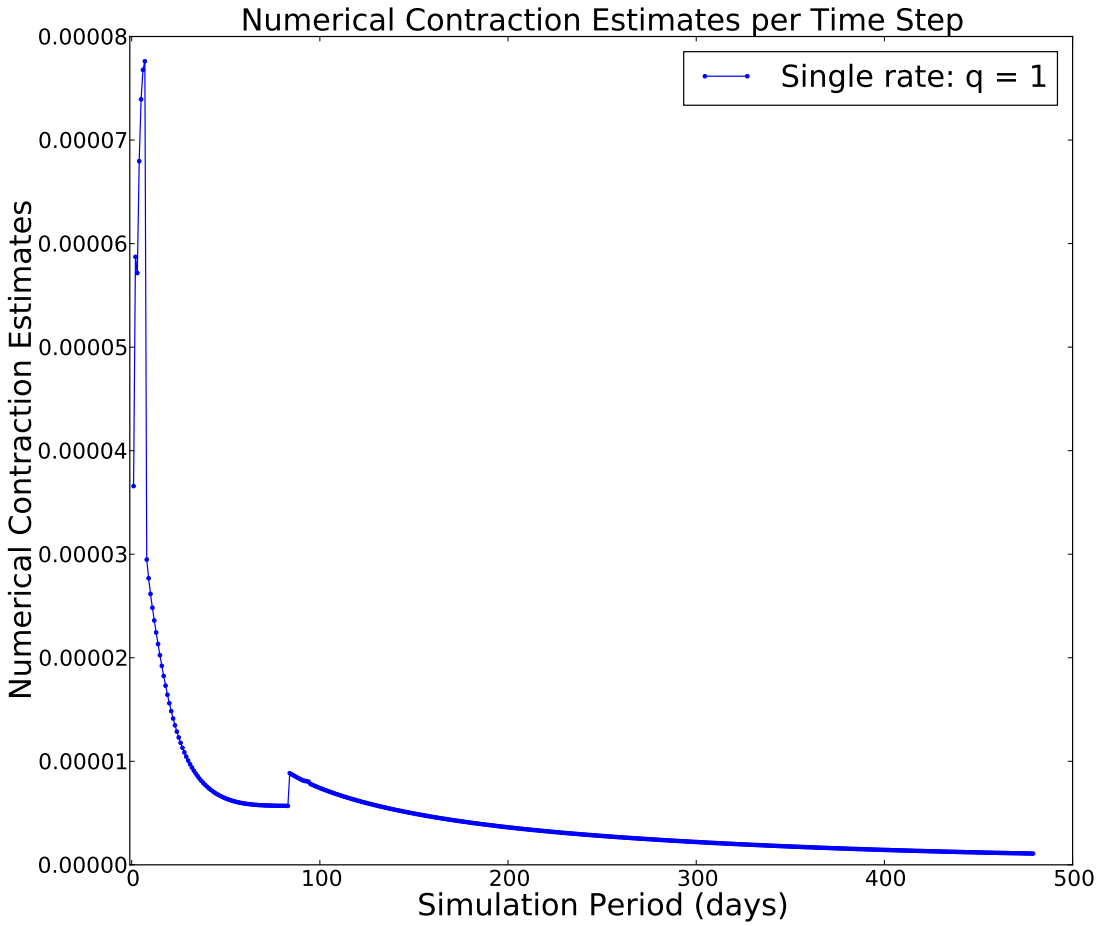

Figure 2.9: Numerical Contraction Estimates per Time Step. The maximum contraction estimate across flow-mechanics coupling iterations is considered for each time step

Effect of Lame Parameters on Contraction Coefficients

Next, we validate the theoretical results obtained in remark 2.3.3. We consider the analysis of the single rate case for simplicity, as the analysis of the multirate case follows in a similar way. The improved contraction estimate for the single rate case, as given in remark 2.3.3 for $q = 1$, is given by $\left\|\delta\sigma_v^{n+1,k}\right\|^2 \leq \left(\frac{C}{C+1}\right)\left(\frac{M\alpha^2}{2\lambda+2M\lambda c_f\varphi_0+M\alpha^2}\right)^2 \left\|\delta\sigma_v^{n,k}\right\|^2$ for a constant $C > 0$, which is difficult to compute in practice. However, we anticipate that it scales monotonically with the values of Lamé's first parameter λ, and Young's modulus E. Therefore, theoretically, we expect the value of the damping factor $\left(\frac{C}{C+1}\right)$ to approach one, as the

value of Young's modulus increases, which means that our derived contraction estimate is sharper for larger Young's modulus values. This behavior is validated numerically for the frio field model in figure 2.10.

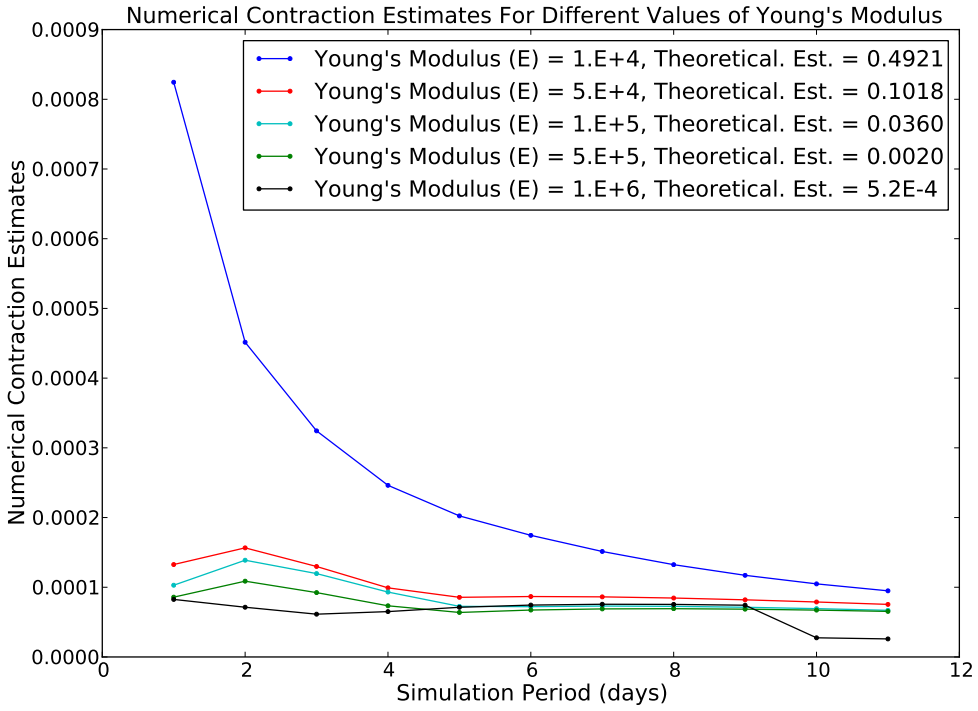

Figure 2.10: Numerical contraction estimates for different values of Young's modulus (E, psi) for the single rate scheme for the first 12 simulation days. As the value of Young's modulus increases, the gap between theoretically predicted contraction estimates and numerically observed values shrinks, validating our theoretical derivations shown in remarks 2.3.3 and 2.3.4.

2.5.3 Two-phase Flow Coupled Problems

2.5.3.1 Two-phase IMPES Numerical Model

The multirate iterative coupling algorithm has been implemented in the two-phase IMPES (implicit pressure explicit saturation) flow model coupled with linear elasticity in IPARS. For completeness, we describe the formulation of the IMPES model, as implemented in IPARS. More details can be found in [86]. For a slightly compressible two phase flow model, we have:

Mass Conservation:

$$\frac{\partial(\rho_j S_j \varphi^*)}{\partial t} + \nabla \cdot (\rho_j \boldsymbol{z}_j) = q_j \qquad \text{in } \Omega \times [0,T] \tag{2.5.147}$$

Darcy Law:

$$\boldsymbol{z}_j = -\boldsymbol{K}\frac{k_{rj}}{\mu_j}(\nabla p_j - \rho_j g \nabla \eta) \qquad \text{in } \Omega \times [0,T] \tag{2.5.148}$$

Constitutive Equations:

$$\varphi^* = \varphi_0 + \alpha \nabla \cdot \boldsymbol{u} + \frac{1}{M}(p - p_r) \tag{2.5.149}$$

$$\rho_j = \rho_{j,r} e^{(c_j(p_j - p_0))} \tag{2.5.150}$$

$$p_o = p_w + p_{cow}(S_w) \tag{2.5.151}$$

$$S_o + S_w = 1 \tag{2.5.152}$$

Boundary and Initial Conditions:

$$p_w = p^D \qquad \text{on } \Gamma_D \times [0,T] \tag{2.5.153}$$

$$S_w = S^D \qquad \text{on } \Gamma_D \times [0,T] \tag{2.5.154}$$

$$\boldsymbol{z}_j \cdot \boldsymbol{n} = 0 \qquad \text{on } \Gamma_N \times [0,T] \tag{2.5.155}$$

$$p_w = p_w^0 \text{ at } t = 0 \qquad \text{in } \Omega \tag{2.5.156}$$

$$S_w = S_w^0 \text{ at } t = 0 \qquad \text{in } \Omega \tag{2.5.157}$$

where the subscript index (j) refers to the oil or water phases ($j = w$ for water phase, and $j = o$ for oil phase), $\boldsymbol{n}$ is the outward unit normal vector on $\partial\Omega, \Gamma_D \cup \Gamma_N = \partial\Omega$, φ^*

is the reservoir porosity (in coupled poromechanics models [86]), ρ_j, μ_j, k_rj and c_j are the density, viscosity, relative permeability, and compressibility of phase (j) respectively. Moreover, p_{cow} is the capillary pressure, which is a function of water saturation (S_w), g is the gravitational constant, η is the distance in the vertical direction (assumed to be constant in time), $\rho_{j,r} > 0$ is reference density (relative to the reference pressure p_j) for phase (j), φ_0 is the initial porosity, q_j is a mass source or sink term taking into account injection into or out of the reservoir. In this model, the water phase saturation S_w, and the water pressure p_w are chosen as the primary unknowns for the two-phase flow model.

Dividing equation (2.5.147) by the reference density of each phase, and summing up the mass balance equations for both the water and oil phases, we obtain:

$$\frac{\partial \varphi^*(\bar{\rho}_w S_w + \bar{\rho}_o S_o)}{\partial t} + \nabla \cdot (\bar{\rho}_w \boldsymbol{z}_w + \bar{\rho}_o \boldsymbol{z}_o) = \bar{q}_w + \bar{q}_o \tag{2.5.158}$$

where $\bar{\rho}_w = \frac{\rho_w}{\rho_{w,r}}$, $\bar{\rho}_o = \frac{\rho_o}{\rho_{o,r}}$, $\bar{q}_w = \frac{q_w}{\rho_{w,r}}$, and $\bar{q}_o = \frac{q_o}{\rho_{o,r}}$. Now, define the total velocity $\boldsymbol{z}_t$ as:

$$\boldsymbol{z}_t = \bar{\rho}_w \boldsymbol{z}_w + \bar{\rho}_o \boldsymbol{z}_o. \tag{2.5.159}$$

Substituting Darcy's law (2.5.148) into (2.5.159), and adding and subtracting the term $(\boldsymbol{K}\bar{\rho}_o \frac{k_{ro}}{\mu_o}\rho_w g \nabla)$ to the right hand side, we have:

$$\begin{aligned}
\boldsymbol{z}_t &= -\boldsymbol{K}\frac{\bar{\rho}_w k_{rw}}{\mu_w}(\nabla p_w - \rho_w g \nabla \eta) - \boldsymbol{K}\frac{\bar{\rho}_o k_{ro}}{\mu_o}(\nabla p_w + \nabla p_{cow} - \rho_o g \nabla \eta) \\
&= -\boldsymbol{K}(\frac{\bar{\rho}_w k_{rw}}{\mu_w} + \frac{\bar{\rho}_o k_{ro}}{\mu_o})(\nabla p_w - \rho_w g \nabla \eta) - \boldsymbol{K}\frac{\bar{\rho}_o k_{ro}}{\mu_o}(\nabla p_{cow} - (\rho_o - \rho_w) g \nabla \eta)
\end{aligned} \tag{2.5.160}$$

Define the normalized total mobility λ_t and the normalized oil mobility λ_o as:

$$\lambda_t = \frac{\bar{\rho}_w k_{rw}}{\mu_w} + \frac{\bar{\rho}_o k_{ro}}{\mu_o}, \qquad \lambda_o = \frac{\bar{\rho}_o k_{ro}}{\mu_o}$$

Then, (2.5.160) can be written as:

$$\boldsymbol{z}_t = -\boldsymbol{K}\lambda_t(\nabla p_w - \rho_w g \nabla \eta) - \boldsymbol{K}\lambda_o(\nabla p_{cow} - (\rho_o - \rho_w) g \nabla \eta) \tag{2.5.161}$$

2.5.3.2 Fully Discrete MFMFE Coupled Model

For a time step $t = t_{k+1}$, and for an iterative coupling iteration "$n + 1$" between two consecutive time steps (t_k and t_{k+1}), the fully discrete formulation reads (remember that

our primary unknowns are water pressure, and saturation):
Find $p_w^{n+1,k+1} \in Q_h$, and $\boldsymbol{z}_w^{n+1,k+1} \in \boldsymbol{Z}_h$ such that (for simplicity, we will drop the subscript (h) for discrete quantities),

Flux Equation:

$$\begin{aligned}\forall \boldsymbol{q}_h \in \boldsymbol{Z}_h\,, \left(\frac{\boldsymbol{K}^{-1}}{\lambda_t^{n+1,k+1}}\boldsymbol{z}_t^{n+1,k+1}, \boldsymbol{q}_h\right)_{Q,E} - \left(p_w^{n+1,k+1}, \nabla\cdot\boldsymbol{q}_h\right)_E - \\ \left(\left(\frac{\lambda_o}{\lambda_t}\right)^{n+1,k+1} p_{cow}^{n+1,k+1}, \nabla\cdot\boldsymbol{q}_h\right)_E = \left(\rho_w^{n+1,k+1} g\nabla\,\eta, \boldsymbol{q}_h\right)_E \\ + \left(\left(\frac{\lambda_o}{\lambda_t}\right)^{n+1,k+1} (\rho_o^{n+1,k+1} - \rho_w^{n+1,k+1}) g\nabla\,\eta, \boldsymbol{q}_h\right)_E \\ - \langle p_w^{n+1,k+1}, \boldsymbol{q}_h\cdot\boldsymbol{n}\rangle_E - \langle\left(\frac{\lambda_o}{\lambda_t}\right)^{n+1,k+1} p_{cow}^{n+1,k+1}, \boldsymbol{q}_h\cdot\boldsymbol{n}\rangle_E \end{aligned} \tag{2.5.162}$$

Mass Balance Equation:

$$\begin{aligned}&\forall\theta_h \in Q_h\,, \\ &\left(\frac{\left(\varphi^*\bar{\rho}_w S_w + \varphi^*\bar{\rho}_o(1-S_w)\right)^{n+1,k+1} - \left(\varphi^*\bar{\rho}_w S_w + \varphi^*\bar{\rho}_o(1-S_w)\right)^{k}}{\Delta t}, \theta_h\right)_E \\ &+ \left(\nabla\cdot\boldsymbol{z}_t^{n+1,k+1}, \theta_h\right)_E = \left(\bar{q}_w^{n+1,k+1} + \bar{q}_o^{n+1,k+1}, \theta_h\right)_E \end{aligned} \tag{2.5.163}$$

We note that the above formulation is nonlinear. Its linearization is given in the next paragraph.

Linearization

For the linearized formulation, we introduce a third index "l" for Newton iterations. For simplicity, we "Newton" iteration lag mobility coefficients. The linearized formulation in terms of the unknowns δp_w, and $\delta\boldsymbol{z}_t$ is as follows:

Flux Equation:

$$\left(\frac{\boldsymbol{K}^{-1}}{\lambda_t^{l,n+1,k+1}}\delta\boldsymbol{z}_t^{l,n+1,k+1},\boldsymbol{q}_h\right)_{Q,E}-\left(\delta p_w^{l,n+1,k+1},\nabla\cdot\boldsymbol{q}_h\right)_E=$$
$$\left(\left(\frac{\lambda_o}{\lambda_t}\right)^{l,n+1,k+1}p_{cow}^{l,n+1,k+1},\nabla\cdot\boldsymbol{q}_h\right)_E-\left(\frac{\boldsymbol{K}^{-1}}{\lambda_t^{l,n+1,k+1}}\boldsymbol{z}_t^{l,n+1,k+1},\boldsymbol{q}_h\right)_{Q,E}$$
$$+\left(p_w^{l,n+1,k+1},\nabla\cdot\boldsymbol{q}_h\right)_E+\left(\rho_w^{l,n+1,k+1}g\nabla\,\eta,\boldsymbol{q}_h\right)_E$$
$$+\left(\left(\frac{\lambda_o}{\lambda_t}\right)^{l,n+1,k+1}(\rho_o^{l,n+1,k+1}-\rho_w^{l,n+1,k+1})g\nabla\,\eta,\boldsymbol{q}_h\right)_E$$
$$-\langle p_w^{l,n+1,k+1},\boldsymbol{q}_h\cdot\boldsymbol{n}\rangle_E-\langle\left(\frac{\lambda_o}{\lambda_t}\right)^{l,n+1,k+1}p_{cow}^{l,n+1,k+1},\boldsymbol{q}_h\cdot\boldsymbol{n}\rangle_E \tag{2.5.164}$$

Mass Balance Equation:

For the mass balance equation, we note that the fixed stress assumption implies that the volumetric mean total stress is kept constant during the flow solve within the iterative coupling iteration. Assuming that the prefix "δ" is used to indicate the difference between two consecutive Newton iterations, the fixed stress assumption implies that:

$$\sigma_v^{l+1,n+1,k+1}-\sigma_v^{l,n+1,k+1}=\delta\sigma_v^{l+1,n+1,k+1}=\lambda\nabla\cdot\delta\boldsymbol{u}^{l+1,n+1,k+1}-\alpha\delta p^{l+1,n+1,k+1}=0$$

This implies that $\nabla\cdot\delta u^{l+1,n+1,k+1}=\frac{\alpha}{\lambda}\delta p^{l+1,n+1,k+1}$, where $\delta\boldsymbol{u}^{l+1,n+1,k+1}=(u^{l+1,n+1,k+1}-\boldsymbol{u}^{l,n+1,k+1})$, and $\delta p^{l+1,n+1,k+1}=(p^{l+1,n+1,k+1}-p^{l+1,n+1,k+1})$. So, we have: $(\delta\varphi^*)^{l+1,n+1,k+1}=\alpha\nabla\cdot\delta\boldsymbol{u}^{l+1,n+1,k+1}+\frac{1}{M}\delta p^{l+1,n+1,k+1}$. Rearranging terms, we can write:

$$\begin{aligned}(\varphi^*)^{l+1,n+1,k+1}&=(\varphi^*)^{l,n+1,k+1}+(\delta\varphi^*)^{l+1,n+1,k+1}\\&=(\varphi^*)^{l,n+1,k+1}+\alpha\nabla\cdot\delta\boldsymbol{u}^{l+1,n+1,k+1}+\frac{1}{M}\delta p^{l+1,n+1,k+1}\\&=(\varphi^*)^{l,n+1,k+1}+\left(\frac{\alpha^2}{\lambda}+\frac{1}{M}\right)\delta p^{l+1,n+1,k+1}\\&=(\varphi^*)^{l,n+1,k+1}+\left(\frac{\alpha^2}{\lambda}+\frac{1}{M}\right)(p^{l+1,n+1,k+1}-p^{l,n+1,k+1})\end{aligned}$$

So, we can approximate the derivative of φ^* by pressure as $\frac{\partial\varphi^{*l+1,n+1,k+1}}{\partial pl+1,n+1,k+1}=\left(\frac{\alpha^2}{\lambda}+\frac{1}{M}\right)$. The last expression will be used in the derivation below. It should be noted that this is a different way of looking at the fixed-stress split iterative coupling method [86]. By the

product rule, the derivative of the first term in (2.5.163) w.r.t. pressure can be written as:

$$
\begin{aligned}
S_w^{l,n+1,k+1} & \frac{\partial\Big(\bar{\rho}_w^{l+1,n+1,k+1}(\varphi^*)^{l+1,n+1,k+1}\Big)}{\partial p^{l+1,n+1,k+1}} \\
&= S_w^{l,n+1,k+1}\left[\frac{\partial\bar{\rho}_w^{l+1,n+1,k+1}}{\partial p^{l+1,n+1,k+1}}\varphi^{*l,n+1,k+1} + \frac{\partial\varphi^{*l+1,n+1,k+1}}{\partial p^{l+1,n+1,k+1}}\bar{\rho}_w^{l,n+1,k+1}\right] \\
&= S_w^{l,n+1,k+1}\left[c_w\bar{\rho}_w^{l,n+1,k+1}(\varphi^*)^{l,n+1,k+1} + \bar{\rho}_w^{l,n+1,k+1}\Big(\frac{\alpha^2}{\lambda}+\frac{1}{M}\Big)\right] \\
&= S_w^{l,n+1,k+1}\bar{\rho}_w^{l,n+1,k+1}\left[c_w(\varphi^*)^{l,n+1,k+1} + \Big(\frac{\alpha^2}{\lambda}+\frac{1}{M}\Big)\right]
\end{aligned}
$$

A similar derivation for the derivative of the oil term can be obtained:

$$
\begin{aligned}
(1-S_w)^{l,n+1,k+1} & \frac{\partial\Big(\bar{\rho}_o^{l+1,n+1,k+1}(\varphi^*)^{l+1,n+1,k+1}\Big)}{\partial p^{l+1,n+1,k+1}} \\
& (1-S_w)^{l,n+1,k+1}\bar{\rho}_o^{l,n+1,k+1}\left[c_o\varphi^{*l,n+1,k+1} + \Big(\frac{\alpha^2}{\lambda}+\frac{1}{M}\Big)\right]
\end{aligned}
$$

The linearized mass balance equation reads:

$$
\begin{aligned}
&\left(S_w^{l,n+1,k+1}\bar{\rho}_w^{l,n+1,k+1}\Big(c_w(\varphi^*)^{l,n+1,k+1}+\frac{\alpha^2}{\lambda}+\frac{1}{M}\Big)\delta p^{l,n+1,k+1},\theta_h\right)_E + \\
&\left(\Big(1-S_w\Big)^{l,n+1,k+1}\bar{\rho}_o^{l,n+1,k+1}\Big(c_o(\varphi^*)^{l,n+1,k+1}+\frac{\alpha^2}{\lambda}+\frac{1}{M}\Big)\delta p^{l,n+1,k+1},\theta_h\right)_E \\
&+\left(\Delta t\nabla\cdot\boldsymbol{z}_t^{l,n+1,k+1},\theta_h\right)_E = \left((\varphi^*)^k\bar{\rho}_w^k S_w^k + (\varphi^*)^k\bar{\rho}_o^k(1-S_w)^k,\theta_h\right)_E \\
&-\left((\varphi^*)^{l,n+1,k+1}\bar{\rho}_w^{l,n+1,k+1}S_w^{l,n+1,k+1} + (\varphi^*)^{l,n+1,k+1}\bar{\rho}_o^{l,n+1,k+1}(1-S_w)^{l,n+1,k+1},\theta_h\right)_E \\
&\qquad -\left(\Delta t\nabla\cdot\boldsymbol{z}_t^{l,n+1,k+1},\theta_h\right)_E + \left(\bar{q}_w^{l,n+1,k+1}+\bar{q}_o^{l,n+1,k+1},\theta_h\right)_E
\end{aligned}
\tag{2.5.165}
$$

Once the value of $p^{l+1,n+1,k+1}$ is obtained, water phase saturation ($S_w^{l,n+1,k+1}$) is updated explicitly by (2.5.147) as follows:

$$
\begin{aligned}
S_w^{l+1,n+1,k+1} = & \frac{1}{\rho_w^{l+1,n+1,k+1}(\varphi^*)^{l+1,n+1,k+1}} \\
& \left[(\varphi^*)^k\bar{\rho}_w^k S_w^k - \Delta t\nabla\cdot(\rho_w^{l+1,n+1,k+1}\boldsymbol{z}_w^{l+1,n+1,k+1}) + \Delta t q_w^{l+1,n+1,k+1}\right]
\end{aligned}
$$

Total Simulation time:	1.024 days
Finer (Unit) time step:	0.0001 days
Number of grids:	4200 grids ($7 \times 20 \times 30$)
Permeabilities: k_{xx}, k_{yy}, k_{zz}	5, 20, 20 md
Capillary Pressure:	0
Initial porosity, φ_0	0.2
Water viscosity, μ_w	1.0 cp
Oil viscosity, μ_o	2.0 cp
Initial oil concentration, c_o	0.0 lb_m/ft^3 **(running as a single phase)**
Initial pressure, p_0	500.0 psi
Water compressibility c_{f_w}:	1.E-6 (1/psi)
Oil compressibility c_{f_o}:	1.E-4 (1/psi)
Rock compressibility:	1.E-6 (1/psi)
Rock density:	165.43 lb_m/ft^3
Initial water density, ρ_w:	62.34 lb_m/ft^3
Initial oil density, ρ_o	56.0 lb_m/ft^3
Young's Modulus (E)	1.1E7 psi
Possion Ratio, ν	0.4
Biot's constant, α	0.75
Biot Modulus, M	0.5E14 psi
L (introduced fixed stress parameter)	$\frac{\alpha^2}{2\lambda}$ (1/psi)

Table 2.5: Input Parameters for the Quarter Wellbore Model

2.5.3.3 Quarter Wellbore Model Results

In this test case, we consider a quarter 3D wellbore model. The model domain is a 25.0 ft $\times$ 25.0 ft $\times$ 25.0 ft cube with a quarter of a cylindrical wellbore centered along one of its edges. The mesh contains 4200 grid elements, with 30 elements in the radial direction, 20 elements in the hoop direction, and 7 elements in the vertical direction. Finer grids are used near the wellbore, and they coarsen as they distance apart from the wellbore. A constant wellbore pressure of 300 psi is enforced on the wellbore surface. No flow boundary conditions are enforced on the rest of the boundary faces. For the mechanics model, we apply a zero displacement boundary condition on top of the cube. For the remaining boundaries, we apply zero normal and zero shear traction boundary conditions. Gravity is neglected in this model. In addition, although the code can handle two-phase flow, we run it as a single phase model by assuming the initial oil concentaion to be zero throughout the whole domain. Detailed specifications of the input parameters can be found in Table 2.5. Moreover, detailed results for this test problem can be found in Almani, *et al* [6].

Convergence Stopping Critera

Similar to the single-phase case, the stopping criteria are based on the difference of two successive iterates of porosity, and are given by

$$\delta\varphi_{flow}^{n,k+q} = \Big(\frac{1}{M} + \frac{\alpha^2}{\lambda}\Big)\delta p_h^{n,k+q} \tag{2.5.166}$$

$$\delta\varphi_{mech}^{n,k+q} = \alpha\nabla\cdot\delta\boldsymbol{u}_h^{n,k+q} + \frac{1}{M}\delta p_h^{n,k+q} \tag{2.5.167}$$

where the pressure variable here is the primary pressure unknown (in this formulation, water pressure). The expression (2.5.167) is the standard definition of the fluid content of the medium [45]. Upon convergence, (2.3.77) leads to $\delta\sigma_v^{n,k+q} = \lambda\nabla\cdot\delta\boldsymbol{u}_h^{n,k+q} - \alpha\delta p_h^{n,k+q} = 0$. Accordingly, we define two convergence stopping criteria as follows: $\left\|\frac{\varphi_{mech}^{n,k+q} - \varphi_{flow}^{n,k+q}}{\varphi_{mech}^{n,k+q}}\right\|_{L^\infty} = \left\|\frac{\alpha\nabla\cdot\boldsymbol{u}_h^{n,k+q} - \frac{\alpha^2}{\lambda}p_h^{n,k+q}}{\varphi_{mech}^{n,k+q}}\right\|_{L^\infty} <$ TOL1, and $\|R_{flow}^{n,k+q+1}\| <$ TOL2, where the latter is the residual of the flow volume conservation equation using the last computed pressure and displacement values $p_h^{n,k+q}$ and $\boldsymbol{u}_h^{n,k+q}$. For the quarter wellbore model, we set TOL1 = TOL2 = 0.0001.

Results and Discussion

Figure 2.11a shows the accumulated CPU run time for the single rate case ($q = 1$), and for multirate cases: $q = 2$, 4, and 8. The case $q = 2$ results in 14.28% reduction in CPU run time compared to the single rate. $q = 4$, and $q = 8$ result in 20.97% and 25.09% reductions in CPU run times respectively. Figure 2.11b explains the reduction in CPU run time observed in the multirate case. By just solving for two flow finer time steps within one coarser mechanics time step ($q = 2$), the total number of mechanics linear iterations was reduced by 45.21% with reference to the single rate case. Multirate couplings ($q = 4$, and $q = 8$) result in 70.46% and 84.36% reductions in the number of mechanics linear iterations respectively, which in turn, reduce the CPU run time as well. For this problem, the total number of flow iterations for both the single rate and multirate coupling algorithms are found to be the same. In addition, all four cases perform the same number of flow/mechanics coupling iterations for each coarse mechanics time step, reducing the number of accumulated mechanics linear iterations for multirate schemes, without affecting the total number of flow linear iterations. This results in multirate coupling schemes to outperform the single rate scheme.

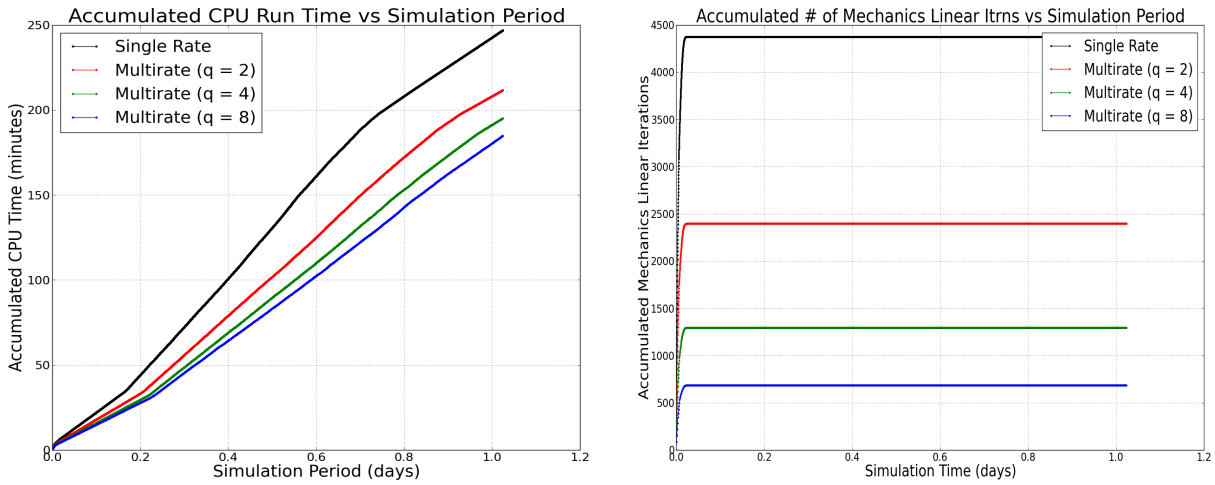

(a) CPU Run Time vs Simulation Days

(b) Total Number of Mechanics Linear Iterations vs Simulation Days

Figure 2.11: Quarter Wellbore Model

We also compare the value of our theoretically driven contraction coefficient against numerically observed contraction coefficient values. Theorem 2.3.4 gives an expression of the contraction coefficient $\left(\frac{M\alpha^2}{2\lambda+2M\lambda c_f\varphi_0+M\alpha^2}\right)^2$ for the multirate algorithm considered in this case ($L = \frac{\alpha^2}{2\lambda}$), leading to linear convergence of the multirate scheme. For this test case, we have $\left(\frac{M\alpha^2}{2\lambda+2M\lambda c_f\varphi_0+M\alpha^2}\right)^2 = 0.006747$. Table 2.6 lists the values of contraction coefficients obtained numerically for $q = 1$, 2, 4, and 8. We consider the iterative coupling iteration for the first coarse mechanics time step, which takes four coupling iterations to converge, according to the stopping criteria described earlier. We compute the values of the volumetric mean stress defined in (2.3.50) for the last two coupling iterations. Ratios of those computed values give estimates of contraction coefficients, obtained numerically, as shown in Table 2.6. We notice that contraction coefficients computed numerically are smaller than the predicted theoretical estimate. This is expected since the extra terms on the left hand side of the contraction result listed in theorem 2.3.4 are not included when computing numerical estimates (i.e. we have not included the effect of the damping factor derived in remark 2.3.4). In addition, we notice that as the number of flow finer time steps solved within one coarser mechanics time step increases, the values of the computed numerical contraction coefficient estimates decrease.

	$q=1$	$q=2$	$q=4$	$q=8$
$\sum_{m=1}^{q} \left\|\delta\sigma_v^{3,m}\right\|^2 \Big/ \sum_{m=1}^{q} \left\|\delta\sigma_v^{2,m}\right\|^2$	0.0009485	0.0007602	0.0004718	0.0001791

Table 2.6: Numerical Contraction Estimates: Contraction estimates observed numerically are shown for different values of q (the number of flow finer time steps within one coarser mechanics time step). These are obtained by taking the ratio of the norms of σ_v computed at the last two iterative coupling iterations during the first coarse time step: Δt, $2\Delta t$,$4\Delta t$, and $8\Delta t$ for $q = 1$, 2, 4, and 8 respectively. The first coarse time step involves four iterative coupling iterations for all the four cases.

2.5.3.4 Frio Field Model Results

Here, we consider the Frio field model, described earlier, but as a two-phase problem coupled with geomechanics. The problem specifications are shown in Table 2.7. Moreover, gravity effects are included in this model.

Convergence Stopping Criteria

For this test case, the convergence stopping criteria are given by:

$$\left\| \frac{\alpha \nabla \cdot \boldsymbol{u}_h^{n,k+q} - \frac{\alpha^2}{\lambda} p_h^{n,k+q}}{\varphi_{mech}^{n,k+q}} \right\|_{L^\infty} < \text{TOL1}$$

$$\left\| \frac{R_{flow}^{n,k+q+1}}{m_{0_{water}} + m_{0_{oil}}} \right\| < \text{TOL2}$$

The first convergence stopping criterion is exactly the same criterion used in the first test case, the quarter wellbore model. The second criterion, involving the residual of the flow volume conservation equation is slightly different. For this one, we scale the norm of the residual by the initial mass of the oil and water, originally found in place. The initial mass of the water, $m_{0_{water}}$, and initial mass of the oil, $m_{0_{oil}}$ are defined as follows: $m_{0_{water}} = \sum_{i,j,k} N_w(i,j,k) V_{por}(i,j,k)$, $m_{0_{oil}} = \sum_{i,j,k} N_o(i,j,k) V_{por}(i,j,k)$, where $N_w(i,j,k)$, $N_o(i,j,k)$, and $V_{por}(i,j,k)$ are the concentration of water, concentration of oil, and the pore volume of the (i,j,k) grid block respectively. We set TOL1 = TOL2 = 10^{-4}.

Wells:	3 production wells, 6 injection well
Injection well (1):	Pressure specified, 4000.0 psi
Injection well (2):	Pressure specified, 3300.0 psi
Injection well (3):	Pressure specified, 4000.0 psi
Injection well (4):	Pressure specified, 4400.0 psi
Injection well (5):	Pressure specified, 3700.0 psi
Injection well (6):	Pressure specified, 4400.0 psi
Production well (1):	Pressure specified, 2000.0 psi
Production well (2):	Pressure specified, 2000.0 psi
Production well (3):	Pressure specified, 2000.0 psi
Total Simulation time:	128.0 days
Finer (Unit) time step:	0.05 days
Number of grids:	891 grids ($33 \times 9 \times 1$)
Absolute Permeabilities: k_{xx}, k_{yy}, k_{zz}	highly varying, range: (5.27E-10, 3.10E+3) md
Initial porosity, φ_0	0.2
Water viscosity, μ_w	1.0 cp
Oil viscosity, μ_o	2.0 cp
Initial oil concentration, c_o	44.8 lb_m/ft^3
Initial oil pressure, p_o	400.0 psi
Water compressibility c_{f_w}:	1.E-6 (1/psi)
Oil compressibility c_{f_o}:	1.E-4 (1/psi)
Rock compressibility:	1.E-6 (1/psi)
Rock density:	165.44 lb_m/ft^3
Initial water density, ρ_w:	56.0 lb_m/ft^3
Initial oil density, ρ_o	62.34 lb_m/ft^3
Young's Modulus (E)	1.2E6 psi
Possion Ratio, ν	0.35
Biot's constant, α	1.0
Biot Modulus, M	1.E8 psi
$\lambda = \frac{E\nu}{(1+\nu)(1-2\nu)}$	1.037E6 psi
L (introduced fixed stress parameter)	$\frac{\alpha^2}{2\lambda}$ (1/psi)
Flow Boundary Conditions:	no flow boundary condition on all 6 boundaries
Mechanics B.C.:	
"X+" boundary (EBCXX1())	$\sigma_{xx} = \sigma \cdot n_x = 10,000 psi$, (overburden pressure)
"X-" - boundary (EBCXXN1())	$\boldsymbol{u} = 0$, zero displacement
"Y+" - boundary (EBCYY1())	$\boldsymbol{u} = 0$, zero displacement
"Y-" - boundary (EBCYYN1())	$\sigma_{yy} = \sigma \cdot n_y = 2000 psi$
"Z+" - boundary (EBCZZ1())	$\boldsymbol{u} = 0$, zero displacement
"Z-" - boundary (EBCZZN1())	$\sigma_{zz} = \sigma \cdot n_z = 1000 psi$

Table 2.7: Input Parameters for the Frio Field Model

Results

Figures 2.13, 2.14, 2.15, and 2.16 show water pressure profile and mechanical displacements in the x, y, and z directions respectively for the Frio field model after 128.0 simulation days. We clearly see that the results for both single rate and multirate implementations are identical.

Figure 2.12a shows the accumulated CPU run time for the single rate case ($q = 1$), and for multirate cases: $q = 2$, 4, and 8. The multirate iterative coupling algorithm with two flow finer time steps within one coarser mechanics time step ($q = 2$) results in 12.25% reduction in CPU run time compared to the single rate case. Multirate couplings ($q = 4$ and $q = 8$) result in 18.18% and 20.05% reductions in CPU run times respectively. Figure 2.12b explains the reduction in CPU run time observed in the multirate case. By just solving for two flow finer time steps within one coarse mechanics time step ($q = 2$), the total number of mechanics linear iterations was reduced by 47.78% with reference to the single rate case. Multirate couplings ($q = 4$ and $q = 8$) result in 73.07% and 85.75% reductions in the number of mechanics linear iterations respectively, which in turn, reduce the CPU run time as well. Figure 2.12c shows the total number of flow linear iterations in the four cases. We see a slight increase in the total number of flow linear iterations for multirate iterative coupling schemes. The case ($q = 2$) results in 1.25% increase in the total number of flow linear iterations. Multirate couplings ($q = 4$) and ($q = 8$) result in 2.89% and 4.82% increase in the total number of flow linear iterations respectively. From these results, we see that the huge decrease in the number of accumulated mechanics linear iterations outperform the overhead introduced by the increase in the number of accumulated flow linear iterations. This is a key factor to the success of the iterative multirate coupling scheme in reducing the overall CPU run time. Figure 2.12d shows the number of flow/mechanics coupling iterations per coarse mechanics time step for the four cases.

2.5.4 Conclusions

We identify three factors that determine the efficiency of multirate schemes:

1. The relative computational cost of the flow solve versus the mechanics solve: if the

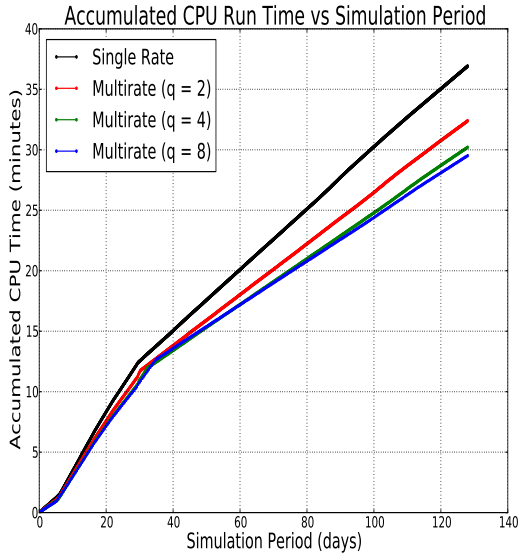

(a) CPU Run Time vs Simulation Days

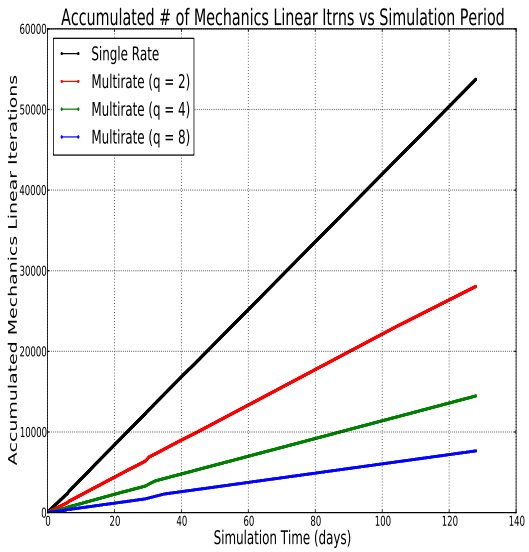

(b) Total Number of Mechanics Linear Iterations vs Simulation Days

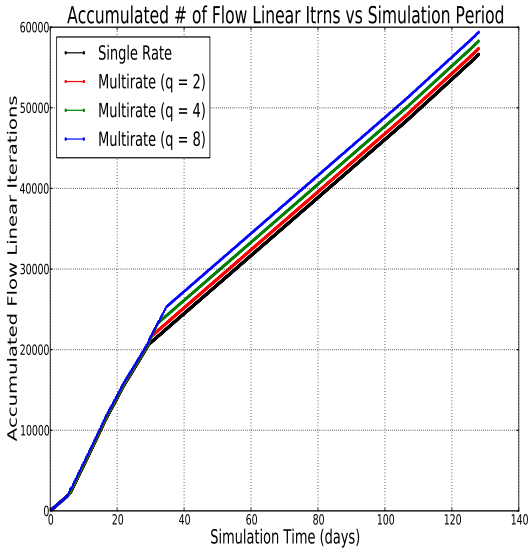

(c) Total Number of Flow Linear Iterations vs Simulation Days

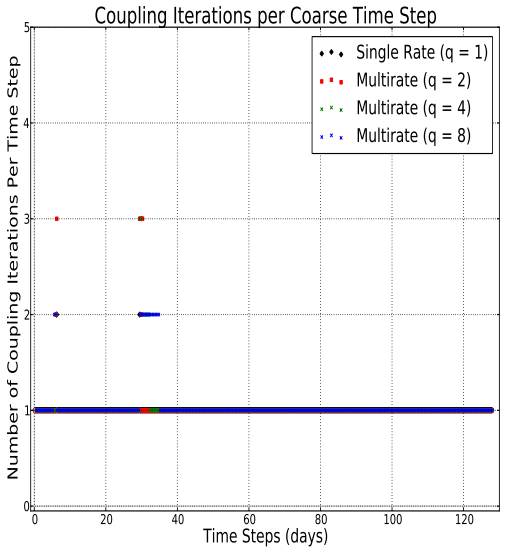

(d) Number of Iterative Coupling Iterations Per Coarser Time Step

Figure 2.12: Frio Field Model

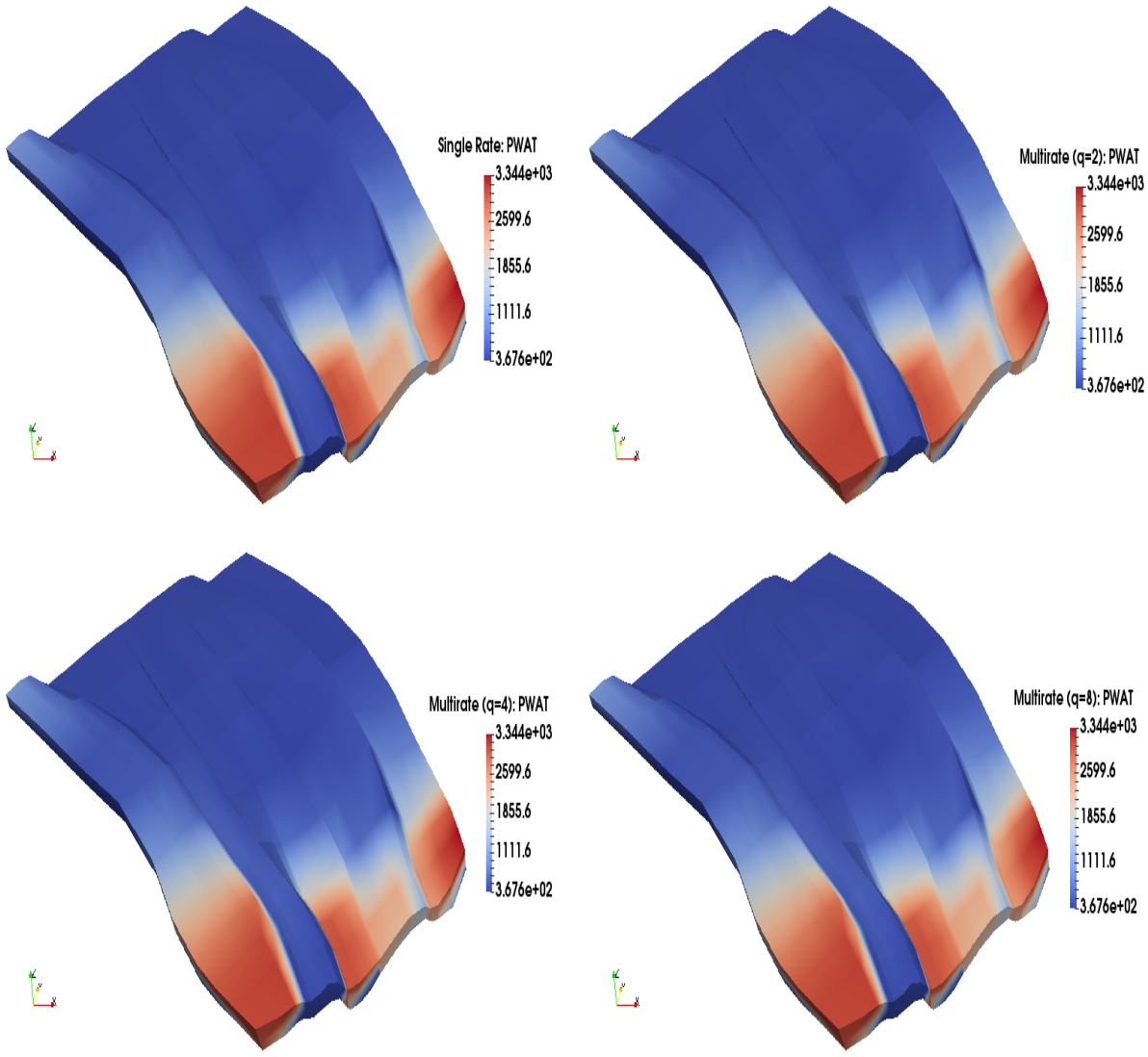

Figure 2.13: Pressure Profiles after 128.0 simulation days (psi)

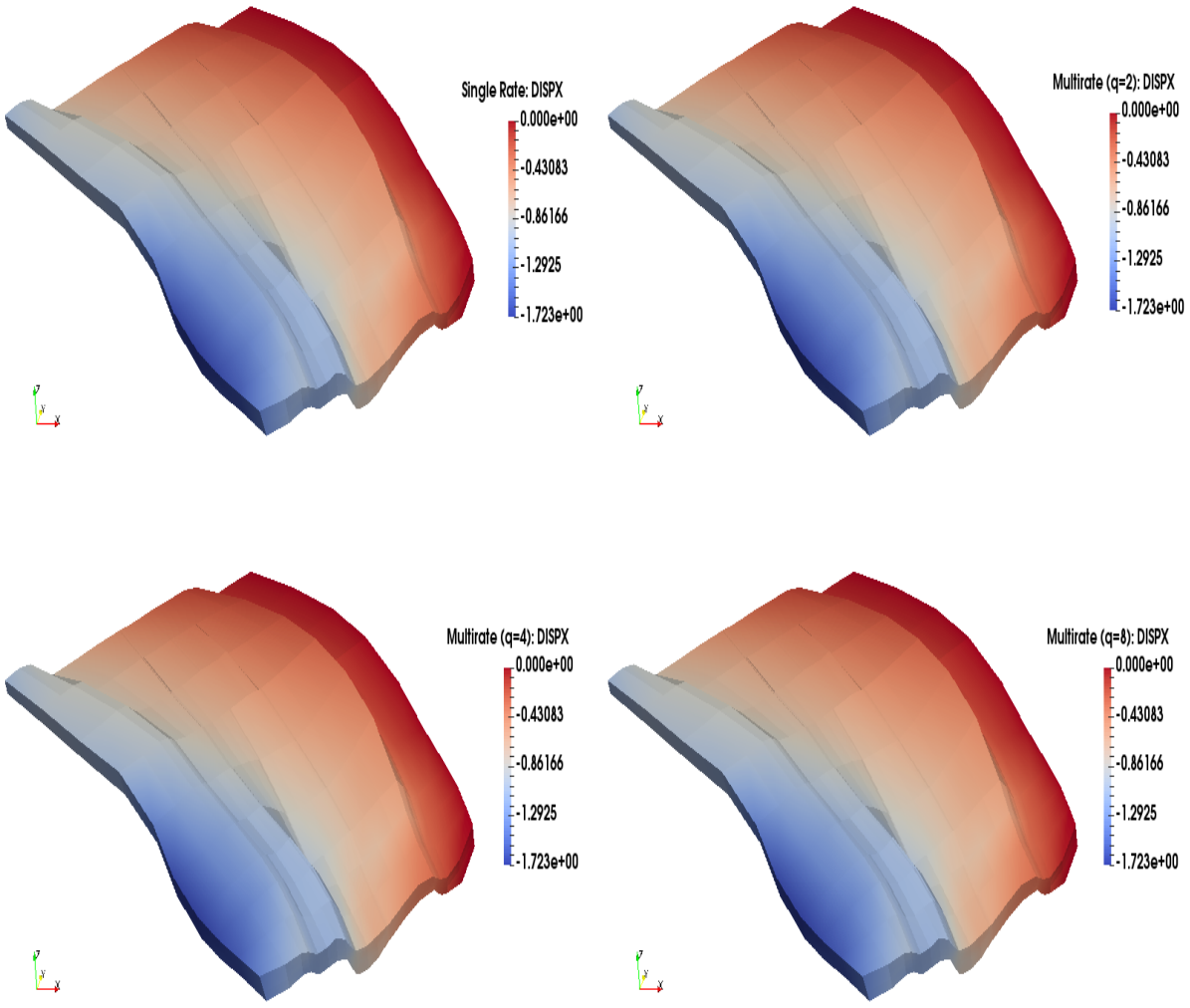

Figure 2.14: Displacement in (x) direction after 128.0 simulation days (ft)

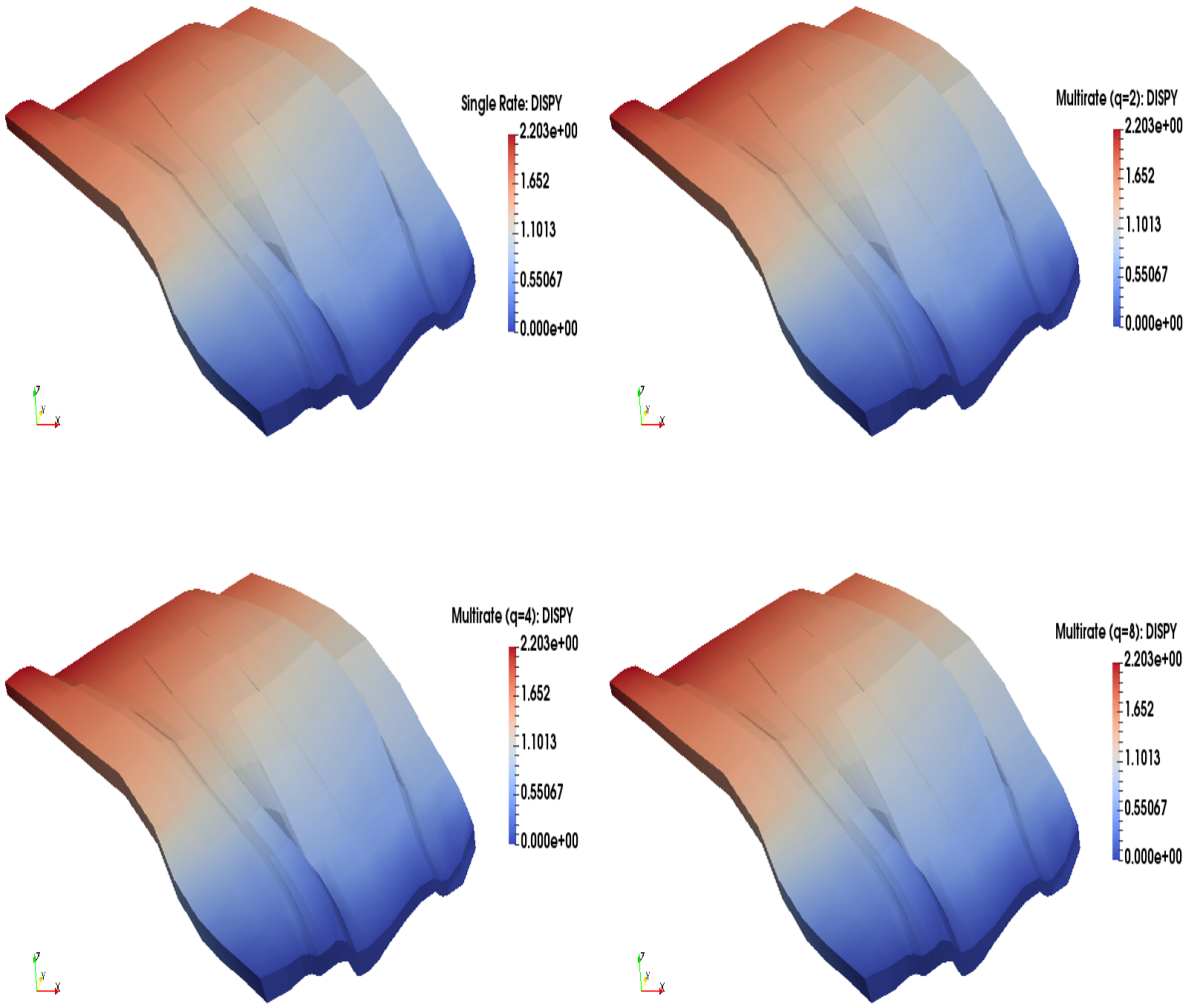

Figure 2.15: Displacement in (y) direction after 128.0 simulation days (ft)

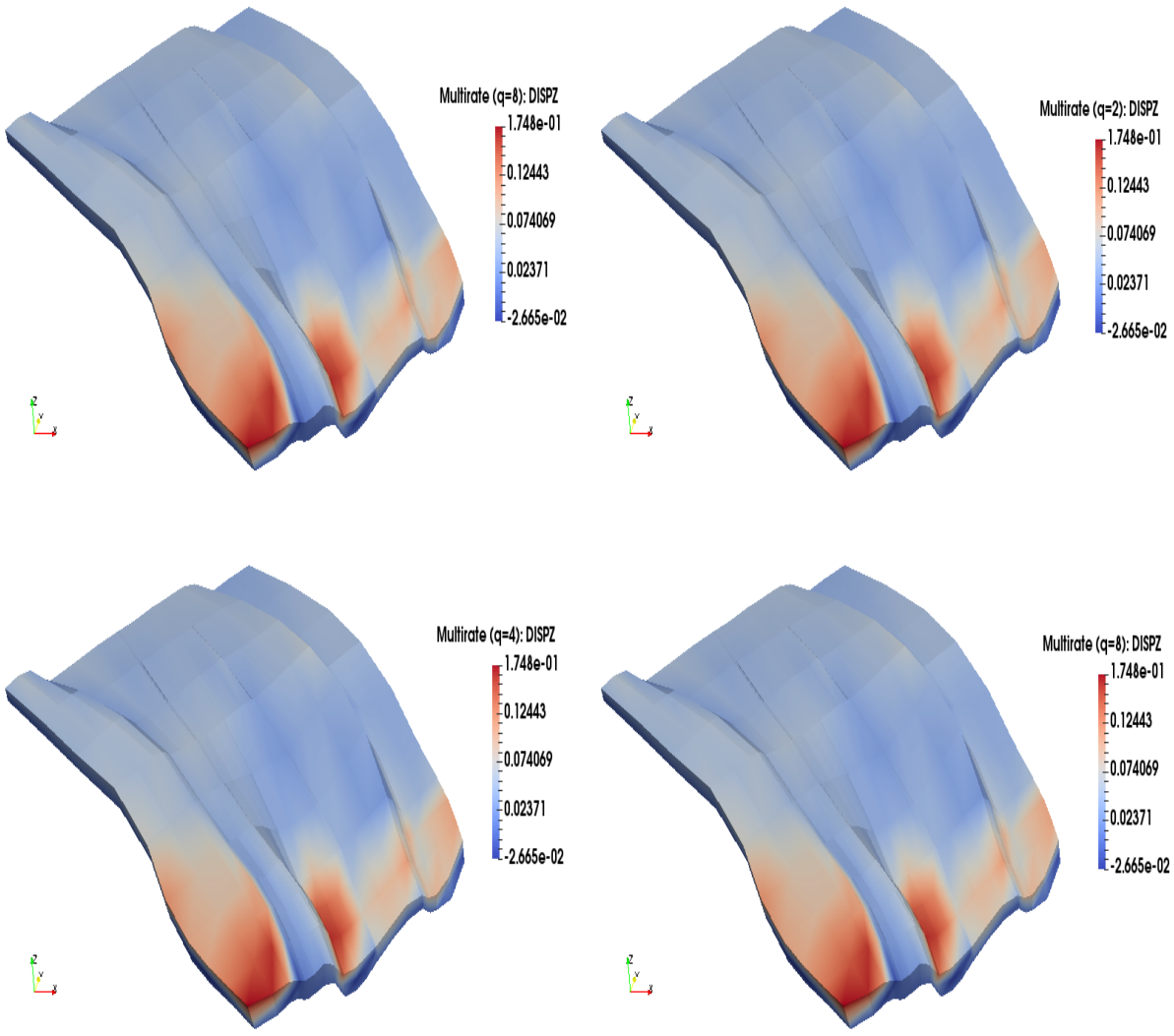

Figure 2.16: Displacement in (z) direction after 128.0 simulation days (ft)

computational cost of solving the coupled problem is dominated by the mechanics solve, then reducing the number of mechanics solve will substantially reduce the overall running time compared to single rate schemes. The multirate schemes are expected to be more useful in this case.

2. Longer simulation periods lead to larger time savings. During early time steps in the simulation, relatively larger numbers of coupling iterations are observed. As the model reaches mechanics equilibrium, the number of iterative coupling iterations per coarse mechanics time step gets reduced. This suggests a dynamic iterative coupling scheme, in which a single rate scheme is employed during early time steps in the simulation, and as the problem approaches mechanics equilibrium, multirate scheme should be employed with adaptive q.

3. Tolerance values used in the convergence stopping criteria affect the efficiency of multirate coupling schemes as well. Loose tolerance values reduce the number of iterative coupling iterations per coarse mechanics time step, which in turn reduces the overall running time. It is a tradeoff between the desired level of accuracy versus computational efficiency and is problem dependent.

Although the theory provided in this work is for single phase flow model, we anticipate that the multirate iterative coupling schemes will be of more importance for nonlinear flow problems coupled with geomechanics, as nonlinearities in the flow problem impose restrictions on the flow time step size. The multirate iterative coupling scheme would be a natural candidate for such nonlinear flow problems coupled with geomechanics.

The work considered in this chapter has been published in [6, 7, 11, 13].

Chapter 3

Error Analysis of Single Rate Iterative Coupling Schemes for Poroelastic Media

The work in this chapter addresses the error analysis for iteratively coupled flow and mechanics problems. More specifically, we derive a priori error estimates for quantifying the error between the solution obtained at any iterate (in iteratively coupled problems) and the true solution. Our approach is based on studying the equations satisfied by the difference of iterates and utilizing a Banach contraction argument to show that the corresponding scheme is a fixed point iteration. Obtained contraction results are then used to derive theoretical convergence error estimates for the single rate iterative coupling scheme.

3.1 Brief Literature Review on Error Estimates for Coupled Flow-Mechanics Problems

We first note that the rigorous mathematical analysis of the iterative and explicit coupling schemes, proposed in literature, has received relatively less attention compared to the proposed linear and nonlinear extensions. To the best of our knowledge, the first asymptotic error estimates for spatially discrete Galerkin approximations of the Biot's model were presented by [69]. Few years later, [40] considered finite difference methods for the Biot's model on staggered grids, derived stability estimates, and analyzed convergence for the discretized system. In a sequence of two papers, [70, 71] studied the continuous in time and fully-discrete Biot's model in which mixed formulation is used for flow and continuous

The theoretical work in this chapter is a collaborative work with Dr. Kundan Kumar, under the supervision of Prof. Mary Wheeler. This work has been presented at the ECMOR XV conference [10], and submitted as an ICES Report [12]. The ECMOR conference paper contains numerical simulations performed in IPARS. The numerical implementation is done primarily by Tameem Almani with helpful discussions with Drs. Kundan Kumar and Gurpreet Singh.

Galerkin is used for mechanics. A priori error estimates are derived in both cases respectively. [34], on the other hand, derived a posteriori error estimates for the quasi-static Biot model, resulting in reliable error bounds with all constants involved in the estimates are being specified. Such error estimators can be used to perform adaptive simulations. Recently, [89] derived a priori error estimates for the quasi-static Biot model in which flow is discretized by the multipoint flux mixed finite element method, and elasticity uses continuous piecewise linear Galerkin finite elements. [75] considered finite element discretizations of the Biot's model based on MINI and stabilized P1-P1 elements, and derived error estimates of the fully discrete system accordingly. The work of [59] considers a formulation of the Biot's system in four unknowns including pore pressure, fluid flux, stress tensor, and solid displacement, using a combination of two-mixed formulations for the flow and mechanics, and derived a priori error estimates of the fully coupled system accordingly. We note here that all previously derived error estimates consider simultaneous coupling of flow and mechanics.

In this work, we consider iterative coupling schemes instead, and drive error estimates for the fixed-stress split iterative coupling scheme for the quasi-static Biot model. The approach we follow in deriving our a priori error estimates utilizes previously established results in a clever way, under the assumption that the solution obtained by the iterative coupling scheme converges to the solution obtained by the simultaneously coupled scheme. Under such assumption, the problem is simplified into estimating the error between the solution obtained by the iterative coupling scheme, and the one obtained by the simultaneously coupled scheme. In fact, we show that the former converges to the later geometrically by a Banach contraction argument. To the best of our knowledge, this is the first rigorous derivation of a priori error estimates for the fixed-stress coupling scheme for the Biot system.

3.2 Model Equations and Discretization

We assume a linear, elastic, heterogeneous, and isotropic poro-elastic medium in which the reservoir is saturated with a slightly compressible fluid. We follow exactly the same quasi-static Biot model [16, 45] described in section 2.2 in Chapter 2. Moreover, the same assumptions listed in 2.2.1 apply here. Furthermore, we will follow the same mixed variational formulation described in section 2.2.4 in Chapter 2.

3.3 Error Analysis for the Fixed-Stress Split Scheme

For a given time step $t = t_k$, and a given iterative coupling iteration $n \geq 0$, we need to estimate $\|\xi_h^{n,k} - \xi(t_k)\|$, where ξ may stand for $p_h, \boldsymbol{z}_h$, and $\boldsymbol{u}_h$. By the triangle inequality, we can write:

$$\|\xi_h^{n,k} - \xi(t_k)\| \leq \|\xi_h^{n,k} - \xi_h^k\| + \|\xi_h^k - \xi(t_k)\|$$

where ξ_h^k is the solution obtained by solving the coupled flow and mechanics equations simultaneously. Error estimates for the second term on the right hand side have been derived in the work of [70, 71]. It only remains to estimate the first term $\|\xi_h^{n,k} - \xi_h^k\|$. This can be done in two steps: first we derive a Banach contraction argument on the difference between the solution obtained at a particular iterative coupling iteration $\xi_h^{n,k}$, and the solution obtained by solving the coupled system simultaneously (fully implicit scheme, ξ_h^k). Then, we derive stability estimates for the fully implicit scheme, and combine the two to bound the term $\|\xi^{n,k} - \xi_h^k\|$. The two steps are detailed below.

3.3.1 Step 1: Banach Contraction Estimate on the Difference between Iterative and Implicit Solutions

We first derive a Banach contraction estimate on the difference: $\|\xi^{n,k} - \xi_h^k\|$. We note that the weak formulation of the fully discrete single-rate fixed-stress split iterative coupling scheme is given in equations (2.3.20) - (2.3.22). In contrast, the weak formulation of the fully discrete implicit scheme reads:

Find $p_h^k \in Q_h$, $\boldsymbol{z}_h^k \in \boldsymbol{Z}_h$, and $\boldsymbol{u}_h^k \in \boldsymbol{V}_h$ such that,

$$\forall \theta_h \in Q_h\,,\ \frac{1}{\Delta t}\Big((\frac{1}{M}+c_f\varphi_0)\Big(p_h^k-p_h^{k-1}\Big),\theta_h\Big)+\frac{1}{\mu_f}\Big(\nabla\cdot\boldsymbol{z}_h^k,\theta_h\Big) = -\frac{\alpha}{\Delta t}\Big(\nabla\cdot\Big(\boldsymbol{u}_h^k-\boldsymbol{u}_h^{k-1}\Big),\theta_h\Big)+\Big(\tilde{q}_h,\theta_h\Big), \tag{3.3.1}$$

$$\forall \boldsymbol{q}_h \in \boldsymbol{Z}_h\,,\ \Big(\boldsymbol{K}^{-1}\boldsymbol{z}_h^k,\boldsymbol{q}_h\Big)=\Big(p_h^k,\nabla\cdot\boldsymbol{q}_h\Big)+\Big(\rho_{f,r}g\nabla\,\eta,\boldsymbol{q}_h\Big), \tag{3.3.2}$$

$$\forall \boldsymbol{v}_h \in V_h\,,\ 2G(\boldsymbol{\varepsilon}(\boldsymbol{u}_h^k),\boldsymbol{\varepsilon}(\boldsymbol{v}_h))+\lambda(\nabla\cdot\boldsymbol{u}_h^k,\nabla\cdot\boldsymbol{v}_h)-\alpha(p_h^k,\nabla\cdot\boldsymbol{v}_h)=(\boldsymbol{f}_h^k,\boldsymbol{v}_h). \tag{3.3.3}$$

Subtracting equations (3.3.3), (3.3.2), and (3.3.1), from (2.3.22), (2.3.21), and (2.3.20) respectively, and noting that $\boldsymbol{f}_h^{n+1,k}=\boldsymbol{f}_h^k$, we get:

$$\forall \theta_h \in Q_h\,,\ \frac{1}{\Delta t}\Big((\frac{1}{M}+c_f\varphi_0)\Big(p_h^{n+1,k}-p_h^k\Big),\theta_h\Big)+\frac{1}{\mu_f}\Big(\nabla\cdot(\boldsymbol{z}_h^{n+1,k}-\boldsymbol{z}_h^k),\theta_h\Big) = -\frac{\alpha}{\Delta t}\Big(\nabla\cdot\Big(\boldsymbol{u}_h^{n,k}-\boldsymbol{u}_h^k\Big),\theta_h\Big)-\frac{L}{\Delta t}\Big(p_h^{n+1,k}-p_h^{n,k},\theta_h\Big), \tag{3.3.4}$$

$$\forall \boldsymbol{q}_h \in \boldsymbol{Z}_h\,,\ \Big(\boldsymbol{K}^{-1}(\boldsymbol{z}_h^{n+1,k}-\boldsymbol{z}_h^k),\boldsymbol{q}_h\Big)=\Big(p_h^{n+1,k}-p_h^k,\nabla\cdot\boldsymbol{q}_h\Big), \tag{3.3.5}$$

$$\forall \boldsymbol{v}_h \in V_h\,,\ 2G(\boldsymbol{\varepsilon}(\boldsymbol{u}_h^{n+1,k}-\boldsymbol{u}_h^k),\boldsymbol{\varepsilon}(\boldsymbol{v}_h))+\lambda(\nabla\cdot(\boldsymbol{u}_h^{n+1,k}-\boldsymbol{u}_h^k),\nabla\cdot\boldsymbol{v}_h)-\alpha(p_h^{n+1,k}-p_h^k,\nabla\cdot\boldsymbol{v}_h). \tag{3.3.6}$$

Define $e_p^{n+1}=p_h^{n+1,k}-p_h^k$, $e_u^{n+1}=\boldsymbol{u}_h^{n+1,k}-\boldsymbol{u}_h^k$, and $e_z^{n+1}=\boldsymbol{z}_h^{n+1,k}-\boldsymbol{z}_h^k$. Equations (3.3.4), (3.3.5), and (3.3.6) can be written as:

$$\forall \theta_h \in Q_h\,,\ \frac{1}{\Delta t}(\frac{1}{M}+c_f\varphi_0+L)\Big(e_p^{n+1},\theta_h\Big)+\frac{1}{\mu_f}\Big(\nabla\cdot e_z^{n+1},\theta_h\Big)=\frac{1}{\Delta t}\Big(-\alpha\nabla\cdot e_u^n+Le_p^n,\theta_h\Big), \tag{3.3.7}$$

$$\forall \boldsymbol{q}_h \in \boldsymbol{Z}_h\,,\ \Big(\boldsymbol{K}^{-1}e_z^{n+1},\boldsymbol{q}_h\Big)=\Big(e_p^{n+1},\nabla\cdot\boldsymbol{q}_h\Big), \tag{3.3.8}$$

$$\forall \boldsymbol{v}_h \in V_h\,,\ 2G(\boldsymbol{\varepsilon}(e_u^{n+1}),\boldsymbol{\varepsilon}(\boldsymbol{v}_h))+\lambda(\nabla\cdot e_u^{n+1},\nabla\cdot\boldsymbol{v}_h)-\alpha(e_p^{n+1},\nabla\cdot\boldsymbol{v}_h)=0. \tag{3.3.9}$$

Let $\beta=\frac{1}{M}+c_f\varphi_0+L$. Testing (3.3.7) with $\theta_h=e_p^{n+1}$, and (3.3.8) with $\boldsymbol{q}_h=e_z^{n+1}$, we obtain:

$$\beta\Big\|e_p^{n+1}\Big\|_\Omega^2+\frac{\Delta t}{\mu_f}(\nabla\cdot e_z^{n+1},e_p^{n+1})_\Omega=\Big(-\alpha\nabla\cdot e_u^n+Le_p^n,e_p^{n+1}\Big)_\Omega. \tag{3.3.10}$$

$$\Big(\boldsymbol{K}^{-1}e_z^{n+1},e_z^{n+1}\Big)_\Omega=\Big(e_p^{n+1},\nabla\cdot e_z^{n+1}\Big)_\Omega. \tag{3.3.11}$$

Substituting (3.3.11) into (3.3.10), defining e_σ^n as $\chi e_\sigma^n = L e_p^n - \alpha \nabla \cdot e_u^n$, where χ is an adjustable parameter, and applying Young's inequality, we obtain:

$$\beta \left\| e_p^{n+1} \right\|_\Omega^2 + \frac{\Delta t}{\mu_f} \left\| \boldsymbol{K}^{-1/2} e_z^{n+1} \right\|_\Omega \leq \frac{1}{2\epsilon} \left\| e_\sigma^n \right\|_\Omega^2 + \frac{\epsilon}{2} \left\| e_p^{n+1} \right\|_\Omega^2.$$

The choice $\epsilon = \beta$ gives (after multiplying by $\frac{2}{\beta}$):

$$\left\| e_p^{n+1} \right\|_\Omega^2 + \frac{2\Delta t}{\beta \mu_f} \left\| \boldsymbol{K}^{-1/2} e_z^{n+1} \right\|_\Omega^2 \leq \frac{1}{\beta^2} \left\| \chi e_\sigma^n \right\|_\Omega^2. \tag{3.3.12}$$

Multiplying the elasticity equation (3.3.9) by a free parameter c_0, and testing with $\boldsymbol{v}_h = e_u^{n+1}$, we get:

$$2Gc_0 \|\boldsymbol{\varepsilon}(e_u^{n+1})\|_\Omega^2 + \lambda c_0 \|\nabla \cdot e_u^{n+1}\|_\Omega^2 - \alpha c_0 (e_p^{n+1}, \nabla \cdot e_u^{n+1})_\Omega = 0. \tag{3.3.13}$$

Combining flow (3.3.12) with elasticity (3.3.13), we obtain:

$$\begin{aligned} 2Gc_0 \|\boldsymbol{\varepsilon}(e_u^{n+1})\|_\Omega^2 + \left\{ \left\| e_p^{n+1} \right\|_\Omega^2 - \alpha c_0 (e_p^{n+1}, \nabla \cdot e_u^{n+1})_\Omega + \lambda c_0 \|\nabla \cdot e_u^{n+1}\|_\Omega^2 \right\} \\ + \frac{2\Delta t}{\beta \mu_f} \left\| \boldsymbol{K}^{-1/2} e_z^{n+1} \right\|_\Omega^2 \leq \frac{\chi^2}{\beta^2} \left\| e_\sigma^n \right\|_\Omega^2. \end{aligned} \tag{3.3.14}$$

Expanding the right hand side to match terms on the left hand side (to form a complete square):

$$\left\| e_\sigma^n \right\|^2 = \frac{L^2}{\chi^2} \left\| e_p^n \right\|_\Omega^2 - \frac{2\alpha L}{\chi^2} \left(e_p^n, \nabla \cdot e_u^n \right)_\Omega + \frac{\alpha^2}{\chi^2} \left\| \nabla \cdot \delta e_u^n \right\|_\Omega^2.$$

The following inequalities should be satisfied: $1 > \frac{L^2}{\chi^2}$, $\frac{2\alpha L}{\chi^2} = \alpha c_0$, and $\lambda c_0 = \frac{\alpha^2}{\chi^2}$. The second and third equalities lead to the following parameter assignments: $c_0 = \frac{2L}{\chi^2}$, and $L = \frac{\alpha^2}{2\lambda}$. The first inequality leads to the condition: $\chi > \frac{\alpha^2}{2\lambda}$. Now, (3.3.14) can be written as:

$$2Gc_0 \|\boldsymbol{\varepsilon}(e_u^{n+1})\|_\Omega^2 + \frac{2\Delta t}{\beta \mu_f} \left\| \boldsymbol{K}^{-1/2} e_z^{n+1} \right\|_\Omega^2 + \left(1 - \frac{L^2}{\chi^2} \right) \left\| e_p^{n+1} \right\|_\Omega^2 + \left\| e_\sigma^{n+1} \right\|_\Omega^2 \leq \left(\frac{\chi}{\beta} \right)^2 \left\| e_\sigma^n \right\|_\Omega^2. \tag{3.3.15}$$

For contraction to hold, we require $\frac{\chi}{\beta} < 1$. Together with the previous condition $\chi > \frac{\alpha^2}{2\lambda}$, the value of χ should be chosen such that

$$\frac{\alpha^2}{2\lambda} < \chi < \frac{1}{M} + c_f \varphi_0 + \frac{\alpha^2}{2\lambda}$$

This imposes the following condition on our given parameters (which corresponds to the condition on the constrained specific storage coefficient in the work of [70, 71]:

$$\frac{1}{M} + c_f \varphi_0 \geq \gamma_0 > 0. \qquad \text{for some positive constant } \gamma_0. \tag{3.3.16}$$

In general, for $n \geq 0$, we can write:

$$\begin{aligned} \left\| e_\sigma^{n+1} \right\|_\Omega^2 &\leq \left(\frac{\chi}{\beta}\right)^2 \left\| e_\sigma^n \right\|_\Omega^2 \\ &\leq \left(\frac{\chi}{\beta}\right)^{2(n+1)} \left\| e_\sigma^0 \right\|_\Omega^2. \\ &\leq \left(\frac{\chi}{\beta}\right)^{2(n+1)} \left\| L e_p^0 - \alpha \nabla \cdot e_u^0 \right\|_\Omega^2. \end{aligned} \tag{3.3.17}$$

Combining (3.3.15) with (3.3.17), together with Young's inequality, we can write:

$$\begin{aligned} \left(1 - \frac{L^2}{\chi^2}\right) \left\| e_p^{n+1} \right\|_\Omega^2 &\leq \left(\frac{\chi}{\beta}\right)^{2(n+1)} \left\| L e_p^0 - \alpha \nabla \cdot e_u^0 \right\|_\Omega^2 \\ &\leq \left(\frac{\chi}{\beta}\right)^{2(n+1)} \left(L^2 \left\| e_p^0 \right\|_\Omega^2 + \alpha^2 \left\| \nabla \cdot e_u^0 \right\|_\Omega^2 - 2L\alpha (e_p^0, \nabla \cdot e_u^0) \right) \\ &\leq \left(\frac{\chi}{\beta}\right)^{2(n+1)} \left(L^2 \left\| e_p^0 \right\|_\Omega^2 + \alpha^2 \left\| \nabla \cdot e_u^0 \right\|_\Omega^2 + 2L\alpha (\frac{1}{2\epsilon} \left\| e_p^0 \right\|_\Omega^2 + \frac{\epsilon}{2} \left\| \nabla \cdot e_u^0 \right\|_\Omega^2) \right) \\ &\leq \left(\frac{\chi}{\beta}\right)^{2(n+1)} \left((L^2 + \frac{L\alpha}{\epsilon}) \left\| e_p^0 \right\|_\Omega^2 + (\alpha^2 + L\alpha\epsilon) \left\| \nabla \cdot e_u^0 \right\|_\Omega^2 \right) \qquad \text{for } \epsilon > 0. \end{aligned} \tag{3.3.18}$$

Similarly, we can write:

$$2Gc_0 \|\boldsymbol{\varepsilon}(e_u^{n+1})\|_\Omega^2 \leq \left(\frac{\chi}{\beta}\right)^{2(n+1)} \left((L^2 + \frac{L\alpha}{\epsilon}) \left\| e_p^0 \right\|_\Omega^2 + (\alpha^2 + L\alpha\epsilon) \left\| \nabla \cdot e_u^0 \right\|_\Omega^2 \right). \tag{3.3.19}$$

$$\frac{2\Delta t}{\beta \mu_f} \left\| \boldsymbol{K}^{-1/2} e_z^{n+1} \right\|_\Omega^2 \leq \left(\frac{\chi}{\beta}\right)^{2(n+1)} \left((L^2 + \frac{L\alpha}{\epsilon}) \left\| e_p^0 \right\|_\Omega^2 + (\alpha^2 + L\alpha\epsilon) \left\| \nabla \cdot e_u^0 \right\|_\Omega^2 \right). \tag{3.3.20}$$

Combining (3.3.18), (3.3.19), and (3.3.20), we have:

$$\begin{aligned} \left\| e_p^{n+1} \right\|_\Omega^2 + \|\boldsymbol{\varepsilon}(e_u^{n+1})\|_\Omega^2 + \left\| \boldsymbol{K}^{-1/2} e_z^{n+1} \right\|_\Omega^2 \leq \\ \left(\frac{\chi}{\beta}\right)^{2(n+1)} C_1 \left((L^2 + \frac{L\alpha}{\epsilon}) \left\| e_p^0 \right\|_\Omega^2 + (\alpha^2 + L\alpha\epsilon) \left\| \nabla \cdot e_u^0 \right\|_\Omega^2 \right). \end{aligned} \tag{3.3.21}$$

where $C_1 = \left[\frac{\chi^2}{\chi^2 - L^2} + \frac{1}{2Gc_0} + \frac{\beta \mu_f}{2\Delta t} \right]$. Noting that: $e_p^0 = p_h^{0,k} - p_h^k = p_h^{k-1} - p_h^k$, and $e_u^0 =$

$\boldsymbol{u}_h^{0,k} - \boldsymbol{u}_h^k = \boldsymbol{u}_h^{k-1} - \boldsymbol{u}_h^k$, (3.3.21) can be written as:

$$\left\|p_h^{n+1,k} - p_h^k\right\|_\Omega^2 + \|\boldsymbol{\varepsilon}(\boldsymbol{u}_h^{n+1,k} - \boldsymbol{u}_h^k)\|_\Omega^2 + \left\|\boldsymbol{K}^{-1/2}\boldsymbol{z}_h^{n+1,k} - \boldsymbol{z}_h^k\right\|_\Omega^2 \leq \left(\frac{\chi}{\beta}\right)^{2(n+1)} C_1\left(L^2 + \frac{L\alpha}{\epsilon}\right)\left\|p_h^k - p_h^{k-1}\right\|_\Omega^2 + \left(\frac{\chi}{\beta}\right)^{2(n+1)} C_1(\alpha^2 + L\alpha\epsilon)\left\|\nabla\cdot\boldsymbol{u}_h^k - \boldsymbol{u}_h^{k-1}\right\|_\Omega^2 \tag{3.3.22}$$

Let $\tilde{\eta}_1 = C_1(L^2 + \frac{L\alpha}{\epsilon})$, and $\tilde{\eta}_2 = C_1(\alpha^2 + L\alpha\epsilon)$ for $\epsilon > 0$, (3.3.22) reduces to:

$$\left\|p_h^{n+1,k} - p_h^k\right\|_\Omega^2 + \|\boldsymbol{\varepsilon}(\boldsymbol{u}_h^{n+1,k} - \boldsymbol{u}_h^k)\|_\Omega^2 + \left\|\boldsymbol{K}^{-1/2}(\boldsymbol{z}_h^{n+1,k} - \boldsymbol{z}_h^k)\right\|_\Omega^2 \leq \left(\frac{\chi}{\beta}\right)^{2(n+1)}\left(\tilde{\eta}_1\left\|p_h^k - p_h^{k-1}\right\|_\Omega^2 + \tilde{\eta}_2\left\|\nabla\cdot\boldsymbol{u}_h^k - \boldsymbol{u}_h^{k-1}\right\|_\Omega^2\right) \tag{3.3.23}$$

3.3.2 Step 2: Stability Estimate for Implicitly Coupled Scheme

The second step involves deriving a stability estimate on $\|\xi_h^k - \xi_h^{k-1}\|$. We recall that the weak formulation of the implicit scheme is given by equations (3.3.1) - (3.3.3). The derivation of the stability estimate for the implicit scheme is carried out in three steps: by first considering the flow equations, followed by the mechanics equation and then combining the two to derive the final estimate. For simplicity, we define $\tilde{c}_f = \frac{1}{M} + c_f\varphi_0$.

3.3.2.1 Flow Equations

Testing (3.3.1) with $\theta_h = p_h^k - p_h^{k-1}$, and multiplying the whole equation by Δt, we obtain

$$\tilde{c}_f\left\|p_h^k - p_h^{k-1}\right\|^2 + \frac{\Delta t}{\mu_f}\left(\nabla\cdot\boldsymbol{z}_h^k, p_h^k - p_h^{k-1}\right) = \alpha\left(\nabla\cdot(\boldsymbol{u}_h^k - \boldsymbol{u}_h^{k-1}), p_h^k - p_h^{k-1}\right) + \left(\tilde{q}_h, p_h^k - p_h^{k-1}\right) \tag{3.3.24}$$

Next, we consider the flux equation (3.3.2). Taking the difference of two consecutive time steps $t = t_k$ and $t = t_{k-1}$ and testing with $\boldsymbol{q}_h = \boldsymbol{z}_h^k$, we obtain:

$$\left(K^{-1}(\boldsymbol{z}_h^k - \boldsymbol{z}_h^{k-1}), \boldsymbol{z}_h^k\right) = \left(p_h^k - p_h^{k-1}, \nabla\cdot\boldsymbol{z}_h^k\right) \tag{3.3.25}$$

Substituting (3.3.25) into (3.3.24), with some algebraic manipulations of the resulting term (using the identity: $a(a-b) = \frac{1}{2}(a^2 - b^2 + (a-b)^2)$), we derive

$$\tilde{c}_f \left\| p_h^k - p_h^{k-1} \right\|^2 + \frac{\Delta t}{2\mu_f} \Big(\left\| K^{-1/2} \boldsymbol{z}_h^k \right\|^2 - \left\| K^{-1/2} \boldsymbol{z}_h^{k-1} \right\|^2 + \left\| K^{-1/2} (\boldsymbol{z}_h^k - \boldsymbol{z}_h^{k-1}) \right\|^2 \Big)$$
$$= -\alpha \Big(\nabla \cdot (\boldsymbol{u}_h^k - \boldsymbol{u}_h^{k-1}), p_h^k - p_h^{k-1} \Big) + \Big(\tilde{q}_h, p_h^k - p_h^{k-1} \Big) \quad (3.3.26)$$

3.3.2.2 Elasticity Equation

Considering (3.3.3) for the difference of two consecutive time steps, $t = t_k$ and $t = t_{k-1}$, and testing with $\boldsymbol{v}_h = \boldsymbol{u}_h^k - \boldsymbol{u}_h^{k-1}$, we obtain

$$2G \left\| \boldsymbol{\varepsilon}(\boldsymbol{u}_h^k - \boldsymbol{u}_h^{k-1}) \right\|^2 + \lambda \left\| \nabla \cdot (\boldsymbol{u}_h^k - \boldsymbol{u}_h^{k-1}) \right\|^2 - \alpha \Big(p_h^k - p_h^{k-1}, \nabla \cdot (\boldsymbol{u}_h^k - \boldsymbol{u}_h^{k-1}) \Big)$$
$$= \Big(\boldsymbol{f}_h^k - \boldsymbol{f}_h^{k-1}, \boldsymbol{u}_h^k - \boldsymbol{u}_h^{k-1} \Big) \quad (3.3.27)$$

3.3.2.3 Combining Flow and Elasticity Equations

Combining (3.3.26) with (3.3.27) yields

$$\tilde{c}_f \left\| p_h^k - p_h^{k-1} \right\|^2 + \frac{\Delta t}{2\mu_f} \Big(\left\| K^{-1/2} \boldsymbol{z}_h^k \right\|^2 - \left\| K^{-1/2} \boldsymbol{z}_h^{k-1} \right\|^2 + \left\| K^{-1/2} (\boldsymbol{z}_h^k - \boldsymbol{z}_h^{k-1}) \right\|^2 \Big)$$
$$+2G \left\| \boldsymbol{\varepsilon}(\boldsymbol{u}_h^k - \boldsymbol{u}_h^{k-1}) \right\|^2 + \lambda \left\| \nabla \cdot (\boldsymbol{u}_h^k - \boldsymbol{u}_h^{k-1}) \right\|^2 = \underbrace{\Big(\tilde{q}_h, p_h^k - p_h^{k-1} \Big)}_{R_1} + \underbrace{\Big(\boldsymbol{f}_h^k - \boldsymbol{f}_h^{k-1}, \boldsymbol{u}_h^k - \boldsymbol{u}_h^{k-1} \Big)}_{R_2} \quad (3.3.28)$$

To bound the terms (R_1 and R_2), we will use Poincaré's (2.1.1) and Korn's inequalities (2.1.2). By Poincaré, Korn, and Young inequalities, we bound R_1 and R_2 as:

$$|R_1| \leq \frac{1}{2\epsilon_1} \left\| \tilde{q}_h \right\|^2 + \frac{\epsilon_1}{2} \left\| p_h^k - p_h^{k-1} \right\|^2$$
$$|R_2| \leq \frac{1}{2\epsilon_2} \left\| \boldsymbol{f}_h^k - \boldsymbol{f}_h^{k-1} \right\|^2 + \frac{\epsilon_2}{2} \left\| \boldsymbol{u}_h^k - \boldsymbol{u}_h^{k-1} \right\|^2$$
$$\leq \frac{1}{2\epsilon_2} \left\| \boldsymbol{f}_h^k - \boldsymbol{f}_h^{k-1} \right\|^2 + \frac{\epsilon_2 \mathcal{P}_\Omega^2 C_\kappa^2}{2} \|\boldsymbol{\varepsilon}(\boldsymbol{u}_h^k - \boldsymbol{u}_h^{k-1})\|^2.$$

for ϵ_1, and $\epsilon_2 > 0$. Choosing $\epsilon_1 = \tilde{c}_f$, and $\epsilon_2 = \frac{2G}{\mathcal{P}_\Omega^2 C_\kappa^2}$, and summing for $1 \leq k \leq N$, where N denotes the total number of time steps (note telescopic cancellations), we derive

$$\frac{\tilde{c}_f}{2}\sum_{k=1}^{N}\left\|p_h^k - p_h^{k-1}\right\|^2 + \frac{\Delta t}{2\mu_f}\Big(\left\|K^{-1/2}\boldsymbol{z}_h^N\right\|^2 + \sum_{k=1}^{N}\left\|K^{-1/2}(\boldsymbol{z}_h^k - \boldsymbol{z}_h^{k-1})\right\|^2\Big)$$
$$+ G\sum_{k=1}^{N}\left\|\boldsymbol{\varepsilon}(\boldsymbol{u}_h^k - \boldsymbol{u}_h^{k-1})\right\|^2 + \lambda\sum_{k=1}^{N}\left\|\nabla\cdot(\boldsymbol{u}_h^k - \boldsymbol{u}_h^{k-1})\right\|^2 \leq \frac{\Delta t}{2\mu_f}\left\|K^{-1/2}\boldsymbol{z}_h^0\right\|^2 + \frac{1}{2\tilde{c}_f}\sum_{k=1}^{N}\left\|\tilde{q}_h\right\|^2$$
$$+ \frac{\mathcal{P}_\Omega^2 C_\kappa^2}{4G}\sum_{k=1}^{N}\left\|\boldsymbol{f}_h^k - \boldsymbol{f}_h^{k-1}\right\|^2. \tag{3.3.29}$$

Therefore, we can write:

$$\sum_{k=1}^{N}\left\|p_h^k - p_h^{k-1}\right\|^2 \leq \frac{\Delta t}{\mu_f\tilde{c}_f}\left\|K^{-1/2}\boldsymbol{z}_h^0\right\|^2 + \frac{1}{\tilde{c}_f^2}\sum_{k=1}^{N}\left\|\tilde{q}_h\right\|^2 + \frac{\mathcal{P}_\Omega^2 C_\kappa^2}{2G\tilde{c}_f}\sum_{k=1}^{N}\left\|\boldsymbol{f}_h^k - \boldsymbol{f}_h^{k-1}\right\|^2, \tag{3.3.30}$$

$$\sum_{k=1}^{N}\left\|\nabla\cdot(\boldsymbol{u}_h^k - \boldsymbol{u}_h^{k-1})\right\|^2 \leq \frac{\Delta t}{2\mu_f\lambda}\left\|K^{-1/2}\boldsymbol{z}_h^0\right\|^2 + \frac{1}{2\tilde{c}_f\lambda}\sum_{k=1}^{N}\left\|\tilde{q}_h\right\|^2 + \frac{\mathcal{P}_\Omega^2 C_\kappa^2}{4G\lambda}\sum_{k=1}^{N}\left\|\boldsymbol{f}_h^k - \boldsymbol{f}_h^{k-1}\right\|^2. \tag{3.3.31}$$

Combining (3.3.30) with (3.3.31), we have:

$$\sum_{k=1}^{N}\left\|p_h^k - p_h^{k-1}\right\|^2 + \sum_{k=1}^{N}\left\|\nabla\cdot(\boldsymbol{u}_h^k - \boldsymbol{u}_h^{k-1})\right\|^2$$
$$\leq \Delta t\tilde{\eta}_3\left\|K^{-1/2}\boldsymbol{z}_h^0\right\|^2 + \tilde{\eta}_4\sum_{k=1}^{N}\left\|\tilde{q}_h\right\|^2 + \tilde{\eta}_5\sum_{k=1}^{N}\left\|\boldsymbol{f}_h^k - \boldsymbol{f}_h^{k-1}\right\|^2 \tag{3.3.32}$$

where $\tilde{\eta}_3 = \frac{1}{\mu_f}C_2$, $\tilde{\eta}_4 = \frac{1}{\tilde{c}_f}C_2$, $\tilde{\eta}_5 = \frac{\mathcal{P}_\Omega^2 C_\kappa^2}{2G}C_2$, and $C_2 = \left(\frac{1}{\tilde{c}_f} + \frac{1}{2\lambda}\right)$. Combining (3.3.23) with (3.3.32), for a generic constant $C_3 > 0$ (which will be revealed by the end of the derivation

but we suppress its value now for the sake of simplicity), we can derive:

$$\begin{aligned}
&\left\|p_h^{n+1,k}-p_h^k\right\|_\Omega^2+\|\boldsymbol{\varepsilon}(\boldsymbol{u}_h^{n+1,k}-\boldsymbol{u}_h^k)\|_\Omega^2+\left\|\boldsymbol{K}^{-1/2}(\boldsymbol{z}_h^{n+1,k}-\boldsymbol{z}_h^k)\right\|_\Omega^2\\
&\qquad\le\left(\frac{\chi}{\beta}\right)^{2(n+1)}\left(\tilde{\eta}_1\left\|p_h^k-p_h^{k-1}\right\|_\Omega^2+\tilde{\eta}_2\left\|\nabla\cdot\boldsymbol{u}_h^k-\boldsymbol{u}_h^{k-1}\right\|_\Omega^2\right)\\
&\qquad\le\left(\frac{\chi}{\beta}\right)^{2(n+1)}C_3\Big[\left\|p_h^k-p_h^{k-1}\right\|_\Omega^2+\left\|\nabla\cdot\boldsymbol{u}_h^k-\boldsymbol{u}_h^{k-1}\right\|_\Omega^2\Big]\\
&\qquad\le\left(\frac{\chi}{\beta}\right)^{2(n+1)}C_3\Big[\sum_{k=1}^{N}\left\|p_h^k-p_h^{k-1}\right\|_\Omega^2+\sum_{k=1}^{N}\left\|\nabla\cdot\boldsymbol{u}_h^k-\boldsymbol{u}_h^{k-1}\right\|_\Omega^2\Big]\\
&\qquad\le\left(\frac{\chi}{\beta}\right)^{2(n+1)}C_3\Big[\Delta t\tilde{\eta}_3\left\|K^{-1/2}\boldsymbol{z}_h^0\right\|^2+\tilde{\eta}_4\sum_{k=1}^{N}\left\|\tilde{q}_h\right\|^2+\tilde{\eta}_5\sum_{k=1}^{N}\left\|\boldsymbol{f}_h^k-\boldsymbol{f}_h^{k-1}\right\|^2\Big]\\
&\qquad\le\left(\frac{\chi}{\beta}\right)^{2(n+1)}C_3\Big[\Delta t\left\|K^{-1/2}\boldsymbol{z}_h^0\right\|^2+\sum_{k=1}^{N}\left\|\tilde{q}_h\right\|^2+\sum_{k=1}^{N}\left\|\boldsymbol{f}_h^k-\boldsymbol{f}_h^{k-1}\right\|^2\Big]
\end{aligned}$$

Therefore, we can write:

$$\begin{aligned}
&\left\|p_h^{n+1,k}-p_h^k\right\|_{L^2(\Omega)}+\|\boldsymbol{\varepsilon}(\boldsymbol{u}_h^{n+1,k}-\boldsymbol{u}_h^k)\|_{L^2(\Omega)}+\left\|\boldsymbol{K}^{-1/2}(\boldsymbol{z}_h^{n+1,k}-\boldsymbol{z}_h^k)\right\|_{L^2(\Omega)}\\
&\qquad\le C_3\Big(\frac{\chi}{\beta}\Big)^{(n+1)}\Big[\Delta t\left\|K^{-1/2}\boldsymbol{z}_h^0\right\|_{L^2(\Omega)}^2+\sum_{k=1}^{N}\left\|\tilde{q}_h\right\|_{L^2(\Omega)}^2+\sum_{k=1}^{N}\left\|\boldsymbol{f}_h^k-\boldsymbol{f}_h^{k-1}\right\|_{L^2(\Omega)}^2\Big]^{1/2}
\end{aligned}\tag{3.3.33}$$

Now, we assume that the permeability tensor $\boldsymbol{K}$ is uniformly bounded and uniformly elliptic. There exits positive constants λ_{min}, and λ_{max}, such that

$$\lambda_{min}\|\xi\|^2\le\xi^t\boldsymbol{K}(x)\xi\le\lambda_{max}\|\xi\|^2.\tag{3.3.34}$$

We can write

$$\|\boldsymbol{K}^{-1/2}(\boldsymbol{z}_h^{n+1,k}-\boldsymbol{z}_h^k)\|_{L^2(\Omega)}\ge\frac{1}{\lambda_{max}^{1/2}}\|\boldsymbol{z}_h^{n+1,k}-\boldsymbol{z}_h^k\|_{L^2(\Omega)}.$$

In addition, by Poincaré's inequality (2.1.1) and Korn's first inequality (2.1.2), we have:

$$\|\boldsymbol{\varepsilon}(\boldsymbol{u}_h^{n+1,k}-\boldsymbol{u}_h^k)\|_{L^2(\Omega)}\ge\frac{1}{\mathcal{P}_\Omega C_\kappa}\|\boldsymbol{u}_h^{n+1,k}-\boldsymbol{u}_h^k\|_{H^1(\Omega)}.$$

Therefore, (3.3.35) can be written as:

$$\begin{aligned}
&\left\|p_h^{n+1,k}-p_h^k\right\|_{L^2(\Omega)}+\left\|\boldsymbol{u}_h^{n+1,k}-\boldsymbol{u}_h^k\right\|_{H^1(\Omega)}+\left\|\boldsymbol{z}_h^{n+1,k}-\boldsymbol{z}_h^k\right\|_{L^2(\Omega)}\\
&\quad\le C_3\Big(\frac{\chi}{\beta}\Big)^{(n+1)}\Big[\Delta t\left\|K^{-1/2}\boldsymbol{z}_h^0\right\|_{L^2(\Omega)}^2+\sum_{k=1}^{N}\left\|\tilde{q}_h\right\|_{L^2(\Omega)}^2+\sum_{k=1}^{N}\left\|\boldsymbol{f}_h^k-\boldsymbol{f}_h^{k-1}\right\|_{L^2(\Omega)}^2\Big]^{1/2}
\end{aligned}\tag{3.3.35}$$

We conclude that for every coupling iteration $n \geq 0$,

$$\begin{aligned}
&\left\|p_h^{n+1,k} - p(t_k)\right\|_{\ell^\infty(L^2)} + \left\|\boldsymbol{u}_h^{n+1,k} - \boldsymbol{u}(t_k)\right\|_{\ell^\infty(H^1)} + \left\|\boldsymbol{z}_h^{n+1,k} - \boldsymbol{z}(t_k)\right\|_{\ell^\infty(L^2)} \\
&\qquad \leq \left\|p_h^{n+1,k} - p_h^k\right\|_{\ell^\infty(L^2)} + \left\|\boldsymbol{u}_h^{n+1,k} - \boldsymbol{u}_h^k\right\|_{\ell^\infty(H^1)} + \left\|\boldsymbol{z}_h^{n+1,k} - \boldsymbol{z}_h^k\right\|_{\ell^\infty(L^2)} \\
&\qquad\qquad + \left\|p_h^k - p(t_k)\right\|_{\ell^\infty(L^2)} + \left\|\boldsymbol{u}_h^k - \boldsymbol{u}(t_k)\right\|_{\ell^\infty(H^1)} + \left\|\boldsymbol{z}_h^k - \boldsymbol{z}(t_k)\right\|_{\ell^\infty(L^2)} \\
&\qquad \leq C_3\Big(\frac{\chi}{\beta}\Big)^{(n+1)}\Big[\Delta t\Big\|K^{-1/2}\boldsymbol{z}_h^0\Big\|_{L^2(\Omega)}^2 + \sum_{k=1}^{N}\Big\|\tilde{q}_h\Big\|_{L^2(\Omega)}^2 + \sum_{k=1}^{N}\Big\|\boldsymbol{f}_h^k - \boldsymbol{f}_h^{k-1}\Big\|_{L^2(\Omega)}^2\Big]^{1/2} \\
&\qquad\qquad + \left\|p_h^k - p(t_k)\right\|_{\ell^\infty(L^2)} + \left\|\boldsymbol{u}_h^k - \boldsymbol{u}(t_k)\right\|_{\ell^\infty(H^1)} + \left\|\boldsymbol{z}_h^k - \boldsymbol{z}(t_k)\right\|_{\ell^2(L^2)}
\end{aligned}$$

3.3.3 Error Estimate Result

By Phillips and Wheeler (2007) [70, 71], we have:

$$\left\|p_h^k - p(t_k)\right\|_{\ell^\infty(L^2)}^2 + \left\|\boldsymbol{u}_h^k - \boldsymbol{u}(t_k)\right\|_{\ell^\infty(H^1)}^2 + \left\|\boldsymbol{z}_h^k - \boldsymbol{z}(t_k)\right\|_{\ell^2(L^2)}^2 \leq C(h^{2r_1+2} + h^{2r_2}) + O(\Delta t^2)$$

for a positive constant $C > 0$ and mesh size h. We note that r_1 denotes the degree of the polynomials used in the mixed space $(Q_h, \boldsymbol{Z}_h)$, and r_2 denotes the degree of the polynomials used in the displacement space $\boldsymbol{V}_h$. In our case, $r_1 = 0$, and $r_2 = 1$. Therefore, our final estimate takes the form:

$$\begin{aligned}
&\left\|p_h^{n+1,k} - p(t_k)\right\|_{\ell^\infty(L^2)} + \left\|\boldsymbol{u}_h^{n+1,k} - \boldsymbol{u}(t_k)\right\|_{\ell^\infty(H^1)} + \left\|\boldsymbol{z}_h^{n+1,k} - \boldsymbol{z}(t_k)\right\|_{\ell^\infty(L^2)} \\
&\quad \leq C_3\Big(\frac{\chi}{\beta}\Big)^{(n+1)}\Big[\Delta t\Big\|K^{-1/2}\boldsymbol{z}_h^0\Big\|_{L^2(\Omega)}^2 + \sum_{k=1}^{N}\Big\|\tilde{q}_h\Big\|_{L^2(\Omega)}^2 + \sum_{k=1}^{N}\Big\|\boldsymbol{f}_h^k - \boldsymbol{f}_h^{k-1}\Big\|_{L^2(\Omega)}^2\Big]^{1/2} \\
&\qquad\qquad + 3\Big(2Ch^2 + O(\Delta t^2)\Big)^{1/2}
\end{aligned}$$

where $C_3 = 3\Big(1 + \mathcal{P}_\Omega C_\kappa + \lambda_{max}^{1/2}\Big)\Big(\mathrm{Max}(\tilde{\eta}_1, \tilde{\eta}_2) \times \mathrm{Max}(\tilde{\eta}_3, \tilde{\eta}_4, \tilde{\eta}_5)\Big)^2$. The above discussions are summarized in the following theorem:

Theorem 3.3.1. *For a particular time step t_k, and a particular flow-mechanics coupling iteration $n \geq 1$, and assuming the lowest order Raviart-Thomas spaces for flow, and continuous piecewise linear approximations for mechanics, and assuming equations* (3.3.16) *and* (3.3.34)*, and sufficient regularity in the true solution, the following finite element error*

estimate, to the leading order in time, for the single rate fixed-stress split iterative coupling scheme holds:

$$\begin{aligned}\Big\|p_h^{n,k}-p(t_k)\Big\|_{\ell^\infty(L^2)}+\Big\|\boldsymbol{u}_h^{n,k}-\boldsymbol{u}(t_k)\Big\|_{\ell^\infty(H^1)}+\Big\|\boldsymbol{z}_h^{n,k}-\boldsymbol{z}(t_k)\Big\|_{\ell^\infty(L^2)}\\ \leq C_1\Big(\tfrac{\chi}{\beta}\Big)^n\Big[\Delta t\Big\|K^{-1/2}\boldsymbol{z}_h^0\Big\|^2_{L^2(\Omega)}+\textstyle\sum_{k=1}^N\Big\|\tilde{q}_h\Big\|^2_{L^2(\Omega)}+\sum_{k=1}^N\Big\|\boldsymbol{f}_h^k-\boldsymbol{f}_h^{k-1}\Big\|^2_{L^2(\Omega)}\Big]^{1/2}\\ +\Big(C_2h^2+O(\Delta t^2)\Big)^{1/2}\end{aligned}$$

where $C_1=3\Big(1+\mathcal{P}_\Omega C_\kappa+\lambda_{max}^{1/2}\Big)\Big(Max(\tilde{\eta}_1,\tilde{\eta}_2)\times Max(\tilde{\eta}_3,\tilde{\eta}_4,\tilde{\eta}_5)\Big)^2$,
and $C_2=C_2(T,\boldsymbol{K},M,c_f,\varphi_0,\mathcal{P}_\Omega,C_\kappa,p_h^k,p_{h,t}^k,\boldsymbol{z}_h^k,\boldsymbol{u}_{h,t}^k)$.

3.4 Error Analysis for the Undrained Split Scheme

In a similar way, we can derive a priori error estimates for the single rate undrained-split iterative coupling scheme, presented in section 2.4 in Chapter 2. In this case, only the first step of the proof (shown in section 3.3.1) needs to be changed. Deriving a Banach contraction estimate on the difference $\|\xi^{n,k}-\xi_h^k\|$ follows similar ideas presented in section 2.4. The second step of the proof present presented in section 3.3.2 remains unchanged, as both the fixed stress split and the undrained split iterative coupling approaches converge to the solution obtained by the simultaneously coupled scheme. Due to space restrictions (in this dissertation), the details are spared.

Deriving a priori error estimates for the multirate coupling schemes is more complicated. We have initial results in that direction under certain assumptions (which require more validation). This will be considered for future work.

Finally, it should be noted that the work involved in this chapter has been presented and published in [10].

Chapter 4

Explicit Coupling Schemes for Poroelastic Media

In this chapter, we consider single rate and multirate explicit schemes for the quasi-static Biot system modeling coupled flow and geomechanics in a poroelastic medium. These schemes are the most widely used in practice that follows a sequential procedure in which the flow and mechanics problems are fully decoupled. In a typical explicit coupling scheme, the flow problem is solved first with time-lagging the displacement term followed by the mechanics solve. The decoupling of the two equations makes it easy to implement and the time marching without any iterations leads to a lower computational cost. The drawback is that this scheme is only conditionally stable. For the single rate scheme, the rigorous stability properties have been investigated in the work of Mikelić and Wheeler [64]. However, in the case when the multiple flow time steps are taken for one mechanics time step, it is unclear how these stability properties change. In this chapter, we focus our attention on the explicit coupling approach, establish its stability theoretically for both fully discrete single rate and multirate schemes, and investigate its computational time savings numerically. More specifically, we will provide fully discrete schemes for both the single rate and multirate approaches that use Backward Euler time discretization, mixed spaces for flow, and conformal Galerkin for mechanics. We perform a rigorous stability analysis and derive the conditions on reservoir parameters and the number of finer flow solves to ensure stability for both schemes. Furthermore, we investigate the computational time savings for explicit coupling schemes against iterative coupling schemes. To the best of our knowledge, this is the first analysis of the multirate explicit coupling scheme for Biot equations.

The theoretical work in this chapter is a collaborative work with Dr. Kundan Kumar, under the supervision of Prof. Mary Wheeler. It has been published as an ICES Report [9], and submitted to the "Computers & Mathematics with Applications" journal. The numerical implementation in IPARS is done primarily by Tameem Almani with helpful discussions with Drs. Kundan Kumar and Gurpreet Singh.

For illustration purposes, figures 4.1a and 4.1b illustrate the differences between single rate versus multirate explicit coupling schemes. Figure 4.1a represents a typical single rate scheme, in which the flow and mechanics problems share the exact same time step. In contrast, Figure 4.1b demonstrates a typical multirate scheme, in which the flow problem takes multiple finer local time steps within one coarser mechanics time step.

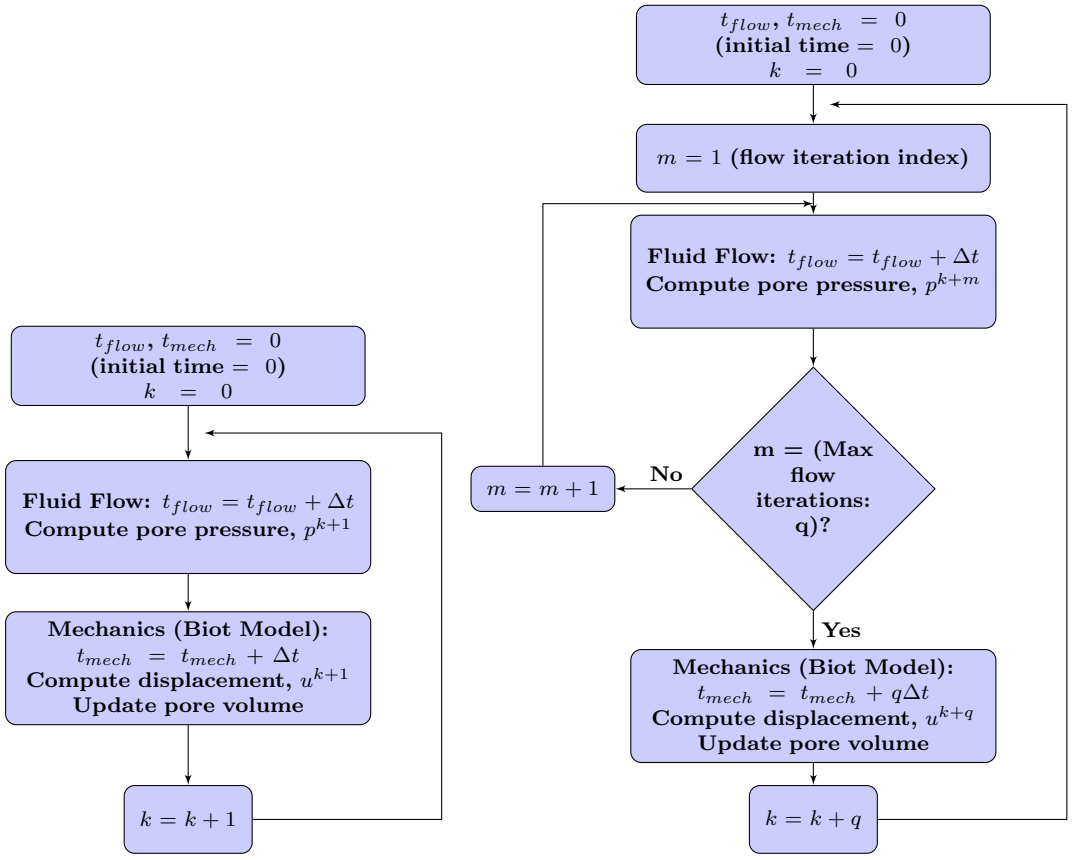

(a) Single Rate (b) Multirate

Figure 4.1: Flowchart for the explicit single rate and multirate time steppings for coupled geomechanics and flow problems

4.1 Model Equations and Discretization

We follow the same model equations and discretization techniques as described in Chapter 2. For this chapter to be self-contained, we briefly discuss the model and its discretizations.

We assume a linear, elastic, homogeneous, and isotropic poro-elastic medium $\Omega \subset \mathbb{R}^d$, $d = 2$ or 3, in which the reservoir is saturated with a slightly compressible fluid.

4.1.1 Assumptions

The fluid is assumed to be slightly compressible and its density is a linear function of pressure, with a constant viscosity $\mu_f > 0$. The reference density of the fluid $\rho_f > 0$, the Lamé coefficients $\lambda > 0$ and $G > 0$, the dimensionless Biot coefficient α, and the pore volume φ^* are all positive. The absolute permeability tensor, $\boldsymbol{K}$, is assumed to be symmetric, bounded, uniformly positive definite in space and constant in time.

A quasi-static Biot model [16, 45] will be employed in this work. The model reads: Find $\boldsymbol{u}$ and p satisfying the equations below for all time $t \in]0, T[$:

Flow Equation:

$$\frac{\partial}{\partial t}\Big((\tfrac{1}{M} + c_f\varphi_0)p + \alpha\nabla\cdot\boldsymbol{u}\Big) - \nabla\cdot\Big(\tfrac{1}{\mu_f}\boldsymbol{K}(\nabla p - \rho_{f,r}g\nabla\eta)\Big) = \tilde{q} \text{ in } \Omega$$

Mechanics Equations:

$$-\mathrm{div}\,\boldsymbol{\sigma}^{\mathrm{por}}(\boldsymbol{u}, p) = \boldsymbol{f} \text{ in } \Omega,$$
$$\boldsymbol{\sigma}^{\mathrm{por}}(\boldsymbol{u}, p) = \boldsymbol{\sigma}(\boldsymbol{u}) - \alpha\, p\, \boldsymbol{I} \text{ in } \Omega,$$
$$\boldsymbol{\sigma}(\boldsymbol{u}) = \lambda(\nabla\cdot\boldsymbol{u})\boldsymbol{I} + 2\,G\boldsymbol{\varepsilon}(\boldsymbol{u}) \text{ in } \Omega$$

Boundary Conditions:

$$\boldsymbol{u} = \boldsymbol{0}\ ,\ \boldsymbol{K}(\nabla p - \rho_{f,r}g\nabla\eta)\cdot\boldsymbol{n} = 0 \text{ on } \partial\Omega$$

Initial Condition $(t = 0)$:

$$\Big((\tfrac{1}{M} + c_f\varphi_0)p + \alpha\nabla\cdot\boldsymbol{u}\Big)(0) = (\tfrac{1}{M} + c_f\varphi_0)p_0 + \alpha\nabla\cdot\boldsymbol{u}_0.$$

where: g is the gravitational constant, η is the distance in the vertical direction (assumed to be constant in time), $\rho_{f,r} > 0$ is a constant reference density (relative to the reference pressure p_r), φ_0 is the initial porosity, M is the Biot constant, $\tilde{q} = \frac{q_s}{\rho_{f,r}}$ where q_s is a mass source or sink term taking into account injection into or out of the reservoir. We remark that the above system is linear and coupled through the Biot coefficient terms.

4.1.2 Mixed Variational Formulation

A mixed finite element formulation for flow and a conformal Galerkin formulation for mechanics will be used. The mixed formulation is a locally mass conservative scheme, and allows for explicit flux computation. The flux is defined as a separate unknown and the flow equation is rewritten as a system of first order equations. Accordingly, for the fully discrete formulation (discrete in time and space), we use a mixed finite element method for space discretization and a backward-Euler time discretization. Let $\mathfrak{T}_h$ denote a regular family of conforming triangular elements of the domain of interest, $\overline{\Omega}$. Using the lowest order Raviart-Thomas (RT) spaces , we have the following discrete spaces ($\boldsymbol{V}_h$ for discrete displacements, Q_h for discrete pressures, and $\boldsymbol{Z}_h$ for discrete velocities (fluxes)):

$$\boldsymbol{V}_h = \{\boldsymbol{v}_h \in H^1(\Omega)^d\,;\, \forall T \in \mathfrak{T}_h, \boldsymbol{v}_{h|T} \in {\mathbb{P}_1}^d, \boldsymbol{v}_{h|\partial\Omega} = \boldsymbol{0}\} \tag{4.1.1}$$

$$Q_h = \{p_h \in L^2(\Omega)\,;\, \forall T \in \mathfrak{T}_h, p_{h|T} \in \mathbb{P}_0\} \tag{4.1.2}$$

$$\boldsymbol{Z}_h = \{\boldsymbol{q}_h \in H(\mathrm{div};\Omega)^d\,;\forall T \in \mathfrak{T}_h, \boldsymbol{q}_{h|T} \in {\mathbb{P}_1}^d,\ \boldsymbol{q}_h \cdot \boldsymbol{n} = 0 \text{ on } \partial\Omega\} \tag{4.1.3}$$

The space of displacements, $\boldsymbol{V}_h$, is equipped with the norm:

$$\|\boldsymbol{v}\|_{V_h} = (\sum_{i=1}^{d} \|v_i\|_{\Omega}^2)^{1/2}.$$

We also assume that the finer time step is given by: $\Delta t = t_k - t_{k-1}$. If we denote the total number of timesteps by N, then the total simulation time is given by T = Δt N, and $t_i = i\Delta t$, $0 \leqslant i \leqslant N$ denote the discrete time points.

For the fully discrete scheme, we have chosen the Raviart-Thomas spaces for the mixed finite element discretization. However, the proof extends to other choices for the mixed spaces, and we will state the results for Multipoint Flux Mixed Finite Element (MFMFE) spaces [90] in Remark 4.3.2.

Remark 4.1.1. Notation: *We adopt the following notations, k denotes the coarser time step iteration index (for indexing mechanics coarse time steps), m is the finer (local) time step iteration index (for indexing flow fine time steps), Δt stands for the unit (finer) time step, and q is the "fixed" number of local flow time steps per coarse mechanics time step.*

4.2 Single Rate Explicit Coupling Formulation and Analysis

4.2.1 Fully Discrete Scheme for Single Rate

As discussed above, using the mixed finite element method in space and the backward Euler finite difference method in time, the weak formulation of the single rate scheme reads as follows.

Definition 4.2.1. *(**flow equation**) Find $p_h^{k+1} \in Q_h$, and $\boldsymbol{z}_h^{k+1} \in \boldsymbol{Z}_h$ such that,*

$$\forall \theta_h \in Q_h, (\frac{1}{M} + c_f\varphi_0)\Big(\frac{p_h^{k+1} - p_h^k}{\Delta t}, \theta_h\Big) + \frac{1}{\mu_f}\Big(\nabla \cdot \boldsymbol{z}_h^{k+1}, \theta_h\Big) + \alpha\Big(\nabla \cdot \frac{\boldsymbol{u}_h^k - \boldsymbol{u}_h^{k-1}}{\Delta t}, \theta_h\Big) = \Big(\tilde{q}_h, \theta_h\Big) \tag{4.2.4}$$

$$\forall \boldsymbol{q}_h \in \boldsymbol{Z}_h, \Big(K^{-1}\boldsymbol{z}_h^{k+1}, \boldsymbol{q}_h\Big) = \Big(p_h^{k+1}, \nabla \cdot \boldsymbol{q}_h\Big) + \Big(\nabla(\rho_{f,r} g\eta), \boldsymbol{q}_h\Big) \tag{4.2.5}$$

Definition 4.2.2. *(**mechanics equation**) Find $\boldsymbol{u}_h^{k+1} \in \boldsymbol{V}_h$ such that,*

$$\forall \boldsymbol{v}_h \in V_h, 2G(\boldsymbol{\varepsilon}(\boldsymbol{u}_h^{k+1}), \boldsymbol{\varepsilon}(\boldsymbol{v}_h)) + \lambda(\nabla \cdot \boldsymbol{u}_h^{k+1}, \nabla \cdot \boldsymbol{v}_h) - \alpha(p_h^{k+1}, \nabla \cdot \boldsymbol{v}_h) = \Big(\boldsymbol{f}_h^{k+1}, \boldsymbol{v}_h\Big) \tag{4.2.6}$$

4.2.2 Single Rate Explicit Coupling Algorithm

We start by analyzing the single-rate explicit coupling algorithm, in which both flow and mechanics share the same time step. To the best of our knowledge, this is the first rigorous mathematical analysis of the fully discrete single-rate explicitly coupled Biot system. In addition, the analysis reveals a more general stability condition compared to the one obtained in [77] by elementary means. The algorithm is given as follows: Note that we begin with $k = 1$ and we require both $\boldsymbol{u}_h^1$ and $\boldsymbol{u}_h^0$ for obtaining p_h^2. In the first step, we use a fully implicit method to solve for $p_h^1, \boldsymbol{u}_h^1$. Alternatively, to keep the problem decoupled, we can use iterative techniques such as fixed stress splitting or undrained splitting [64].

4.2.2.1 Assumptions

For notational convenience, we define

$$\beta = (\frac{1}{M} + c_f\varphi_0).$$

Algorithm 6: Single Rate Explicit Coupling Algorithm

Given initial conditions $\boldsymbol{u}_h^0$ *and* p_h^0*, solve fully implicitly for* $p_h^1, \boldsymbol{u}_h^1$ *satisfying Biot model*

for $k = 1, 2, \ldots$ **do** `/* time step index */`

  First Step: Flow equations

  Given $\boldsymbol{u}_h^k$ *and* $\boldsymbol{u}_h^{k-1}$*:*

    Solve for p_h^{k+1} *and* $\boldsymbol{z}_h^{k+1}$ *satisfying definition 4.2.1*

  Second Step: Mechanics equations

  Given p_h^{k+1} *and,* $\boldsymbol{z}_h^{k+1}$*:*

    Solve for $\boldsymbol{u}_h^{k+1}$ *satisfying definition 4.2.2*

For stability to hold, we assume the following:

$$(\mathbf{A_1}) \quad \beta > \tfrac{\alpha^2}{\lambda}.$$

4.2.2.2 Result

Our results make explicit the dependence of the stability on the difference of the above quantities. we have the following stability result.

Theorem 4.2.1. *[Single rate] Under the Assumption* $\mathbf{A_1}$ *above, the following stability result holds for the single rate explicit coupling scheme for time steps* $t_0 \leq t_k \leq t_J$*:*

$$\frac{\Delta t}{\lambda \mu_f}\Big(\Big\|K^{-1/2}\boldsymbol{z}_h^{J+1}\Big\|^2 + \sum_{k=1}^{J}\Big\|K^{-1/2}(\boldsymbol{z}_h^{k+1} - \boldsymbol{z}_h^k)\Big\|^2\Big) + \frac{2G}{\lambda}\sum_{k=1}^{J}\Big\|\boldsymbol{\varepsilon}(\boldsymbol{u}_h^{k+1} - \boldsymbol{u}_h^k)\Big\|^2$$
$$+ \Big\|\nabla\cdot(\boldsymbol{u}_h^{J+1} - \boldsymbol{u}_h^J)\Big\|^2 \leq C\Delta t + \frac{\Delta t^2}{2\lambda(\beta - \frac{\alpha^2}{\lambda})}\sum_{k=1}^{J}\Big\|\tilde{q}_h\Big\|^2 + \frac{\mathcal{P}_\Omega^2 C_\kappa^2}{2G\lambda}\sum_{k=1}^{J}\Big\|\boldsymbol{f}_h^{k+1} - \boldsymbol{f}_h^k\Big\|^2$$

4.2.3 Stability Analysis

The proof of the above theorem is carried out in three steps by considering the flow equation, the mechanics equation and then combining the two together. Recall that $\beta = \frac{1}{M} + c_f\varphi_0$.

Proof. • **Step 1: Flow equations**

Testing (4.2.4) with $\theta_h = p_h^{k+1} - p_h^k$, we obtain

$$\beta \frac{1}{\Delta t}\left\| p_h^{k+1} - p_h^k \right\|^2 + \frac{1}{\mu_f}\Big(\nabla \cdot \boldsymbol{z}_h^{k+1}, p_h^{k+1} - p_h^k\Big) + \frac{\alpha}{\Delta t}\Big(\nabla \cdot (\boldsymbol{u}_h^k - \boldsymbol{u}_h^{k-1}), p_h^{k+1} - p_h^k\Big) = \Big(\tilde{q}_h, p_h^{k+1} - p_h^k\Big) \tag{4.2.7}$$

Next, we consider the flux equation (4.2.5). Taking the difference of two consecutive time steps $t = t_{k+1}$ and $t = t_k$ and testing with $\boldsymbol{q}_h = \boldsymbol{z}_h^{k+1}$, we obtain:

$$\Big(K^{-1}(\boldsymbol{z}_h^{k+1} - \boldsymbol{z}_h^k), \boldsymbol{z}_h^{k+1}\Big) = \Big(p_h^{k+1} - p_h^k, \nabla \cdot \boldsymbol{z}_h^{k+1}\Big) \tag{4.2.8}$$

Substituting (4.2.8) into (4.2.7), after some algebraic manipulations of the resulting term (using: $a(a-b) = \frac{1}{2}(a^2 - b^2 + (a-b)^2)$), we derive

$$\frac{\beta}{\Delta t}\left\| p_h^{k+1} - p_h^k \right\|^2 + \frac{1}{2\mu_f}\Big(\left\| K^{-1/2}\boldsymbol{z}_h^{k+1} \right\|^2 - \left\| K^{-1/2}\boldsymbol{z}_h^k \right\|^2 + \left\| K^{-1/2}(\boldsymbol{z}_h^{k+1} - \boldsymbol{z}_h^k) \right\|^2\Big) + \frac{\alpha}{\Delta t}\Big(\nabla \cdot \boldsymbol{u}_h^k - \boldsymbol{u}_h^{k-1}, p_h^{k+1} - p_h^k\Big) = \Big(\tilde{q}_h, p_h^{k+1} - p_h^k\Big) \tag{4.2.9}$$

• **Step 2: Elasticity equation**

Considering (4.2.6) for the difference of two consecutive time steps, $t = t_{k+1}$ and $t = t_k$, and testing with $\boldsymbol{v}_h = \frac{\boldsymbol{u}_h^{k+1} - \boldsymbol{u}_h^k}{\Delta t}$, we obtain

$$\frac{2G}{\Delta t}\left\| \boldsymbol{\varepsilon}(\boldsymbol{u}_h^{k+1} - \boldsymbol{u}_h^k) \right\|^2 + \frac{\lambda}{\Delta t}\left\| \nabla \cdot (\boldsymbol{u}_h^{k+1} - \boldsymbol{u}_h^k) \right\|^2 - \frac{\alpha}{\Delta t}\Big(p_h^{k+1} - p_h^k, \nabla \cdot (\boldsymbol{u}_h^{k+1} - \boldsymbol{u}_h^k)\Big) = \frac{1}{\Delta t}\Big(\boldsymbol{f}_h^{k+1} - \boldsymbol{f}_h^k, \boldsymbol{u}_h^{k+1} - \boldsymbol{u}_h^k\Big) \tag{4.2.10}$$

- **Step 3: Combining flow and elasticity equations**

  Combining (4.2.9) with (4.2.10) yields

$$\frac{\beta}{\Delta t}\left\|p_h^{k+1}-p_h^k\right\|^2+\frac{1}{2\mu_f}\left(\left\|K^{-1/2}\boldsymbol{z}_h^{k+1}\right\|^2-\left\|K^{-1/2}\boldsymbol{z}_h^k\right\|^2+\left\|K^{-1/2}(\boldsymbol{z}_h^{k+1}-\boldsymbol{z}_h^k)\right\|^2\right)$$
$$+\frac{2G}{\Delta t}\left\|\boldsymbol{\varepsilon}(\boldsymbol{u}_h^{k+1}-\boldsymbol{u}_h^k)\right\|^2+\frac{\lambda}{\Delta t}\left\|\nabla\cdot(\boldsymbol{u}_h^{k+1}-\boldsymbol{u}_h^k)\right\|^2=\underbrace{-\frac{\alpha}{\Delta t}\left(\nabla\cdot(\boldsymbol{u}_h^k-\boldsymbol{u}_h^{k-1}),p_h^{k+1}-p_h^k\right)}_{R_1}$$
$$+\underbrace{\frac{\alpha}{\Delta t}\left(p_h^{k+1}-p_h^k,\nabla\cdot(\boldsymbol{u}_h^{k+1}-\boldsymbol{u}_h^k)\right)}_{R_2}+\underbrace{\left(\tilde{q}_h,p_h^{k+1}-p_h^k\right)}_{R_3}+\underbrace{\frac{1}{\Delta t}\left(\boldsymbol{f}_h^{k+1}-\boldsymbol{f}_h^k,\boldsymbol{u}_h^{k+1}-\boldsymbol{u}_h^k\right)}_{R_4} \tag{4.2.11}$$

  Denoting by R_1, R_2, R_3, and R_4 the terms on the right hand side, together with Poincaré's, Korn's, and Young's inequalities, we estimate

$$\begin{aligned}
|R_1| &\le \frac{\alpha}{\Delta t}\frac{1}{2\epsilon_1}\left\|\nabla\cdot(\boldsymbol{u}_h^k-\boldsymbol{u}_h^{k-1})\right\|^2+\frac{\alpha}{\Delta t}\frac{\epsilon_1}{2}\left\|p_h^{k+1}-p_h^k\right\|^2\\
|R_2| &\le \frac{\alpha}{2\Delta t\epsilon_2}\left\|\nabla\cdot(\boldsymbol{u}_h^{k+1}-\boldsymbol{u}_h^k)\right\|^2+\frac{\alpha\epsilon_2}{2\Delta t}\left\|p_h^{k+1}-p_h^k\right\|^2\\
|R_3| &\le \frac{1}{2\epsilon_3}\left\|\tilde{q}_h\right\|^2+\frac{\epsilon_3}{2}\left\|p_h^{k+1}-p_h^k\right\|^2\\
|R_4| &\le \frac{1}{2\Delta t\epsilon_4}\left\|\boldsymbol{f}_h^{k+1}-\boldsymbol{f}_h^k\right\|^2+\frac{\epsilon_4}{2\Delta t}\left\|\boldsymbol{u}_h^{k+1}-\boldsymbol{u}_h^k\right\|^2\\
&\le \frac{1}{2\Delta t\epsilon_4}\left\|\boldsymbol{f}_h^{k+1}-\boldsymbol{f}_h^k\right\|^2+\frac{\epsilon_4\mathcal{P}_\Omega^2C_\kappa^2}{2\Delta t}\|\boldsymbol{\varepsilon}(\boldsymbol{u}_h^{k+1}-\boldsymbol{u}_h^k)\|^2.
\end{aligned}$$

  for $\epsilon_1,\epsilon_2,\epsilon_3,$ and $\epsilon_4>0$. Choosing $\epsilon_1=\epsilon_2=\frac{\alpha}{\lambda}$, $\epsilon_3=\frac{2}{\Delta t}(\beta-\frac{\alpha^2}{\lambda})$, $\epsilon_4=\frac{2G}{\mathcal{P}_\Omega^2C_\kappa^2}$ and multiplying (4.2.11) by $\frac{2\Delta t}{\lambda}$, we derive

$$\frac{\Delta t}{\lambda\mu_f}\left(\left\|K^{-1/2}\boldsymbol{z}_h^{k+1}\right\|^2-\left\|K^{-1/2}\boldsymbol{z}_h^k\right\|^2+\left\|K^{-1/2}(\boldsymbol{z}_h^{k+1}-\boldsymbol{z}_h^k)\right\|^2\right)+\frac{2G}{\lambda}\left\|\boldsymbol{\varepsilon}(\boldsymbol{u}_h^{k+1}-\boldsymbol{u}_h^k)\right\|^2$$
$$+\left\|\nabla\cdot(\boldsymbol{u}_h^{k+1}-\boldsymbol{u}_h^k)\right\|^2\le\left\|\nabla\cdot(\boldsymbol{u}_h^k-\boldsymbol{u}_h^{k-1})\right\|^2+\frac{\Delta t^2}{2\beta\lambda-2\alpha^2}\left\|\tilde{q}_h\right\|^2+\frac{\mathcal{P}_\Omega^2C_\kappa^2}{2G\lambda}\left\|\boldsymbol{f}_h^{k+1}-\boldsymbol{f}_h^k\right\|^2 \tag{4.2.12}$$

Summing up (4.2.12) for $1 \leq k \leq J$, for J time steps, with telescopic cancellations, we get:

$$\frac{\Delta t}{\lambda \mu_f}\Big(\Big\|K^{-1/2}\boldsymbol{z}_h^{J+1}\Big\|^2 + \sum_{k=1}^{J}\Big\|K^{-1/2}(\boldsymbol{z}_h^{k+1}-\boldsymbol{z}_h^k)\Big\|^2\Big) + \frac{2G}{\lambda}\sum_{k=1}^{J}\Big\|\boldsymbol{\varepsilon}(\boldsymbol{u}_h^{k+1}-\boldsymbol{u}_h^k)\Big\|^2$$
$$+ \Big\|\nabla\cdot(\boldsymbol{u}_h^{J+1}-\boldsymbol{u}_h^J)\Big\|^2 \leq \Big\|\nabla\cdot(\boldsymbol{u}_h^1-\boldsymbol{u}_h^0)\Big\|^2 + \frac{\Delta t}{\lambda\mu_f}\Big\|K^{-1/2}\boldsymbol{z}_h^1\Big\|^2$$
$$+ \frac{\Delta t^2}{2\lambda(\beta-\frac{\alpha^2}{\lambda})}\sum_{k=1}^{J}\Big\|\tilde{q}_h\Big\|^2 + \frac{\mathcal{P}_\Omega^2 C_\kappa^2}{2G\lambda}\sum_{k=1}^{J}\Big\|\boldsymbol{f}_h^{k+1}-\boldsymbol{f}_h^k\Big\|^2, \tag{4.2.13}$$

Recall that $\boldsymbol{u}_h^1, \boldsymbol{z}_h^1$ have been computed using the fully implicit time discretization. Using standard a priori estimates for the coupled Biot model (refer to equations (3.3.29) and (3.3.31)), we conclude that $\|\nabla\cdot\boldsymbol{u}_h^1 - \nabla\cdot\boldsymbol{u}_h^0\|^2 \leq C\Delta t$ and $\Big\|K^{-1/2}\boldsymbol{z}_h^1\Big\|^2 \leq C$. This completes the derivation.

□

Remark 4.2.1. The above proof also provides a way to devise an explicitly coupled algorithm that is unconditionally stable. For the single rate algorithm, we replace (4.2.4) by the following equation:

(**flow equation**) Find $p_h^{k+1} \in Q_h$ and $\boldsymbol{z}_h^{k+1} \in \boldsymbol{Z}_h$ such that,

$$\forall \theta_h \in Q_h, (\frac{1}{M} + c_f\varphi_0 + \frac{\alpha^2}{\lambda})\Big(\frac{p_h^{k+1}-p_h^k}{\Delta t}, \theta_h\Big) + \frac{1}{\mu_f}\Big(\nabla\cdot\boldsymbol{z}_h^{k+1}, \theta_h\Big) + \alpha\Big(\nabla\cdot\frac{\boldsymbol{u}_h^k-\boldsymbol{u}_h^{k-1}}{\Delta t}, \theta_h\Big)$$
$$= \Big(\tilde{q}_h, \theta_h\Big). \tag{4.2.14}$$

Note that the stabilisation term $\frac{\alpha^2}{\lambda\Delta t}(p_h^{k+1}-p_h^k)$ has been added above in contrast to (4.2.4). The stability result is then obtained with the assumption ($\mathbf{A_1}$) relaxed. The consistence error is expected to be of order $O(\Delta t)$ which is also expected for the scheme. This follows by a very similar procedure as in [46] (the section of time-consistency error).

To see the unconditional stability of the new scheme, consider the analog of (4.2.11) and

proceed as in the previous case,

$$\frac{\beta+\frac{\alpha^2}{\lambda}}{\Delta t}\left\|p_h^{k+1}-p_h^k\right\|^2+\frac{1}{2\mu_f}\left(\left\|K^{-1/2}\boldsymbol{z}_h^{k+1}\right\|^2-\left\|K^{-1/2}\boldsymbol{z}_h^k\right\|^2+\left\|K^{-1/2}(\boldsymbol{z}_h^{k+1}-\boldsymbol{z}_h^k)\right\|^2\right)$$
$$+\frac{2G}{\Delta t}\left\|\boldsymbol{\varepsilon}(\boldsymbol{u}_h^{k+1}-\boldsymbol{u}_h^k)\right\|^2+\frac{\lambda}{\Delta t}\left\|\nabla\cdot(\boldsymbol{u}_h^{k+1}-\boldsymbol{u}_h^k)\right\|^2=\underbrace{-\frac{\alpha}{\Delta t}\left(\nabla\cdot(\boldsymbol{u}_h^k-\boldsymbol{u}_h^{k-1}),p_h^{k+1}-p_h^k\right)}_{R_1}$$
$$+\underbrace{\frac{\alpha}{\Delta t}\left(p_h^{k+1}-p_h^k,\nabla\cdot(\boldsymbol{u}_h^{k+1}-\boldsymbol{u}_h^k)\right)}_{R_2}+\underbrace{\left(\tilde{q}_h,p_h^{k+1}-p_h^k\right)}_{R_3}+\underbrace{\frac{1}{\Delta t}\left(\boldsymbol{f}_h^{k+1}-\boldsymbol{f}_h^k,\boldsymbol{u}_h^{k+1}-\boldsymbol{u}_h^k\right)}_{R_4}. \tag{4.2.15}$$

Denoting by R_1, R_2, R_3, and R_4 the terms on the right hand side, together with Poincaré's, Korn's, and Young's inequalities, we estimate

$$\begin{aligned}
|R_1| &\le \frac{\alpha}{\Delta t}\frac{1}{2\epsilon_1}\left\|\nabla\cdot(\boldsymbol{u}_h^k-\boldsymbol{u}_h^{k-1})\right\|^2+\frac{\alpha}{\Delta t}\frac{\epsilon_1}{2}\left\|p_h^{k+1}-p_h^k\right\|^2\\
|R_2| &\le \frac{\alpha}{2\Delta t\epsilon_2}\left\|\nabla\cdot(\boldsymbol{u}_h^{k+1}-\boldsymbol{u}_h^k)\right\|^2+\frac{\alpha\epsilon_2}{2\Delta t}\left\|p_h^{k+1}-p_h^k\right\|^2\\
|R_3| &\le \frac{1}{2\epsilon_3}\left\|\tilde{q}_h\right\|^2+\frac{\epsilon_3}{2}\left\|p_h^{k+1}-p_h^k\right\|^2\\
|R_4| &\le \frac{1}{2\Delta t\epsilon_4}\left\|\boldsymbol{f}_h^{k+1}-\boldsymbol{f}_h^k\right\|^2+\frac{\epsilon_4}{2\Delta t}\left\|\boldsymbol{u}_h^{k+1}-\boldsymbol{u}_h^k\right\|^2\\
&\le \frac{1}{2\Delta t\epsilon_4}\left\|\boldsymbol{f}_h^{k+1}-\boldsymbol{f}_h^k\right\|^2+\frac{\epsilon_4\mathcal{P}_\Omega^2C_\kappa^2}{2\Delta t}\|\boldsymbol{\varepsilon}(\boldsymbol{u}_h^{k+1}-\boldsymbol{u}_h^k)\|^2.
\end{aligned}$$

for $\epsilon_1,\epsilon_2,$and $\epsilon_4>0$. Choosing $\epsilon_1=\frac{\alpha}{\lambda}$, $\epsilon_2=\frac{\alpha}{\lambda}$, $\epsilon_3=\frac{2\beta}{\Delta t}$, and $\epsilon_4=\frac{2G}{\mathcal{P}_\Omega^2C_\kappa^2}$ and multiplying (4.2.15) by $\frac{2\Delta t}{\lambda}$, we derive

$$\frac{\Delta t}{\lambda\mu_f}\left(\left\|K^{-1/2}\boldsymbol{z}_h^{k+1}\right\|^2-\left\|K^{-1/2}\boldsymbol{z}_h^k\right\|^2+\left\|K^{-1/2}(\boldsymbol{z}_h^{k+1}-\boldsymbol{z}_h^k)\right\|^2\right)+\frac{2G}{\lambda}\left\|\boldsymbol{\varepsilon}(\boldsymbol{u}_h^{k+1}-\boldsymbol{u}_h^k)\right\|^2$$
$$+\left\|\nabla\cdot(\boldsymbol{u}_h^{k+1}-\boldsymbol{u}_h^k)\right\|^2\le\left\|\nabla\cdot(\boldsymbol{u}_h^k-\boldsymbol{u}_h^{k-1})\right\|^2+\frac{\Delta t^2}{2\beta\lambda}\left\|\tilde{q}_h\right\|^2+\frac{\mathcal{P}_\Omega^2C_\kappa^2}{2G\lambda}\left\|\boldsymbol{f}_h^{k+1}-\boldsymbol{f}_h^k\right\|^2 \tag{4.2.16}$$

and rest of the steps proceeds as follows.

4.3 Multirate Explicit Coupling Formulation and Analysis

Recall that in the multirate explicit coupling approach, the flow problem is solved q times (with a finer time step) within a coarser mechanics time step.

4.3.1 Fully Discrete Scheme for Multirate

The weak formulation of the multirate scheme reads as follows.

Definition 4.3.1. *(**flow equation**) For $1 \leq m \leq q$, find $p_h^{m+k} \in Q_h$, and $\boldsymbol{z}_h^{m+k} \in \boldsymbol{Z}_h$ such that,*

$$\forall \theta_h \in Q_h \,, \frac{1}{\Delta t}\Big((\frac{1}{M} + c_f\varphi_0)\Big(p_h^{m+k} - p_h^{m-1+k}\Big), \theta_h\Big) + \frac{1}{\mu_f}(\nabla \cdot \boldsymbol{z}_h^{m+k}, \theta_h) = \\ - \frac{\alpha}{q\Delta t}\Big(\nabla \cdot \Big(\boldsymbol{u}_h^{k} - \boldsymbol{u}_h^{k-q}\Big), \theta_h\Big) + \Big(\tilde{q}_h, \theta_h\Big), \tag{4.3.17}$$

$$\forall \boldsymbol{q}_h \in \boldsymbol{Z}_h \,, \Big(\boldsymbol{K}^{-1}\boldsymbol{z}_h^{m+k}, \boldsymbol{q}_h\Big) = \Big(p_h^{m+k}, \nabla \cdot \boldsymbol{q}_h\Big) + \Big(\rho_{f,r} g \nabla \eta, \boldsymbol{q}_h\Big), \tag{4.3.18}$$

Definition 4.3.2. *(**mechanics equation**) Find $\boldsymbol{u}_h^{k+q} \in \boldsymbol{V}_h$ such that,*

$$\forall \boldsymbol{v}_h \in V_h \,, 2G(\boldsymbol{\varepsilon}(\boldsymbol{u}_h^{k+q}), \boldsymbol{\varepsilon}(\boldsymbol{v}_h)) + \lambda(\nabla \cdot \boldsymbol{u}_h^{k+q}, \nabla \cdot \boldsymbol{v}_h) - \alpha(p_h^{k+q}, \nabla \cdot \boldsymbol{v}_h) = (\boldsymbol{f}_h^{k+q}, \boldsymbol{v}_h). \tag{4.3.19}$$

4.3.2 Multirate Explicit Coupling Algorithm

Algorithm 7: Multirate Explicit Coupling Algorithm

Given initial conditions $\boldsymbol{u}_h^0$ and p_h^0, solve implicitly for $\boldsymbol{u}_h^m, p_h^m, \boldsymbol{z}_h^m, m = 1, 2, \ldots, q$ satisfying fully coupled multirate Biot model

for $k = q, 2q, 3q, ..$ **do** `/* mechanics time step iteration index */`

  First Step: Flow equations

  Given $\boldsymbol{u}_h^k$

  for $m = 1, 2, .., q$ **do** `/* flow finer time steps iteration index */`

    Solve for p_h^{m+k} and $\boldsymbol{z}_h^{m+k}$ satisfying definition 4.3.1

  Second Step: Mechanics equations

  Given p_h^{k+q} and, $\boldsymbol{z}_h^{k+q}$

    Solve for $\boldsymbol{u}_h^{k+q}$ satisfying definition 4.3.2

4.3.2.1 Assumptions

The stability assumption in the multirate case takes the form:

$$(\mathbf{A_q}) \quad \beta > \tfrac{1}{2}(\tfrac{1}{q} + q)\tfrac{\alpha^2}{\lambda} \qquad \text{for} \qquad q \geq 1,$$

where q is the number of flow finer time steps within one coarse mechanics time step.
As in the single rate case, we need to prepare the initial data for starting the time stepping. Accordingly, in the first step of the multirate algorithm (Algorithm 7), for $k = 0$, and $m = 1, 2, \ldots, q$, the initial conditions are computed by solving the coupled Biot system with fully implicit time discretization (with a time step of size Δt for the "q" coupled solves). Alternatively, decoupled iterative schemes [8, 11] such as fixed stress iterative single rate scheme can be used to compute $\boldsymbol{u}_h^m, p_h^m, \boldsymbol{z}_h^m, m = 1, 2, \ldots, q$. Note that if $q = 1$, the multirate condition $(\mathbf{A_q})$ is identical to the single rate condition $(\mathbf{A_1})$. Our main result is the following stability estimate.

Theorem 4.3.1. *[Multirate] Under the assumption* $(\mathbf{A_q})$*, the following stability result holds for the multirate explicit coupling scheme for mechanics time steps* $t_0 \leq t_k \leq t_J$*,* $k = q, 2q, ..$*:*

$$\frac{2G}{\lambda}\sum_{k=q}^{J}\left\|\boldsymbol{\varepsilon}(\boldsymbol{u}_h^{k+q}-\boldsymbol{u}_h^k)\right\|^2+\frac{\Delta t}{\lambda\mu_f}\left(\left\|K^{-1/2}\boldsymbol{z}_h^{J+q}\right\|^2+\sum_{k=q}^{J}\sum_{m=1}^{q}\left\|K^{-1/2}(\boldsymbol{z}_h^{m+k}-\boldsymbol{z}_h^{m-1+k})\right\|^2\right)$$
$$+\left\|\nabla\cdot(\boldsymbol{u}_h^{J+q}-\boldsymbol{u}_h^J)\right\|^2\leq C\Delta t+\frac{q\Delta t^2}{2\lambda\left(\beta-\frac{1}{2}(\frac{1}{q}+q)\frac{\alpha^2}{\lambda}\right)}\sum_{k=q}^{J}\left\|\tilde{q}_h\right\|^2+\frac{\mathcal{P}_\Omega^2C_\kappa^2}{2\lambda G}\sum_{k=q}^{J}\left\|\boldsymbol{f}_h^{k+q}-\boldsymbol{f}_h^k\right\|^2. \tag{4.3.20}$$

4.3.3 Stability Analysis

The proof for the stability analysis follows the same ideas as in the single rate proof, however the use of multiple time steps requires additional estimates. We follow the same principle of estimating the flow equation followed by mechanics equation and then combining the two together to obtain the stability estimates.

Proof. • **Step 1: Flow equations**

Testing (4.3.17) with $\theta_h = p_h^{m+k} - p_h^{m-1+k}$, we get

$$\frac{\beta}{\Delta t}\left\|p_h^{m+k}-p_h^{m-1+k}\right\|^2+\frac{1}{\mu_f}\left(\nabla\cdot\boldsymbol{z}_h^{m+k},p_h^{m+k}-p_h^{m-1+k}\right)$$
$$+\frac{\alpha}{q\Delta t}\left(\nabla\cdot(\boldsymbol{u}_h^k-\boldsymbol{u}_h^{k-q}),p_h^{m+k}-p_h^{m-1+k}\right)=\left(\tilde{q}_h,p_h^{m+k}-p_h^{m-1+k}\right) \tag{4.3.21}$$

In the flux equation (4.3.18), considering the difference for two consecutive finer time steps $t = t_{m+k}$ and $t = t_{m-1+k}$, and testing with $\boldsymbol{q}_h = \boldsymbol{z}_h^{m+k}$, we obtain

$$\Big(K^{-1}(\boldsymbol{z}_h^{m+k} - \boldsymbol{z}_h^{m-1+k}), \boldsymbol{z}_h^{m+k}\Big) = \Big(p_h^{m+k} - p_h^{m-1+k}, \nabla \cdot \boldsymbol{z}_h^{m+k}\Big). \tag{4.3.22}$$

Substituting (4.3.22) into (4.3.21), we derive

$$\begin{aligned}\beta\Big\|p_h^{m+k} - p_h^{m-1+k}\Big\|^2 + \frac{\Delta t}{\mu_f}\Big(K^{-1}(\boldsymbol{z}_h^{m+k} - \boldsymbol{z}_h^{m-1+k}), \boldsymbol{z}_h^{m+k}\Big) \\ = -\frac{\alpha}{q}\Big(\nabla \cdot (\boldsymbol{u}_h^k - \boldsymbol{u}_h^{k-q}), p_h^{m+k} - p_h^{m-1+k}\Big) + \Delta t\Big(\tilde{q}_h, p_h^{m+k} - p_h^{m-1+k}\Big)\end{aligned}$$

Summing across flow finer time steps $1 \le m \le q$, we get (use $a(a-b) = \frac{1}{2}(a^2 - b^2 + (a-b)^2)$ and the telescopic cancellations)

$$\begin{aligned}&\beta \sum_{m=1}^{q} \Big\|p_h^{m+k} - p_h^{m-1+k}\Big\|^2 + \frac{\Delta t}{2\mu_f}\Big(\Big\|K^{-1/2}\boldsymbol{z}_h^{k+q}\Big\|^2 - \Big\|K^{-1/2}\boldsymbol{z}_h^{k}\Big\|^2 \\ &+ \sum_{m=1}^{q} \Big\|K^{-1/2}(\boldsymbol{z}_h^{m+k} - \boldsymbol{z}_h^{m-1+k})\Big\|^2\Big) = -\frac{\alpha}{q}\Big(\nabla \cdot (\boldsymbol{u}_h^k - \boldsymbol{u}_h^{k-q}), \sum_{m=1}^{q}(p_h^{m+k} - p_h^{m-1+k})\Big) \\ &\qquad + \Delta t\Big(\tilde{q}_h, \sum_{m=1}^{q}(p_h^{m+k} - p_h^{m-1+k})\Big)\end{aligned} \tag{4.3.23}$$

- **Step 2: Elasticity equation**

  Considering (4.3.19) for the difference of two consecutive mechanics time steps, $t = t_k$ and $t = t_{k+q}$, and testing with $\boldsymbol{v}_h = \boldsymbol{u}_h^{k+q} - \boldsymbol{u}_h^k$, we obtain

$$\begin{aligned}2G\Big\|\boldsymbol{\varepsilon}(\boldsymbol{u}_h^{k+q} - \boldsymbol{u}_h^k)\Big\|^2 + \lambda\Big\|\nabla \cdot (\boldsymbol{u}_h^{k+q} - \boldsymbol{u}_h^k)\Big\|^2 - \alpha(p_h^{k+q} - p_h^k, \nabla \cdot (\boldsymbol{u}_h^{k+q} - \boldsymbol{u}_h^k)) = \\ \Big(\boldsymbol{f}_h^{k+q} - \boldsymbol{f}_h^k, \boldsymbol{u}_h^{k+q} - \boldsymbol{u}_h^k\Big).\end{aligned} \tag{4.3.24}$$

- **Step 3: Combining flow and elasticity equations**

  Combining (4.3.23) with (4.3.24) gives

$$\begin{aligned}
&\beta \sum_{m=1}^{q} \left\| p_h^{m+k} - p_h^{m-1+k} \right\|^2 + 2G \left\| \boldsymbol{\varepsilon}(\boldsymbol{u}_h^{k+q} - \boldsymbol{u}_h^k) \right\|^2 + \lambda \left\| \nabla \cdot (\boldsymbol{u}_h^{k+q} - \boldsymbol{u}_h^k) \right\|^2 \\
&\quad + \frac{\Delta t}{2\mu_f} \Big(\left\| K^{-1/2} \boldsymbol{z}_h^{k+q} \right\|^2 - \left\| K^{-1/2} \boldsymbol{z}_h^k \right\|^2 + \sum_{m=1}^{q} \left\| K^{-1/2} (\boldsymbol{z}_h^{m+k} - \boldsymbol{z}_h^{m-1+k}) \right\|^2 \Big) \\
&= \underbrace{-\frac{\alpha}{q} \Big(\nabla \cdot (\boldsymbol{u}_h^k - \boldsymbol{u}_h^{k-q}), \sum_{m=1}^{q} (p_h^{m+k} - p_h^{m-1+k}) \Big)}_{R_1} + \underbrace{\Delta t \Big(\tilde{q}_h, \sum_{m=1}^{q} (p_h^{m+k} - p_h^{m-1+k}) \Big)}_{R_2} \\
&+ \underbrace{\alpha (p_h^{k+q} - p_h^k, \nabla \cdot (\boldsymbol{u}_h^{k+q} - \boldsymbol{u}_h^k))}_{R_3} + \underbrace{\Big(\boldsymbol{f}_h^{k+q} - \boldsymbol{f}_h^k, \boldsymbol{u}_h^{k+q} - \boldsymbol{u}_h^k \Big)}_{R_4}.
\end{aligned} \tag{4.3.25}$$

  Denoting by R_1 and R_2 the first two terms on the right hand side, Youngs's and triangle's inequalities give

$$\begin{aligned}
|R_1| &\leq \frac{\alpha}{q} \Big(\frac{\epsilon_1}{2} \sum_{m=1}^{q} \left\| p_h^{m+k} - p_h^{m-1+k} \right\|^2 + \frac{q}{2\epsilon_1} \left\| \nabla \cdot (\boldsymbol{u}_h^k - \boldsymbol{u}_h^{k-q}) \right\|^2 \Big), \\
|R_2| &\leq \Delta t \Big(\frac{\epsilon_2}{2} \sum_{m=1}^{q} \left\| p_h^{m+k} - p_h^{m-1+k} \right\|^2 + \frac{q}{2\epsilon_2} \left\| \tilde{q}_h \right\|^2 \Big)
\end{aligned}$$

  Using the fact that $p_h^{k+q} - p_h^k = \sum_{m=1}^{q} \left(p_h^{m+k} - p_h^{m-1+k} \right)$ together with Young's and triangle's inequalities, the third term on the right hand side of (4.3.25), denoted by R_3, can be written as

$$|R_3| \leq \frac{\alpha \epsilon_3}{2} \sum_{m=1}^{q} \left\| p_h^{m+k} - p_h^{m-1+k} \right\|^2 + \frac{q\alpha}{2\epsilon_3} \left\| \nabla \cdot (\boldsymbol{u}_h^{k+q} - \boldsymbol{u}_h^k) \right\|^2 \tag{4.3.26}$$

  By Poincaré's, Korn's, and Young's inequalities, the last term on the right hand side of (4.3.25), denoted by R_4, can be written as

$$\begin{aligned}
|R_4| &\leq \frac{1}{2\epsilon_4} \left\| \boldsymbol{f}_h^{k+q} - \boldsymbol{f}_h^k \right\|^2 + \frac{\epsilon_4}{2} \left\| \boldsymbol{u}_h^{k+q} - \boldsymbol{u}_h^k \right\|^2 \\
&\leq \frac{1}{2\epsilon_4} \left\| \boldsymbol{f}_h^{k+q} - \boldsymbol{f}_h^k \right\|^2 + \frac{\epsilon_4 \mathcal{P}_\Omega^2 C_\kappa^2}{2} \left\| \boldsymbol{\varepsilon}(\boldsymbol{u}_h^{k+q} - \boldsymbol{u}_h^k) \right\|^2.
\end{aligned}$$

Choosing $\epsilon_1 = \frac{\alpha}{\lambda}$, $\epsilon_2 = \frac{2}{\Delta t}\Big(\beta - \frac{1}{2}(\frac{1}{q}+q)\frac{\alpha^2}{\lambda}\Big)$, $\epsilon_3 = \frac{q\alpha}{\lambda}$, $\epsilon_4 = \frac{2G}{\mathcal{P}_\Omega^2 C_\kappa^2}$, and multiplying by $\frac{2}{\lambda}$ we derive

$$\begin{aligned}\frac{\Delta t}{\lambda\mu_f}\Big(\Big\|K^{-1/2}\boldsymbol{z}_h^{k+q}\Big\|^2 - \Big\|K^{-1/2}\boldsymbol{z}_h^{k}\Big\|^2 + \sum_{m=1}^{q}\Big\|K^{-1/2}(\boldsymbol{z}_h^{m+k} - \boldsymbol{z}_h^{m-1+k})\Big\|^2\Big) \\ + \frac{2G}{\lambda}\Big\|\boldsymbol{\varepsilon}(\boldsymbol{u}_h^{k+q} - \boldsymbol{u}_h^{k})\Big\|^2 + \Big\|\nabla\cdot(\boldsymbol{u}_h^{k+q} - \boldsymbol{u}_h^{k})\Big\|^2 \leq \Big\|\nabla\cdot(\boldsymbol{u}_h^{k} - \boldsymbol{u}_h^{k-q})\Big\|^2 \\ + \frac{q\Delta t^2}{2\lambda\Big(\beta - \frac{1}{2}(\frac{1}{q}+q)\frac{\alpha^2}{\lambda}\Big)}\Big\|\tilde{q}_h\Big\|^2 + \frac{\mathcal{P}_\Omega^2 C_\kappa^2}{2\lambda G}\Big\|\boldsymbol{f}_h^{k+q} - \boldsymbol{f}_h^{k}\Big\|^2. \qquad (4.3.27)\end{aligned}$$

We need to impose the following condition: $\beta - \frac{1}{2}(\frac{1}{q}+q)\frac{\alpha^2}{\lambda} > 0$, which is nothing but the Assumption $\mathbf{A_q}$. Summing up equation (4.3.27) for $q \leq k \leq J$ (k is a multiple of q, that is, $k = q, 2q, ..$), we write

$$\begin{aligned}\frac{2G}{\lambda}\sum_{k=q}^{J}\Big\|\boldsymbol{\varepsilon}(\boldsymbol{u}_h^{k+q} - \boldsymbol{u}_h^{k})\Big\|^2 + \frac{\Delta t}{\lambda\mu_f}\Big(\Big\|K^{-1/2}\boldsymbol{z}_h^{J+q}\Big\|^2 + \sum_{k=q}^{J}\sum_{m=1}^{q}\Big\|K^{-1/2}(\boldsymbol{z}_h^{m+k} - \boldsymbol{z}_h^{m-1+k})\Big\|^2\Big) \\ + \Big\|\nabla\cdot(\boldsymbol{u}_h^{J+q} - \boldsymbol{u}_h^{J})\Big\|^2 \leq \frac{\Delta t}{\lambda\mu_f}\Big\|K^{-1/2}\boldsymbol{z}_h^{q}\Big\|^2 + \Big\|\nabla\cdot(\boldsymbol{u}_h^{q} - \boldsymbol{u}_h^{0})\Big\|^2 \\ + \frac{q\Delta t^2}{2\lambda\Big(\beta - \frac{1}{2}(\frac{1}{q}+q)\frac{\alpha^2}{\lambda}\Big)}\sum_{k=q}^{J}\Big\|\tilde{q}_h\Big\|^2 + \frac{\mathcal{P}_\Omega^2 C_\kappa^2}{2\lambda G}\sum_{k=q}^{J}\Big\|\boldsymbol{f}_h^{k+q} - \boldsymbol{f}_h^{k}\Big\|^2. \qquad (4.3.28)\end{aligned}$$

To estimate the first two terms on the right hand side, we need to obtain a priori estimates for the fully implicit scheme for the multirate Biot. This a priori estimate is obtained by a slight variation of the technique from the single rate scheme and yields $\Big\|\nabla\cdot(\boldsymbol{u}_h^q - \boldsymbol{u}_h^0)\Big\|^2 \leq Cq\Delta t$ and $\Big\|K^{-1/2}\boldsymbol{z}_h^q\Big\| \leq C$. We spare the details of obtaining these a priori estimates (with reference to (3.3.29), we immediately conclude by triangles inequality that $\Big\|\nabla\cdot(\boldsymbol{u}_h^q - \boldsymbol{u}_h^0)\Big\| \leq \sum_{m=0}^{q}\Big\|\nabla\cdot(\boldsymbol{u}_h^{m+1} - \boldsymbol{u}_h^{m})\Big\| \leq q(C\Delta t)^{1/2}$. Squaring both sides gives the desired result for a generic constant C in which one "q" is absorbed in the constant). Putting together, we conclude the result.

□

Remark 4.3.1. As in the single rate case in remark 4.2.1, the multirate case can also be made unconditionally stable by adding a stabilisation term. In the definition 4.3.1, we

modify the flow equation (2.3.33) by adding a stabilisation term $\gamma\frac{\alpha^2}{\lambda\Delta t}(p_h^{m+k} - p_h^{m-1+k})$, where $\gamma = \frac{1}{2}(\frac{1}{q} + q)$. The modified equation reads:

(**flow equation**) For $1 \leq m \leq q$, find $p_h^{m+k} \in Q_h$, and $\boldsymbol{z}_h^{m+k} \in \boldsymbol{Z}_h$ such that,

$$\forall \theta_h \in Q_h\,, \frac{1}{\Delta t}\Big((\frac{1}{M} + c_f\varphi_0 + \frac{\gamma\alpha^2}{\lambda})\Big(p_h^{m+k} - p_h^{m-1+k}\Big), \theta_h\Big) + \frac{1}{\mu_f}(\nabla\cdot\boldsymbol{z}_h^{m+k}, \theta_h) = \\ - \frac{\alpha}{q\Delta t}\Big(\nabla\cdot\Big(\boldsymbol{u}_h^k - \boldsymbol{u}_h^{k-q}\Big), \theta_h\Big) + \Big(\tilde{q}_h, \theta_h\Big). \tag{4.3.29}$$

The proof for the unconditional stability follows the same ideas as in the single rate case and is skipped here.

Remark 4.3.2. For the numerical simulations we will be using the multipoint flux mixed finite element method (MFMFE) [88,90] for the flow discretization. All our obtained results remain valid for this discretization. Indeed, for such a scheme, the stability results (4.3.28) translates to,

$$\frac{\Delta t}{\lambda\mu_f}\Big(K^{-1}\boldsymbol{z}_h^{J+q}, \boldsymbol{z}_h^{J+q}\Big)_Q + \frac{\Delta t}{\lambda\mu_f}\sum_{k=q}^{J}\sum_{m=1}^{q}\Big(K^{-1}(\boldsymbol{z}_h^{m+k} - \boldsymbol{z}_h^{m-1+k}), (\boldsymbol{z}_h^{m+k} - \boldsymbol{z}_h^{m-1+k})\Big)_Q \\ + \frac{2G}{\lambda}\sum_{k=q}^{J}\Big\|\boldsymbol{\varepsilon}(\boldsymbol{u}_h^{k+q} - \boldsymbol{u}_h^k)\Big\|^2 + \Big\|\nabla\cdot(\boldsymbol{u}_h^{J+q} - \boldsymbol{u}_h^J)\Big\|^2 \leq \frac{\Delta t}{\lambda\mu_f}\Big(K^{-1}\boldsymbol{z}_h^q, \boldsymbol{z}_h^q\Big)_Q \tag{4.3.30}$$
$$+ \Big\|\nabla\cdot(\boldsymbol{u}_h^q - \boldsymbol{u}_h^0)\Big\|^2 + \frac{q\Delta t^2}{2\lambda\Big(\beta - \frac{1}{2}(\frac{1}{q} + q)\frac{\alpha^2}{\lambda}\Big)}\sum_{k=q}^{J}\Big\|\tilde{q}_h\Big\|^2 + \frac{\mathcal{P}_\Omega^2 C_\kappa^2}{2\lambda G}\sum_{k=q}^{J}\Big\|\boldsymbol{f}_h^{k+q} - \boldsymbol{f}_h^k\Big\|^2,$$

where $(K^{-1}.,.)_Q$ is the quadrature rule defined in [90] for the MFMFE corresponding spaces. It was shown by Wheeler and Yotov in [90], and then extended to distorted quadrilaterals and hexahedra in [88], that for any $\boldsymbol{z}_h \in \boldsymbol{Z}_h, C_1\|\boldsymbol{z}_h\|^2 \leq (K^{-1}\boldsymbol{z}_h, \boldsymbol{z}_h)_Q \leq C_2\|\boldsymbol{z}_h\|^2$, for a constant $C_1, C_2 > 0$. This immediately leads to a similar stability result. The same argument holds for single rate case.

Remark 4.3.3. The well source/sink term $(\tilde{q}_h)$ can be assumed to be varying with discrete fine/coarse time steps, and all obtained results remain valid.

4.4 Numerical Results

4.4.1 Iterative vs. Explicit Coupling Schemes

In this section, we compare single rate and multirate explicit coupling schemes versus iterative coupling schemes. Both schemes are implemented in the Integrated Parallel Accurate Reservoir Simulator (IPARS) on top of a single-phase flow model coupled with a linear poroelasticity model. The Multipoint Flux Mixed Finite Element Method (MFMFE) is used for flow discretization and Conformal Galerkin is used for elasticity discretization. Mikelić and Wheeler [64] have analyzed different iterative coupling schemes, and have shown that the two often used techniques known as the fixed-stress split and the undrained-split coupling algorithms are unconditionally stable. The numerical computations in [63] show the relative performances of the two methods with fixed stress splitting performing better. In the multirate case the unconditional stability of these two schemes have been studied in Almani, et. al. [8, 11]. For our numerical tests, we consider the iterative fixed-stress coupling algorithm when comparing the efficiency of the iterative coupling schemes versus explicit coupling schemes. Details about the single-phase flow model implementation in IPARS can be found in section 2.5.2.1. We note that in explicit coupling schemes, the fixed-stress regularization terms are not added to the mass balance equation.

4.4.1.1 Brugge Fileld Model

We consider the Brugge field model [82] for comparing the accuracy and efficiency of iterative versus explicit coupling schemes. The model consists of a $9 \times 48 \times 139$ general hexahedral elements capturing the field geometry, with 30 bottom-hole pressure specified wells, 10 of which are injectors at a pressure of 4600 psi, and 20 are producers at a pressure of 1200 psi. Producers are located at a higher elevation compared to injectors. No flow boundary condition is enforced across all external boundaries. For the mechanics model, we apply a mixture of zero displacement and traction boundary conditions. we also include the effects of gravity. Detailed specifications of the input parameters can be found in Table 4.1. We note here that assumptions $(\mathbf{A_1})$ and $(\mathbf{A_q})$ are both satisfied for the single rare and multirate explicit coupling cases ($q = 4$ and 8), respectively.

Total Simulation time:	64.0 days	k_{xx}	Range: (0.002122, 350.1372) md
Finer (Unit) time step:	1.0 days	k_{yy}	Range: (0.022143, 4135.124) md
Number of grids:	60048 grids (9×48×139)	k_{zz}	Range: (0.022493, 4163.053) md
Possion Ratio, ν	0.35	Biot Modulus, M	1.E8 psi
Biot's constant, α	0.9	$\lambda = \frac{E\nu}{(1+\nu)(1-2\nu)}$	4.32E7 psi
Initial porosity, φ_0	Range: (0.054244, 0.260265)	Flow Boundary Conditions:	zero flow B.C.
Fluid viscosity, μ_w	1.0 cp	Mechanics B.C.:	
Initial fluid pressure, p_0	1000.0 psi	"X+" boundary	$\sigma_{xx} = \sigma \cdot n_x = 10,000 psi$
fluid compressibility c_{f_w}:	1.E-6 (1/psi)	"X-" - boundary	$\boldsymbol{u} = 0$, zero displacement
Rock compressibility:	1.E-6 (1/psi)	"Y+" - boundary	$\boldsymbol{u} = 0$, zero displacement
Rock density:	165.44 lb_m/ft^3	"Y-" - boundary	$\sigma_{yy} = \sigma \cdot n_y = 2000 psi$
Initial fluid density, ρ_o	62.34 lb_m/ft^3	"Z+" - boundary	$\boldsymbol{u} = 0$, zero displacement
Young's Modulus (E)	5.0E7 psi	"Z-" - boundary	$\sigma_{zz} = \sigma \cdot n_z = 1000 psi$

Table 4.1: Input Parameters for the Brugge Field Model

% of Reduction in:	$q = 1$	$q = 4$	$q = 8$
CPU run time	62.24%	79.51%	79.75%
Number of flow linear iterations	51.50%	76.88%	77.85%
Number of mechanics linear iterations	54.50%	76.75%	77.72%

Table 4.2: Computational savings of explicit coupling schemes versus iterative coupling schemes for different values of "q" (the number of flow fine time steps within one coarse mechanics time step).

4.4.1.2 Results and Discussion

Figure 4.2a shows the accumulated CPU run time for the single rate case ($q = 1$), and for multirate cases: $q = 4$ and 8, for both iterative and explicit coupling schemes. In general, for a fixed q, explicit coupling schemes are more efficient, compared to their counterpart iterative coupling schemes. This is expected as explicit schemes eliminate any coupling iteration between the two problems. This results in a huge reduction in the total number of flow and mechanics linear iterations for explicit coupling schemes, as shown in Figures 4.2c, and 4.2b respectively. The results obtained show that explicit coupling schemes can reduce the accumulative number of flow linear iterations for the whole simulation run by more than 50.0% compared to iterative coupling schemes. In addition, the accumulative number of mechanics linear iterations is reduced as well when comparing an explicit coupling scheme to an iterative scheme for a fixed value of q. As shown in figure 4.2b, the single rate iterative coupling scheme results in the highest number of total mechanics linear iterations.

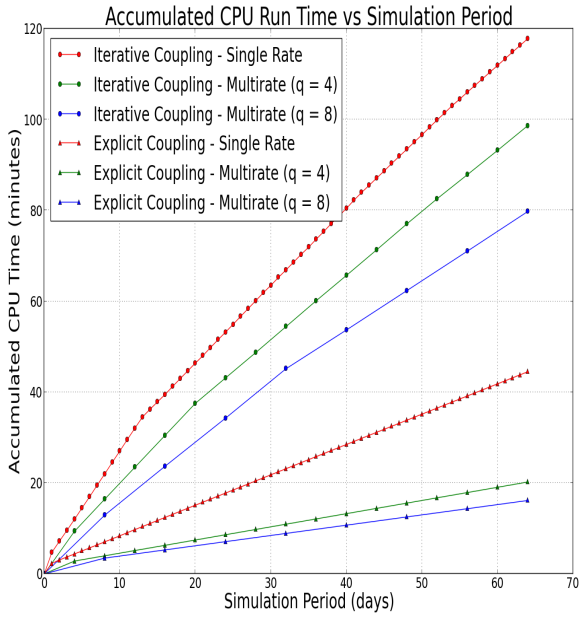

(a) CPU Run Time vs Simulation Days

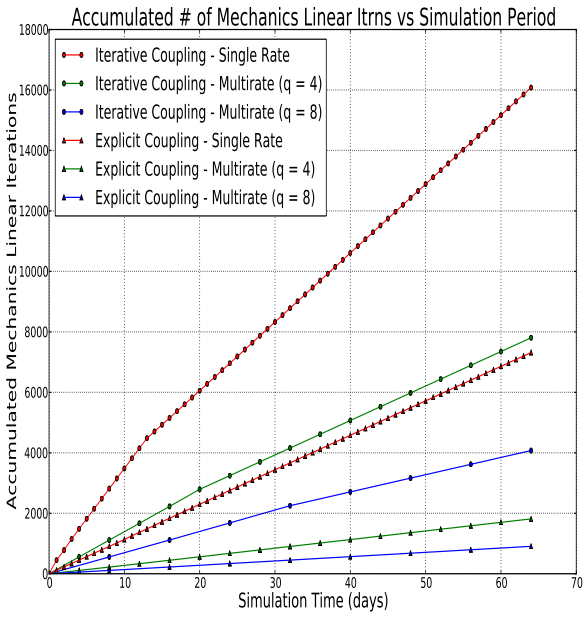

(b) Total Number of Mechanics Linear Iterations vs Simulation Days

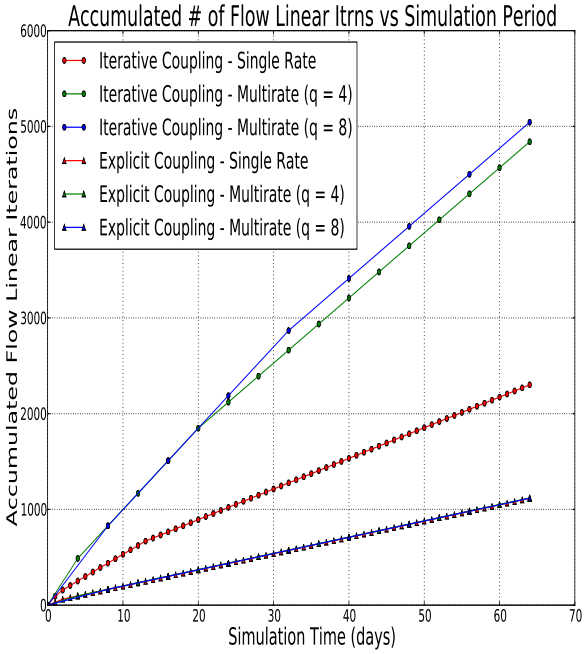

(c) Total Number of Flow Linear Iterations vs Simulation Days

Figure 4.2: Brugge Field Model Numerical Results

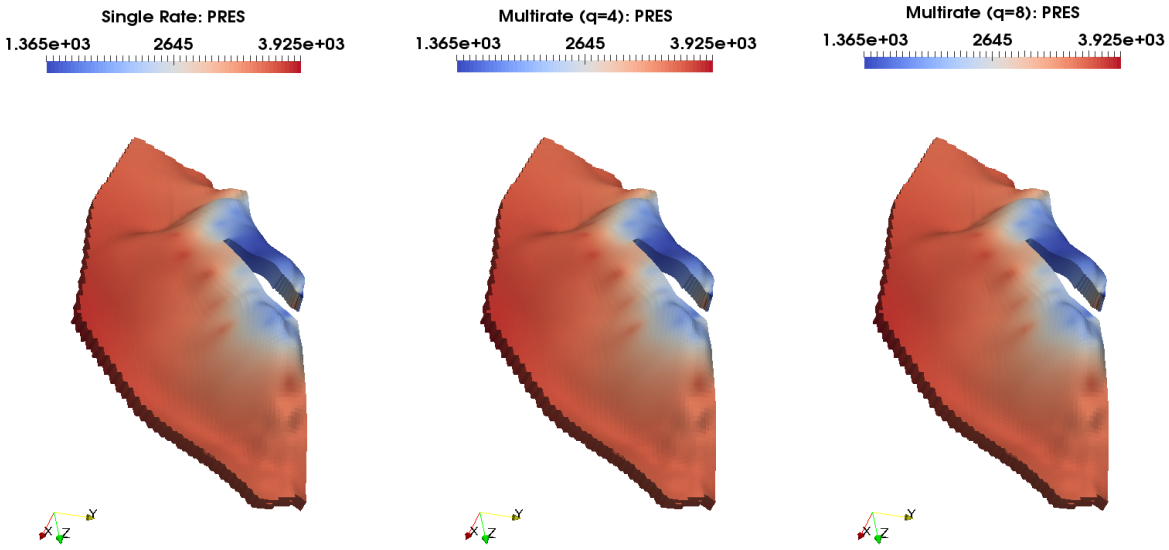

(a) Pressure field at 64.0 days (Iterative Coupling) (psi)

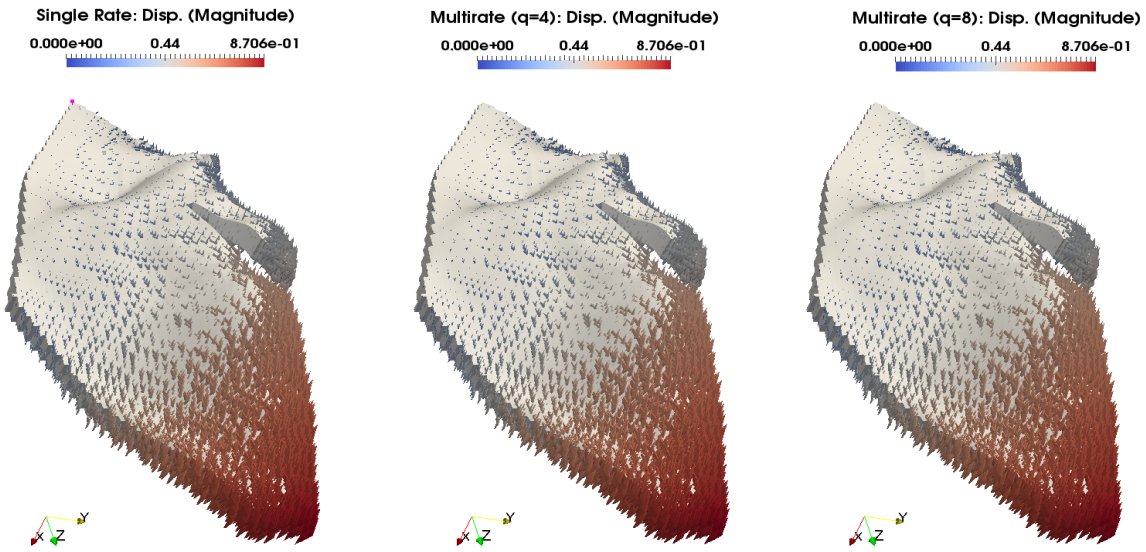

(b) Displacement field at 64.0 days (Iterative Coupling) (ft)

Figure 4.3: Iterative Coupling Pressure and Displacement Fields

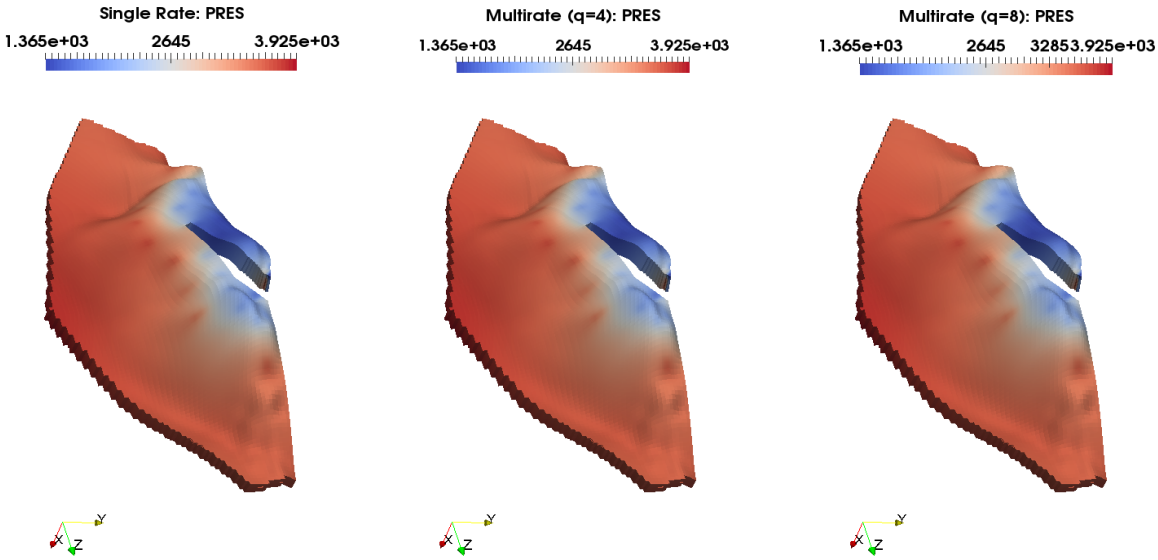

(a) Pressure field at 64.0 days (Explicit Coupling) (psi)

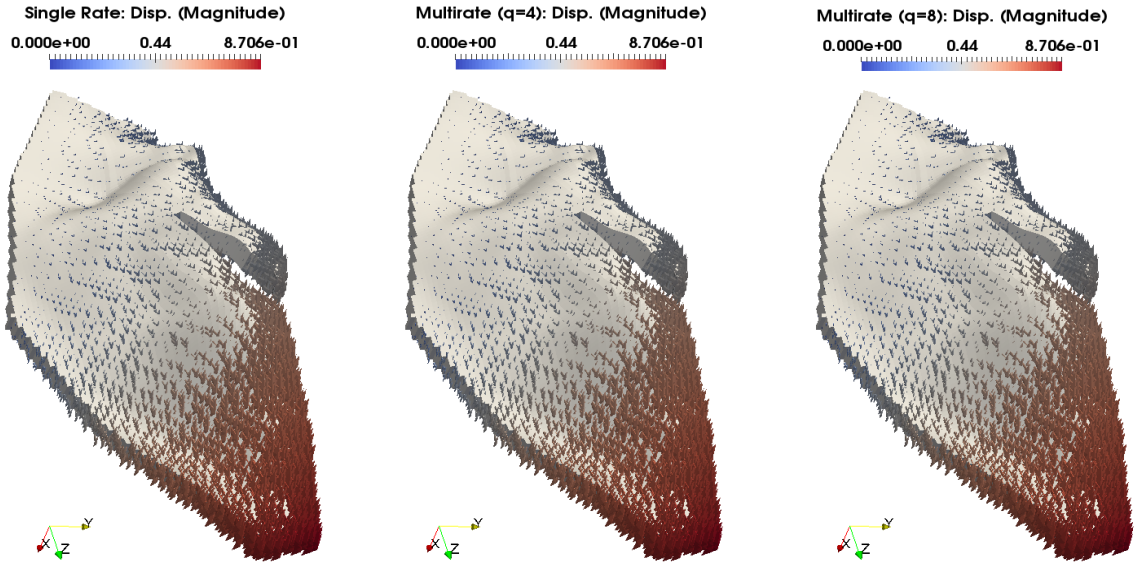

(b) Displacement field at 64.0 days (Explicit Coupling) (ft)

Figure 4.4: Explicit Coupling Pressure and Displacement Fields

In contrast, the multirate explicit coupling scheme ($q = 8$) results in the lowest number of mechanics linear iterations for the whole simulation run. Computational savings of explicit coupling schemes versus iterative coupling schemes are shown in Table 4.2.
Figures 4.3a and 4.3b show the pressure and displacement fields for the iterative coupling scheme after 64.0 days of simulation of the Brugge field case. Figures 4.4a and 4.4b show the corresponding fields for the explicit coupling scheme. The solutions for both the approaches are fairly close with a slight difference between the iterative and explicit coupling being more apparent for pressure fields. The differences in displacement fields for both schemes are negligible.

4.4.2 Validating Theoretical Assumptions

In this section, we try to validate our theoretically induced assumptions for the single rate and multirate explicit coupling schemes against the Frio field model (considered in Chapter 2 earlier). We recall that the Frio field model is an existing oil field located on the Gulf Coast, near Dayton, Texas. It is a field-scale problem with a geometrically challenging geological formation [48]. The field is curved in the depth direction, with several thin curved faults [48]. In this work, we consider the challenging geometry of the field, and its real permeability distribution. Gravity effects are included in this model. Other input specifications are shown in Table 4.3.

4.4.2.1 Results and Discussion

We recall that for the single rate case, the stability assumption is $(\frac{1}{M} + c_f\varphi_0) > \frac{\alpha^2}{\lambda}$ and in the multirate case it reads $(\frac{1}{M} + c_f\varphi_0) > \frac{1}{2}(\frac{1}{q} + q)\,\frac{\alpha^2}{\lambda}$. We consider a particular choice for $q = 2$ and for the parameters shown in Table 4.3, our assumption requires $(\frac{1}{M} + c_f\varphi_0) > (1.06 \times 10^{-5})$. For the numerical test cases, we consider two different compressibility values corresponding to (1) satisfying the stability condition and (2) the stability assumption is violated.

In the first case, we choose $c_f = 1.0 \times 10^{-4}$ (1/psi) satisfying the stability assumption. The pressure profile after 4010 simulation days is shown in figure 4.5a. Resulting pressures lie

Wells:	3 production wells, 6 injection well
Injection well (1):	Pressure specified, 14000.0 psi
Injection well (2):	Pressure specified, 8300.0 psi
Injection well (3):	Pressure specified, 8000.0 psi
Injection well (4):	Pressure specified, 8400.0 psi
Injection well (5):	Pressure specified, 8700.0 psi
Injection well (6):	Pressure specified, 4400.0 psi
Production well (1):	Pressure specified, 2000.0 psi
Production well (2):	Pressure specified, 2000.0 psi
Production well (3):	Pressure specified, 2000.0 psi
Total Simulation time:	4010.0 days
Finer flow (Unit) time step:	1.0 days
Coarse mechanics time step:	2.0 days ($q = 2$)
Number of grids:	891 grids ($33 \times 9 \times 3$)
Permeabilities: k_{xx}, k_{yy}, k_{zz}	highly varying, range: (5.27E-10, 3.10E+3) md
Initial porosity, φ_0:	0.2
Fluid viscosity, μ_f:	1.0 cp
Initial pressure, p_0:	400.0 psi
Fluid compressibilities:	
Case (1), condition is satisfied, c_f:	1.E-4 (1/psi)
Case (2), condition is not satisfied, c_f:	1.E-13 (1/psi)
Case (3), condition is not satisfied, c_f:	1.E-8 (1/psi)
Rock compressibility:	1.E-6 (1/psi)
Rock density:	165.44 lb_m/ft^3
Initial fluid density, ρ_f:	62.34 lb_m/ft^3
Young's Modulus (E):	1.E5 psi
Possion Ratio, ν:	0.3
Biot's constant, α:	0.7
Biot Modulus, M:	1.0E8 psi
$\lambda = \frac{E\nu}{(1+\nu)(1-2\nu)}$:	57692.3 psi
Flow Boundary Conditions:	no flow boundary condition on all 6 boundaries
Mechanics B.C.:	
"X+" boundary (EBCXX1()):	$\sigma_{xx} = \sigma \cdot n_x = 10,000 psi$, (overburden pressure)
"X-" - boundary (EBCXXN1()):	$\boldsymbol{u} = 0$, zero displacement
"Y+" - boundary (EBCYY1()):	$\boldsymbol{u} = 0$, zero displacement
"Y-" - boundary (EBCYYN1()):	$\sigma_{yy} = \sigma \cdot n_y = 2000 psi$
"Z+" - boundary (EBCZZ1()):	$\boldsymbol{u} = 0$, zero displacement
"Z-" - boundary (EBCZZN1()):	$\sigma_{zz} = \sigma \cdot n_z = 1000 psi$

Table 4.3: Input Parameters for the Frio Field Model

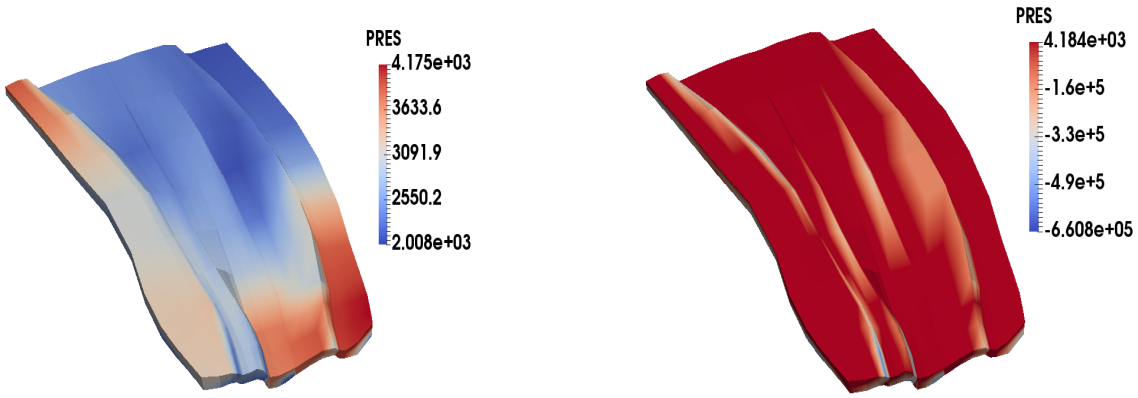

(a) Pressure profile (psi) when the compressibility of the fluid satisfies the derived stability condition ($c_f = 1 \times 10^{-4}(1/psi)$). Results are physically correct, and lie between the expected range of values.

(b) Pressure profile (psi) when the compressibility of the fluid does not satisfy the derived stability condition ($c_f = 1 \times 10^{-8}(1/psi)$). Results are not physically correct, as pressure values drop below zero.

Figure 4.5: Pressure profiles of the multirate explicit coupling scheme ($q = 2$) for the Frio field model.

in the expected range of values, based on wells' injection and production rates specified in table 4.3.

Next, we consider the case when we choose $c_f = 1.0 \times 10^{-13}$ (1/psi), that strongly violates the stability condition. In this case, the coupling iteration did not converge, as a result of producing extremely high pressure values (in magnitudes), and that, in turn, triggered the pore-volume values of grid blocks to exceed their corresponding bulk-volume values, which is physically meaningless. To further test the effect of compressibility, we increase the compressibility and choose ($c_f = 1.0 \times 10^{-8}$ (1/psi), still violating the stability condition). In this case, the pressure profile after 4010 simulation days is shown in figure 4.5b. It is clear from the figure that the pressure profile is unphysical since pressure values drop below zero. Given the values of the initial pressure, and wells' injection and production rates specified in table 4.3, this is a non-physical solution.

4.5 Conclusions

In this chapter, we considered single rate and multirate explicit coupling schemes for coupling flow with geomechanics in poro-elastic media. We derived stability criteria for both multirate and single rate schemes and derived the assumptions on reservoir parameters for the stability to hold. In addition, we perform the numerical experiments where we compare the time savings in the explicit coupling schemes compared to the iterative fixed stress schemes. The multirate iterative schemes have been proven to be geometrically convergent. Our computational results show that, if the parameters satisfy the stability condition, the explicit coupling schemes reduce CPU run time efficiently as compared to the iterative coupling schemes.

Chapter 5

Localized Banach Contraction Estimates for Heterogeneous Poroelastic Media

In this chapter, we consider iterative coupling schemes for spatially and temporally heterogeneous poroelastic media. All our previously established Banach contraction estimates are valid for temporally heterogenous poroelastic media (as the analysis was done for one coarse mechanics time step only, and thus parameters can change across different coarse mechanics time steps). However, we assumed spatially homogeneous flow and mechanics parameters for the whole domain of consideration (or at least some degree of uniformity should be imposed, see remark 5.4.2). Although this is a nice theoretical assumption, it is not realistically true, especially for fluid parameters. This chapter tries to bridge this gap by assuming (spatially and temporally) heterogeneous flow and mechanics parameters.

Due to space restrictions (in this dissertation), we will consider only single rate and multi-rate fixed-stress split iterative coupling schemes for the quasi-static Biot model. However, our proof outlines a general strategy that is very likely to be useful for obtaining similar localized estimates for other iterative and explicit coupling schemes.

5.1 Model Equations and Discretization

We assume a linear, elastic, heterogeneous, and isotropic poro-elastic medium in which the reservoir is saturated with a slightly compressible fluid. We follow exactly the same quasi-static Biot model [16,45] described in section 2.2 in Chapter 2, except that the parameters $\boldsymbol{K}, \alpha, G, M, \lambda, c_f, \mu_f$ and φ_0 can vary spatially (when discretized). Moreover, the same assumptions listed in 2.2.1 apply here (except for the homogenous medium assumption). Furthermore, we will follow the same mixed variational formulation described in section

2.2.4 in Chapter 2.

For our spatial discretization, we assume the following:

- The spatial domain is denoted by $\Omega \subset \mathbb{R}^d$, $d = 1$, 2, or 3. Its external boundary is denoted by $\partial\Omega$, with an outward unit normal vector $\boldsymbol{n}$.
- The spatial domain is discretized into N_Ω conforming grid elements E_i such that: $\overline{\Omega} = \bigcup_{i=1}^{N_\Omega} E_i$.
- Each grid element E_i has its own, independent, set of flow and mechanics parameters: $\boldsymbol{K}_i, \alpha_i, G_i, M_i, \lambda_i, c_{f_i}, \mu_{f_i}$ and φ_{0i}. Moreover, we assume that the localized permeabilities $\boldsymbol{K}_i$ include viscosities μ_{f_i} (i.e. $\boldsymbol{K}_i = \frac{\boldsymbol{K}_i}{\mu_{f_i}}$).
- The outward normal vector for each grid element E_i is denoted by $\boldsymbol{n}_i$. In addition, for two adjacent grid elements E_i and E_{i-1} sharing a common boundary interface, $\boldsymbol{n}_i = -\boldsymbol{n}_{i-1}$ across the common boundary.

5.2 Localized Single Rate Formulation and Analysis

5.2.1 Continuous in Space Global Weak Formulation

Step (a): Find $p^{n+1,k} \in H^1(\Omega)$, $\boldsymbol{z}^{n+1,k} \in H(\mathrm{div};\Omega)^d \cap \{\boldsymbol{z}^{n+1,k} \cdot n = 0 \text{ on } \partial\Omega\}$ such that:

$$\forall \theta \in L^2(\Omega)\,, \sum_{i=1}^{N_\Omega} \Big((\frac{1}{M_i} + c_{f_i}\varphi_{0i} + L_i)(\frac{p^{n+1,k} - p^{k-1}}{\Delta t}), \theta \Big)_{E_i} + \sum_{i=1}^{N_\Omega} (\nabla \cdot \boldsymbol{z}^{n+1,k}, \theta)_{E_i}$$
$$= \sum_{i=1}^{N_\Omega} \Big(L_i(\frac{p^{n,k} - p^{k-1}}{\Delta t}) - \alpha_i \nabla \cdot (\frac{\boldsymbol{u}^{n,k} - \boldsymbol{u}^{k-1}}{\Delta t}), \theta \Big)_{E_i} + \sum_{i=1}^{N_\Omega} (\tilde{q}, \theta)_{E_i} \tag{5.2.1}$$

$$\forall \boldsymbol{q} \in H(\mathrm{div};\Omega)^d \cap \{\boldsymbol{q} \cdot n = 0 \text{ on } \partial\Omega\}\,,$$
$$\sum_{i=1}^{N_\Omega} (\boldsymbol{K}_i^{-1} \boldsymbol{z}^{n+1,k}, \boldsymbol{q})_{E_i} = \sum_{i=1}^{N_\Omega} (p^{n+1,k}, \nabla \cdot \boldsymbol{q})_{E_i} - \sum_{i=1}^{N_\Omega} \langle p^{n+1,k}, \boldsymbol{q} \cdot \boldsymbol{n} \rangle_{\partial E_i} + \sum_{i=1}^{N_\Omega} (\nabla(\rho_{f,r} g \eta), \boldsymbol{q})_{E_i} \tag{5.2.2}$$

Step (b): Given $p^{n+1,k}, \boldsymbol{z}^{n+1,k}$, find $\boldsymbol{u}^{n+1,k} \in H^1(\Omega)^d \cap \{\boldsymbol{u} = 0 \text{ on } \partial\Omega\}$ such that,

$$\forall \boldsymbol{v} \in H^1(\Omega)^d \cap \{\boldsymbol{v} = 0 \text{ on } \partial\Omega\}, \sum_{i=1}^{N_\Omega} 2(G_i \boldsymbol{\varepsilon}(\boldsymbol{u}^{n+1,k}), \boldsymbol{\varepsilon}(\boldsymbol{v}))_{E_i} + \sum_{i=1}^{N_\Omega} (\lambda_i \nabla \cdot \boldsymbol{u}^{n+1,k}, \nabla \cdot \boldsymbol{v})_{E_i}$$
$$- \sum_{i=1}^{N_\Omega} (\alpha_i p^{n+1,k}, \nabla \cdot \boldsymbol{v})_{E_i} - \sum_{i=1}^{N_\Omega} \langle \boldsymbol{\sigma}(\boldsymbol{u}^{n+1,k})\boldsymbol{n}, \boldsymbol{v} \rangle_{\partial E_i} + \sum_{i=1}^{N_\Omega} \langle \alpha_i p^{n+1,k} \underline{\underline{\boldsymbol{I}}} \boldsymbol{n}, \boldsymbol{v} \rangle_{\partial E_i} = \sum_{i=1}^{N_\Omega} (\boldsymbol{f}, \boldsymbol{v})_{E_i} \tag{5.2.3}$$

We note that at the continuum level, the Cauchy stress tensor, given by $\boldsymbol{\sigma}^{por}(\boldsymbol{u}, p) = \boldsymbol{\sigma}(\boldsymbol{u}) - \alpha p \underline{\underline{\boldsymbol{I}}}$, is continuous at grid boundaries. Thus, the boundary terms in equation (5.2.3) can be grouped as:

$$- \sum_{i=1}^{N_\Omega} \langle \boldsymbol{\sigma}(\boldsymbol{u}^{n+1,k})\boldsymbol{n}, \boldsymbol{v} \rangle_{\partial E_i} + \sum_{i=1}^{N_\Omega} \langle \alpha_i p^{n+1,k} \underline{\underline{\boldsymbol{I}}} \boldsymbol{n}, \boldsymbol{v} \rangle_{\partial E_i} = - \sum_{i=1}^{N_\Omega} \langle \boldsymbol{\sigma}^{por}(\boldsymbol{u}^{n+1,k})\boldsymbol{n}, \boldsymbol{v} \rangle_{\partial E_i} = 0$$

due to the continuity of $\boldsymbol{\sigma}^{por}$ at grid boundaries and the fact that the normal vector has a different sign in each two adjacent grid elements sharing a common boundary. For the outer boundary, we require that $\boldsymbol{v} = 0$ on $\partial\Omega$.

The boundary term in the flux equation (5.2.2) also vanishes due to similar reasons. The pressure unknown is assumed to be continuous at the continuum level (otherwize ∇p is not defined). In addition, $\boldsymbol{q} \cdot \boldsymbol{n}$ is continuous across element boundaries, as $\boldsymbol{q} \in H(\text{div}; \Omega)^d$. This results in cancelling all inner boundary terms in equation (5.2.2). For outer boundary terms, we restricted the test space such that $\boldsymbol{q} \cdot \boldsymbol{n} = 0$ on $\partial\Omega$. Therefore, we have:

$$\sum_{i=1}^{N_\Omega} \langle p^{n+1,k}, \boldsymbol{q} \cdot \boldsymbol{n} \rangle_{\partial E_i} = 0.$$

The weak formulation now reads:

Step (a): Find $p^{n+1,k} \in H^1(\Omega)$, $\boldsymbol{z}^{n+1,k} \in H(\mathrm{div};\Omega)^d \cap \{\boldsymbol{z}^{n+1,k} \cdot n = 0 \text{ on } \partial\Omega\}$ such that:

$$\forall \theta \in L^2(\Omega)\,, \sum_{i=1}^{N_\Omega} \Big((\frac{1}{M_i} + c_{f_i}\varphi_{0i} + L_i)(\frac{p^{n+1,k} - p^{k-1}}{\Delta t}), \theta \Big)_{E_i} + \sum_{i=1}^{N_\Omega} (\nabla \cdot \boldsymbol{z}^{n+1,k}, \theta)_{E_i}$$
$$= \sum_{i=1}^{N_\Omega} \Big(L_i(\frac{p^{n,k} - p^{k-1}}{\Delta t}) - \alpha_i \nabla \cdot (\frac{\boldsymbol{u}^{n,k} - \boldsymbol{u}^{k-1}}{\Delta t}), \theta \Big)_{E_i} + \sum_{i=1}^{N_\Omega} (\tilde{q}, \theta)_{E_i} \tag{5.2.4}$$

$$\forall \boldsymbol{q} \in H(\mathrm{div};\Omega)^d \cap \{\boldsymbol{q} \cdot n = 0 \text{ on } \partial\Omega\}\,,$$
$$\sum_{i=1}^{N_\Omega} (\boldsymbol{K}_i^{-1} \boldsymbol{z}^{n+1,k}, \boldsymbol{q})_{E_i} = \sum_{i=1}^{N_\Omega} (p^{n+1,k}, \nabla \cdot \boldsymbol{q})_{E_i} + \sum_{i=1}^{N_\Omega} (\nabla(\rho_{f,r} g \eta), \boldsymbol{q})_{E_i} \tag{5.2.5}$$

Step (b): Given $p^{n+1,k}, \boldsymbol{z}^{n+1,k}$, find $\boldsymbol{u}^{n+1,k} \in H^1(\Omega)^d \cap \{\boldsymbol{u} = 0 \text{ on } \partial\Omega\}$ such that,

$$\forall \boldsymbol{v} \in H^1(\Omega)^d \cap \{\boldsymbol{v} = 0 \text{ on } \partial\Omega\}\,,$$
$$\sum_{i=1}^{N_\Omega} 2(G_i \boldsymbol{\varepsilon}(\boldsymbol{u}^{n+1,k}), \boldsymbol{\varepsilon}(\boldsymbol{v}))_{E_i} + \sum_{i=1}^{N_\Omega} (\lambda_i \nabla \cdot \boldsymbol{u}^{n+1,k}, \nabla \cdot \boldsymbol{v})_{E_i} - \sum_{i=1}^{N_\Omega} (\alpha_i p^{n+1,k}, \nabla \cdot \boldsymbol{v})_{E_i} = \sum_{i=1}^{N_\Omega} (\boldsymbol{f}, \boldsymbol{v})_{E_i} \tag{5.2.6}$$

5.2.2 Fully Discrete Weak formulation

Now, we mimic the spatially continuous weak formulation ((5.2.4), (5.2.5), and (5.2.6)) to obtain the fully discrete formulation (discrete in time and space). We recall that a mixed formulation will be used for flow, and continuous Galerkin will be used for mechanics. A Backward-Euler scheme will be used for temporal discretization. Using the lowest order RT (Raviart and Thomas, 1977) spaces, we have the following discrete spaces:

$$\begin{aligned}
\textit{Displacement} \qquad & \boldsymbol{V}_h = \{\boldsymbol{v}_h \in H^1(\Omega)^d\,;\, \forall E \in \mathfrak{T}_h, \boldsymbol{v}_{h|E} \in {\mathbb{P}_1}^d, \boldsymbol{v}_{h|\partial\Omega} = \boldsymbol{0}\} \\
\textit{Pressue} \qquad & Q_h = \{p_h \in L^2(\Omega)\,;\, \forall E \in \mathfrak{T}_h, p_{h|E} \in \mathbb{P}_0\} \\
\textit{Flux} \qquad & \boldsymbol{Z}_h = \{\boldsymbol{q}_h \in H(\mathrm{div};\Omega)^d\,; \forall E \in \mathfrak{T}_h, \boldsymbol{q}_{h|E} \in {\mathbb{P}_1}^d,\ \boldsymbol{q}_h \cdot \boldsymbol{n} = 0 \text{ on } \partial\Omega\}
\end{aligned}$$

Moreover, we assume no flow boundary conditions for the outer boundary, and zero displacement boundary conditions for mechanics.

The fully-discrete weak formulation now reads:

Step (a): Find $p_h^{n+1,k} \in Q_h$, $\boldsymbol{z}_h^{n+1,k} \in \boldsymbol{Z}_h$ such that:

$$\forall \theta_h \in Q_h \,,\, \sum_{i=1}^{N_\Omega} \Big((\frac{1}{M_i} + c_{f_i}\varphi_{0i} + L_i)(\frac{p_h^{n+1,k} - p_h^{k-1}}{\Delta t}), \theta_h \Big)_{E_i} + \sum_{i=1}^{N_\Omega} (\nabla \cdot \boldsymbol{z}_h^{n+1,k}, \theta_h)_{E_i}$$
$$= \sum_{i=1}^{N_\Omega} \Big(L_i(\frac{p_h^{n,k} - p_h^{k-1}}{\Delta t}) - \alpha_i \nabla \cdot (\frac{\boldsymbol{u}_h^{n,k} - \boldsymbol{u}_h^{k-1}}{\Delta t}), \theta_h \Big)_{E_i} + \sum_{i=1}^{N_\Omega} (\tilde{q}, \theta_h)_{E_i} \tag{5.2.7}$$

$$\forall \boldsymbol{q}_h \in \boldsymbol{Z}_h \,,\, \sum_{i=1}^{N_\Omega} (\boldsymbol{K}_i^{-1} \boldsymbol{z}_h^{n+1,k}, \boldsymbol{q}_h)_{E_i} = \sum_{i=1}^{N_\Omega} (p_h^{n+1,k}, \nabla \cdot \boldsymbol{q}_h)_{E_i} + \sum_{i=1}^{N_\Omega} (\nabla(\rho_{f,r} g \eta), \boldsymbol{q}_h)_{E_i} \tag{5.2.8}$$

Step (b): Given $p_h^{n+1,k}, \boldsymbol{z}_h^{n+1,k}$, find $\boldsymbol{u}_h^{n+1,k} \in \boldsymbol{V}_h$ such that,

$$\forall \boldsymbol{v}_h \in \boldsymbol{V}_h \,,\, \sum_{i=1}^{N_\Omega} 2(G_i \boldsymbol{\varepsilon}(\boldsymbol{u}_h{}^{n+1,k}), \boldsymbol{\varepsilon}(\boldsymbol{v}_h))_{E_i} + \sum_{i=1}^{N_\Omega} (\lambda_i \nabla \cdot \boldsymbol{u}_h^{n+1,k}, \nabla \cdot \boldsymbol{v}_h)_{E_i}$$
$$- \sum_{i=1}^{N_\Omega} (\alpha_i p_h^{n+1,k}, \nabla \cdot \boldsymbol{v}_h)_{E_i} = \sum_{i=1}^{N_\Omega} (\boldsymbol{f}, \boldsymbol{v}_h)_{E_i} \tag{5.2.9}$$

In terms of differences between coupling iterations, equations (5.2.7), (5.2.8), and (5.2.9) read:

$$\forall \theta_h \in Q_h \,,\, \frac{1}{\Delta t} \sum_{i=1}^{N_\Omega} \Big((\frac{1}{M_i} + c_{f_i}\varphi_{0i} + L_i) \delta p_h^{n+1,k}, \theta_h \Big)_{E_i} + \sum_{i=1}^{N_\Omega} (\nabla \cdot \delta \boldsymbol{z}_h^{n+1,k}, \theta_h)_{E_i}$$
$$= \frac{1}{\Delta t} \sum_{i=1}^{N_\Omega} \Big(L_i \delta p_h^{n,k} - \alpha_i \nabla \cdot \delta \boldsymbol{u}_h^{n,k}, \theta_h \Big)_{E_i} \tag{5.2.10}$$

$$\forall \boldsymbol{q}_h \in \boldsymbol{Z}_h \,,\, \sum_{i=1}^{N_\Omega} (\boldsymbol{K}_i^{-1} \delta \boldsymbol{z}_h^{n+1,k}, \boldsymbol{q}_h)_{E_i} = \sum_{i=1}^{N_\Omega} (\delta p_h^{n+1,k}, \nabla \cdot \boldsymbol{q}_h)_{E_i} \tag{5.2.11}$$

$$\forall \boldsymbol{v}_h \in \boldsymbol{V}_h \,,\, \sum_{i=1}^{N_\Omega} 2(G_i \boldsymbol{\varepsilon}(\delta \boldsymbol{u}_h{}^{n+1,k}), \boldsymbol{\varepsilon}(\boldsymbol{v}_h))_{E_i} + \sum_{i=1}^{N_\Omega} (\lambda_i \nabla \cdot \delta \boldsymbol{u}_h^{n+1,k}, \nabla \cdot \boldsymbol{v}_h)_{E_i}$$
$$- \sum_{i=1}^{N_\Omega} (\alpha_i \delta p_h^{n+1,k}, \nabla \cdot \boldsymbol{v}_h)_{E_i} = 0 \tag{5.2.12}$$

5.2.3 Proof of Contraction

For each grid element E_i, let $\beta_i = \frac{1}{M_i} + c_{f_i}\varphi_{0i} + L_i$, testing (5.2.10) with $\theta_h = \delta p_h^{n+1,k}$, and multiplying by Δt, we obtain:

$$\sum_{i=1}^{N_\Omega} \left\| \beta_i^{1/2} \delta p_h^{n+1,k} \right\|_{E_i}^2 + \Delta t \sum_{i=1}^{N_\Omega} (\nabla \cdot \delta \boldsymbol{z}_h^{n+1,k}, \delta p_h^{n+1,k})_{E_i} = \sum_{i=1}^{N_\Omega} \left(L_i \delta p_h^{n,k} - \alpha_i \nabla \cdot \delta \boldsymbol{u}_h^{n,k}, \delta p_h^{n+1,k} \right)_{E_i}. \tag{5.2.13}$$

Testing (5.2.11) with $\boldsymbol{q}_h = \delta \boldsymbol{z}_h^{n+1,k}$, we obtain:

$$\sum_{i=1}^{N_\Omega} \left(\boldsymbol{K}_i^{-1} \delta \boldsymbol{z}_h^{n+1,k}, \delta \boldsymbol{z}_h^{n+1,k} \right)_{E_i} = \sum_{i=1}^{N_\Omega} \left(\delta p_h^{n+1,k}, \nabla \cdot \delta \boldsymbol{z}_h^{n+1,k} \right)_{E_i}. \tag{5.2.14}$$

Substituting (5.2.14) into (5.2.13), together with Young's inequality, we obtain:

$$\sum_{i=1}^{N_\Omega} \left\| \beta_i^{1/2} \delta p_h^{n+1,k} \right\|_{E_i}^2 + \Delta t \sum_{i=1}^{N_\Omega} \left(\boldsymbol{K}_i^{-1} \delta \boldsymbol{z}_h^{n+1,k}, \delta \boldsymbol{z}_h^{n+1,k} \right)_{E_i} \leq \sum_{i=1}^{N_\Omega} \frac{1}{2\epsilon_i} \left\| L_i \delta p_h^{n,k} - \alpha_i \nabla \cdot \delta \boldsymbol{u}_h^{n,k} \right\|_{E_i}^2 + \sum_{i=1}^{N_\Omega} \frac{\epsilon_i}{2} \left\| \delta p_h^{n+1,k} \right\|_{E_i}^2.$$

Introducing a new parameter χ_i for each grid element E_i, we define a local quantity of contraction for each E_i as: $\chi_i \delta \sigma_v^{n,k} = L_i \delta p_h^{n,k} - \alpha_i \nabla \cdot \delta \boldsymbol{u}_h^{n,k}$. The choice $\epsilon_i = \beta_i$ for each E_i gives:

$$\sum_{i=1}^{N_\Omega} \frac{\beta_i}{2} \left\| \delta p_h^{n+1,k} \right\|_{E_i}^2 + \Delta t \sum_{i=1}^{N_\Omega} \left\| \boldsymbol{K}_i^{-1/2} \delta \boldsymbol{z}_h^{n+1,k} \right\|_{E_i}^2 \leq \sum_{i=1}^{N_\Omega} \frac{1}{2\beta_i} \left\| \chi_i \delta \sigma_v^{n,k} \right\|_{E_i}^2. \tag{5.2.15}$$

Now, test the elasticity equation (5.2.12) with $\boldsymbol{v}_h = \delta \boldsymbol{u}_h^{n+1,k}$ to get:

$$\sum_{i=1}^{N_\Omega} 2G_i \|\boldsymbol{\varepsilon}(\delta \boldsymbol{u}_h^{n+1,k})\|_{E_i}^2 + \sum_{i=1}^{N_\Omega} \lambda_i \|\nabla \cdot \delta \boldsymbol{u}_h^{n+1,k}\|_{E_i}^2 - \sum_{i=1}^{N_\Omega} \alpha_i (\delta p_h^{n+1,k}, \nabla \cdot \delta \boldsymbol{u}_h^{n+1,k})_{E_i} = 0. \tag{5.2.16}$$

Combining flow (5.2.15) with elasticity (5.2.16), we obtain:

$$\sum_{i=1}^{N_\Omega} 2G_i \|\boldsymbol{\varepsilon}(\delta \boldsymbol{u}_h^{n+1,k})\|_{E_i}^2 + \Delta t \sum_{i=1}^{N_\Omega} \left\| \boldsymbol{K}_i^{-1/2} \delta \boldsymbol{z}_h^{n+1,k} \right\|_{E_i}^2 + \sum_{i=1}^{N_\Omega} \left\{ \frac{\beta_i}{2} \left\| \delta p_h^{n+1,k} \right\|_{E_i}^2 - \alpha_i (\delta p_h^{n+1,k}, \nabla \cdot \delta \boldsymbol{u}_h^{n+1,k})_{E_i} + \lambda_i \|\nabla \cdot \delta \boldsymbol{u}_h^{n+1,k}\|_{E_i}^2 \right\} \leq \sum_{i=1}^{N_\Omega} \frac{\chi_i^2}{2\beta_i} \left\| \delta \sigma_v^{n,k} \right\|_{E_i}^2. \tag{5.2.17}$$

Now, for each grid element E_i, expand the RHS to match terms on the left hand side and form a square:

$$\left\|\delta\sigma_v^{n,k}\right\|_{E_i}^2 = \frac{L_i^2}{{\chi_i}^2}\left\|\delta p_h^{n,k}\right\|_{E_i}^2 - \frac{2\alpha_i L_i}{\chi_i^2}\left(\delta p_h^{n,k}, \nabla\cdot\delta\boldsymbol{u}_h^{n,k}\right)_{E_i} + \frac{\alpha_i^2}{\chi_i^2}\left\|\nabla\cdot\delta\boldsymbol{u}_h^{n,k}\right\|_{E_i}^2.$$

For each E_i, the following inequalities should be satisfied: $\frac{\beta_i}{2} \geq \frac{L_i^2}{{\chi_i}^2}$, $\frac{2\alpha_i L_i}{\chi_i^2} = \alpha_i$, and $\lambda_i \geq \frac{\alpha_i^2}{\chi_i^2}$. The first and second inequalities give: $\chi_i^2 = 2L_i$, and $\frac{1}{M_i} + c_{f_i}\varphi_{0i} \geq 0$, which is trivially satisfied. The third inequality gives: $L_i = \frac{\alpha_i^2}{2\lambda_i}$. With: $L_i = \frac{\alpha_i^2}{2\lambda_i}$ and $\chi_i^2 = 2L_i$, we have:

$$\sum_{i=1}^{N_\Omega} 2G_i\|\boldsymbol{\varepsilon}(\delta\boldsymbol{u}_h^{n+1,k})\|_{E_i}^2 + \sum_{i=1}^{N_\Omega}\frac{1}{2}\left(\frac{1}{M_i} + c_{f_i}\varphi_{0i}\right)\left\|\delta p_h^{n+1,k}\right\|_{E_i}^2 + \Delta t\sum_{i=1}^{N_\Omega}\left\|{\boldsymbol{K}_i}^{-1/2}\delta\boldsymbol{z}_h^{n+1,k}\right\|_{E_i}^2 + \sum_{i=1}^{N_\Omega}\left\|\delta\sigma_v^{n+1,k}\right\|_{E_i}^2 \leq \sum_{i=1}^{N_\Omega}\left(\frac{L_i}{\frac{1}{M_i} + c_{f_i}\varphi_{0i} + L_i}\right)\left\|\delta\sigma_v^{n,k}\right\|_{E_i}^2. \tag{5.2.18}$$

We finally have, for each $E_i \in \Omega, 1 \leq i \leq N_\Omega$:

$$2\sum_{i=1}^{N_\Omega} G_i\|\boldsymbol{\varepsilon}(\delta\boldsymbol{u}_h^{n+1,k})\|_{E_i}^2 + \frac{1}{2}\sum_{i=1}^{N_\Omega}\left(\frac{1}{M_i} + c_{f_i}\varphi_{0i}\right)\left\|\delta p_h^{n+1,k}\right\|_{E_i}^2 + \Delta t\sum_{i=1}^{N_\Omega}\left\|{\boldsymbol{K}_i}^{-1/2}\delta\boldsymbol{z}_h^{n+1,k}\right\|_{E_i}^2 + \sum_{i=1}^{N_\Omega}\left\|\delta\sigma_v^{n+1,k}\right\|_{E_i}^2 \leq \max_{1\leq i\leq N_\Omega}\left(\frac{L_i}{\frac{1}{M_i} + c_{f_i}\varphi_{0i} + L_i}\right)\sum_{i=1}^{N_\Omega}\left\|\delta\sigma_v^{n,k}\right\|_{E_i}^2. \tag{5.2.19}$$

Theorem 5.2.1. *[Localized Single Rate Banach Contraction Estimate] The localized multirate iterative scheme is a contraction given by*

$$2\sum_{i=1}^{N_\Omega} G_i\|\boldsymbol{\varepsilon}(\delta\boldsymbol{u}_h^{n+1,k})\|_{E_i}^2 + \frac{1}{2}\sum_{i=1}^{N_\Omega}\left(\frac{1}{M_i} + c_{f_i}\varphi_{0i}\right)\left\|\delta p_h^{n+1,k}\right\|_{E_i}^2 + \Delta t\sum_{i=1}^{N_\Omega}\left\|{\boldsymbol{K}_i}^{-1/2}\delta\boldsymbol{z}_h^{n+1,k}\right\|_{E_i}^2 + \sum_{i=1}^{N_\Omega}\left\|\delta\sigma_v^{n+1,k}\right\|_{E_i}^2 \leq \max_{1\leq i\leq N_\Omega}\left(\frac{L_i}{\frac{1}{M_i} + c_{f_i}\varphi_{0i} + L_i}\right)\sum_{i=1}^{N_\Omega}\left\|\delta\sigma_v^{n,k}\right\|_{E_i}^2.$$

5.3 Localized Multirate Formulation and Analysis

In a similar way, we can derive a localized Banach contraction estimate for the multirate case. We start by writing the localized spatially continuous multirate weak formulation. We note that the localized permeability tensor $\boldsymbol{K}_i$ includes the viscosity μ_i.

5.3.1 Continuous in Space Global Weak Formulation

- Step (a): For $1 \leq m \leq q$, find $p^{n+1,m+k} \in H^1(\Omega)$, and $\boldsymbol{z}^{n+1,m+k} \in H(\mathrm{div};\Omega)^d \cap \{\boldsymbol{z}^{n+1,k} \cdot n = 0 \text{ on } \partial\Omega\}$ such that,

$$\forall \theta \in L^2(\Omega)\,,\ \frac{1}{\Delta t}\sum_{i=1}^{N_\Omega}\Big((\frac{1}{M_i}+c_{f_i}\varphi_{0i}+L_i)\Big(p^{n+1,m+k}-p^{n+1,m-1+k}\Big),\theta\Big)_{E_i} + \sum_{i=1}^{N_\Omega}(\nabla\cdot\boldsymbol{z}^{n+1,m+k},\theta)_{E_i} = \frac{1}{\Delta t}\sum_{i=1}^{N_\Omega}\Big(L_i\Big(p^{n,m+k}-p^{n,m-1+k}\Big)-\frac{\alpha_i}{q}\nabla\cdot\Big(\boldsymbol{u}^{n,k+q}-\boldsymbol{u}^{n,k}\Big),\theta\Big)_{E_i}+\sum_{i=1}^{N_\Omega}\Big(\tilde{q},\theta\Big)_{E_i}, \tag{5.3.20}$$

$$\forall \boldsymbol{q} \in H(\mathrm{div};\Omega)^d \cap \{\boldsymbol{q}\cdot n = 0 \text{ on } \partial\Omega\}\,,\ \sum_{i=1}^{N_\Omega}\Big(\boldsymbol{K}_i{}^{-1}\boldsymbol{z}^{n+1,m+k},\boldsymbol{q}\Big)_{E_i} = \sum_{i=1}^{N_\Omega}\Big(p^{n+1,m+k},\nabla\cdot\boldsymbol{q}\Big)_{E_i} - \sum_{i=1}^{N_\Omega}\langle p^{n+1,m+k},\boldsymbol{q}\cdot\boldsymbol{n}\rangle_{\partial E_i}+\sum_{i=1}^{N_\Omega}\Big(\rho_{f,r}g\nabla\eta,\boldsymbol{q}\Big)_{E_i}, \tag{5.3.21}$$

- Step (b): Given $p^{n+1,k+q}$ and, $\boldsymbol{z}^{n+1,k+q}$, find $\boldsymbol{u}^{n+1,k+q} \in H^1(\Omega)^d \cap \{\boldsymbol{u} = 0 \text{ on } \partial\Omega\}$ such that,

$$\forall \boldsymbol{v} \in H^1(\Omega)^d \cap \{\boldsymbol{v} = 0 \text{ on } \partial\Omega\}\,,\ 2\sum_{i=1}^{N_\Omega}(G_i\boldsymbol{\varepsilon}(\boldsymbol{u}^{n+1,k+q}),\boldsymbol{\varepsilon}(\boldsymbol{v}))_{E_i}+\sum_{i=1}^{N_\Omega}(\lambda_i\nabla\cdot\boldsymbol{u}^{n+1,k+q},\nabla\cdot\boldsymbol{v})_{E_i}-\sum_{i=1}^{N_\Omega}(\alpha_i p^{n+1,k+q},\nabla\cdot\boldsymbol{v})_{E_i} - \sum_{i=1}^{N_\Omega}\langle\boldsymbol{\sigma}(\boldsymbol{u}^{n+1,k+q})\boldsymbol{n},\boldsymbol{v}\rangle_{\partial E_i}+\sum_{i=1}^{N_\Omega}\langle\alpha_i p^{n+1,k+q}\underline{\underline{\boldsymbol{I}}}\boldsymbol{n},\boldsymbol{v}\rangle_{\partial E_i} = \sum_{i=1}^{N_\Omega}(\boldsymbol{f},\boldsymbol{v})_{E_i}. \tag{5.3.22}$$

In a similar way, as detailed in the single rate case, all boundary terms vanish. The continuous-in-space weak formulation then reads:

- Step (a): For $1 \leq m \leq q$, find $p^{n+1,m+k} \in H^1(\Omega)$, and $\boldsymbol{z}^{n+1,m+k} \in H(\mathrm{div};\Omega)^d \cap$

$\{\boldsymbol{z}^{n+1,k} \cdot n = 0 \text{ on } \partial\Omega\}$ such that,

$$\forall \theta \in L^2(\Omega)\,,\ \frac{1}{\Delta t}\sum_{i=1}^{N_\Omega}\Big((\frac{1}{M_i}+c_{f_i}\varphi_{0i}+L_i)\Big(p^{n+1,m+k}-p^{n+1,m-1+k}\Big),\theta\Big)_{E_i}$$
$$+\sum_{i=1}^{N_\Omega}(\nabla\cdot\boldsymbol{z}^{n+1,m+k},\theta)_{E_i}=$$
$$\frac{1}{\Delta t}\sum_{i=1}^{N_\Omega}\Big(L_i\Big(p^{n,m+k}-p^{n,m-1+k}\Big)-\frac{\alpha_i}{q}\nabla\cdot\Big(\boldsymbol{u}^{n,k+q}-\boldsymbol{u}^{n,k}\Big),\theta\Big)_{E_i}+\sum_{i=1}^{N_\Omega}\Big(\tilde{q},\theta\Big)_{E_i}, \tag{5.3.23}$$

$$\forall \boldsymbol{q} \in H(\mathrm{div};\Omega)^d \cap \{\boldsymbol{q}\cdot n = 0 \text{ on } \partial\Omega\}\,,$$
$$\sum_{i=1}^{N_\Omega}\Big({\boldsymbol{K}_i}^{-1}\boldsymbol{z}^{n+1,m+k},\boldsymbol{q}\Big)_{E_i}=\sum_{i=1}^{N_\Omega}\Big(p^{n+1,m+k},\nabla\cdot\boldsymbol{q}\Big)_{E_i}+\sum_{i=1}^{N_\Omega}\Big(\rho_{f,r}g\nabla\,\eta,\boldsymbol{q}\Big)_{E_i}, \tag{5.3.24}$$

- Step (b): Given $p^{n+1,k+q}$ and, $\boldsymbol{z}^{n+1,k+q}$, find $\boldsymbol{u}^{n+1,k+q} \in H^1(\Omega)^d \cap \{\boldsymbol{u} = 0 \text{ on } \partial\Omega\}$ such that,

$$\forall \boldsymbol{v} \in H^1(\Omega)^d \cap \{\boldsymbol{v} = 0 \text{ on } \partial\Omega\}\,,$$
$$2\sum_{i=1}^{N_\Omega}(G_i\boldsymbol{\varepsilon}(\boldsymbol{u}^{n+1,k+q}),\boldsymbol{\varepsilon}(\boldsymbol{v}))_{E_i}+\sum_{i=1}^{N_\Omega}(\lambda_i\nabla\cdot\boldsymbol{u}^{n+1,k+q},\nabla\cdot\boldsymbol{v})_{E_i}-\sum_{i=1}^{N_\Omega}(\alpha_i p^{n+1,k+q},\nabla\cdot\boldsymbol{v})_{E_i}$$
$$=\sum_{i=1}^{N_\Omega}(\boldsymbol{f},\boldsymbol{v})_{E_i}. \tag{5.3.25}$$

5.3.2 Fully Discrete Weak formulation

We mimic the spatially continuous weak formulation ((5.3.23), (5.3.24), and (5.3.25)) and obtain the fully discrete formulation (discrete in time and space) as follows:

- Step (a): For $1 \leq m \leq q$, find $p_h^{n+1,m+k} \in Q_h$, and $\boldsymbol{z}_h^{n+1,m+k} \in \boldsymbol{Z}_h$ such that,

$$\forall \theta_h \in Q_h\,,\ \frac{1}{\Delta t}\sum_{i=1}^{N_\Omega}\Big((\frac{1}{M_i}+c_{f_i}\varphi_{0i}+L_i)\Big(p_h^{n+1,m+k}-p_h^{n+1,m-1+k}\Big),\theta_h\Big)_{E_i}$$
$$+\sum_{i=1}^{N_\Omega}(\nabla\cdot\boldsymbol{z}_h^{n+1,m+k},\theta_h)_{E_i}=$$
$$\frac{1}{\Delta t}\sum_{i=1}^{N_\Omega}\Big(L_i\Big(p_h^{n,m+k}-p_h^{n,m-1+k}\Big)-\frac{\alpha_i}{q}\nabla\cdot\Big(\boldsymbol{u}_h^{n,k+q}-\boldsymbol{u}_h^{n,k}\Big),\theta_h\Big)_{E_i}+\sum_{i=1}^{N_\Omega}\Big(\tilde{q}_h,\theta_h\Big)_{E_i}, \tag{5.3.26}$$

$$\forall \boldsymbol{q}_h \in \boldsymbol{Z}_h\,,$$
$$\sum_{i=1}^{N_\Omega}\Big({\boldsymbol{K}_i}^{-1}\boldsymbol{z}_h^{n+1,m+k},\boldsymbol{q}_h\Big)_{E_i}=\sum_{i=1}^{N_\Omega}\Big(p_h^{n+1,m+k},\nabla\cdot\boldsymbol{q}_h\Big)_{E_i}+\sum_{i=1}^{N_\Omega}\Big(\rho_{f,r}g\nabla\,\eta,\boldsymbol{q}_h\Big)_{E_i}, \tag{5.3.27}$$

- Step (b): Given $p_h^{n+1,k+q}$ and, $\boldsymbol{z}_h^{n+1,k+q}$, find $\boldsymbol{u}_h^{n+1,k+q} \in \boldsymbol{V}_h$ such that,

$$\forall \boldsymbol{v}_h \in \boldsymbol{V}_h\,,\ 2\sum_{i=1}^{N_\Omega}(G_i\boldsymbol{\varepsilon}(\boldsymbol{u}_h^{n+1,k+q}),\boldsymbol{\varepsilon}(\boldsymbol{v}_h))_{E_i}+\sum_{i=1}^{N_\Omega}(\lambda_i\nabla\cdot\boldsymbol{u}_h^{n+1,k+q},\nabla\cdot\boldsymbol{v}_h)_{E_i}$$
$$-\sum_{i=1}^{N_\Omega}(\alpha_i p_h^{n+1,k+q},\nabla\cdot\boldsymbol{v}_h)_{E_i}=\sum_{i=1}^{N_\Omega}(\boldsymbol{f}_h,\boldsymbol{v}_h)_{E_i}. \tag{5.3.28}$$

5.3.3 Proof of Contraction

Recall that for a given time step $t = t_k$, we define the difference between two coupling iterates as:

$$\delta\xi^{n+1,k}=\xi^{n+1,k}-\xi^{n,k},$$

where ξ may stand for $p_h, \boldsymbol{z}_h$, or $\boldsymbol{u}_h$.

- **Step 1: Flow equations**

  For each grid element E_i, let $\beta_i = \frac{1}{M_i}+c_{f_i}\varphi_{0i}+L_i$. . For $n \geq 1$, by taking the difference of two successive iterates of (5.3.26), which corresponds to one local flow iteration and its corresponding local flow iteration in the previous flow and geomechanics iterative

coupling iteration, testing with $\theta_h = \delta p_h^{n+1,m+k} - \delta p_h^{n+1,m-1+k}$, we obtain

$$\sum_{i=1}^{N_\Omega} \beta_i \left\| \delta p_h^{n+1,m+k} - \delta p_h^{n+1,m-1+k} \right\|_{E_i}^2 + \Delta t \sum_{i=1}^{N_\Omega} (\nabla \cdot \delta \boldsymbol{z}_h^{n+1,m+k}, \delta p_h^{n+1,m+k} - \delta p_h^{n+1,m-1+k})_{E_i} = \sum_{i=1}^{N_\Omega} \left(L_i(\delta p_h^{n,m+k} - \delta p_h^{n,m-1+k}) - \frac{\alpha_i}{q} \nabla \cdot \delta \boldsymbol{u}_h^{n,k+q}, \delta p_h^{n+1,m+k} - \delta p_h^{n+1,m-1+k} \right)_{E_i}. \tag{5.3.29}$$

Similarly, for the flux equation (5.3.27), by taking the difference of two successive iterates, followed by taking the difference at two consecutive finer time steps, $t = t_{m+k}$, and $t = t_{m-1+k}$, and testing with $\boldsymbol{q}_h = \delta \boldsymbol{z}_h^{n+1,m+k}$, we obtain

$$\sum_{i=1}^{N_\Omega} \left({\boldsymbol{K}_i}^{-1} \left(\delta \boldsymbol{z}_h^{n+1,m+k} - \delta \boldsymbol{z}_h^{n+1,m-1+k} \right), \delta \boldsymbol{z}_h^{n+1,m+k} \right)_{E_i} = \sum_{i=1}^{N_\Omega} \left(\delta p_h^{n+1,m+k} - \delta p_h^{n+1,m-1+k}, \nabla \cdot \delta \boldsymbol{z}_h^{n+1,m+k} \right)_{E_i}. \tag{5.3.30}$$

We combine (5.3.29) with (5.3.30), apply Young's inequality (for each grid E_i) to obtain

$$\begin{aligned} &\sum_{i=1}^{N_\Omega} \beta_i \left\| \delta p_h^{n+1,m+k} - \delta p_h^{n+1,m-1+k} \right\|_{E_i}^2 \\ &+ \Delta t \sum_{i=1}^{N_\Omega} \left({\boldsymbol{K}_i}^{-1} \left(\delta \boldsymbol{z}_h^{n+1,m+k} - \delta \boldsymbol{z}_h^{n+1,m-1+k} \right), \delta \boldsymbol{z}_h^{n+1,m+k} \right)_{E_i} \\ &\quad \leq \sum_{i=1}^{N_\Omega} \frac{1}{2\epsilon_i} \left\| L_i(\delta p_h^{n,m+k} - \delta p_h^{n,m-1+k}) - \frac{\alpha_i}{q} \nabla \cdot \delta \boldsymbol{u}_h^{n,k+q} \right\|_{E_i}^2 \\ &\quad + \sum_{i=1}^{N_\Omega} \frac{\epsilon_i}{2} \left\| \delta p_h^{n+1,m+k} - \delta p_h^{n+1,m-1+k} \right\|_{E_i}^2. \end{aligned}$$

For each E_i, the choice $\epsilon_i = \beta_i$ absorbs the pressure term on the right hand side. Together with a simple expansion of the flux product, we derive

$$\begin{aligned}
&\sum_{i=1}^{N_\Omega} \frac{\beta_i}{2} \left\| \delta p_h^{n+1,m+k} - \delta p_h^{n+1,m-1+k} \right\|_{E_i}^2 \\
&+ \frac{\Delta t}{2} \sum_{i=1}^{N_\Omega} \left\{ \left\| \boldsymbol{K}_i{}^{-1/2} \delta \boldsymbol{z}_h^{n+1,m+k} \right\|_{E_i}^2 - \left\| \boldsymbol{K}_i{}^{-1/2} \delta \boldsymbol{z}_h^{n+1,m-1+k} \right\|_{E_i}^2 \right. \\
&\qquad \left. + \left\| \boldsymbol{K}_i{}^{-1/2} (\delta \boldsymbol{z}_h^{n+1,m+k} - \delta \boldsymbol{z}_h^{n+1,m-1+k}) \right\|_{E_i}^2 \right\} \\
&\qquad \leq \sum_{i=1}^{N_\Omega} \frac{1}{2\beta_i} \left\| L_i (\delta p_h^{n,m+k} - \delta p_h^{n,m-1+k}) - \frac{\alpha_i}{q} \nabla \cdot \delta \boldsymbol{u}_h^{n,k+q} \right\|_{E_i}^2 . \qquad (5.3.31)
\end{aligned}$$

The right hand side constitutes an expression for a quantity to be contracted on. Introducing a new parameter χ_i for each E_i, we define the localized volumetric mean stress for $(1 \leq m \leq q)$ as

$$\chi_i \delta \sigma_v^{n,m+k} = L_i (\delta p_h^{n,m+k} - \delta p_h^{n,m-1+k}) - \frac{\alpha_i}{q} \nabla \cdot \delta \boldsymbol{u}_h^{n,k+q}. \qquad (5.3.32)$$

The value of χ_i for each E_i will be chosen such that contraction can be achieved on the spatial summation of the localized norms of $\sigma_v^{n,m+k}$, summed over q flow finer time steps, within one coarser mechanics time step. Summing up (5.3.31) for $1 \leq m \leq q$, substituting the new definition of the localized volumetric mean stress (5.3.32), and noting that $\delta \boldsymbol{z}_h^{n+1,k} = 0$, we obtain

$$\begin{aligned}
&\sum_{m=1}^{q} \sum_{i=1}^{N_\Omega} \frac{\beta_i}{2} \left\| \delta p_h^{n+1,m+k} - \delta p_h^{n+1,m-1+k} \right\|_{E_i}^2 + \frac{\Delta t}{2} \sum_{i=1}^{N_\Omega} \left\| \boldsymbol{K}_i{}^{-1/2} \delta \boldsymbol{z}_h^{n+1,k+q} \right\|_{E_i}^2 \\
&+ \frac{\Delta t}{2} \sum_{m=1}^{q} \sum_{i=1}^{N_\Omega} \left\| \boldsymbol{K}_i{}^{-1/2} (\delta \boldsymbol{z}_h^{n+1,m+k} - \delta \boldsymbol{z}_h^{n+1,m-1+k}) \right\|_{E_i}^2 \leq \sum_{m=1}^{q} \sum_{i=1}^{N_\Omega} \frac{1}{2\beta_i} \left\| \chi_i \delta \sigma_v^{n,m+k} \right\|_{E_i}^2 .
\end{aligned} \qquad (5.3.33)$$

- **Step 2: Elasticity equation**

For $n \geq 1$, we take the difference of successive iterates of the mechanics equation

(5.3.28), and test with $\boldsymbol{v}_h = \delta \boldsymbol{u}_h^{n+1,k+q}$ to get

$$2\sum_{i=1}^{N_\Omega} G_i \|\boldsymbol{\varepsilon}(\delta \boldsymbol{u}_h^{n+1,k+q})\|_{E_i}^2 + \sum_{i=1}^{N_\Omega} \lambda_i \|\nabla \cdot \delta \boldsymbol{u}_h^{n+1,k+q}\|_{E_i}^2 - \sum_{i=1}^{N_\Omega} \alpha_i (\delta p_h^{n+1,k+q}, \nabla \cdot \delta \boldsymbol{u}_h^{n+1,k+q})_{E_i} = 0. \tag{5.3.34}$$

For the iterative scheme to be contractive, a quantity similar to the right hand side of (5.3.33), for the next iterative coupling iteration, $n+1$, has to be formed. To achieve that, we introduce a term involving a summation over all flow finer time steps in (5.3.34) by noticing that

$$\sum_{m=1}^{q} \left(\delta p_h^{n+1,m+k} - \delta p_h^{n+1,m-1+k} \right) = \delta p_h^{n+1,k+q}. \tag{5.3.35}$$

Substituting (5.3.35) into (5.3.34) leads to

$$2\sum_{i=1}^{N_\Omega} G_i \|\boldsymbol{\varepsilon}(\delta \boldsymbol{u}_h^{n+1,k+q})\|_{E_i}^2 + \sum_{i=1}^{N_\Omega} \lambda_i \|\nabla \cdot \delta \boldsymbol{u}_h^{n+1,k+q}\|_{E_i}^2 - \sum_{i=1}^{N_\Omega} \alpha_i \Big(\sum_{m=1}^{q} \left(\delta p_h^{n+1,m+k} - \delta p_h^{n+1,m-1+k} \right), \nabla \cdot \delta \boldsymbol{u}_h^{n+1,k+q} \Big)_{E_i} = 0. \tag{5.3.36}$$

- **Step 3: Combining flow and elasticity equations**

  By combining (5.3.36) with (5.3.33), and rearranging terms, we form a square term, in expanded form, summed over flow finer time steps within one coarser mechanics time step for each grid element E_i,

$$\begin{aligned} &2\sum_{i=1}^{N_\Omega} G_i \|\boldsymbol{\varepsilon}(\delta \boldsymbol{u}_h^{n+1,k+q})\|_{E_i}^2 + \sum_{m=1}^{q} \sum_{i=1}^{N_\Omega} \Big\{ \frac{\beta_i}{2} \left\| \delta p_h^{n+1,m+k} - \delta p_h^{n+1,m-1+k} \right\|_{E_i}^2 \\ &+ \frac{\lambda_i}{q} \left\| \nabla \cdot \delta \boldsymbol{u}_h^{n+1,k+q} \right\|_{E_i}^2 - \alpha_i \left(\delta p_h^{n+1,m+k} - \delta p_h^{n+1,m-1+k}, \nabla \cdot \delta \boldsymbol{u}_h^{n+1,k+q} \right)_{E_i} \Big\} \\ &+ \frac{\Delta t}{2} \sum_{i=1}^{N_\Omega} \left\| \boldsymbol{K}_i^{-1/2} \delta \boldsymbol{z}_h^{n+1,k+q} \right\|_{E_i}^2 + \frac{\Delta t}{2} \sum_{m=1}^{q} \sum_{i=1}^{N_\Omega} \left\| \boldsymbol{K}_i^{-1/2} (\delta \boldsymbol{z}_h^{n+1,m+k} - \delta \boldsymbol{z}_h^{n+1,m-1+k}) \right\|_{E_i}^2 \\ &\leq \sum_{m=1}^{q} \sum_{i=1}^{N_\Omega} \frac{\chi_i^2}{2\beta_i} \left\| \delta \sigma_v^{n,m+k} \right\|_{E_i}^2. \end{aligned} \tag{5.3.37}$$

It remains to choose the values of our newly introduced parameters, χ_i and L_i, such that the coefficients of the expanded square contributes only positive terms to the left hand side of (5.3.37). Therefore, we expand the right hand side of (5.3.37) for each E_i as

$$\begin{aligned}\Big\|\delta\sigma_v^{n,m+k}\Big\|_{E_i}^2 &= \frac{L_i^2}{{\chi_i}^2}\Big\|\delta p_h^{n,m+k} - \delta p_h^{n,m-1+k}\Big\|_{E_i}^2 \\ &- \frac{2\alpha_i L_i}{q\chi_i^2}\Big(\delta p_h^{n,m+k} - \delta p_h^{n,m-1+k}, \nabla\cdot\delta\boldsymbol{u}_h^{n,k+q}\Big)_{E_i} + \frac{\alpha_i^2}{\chi_i^2 q^2}\Big\|\nabla\cdot\delta\boldsymbol{u}_h^{n,k+q}\Big\|_{E_i}^2. \end{aligned} \tag{5.3.38}$$

Now, we match the coefficients of the expansion in (5.3.38) to the coefficients of the expanded square on the right hand side of (5.3.37), hence, deduce the values of χ_i and L_i for each grid element E_i, respectively. For the left hand side of (5.3.37) to remain positive, the following inequalities should be satisfied

$$\frac{\beta_i}{2} \geq \frac{L_i^2}{{\chi_i}^2}, \qquad \frac{2\alpha_i L_i}{q\chi_i^2} = \alpha_i, \qquad \frac{\lambda_i}{q} \geq \frac{\alpha_i^2}{\chi_i^2 q^2}.$$

The second and third inequalities give rise to the following condition

$$L_i \geq \frac{\alpha_i^2}{2\lambda_i} \quad \text{for each } E_i.$$

The first inequality gives rise to $q \leq \frac{\beta_i}{L_i}$. For $L_i = \frac{\alpha_i^2}{2\lambda_i}, \chi_i^2 = \frac{\alpha_i^2}{q\lambda_i}$, we derive the following condition on the number of flow finer time steps within one coarse mechanics time step

$$q \leq \frac{2\lambda_i}{{\alpha_i}^2}\Big(\frac{1}{M_i} + c_{f_i}\varphi_{0i}\Big) + 1 \quad \text{for each } E_i, \tag{5.3.39}$$

which is not restrictive as typically in practice the values of λ_i are quite large. Now, we group the terms of the expanded square on the left hand side of (5.3.37) to form the quantity of contraction for the next iterative coupling iteration, $n+1$, as

$$\begin{aligned} &2\sum_{i=1}^{N_\Omega} G_i\|\boldsymbol{\varepsilon}(\delta\boldsymbol{u}_h^{n+1,k+q})\|_{E_i}^2 + \sum_{m=1}^{q}\sum_{i=1}^{N_\Omega}\Big(\frac{\beta_i}{2} - \frac{L_i^2}{\chi_i^2}\Big)\Big\|\delta p_h^{n+1,m+k} - \delta p_h^{n+1,m-1+k}\Big\|_{E_i}^2 \\ &+ \sum_{m=1}^{q}\sum_{i=1}^{N_\Omega}\Big\|\delta\sigma_v^{n+1,m+k}\Big\|_{E_i}^2 + \frac{\Delta t}{2}\sum_{i=1}^{N_\Omega}\Big\|{\boldsymbol{K}_i}^{-1/2}\delta\boldsymbol{z}_h^{n+1,k+q}\Big\|_{E_i}^2 \\ &+ \frac{\Delta t}{2}\sum_{m=1}^{q}\sum_{i=1}^{N_\Omega}\Big\|{\boldsymbol{K}_i}^{-1/2}(\delta\boldsymbol{z}_h^{n+1,m+k} - \delta\boldsymbol{z}_h^{n+1,m-1+k})\Big\|_{E_i}^2 \leq \sum_{m=1}^{q}\sum_{i=1}^{N_\Omega}\frac{\chi_i^2}{2\beta_i}\Big\|\delta\sigma_v^{n,m+k}\Big\|_{E_i}^2. \end{aligned}$$

Substituting $\chi_i^2 = \frac{2L_i}{q}$, $\beta_i = \frac{1}{M_i} + c_{f_i}\varphi_{0i} + L_i$ for each E_i, with further algebraic simplifications, we obtain

$$
\begin{aligned}
&2\sum_{i=1}^{N_\Omega} G_i \|\boldsymbol{\varepsilon}(\delta \boldsymbol{u}_h^{n+1,k+q})\|_{E_i}^2 \\
&+ \frac{1}{2}\sum_{m=1}^{q}\sum_{i=1}^{N_\Omega}\Big(\frac{1}{M_i} + c_{f_i}\varphi_{0i} + (1-q)L_i\Big)\Big\|\delta p_h^{n+1,m+k} - \delta p_h^{n+1,m-1+k}\Big\|_{E_i}^2 \\
&+ \frac{\Delta t}{2}\sum_{i=1}^{N_\Omega}\Big\|\boldsymbol{K}_i^{-1/2}\delta \boldsymbol{z}_h^{n+1,k+q}\Big\|_{E_i}^2 + \frac{\Delta t}{2}\sum_{m=1}^{q}\sum_{i=1}^{N_\Omega}\Big\|\boldsymbol{K}_i^{-1/2}(\delta \boldsymbol{z}_h^{n+1,m+k} - \delta \boldsymbol{z}_h^{n+1,m-1+k})\Big\|_{E_i}^2 \\
&+ \sum_{m=1}^{q}\sum_{i=1}^{N_\Omega}\Big\|\delta\sigma_v^{n+1,m+k}\Big\|_{E_i}^2 \leq \max_{1\leq i\leq N_\Omega}\Big(\frac{L_i}{q(\frac{1}{M_i} + c_{f_i}\varphi_{0i} + L_i)}\Big)\sum_{m=1}^{q}\sum_{i=1}^{N_\Omega}\Big\|\delta\sigma_v^{n,m+k}\Big\|_{E_i}^2.
\end{aligned}
\tag{5.3.40}
$$

The contraction coefficient: $\max_{1\leq i\leq N_\Omega}\Big(\frac{L_i}{q(\frac{1}{M_i}+c_{f_i}\varphi_{0i}+L_i)}\Big) < 1$ for $q \geq 1$. This is trivially satisfied (at least we take one flow time step followed by one mechanics time step).

Theorem 5.3.1. *[Localized Multirate Contraction Estimate] For* $q \leq 1 + \min_{1\leq i\leq N_\Omega}\frac{2\lambda_i}{\alpha_i{}^2}\Big(\frac{1}{M_i} + c_{f_i}\varphi_{0i}\Big)$, $L_i = \frac{\alpha_i^2}{2\lambda_i}$ *and* $\chi_i^2 = \frac{2L_i}{q}$, *the localized multirate iterative scheme is a contraction given by*

$$
\begin{aligned}
&2\textstyle\sum_{i=1}^{N_\Omega} G_i \|\boldsymbol{\varepsilon}(\delta \boldsymbol{u}_h^{n+1,k+q})\|_{E_i}^2 \\
&+\tfrac{1}{2}\textstyle\sum_{m=1}^{q}\sum_{i=1}^{N_\Omega}\Big(\frac{1}{M_i} + c_{f_i}\varphi_{0i} + (1-q)L_i\Big)\Big\|\delta p_h^{n+1,m+k} - \delta p_h^{n+1,m-1+k}\Big\|_{E_i}^2 \\
&+\tfrac{\Delta t}{2}\textstyle\sum_{i=1}^{N_\Omega}\Big\|K_i{}^{-1/2}\delta \boldsymbol{z}_h^{n+1,k+q}\Big\|_{E_i}^2 \\
&+\tfrac{\Delta t}{2}\textstyle\sum_{m=1}^{q}\sum_{i=1}^{N_\Omega}\Big\|K_i{}^{-1/2}(\delta \boldsymbol{z}_h^{n+1,m+k} - \delta \boldsymbol{z}_h^{n+1,m-1+k})\Big\|_{E_i}^2 + \textstyle\sum_{m=1}^{q}\sum_{i=1}^{N_\Omega}\Big\|\delta\sigma_v^{n+1,m+k}\Big\|_{E_i}^2 \\
&\leq \max_{1\leq i\leq N_\Omega}\Big(\frac{L_i}{q(\frac{1}{M_i}+c_{f_i}\varphi_{0i}+L_i)}\Big)\textstyle\sum_{m=1}^{q}\sum_{i=1}^{N_\Omega}\Big\|\delta\sigma_v^{n,m+k}\Big\|_{E_i}^2.
\end{aligned}
$$

5.4 Multirate Banach Contraction Estimates for Homogeneous vs Heterogeneous (Localized) Poroelastic Media

Table 5.1 compares the Banach contraction result obtained in Theorem 2.3.4 against the one obtained above.

	Original Contraction Estimates for Poroelastic Media	**Localized Contraction Estimates for Heterogeneous Poroelastic Media**
Conditions on Parameters:	A degree of spatial uniformity should be imposed as described in remark 5.4.2	Parameters can be heterogeneous.
Contraction Coefficient:	$\left(\frac{L}{\frac{1}{M}+c_f\varphi_0+L}\right)^2$	$\max\limits_{1\leq i\leq N_\Omega}\left(\frac{L_i}{q(\frac{1}{M_i}+c_{f\,i}\varphi_{0\,i}+L_i)}\right)$ for $L_i=\frac{\alpha_i^2}{2\lambda_i}$ for all $E_i\in\Omega$
Condition on q:	none	$q\leq 1+\min\limits_{1\leq i\leq N_\Omega}\frac{2\lambda_i}{{\alpha_i}^2}\left(\frac{1}{M_i}+c_{f\,i}\varphi_{0\,i}\right)$.
When do Contraction Coefficients Match?	For $L=\frac{\alpha^2}{2\lambda}$, $\left(\frac{M\alpha^2}{2(\lambda+M\lambda c_f\varphi_0)+M\alpha^2}\right)^2$	For q = upper limit, and $L_i=\frac{\alpha_i^2}{2\lambda_i}$ for all $E_i\in\Omega$, contraction estimate $=\max\limits_{1\leq i\leq N_\Omega}\left(\frac{M_i{\alpha_i}^2}{2(\lambda_i+M_i\lambda_i c_{f\,i}\varphi_{0\,i})+M_i\alpha_i^2}\right)^2$. Exact Match.

Table 5.1: Banach Contraction Estimates for Homogeneous vs Heterogeneous (Localized) Poro-elastic Media

Remark 5.4.1. *Our localized Banach estimates work provides another strong justification for introducing the modified multirate iterative coupling scheme presented in section* (2.3.3.5)*. Following a similar approach to the proof presented above, the localized modified multirate iterative coupling scheme will not impose any upper bound on the number of flow finer time steps taken within one coarse mechanics time steps. This follows immediately as the quantity of contraction in the modified scheme is independent of q. The details are spared.*

Remark 5.4.2. *For our earlier obtained results, the word "homogeneous" is not as restrictive as it sounds. In fact, some degree of uniformity in the flow and mechanics parameters should be imposed in this case. However, parameter values can change smoothly across the spatial domain. The fixed stress stabilization term in this case should take the form* $L=\frac{\alpha_{max}^2}{2\lambda_{min}}$*, and this value will be added to the main diagonal of the linear system in a homogeneous manner. In fact, this leads to slower convergence rate, as the contraction coefficient increases monotinially with L. The power of the localized contraction result is that it allows us to add localized fixed-stress regularization terms which can vary across grid cells, yet the scheme is still contractive.*

Chapter 6

Iterative Coupling Schemes for Fractured Poroelastic Media

6.1 Introduction

In this chapter, we consider single rate and multirate iterative coupling schemes for coupling flow with linear elasticity in fractured poro-elastic media. Our proposed multirate iterative coupling schemes are extensions of the fixed-stress split iterative coupling algorithm, described in [43], in the presence of fractures. Two different multirate iterative coupling schemes will be proposed, along with rigorous derivations of their convergence properties. The single rate and multirate iterative coupling schemes for fractured poro-elastic media are shown in figures 6.1a and 6.1b respectively. It should be noted that in our mathematical analysis, we make the assumption that the flow in the reservoir and the fracture are solved monolithically.

6.1.1 Notation

We will follow a similar notation to the one presented in [45]. Let Ω be an open, connected, and bounded domain of $\mathbb{R}^d$, $d = 2$ or 3. The boundary of the domain, $\partial\Omega$, is assumed to be Lipschitz continuous. We denote by Γ the part of the boundary $\partial\Omega$ with a positive measure. In addition, the boundary of Γ is assumed to be Lipschitz continuous for $d = 3$. We recall from Chapter 2 that $\mathfrak{D}(\Omega)$ denotes the space of infinitely differentiable functions with compact support in Ω. Moreover, we recall that $\mathfrak{D}'(\Omega)$ is the dual space of $\mathfrak{D}(\Omega)$ which constitutes the space of distributions in Ω. As usual, $H^1(\Omega)$ denotes the classical Sobolev space

$$H^1(\Omega) = \{v \in L^2(\Omega)\,;\, \nabla v \in L^2(\Omega)^d\},$$

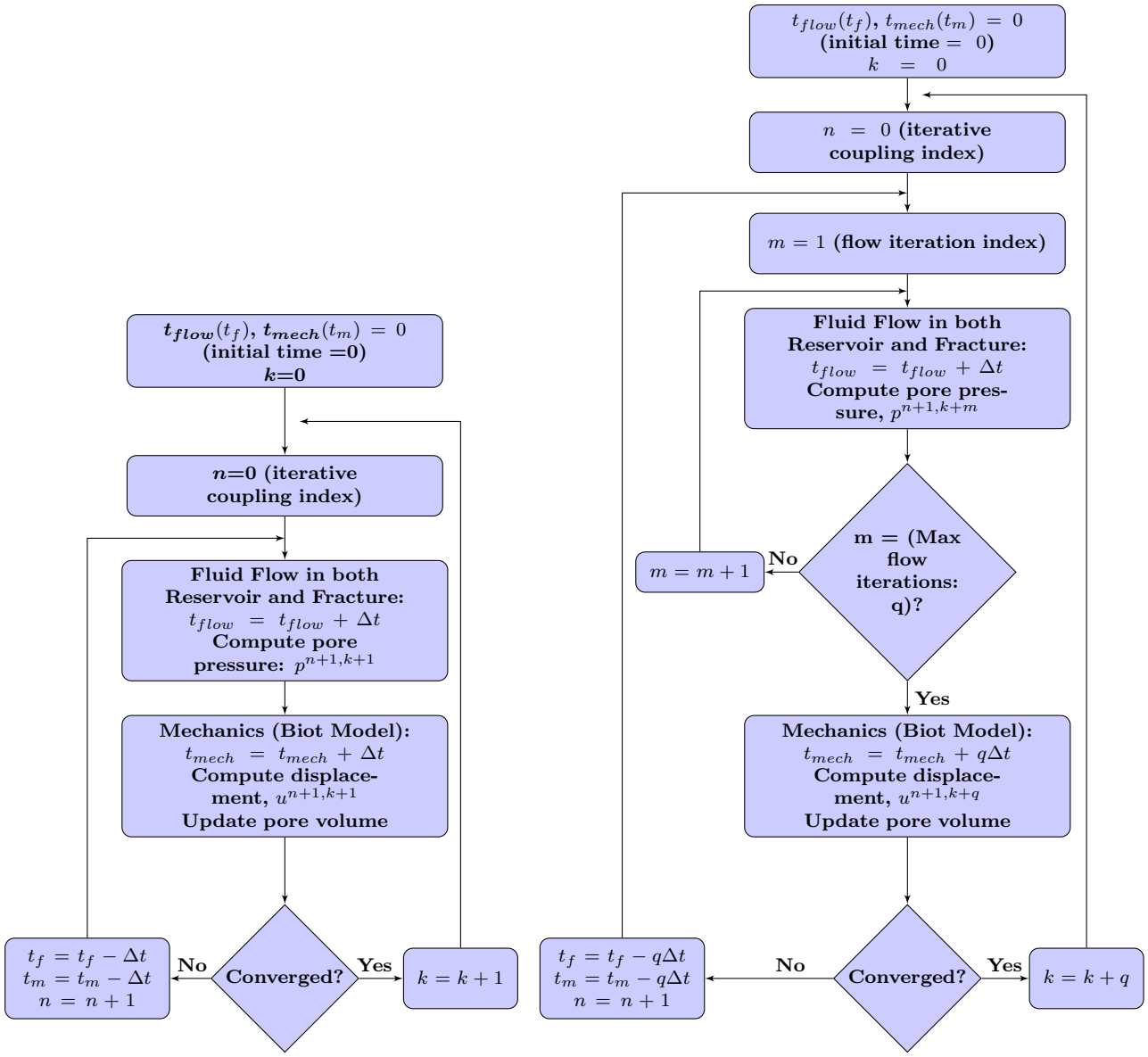

(a) Single Rate (b) Multirate

Figure 6.1: Flowchart for the iterative flow and mechanics coupling algorithm using single rate and multirate time stepping in fractured poro-elastic media. We assume that the flow in the reservoir and the fracture are solved monolithically.

equipped with the semi-norm and norm:

$$|v|_{H^1(\Omega)} = \|\nabla v\|_{L^2(\Omega)^d} \quad , \quad \|v\|_{H^1(\Omega)} = \left(\|v\|^2_{L^2(\Omega)} + |v|^2_{H^1(\Omega)}\right)^{1/2}.$$

In addition, we recall from Chapter 2 that for $1 \leq p < \infty$, $W^{1,p}(\Omega)$ is the space

$$W^{1,p}(\Omega) = \{v \in L^p(\Omega)\,;\, \nabla\, v \in L^p(\Omega)^d\},$$

normed by

$$|v|_{W^{1,p}(\Omega)} = \|\nabla\, v\|_{L^p(\Omega)} \quad , \quad \|v\|_{W^{1,p}(\Omega)} = (\|v\|^p_{L^p(\Omega)} + |v|^p_{W^{1,p}(\Omega)})^{1/p},$$

Moreover, we denote by $H^{1/2}(\Gamma)$ the space of traces of functions of $H^1(\Omega)$ on Γ (or generally Lipschitz curve in $\overline{\Omega}$). We note that $H^{1/2}(\Gamma) \subset L^2(\Gamma)$. The dual space of $H^{1/2}(\Gamma)$ is denoted by $H^{-1/2}(\Gamma)$, and is equipped with the norm [43]

$$|v|_{H^{1/2}(\Gamma)} = \Big(\int_\Gamma \int_\Gamma \frac{|v(\boldsymbol{x}) - v(\boldsymbol{y})|^2}{|\boldsymbol{x} - \boldsymbol{y}|^d} d\boldsymbol{x}\, d\boldsymbol{y}\Big)^{1/2} \;,\; \|v\|_{H^{1/2}(\Gamma)} = (\|v\|^2_{L^2(\Gamma)} + |v|^2_{H^{1/2}(\Gamma)})^{1/2}. \quad (6.1.1)$$

We also define

$$H^1_0(\Omega) = \{v \in H^1(\Omega)\,;\, v|_{\partial\Omega} = 0\},$$

and more generally

$$H^1_{0,\Gamma}(\Omega) = \{v \in H^1(\Omega)\,;\, v|_\Gamma = 0\}.$$

Moreover, we recall from Chapter 2 that for a vector $\boldsymbol{v}$ in $\mathbb{R}^d$, the strain tensor $\boldsymbol{\varepsilon}(\boldsymbol{v})$ is defined as:

$$\boldsymbol{\varepsilon}(\boldsymbol{v}) = \frac{1}{2}(\nabla\, \boldsymbol{v} + (\nabla\, \boldsymbol{v})^T).$$

In the analysis we carry out in this chapter, we shall use Korn's, Poincaré's, and traces inequalities, listed as follows:

- Korn's first inequality in $H^1_{0,\Gamma}(\Omega)^d$: there exists a constant C_κ which depends on Ω and Γ such that

$$\forall \boldsymbol{v} \in H^1_{0,\Gamma}(\Omega)^d\,,\; |\boldsymbol{v}|_{H^1(\Omega)^d} \leq C_\kappa \|\boldsymbol{\varepsilon}(\boldsymbol{v})\|_{L^2(\Omega)^{d\times d}}. \quad (6.1.2)$$

- Poincaré's inequality in $H^1_{0,\Gamma}(\Omega)$ reads: there exists a constant $\mathcal{P}_\Gamma$ which depends on Γ and Ω such that

$$\forall v \in H^1_{0,\Gamma}(\Omega)\,,\; \|v\|_{L^2(\Omega)} \leq \mathcal{P}_\Gamma |v|_{H^1(\Omega)}. \quad (6.1.3)$$

- Trace inequality in $H^1(\Omega)$: there exists a constant C_τ which depends on Γ and Ω such that

$$\forall \varepsilon > 0\,,\ \forall v \in H^1(\Omega)\,,\ \|v\|_{L^2(\Gamma)} \leq \varepsilon \|\nabla v\|_{L^2(\Omega)} + (\frac{C_\tau}{\varepsilon} + \varepsilon)\|v\|_{L^2(\Omega)}. \tag{6.1.4}$$

  This follows directly from the Young's inequality and the interpolation inequality [21, 43]:

$$\forall v \in H^1(\Omega)\,,\ \|v\|_{L^2(\Gamma)} \leq C\|v\|^{1/2}_{L^2(\Omega)}\|v\|^{1/2}_{H^1(\Omega)}.$$

Furthermore, we recall that the $H(\mathrm{div};\Omega)$ space is defined as follows:

$$H(\mathrm{div};\Omega) = \{\boldsymbol{v} \in L^2(\Omega)^d\,;\ \nabla \cdot \boldsymbol{v} \in L^2(\Omega)\},$$

and equipped with the norm

$$\|\boldsymbol{v}\|_{H(\mathrm{div};\Omega)} = (\|\boldsymbol{v}\|^2_{L^2(\Omega)} + \|\nabla \cdot \boldsymbol{v}\|^2_{L^2(\Omega)})^{1/2}.$$

6.1.2 Reservoir and Fracture Domains

In this work, the reservoir is represented by Ω, a bounded domain of $\mathbb{R}^d$, $d = 2$ or 3, with a Lipschitz continuous boundary $\partial\Omega$, and outward normal $\boldsymbol{n}$. The fracture is modeled as an interface $\mathcal{C}$ which is a closed subset of Ω. For $d = 2$, $\mathcal{C}$ represents a simple piecewise smooth curve. For $d = 3$, it represents a simple piecewise smooth surface with piecewise smooth Lipschitz boundary $\partial\mathcal{C}$. The reservoir matrix is thus denoted by $\Omega\backslash\mathcal{C}$.

For discretization purposes (will be described in details later), we introduce an auxiliary partition of Ω into two non-overlapping subdomains Ω^+ and Ω^-. The interface between the two subdomains is assumed to be Lipschitz and denoted by Γ. The fracture $\mathcal{C}$ is contained within Γ: $\mathcal{C} \subset \Gamma$. We will distinguish the two sides (or faces) of the fracture, $\mathcal{C}$, by the superscripts $+$ and $-$ (following a similar notation as the one presented in [43]). We will use the superscript $\star$ to denote either $+$ or $-$. Let $\Omega^\star$ denote the part of Ω adjacent to $\mathcal{C}^\star$ and let $\boldsymbol{n}^\star$ denote the unit normal vector to $\mathcal{C}$ exterior to $\Omega^\star$, $\star = +, -$. The fracture is represented by two coincident sides/surfaces, so we have $\boldsymbol{n}^- = -\boldsymbol{n}^+$. Moreover, we let $\Gamma^\star = \partial\Omega^\star\backslash\Gamma$. Figure 6.2 summarizes the above discussion.

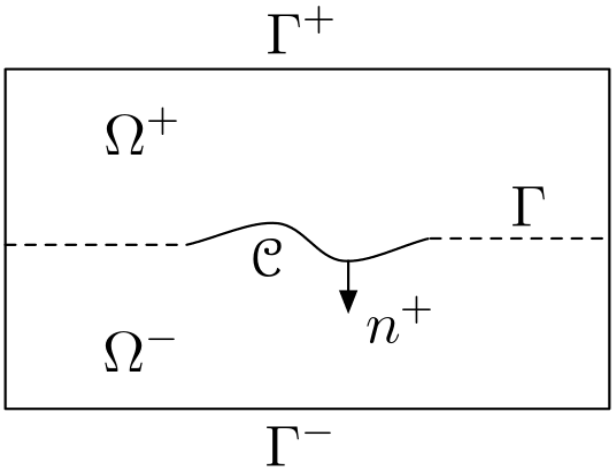

Figure 6.2: Reservoir and fracture domains (image courtesy of [45])

6.2 Model Equations and Discretization

6.2.1 Fractured Poroelastic Model

We recall that we assume a linear, elastic, homogeneous, and isotropic porous medium $\Omega \subset \mathbb{R}^3$, in which the reservoir is saturated with a slightly compressible fluid. Fractures are treated as possibly non-planar interfaces denoted by $\mathcal{C}$. As described earlier in Chapter 2 (section 2.2.2), using a quasi-static (i.e. ignoring the second order time derivative of the displacement) Biot approach to obtain the displacements (see [16]), the "geomechanics" model is as follows:

$$\boldsymbol{\sigma}^{\text{por}}(\boldsymbol{u}, p) = \boldsymbol{\sigma}(\boldsymbol{u}) - \alpha\, p\, \boldsymbol{I}, \tag{6.2.5}$$

$$\boldsymbol{\sigma}(\boldsymbol{u}) = \lambda(\nabla \cdot \boldsymbol{u})\boldsymbol{I} + 2\, G\boldsymbol{\varepsilon}(\boldsymbol{u}), \tag{6.2.6}$$

$$-\operatorname{div} \boldsymbol{\sigma}^{\text{por}}(\boldsymbol{u}, p) = \boldsymbol{f} \quad \text{in}\, \Omega \setminus \mathcal{C}, \tag{6.2.7}$$

where $\boldsymbol{\sigma}^{\text{por}}$ is the Cauchy stress tensor, $\boldsymbol{I}$ is the identity tensor, $\boldsymbol{u}$ is the solid's displacement, p is the fluid pressure in the reservoir, $\alpha > 0$ is the dimensionless Biot coefficient, $\boldsymbol{\sigma}$ is the effective linear elastic stress tensor, $\lambda > 0$ and $G > 0$ are the Lamé constants, $\boldsymbol{f}$ is a body force, which is usually assumed to be a gravity loading term.

In addition, as described in section 2.2.3 of Chapter 2, we assume a linearized slightly compressible single-phase flow model for the fluid (in both the reservoir and the fracture).

The fluid density, ρ_f, is a linear function of pressure: $\rho_f = \rho_{f,r}(1 + c_f(p - p_r))$. The porosity, denoted by φ^*, is given by: $\varphi^* = \varphi_0 + \alpha\nabla \cdot \boldsymbol{u} + \frac{1}{M}p$, where φ_0 is the initial porosity, and M is the Biot modulus. The fluid mass balance in the reservoir $\Omega \setminus \mathcal{C}$ reads: $\frac{\partial}{\partial t}(\rho_f \varphi^*) + \nabla \cdot (\rho_f \boldsymbol{v}^D) = q_s$, where q_s is a mass source or sink term, and $\boldsymbol{v}^D$ is the velocity of the fluid in $\Omega \setminus \mathcal{C}$, $\boldsymbol{v}^D = -\frac{1}{\mu_f}\boldsymbol{K}(\nabla p - \rho_f g \nabla \eta)$. Substituting the definitions of $\boldsymbol{v}^D$, ρ_f, and φ^* into the mass balance equation, and following the same approach as in section 2.2.3 of Chapter 2, we derive:

$$\frac{\partial}{\partial t}\Big((\frac{1}{M} + c_f\varphi_0)p + \alpha\nabla \cdot \boldsymbol{u}\Big) - \nabla \cdot \Big(\frac{1}{\mu_f}\boldsymbol{K}(\nabla p - \rho_{f,r} g \nabla \eta)\Big) = \tilde{q}. \tag{6.2.8}$$

where $\tilde{q} = \frac{q_s}{\rho_{f,r}}$. This completes the derivation of the poro-elastic equations, modeling the displacement $\boldsymbol{u}$ and pressure p in $\Omega \setminus \mathcal{C}$.

The fluid in the fracture is also assumed to be slightly compressible. Following a similar model as in [45], the conservation of mass in the fracture can be written as:

$$\frac{\partial(\rho_f w)}{\partial t} - \overline{\nabla} \cdot (\rho_f \frac{K_{\mathcal{C}}}{12\mu_f}(\overline{\nabla} p_f - \rho_r g \overline{\nabla} \eta)) = q_W - q_L.$$

For a slightly compressible fluid in the fracture, we can write: $\rho_f = \rho_{f,r}(1 + c_f(p_f - p_{c,r}))$, where p_f is the pressure in the fracture, $p_{c,r}$ is the reference pressure in the fracture, and c_f is the compressibility of the fluid. Assuming that c_f is in the order of 10^{-5} or 10^{-6}, we can approximate ρ_f as: $\rho_f \approx \rho_{f,r}$. Now, we write the mass balance equation in the fracture as follows:

$$\rho_{f,r}\frac{\partial w}{\partial t} + w\frac{\partial \rho_f}{\partial t} - \overline{\nabla} \cdot (\rho_{f,r} \frac{K_{\mathcal{C}}}{12\mu_f}(\overline{\nabla} p_f - \rho_{f,r} g \overline{\nabla} \eta)) = q_W - q_L.$$

Dividing by $\rho_{f,r}$ (defining $\tilde{q}_W = \frac{q_W}{\rho_{f,r}}$, and $\tilde{q}_L = \frac{q_L}{\rho_{f,r}}$), and substituting $\frac{\partial \rho_f}{\partial t} = \rho_{f,r} c_f \frac{\partial p_f}{\partial t}$, we obtain:

$$\frac{\partial w}{\partial t} + c_f w\frac{\partial p_f}{\partial t} - \overline{\nabla} \cdot (\frac{K_{\mathcal{C}}}{12\mu_f}(\overline{\nabla} p_f - \rho_{f,r} g \overline{\nabla} \eta)) = \tilde{q}_W - \tilde{q}_L.$$

The second term in the equation above is not linear. To linearize it, we redefine the compressibility of the fluid in the fracture as: $c_{f_c} = c_f w$, and assume it to be constant. Thus, the mass conservation equation in the fracture $\mathcal{C}$ reads:

$$c_f \frac{\partial p_f}{\partial t} + \frac{\partial}{\partial t} w - \overline{\nabla} \cdot (\frac{K_{\mathcal{C}}}{12\mu_f} (\overline{\nabla}\, p_f - \rho_{f,r} g \overline{\nabla}\, \eta)) = \tilde{q}_W - \tilde{q}_L. \tag{6.2.9}$$

The term $\frac{\partial}{\partial t} w$ accounts for the change in width of the fracture due to mechanical deformation. The term $\tilde{q}_W$ represents the injection term and $\tilde{q}_L$ represents the leakage term which connects the fracture flow model to the reservoir flow model. We will assume that $K_{\mathcal{C}}$ is a positive definite permeability tensor in our analysis.

For any function g defined in $\Omega \setminus \mathcal{C}$ with a trace, let $g^\star$ denote the trace of g on $\mathcal{C}^\star$, $\star = +, -$. The jump of g on $\mathcal{C}$ in the direction of $\boldsymbol{n}^+$ is defined by $[g]_{\mathcal{C}} = g^+ - g^-$. The width of the fracture, w, is the jump of $\boldsymbol{u} \cdot \boldsymbol{n}^-$ on $\mathcal{C}$, therefore, we have $w = -[\boldsymbol{u}]_{\mathcal{C}} \cdot \boldsymbol{n}^+$. Following this approach, we note that the leakoff term $\tilde{q}_L$ is the only unknown in equation (6.2.9) (recall that p_f is the trace of p on $\mathcal{C}$, i.e. $p_f = p|_{\mathcal{C}}$ on $\mathcal{C}$).

For the interface and boundary conditions, we will follow the same approach as in [43, 45]. Let $\boldsymbol{\tau}_j^\star$, $1 \le j \le d-1$, be a set of orthonormal tangent vectors on $\mathcal{C}^\star$, $\star = +, -$. The conservation of mass and the balance of the normal traction vector gives the interface conditions on each face (or side) of $\mathcal{C}$:

$$(\boldsymbol{\sigma}^{\mathrm{por}}(\boldsymbol{u}, p))^\star \boldsymbol{n}^\star = -p_f \boldsymbol{n}^\star \ , \ \star = +, -. \tag{6.2.10}$$

The continuity of p_f on $\mathcal{C}$ gives

$$[\boldsymbol{\sigma}^{\mathrm{por}}(\boldsymbol{u}, p)]_{\mathcal{C}} \boldsymbol{n}^\star = \boldsymbol{0}.$$

We simply derive:

$$\boldsymbol{\sigma}^{\mathrm{por}}(\boldsymbol{u}, p) \boldsymbol{n}^\star \cdot \boldsymbol{n}^\star = -p_f \ , \ \boldsymbol{\sigma}^{\mathrm{por}}(\boldsymbol{u}, p) \boldsymbol{n}^\star \cdot \boldsymbol{\tau}_j^\star = 0, \qquad 1 \le j \le d-1. \tag{6.2.11}$$

The jump in reservoir flux is equal to the leakage term, so, the conservation of mass equation at the interface gives:

$$\frac{1}{\mu_f} [\boldsymbol{K}(\nabla\, p - \rho_{f,r} g \nabla\, \eta)]_{\mathcal{C}} \cdot \boldsymbol{n}^+ = \tilde{q}_L. \tag{6.2.12}$$

We assume that the displacement, $\boldsymbol{u}$, and the normal component of the flux, $\boldsymbol{K}(\nabla p - \rho_{f,r} g \nabla \eta) \cdot \boldsymbol{n}$, vanish on $\partial\Omega$. We also assume that w is bounded in $\mathcal{C}$ and vanishes on $\partial\mathcal{C}$. Finally, since the time derivative in (6.2.8) acts on $(\frac{1}{M} + c_f\varphi_0)p + \alpha\nabla\cdot\boldsymbol{u}$, the initial condition is prescribed by (see [81]):

$$\Big((\frac{1}{M} + c_f\varphi_0)p + \alpha\nabla\cdot\boldsymbol{u}\Big)(0) = (\frac{1}{M} + c_f\varphi_0)p_0 + \alpha\nabla\cdot\boldsymbol{u}_0, \tag{6.2.13}$$

where $\boldsymbol{u}_0$ a given initial displacement and p_0 is a given initial pressure. We note that $\boldsymbol{u}_0$ and p_0 are not independent, as $\boldsymbol{u}_0$ is computed by solving the elasticity equation given p_0 and $(p_f|_{t=0} = p_0|_{\mathcal{C}})$ [43, 45].

The continuos in time formulation now reads: Find $\boldsymbol{u}$, p, and $\tilde{q}_L$ satisfying the equations below for all time $t \in]0, T[$:

$$
\begin{gathered}
-\operatorname{div}\boldsymbol{\sigma}^{\mathrm{por}}(\boldsymbol{u}, p) = \boldsymbol{f} \ \text{ in } \Omega\setminus\mathcal{C},\\
\boldsymbol{\sigma}^{\mathrm{por}}(\boldsymbol{u}, p) = \boldsymbol{\sigma}(\boldsymbol{u}) - \alpha\, p\, \boldsymbol{I} \ \text{ in } \Omega\setminus\mathcal{C},\\
\tfrac{\partial}{\partial t}\Big((\tfrac{1}{M} + c_f\varphi_0)p + \alpha\nabla\cdot\boldsymbol{u}\Big) - \nabla\cdot\Big(\tfrac{1}{\mu_f}\boldsymbol{K}(\nabla p - \rho_{f,r} g\nabla\eta)\Big) = \tilde{q} \ \text{ in } \Omega\setminus\mathcal{C},\\
c_f\tfrac{\partial p_f}{\partial t} + \tfrac{\partial}{\partial t}w - \overline{\nabla}\cdot(\tfrac{K_{\mathcal{C}}}{12\mu_f}(\overline{\nabla} p_f - \rho_{f,r} g\overline{\nabla}\eta)) = \tilde{q}_W - \tilde{q}_L \ \text{ in } \mathcal{C},\\
(\boldsymbol{\sigma}^{\mathrm{por}}(\boldsymbol{u}, p))^{\star}\boldsymbol{n}^{\star} = -p|_{\mathcal{C}}\boldsymbol{n}^{\star}\ ,\ \star = +, - \ \text{ on } \mathcal{C},\\
\tfrac{1}{\mu_f}[\boldsymbol{K}(\nabla p - \rho_{f,r} g\nabla\eta)]_{\mathcal{C}}\cdot\boldsymbol{n}^{+} = \tilde{q}_L \ \text{ on } \mathcal{C},\\
\text{where} \quad w = -[\boldsymbol{u}]_{\mathcal{C}}\cdot\boldsymbol{n}^{+},\\
\text{Boundary Conditions: } \boldsymbol{u} = \boldsymbol{0}\ ,\ \boldsymbol{K}(\nabla p - \rho_{f,r} g\nabla\eta)\cdot\boldsymbol{n} = 0 \ \text{ on } \partial\Omega,\\
\text{Initial Condition } \ (t=0): \ \Big((\tfrac{1}{M} + c_f\varphi_0)p + \alpha\nabla\cdot\boldsymbol{u}\Big)(0) =\\
(\tfrac{1}{M} + c_f\varphi_0)p_0 + \alpha\nabla\cdot\boldsymbol{u}_0.
\end{gathered}
$$

where: $\boldsymbol{K}$ is the absolute permeability tensor, g is the gravitation constant, $\mu_f > 0$ is the constant fluid viscosity, η is the distance in the vertical direction (assumed to be constant in time), $\rho_{f,r} > 0$ a constant reference density (relative to the reference pressure p_r), φ_0 is the initial porosity, M is the Biot modulus, $\tilde{q} = \frac{q}{\rho_{f,r}}$ where q is a mass source or sink term taking into account injection into or out of the reservoir, $\frac{\partial}{\partial t}w$ represents the change in fracture width due to mechanical deformation, $\tilde{q}_W$ represents the injection term and $\tilde{q}_L$

represents the leakage term which connects it to the reservoir flow model, and $\boldsymbol{n}^+$ is the normal vector out of the fracture surface.

6.2.2 Assumptions

The assumptions on the model and data are summarized as follows:

1. The reservoir is assumed to be homogeneous, isotropic and saturated poro-elastic medium. The reference density of the fluid (in the reservoir and fracture, $\rho_{f,r}$) and viscosity, μ_f, are given and positive. Moreover, $\mu_f > 0$ is assumed to be constant.

2. The dimensionless Biot coefficient α, the Lamé coefficients $\lambda > 0$ and $G > 0$, and the pore volume φ^* are all positive.

3. The absolute permeability tensors ($\boldsymbol{K}$ and $\boldsymbol{K}_c$) are assumed to be bounded, symmetric, uniformly positive definite in space and constant in time (for discrete time intervals).

4. The fluids are assumed to be slightly compressible (their densities are linear functions of the corresponding pressure).

5. For the single rate iterative coupling algorithm and the modified multirate iterative coupling algorithm, the Lamé coefficients λ, G and the compressibilities of the fluid satisfy

$$4GC^* > \frac{\lambda}{\alpha^2 c_{f_c}} \left(\frac{1}{M} + c_f \varphi_0 \right), \tag{6.2.14}$$

   where C^* is a product of optimal constants in Korn's, Poincare, and trace inequalities (defined in (6.4.55)).

   For the first multirate algorithm considered in this chapter, we assume:

$$\frac{\alpha^2}{\lambda} > \frac{1}{2GC^*} \qquad \& \qquad c_{f_c} > \frac{1}{M} + c_f \varphi_0$$

As explained in [43, 45], assumptions involving the constant C^* are not very restrictive provided that its value does not become very small. The shear modulus G and the bulk modulus λ are almost of the same order. Similarly, the compressibilities (c_f and c_{f_c}) and the reciprocal of the Biot modulus $1/M$ can be assumed to be of the same order. As stated in [43, 45], the shape of the fracture plays a role in the convergence of the iterative scheme since the constant C^* depends on the constant of the trace inequality. We note that the existence and uniqueness of the solution to the continuous formulation is given in [43].

6.2.3 Mixed Variational Formulation

In this section, we formulate and study a space-time discretization of the fractured poro-elastic system described above. Temporal discretization follows the usual backward-Euler scheme. A mixed finite element formulation is used to descretize flow equations in the reservoir and the fracture, while continuous Galerkin is used to descretize the elasticity equation. As described in Chapter 2, the mixed form defines the flux as a separate unknown and rewrites the flow equation as a system of first order equations. For the mixed formulation involved, we assume the lowest order RT (Raviart and Thomas, 1977) spaces. Let $\mathfrak{T}_h$ denote a regular family of conforming triangulation of the domain of interest $\overline{\Omega}$. We assume that $\mathfrak{T}_h$ triangulates both Ω^+ and Ω^-.

We define the space of discrete displacements $\boldsymbol{V}_h$, the space of discrete pressures in the reservoir Q_h, the space of discrete pressures in the fracture Q_{c_h}, the space of discrete velocities (fluxes) in the reservoir $\boldsymbol{Z}_h$, and the space of discrete velocities (fluxes) in the fracture $\boldsymbol{Z}_{\mathcal{C}h}$ as follows:

$$\boldsymbol{V}_h = \{\boldsymbol{v}_h \in H^1(\Omega^+ \cup \Omega^-)^d\,;\, \forall T \in \mathfrak{T}_h, \boldsymbol{v}_h|_T \in \mathbb{P}_1^d, [\boldsymbol{v}_h]_{\Gamma\setminus\mathcal{C}} = \boldsymbol{0}, \boldsymbol{v}_h^\star|_{\Gamma^\star} = \boldsymbol{0}, \star = +, -\}$$

$$Q_h = \{p_h \in L^2(\Omega)\,;\, \forall T \in \mathfrak{T}_h, p_h|_T \in \mathbb{P}_0\}$$

$$Q_{c_h} = \{p_{f_h} \in H^{1/2}(\mathcal{C})\,;\, \forall T \in \mathfrak{T}_h, p_{f_h}|_T \in \mathbb{P}_1\}$$

$$\boldsymbol{Z}_h = \{\boldsymbol{q}_h \in H(\mathrm{div}; \Omega^+ \cup \Omega^-)^d\,; \forall T \in \mathfrak{T}_h, \boldsymbol{q}_h|_T \in \mathbb{P}_1^d,$$
$$[\boldsymbol{q}_h] \cdot \boldsymbol{n}^+ = 0 \text{ on } \Gamma \setminus \mathcal{C}, \boldsymbol{q}_h \cdot \boldsymbol{n} = 0 \text{ on } \partial\Omega\}$$

$$\boldsymbol{Z}_{\mathcal{C}h} = \{\boldsymbol{\mu}_{f_h} \in \boldsymbol{Z}_{\mathcal{C}}\,;\, \forall T \in \mathfrak{T}_h, \boldsymbol{\mu}_{f_h}|_T \in \mathbb{P}_1^d\}$$

where $\boldsymbol{Z}_{\mathcal{C}}$ represents the space of continuous velocities in the fracture, and is defined as follows:

$$\boldsymbol{Z}_{\mathcal{C}} = \{\boldsymbol{\mu}_f \in L^2(\mathcal{C})^{d-1}\,;\, \overline{\nabla}\cdot\boldsymbol{\mu}_f \in H^{-1/2}(\mathcal{C})\}, \tag{6.2.15}$$

normed by:

$$\|\boldsymbol{\mu}_f\|_{\boldsymbol{Z}_{\mathcal{C}}} = (\|\boldsymbol{\mu}_f\|^2_{L^2(\mathcal{C})} + \|\overline{\nabla}\cdot\boldsymbol{\mu}_f\|^2_{H^{-1/2}(\mathcal{C})})^{1/2}. \tag{6.2.16}$$

In addition, the Space Q_{c_h} is equipped with the norm:

$$|v|_{H^{1/2}(\mathcal{C})} = \Big(\int_{\mathcal{C}}\int_{\mathcal{C}} \frac{|v(\boldsymbol{x}) - v(\boldsymbol{y})|^2}{|\boldsymbol{x}-\boldsymbol{y}|^d} d\boldsymbol{x}\, d\boldsymbol{y}\Big)^{1/2}\ ,\ \|v\|_{H^{1/2}(\mathcal{C})} = (\|v\|^2_{L^2(\mathcal{C})} + |v|^2_{H^{1/2}(\mathcal{C})})^{1/2}. \tag{6.2.17}$$

The space of displacements $\boldsymbol{V}_h$ is equipped with the norm:

$$\|\boldsymbol{v}_h\|_{V_h} = \Big(\sum_{i=1}^{d} \|\boldsymbol{v}_{hi}\|^2_{\Omega^+\cup\Omega^-}\Big)^{1/2} = \Big(\sum_{i=1}^{d}\Big(\|\boldsymbol{v}_{h_i}^{+}\|^2_{H^1(\Omega^+)} + \|\boldsymbol{v}_{h_i}^{-}\|^2_{H^1(\Omega^-)}\Big)\Big)^{1/2}.$$

Moreover, the space of reservoir matrix velocity is normed by:

$$\|\boldsymbol{q}_h\|_{\boldsymbol{Z}_h} = (\|\boldsymbol{q}_h\|^2_{H(div;\Omega^+\cup\Omega^-)})^{1/2} = \Big(\|\boldsymbol{q}_h^{+}\|^2_{H(div;\Omega^+)} + \|\boldsymbol{q}_h^{-}\|^2_{H(div;\Omega^-)}\Big)^{1/2}.$$

The space Q_h is normed by the usual L^2 norm.

We can also assume that the discrete leakage term is in $H^{-1/2}(\mathcal{C})$. However, it will be eliminated completely by substituting (6.2.12) into the fracture flow equation.

Following the same approach described in the earlier chapters, we assume that a local time step is given by: $\Delta t = t_k - t_{k-1}$. If we denote the total number of time steps by N, then the total simulation time is given by T = Δt N, and $t_i = i\Delta t$, $0 \leqslant i \leqslant N$ denote the discrete time points.

In the following section, we describe an extension of the fixed-stress split iterative coupling algorithm to the fractured poro-elastic media.

6.3 Fixed Stress Split Algorithm For Fractured Poroelastic Media

We will follow the fixed stress split formulation introduced in [43]. Although we use the splitting scheme at the discrete level, it is easier to see its details at the continuum level (we note here that the superscript n denotes the iterative coupling iteration index). In this iterative coupling algorithm, we first solve the flow problem in the reservoir and the fracture in a monolithic manner:

Step (a) [Flow] Given $\boldsymbol{u}^n$, we solve for $p^{n+1}, \boldsymbol{z}^{n+1}, p_f^{n+1}, \boldsymbol{\zeta}^{n+1}$

$$\begin{gathered}(\tfrac{1}{M} + c_f\varphi_0 + \tfrac{\alpha^2}{\lambda})\tfrac{\partial}{\partial t}p^{n+1} + \tfrac{1}{\mu_f}\nabla\cdot\boldsymbol{z}^{n+1} = \tfrac{\alpha^2}{\lambda}\tfrac{\partial}{\partial t}p^{n} - \alpha\nabla\cdot\tfrac{\partial}{\partial t}\boldsymbol{u}^n + \tilde{q} \text{ in } \Omega\setminus\mathcal{C},\\ \boldsymbol{z}^{n+1} = -\boldsymbol{K}(\nabla\, p^{n+1} - \rho_{f,r}g\nabla\,\eta),\end{gathered}$$

$$\begin{gathered}(\gamma_c + c_{fc})\,\tfrac{\partial}{\partial t}\,p_f^{n+1} + \tfrac{\partial}{\partial t}w^n + \tfrac{1}{12\mu_f}\overline{\nabla}\cdot\boldsymbol{\zeta}^{n+1} = \gamma_c\,\tfrac{\partial}{\partial t}p_f^n + \tilde{q}_W + [\boldsymbol{z}]_{\mathcal{C}}^{n+1}\cdot\boldsymbol{n}^+ \text{ in } \mathcal{C},\\ \boldsymbol{\zeta}^{n+1} = -K_{\mathcal{C}}(\overline{\nabla}\,p_f^{n+1} - \rho_{f,r}g\overline{\nabla}\,\eta) \text{ in } \mathcal{C}\end{gathered}$$

Once the flow is computed, we update the displacement solution.

Step (b) [Mechanics] Given $p^{n+1}, \boldsymbol{z}^{n+1}, p_f^{n+1}, \boldsymbol{\zeta}^{n+1}$, we solve for $\boldsymbol{u}^{n+1}$ satisfying

$$\begin{gathered}-\mathrm{div}\,\boldsymbol{\sigma}^{\mathrm{por}}(\boldsymbol{u}^{n+1}, p^{n+1}) = \boldsymbol{f} \text{ in } \Omega\setminus\mathcal{C},\\ \boldsymbol{\sigma}^{\mathrm{por}}(\boldsymbol{u}^{n+1}, p^{n+1}) = \boldsymbol{\sigma}(\boldsymbol{u}^{n+1}) - \alpha\, p^{n+1}\,\boldsymbol{I} \text{ in } \Omega\setminus\mathcal{C},\\ (\boldsymbol{\sigma}^{\mathrm{por}}(\boldsymbol{u}^{n+1}, p^{n+1}))^{\star}\boldsymbol{n}^{\star} = -p_f^{n+1}|_{\mathcal{C}}\boldsymbol{n}^{\star}\ ,\ \star = +,- \text{ on } \mathcal{C}.\end{gathered}$$

γ_c is an adjustable coefficient which is going to be revealed by the proof of the contraction.

In what follows, we still denote the scalar products in space by parentheses. If the domain of integration is not indicated, then it is understood that the integrals are taken over $\Omega^+\cup\Omega^-$. Let the solution at time t_{k-1} be known. That is, the values of $\boldsymbol{u}^{k-1}$, p^{k-1}, ${p_f}^{k-1}$, $\boldsymbol{z}^{k-1}$, and $\boldsymbol{\zeta}^{k-1}$ are computed and known from the last time step (the superscript k here denotes the time step index). We also assume appropriate initial values of our unknowns: $\boldsymbol{u}^0$, p^0, ${p_f}^0$, $\boldsymbol{z}^0$, and $\boldsymbol{\zeta}^0$. Moreover, we will follow the same notation as the one used in Chapter 2, listed below for completeness.

Remark 6.3.1. Notation: *We briefly recall the notation introduced earlier: n denotes the flow/mechanics coupling iteration index and k denotes the time step index. For multirate*

iterative coupling schemes, k denotes the coarser time step index (for indexing mechanics coarse time steps), and m denotes the finer (local) time step index (for indexing flow fine time steps). Moreover, Δt stands for the fine time step size, and q is the "fixed" number of finer flow time steps per coarse mechanics time step.

6.4 Single Rate Formulation and Analysis

6.4.1 Fully Discrete Scheme for Single Rate

As for the pure Biot system (without including fractures), using the mixed finite element method in space (for flow), continuous Galerkin (CG) for mechanics, and the backward Euler finite difference method in time, the weak formulation of the single rate scheme reads as follows.

Definition 6.4.1. *Find $p_h^k \in Q_h$, $p_{f_h}^k \in Q_{c_h}$, $\boldsymbol{z}_h^k \in \boldsymbol{Z}_h$, and $\boldsymbol{\zeta}_h^k \in \boldsymbol{Z}_{\mathcal{E}h}$ such that,*

*(***flow equation***)*

$$\forall \theta_h \in Q_h\,, \frac{1}{\Delta t}\Big((\frac{1}{M}+c_f\varphi_0)\Big(p_h^k-p_h^{k-1}\Big),\theta_h\Big)+\frac{1}{\mu_f}(\nabla\cdot\boldsymbol{z}_h^k,\theta_h)= \\ -\frac{\alpha}{\Delta t}\Big(\nabla\cdot\Big(\boldsymbol{u}_h^k-\boldsymbol{u}_h^{k-1}\Big),\theta_h\Big)+\Big(\tilde{q}_h,\theta_h\Big)\,, \tag{6.4.18}$$

$$\forall \boldsymbol{q}_h \in \boldsymbol{Z}_h\,, \Big(\boldsymbol{K}^{-1}\boldsymbol{z}_h^k,\boldsymbol{q}_h\Big)=\Big(p_h^k,\nabla\cdot\boldsymbol{q}_h\Big)-\Big(p_{f_h}^k,[\boldsymbol{q}_h]_{\mathcal{E}}\cdot n^+\Big)_{\mathcal{E}}+\Big(\rho_{f,r}g\nabla\eta,\boldsymbol{q}_h\Big)\,, \tag{6.4.19}$$

$$\forall \theta_{c_h} \in Q_{c_h}\,, \frac{c_{f_c}}{\Delta t}\Big(p_{f_h}^k-p_{f_h}^{k-1},\theta_{c_h}\Big)_{\mathcal{E}}+\frac{1}{12\mu_f}\Big(\overline{\nabla}\cdot\delta\boldsymbol{\zeta}_h^k,\theta_{c_h}\Big)_{\mathcal{E}}-\frac{1}{\mu_f}\Big(\Big[\boldsymbol{z}_h^k\Big]_{\mathcal{E}}\cdot\boldsymbol{n}^+,\theta_{c_h}\Big)_{\mathcal{E}} \\ =\frac{1}{\Delta t}\Big([\boldsymbol{u}_h^k]_{\mathcal{E}}\cdot\boldsymbol{n}^+-[\boldsymbol{u}_h^{k-1}]_{\mathcal{E}}\cdot\boldsymbol{n}^+,\theta_{c_h}\Big)_{\mathcal{E}}+(q_{\tilde{W}h},\theta_{c_h})_{\mathcal{E}}\,, \tag{6.4.20}$$

$$\forall \boldsymbol{\mu}_{f_h} \in \boldsymbol{Z}_{\mathcal{E}h}\,, (K_{\mathcal{E}}^{-1}\boldsymbol{\zeta}_h^k,\boldsymbol{\mu}_{f_h})_{\mathcal{E}}=(p_{f_h}^k,\overline{\nabla}\cdot(\boldsymbol{\mu}_{f_h}))_{\mathcal{E}}+(\overline{\nabla}(\rho_{f,r}g\eta),\boldsymbol{\mu}_{f_h})_{\mathcal{E}}\,, \tag{6.4.21}$$

*and (***mechanics equation***)*

find $\boldsymbol{u}_h^k \in \boldsymbol{V}_h$ such that,

$$\forall \boldsymbol{v}_h \in V_h\,, 2G(\boldsymbol{\varepsilon}(\boldsymbol{u}_h^k),\boldsymbol{\varepsilon}(\boldsymbol{v}_h))+\lambda(\nabla\cdot\boldsymbol{u}_h^k,\nabla\cdot\boldsymbol{v}_h)-\alpha(p_h^k,\nabla\cdot\boldsymbol{v}_h) \\ +(p_{f_h}^k,[\boldsymbol{v}_h]_{\mathcal{E}}\cdot\boldsymbol{n}^+)_{\mathcal{E}}=(\boldsymbol{f},\boldsymbol{v}_h)\,, \tag{6.4.22}$$

with the initial condition for the first discrete time step,

$$\Big((\frac{1}{M}+c_f\varphi_0)p_h^0+\alpha\nabla\cdot\boldsymbol{u}_h^0\Big)(0)=(\frac{1}{M}+c_f\varphi_0)p_0+\alpha\nabla\cdot\boldsymbol{u}_0. \tag{6.4.23}$$

6.4.2 Single Rate Iterative Scheme

In what follows, we consider the fully discrete scheme of the fixed stress split iterative coupling algorithm presented above. The proof of contraction for the single rate case is a direct generalization of the proof presented in the work of Girault *et al.* [43] at the continuum level (continuous in time and space formulation). It should be noted that this proof can be optimized by assuming the coefficients of the fixed-stress split regularization terms (in equations (6.4.24) and (6.4.26)) to be free-parameters, determined by the proof of contraction. The quantity of contraction in this case will change accordingly. This approach is going to be followed in the multirate case. We start by presenting the fully-discrete single rate iterative coupling algorithm.

Algorithm 8: Single Rate Iterative Coupling Algorithm for Fractured Poroleastic Media

for $k = 0, 1, 2, 3, ..$ **do** /* Time step iteration index */

  for $n = 1, 2, ..$ **do** /* coupling iteration index */

    First Step: Flow equations

    Given $\boldsymbol{u}_h^{n,k}$ *(assuming an initial value is given for the first iteration:* $\boldsymbol{u}_h^{0,k}$*)*

    Solve for $p_h^{n+1,k}, \boldsymbol{z}_h^{n+1,k}, {p_f}_h^{n+1,k}$, *and* $\boldsymbol{\zeta}_h^{n+1,k}$ *satisfying:*

$$(\frac{1}{M} + c_f\varphi_0 + \frac{\alpha^2}{\lambda})\frac{p_h^{n+1,k} - p_h^{k-1}}{\Delta t} + \frac{1}{\mu_f}\nabla \cdot \boldsymbol{z}_h^{n+1,k} =$$
$$\frac{\alpha^2}{\lambda}\frac{p_h^{n,k} - p_h^{k-1}}{\Delta t} - \alpha\nabla \cdot \frac{\boldsymbol{u}_h^{n,k} - \boldsymbol{u}_h^{k-1}}{\Delta t} + \tilde{q}_h \text{ in } \Omega \setminus \mathcal{C}, \tag{6.4.24}$$

$$\boldsymbol{z}_h^{n+1,k} = -\boldsymbol{K}(\nabla p_h^{n+1,k} - \rho_{f,r} g \nabla \eta), \tag{6.4.25}$$

$$(\gamma_c + c_{fc})\frac{{p_f}_h^{n+1,k} - {p_f}_h^{k-1}}{\Delta t} + \frac{w_h^{n,k} - w_h^{k-1}}{\Delta t} + \frac{1}{12\mu_f}\overline{\nabla} \cdot \boldsymbol{\zeta}_h^{n+1,k} =$$
$$\gamma_c\frac{{p_f}_h^{n,k} - {p_f}_h^{k-1}}{\Delta t} + \tilde{q}_{W_h} - \tilde{q_L}_h^{n+1,k} \text{ in } \mathcal{C} \tag{6.4.26}$$

$$\boldsymbol{\zeta}_h^{n+1,k} = \boldsymbol{K}_{\mathcal{C}}(\overline{\nabla}\, {p_f}_h^{n+1,k} - \rho_{f,r} g \overline{\nabla}\, \eta), \tag{6.4.27}$$

$$\frac{1}{\mu_f}[\boldsymbol{K}(\nabla p_h^{n+1,k} - \rho_{f,r} g \nabla \eta)]_{\mathcal{C}} \cdot \boldsymbol{n}^+ = \tilde{q_L}_h^{n+1,k} \text{ on } \mathcal{C} \tag{6.4.28}$$

$$w_h^{n,k} = -[\boldsymbol{u}_h^{n,k}]_{\mathcal{C}} \cdot \boldsymbol{n}^+, \tag{6.4.29}$$

    Second Step: Mechanics equations

    Given $p_h^{n+1,k}, \boldsymbol{z}_h^{n+1,k}, {p_f}_h^{n+1,k}$, *and* $\boldsymbol{\zeta}_h^{n+1,k}$, *solve for* $\boldsymbol{u}_h^{n+1,k}$ *satisfying:*

$$-\operatorname{div} \boldsymbol{\sigma}^{\text{por}}(\boldsymbol{u}_h^{n+1,k}, p_h^{n+1,k}) = \boldsymbol{f} \text{ in } \Omega \setminus \mathcal{C} \tag{6.4.30}$$

$$\boldsymbol{\sigma}^{\text{por}}(\boldsymbol{u}_h^{n+1,k}, p_h^{n+1,k}) = \boldsymbol{\sigma}(\boldsymbol{u}_h^{n+1,k}) - \alpha\, p_h^{n+1,k}\, \boldsymbol{I} \text{ in } \Omega \setminus \mathcal{C} \tag{6.4.31}$$

$$(\boldsymbol{\sigma}^{\text{por}}(\boldsymbol{u}_h^{n+1,k}, p_h^{n+1,k}))^\star \boldsymbol{n}^\star = -{p_f}_h^{n+1,k} \boldsymbol{n}^\star \ , \ \star = +, - \text{ on } \mathcal{C} \tag{6.4.32}$$

The weak formulation of the above equations reads:

Step (a): Find $\boldsymbol{u}_h^{n+1,k} \in \boldsymbol{V}_h$, $p_h^{n+1,k} \in Q_h$, $p_{f_h}^{n+1,k} \in Q_{c_h}$, $\boldsymbol{z}_h^{n+1,k} \in \boldsymbol{Z}_h$, and $\boldsymbol{\zeta}_h^{n+1,k} \in \boldsymbol{Z}_{\mathcal{E}h}$ such that:

$$\forall \theta_h \in Q_h\,,\ \Big((\frac{1}{M}+c_f\varphi_0+\frac{\alpha^2}{\lambda})(\frac{p_h^{n+1,k}-p_h^{k-1}}{\Delta t}),\theta_h\Big)+\frac{1}{\mu_f}(\nabla\cdot\boldsymbol{z}_h^{n+1,k},\theta_h)= \\ \Big(-\frac{\alpha}{\lambda}(-\alpha(\frac{p_h^{n+1,k}-p_h^{k-1}}{\Delta t})+\lambda\nabla\cdot(\frac{\boldsymbol{u}_h^{n+1,k}-\boldsymbol{u}_h^{k-1}}{\Delta t})),\theta_h\Big)+(\tilde{q}_h,\theta_h) \tag{6.4.33}$$

$$\forall \theta_{c_h} \in Q_{c_h}\,,\ \Big((c_{fc}+\gamma_c)\frac{p_{f_h}^{n+1,k}-p_{f_h}^{k-1}}{\Delta t},\theta_{c_h}\Big)+\frac{1}{12\mu_f}(\overline{\nabla}\cdot(\boldsymbol{\zeta}_h^{n+1,k}),\theta_{c_h})_{\mathcal{E}} \\ -\frac{1}{\mu_f}([\boldsymbol{z}_h^{n+1,k}]_{\mathcal{E}}\cdot\boldsymbol{n}^+,\theta_{c_h})_{\mathcal{E}}=\Big(\gamma_c\frac{p_{f_h}^{n,k}-p_{f_h}^{k-1}}{\Delta t},\theta_{c_h}\Big) \\ +(\frac{[\boldsymbol{u}_h^{n,k}]_{\mathcal{E}}\cdot\boldsymbol{n}^+-[\boldsymbol{u}_h^{k-1}]_{\mathcal{E}}\cdot\boldsymbol{n}^+}{\Delta t},\theta_{c_h})_{\mathcal{E}}+(\tilde{q_{W}}_h,\theta_{c_h})_{\mathcal{E}} \tag{6.4.34}$$

$$\forall \boldsymbol{q}_h \in \boldsymbol{Z}_h\,,\ (\boldsymbol{K}^{-1}\boldsymbol{z}_h^{n+1,k},\boldsymbol{q}_h)=(p_h^{n+1,k},\nabla\cdot\boldsymbol{q}_h)-(p_{f_h}^{n+1,k},[\boldsymbol{q}_h]_{\mathcal{E}}\cdot\boldsymbol{n}^+)_{\mathcal{E}}+(\nabla(\rho_{f,r}g\eta),\boldsymbol{q}_h) \tag{6.4.35}$$

$$\forall \boldsymbol{\mu}_{f_h} \in \boldsymbol{Z}_{\mathcal{E}h}\,,\ (\boldsymbol{K}_{\mathcal{E}}^{-1}\boldsymbol{\zeta}_h^{n+1,k},\boldsymbol{\mu}_{f_h})_{\mathcal{E}}=(p_{f_h}^{n+1,k},\overline{\nabla}\cdot(\boldsymbol{\mu}_{f_h}))_{\mathcal{E}}+(\overline{\nabla}(\rho_{f,r}g\eta),\boldsymbol{\mu}_{f_h})_{\mathcal{E}}. \tag{6.4.36}$$

Step (b): Given $p_h^{n+1,k}, \boldsymbol{z}_h^{n+1,k}, p_{f_h}^{n+1,k}, \boldsymbol{\zeta}_h^{n+1,k}$, find $\boldsymbol{u}_h^{n+1,k} \in \boldsymbol{V}_h$,

$$\forall \boldsymbol{v}_h \in V_h\,,\ 2G(\boldsymbol{\varepsilon}(\boldsymbol{u}_h^{n+1,k}),\boldsymbol{\varepsilon}(\boldsymbol{v}_h))+\lambda(\nabla\cdot\boldsymbol{u}_h^{n+1,k},\nabla\cdot\boldsymbol{v}_h)-\alpha(p_h^{n+1,k},\nabla\cdot\boldsymbol{v}_h) \\ +(p_{f_h}^{n+1,k},[\boldsymbol{v}_h]_{\mathcal{E}}\cdot\boldsymbol{n}^+)_{\mathcal{E}}=(\boldsymbol{f},\boldsymbol{v}_h)\,, \tag{6.4.37}$$

To begin the iteration (at the beginning of time step t_k), for $n=1$, we assign the initial condition (compare to (6.2.13)):

$$\Big((\frac{1}{M}+c_f\varphi_0)p_h^{1,k}+\alpha\nabla\cdot\boldsymbol{u}_h^{1,k}\Big)(t_{k-1})=(\frac{1}{M}+c_f\varphi_0)p^{k-1}+\alpha\nabla\cdot\boldsymbol{u}^{k-1}.$$

where the terms $\frac{\alpha^2}{\lambda}\frac{p_h^{n+1,k}-p_h^{k-1}}{\Delta t}$ and $\frac{\alpha^2}{\lambda}\frac{p_h^{n,k}-p_h^{k-1}}{\Delta t}$ on the right and left hand sides of (6.4.33) are the usual fixed-stress split regularization terms. In a similar way, we have introduced fixed-stress split regularization terms for the fracture equation. The term $\gamma_c\frac{p_{f_h}^{n+1,k}-p_{f_h}^{k-1}}{\Delta t}$ is added to the left hand side of (6.4.34), and a corresponding term $\gamma_c\frac{p_{f_h}^{n,k}-p_{f_h}^{k-1}}{\Delta t}$ is added

to the right hand side of the same equation for consistency. The carried out mathematical analysis will result in an appropriate estimate for γ_c, which depends on the trace and Korn's inequalities' constants (following a similar approach to the one presented in Girault *et al.* [43], but for the fully discrete case) . We note that the presence of the newly introduced terms does not affect obtained solution upon convergence. However, their presence is necessary to show that the scheme is contractive.

For the single rate fully discrete formulation, we define the volumetric mean stress (or the quantity to be contracted on) as follows:

$$\sigma_v^k = \sigma_v^{k-1} + \lambda \nabla \cdot \boldsymbol{u}_h^k - \alpha(p_h^k - p_h^{k-1}). \tag{6.4.38}$$

Incorporating the coupling-iteration index, we have:

$$\sigma_v^{n,k} = \sigma_v^{k-1} + \lambda \nabla \cdot \boldsymbol{u}_h^{n,k} - \alpha(p_h^{n,k} - p_h^{k-1}). \tag{6.4.39}$$

Recalling the notation used for the difference between two consecutive iterates:

$$\delta\xi^{n+1} = \xi^{n+1} - \xi^n,$$

where ξ may stand for $p_h, p_{f_h}, \boldsymbol{z}_h$, $\boldsymbol{\zeta}_h, \sigma_v$, or $\boldsymbol{u}_h$. We write the volumetric mean stress in terms of coupling iteration differences as follows:

$$\delta\sigma_v^{n,k} = \lambda \nabla \cdot \delta\boldsymbol{u}_h^{n,k} - \alpha \delta p_h^{n,k} \tag{6.4.40}$$

In addition, we define a corresponding quantity for the flow in the fracture as follows:

$$\chi\sigma_f^{n,k} = \gamma_c {p_f}_h^{n,k} - w_n^k, \tag{6.4.41}$$

where χ and γ_c are unknown coefficients, to be determined by the proof of contraction. In terms of coupling iteration differences, (6.4.41) can be written as:

$$\chi\delta\sigma_f^{n,k} = \gamma_c \delta {p_f}_h^{n,k} - \delta w_n^k, \tag{6.4.42}$$

Equation (6.4.40) can also be written as $-\frac{\alpha}{\lambda}\delta\sigma_v^{n,k} = \frac{\alpha^2}{\lambda}\delta p_h^{n,k} - \alpha\nabla \cdot \delta\boldsymbol{u}_h^{n,k}$ which will appear on the right hand side of the mass balance equation for the flow in the matrix. In terms of

coupling iteration differences, equations (6.4.33), (6.4.34), (6.4.35), (6.4.36), and (6.4.37) can be written as follows:

$$\forall \theta_h \in Q_h\,,\ \Big(\frac{1}{\Delta t}(\frac{1}{M}+c_f\varphi_0+\frac{\alpha^2}{\lambda})\delta p_h^{n+1,k},\theta_h\Big)+\frac{1}{\mu_f}(\nabla\cdot\delta\boldsymbol{z}_h^{n+1,k},\theta_h)=\Big(-\frac{\alpha}{\lambda\Delta t}\delta\sigma_v^{n,k},\theta_h\Big) \tag{6.4.43}$$

$$\begin{aligned}\forall \theta_{c_h} \in Q_{c_h}\,,\ \Big(\frac{1}{\Delta t}(c_{fc}+\gamma_c)\delta p_{f_h}^{n+1,k},\theta_{c_h}\Big)+\frac{1}{12\mu_f}(\overline{\nabla}\cdot(\delta\boldsymbol{\zeta}_h^{n+1,k}),\theta_{c_h})_{\mathcal{E}}\\ -\frac{1}{\mu_f}([\delta\boldsymbol{z}_h^{n+1,k}]_{\mathcal{E}}\cdot\boldsymbol{n}^+,\theta_{c_h})_{\mathcal{E}}=\Big(\frac{\gamma_c}{\Delta t}\delta p_{f_h}^{n,k},\theta_{c_h}\Big)+(\frac{1}{\Delta t}[\delta\boldsymbol{u}_h^{n,k}]_{\mathcal{E}}\cdot\boldsymbol{n}^+,\theta_{c_h})_{\mathcal{E}}\end{aligned} \tag{6.4.44}$$

$$\forall \boldsymbol{q}_h \in \boldsymbol{Z}_h\,,\ (\boldsymbol{K}^{-1}\delta\boldsymbol{z}_h^{n+1,k},\boldsymbol{q}_h)=(\delta p_h^{n+1,k},\nabla\cdot\boldsymbol{q}_h)-(\delta p_{f_h}^{n+1,k},[\boldsymbol{q}_h]_{\mathcal{E}}\cdot\boldsymbol{n}^+)_{\mathcal{E}} \tag{6.4.45}$$

$$\forall \boldsymbol{\mu}_{f_h} \in \boldsymbol{Z}_{\mathcal{E}h}\,,\ (\boldsymbol{K}_{\mathcal{E}}^{-1}\delta\boldsymbol{\zeta}_h^{n+1,k},\boldsymbol{\mu}_{f_h})_{\mathcal{E}}=(\delta p_{f_h}^{n+1,k},\overline{\nabla}\cdot(\boldsymbol{\mu}_{f_h}))_{\mathcal{E}} \tag{6.4.46}$$

$$\begin{aligned}\forall \boldsymbol{v}_h \in V_h\,,\ 2G(\boldsymbol{\varepsilon}(\delta\boldsymbol{u}_h^{n+1,k}),\boldsymbol{\varepsilon}(\boldsymbol{v}_h))+\lambda(\nabla\cdot\delta\boldsymbol{u}_h^{n+1,k},\nabla\cdot\boldsymbol{v}_h)-\alpha(\delta p_h^{n+1,k},\nabla\cdot\boldsymbol{v}_h)\\ +(\delta p_{f_h}^{n+1,k},[\boldsymbol{v}_h]_{\mathcal{E}}\cdot\boldsymbol{n}^+)_{\mathcal{E}}=0\end{aligned} \tag{6.4.47}$$

6.4.3 Proof of Contraction

We first group our constants as follows:

$$\beta=\frac{1}{M\alpha^2}+\frac{c_f}{\alpha^2}\varphi_0+\frac{1}{\lambda},\quad \beta_c=c_f+\gamma_c. \tag{6.4.48}$$

Note that β and β_c are the coefficients of the pressure terms in (6.4.43) and (6.4.44) respectively.

- **Step (1): Flow equations**

  Consider (6.4.43), and test it with $\theta_h=\delta p_h^{n+1,k}$ to obtain

  $$\Big(\frac{1}{\Delta t}\alpha^2\beta\delta p_h^{n+1,k},\delta p_h^{n+1,k}\Big)+\frac{1}{\mu_f}\Big(\nabla\cdot\delta\boldsymbol{z}_h^{n+1,k},\delta p_h^{n+1,k}\Big)=-\frac{\alpha}{\lambda\Delta t}\Big(\delta\sigma_v^{n,k},\delta p_h^{n+1,k}\Big).$$

  By Young's inequality, we have

  $$\begin{aligned}\frac{\beta}{\Delta t}\Big\|\alpha\delta p_h^{n+1,k}\Big\|^2+\frac{1}{\mu_f}\Big(\nabla\cdot\delta\boldsymbol{z}_h^{n+1,k},\delta p_h^{n+1,k}\Big)&=\frac{1}{\Delta t}\Big((-\alpha\epsilon\delta p_h^{n+1,k}),(\frac{1}{\epsilon\lambda})\sigma_v^{n,k}\Big)\\ &\le\frac{1}{\Delta t}\Big(\frac{\epsilon^2}{2}\Big\|\alpha\delta p_h^{n+1,k}\Big\|^2+\frac{1}{2\epsilon^2\lambda^2}\Big\|\frac{\partial}{\partial t}\delta\sigma_v^{n,k}\Big\|^2\Big)\end{aligned}$$

Letting $\epsilon^2 = \beta$, we obtain

$$\beta\Big\|\alpha\delta p_h^{n+1,k}\Big\|^2 + \frac{2\Delta t}{\mu_f}(\nabla\cdot\delta\boldsymbol{z}_h^{n+1,k}, \delta p_h^{n+1,k}) \leq \frac{1}{\beta\lambda^2}\Big\|\delta\sigma_v^{n,k}\Big\|^2. \tag{6.4.49}$$

Now, consider the equation of flux in the reservoir (6.4.45), and test it with $\boldsymbol{q}_h = \delta\boldsymbol{z}_h^{n+1,k}$ to obtain

$$(\boldsymbol{K}^{-1}\delta\boldsymbol{z}_h^{n+1,k}, \delta\boldsymbol{z}_h^{n+1,k}) = (\delta p_h^{n+1,k}, \nabla\cdot\delta\boldsymbol{z}_h^{n+1,k}) - (\delta {p_f}_h^{n+1,k}, [\delta\boldsymbol{z}_h^{n+1,k}]_{\mathcal{E}}\cdot\boldsymbol{n}^+)_{\mathcal{E}}. \tag{6.4.50}$$

For the pressure in the fracture, consider (6.4.44) and test it with θ_{c_h} to be $\theta_{c_h} = \delta {p_f}_h^{n+1,k}$ to obtain

$$\begin{aligned}
&\Big(\frac{1}{\Delta t}(c_{fc}+\gamma_c)\delta {p_f}_h^{n+1,k}, \delta {p_f}_h^{n+1,k}\Big)_{\mathcal{E}} + \frac{1}{12\mu_f}(\overline{\nabla}\cdot(\delta\boldsymbol{\zeta}_h^{n+1,k}), \delta {p_f}_h^{n+1,k})_{\mathcal{E}} \\
&- \frac{1}{\mu_f}([\delta\boldsymbol{z}_h^{n+1,k}]_{\mathcal{E}}\cdot\boldsymbol{n}^+, \delta {p_f}_h^{n+1,k})_{\mathcal{E}} = \Big(\frac{\gamma_c}{\Delta t}\delta {p_f}_h^{n,k}, \delta {p_f}_h^{n+1,k}\Big)_{\mathcal{E}} + (\frac{1}{\Delta t}[\delta\boldsymbol{u}_h^{n,k}]_{\mathcal{E}}\cdot\boldsymbol{n}^+, \delta {p_f}_h^{n+1,k})_{\mathcal{E}} \\
&\qquad = \frac{1}{\Delta t}\Big(\frac{1}{\epsilon}(\gamma_c\delta {p_f}_h^{n,k} + [\delta\boldsymbol{u}_h^{n,k}]_{\mathcal{E}}\cdot\boldsymbol{n}^+), \epsilon\delta {p_f}_h^{n+1,k}\Big) \\
&\qquad \leq \frac{1}{\Delta t}\Big(\frac{1}{2\epsilon^2}\Big\|\gamma_c\delta {p_f}_h^{n,k} + \delta[\boldsymbol{u}_h^{n,k}]_{\mathcal{E}}\cdot\boldsymbol{n}^+\Big\|_{\mathcal{E}}^2 + \frac{\epsilon^2}{2}\Big\|\delta {p_f}_h^{n+1,k}\Big\|_{\mathcal{E}}^2\Big)
\end{aligned} \tag{6.4.51}$$

by Young's inequality. Choosing $\epsilon^2 = (c_{fc}+\gamma_c)$ and multiplying the whole equation by $2\Delta t$, we derive:

$$\begin{aligned}
&(c_{fc}+\gamma_c)\Big\|\delta {p_f}_h^{n+1,k}\Big\|_{\mathcal{E}}^2 + \frac{\Delta t}{6\mu_f}(\overline{\nabla}\cdot(K_{\mathcal{E}}^{-1}\delta\boldsymbol{\zeta}_h^{n+1,k}), \delta {p_f}_h^{n+1,k})_{\mathcal{E}} \\
&\quad - \frac{2\Delta t}{\mu_f}([\delta\boldsymbol{z}_h^{n+1,k}]_{\mathcal{E}}\cdot\boldsymbol{n}^+, \delta {p_f}_h^{n+1,k})_{\mathcal{E}} \leq \frac{1}{(c_{fc}+\gamma_c)}\Big\|\gamma_c\delta {p_f}_h^{n,k} + \delta[\boldsymbol{u}_h^{n,k}]_{\mathcal{E}}\cdot\boldsymbol{n}^+\Big\|_{\mathcal{E}}^2.
\end{aligned}$$

For flux in the fracture, consider (6.4.46) and test it with $\boldsymbol{\mu}_f = \delta\boldsymbol{\zeta}_h^{n+1,k}$ to obtain

$$(K_{\mathcal{E}}^{-1}\delta\boldsymbol{\zeta}_h^{n+1,k}, \delta\boldsymbol{\zeta}_h^{n+1,k})_{\mathcal{E}} = (\delta {p_f}_h^{n+1,k}, \overline{\nabla}\cdot(\delta\boldsymbol{\zeta}_h^{n+1,k}))_{\mathcal{E}} \tag{6.4.52}$$

Combining (6.4.49), (6.4.50), (6.4.51), and (6.4.52), we derive:

$$\begin{aligned}
&\Big\|\alpha\delta p_h^{n+1,k}\Big\|^2 + \frac{2\Delta t}{\beta\mu_f}\|K^{-1/2}\delta\boldsymbol{z}_h^{n+1,k}\|^2 + \frac{2\beta_c}{\beta}\|\delta {p_f}_h^{n+1,k}\|_{\mathcal{E}}^2 + \frac{\Delta t}{6\mu_f\beta}\|K_{\mathcal{E}}^{-1/2}\delta\boldsymbol{\zeta}_h^{n+1,k}\|_{\mathcal{E}}^2 \\
&\qquad \leq \frac{1}{\beta^2\lambda^2}\Big\|\delta\sigma_v^{n,k}\Big\|^2 + \frac{2}{\beta}(\gamma_c\delta {p_f}_h^{n,k} + [\delta\boldsymbol{u}_h^{n,k}]_{\mathcal{E}}\cdot\boldsymbol{n}^+, \delta {p_f}_h^{n+1,k})_{\mathcal{E}}
\end{aligned} \tag{6.4.53}$$

- **Step 2: Elasticity equation**

  Testing (6.4.47) with $\boldsymbol{v}_h = \delta \boldsymbol{u}_h^{n+1,k}$, we derive:

$$2G\|\boldsymbol{\varepsilon}(\delta \boldsymbol{u}_h^{n+1,k})\|^2 + \lambda\|\nabla \cdot \delta \boldsymbol{u}_h^{n+1,k}\|^2 - \alpha(\delta p_h^{n+1,k}, \nabla \cdot \delta \boldsymbol{u}_h^{n+1,k}) \\ +(\delta p_{f_h}^{n+1,k}, [\delta \boldsymbol{u}_h^{n+1,k}]_{\mathcal{C}} \cdot \boldsymbol{n}^+)_{\mathcal{C}} = 0. \tag{6.4.54}$$

The term $\|\boldsymbol{\varepsilon}(\delta \boldsymbol{u}_h^{n+1,k})\|^2$ can be related to the width of the fracture, w, as follows (following exactly the same approach described in [43]). Let $C_T^\star$, $\mathcal{P}_\Gamma^\star$, and $C_\kappa^\star$ denote respectively the constants of the trace, Poincaré, and Korn inequality in $\Omega^\star$, $\star = +, -$:

$$\|\boldsymbol{u}_h|_\Omega^\star\|_{L^2(\mathcal{C})} \leq C_T^\star \|\boldsymbol{u}_h\|_{H^1(\Omega^\star)} \ , \ \|\boldsymbol{u}_h\|_{L^2(\Omega^\star)} \leq \mathcal{P}_\Gamma^\star |\boldsymbol{u}_h|_{H^1(\Omega^\star)} \ , \ |\boldsymbol{u}_h|_{H^1(\Omega^\star)} \leq C_\kappa^\star \|\boldsymbol{\varepsilon}(\boldsymbol{u}_h)\|_{L^2(\Omega^\star)}.$$

Let $C_T = \max(C_T^+, C_T^-)$, $C_\kappa = \max(C_\kappa^+, C_\kappa^-)$, and $\mathcal{P}_\Gamma = \max(\mathcal{P}_\Gamma^+, \mathcal{P}_\Gamma^-)$. By combining these three inequalities we derive for any $\boldsymbol{v}_h$ in V_h

$$\begin{aligned}
\|[\boldsymbol{v}_h]_{\mathcal{C}}\|_{L^2(\mathcal{C})}^2 &\leq \|\boldsymbol{v}_h|_{\Omega^+}\|_{L^2(\mathcal{C})}^2 + |2(\boldsymbol{v}_h|_{\Omega^+}, \boldsymbol{v}_h|_{\Omega^-})_{\mathcal{C}}| + \|\boldsymbol{v}_h|_{\Omega^-}\|_{L^2(\mathcal{C})}^2 \\
&\leq \|\boldsymbol{v}_h|_{\Omega^+}\|_{L^2(\mathcal{C})}^2 + 2 \times \frac{1}{2}\Big(\|\boldsymbol{v}_h|_{\Omega^+}\|_{L^2(\mathcal{C})}^2 + \|\boldsymbol{v}_h|_{\Omega^-}\|_{L^2(\mathcal{C})}^2\Big) + \|\boldsymbol{v}_h|_{\Omega^-}\|_{L^2(\mathcal{C})}^2 \\
&\leq 2\|\boldsymbol{v}_h|_{\Omega^+}\|_{L^2(\mathcal{C})}^2 + 2\|\boldsymbol{v}_h|_{\Omega^-}\|_{L^2(\mathcal{C})}^2 \\
&\leq 2C_T^2 \|\boldsymbol{v}_h\|_{H^1(\Omega^+ \cup \Omega^-)}^2 \\
&\leq 2C_T^2(\mathcal{P}_\Gamma^2 + 1)|\boldsymbol{v}_h|_{H^1(\Omega^+ \cup \Omega^-)}^2 \\
&\leq 2C_T^2(\mathcal{P}_\Gamma^2 + 1)C_\kappa^2 \|\boldsymbol{\varepsilon}(\boldsymbol{v}_h)\|_{L^2(\Omega^+ \cup \Omega^-)} = 2C_T^2(\mathcal{P}_\Gamma^2 + 1)C_\kappa^2 \|\boldsymbol{\varepsilon}(\boldsymbol{v}_h)\|_{L^2(\Omega \setminus \mathcal{C})}.
\end{aligned}$$

Hence

$$\|\boldsymbol{\varepsilon}(\boldsymbol{u}_h)\|_{L^2(\Omega \setminus \mathcal{C})}^2 \geq C^\star \|[\boldsymbol{u}_h]_{\mathcal{C}}\|_{L^2(\mathcal{C})}^2 \geq C^\star \|[\boldsymbol{u}_h]_{\mathcal{C}} \cdot \boldsymbol{n}^+\|_{L^2(\mathcal{C})}^2,$$

where $C^\star = (2C_T^2(\mathcal{P}_\Gamma^2 + 1)C_\kappa^2)^{-1}$. So, we have:

$$C^\star \|w_h\|_{L^2(\mathcal{C})}^2 = C^\star \|[\boldsymbol{u}_h]_{\mathcal{C}} \cdot \boldsymbol{n}^+\|_{L^2(\mathcal{C})}^2 \leq \|\boldsymbol{\varepsilon}(\boldsymbol{u}_h)\|_{L^2(\Omega \setminus \mathcal{C})}^2 \tag{6.4.55}$$

Applying (6.4.55) to (6.4.54) and multiplying by 2λ, we obtain:

$$4G\lambda C^* \|\delta w_h^{n+1,k}\|^2 + 2\lambda^2 \|\nabla \cdot \delta \boldsymbol{u}_h^{n+1,k}\|^2 - 2\lambda\alpha(\delta p_h^{n+1,k}, \nabla \cdot \delta \boldsymbol{u}_h^{n+1,k}) \\ +2\lambda(\delta p_{f_h}^{n+1,k}, \delta w_h^{n+1,k} \cdot \boldsymbol{n}^+)_{\mathcal{C}} = 0, \tag{6.4.56}$$

Combining (6.4.53) and (6.4.56) and re-arranging terms, we derive:

$$\begin{aligned}
&\left\{\left\|\alpha\delta p_h^{n+1,k}\right\|^2 - 2\lambda\alpha(\delta p_h^{n+1,k}, \nabla\cdot\delta\boldsymbol{u}_h^{n+1,k}) + \lambda^2\|\nabla\cdot\delta\boldsymbol{u}_h^{n+1,k}\|^2\right\} \\
+\lambda^2\|\nabla\cdot\delta\boldsymbol{u}_h^{n+1,k}\|^2 &+ \frac{2\Delta t}{\beta\mu_f}\|K^{-1/2}\delta\boldsymbol{z}_h^{n+1,k}\|^2 + \frac{\Delta t}{6\mu_f\beta}\|K_{\mathfrak{e}}^{-1/2}\delta\boldsymbol{\zeta}_h^{n+1,k}\|_{\mathfrak{e}}^2 \\
+\left\{\frac{2\beta_c}{\beta}\|\delta {p_f}_h^{n+1,k}\|_{\mathfrak{e}}^2 + 4G\lambda C^*\|\delta w_h^{n+1,k}\|_{\mathfrak{e}}^2 - 2\lambda(\delta {p_f}_h^{n+1,k}, \delta w_h^{n+1,k})_{\mathfrak{e}}\right\} & \\
\leq \frac{1}{\beta^2\lambda^2}\left\|\delta\sigma_v^{n,k}\right\|^2 + \frac{2}{\beta}(\gamma_c\delta {p_f}_h^{n,k} - \delta w_h^{n,k}, \delta {p_f}_h^{n+1,k})_{\mathfrak{e}} &\qquad (6.4.57)
\end{aligned}$$

Using Young's inequality for the second term on the right hand side of (6.4.57),

$$\begin{aligned}
\frac{2}{\beta}\Big(\gamma_c\delta {p_f}_h^{n,k} - \delta w_h^{n,k}, \delta {p_f}_h^{n+1,k}\Big) &\leq \frac{2}{\beta}\Big(\frac{1}{2\beta_c}\left\|\gamma_c\delta {p_f}_h^{n,k} - \delta w_h^{n,k}\right\|_{\mathfrak{e}}^2 + \frac{\beta_c}{2}\left\|\delta {p_f}_h^{n+1,k}\right\|_{\mathfrak{e}}^2\Big) \\
&= \frac{1}{\beta\beta_c}\left\|\gamma_c\delta {p_f}_h^{n,k} - \delta w_h^{n,k}\right\|_{\mathfrak{e}}^2 + \frac{\beta_c}{\beta}\left\|\delta {p_f}_h^{n+1,k}\right\|_{\mathfrak{e}}^2 \qquad (6.4.58)
\end{aligned}$$

Substituting (6.4.58) into (6.4.57), we obtain:

$$\begin{aligned}
&\left\{\left\|\alpha\delta p_h^{n+1,k}\right\|^2 - 2\lambda(\alpha\delta p_h^{n+1,k}, \nabla\cdot\delta\boldsymbol{u}_h^{n+1,k}) + \lambda^2\|\nabla\cdot\delta\boldsymbol{u}_h^{n+1,k}\|^2\right\} \\
+\lambda^2\|\nabla\cdot\delta\boldsymbol{u}_h^{n+1,k}\|^2 &+ \frac{2\Delta t}{\beta\mu_f}\|K^{-1/2}\delta\boldsymbol{z}_h^{n+1,k}\|^2 + \frac{\Delta t}{6\mu_f\beta}\|K_{\mathfrak{e}}^{-1/2}\delta\boldsymbol{\zeta}_h^{n+1,k}\|_{\mathfrak{e}}^2 \\
+\left\{\frac{\beta_c}{\beta}\|\delta {p_f}_h^{n+1,k}\|_{\mathfrak{e}}^2 + 4G\lambda C^*\|\delta w_h^{n+1,k}\|_{\mathfrak{e}}^2 - 2\lambda(\delta {p_f}_h^{n+1,k}, \delta w_h^{n+1,k})_{\mathfrak{e}}\right\} & \\
\leq \frac{1}{\beta^2\lambda^2}\left\|\delta\sigma_v^{n,k}\right\|^2 + \frac{1}{\beta\beta_c}\left\|\gamma_c\delta {p_f}_h^{n,k} - \delta w_h^{n,k}\right\|_{\mathfrak{e}}^2 &\qquad (6.4.59)
\end{aligned}$$

The first three terms on the left hand side is an expanded square, which forms the quantity of contraction in the reservoir matrix. To form a quantity of contraction on the last three terms on the left hand side, we will match their coefficients with the coefficients of the expanded square of (6.4.41). Expanding (6.4.41) yields

$$\begin{aligned}
\left\|\chi\sigma_f^{n+1,k}\right\|^2 &= \frac{\gamma_c^2}{\chi^2}\|_{\mathfrak{e}}^2\delta {p_f}_h^{n+1,k}\|^2 + \|\delta w_h^{n+1,k}\|_{\mathfrak{e}}^2 - 2\frac{\gamma_c}{\chi^2}(\delta {p_f}_h^{n+1,k}, \delta w_h^{n+1,k})_{\mathfrak{e}}, \\
&= \frac{\beta_c}{\beta}\|\delta {p_f}_h^{n+1,k}\|_{\mathfrak{e}}^2 + 4G\lambda C^*\|\delta w_h^{n+1,k}\|_{\mathfrak{e}}^2 - 2\lambda(\delta {p_f}_h^{n+1,k}, \delta w_h^{n+1,k})_{\mathfrak{e}}
\end{aligned}$$

Choosing,

$$\frac{\beta_c}{\beta} = \frac{\gamma_c^2}{\chi^2}, \quad \frac{\gamma_c}{\chi^2} = \lambda, \quad 4\lambda GC^* = \left(4\lambda GC^* - \frac{1}{\chi^2}\right) + \frac{1}{\chi^2}.$$

With β and β_c defined in (6.4.48), we compute

$$\gamma_c = \frac{c_{f_c}}{\lambda\beta - 1}, \quad \chi = \left\{ \frac{c_{f_c}}{\lambda^2\beta - \lambda} \right\}^{1/2}. \tag{6.4.60}$$

Note that $\lambda\beta > 1$ and hence, γ_c is a positive quantity. Substituting the above into (6.4.59), we obtain:

$$\begin{aligned} &\|\delta\sigma_v^{n+1,k}\|^2 + \lambda^2\|\nabla\cdot\delta\boldsymbol{u}_h^{n+1,k}\|^2 + \tfrac{2\Delta t}{\beta\mu_f}\|K^{-1/2}\delta\boldsymbol{z}_h^{n+1,k}\|^2 + \tfrac{\Delta t}{6\mu_f\beta}\|K_{\mathcal{C}}^{-1/2}\delta\boldsymbol{\zeta}_h^{n+1,k}\|_{\mathcal{C}}^2 \\ &+\|\delta\sigma_f^{n+1,k}\|_{\mathcal{C}}^2 + (4G\lambda C^* - \tfrac{1}{\chi^2})\|\delta w_h^{n+1,k}\|_{\mathcal{C}}^2 \leq \tfrac{1}{\beta^2\lambda^2}\left\|\delta\sigma_v^{n,k}\right\|^2 + \tfrac{\chi^2}{\beta_c\beta}\|\delta\sigma_f^{n,k}\|_{\mathcal{C}}^2. \end{aligned} \tag{6.4.61}$$

For contraction to hold, we require,

$$4G\lambda C^* \geq \frac{1}{\chi^2}, \quad \frac{1}{\beta^2\lambda^2} < 1, \quad \frac{\chi^2}{\beta_c\beta} < 1,$$

By (6.4.60), the first inequality implies

$$4GC^* \geq \frac{\lambda}{c_{f_c}}\left(\frac{1}{M\alpha^2} + \frac{c_f}{\alpha^2}\varphi_0\right) \tag{6.4.62}$$

which is satisfied by the assumption (6.2.14). In fact, (6.2.14) is a sharper assumption (strict inequality versus inequality), since it is needed to prove strong convergence of the term involving $w_h^{n,k}$. The second inequality is trivially satisfied by (6.4.48). For the last inequality, a simple calculation reveals

$$\gamma_c < \lambda\beta(c_{fc} + \gamma_c) \Rightarrow (1 - \lambda\beta)\gamma_c < \lambda\beta c_{fc}$$

which is also satisfied using the value of γ_c derived in (6.4.60).

6.4.4 Convergence to the Continuous Form

From the discussion above, we obtain the following lemma.

Lemma 6.4.1. *There exist limit functions $p_h^k, \boldsymbol{u}_h^k, \boldsymbol{z}_h^k, \boldsymbol{\zeta}_h^k, p_{f_h}^k, w_h^k$ such that*

$$\begin{array}{llll} p_h^{n,k} \to p_h^k, , & \text{in } L^2(\Omega^+\cup\Omega^-), & \boldsymbol{u}_h^{n,k} \to \boldsymbol{u}_h^k, & \text{in } H^1(\Omega^+\cup\Omega^-)^d \\ \boldsymbol{z}_h^{n,k} \to \boldsymbol{z}_h^k, & \text{in } \boldsymbol{Z}_h, & \boldsymbol{\zeta}_h^{n,k} \to \boldsymbol{\zeta}_h^k, & \text{in } \boldsymbol{Z}_{\mathcal{C}h} \\ p_{f_h}^{n,k} \to p_{f_h}^k & \text{in } L^2(\mathcal{C}), & w_h^{n,k} \to w_h^k & \text{in } L^2(\mathcal{C}) \end{array}$$

converge strongly in the norms of the above spaces.

Proof. The result (6.4.61) implies that $\sigma_v^{n,k}$, $\nabla \cdot \boldsymbol{u}_h^{n,k}$ and $\sigma_{fh}^{n,k}$ are Cauchy sequences (the first two in $L^2(\Omega \setminus \mathcal{C})$ and the third in and $L^2(\mathcal{C})$), with geometric convergence. The sharper hypothesis (6.2.14) with strict inequality implies that $w_h^{n,k}$ is also a Cauchy sequence in $L^2(\mathcal{C})$ with geometric convergence. Moreover, the same result implies that $\boldsymbol{z}_h^{n,k}$ and $\boldsymbol{\zeta}_h^{n,k}$ are Cauchy sequences with geometric convergence in $L^2(\Omega \setminus \mathcal{C})$ and $L^2(\mathcal{C})$ respectively. From the definitions of $\sigma_v^{n,k}$ and $\sigma_{fh}^{n,k}$: (6.4.39) and (6.4.41), and the fact that the addition of two Cauchy sequences is still a Cauchy sequence, we conclude that $p_h^{n+1,k}$ and $p_{fh}^{n+1,k}$ are Cauchy sequences with geometric convergence in $L^2(\Omega \setminus \mathcal{C})$ and $L^2(\mathcal{C})$, both are Hilbert (complete) spaces, therefore $p_h^{n+1,k}$ and $p_{fh}^{n+1,k}$ have unique limits in $L^2(\Omega \setminus \mathcal{C})$ and $L^2(\mathcal{C})$ respectively.

To obtain convergence of the displacement, we use Young's inequality in (6.4.54):

$$2G\|\boldsymbol{\varepsilon}(\delta\boldsymbol{u}_h^{n+1,k})\|^2 + \lambda\|\nabla\cdot\delta\boldsymbol{u}_h^{n+1,k}\|^2 \leq \frac{\alpha^2}{2\lambda}\left\|\delta p_h^{n+1,k}\right\|^2 + \frac{\lambda}{2}\left\|\nabla\cdot\delta\boldsymbol{u}_h^{n+1,k}\right\|^2 + \frac{1}{4GC^*}\left\|\delta p_{fh}^{n+1,k}\right\|_{\mathcal{C}}^2 + GC^*\left\|\delta w_h^{n+1,k}\right\|_{\mathcal{C}}^2$$

where C^* is the constant in (6.4.55). Applying (6.4.55) to the left hand side above, we get:

$$G\|\boldsymbol{\varepsilon}(\delta\boldsymbol{u}_h^{n+1,k})\|^2 + GC^*\|\delta w_h^{n+1,k}\|^2 + \lambda\|\nabla\cdot\delta\boldsymbol{u}_h^{n+1,k}\|^2 \leq \frac{\alpha^2}{2\lambda}\left\|\delta p_h^{n+1,k}\right\|^2 + \frac{\lambda}{2}\left\|\nabla\cdot\delta\boldsymbol{u}_h^{n+1,k}\right\|^2 + \frac{1}{4GC^*}\left\|\delta p_{fh}^{n+1,k}\right\|_{\mathcal{C}}^2 + GC^*\left\|\delta w_h^{n+1,k}\right\|_{\mathcal{C}}^2$$

$\Rightarrow$

$$G\|\boldsymbol{\varepsilon}(\delta\boldsymbol{u}_h^{n+1,k})\|^2 + \frac{\lambda}{2}\|\nabla\cdot\delta\boldsymbol{u}_h^{n+1,k}\|^2 \leq \frac{\alpha^2}{2\lambda}\left\|\delta p_h^{n+1,k}\right\|^2 + \frac{1}{4GC^*}\left\|\delta p_{fh}^{n+1,k}\right\|_{\mathcal{C}}^2$$

The right-hand side of the above equation converges geometrically to 0. We conclude that $\boldsymbol{\varepsilon}(\boldsymbol{u}_h^{n+1,k})$ also converges geometrically in $L^2(\Omega \setminus \mathcal{C})$ implying that $\boldsymbol{u}_h^{n+1,k}$ converges geometrically in $H^1(\Omega^+ \cup \Omega^-)^d$.

For estimating the divergence of the fluxes, we observe that (6.4.43) amounts to the following equality a.e. in $L^2(\Omega \setminus \mathcal{C})$

$$-\nabla\cdot\delta\boldsymbol{z}_h^{n+1,k} = \left(\frac{\mu_f}{\Delta t}\right)\left(\frac{1}{M} + c_f\varphi_0 + \frac{\alpha^2}{\lambda}\right)\delta p_h^{n+1,k} + \left(\frac{\mu_f\alpha}{\lambda\Delta t}\right)\delta\sigma_v^{n,k}$$

The convergence of $\nabla\cdot\boldsymbol{z}_h^{n+1,k}$ in $L^2(\Omega\setminus\mathcal{C})$ follows from the convergence of $p_h^{n+1,k}$ and $\sigma_v^{n,k}$ in $L^2(\Omega\setminus\mathcal{C})$. Therefore, we have both $\nabla\cdot\boldsymbol{z}_h^{n+1,k}$ and $\boldsymbol{z}_h^{n+1,k}$ converging geometrically to unique

limits in $L^2(\Omega \setminus \mathcal{C})$, hence $\boldsymbol{z}_h^{n+1,k}$ converges to a unique limit in $\boldsymbol{Z}_h$. With Green's formula, we have the convergence of $[\delta \boldsymbol{z}_h^{n+1,k}]_{\mathcal{C}} \cdot \mathbf{n}^+$ in $H^{-1/2}(\mathcal{C})$. In a similar way, the convergence of $\overline{\nabla} \cdot \boldsymbol{\zeta}_h^{n,k}$ follows from the previous convergences and the fact that (6.4.44) gives the following equality a.e. in $H^{-1/2}(\mathcal{C})$:

$$\begin{aligned}\overline{\nabla} \cdot (\delta \boldsymbol{\zeta}_h^{n+1,k}) = -\Big(\frac{12\mu_f}{\Delta t}\Big)(c_{fc} + \gamma_c)\delta {p_f}_h^{n+1,k} + 12[\delta \boldsymbol{z}_h^{n+1,k}]_{\mathcal{C}} \cdot \boldsymbol{n}^+ \\ + \Big(\frac{12\mu_f \gamma_c}{\Delta t}\Big)\delta {p_f}_h^{n,k} + \Big(\frac{12\mu_f}{\Delta t}\Big)[\delta \boldsymbol{u}_h^{n,k}]_{\mathcal{C}} \cdot \boldsymbol{n}^+\end{aligned}$$

which can be written as,

$$\overline{\nabla} \cdot (\delta \boldsymbol{\zeta}_h^{n+1,k}) = -\Big(\frac{12\mu_f}{\Delta t}\Big)(c_{fc} + \gamma_c)\delta {p_f}_h^{n+1,k} + 12[\delta \boldsymbol{z}_h^{n+1,k}]_{\mathcal{C}} \cdot \boldsymbol{n}^+ + \Big(\frac{12\mu_f \chi}{\Delta t}\Big)\delta \sigma_f^{n+1,k}$$

All sequences on the right hand side converge in $H^{-1/2}(\mathcal{C})$. Therefore, we have the convergence of $\overline{\nabla} \cdot \boldsymbol{\zeta}_h^{n,k}$ in $H^{-1/2}(\mathcal{C})$ as well. Together with the previous deduced result that $\boldsymbol{\zeta}_h^{n,k}$ converges strongly to a unique limit in $L^2(\mathcal{C})$, we have the convergence of $\boldsymbol{\zeta}_h^{n,k}$ to a unique limit in $Z_{\mathcal{C}h}$.

Therefore, all sequences considered converge strongly. The existence of the limiting functions in the corresponding spaces follows immediately from the completeness of these spaces. □

It remains to pass to the limit in (6.4.33)–(6.4.37). This follows immediately since the equations are linear and all operators involved are continuous in the spaces invoked in the statement of Lemma 6.4.1. Moreover the convergences are strong. Therefore, we easily retrieve the fully discrete formulation.

The above discussions are summarized in the following main result of this work.

Theorem 6.4.1. *The iterative scheme is a contraction given by*

$$\begin{aligned}&\|\delta \sigma_v^{n+1,k}\|_{\Omega^+ \cup \Omega^-} + \lambda^2 \|\nabla \cdot \delta \boldsymbol{u}_h^{n+1,k}\|_{\Omega^+ \cup \Omega^-} + \tfrac{2\Delta t}{\beta \mu_f}\|K^{-1/2}\delta \boldsymbol{z}_h^{n+1,k}\|_{\Omega^+ \cup \Omega^-} \\ &+ \tfrac{\Delta t}{6\mu_f \beta}\|K_{\mathcal{C}}^{-1/2}\delta \boldsymbol{\zeta}_h^{n+1,k}\|_{\mathcal{C}} + \|\delta \sigma_f^{n+1,k}\|_{\mathcal{C}} + (4G\lambda C^* - \tfrac{1}{\chi^2})\|\delta w_h^{n+1,k}\|_{\mathcal{C}} \\ &\qquad \leq \max\left\{ \frac{1/\lambda^2}{\left(\frac{1}{M\alpha^2} + \frac{c_f}{\alpha^2}\varphi_0 + \frac{1}{\lambda}\right)^2}, \frac{\gamma_c}{(c_{fc}+\gamma_c)\lambda\left(\frac{1}{M\alpha^2} + \frac{c_f}{\alpha^2}\varphi_0 + \frac{1}{\lambda}\right)} \right\} \left(\left\| \delta \sigma_v^{n,k} \right\|_{\Omega^+ \cup \Omega^-} + \|\delta \sigma_f^{n,k}\|_{\mathcal{C}} \right).\end{aligned}$$

Furthermore, the converged solution is a unique solution to the weak formulation (6.4.18) - (6.4.22).

6.5 Multirate Formulation and Analysis

In this section, we consider a multirate formulation of the fixed stress split iterative coupling algorithm in fractured poro-elastic media, and rigorously analyze its convergence properties. We recall from previous chapters that the multirate algorithm allows for multiple finer flow time steps within one coarser mechanics time step. We will formulate a multirate iterative coupling scheme and show that it is Banach contractive with respect to a correctly chosen metric. We adopt exactly the same notation as the one used in Chapter 2.

6.5.1 Fully Discrete Scheme for Multirate

Using the mixed finite element method in space (for flow), continuous Galerkin for mechanics, and the backward Euler finite difference method in time, the weak formulation of the multirate scheme in fractured poro-elastic media reads as follows.

Definition 6.5.1. *For $k = iq$, $i \in \mathbb{N}$, and $1 \leq m \leq q$, find $p_h^{m+k} \in Q_h$, $p_{f_h}^{m+k} \in Q_{c_h}$, $\boldsymbol{z}_h^{m+k} \in \boldsymbol{Z}_h$, and $\boldsymbol{\zeta}_h^{m+k} \in \boldsymbol{Z}_{\mathcal{e}h}$ such that,*

*(***flow equation***)*

$$\forall \theta_h \in Q_h\,, \frac{1}{\Delta t}\Big((\frac{1}{M}+c_f\varphi_0)\Big(p_h^{m+k}-p_h^{m-1+k}\Big),\theta_h\Big)+\frac{1}{\mu_f}(\nabla\cdot\boldsymbol{z}_h^{m+k},\theta_h)= \\ -\frac{1}{\Delta t}\Big(\frac{\alpha}{q}\nabla\cdot\Big(\boldsymbol{u}_h^{k+q}-\boldsymbol{u}_h^{k}\Big),\theta_h\Big)+\Big(\tilde{q}_h,\theta_h\Big)\,, \tag{6.5.63}$$

$$\forall \boldsymbol{q}_h \in \boldsymbol{Z}_h\,, \Big(\boldsymbol{K}^{-1}\boldsymbol{z}_h^{m+k},\boldsymbol{q}_h\Big)=\Big(p_h^{m+k},\nabla\cdot\boldsymbol{q}_h\Big)-\Big(p_{f_h}^{m+k},[\boldsymbol{q}_h]_{\mathcal{e}}\cdot n^+\Big)_{\mathcal{e}}+\Big(\rho_{f,r}g\nabla\eta,\boldsymbol{q}_h\Big)\,, \tag{6.5.64}$$

$$\forall \theta_{c_h} \in Q_{c_h}\,, \frac{c_{f_c}}{\Delta t}\Big(p_{f_h}^{m+k}-p_{f_h}^{m-1+k},\theta_{c_h}\Big)_{\mathcal{e}}+\frac{1}{12\mu_f}\Big(\overline{\nabla}\cdot\delta\boldsymbol{\zeta}_h^{m+k},\theta_{c_h}\Big)_{\mathcal{e}} \\ -\frac{1}{\mu_f}\Big(\Big[\boldsymbol{z}_h^{m+k}\Big]_{\mathcal{e}}\cdot\boldsymbol{n}^+,\theta_{c_h}\Big)_{\mathcal{e}}=\frac{1}{q\Delta t}\Big([\boldsymbol{u}_h^{k+q}]_{\mathcal{e}}\cdot\boldsymbol{n}^+-[\boldsymbol{u}_h^{k}]_{\mathcal{e}}\cdot\boldsymbol{n}^+,\theta_{c_h}\Big)_{\mathcal{e}} \\ +(\tilde{q_W}_h,\theta_{c_h})_{\mathcal{e}}\,, \tag{6.5.65}$$

$$\forall \boldsymbol{\mu}_{f_h} \in \boldsymbol{Z}_{\mathcal{e}h}\,, (K_{\mathcal{e}}^{-1}\boldsymbol{\zeta}_h^{m+k},\boldsymbol{\mu}_{f_h})_{\mathcal{e}}=(p_{f_h}^{m+k},\overline{\nabla}\cdot(\boldsymbol{\mu}_{f_h}))_{\mathcal{e}}+(\overline{\nabla}(\rho_{f,r}g\eta),\boldsymbol{\mu}_{f_h})_{\mathcal{e}}\,, \tag{6.5.66}$$

*and (***mechanics equation***)*

find $\boldsymbol{u}_h^{k+q} \in \boldsymbol{V}_h$ *such that,*

$$\forall \boldsymbol{v}_h \in V_h\,,\; 2G(\boldsymbol{\varepsilon}(\boldsymbol{u}_h^{k+q}), \boldsymbol{\varepsilon}(\boldsymbol{v}_h)) + \lambda(\nabla \cdot \boldsymbol{u}_h^{k+q}, \nabla \cdot \boldsymbol{v}_h) - \alpha(p_h^{k+q}, \nabla \cdot \boldsymbol{v}_h) + (p_{f_h}^{k+q}, [\boldsymbol{v}_h]_{\mathcal{C}} \cdot \boldsymbol{n}^+)_{\mathcal{C}} = (\boldsymbol{f}, \boldsymbol{v}_h)\,, \tag{6.5.67}$$

with the initial condition for the first discrete time step,

$$\Big((\frac{1}{M} + c_f\varphi_0)p_h^0 + \alpha\nabla \cdot \boldsymbol{u}_h^0\Big)(0) = (\frac{1}{M} + c_f\varphi_0)p_0 + \alpha\nabla \cdot \boldsymbol{u}_0. \tag{6.5.68}$$

Note that the pressure unknowns p_h, p_{f_h} and flux unknowns $\boldsymbol{z}_h, \boldsymbol{\zeta}_h$ are solved at finer time steps $t_{k+m}, m = 0, \ldots, q$ whereas the mechanics variables $\boldsymbol{u}_h$ are being solved at $t_{iq}, i \in \mathbb{N}$. Therefore, for each mechanics time step of size $q\Delta t$, there are q flow solves justifying the nomenclature of multirate (as described in Chapter 2). In addition, the above system of PDEs is linear but coupled with the coupling terms being computed at the coarse mechanics time steps. Instead of solving the system in a simultaneously coupled manner, a splitting algorithm (in particular, the fixed stress split algorithm as described in the single rate case) will be applied to decouple the two equations and iterate between them until the solutions satisfying the above system (6.5.63) – (6.5.68) are obtained.

6.5.2 Multirate Iterative Coupling Scheme

We begin by describing the algorithm:

Algorithm 9: Multirate Iterative Coupling Algorithm for Fractured Poroleastic Media

for $k = 0, q, 2q, 3q, ..$ **do** `/* mechanics time step iteration index */`

  for $n = 1, 2, ..$ **do** `/* coupling iteration index */`

    First Step: Flow equations

    Given $\boldsymbol{u}_h^{n,k+q}$ *(assuming an initial value is given for the first iteration:* $\boldsymbol{u}_h^{0,k+q}$*)*

    for $m = 1, 2, .., q$ **do** `/* flow finer time steps iteration index */`

      Solve for $p_h^{n+1,m+k}, \boldsymbol{z}_h^{n+1,m+k}, {p_f}_h^{n+1,m+k}$, *and* $\boldsymbol{\zeta}_h^{n+1,m+k}$ *satisfying:*

$$(\frac{1}{M} + c_f\varphi_0 + L)\frac{p_h^{n+1,m+k} - p_h^{n+1,m-1+k}}{\Delta t} + \frac{1}{\mu_f}\nabla \cdot \boldsymbol{z}_h^{n+1,m+k} = L\frac{p_h^{n,m+k} - p_h^{m-1+k}}{\Delta t} - \alpha\nabla \cdot \frac{\boldsymbol{u}_h^{n,k+q} - \boldsymbol{u}_h^{n,k}}{q\Delta t} + \tilde{q}_h \text{ in } \Omega \setminus \mathcal{C}, \tag{6.5.69}$$

$$\boldsymbol{z}_h^{n+1,m+k} = -\boldsymbol{K}(\nabla\, p_h^{n+1,m+k} - \rho_{f,r} g \nabla\, \eta), \tag{6.5.70}$$

$$(\gamma_c + c_{fc})\frac{{p_f}_h^{n+1,m+k} - {p_f}_h^{n+1,m-1+k}}{\Delta t} + \frac{w_h^{n,k+q} - w_h^{n,k}}{q\Delta t} + \frac{1}{12\mu_f}\overline{\nabla} \cdot \boldsymbol{\zeta}_h^{n+1,m+k} = \gamma_c\frac{{p_f}_h^{n,m+k} - {p_f}_h^{n,m-1+k}}{\Delta t} + \tilde{q}_{W_h} - \tilde{q_L}_h^{n+1,m+k} \text{ in } \mathcal{C} \tag{6.5.71}$$

$$\boldsymbol{\zeta}_h^{n+1,m+k} = -\boldsymbol{K}_{\mathcal{C}}(\overline{\nabla}\, {p_f}_h^{n+1,m+k} - \rho_{f,r} g \overline{\nabla}\, \eta), \tag{6.5.72}$$

$$\frac{1}{\mu_f}[\boldsymbol{K}(\nabla\, p_h^{n+1,m+k} - \rho_{f,r} g \nabla\, \eta)]_{\mathcal{C}} \cdot \boldsymbol{n}^+ = \tilde{q_L}_h^{n+1,m+k} \text{ on } \mathcal{C} \tag{6.5.73}$$

$$w_h^{n,k+q} = -[\boldsymbol{u}_h^{n,k+q}]_{\mathcal{C}} \cdot \boldsymbol{n}^+, \tag{6.5.74}$$

    Second Step: Mechanics equations

    Given $p_h^{n+1,k+q}, \boldsymbol{z}_h^{n+1,k+q}, {p_f}_h^{n+1,k+q}$, *and* $\boldsymbol{\zeta}_h^{n+1,k+q}$, *solve for* $\boldsymbol{u}_h^{n+1,k+q}$ *satisfying:*

$$-\operatorname{div} \boldsymbol{\sigma}^{\text{por}}(\boldsymbol{u}_h^{n+1,k+q}, p_h^{n+1,k+q}) = \boldsymbol{f} \text{ in } \Omega \setminus \mathcal{C} \tag{6.5.75}$$

$$\boldsymbol{\sigma}^{\text{por}}(\boldsymbol{u}_h^{n+1,k+q}, p_h^{n+1,k+q}) = \boldsymbol{\sigma}(\boldsymbol{u}_h^{n+1,k+q}) - \alpha\, p_h^{n+1,k+q}\boldsymbol{I} \text{ in } \Omega \setminus \mathcal{C} \tag{6.5.76}$$

$$(\boldsymbol{\sigma}^{\text{por}}(\boldsymbol{u}_h^{n+1,k+q}, p_h^{n+1,k+q}))^\star \boldsymbol{n}^\star = -{p_f}_h^{n+1,k+q}\boldsymbol{n}^\star \ , \ \star = +, - \text{ on } \mathcal{C} \tag{6.5.77}$$

In the algorithm above, L and γ_c are adjustable fixed-stress regularization parameters which will be determined appropriately by the proof of contraction.

6.5.3 Proof of Contraction

Considering the difference between one finer flow iteration and its corresponding finer flow iteration in the previous coupling iteration, equations (6.5.69), (6.5.70), (6.5.71), (6.5.72) can be written as follows (substituting (6.5.73) and (6.5.74) into (6.5.69), (6.5.70), (6.5.71), and (6.5.72)):

$$(\frac{1}{M}+c_f\varphi_0+L)\Big(\frac{\delta p_h^{n+1,m+k}-\delta p_h^{n+1,m-1+k}}{\Delta t}\Big)+\frac{1}{\mu_f}\nabla\cdot\delta\boldsymbol{z}_h^{n+1,m+k}= \\ \frac{1}{\Delta t}\Big(L(\delta p_h^{n,m+k}-\delta p_h^{n,m-1+k})-\frac{\alpha}{q}\nabla\cdot(\delta\boldsymbol{u}_h^{n,k+q}-\delta\boldsymbol{u}_h^{n,k})\Big) \tag{6.5.78}$$

$$\delta\boldsymbol{z}_h^{n+1,m+k}=-\boldsymbol{K}\nabla\delta p_h^{n+1,m+k} \tag{6.5.79}$$

$$(\frac{\gamma_c+c_{f_c}}{\Delta t})\Big(\delta {p_f}_h^{n+1,m+k}-\delta {p_f}_h^{n+1,m-1+k}\Big)+\frac{1}{12\mu_f}\overline{\nabla}\cdot\delta\boldsymbol{\zeta}_h^{n+1,m+k}-\frac{1}{\mu_f}[\delta\boldsymbol{z}_h^{n+1,m+k}]\cdot\boldsymbol{n}^+ \\ =\gamma_c\Big(\frac{\delta {p_f}_h^{n,m+k}-\delta {p_f}_h^{n,m-1+k}}{\Delta t}\Big)+\frac{1}{q\Delta t}\Big([\delta\boldsymbol{u}_h^{n,k+q}]_{\mathfrak{e}}\cdot\boldsymbol{n}^+-[\delta\boldsymbol{u}_h^{n,k}]_{\mathfrak{e}}\cdot\boldsymbol{n}^+\Big) \tag{6.5.80}$$

$$\delta\boldsymbol{\zeta}_h^{n+1,m+k}=-K_{\mathfrak{e}}\overline{\nabla}\delta {p_f}_h^{n+1,m+k} \tag{6.5.81}$$

The weak formulation of the flow equations (6.5.78), (6.5.79), (6.5.80), and (6.5.81), and the mechanics equation (considered for the difference between two consecutive iterative coupling iterations, compare to (6.4.47) in the single rate case) reads:

$$\forall\theta_h\in Q_h\,,\ \frac{1}{\Delta t}(\frac{1}{M}+c_f\varphi_0+L)\Big(\delta p_h^{n+1,m+k}-\delta p_h^{n+1,m-1+k},\theta_h\Big) \\ +\frac{1}{\mu_f}(\nabla\cdot\delta\boldsymbol{z}_h^{n+1,m+k},\theta_h)=\frac{1}{\Delta t}\Big(L\Big(\delta p_h^{n,m+k}-\delta p_h^{n,m-1+k}\Big)-\frac{\alpha}{q}\nabla\cdot\boldsymbol{u}_h^{n,k+q},\theta_h\Big) \tag{6.5.82}$$

$$\forall\boldsymbol{q}_h\in\boldsymbol{Z}_h\,,\ \Big(\boldsymbol{K}^{-1}\delta\boldsymbol{z}_h^{n+1,m+k},\boldsymbol{q}_h\Big)=\Big(\delta p_h^{n+1,m+k},\nabla\cdot\boldsymbol{q}_h\Big)-\Big(\delta {p_f}_h^{n+1,m+k},[\boldsymbol{q}_h]_{\mathfrak{e}}\cdot n^+\Big)_{\mathfrak{e}} \tag{6.5.83}$$

$$\forall \theta_{c_h} \in Q_{c_h}\,, \frac{(\gamma_c + c_{f_c})}{\Delta t}\Big(\delta {p_{f}}_h^{n+1,m+k} - \delta {p_{f}}_h^{n+1,m-1+k}, \theta_{c_h}\Big)_{\mathcal{C}} + \frac{1}{12\mu_f}\Big(\overline{\nabla}\cdot\delta\boldsymbol{\zeta}_h^{n+1,m+k}, \theta_{c_h}\Big)_{\mathcal{C}}$$
$$- \frac{1}{\mu_f}\Big(\Big[\delta\boldsymbol{z}_h^{n+1,m+k}\Big]_{\mathcal{C}}\cdot\boldsymbol{n}^+, \theta_{c_h}\Big)_{\mathcal{C}} = \frac{\gamma_c}{\Delta t}\Big(\delta {p_{f}}_h^{n,m+k} - \delta {p_{f}}_h^{n,m-1+k}, \theta_{c_h})_{\mathcal{C}}$$
$$+ \frac{1}{q\Delta t}\Big([\boldsymbol{u}_h^{n,k+q}]_{\mathcal{C}}\cdot\boldsymbol{n}^+, \theta_{c_h}\Big)_{\mathcal{C}} \tag{6.5.84}$$

$$\forall \boldsymbol{\mu}_{f_h} \in \boldsymbol{Z}_{\mathcal{C}h}\,, \Big({K_{\mathcal{C}}}^{-1}\delta\boldsymbol{\zeta}_h^{n+1,m+k}, \boldsymbol{\mu}_{f_h})_{\mathcal{C}} = \Big(\delta {p_{f}}_h^{n+1,m+k}, \overline{\nabla}\cdot(\boldsymbol{\mu}_{f_h})\Big)_{\mathcal{C}} \tag{6.5.85}$$

$$\forall \boldsymbol{v}_h \in V_h\,, 2G(\boldsymbol{\varepsilon}(\delta\boldsymbol{u}_h^{n+1,k+q}), \boldsymbol{\varepsilon}(\boldsymbol{v}_h)) + \lambda(\nabla\cdot\delta\boldsymbol{u}_h^{n+1,k+q}, \nabla\cdot\boldsymbol{v}_h) - \alpha(\delta p_h^{n+1,k+q}, \nabla\cdot\boldsymbol{v}_h)$$
$$+ (\delta {p_{f}}_h^{n+1,k+q}, [\boldsymbol{v}_h]_{\mathcal{C}}\cdot\boldsymbol{n}^+)_{\mathcal{C}} = 0 \tag{6.5.86}$$

Let $\beta = \frac{1}{M} + c_{f_c}\varphi_0 + L$, test (6.5.82) with $\theta_h = \delta p_h^{n+1,m+k} - \delta p_h^{n+1,m-1+k}$, and multiply the whole equation by Δt to get:

$$\beta\Big\|\delta p_h^{n+1,m+k} - \delta p_h^{n+1,m-1+k}\Big\|^2 + \frac{\Delta t}{\mu_f}(\nabla\cdot\delta\boldsymbol{z}_h^{n+1,m+k}, \delta p_h^{n+1,m+k} - \delta p_h^{n+1,m-1+k}) =$$
$$\Big(L\Big(\delta p_h^{n,m+k} - \delta p_h^{n,m-1+k}\Big) - \frac{\alpha}{q}\nabla\cdot\boldsymbol{u}_h^{n,k+q}, \delta p_h^{n+1,m+k} - \delta p_h^{n+1,m-1+k}\Big). \tag{6.5.87}$$

Consider (6.5.83) for the difference between two consecutive time steps (t_{m+k} and t_{m-1+k}) and test with $\boldsymbol{q}_h = \delta\boldsymbol{z}_h^{n+1,m+k}$ to obtain:

$$\Big(\delta p_h^{n+1,m+k} - \delta p_h^{n+1,m-1+k}, \nabla\cdot\delta\boldsymbol{z}_h^{n+1,m+k}\Big)$$
$$= \Big(\boldsymbol{K}^{-1}(\delta\boldsymbol{z}_h^{n+1,m+k} - \delta\boldsymbol{z}_h^{n+1,m-1+k}), \delta\boldsymbol{z}_h^{n+1,m+k}\Big)$$
$$+ \Big(\delta {p_{f}}_h^{n+1,m+k} - \delta {p_{f}}_h^{n+1,m-1+k}, [\delta\boldsymbol{z}_h^{n+1,m+k}]_{\mathcal{C}}\cdot n^+\Big)_{\mathcal{C}}. \tag{6.5.88}$$

Substitute (6.5.88) into (6.5.87) to derive:

$$\beta\Big\|\delta p_h^{n+1,m+k} - \delta p_h^{n+1,m-1+k}\Big\|^2 + \frac{\Delta t}{\mu_f}\Big[\Big(\boldsymbol{K}^{-1}(\delta\boldsymbol{z}_h^{n+1,m+k} - \delta\boldsymbol{z}_h^{n+1,m-1+k}), \delta\boldsymbol{z}_h^{n+1,m+k}\Big)$$
$$+ \Big(\delta {p_{f}}_h^{n+1,m+k} - \delta {p_{f}}_h^{n+1,m-1+k}, [\delta\boldsymbol{z}_h^{n+1,m+k}]_{\mathcal{C}}\cdot n^+\Big)_{\mathcal{C}}\Big]$$
$$= \Big(L\Big(\delta p_h^{n,m+k} - \delta p_h^{n,m-1+k}\Big) - \frac{\alpha}{q}\nabla\cdot\boldsymbol{u}_h^{n,k+q}, \delta p_h^{n+1,m+k} - \delta p_h^{n+1,m-1+k}\Big).$$

By Young's inequality, we have:

$$\beta\Big\|\delta p_h^{n+1,m+k}-\delta p_h^{n+1,m-1+k}\Big\|^2+\frac{\Delta t}{\mu_f}\Big[\Big(\boldsymbol{K}^{-1}(\delta\boldsymbol{z}_h^{n+1,m+k}-\delta\boldsymbol{z}_h^{n+1,m-1+k}),\delta\boldsymbol{z}_h^{n+1,m+k}\Big)$$
$$+\Big(\delta p_{f_h}^{n+1,m+k}-\delta p_{f_h}^{n+1,m-1+k},[\delta\boldsymbol{z}_h^{n+1,m+k}]_{\mathcal{E}}\cdot n^+\Big)_{\mathcal{E}}\Big]\leq$$
$$\Big(\frac{1}{2\epsilon}\Big\|L\Big(\delta p_h^{n,m+k}-\delta p_h^{n,m-1+k}\Big)-\frac{\alpha}{q}\nabla\cdot\boldsymbol{u}_h^{n,k+q}\Big\|^2+\frac{\epsilon}{2}\Big\|\delta p_h^{n+1,m+k}-\delta p_h^{n+1,m-1+k}\Big\|^2\Big). \tag{6.5.89}$$

Let $\epsilon=\beta$ to obtain:

$$\frac{\beta}{2}\Big\|\delta p_h^{n+1,m+k}-\delta p_h^{n+1,m-1+k}\Big\|^2+\frac{\Delta t}{\mu_f}\Big[\Big(\boldsymbol{K}^{-1}(\delta\boldsymbol{z}_h^{n+1,m+k}-\delta\boldsymbol{z}_h^{n+1,m-1+k}),\delta\boldsymbol{z}_h^{n+1,m+k}\Big)$$
$$+\Big(\delta p_{f_h}^{n+1,m+k}-\delta p_{f_h}^{n+1,m-1+k},[\delta\boldsymbol{z}_h^{n+1,m+k}]_{\mathcal{E}}\cdot n^+\Big)_{\mathcal{E}}\Big]\leq$$
$$\frac{1}{2\beta}\Big\|L\Big(\delta p_h^{n,m+k}-\delta p_h^{n,m-1+k}\Big)-\frac{\alpha}{q}\nabla\cdot\boldsymbol{u}_h^{n,k+q}\Big\|^2.$$

Now, define the quantity of contraction for the flow in the reservoir matrix within one coarse mechanics time step (between coarse time steps t_k and t_{k+q}) as follows:

$$\chi_M\delta\sigma_v^{n,m+k}=L(\delta p_h^{n,m+k}-\delta p_h^{n,m-1+k})-\frac{\alpha}{q}\nabla\cdot\delta\boldsymbol{u}_h^{n,k+q}\quad\text{ for }\quad 1\leq m\leq q. \tag{6.5.90}$$

Then, we have (multiplying the whole equation by 2, with further simplifications):

$$\begin{aligned}&\beta\Big\|\delta p_h^{n+1,m+k}-\delta p_h^{n+1,m-1+k}\Big\|^2+\frac{\Delta t}{\mu_f}\Big(\Big\|\boldsymbol{K}^{-1/2}\delta\boldsymbol{z}_h^{n+1,m+k}\Big\|^2\\&-\Big\|\boldsymbol{K}^{-1/2}\delta\boldsymbol{z}_h^{n+1,m-1+k}\Big\|^2+\Big\|\boldsymbol{K}^{-1/2}(\delta\boldsymbol{z}_h^{n+1,m+k}-\delta\boldsymbol{z}_h^{n+1,m-1+k})\Big\|^2\Big)\\&+\frac{2\Delta t}{\mu_f}\Big(\delta p_{f_h}^{n+1,m+k}-\delta p_{f_h}^{n+1,m-1+k},[\delta\boldsymbol{z}_h^{n+1,m+k}]_{\mathcal{E}}\cdot n^+\Big)_{\mathcal{E}}\leq\frac{1}{\beta}\Big\|\chi_M\delta\sigma_v^{n,m+k}\Big\|^2.\end{aligned} \tag{6.5.91}$$

Now, we consider the flow in the fracture. Testing (6.5.84) with $\theta_h=\delta p_{f_h}^{n+1,m+k}-\delta p_{f_h}^{n+1,m-1+k}$, we obtain:

$$\begin{aligned}\frac{\gamma_c+c_{f_c}}{\Delta t}\Big\|\delta p_{f_h}^{n+1,m+k}-\delta p_{f_h}^{n+1,m-1+k}\Big\|_{\mathcal{E}}^2&+\frac{1}{12\mu_f}\Big(\overline{\nabla}\cdot\delta\boldsymbol{\zeta}_h^{n+1,m+k},\delta p_{f_h}^{n+1,m+k}-\delta p_{f_h}^{n+1,m-1+k}\Big)_{\mathcal{E}}\\&-\frac{1}{\mu_f}\Big(\Big[\delta\boldsymbol{z}_h^{n+1,m+k}\Big]_{\mathcal{E}}\cdot\boldsymbol{n}^+,\delta p_{f_h}^{n+1,m+k}-\delta p_{f_h}^{n+1,m-1+k}\Big)_{\mathcal{E}}\\&=\frac{\gamma_c}{\Delta t}\Big(\delta p_{f_h}^{n,m+k}-\delta p_{f_h}^{n,m-1+k},\delta p_{f_h}^{n+1,m+k}-\delta p_{f_h}^{n+1,m-1+k})_{\mathcal{E}}\\&+\frac{1}{q\Delta t}\Big([\boldsymbol{u}_h^{n,k+q}]_{\mathcal{E}}\cdot\boldsymbol{n}^+,\delta p_{f_h}^{n+1,m+k}-\delta p_{f_h}^{n+1,m-1+k}\Big)_{\mathcal{E}}.\end{aligned} \tag{6.5.92}$$

Next, consider (6.5.85) for the difference between two consecutive time steps (t_{m+k} and t_{m-1+k}) and test with $\boldsymbol{\mu}_{f_h} = \delta\boldsymbol{\zeta}_h^{n+1,m+k}$ to obtain:

$$\Big(K_{\mathfrak{e}}{}^{-1}(\delta\boldsymbol{\zeta}_h^{n+1,m+k} - \delta\boldsymbol{\zeta}_h^{n+1,m-1+k}), \delta\boldsymbol{\zeta}_h^{n+1,m+k}\Big)_{\mathfrak{e}} = \Big(\delta p_{f_h}^{n+1,m+k} - \delta p_{f_h}^{n+1,m+k}, \overline{\nabla}\cdot(\delta\boldsymbol{\zeta}_h^{n+1,m+k})\Big)_{\mathfrak{e}} \tag{6.5.93}$$

Substitute (6.5.93) into (6.5.92) and multiply by $2\Delta t$ to derive:

$$\begin{aligned}
&2(\gamma_c + c_{f_c})\Big\|\delta p_{f_h}^{n+1,m+k} - \delta p_{f_h}^{n+1,m-1+k}\Big\|_{\mathfrak{e}}^2 \\
&+ \frac{\Delta t}{6\mu_f}\Big(K_{\mathfrak{e}}{}^{-1}(\delta\boldsymbol{\zeta}_h^{n+1,m+k} - \delta\boldsymbol{\zeta}_h^{n+1,m-1+k}), \delta\boldsymbol{\zeta}_h^{n+1,m+k}\Big)_{\mathfrak{e}} \\
&- \frac{2\Delta t}{\mu_f}\Big(\Big[\delta\boldsymbol{z}_h^{n+1,m+k}\Big]_{\mathfrak{e}}\cdot\boldsymbol{n}^+, \delta p_{f_h}^{n+1,m+k} - \delta p_{f_h}^{n+1,m-1+k}\Big)_{\mathfrak{e}} \\
&= 2\Big(\gamma_c(\delta p_{f_h}^{n,m+k} - \delta p_{f_h}^{n,m-1+k}) + \frac{1}{q}[\boldsymbol{u}_h^{n,k+q}]_{\mathfrak{e}}\cdot\boldsymbol{n}^+, \delta p_{f_h}^{n+1,m+k} - \delta p_{f_h}^{n+1,m-1+k}\Big)_{\mathfrak{e}}.
\end{aligned} \tag{6.5.94}$$

With further simplifications, we have:

$$\begin{aligned}
&2(\gamma_c + c_{f_c})\Big\|\delta p_{f_h}^{n+1,m+k} - \delta p_{f_h}^{n+1,m-1+k}\Big\|_{\mathfrak{e}}^2 + \frac{\Delta t}{12\mu_f}\Big[\Big\|K_{\mathfrak{e}}{}^{-1/2}\delta\boldsymbol{\zeta}_h^{n+1,m+k}\Big\|_{\mathfrak{e}}^2 \\
&- \Big\|K_{\mathfrak{e}}{}^{-1/2}\delta\boldsymbol{\zeta}_h^{n+1,m-1+k}\Big\|_{\mathfrak{e}}^2 + \Big\|K_{\mathfrak{e}}{}^{-1/2}(\delta\boldsymbol{\zeta}_h^{n+1,m+k} - \delta\boldsymbol{\zeta}_h^{n+1,m-1+k})\Big\|_{\mathfrak{e}}^2\Big] \\
&- \frac{2\Delta t}{\mu_f}\Big(\Big[\delta\boldsymbol{z}_h^{n+1,m+k}\Big]_{\mathfrak{e}}\cdot\boldsymbol{n}^+, \delta p_{f_h}^{n+1,m+k} - \delta p_{f_h}^{n+1,m-1+k}\Big)_{\mathfrak{e}} \\
&= 2\Big(\gamma_c(\delta p_{f_h}^{n,m+k} - \delta p_{f_h}^{n,m-1+k}) + \frac{1}{q}[\boldsymbol{u}_h^{n,k+q}]_{\mathfrak{e}}\cdot\boldsymbol{n}^+, \delta p_{f_h}^{n+1,m+k} - \delta p_{f_h}^{n+1,m-1+k}\Big)_{\mathfrak{e}}.
\end{aligned} \tag{6.5.95}$$

Now, add equation (6.5.91) to (6.5.95) and divide the result by β to obtain:

$$\begin{aligned}
&\Big\|\delta p_h^{n+1,m+k} - \delta p_h^{n+1,m-1+k}\Big\|^2 + \frac{\Delta t}{\mu_f\beta}\Big[\Big\|\boldsymbol{K}^{-1/2}\delta\boldsymbol{z}_h^{n+1,m+k}\Big\|^2 \\
&- \Big\|\boldsymbol{K}^{-1/2}\delta\boldsymbol{z}_h^{n+1,m-1+k}\Big\|^2 + \Big\|\boldsymbol{K}^{-1/2}(\delta\boldsymbol{z}_h^{n+1,m+k} - \delta\boldsymbol{z}_h^{n+1,m-1+k})\Big\|^2\Big] \\
&+ \frac{2}{\beta}(\gamma_c + c_{f_c})\Big\|\delta p_{f_h}^{n+1,m+k} - \delta p_{f_h}^{n+1,m-1+k}\Big\|_{\mathfrak{e}}^2 + \frac{\Delta t}{12\mu_f\beta}\Big[\Big\|K_{\mathfrak{e}}{}^{-1/2}\delta\boldsymbol{\zeta}_h^{n+1,m+k}\Big\|_{\mathfrak{e}}^2 \\
&- \Big\|K_{\mathfrak{e}}{}^{-1/2}\delta\boldsymbol{\zeta}_h^{n+1,m-1+k}\Big\|_{\mathfrak{e}}^2 + \Big\|K_{\mathfrak{e}}{}^{-1/2}(\delta\boldsymbol{\zeta}_h^{n+1,m+k} - \delta\boldsymbol{\zeta}_h^{n+1,m-1+k})\Big\|_{\mathfrak{e}}^2\Big] \le \frac{1}{\beta^2}\Big\|\chi_M\delta\sigma_v^{n,m+k}\Big\|^2 \\
&\quad + \frac{2}{\beta}\Big(\gamma_c(\delta p_{f_h}^{n,m+k} - \delta p_{f_h}^{n,m-1+k}) + \frac{1}{q}[\boldsymbol{u}_h^{n,k+q}]_{\mathfrak{e}}\cdot\boldsymbol{n}^+, \delta p_{f_h}^{n+1,m+k} - \delta p_{f_h}^{n+1,m-1+k}\Big)_{\mathfrak{e}}.
\end{aligned} \tag{6.5.96}$$

Let $\beta_c = \gamma_c + c_{f_c}$ and apply Young's inequality to the last term on the right hand side to derive:

$$\begin{aligned}
&\left\|\delta p_h^{n+1,m+k} - \delta p_h^{n+1,m-1+k}\right\|^2 + \frac{\Delta t}{\mu_f \beta}\Big[\left\|\boldsymbol{K}^{-1/2}\delta \boldsymbol{z}_h^{n+1,m+k}\right\|^2 - \left\|\boldsymbol{K}^{-1/2}\delta \boldsymbol{z}_h^{n+1,m-1+k}\right\|^2 \quad (6.5.97)\\
&+ \left\|\boldsymbol{K}^{-1/2}(\delta \boldsymbol{z}_h^{n+1,m+k} - \delta \boldsymbol{z}_h^{n+1,m-1+k})\right\|^2\Big] + \frac{2\beta_c}{\beta}\left\|\delta {p_f}_h^{n+1,m+k} - \delta {p_f}_h^{n+1,m-1+k}\right\|_{\mathfrak{e}}^2\\
&+\frac{\Delta t}{12\mu_f\beta}\Big[\left\|{K_{\mathfrak{e}}}^{-1/2}\delta \boldsymbol{\zeta}_h^{n+1,m+k}\right\|_{\mathfrak{e}}^2 - \left\|{K_{\mathfrak{e}}}^{-1/2}\delta \boldsymbol{\zeta}_h^{n+1,m-1+k}\right\|_{\mathfrak{e}}^2 + \left\|{K_{\mathfrak{e}}}^{-1/2}(\delta \boldsymbol{\zeta}_h^{n+1,m+k} - \delta \boldsymbol{\zeta}_h^{n+1,m-1+k})\right\|_{\mathfrak{e}}^2\Big]\\
&\leq \frac{1}{\beta^2}\left\|\chi_M \delta \sigma_v^{n,m+k}\right\|^2 + \frac{2}{\beta}\Big[\frac{1}{2\epsilon}\left\|\gamma_c(\delta {p_f}_h^{n,m+k} - \delta {p_f}_h^{n,m-1+k}) - \frac{1}{q}\delta w_h^{n,k+q}\right\|_{\mathfrak{e}}^2\\
&+ \frac{\epsilon}{2}\left\|\delta {p_f}_h^{n+1,m+k} - \delta {p_f}_h^{n+1,m-1+k}\right\|_{\mathfrak{e}}^2\Big]
\end{aligned}$$

The choice $\epsilon = \beta_c$ gives:

$$\begin{aligned}
&\left\|\delta p_h^{n+1,m+k} - \delta p_h^{n+1,m-1+k}\right\|^2 + \frac{\Delta t}{\mu_f \beta}\Big[\left\|\boldsymbol{K}^{-1/2}\delta \boldsymbol{z}_h^{n+1,m+k}\right\|^2\\
&- \left\|\boldsymbol{K}^{-1/2}\delta \boldsymbol{z}_h^{n+1,m-1+k}\right\|^2 + \left\|\boldsymbol{K}^{-1/2}(\delta \boldsymbol{z}_h^{n+1,m+k} - \delta \boldsymbol{z}_h^{n+1,m-1+k})\right\|^2\Big]\\
&+ \frac{\beta_c}{\beta}\left\|\delta {p_f}_h^{n+1,m+k} - \delta {p_f}_h^{n+1,m-1+k}\right\|_{\mathfrak{e}}^2 + \frac{\Delta t}{12\mu_f\beta}\Big[\left\|{K_{\mathfrak{e}}}^{-1/2}\delta \boldsymbol{\zeta}_h^{n+1,m+k}\right\|_{\mathfrak{e}}^2 - \quad (6.5.98)\\
&\left\|{K_{\mathfrak{e}}}^{-1/2}\delta \boldsymbol{\zeta}_h^{n+1,m-1+k}\right\|_{\mathfrak{e}}^2 + \left\|{K_{\mathfrak{e}}}^{-1/2}(\delta \boldsymbol{\zeta}_h^{n+1,m+k} - \delta \boldsymbol{\zeta}_h^{n+1,m-1+k})\right\|_{\mathfrak{e}}^2\Big]\\
&\leq \frac{1}{\beta^2}\left\|\chi_M \delta \sigma_v^{n,m+k}\right\|^2 + \frac{1}{\beta\beta_c}\left\|\gamma_c(\delta {p_f}_h^{n,m+k} - \delta {p_f}_h^{n,m-1+k}) - \frac{1}{q}\delta w_h^{n,k+q}\right\|_{\mathfrak{e}}^2
\end{aligned}$$

Now, we sum up equation (6.5.98) for q flow finer time steps. Noting that $\left\|K^{-1/2}\delta \boldsymbol{z}_h^{n+1,k}\right\|^2 = 0$, and $\left\|K_{\mathfrak{e}}^{-1/2}\delta \boldsymbol{\zeta}_h^{n+1,k}\right\|_{\mathfrak{e}}^2 = 0$ with further telescopic cancellations, we obtain:

$$\begin{aligned}
&\sum_{m=1}^{q}\left\|\delta p_h^{n+1,m+k} - \delta p_h^{n+1,m-1+k}\right\|^2 + \frac{\Delta t}{\mu_f \beta}\Big[\left\|\boldsymbol{K}^{-1/2}\delta \boldsymbol{z}_h^{n+1,k+q}\right\|^2\\
&+ \sum_{m=1}^{q}\left\|\boldsymbol{K}^{-1/2}(\delta \boldsymbol{z}_h^{n+1,m+k} - \delta \boldsymbol{z}_h^{n+1,m-1+k})\right\|^2\Big] + \frac{\beta_c}{\beta}\sum_{m=1}^{q}\left\|\delta {p_f}_h^{n+1,m+k} - \delta {p_f}_h^{n+1,m-1+k}\right\|_{\mathfrak{e}}^2\\
&+ \frac{\Delta t}{12\mu_f\beta}\Big[\left\|{K_{\mathfrak{e}}}^{-1/2}\delta \boldsymbol{\zeta}_h^{n+1,m+k}\right\|_{\mathfrak{e}}^2 + \sum_{m=1}^{q}\left\|{K_{\mathfrak{e}}}^{-1/2}(\delta \boldsymbol{\zeta}_h^{n+1,m+k} - \delta \boldsymbol{\zeta}_h^{n+1,m-1+k})\right\|_{\mathfrak{e}}^2\Big]\\
&\leq \frac{1}{\beta^2}\sum_{m=1}^{q}\left\|\chi_M \delta \sigma_v^{n,m+k}\right\|^2 + \frac{1}{\beta\beta_c}\sum_{m=1}^{q}\left\|\gamma_c(\delta {p_f}_h^{n,m+k} - \delta {p_f}_h^{n,m-1+k}) - \frac{1}{q}\delta w_h^{n,k+q}\right\|_{\mathfrak{e}}^2 \quad (6.5.99)
\end{aligned}$$

Now, consider (6.5.86) for the elasticity equation and test with $\boldsymbol{v}_h = \delta \boldsymbol{u}_h^{n+1,k+q}$ to obtain:

$$2G\left\|\boldsymbol{\varepsilon}(\delta \boldsymbol{u}_h^{n+1,k+q})\right\|^2 + \lambda\left\|\nabla \cdot \delta \boldsymbol{u}_h^{n+1,k+q}\right\|^2 - \alpha(\delta p_h^{n+1,k+q}, \nabla \cdot \delta \boldsymbol{u}_h^{n+1,k+q}) + (\delta p_{f_h}^{n+1,k+q}, [\delta \boldsymbol{u}_h^{n+1,k+q}]_{\mathcal{E}} \cdot \boldsymbol{n}^+)_{\mathcal{E}} = 0 \tag{6.5.100}$$

Noting that

$$\sum_{m=1}^{q}\left(\delta p_h^{n+1,m+k} - \delta p_h^{n+1,m-1+k}\right) = \delta p_h^{n+1,k+q}, \sum_{m=1}^{q}\left(\delta p_{f_h}^{n+1,m+k} - \delta p_{f_h}^{n+1,m-1+k}\right) = \delta p_{f_h}^{n+1,k+q},$$

equation (6.5.100) can be written as:

$$2G\left\|\boldsymbol{\varepsilon}(\delta \boldsymbol{u}_h^{n+1,k+q})\right\|^2 + \lambda\left\|\nabla \cdot \delta \boldsymbol{u}_h^{n+1,k+q}\right\|^2 - \alpha(\sum_{m=1}^{q}\left(\delta p_h^{n+1,m+k} - \delta p_h^{n+1,m-1+k}\right), \nabla \cdot \delta \boldsymbol{u}_h^{n+1,k+q}) + (\sum_{m=1}^{q}\left(\delta p_{f_h}^{n+1,m+k} - \delta p_{f_h}^{n+1,m-1+k}\right), [\delta \boldsymbol{u}_h^{n+1,k+q}]_{\mathcal{E}} \cdot \boldsymbol{n}^+)_{\mathcal{E}} = 0 \tag{6.5.101}$$

Now, bound the first term on the left hand side from below by (6.4.55) and multiply the whole equation by a free parameter c_0 (the specific value of c_0 which will be determined in subsequent derivations) to obtain:

$$2GC^* c_0\left\|\delta w_h^{n+1,k+q}\right\|^2 + \lambda c_0\left\|\nabla \cdot \delta \boldsymbol{u}_h^{n+1,k+q}\right\|^2 - \alpha c_0(\sum_{m=1}^{q}\left(\delta p_h^{n+1,m+k} - \delta p_h^{n+1,m-1+k}\right), \nabla \cdot \delta \boldsymbol{u}_h^{n+1,k+q}) - c_0(\sum_{m=1}^{q}\left(\delta p_{f_h}^{n+1,m+k} - \delta p_{f_h}^{n+1,m-1+k}\right), \delta w_h^{n+1,k+q})_{\mathcal{E}} \leq 0. \tag{6.5.102}$$

Add (6.5.99) to (6.5.102) to get:

$$\sum_{m=1}^{q}\Big[\Big\|\delta p_h^{n+1,m+k}-\delta p_h^{n+1,m-1+k}\Big\|^2-\alpha c_0(\Big(\delta p_h^{n+1,m+k}-\delta p_h^{n+1,m-1+k}\Big),\nabla\cdot\delta\boldsymbol{u}_h^{n+1,k+q})$$
$$+\frac{\lambda c_0}{q}\Big\|\nabla\cdot\delta\boldsymbol{u}_h^{n+1,k+q}\Big\|^2\Big]$$
$$+\sum_{m=1}^{q}\Big[\frac{\beta_c}{\beta}\Big\|\delta p_{f_h}^{n+1,m+k}-\delta p_{f_h}^{n+1,m-1+k}\Big\|_{\mathfrak{C}}^2-c_0(\Big(\delta p_{f_h}^{n+1,m+k}-\delta p_{f_h}^{n+1,m-1+k}\Big),\delta w_h^{n+1,k+q})_{\mathfrak{C}}$$
$$+\frac{2GC^*c_0}{q}\Big\|\delta w_h^{n+1,k+q}\Big\|^2\Big]$$
$$+\frac{\Delta t}{\mu_f\beta}\Big[\Big\|\boldsymbol{K}^{-1/2}\delta\boldsymbol{z}_h^{n+1,k+q}\Big\|^2+\sum_{m=1}^{q}\Big\|\boldsymbol{K}^{-1/2}(\delta\boldsymbol{z}_h^{n+1,m+k}-\delta\boldsymbol{z}_h^{n+1,m-1+k})\Big\|^2\Big]$$
$$+\frac{\Delta t}{12\mu_f\beta}\Big[\Big\|{K_{\mathfrak{C}}}^{-1/2}\delta\boldsymbol{\zeta}_h^{n+1,m+k}\Big\|_{\mathfrak{C}}^2+\sum_{m=1}^{q}\Big\|{K_{\mathfrak{C}}}^{-1/2}(\delta\boldsymbol{\zeta}_h^{n+1,m+k}-\delta\boldsymbol{\zeta}_h^{n+1,m-1+k})\Big\|_{\mathfrak{C}}^2\Big]$$
$$\leq\frac{1}{\beta^2}\sum_{m=1}^{q}\Big\|\chi_M\delta\sigma_v^{n,m+k}\Big\|^2+\frac{1}{\beta\beta_c}\sum_{m=1}^{q}\Big\|\gamma_c(\delta p_{f_h}^{n,m+k}-\delta p_{f_h}^{n,m-1+k})-\frac{1}{q}\delta w_h^{n,k+q}\Big\|_{\mathfrak{C}}^2. \quad (6.5.103)$$

Define the quantity of contraction for the flow in the fracture within one coarse mechanics time step (between coarse time steps t_k and t_{k+q}) as follows:

$$\chi_c\delta\sigma_f^{n,m+k}=\gamma_c(\delta p_{f_h}^{n,m+k}-\delta p_{f_h}^{n,m-1+k})-\frac{1}{q}\delta w_h^{n,k+q}\quad\text{for}\quad 1\leq m\leq q. \quad (6.5.104)$$

We emphasize that the parameters χ_M, L, χ_c, γ_c, and c_0 are to be determined such that contraction is obtained on $\sigma_v^{n,m+k}$ and $\sigma_f^{n,m+k}$ defined above . This will be carried out in a very systematic way shown below. We first write the quantity of contraction for the reservoir matrix (6.5.90) as:

$$\delta\sigma_v^{n,m+k}=\frac{L}{\chi_M}(\delta p_h^{n,m+k}-\delta p_h^{n,m-1+k})-\frac{\alpha}{\chi_M q}\nabla\cdot\delta\boldsymbol{u}_h^{n,k+q}.$$

Next, expand the square of its L^2 norm as

$$\Big\|\delta\sigma_v^{n,m+k}\Big\|^2=\frac{L^2}{\chi_M^2}\Big\|\delta p_h^{n,m+k}-\delta p_h^{n,m-1+k}\Big\|^2$$
$$-\frac{2\alpha L}{\chi_M^2 q}(\delta p_h^{n,m+k}-\delta p_h^{n,m-1+k},\nabla\cdot\delta\boldsymbol{u}_h^{n,k+q})+\frac{\alpha^2}{{\chi_M}^2q^2}\Big\|\nabla\cdot\delta\boldsymbol{u}_h^{n,k+q}\Big\|^2. \quad (6.5.105)$$

In order to determine the values of our additional unknown parameters, we need to match the coefficients of the terms in the expansion above (6.5.105) to the coefficients of the first

three terms in equation (6.5.103) as follows:

$$\frac{L^2}{\chi_M^2} \leq 1, \qquad \alpha c_0 = \frac{2\alpha L}{\chi_M^2 q}, \qquad \frac{\alpha^2}{\chi_M^2 q^2} \leq \frac{\lambda c_0}{q}$$

The second equality gives: $c_0 = \frac{2L}{q\chi_M^2}$. Substituting the value of c_0 into the third inequality gives: $L \geq \frac{1}{2}\frac{\alpha^2}{\lambda}$. The first inequality gives rise to (assuming positive values of all undetermined parameters): $\chi_M \geq L$. Therefore, we have the following combined condition on L:

$$\frac{\alpha^2}{2\lambda} \leq L \leq \chi_M. \tag{6.5.106}$$

In a similar way, we write the expression for the quantity of contraction in the fracture (6.5.104) as follows:

$$\delta\sigma_f^{n,m+k} = \frac{\gamma_c}{\chi_c}(\delta p_{f_h}^{n,m+k} - \delta p_{f_h}^{n,m-1+k}) - \frac{1}{q\chi_c}\delta w_h^{n,k+q}$$

Expanding the square of its L^2 norm gives

$$\left\|\delta\sigma_f^{n,m+k}\right\|_{\mathcal{E}}^2 = \frac{\gamma_c^2}{\chi_c^2}\left\|\delta p_{f_h}^{n,m+k} - \delta p_{f_h}^{n,m-1+k}\right\|_{\mathcal{E}}^2 - \frac{2\gamma_c}{\chi_c^2 q}(\delta p_{f_h}^{n,m+k} - \delta p_{f_h}^{n,m-1+k}, \delta w_h^{n,k+q})_{\mathcal{E}} + \frac{1}{q^2\chi_c^2}\left\|\delta w_h^{n,k+q}\right\|_{\mathcal{E}}^2 \tag{6.5.107}$$

Now, we match the coefficients of the terms in the expansion above (6.5.107) to the coefficients of the second three terms in equation (6.5.103) as follows:

$$\frac{\gamma_c^2}{\chi_c^2} \leq \frac{\beta_c}{\beta}, \qquad \frac{2\gamma_c}{\chi_c^2 q} = c_0, \qquad \frac{1}{q^2\chi_c^2} \leq \frac{2GC^* c_0}{q}$$

The second equality gives rise to $\frac{2\gamma_c}{q\chi_c^2} = \frac{2L}{q\chi_M^2}$. Therefore, we need to maintain the following relation:

$$\frac{L}{\chi_M^2} = \frac{\gamma_c}{\chi_c^2} \tag{6.5.108}$$

between our unknown parameters L, γ_c, χ_M, and χ_c. The third inequality results in the condition:

$$\gamma_c \geq \frac{1}{4GC^*}. \tag{6.5.109}$$

The first inequality results in the condition:

$$\frac{\gamma_c}{\beta_c} \leq \frac{\chi_M^2}{L\beta}. \tag{6.5.110}$$

Now, for $L = \gamma_c = \chi_M = \chi_c = \frac{\alpha^2}{2\lambda}$, conditions (6.5.106) and (6.5.108) are trivially satisfied. Conditions (6.5.109) and (6.5.110) translate to

$$\frac{\alpha^2}{\lambda} > \frac{1}{2GC^*} \qquad \text{and} \qquad c_{f_c} > \Big(\frac{1}{M} + c_f\varphi_0\Big). \tag{6.5.111}$$

respectively. So, in summary, for $c_0 = \frac{4\lambda}{q\alpha^2}$, and $L = \gamma_c = \chi_M = \chi_c = \frac{\alpha^2}{2\lambda}$, and under condition (6.5.111), the following equalities and inequalities are satisfied:

$$\frac{L^2}{\chi_M^2} = 1, \qquad \alpha c_0 = \frac{2\alpha L}{\chi_M^2 q}, \qquad \frac{\alpha^2}{\chi_M^2 q^2} = \frac{\lambda c_0}{q},$$
$$\frac{\gamma_c^2}{\chi_c^2} \leq \frac{\beta_c}{\beta}, \qquad \frac{2\gamma_c}{\chi_c^2 q} = c_0, \qquad \frac{1}{q^2\chi_c^2} \leq \frac{2GC^* c_0}{q}.$$

Substituting (6.5.105) and (6.5.107) into (6.5.103) together with the above equalities and inequalities, equation (6.5.103) can be written as:

$$\begin{aligned}
&\Big(\frac{\beta_c}{\beta} - \frac{{\gamma_c}^2}{{\chi_c}^2}\Big)\sum_{m=1}^{q}\Big\|\delta p_{f_h}^{n+1,m+k} - \delta p_{f_h}^{n+1,m-1+k}\Big\|_{\mathfrak{e}}^2 + \Big(\frac{2GC^*c_0}{q} - \frac{1}{q^2\chi_c^2}\Big)\sum_{m=1}^{q}\Big\|\delta w_h^{n+1,k+q}\Big\|_{\mathfrak{e}}^2 \\
&+ \sum_{m=1}^{q}\Big\|\delta\sigma_v^{n+1,m+k}\Big\|^2 + \sum_{m=1}^{q}\Big\|\delta\sigma_f^{n+1,m+k}\Big\|_{\mathfrak{e}}^2 \\
&+ \frac{\Delta t}{\mu_f\beta}\Big[\Big\|\boldsymbol{K}^{-1/2}\delta\boldsymbol{z}_h^{n+1,k+q}\Big\|^2 + \sum_{m=1}^{q}\Big\|\boldsymbol{K}^{-1/2}(\delta\boldsymbol{z}_h^{n+1,m+k} - \delta\boldsymbol{z}_h^{n+1,m-1+k})\Big\|^2\Big] \\
&+ \frac{\Delta t}{12\mu_f\beta}\Big[\Big\|{K_{\mathfrak{e}}}^{-1/2}\delta\boldsymbol{\zeta}_h^{n+1,m+k}\Big\|_{\mathfrak{e}}^2 + \sum_{m=1}^{q}\Big\|{K_{\mathfrak{e}}}^{-1/2}(\delta\boldsymbol{\zeta}_h^{n+1,m+k} - \delta\boldsymbol{\zeta}_h^{n+1,m-1+k})\Big\|_{\mathfrak{e}}^2\Big] \\
&\leq \frac{\chi_M^2}{\beta^2}\sum_{m=1}^{q}\Big\|\delta\sigma_v^{n,m+k}\Big\|^2 + \frac{\chi_c^2}{\beta\beta_c}\sum_{m=1}^{q}\Big\|\delta\sigma_f^{n,m+k}\Big\|_{\mathfrak{e}}^2.
\end{aligned} \tag{6.5.112}$$

Now, it remains to check that the contraction coefficients are strictly less than one. For $\frac{\chi_M^2}{\beta^2}$, we have:

$$\frac{\chi_M^2}{\beta^2} = \Big(\frac{L}{\frac{1}{M} + c_f\varphi_0 + L}\Big)^2 < 1.$$

For $\frac{\chi_c^2}{\beta\beta_c}$, we have:

$$\frac{\chi_c^2}{\beta\beta_c} = \frac{L^2}{c_{f_c}\beta + L(\frac{1}{M} + c_f\varphi_0) + L^2} < 1.$$

The above discussions are summarized in the following contraction result:

$$\Big(\frac{\beta_c}{\beta}-1\Big)\sum_{m=1}^{q}\Big\|\delta {p_f}_h^{n+1,m+k}-\delta {p_f}_h^{n+1,m-1+k}\Big\|_{\mathcal{C}}^2+\frac{4\lambda}{\alpha^2q^2}\Big(2GC^*-\frac{\lambda}{\alpha^2}\Big)\sum_{m=1}^{q}\Big\|\delta w_h^{n+1,k+q}\Big\|_{\mathcal{C}}^2$$
$$+\frac{\Delta t}{\mu_f\beta}\Big[\Big\|\boldsymbol{K}^{-1/2}\delta\boldsymbol{z}_h^{n+1,k+q}\Big\|^2+\sum_{m=1}^{q}\Big\|\boldsymbol{K}^{-1/2}(\delta\boldsymbol{z}_h^{n+1,m+k}-\delta\boldsymbol{z}_h^{n+1,m-1+k})\Big\|^2\Big]$$
$$+\frac{\Delta t}{12\mu_f\beta}\Big[\Big\|{K_{\mathcal{C}}}^{-1/2}\delta\boldsymbol{\zeta}_h^{n+1,m+k}\Big\|_{\mathcal{C}}^2+\sum_{m=1}^{q}\Big\|{K_{\mathcal{C}}}^{-1/2}(\delta\boldsymbol{\zeta}_h^{n+1,m+k}-\delta\boldsymbol{\zeta}_h^{n+1,m-1+k})\Big\|_{\mathcal{C}}^2\Big]$$
$$+\sum_{m=1}^{q}\Big\|\delta\sigma_v^{n+1,m+k}\Big\|^2+\sum_{m=1}^{q}\Big\|\delta\sigma_f^{n+1,m+k}\Big\|_{\mathcal{C}}^2$$
$$\leq Max(\frac{L^2}{\beta^2},\frac{L^2}{\beta\beta_c})\sum_{m=1}^{q}\left(\Big\|\delta\sigma_v^{n,m+k}+\Big\|^2+\Big\|\delta\sigma_f^{n,m+k}\Big\|_{\mathcal{C}}^2\right). \quad (6.5.113)$$

6.5.4 Convergence to Discrete Multirate Formulation

We will now establish convergence of the sequences generated by the multirate fixed stress split coupling algorithm (in fractured poro-elastic meida) and show that the converged quantities satisfy the weak formulation (6.5.63) – (6.5.68). Following a similar approach to the one used in Chapter 2 for the Biot system, the proof uses a mathematical induction argument for the finer flow equations combined with the contraction estimates obtained above.

Lemma 6.5.1. *For every coarser mechanics time step, $t = t_k$, there exist limit functions $\boldsymbol{u}_h^k$, and w_h^k such that*

$$\boldsymbol{u}_h^{n,k}\to\boldsymbol{u}_h^k \quad \text{in } H^1(\Omega^+\cup\Omega^-)^d, \quad w_h^{n,k}\to w_h^k, \quad \text{in } L^2(\mathcal{C}),$$

with strong convergence in the norms of the above spaces.

Proof. For a coarser time step $t = t_k$, the contraction result in (6.5.113) with the condition (6.5.111) (with strict inequalities) implies that $w_h^{n,k}$ is a Cauchy sequence converging geometrically to a unique limit in $L^2(\mathcal{C})$, being a Hilbert space. For the convergence of the

displacements, by applying (6.4.55) to half of the first term in (6.5.101) we get:

$$
\begin{aligned}
&G\Big\|\boldsymbol{\varepsilon}(\delta\boldsymbol{u}_h^{n,k+q})\Big\|^2+GC^*\Big\|\delta w_h^{n,k+q}\Big\|^2+\lambda\Big\|\nabla\cdot\delta\boldsymbol{u}_h^{n,k+q}\Big\|^2\\
&\leq\alpha\left|\Big(\sum_{m=1}^{q}\Big(\delta p_h^{n,m+k}-\delta p_h^{n,m-1+k}\Big),\nabla\cdot\delta\boldsymbol{u}_h^{n,k+q}\Big)\right|\\
&\qquad\qquad+\left|\Big(\sum_{m=1}^{q}\Big(\delta p_{f_h}^{n,m+k}-\delta p_{f_h}^{n,m-1+k}\Big),[\delta\boldsymbol{u}_h^{n,k+q}]_{\mathfrak{C}}\cdot\boldsymbol{n}^+\Big)_{\mathfrak{C}}\right|\\
&\leq\frac{\alpha}{2\epsilon_1}\sum_{m=1}^{q}\|\delta p_h^{n,m+k}-\delta p_h^{n,m-1+k}\|^2+\frac{q\alpha\epsilon_1}{2}\|\nabla\cdot\delta\boldsymbol{u}_h^{n,k+q}\|^2\\
&\qquad\qquad+\frac{1}{2\epsilon_2}\sum_{m=1}^{q}\|\delta p_{f_h}^{n,m+k}-\delta p_{f_h}^{n,m-1+k}\|_{\mathfrak{C}}^2+\frac{q\epsilon_2}{2}\|\delta w_h^{n,k+q}\|_{\mathfrak{C}}^2
\end{aligned}
$$

by the triangle inequality and Young's inequality.

Now, we set: $\epsilon_1=\frac{\lambda}{q\alpha}$, and $\epsilon_2=\frac{2GC^*}{q}$ to get:

$$
\begin{aligned}
&G\Big\|\boldsymbol{\varepsilon}(\delta\boldsymbol{u}_h^{n,k+q})\Big\|^2+\frac{\lambda}{2}\Big\|\nabla\cdot\delta\boldsymbol{u}_h^{n,k+q}\Big\|^2\\
&\quad\leq\frac{q\alpha^2}{2\lambda}\sum_{m=1}^{q}\|\delta p_h^{n,m+k}-\delta p_h^{n,m-1+k}\|^2+\frac{q}{4GC^*}\sum_{m=1}^{q}\|\delta p_{f_h}^{n,m+k}-\delta p_{f_h}^{n,m-1+k}\|_{\mathfrak{C}}^2 \qquad (6.5.114)
\end{aligned}
$$

The contraction result in (6.5.113) implies that $\sum_{m=1}^{q}\|\delta p_{f_h}^{n,m+k}-\delta p_{f_h}^{n,m-1+k}\|_{\mathfrak{C}}^2$ converges geometrically to zero. It remains to show that $\sum_{m=1}^{q}\|\delta p_h^{n,m+k}-\delta p_h^{n,m-1+k}\|^2$ converges geometrically to zero. By a similar argument, the contraction result in (6.5.113) implies that $\sum_{m=1}^{q}\Big\|\boldsymbol{K}^{-1/2}(\delta\boldsymbol{z}_h^{n+1,m+k}-\delta\boldsymbol{z}_h^{n+1,m-1+k})\Big\|^2$ converges geometrically to zero. This implies that for every $1\leq m\leq q$, the finer time step differences $(\delta\boldsymbol{z}_h^{n+1,m+k}-\delta\boldsymbol{z}_h^{n+1,m-1+k})$ converge geometrically to zero. By (6.5.70), and Poincare inequality, it follows that $(\delta p_h^{n+1,m+k}-\delta p_h^{n+1,m-1+k})$ converges geometrically to zero. Therefore, the right hand side of (6.5.114) converges geometrically to zero. We conclude that for a coarser time step $t=t_k$, $\|\boldsymbol{\varepsilon}(\delta\boldsymbol{u}_h^{n,k})\|$ converges geometrically to zero. This implies that $\boldsymbol{\varepsilon}(\boldsymbol{u}_h^{n,k})$ is a Cauchy sequence converging geometrically to a unique limit in $L^2(\Omega^+\cup\Omega^-)$. By Korn's inequality, $|\boldsymbol{u}_h|_{H^1(\Omega^\star)}\leq C_\kappa^\star\|\boldsymbol{\varepsilon}(\boldsymbol{u}_h)\|_{L^2(\Omega^\star)}$, and Poincare inequality, $\|\boldsymbol{u}_h\|_{L^2(\Omega^\star)}\leq\mathcal{P}_{\Gamma^\star}|\boldsymbol{u}_h|_{H^1(\Omega^\star)}$, for $C_\kappa^\star>0,\mathcal{P}_{\Gamma^\star}>0,\star=+,-$, and noting that $\forall n\geq 0,\boldsymbol{u}_h^{n,k}|_{\partial\Omega}=0$, it follows immediately that $\boldsymbol{u}_h^{n,k}$ is a Cauchy sequence converging geometrically to a unique limit in $H^1(\Omega^+\cup\Omega^-)^d$, being a Hilbert space. □

Lemma 6.5.2. *For every two consecutive coarser mechanics time steps, $t = t_k$, and $t = t_{k+q}$, and for every $1 \leq m \leq q$, there exist limit functions $p_h^{m+k}, {p_f}_h^{m+k}, \boldsymbol{z}_h^{m+k}, \boldsymbol{\zeta}_h^{m+k}$ such that*

$$\begin{array}{llll} p_h^{n,m+k} \to p_h^{m+k},, & \text{in } L^2(\Omega^+ \cup \Omega^-), & {p_f}_h^{n,m+k} \to {p_f}_h^{m+k} & \text{in } L^2(\mathcal{C}) \\ \boldsymbol{z}_h^{n,m+k} \to \boldsymbol{z}_h^{m+k}, & \text{in } \boldsymbol{Z}_h, & \boldsymbol{\zeta}_h^{n,m+k} \to \boldsymbol{\zeta}_h^{m+k}, & \text{in } Z_{\mathcal{C}} \end{array}$$

converge strongly in the norms of the above spaces.

Proof. The contraction result in (6.5.113) implies that the quantities

$$\left\|\delta w_h^{n,k+q}\right\|_{\mathcal{C}}^2, \sum_{m=1}^{q} \left\|\delta {p_f}_h^{n,m+k} - \delta {p_f}_h^{n,m-1+k}\right\|^2,$$

$$\sum_{m=1}^{q} \left\|K^{-1/2}(\delta \boldsymbol{z}_h^{n,m+k} - \delta \boldsymbol{z}_h^{n,m-1+k})\right\|^2, \sum_{m=1}^{q} \left\|{K_{\mathcal{C}}}^{-1/2}(\delta \boldsymbol{\zeta}_h^{n,m+k} - \delta \boldsymbol{\zeta}_h^{n,m-1+k})\right\|_{\mathcal{C}}^2,$$

$$\sum_{m=1}^{q} \left\|\delta \sigma_f^{n,m+k}\right\|_{\mathcal{C}}^2, \text{ and } \sum_{m=1}^{q} \left\|\delta \sigma_v^{n,m+k}\right\|^2$$

converge geometrically to zero. It follows that for $1 \leq m \leq q$, $\left\|\delta {p_f}_h^{n,m+k} - \delta {p_f}_h^{n,m-1+k}\right\|^2$, $\left\|K^{-1/2}(\delta \boldsymbol{z}_h^{n,m+k} - \delta \boldsymbol{z}_h^{n,m-1+k})\right\|^2$, $\left\|{K_{\mathcal{C}}}^{-1/2}(\delta \boldsymbol{\zeta}_h^{n,m+k} - \delta \boldsymbol{\zeta}_h^{n,m-1+k})\right\|_{\mathcal{C}}^2$, $\left\|\delta \sigma_v^{n,m+k}\right\|^2$, and $\left\|\delta \sigma_f^{n,m+k}\right\|_{\mathcal{C}}^2$ converge geometrically to zero, in their corresponding spaces. This implies that for every $1 \leq m \leq q$, the finer time step differences $(\boldsymbol{z}_h^{n,m+k} - \boldsymbol{z}_h^{n,m-1+k})$, and $\sigma_v^{n+1,m+k}$ are Cauchy sequences converging to unique limits in $L^2(\Omega^+ \cup \Omega^-)$. By (6.5.70), and Poincare inequality, it follows that $(\delta p_h^{n,m+k} - \delta p_h^{n,m-1+k})$ converges geometrically to zero in $L^2(\Omega^+ \cup \Omega^-)$, which implies that for every $1 \leq m \leq q$, $(p_h^{n,m+k} - p_h^{n,m-1+k})$ is a Cauchy sequence converging to a unique limit in $L^2(\Omega^+ \cup \Omega^-)$. Similarly, the finer time step difference $({p_f}_h^{n,m+k} - {p_f}_h^{n,m-1+k})$, $(\boldsymbol{\zeta}_h^{n,m+k} - \boldsymbol{\zeta}_h^{n,m-1+k})$ and $\sigma_f^{n,m+k}$ are Cauchy sequences converging to unique limits in $L^2(\mathcal{C})$. We will show strong convergence of the pressure finer time step sequences $p_h^{n,m+k}$, for $1 \leq m \leq q$, by induction. The proof of strong convergences for the sequences corresponding to the pressure in the fracture ${p_f}_h^{n,m+k}$ and the flux in the reservoir $\boldsymbol{z}_h^{n,m+k}$ and in the fracture $\boldsymbol{\zeta}_h^{n,m+k}$ follow in the same way. Given an initial pressure value for $t = t_0$: $p_h^{n,0} = p_0$, from the above discussion, $(p_h^{n,1} - p_0)$ is a Cauchy sequence in $L^2(\Omega^+ \cup \Omega^-)$, and, in turn, $p_h^{n,1}$ is a Cauchy sequence in the complete space $L^2(\Omega^+ \cup \Omega^-)$, and thus has a unique limit. This

completes the base case for induction. For the inductive hypothesis, we assume that for any coarser mechanics time step $t = t_k$, and for any $1 \leq m \leq q$, $p_h^{n,m+k}$ is a Cauchy sequence converging to a unique limit in $L^2(\Omega^+ \cup \Omega^-)$: $p_h^{n,m+k} \to p_h^{m+k}$ in $L^2(\Omega^+ \cup \Omega^-)$. We will show that $p_h^{n,m+k+1}$ is also a Cauchy sequence converging to a unique limit in $L^2(\Omega^+ \cup \Omega^-)$. However, this follows immediately, as $(p_h^{n,m+k+1} - p_h^{n,m+k})$ is a Cauchy sequence converging to a unique limit in $L^2(\Omega^+ \cup \Omega^-)$. This completes the inductive step. Therefore, we obtain that for all coarser mechanics time steps $t = t_k$, and for $1 \leq m \leq q$, $p_h^{n,m+k}, \boldsymbol{z}_h^{n,m+k}$ are Cauchy sequences converging geometrically to unique limits in $L^2(\Omega^+ \cup \Omega^-)$, and ${p_f}_h^{n,m+k}, \boldsymbol{\zeta}_h^{n,m+k}$ are Cauchy sequences converging geometrically to unique limits in $L^2(\mathcal{C})$.

For the divergence of the reservoir flux, we note that (6.5.78) amounts to the following equality a.e. in $L^2(\Omega^+ \cup \Omega^-)$:

$$\nabla \cdot \delta \boldsymbol{z}_h^{n+1,m+k} = -\frac{\beta \mu_f}{\Delta t}(\delta p_h^{n+1,m+k} - \delta p_h^{n+1,m-1+k}) - \frac{\mu_f \chi_M}{\Delta t} \delta \sigma_v^{n+1,m+k}.$$

The convergence of $\nabla \cdot \boldsymbol{z}_h^{n,m+k}$ in $L^2(\Omega^+ \cup \Omega^-)$ follows from the convergence of the difference $(p_h^{n,m+k} - p_h^{n,m+k})$ and $\sigma_v^{n,m+k}$ in $L^2(\Omega^+ \cup \Omega^-)$, established above. Thus, we have both $\nabla \cdot \boldsymbol{z}_h^{n,m+k}$ and $\boldsymbol{z}_h^{n,m+k}$ converging geometrically to unique limits in $L^2(\Omega^+ \cup \Omega^-)$, and hence $\boldsymbol{z}_h^{n+1,k}$ converges to a unique limit in $\boldsymbol{Z}_h$. With Green's formula, we have the convergence of $[\boldsymbol{z}_h^{n,k}]_{\mathcal{C}} \cdot \mathbf{n}^+$ in $H^{-1/2}(\mathcal{C})$. In a similar manner, the convergence of $\overline{\nabla} \cdot \boldsymbol{\zeta}_h^{n,k}$ follows from the previous convergences and the fact that (6.5.80) gives the following equality a.e. in $H^{-1/2}(\mathcal{C})$:

$$\begin{aligned}\overline{\nabla} \cdot (\delta \boldsymbol{\zeta}_h^{n+1,m+k}) = &-\frac{12\mu_f(c_{fc} + \gamma_c)}{\Delta t}(\delta {p_f}_h^{n+1,m+k} - \delta {p_f}_h^{n+1,m-1+k}) + 12[\delta \boldsymbol{z}_h^{n+1,m+k}]_{\mathcal{C}} \cdot \boldsymbol{n}^+ \\ &+ \Big(\frac{12\mu_f \gamma_c}{\Delta t}\Big)(\delta {p_f}_h^{n,m+k} - \delta {p_f}_h^{n,m-1+k}) + \Big(\frac{12\mu_f}{q\Delta t}\Big)[\delta \boldsymbol{u}_h^{n,k+q}]_{\mathcal{C}} \cdot \boldsymbol{n}^+\end{aligned}$$

which can be written as:

$$\begin{aligned}\overline{\nabla} \cdot (\delta \boldsymbol{\zeta}_h^{n+1,m+k}) = &-\frac{12\mu_f(c_{fc} + \gamma_c)}{\Delta t}(\delta {p_f}_h^{n+1,m+k} - \delta {p_f}_h^{n+1,m-1+k}) + 12[\delta \boldsymbol{z}_h^{n+1,m+k}]_{\mathcal{C}} \cdot \boldsymbol{n}^+ \\ &+ \Big(\frac{12\mu_f \chi_c}{\Delta t}\Big)\delta \sigma_f^{n,m+k}\end{aligned}$$

All sequences on the right hand side converge in $H^{-1/2}(\mathcal{C})$. Therefore, we have the convergence of $\overline{\nabla} \cdot \boldsymbol{\zeta}_h^{n,k}$ in $H^{-1/2}(\mathcal{C})$ as well. Together with the previously obtained result that $\boldsymbol{\zeta}_h^{n,k}$

converges strongly in $L^2(\mathcal{C})$ to a unique limit, we have the convergence of $\boldsymbol{\zeta}_h^{n,k}$ to a unique limit in $Z_{\mathcal{C}}$. Therefore, all considered sequences converge strongly. The existence of the limiting functions in the corresponding spaces follows immediately by the completeness of the corresponding spaces. □

It remains to pass to the limit in (6.5.63)–(6.5.67). As described in Chapter 2 for the Biot system, this is trivially satisfied as the equations are linear and all operators involved are continuous in the spaces invoked in the statements of Lemmas 6.5.1 and 6.5.2. Furthermore, the convergences are strong and we easily retrieve the fully discrete formulation.

The above discussions are summarized in the following main result: We have the following theorem:

Theorem 6.5.1. *[Multirate] For $L = \gamma_c = \chi_M = \chi_c = \frac{\alpha^2}{2\lambda}$, and under condition* (6.5.111)*, the proposed multirate iterative scheme is a contraction given by*

$$\begin{aligned}
&\left(\tfrac{\beta_c}{\beta} - 1\right) \textstyle\sum_{m=1}^{q} \left\| \delta p_{f_h}^{n+1,m+k} - \delta p_{f_h}^{n+1,m-1+k} \right\|_{\mathcal{C}}^2 + \tfrac{4\lambda}{\alpha^2 q^2} \left(2GC^* - \tfrac{\lambda}{\alpha^2}\right) \textstyle\sum_{m=1}^{q} \left\| \delta w_h^{n+1,k+q} \right\|_{\mathcal{C}}^2 \\
&+ \tfrac{\Delta t}{\beta \mu_f} \| K^{-1/2} \delta \boldsymbol{z}_h^{n+1,k+q} \|_{\Omega^+ \cup \Omega^-}^2 + \tfrac{\Delta t}{12 \mu_f \beta} \| K_{\mathcal{C}}^{-1/2} \delta \boldsymbol{\zeta}_h^{n+1,k+q} \|_{\mathcal{C}}^2 \\
&+ \tfrac{\Delta t}{\beta \mu_f} \textstyle\sum_{m=1}^{q} \| K^{-1/2} (\delta \boldsymbol{z}_h^{n+1,m+k} - \delta \boldsymbol{z}_h^{n+1,m-1+k}) \|_{\Omega^+ \cup \Omega^-}^2 \\
&+ \tfrac{\Delta t}{12 \mu_f \beta} \textstyle\sum_{m=1}^{q} \| K_{\mathcal{C}}^{-1/2} (\delta \boldsymbol{\zeta}_h^{n+1,m+k} - \delta \boldsymbol{\zeta}_h^{n+1,m-1+k}) \|_{\mathcal{C}}^2 \\
&+ \textstyle\sum_{m=1}^{q} \left(\| \delta \sigma_v^{n+1,m+k} \|_{\Omega^+ \cup \Omega^-}^2 + \| \delta \sigma_f^{n+1,m+k} \|_{\mathcal{C}}^2 \right) \\
&\quad \leq Max\left(\tfrac{L^2}{\beta^2}, \tfrac{L^2}{\beta \beta_c}\right) \textstyle\sum_{m=1}^{q} \left(\| \delta \sigma_v^{n+1,m+k} \|_{\Omega^+ \cup \Omega^-}^2 + \| \delta \sigma_f^{n+1,m+k} \|_{\mathcal{C}}^2 \right)
\end{aligned}$$

Furthermore, the sequences defined by this scheme converge to the unique solution of the weak formulation (6.5.63)–(6.5.67)*.*

6.6 Modified Multirate Formulation and Analysis

In this section, we present a modified multirate iterative coupling algorithm, which results in a Banach contraction estimate on the volumetric mean total stresses (or to be more

accurate on the quantities of contractions) as defined by Girualt *et al.* [43], for the single rate fixed stress split scheme. This algorithm involves a slight modification to the original multirate iterative coupling scheme in which we employ "successive corrections" in the flow problem which will cancel out in the limit. This is quite similar to the addition of regularization terms in the fixed stress split scheme. In this case, the iterative coupling iteration is split into even and odd iterations, in which flux corrections terms are added in even coupling iterations. Those added flux correction terms result in eliminating the excessive flux accumulation contributions which appear as a result of taking more than one flow time step within one coarse mechanics time step and yield theoretical results identical to those of the single rate case.
The rational behind introducing this scheme can be summarized as follows:

- The weak formulation of the modified scheme reduces to that of the single rate scheme. As a result, all established theoretical results for the single rate scheme will be applicable for the modified multirate scheme.

- A key advantage of this scheme is the fact that its quantity of contraction is independent of q (the number of flow fine time steps within one coarse mechanics time steps). This is not the case in the original multirate iterative coupling scheme, considered earlier, as the volumetric strain term and also the term involving the jump in displacement across the fracture are both divided by q in the quantities of contraction (6.5.90) and (6.5.104), respectively. This means that as the value of q increases, the mechanics contribution to the quantities of contraction gets reduced. For larger values of q, the scheme mostly contracts on differences in pressures in both the reservoir matrix and the fracture. This restriction is completely eliminated in the modified multirate iterative coupling scheme.

- Compared to the combined condition (6.5.111) imposed in the first multirate scheme, the modified multirate scheme only imposes the condition (6.4.62).

We adopt exactly the same notation as the one used earlier.

6.6.1 Modified Multirate Iterative Coupling Scheme

Algorithm 10: Modified Multirate Iterative Coupling Algorithm

for $k = 0, q, 2q, 3q, ..$ **do** /* mechanics time step iteration index */

  for $n = 1, 2, ..$ **do** /* coupling iteration index */

    First Step: Flow equations

    Given $\boldsymbol{u}_h^{n,k+q}$ *(assuming an initial value is given for the first iteration:* $\boldsymbol{u}_h^{0,k+q}$*)*

    For the first local flow time step iteration, solve for $p_h^{n+1,1+k}$, $\boldsymbol{z}_h^{n+1,1+k}$, $p_{f_h}^{n+1,1+k}$, *and* $\boldsymbol{\zeta}_h^{n+1,1+k}$ *satisfying:*

$$
\begin{aligned}
&(\frac{1}{M} + c_f\varphi_0 + \frac{\alpha^2}{\lambda})\Big(\frac{p_h^{n+1,1+k} - p_h^{n+1,k}}{\Delta t}\Big) + \frac{1}{\mu_f}\nabla\cdot\boldsymbol{z}_h^{n+1,1+k} = \\
&\qquad \frac{\alpha^2}{\lambda}\Big(\frac{p_h^{n,1+k} - p_h^{k}}{\Delta t}\Big) - \alpha\nabla\cdot\Big(\frac{\boldsymbol{u}_h^{n,k+q} - \boldsymbol{u}_h^{n,k}}{q\Delta t}\Big) + \tilde{q}_h \ \text{ in } \Omega\setminus\mathcal{C}, \\
&(\gamma_c + c_{fc})\Big(\frac{{p_f}_h^{n+1,1+k} - {p_f}_h^{n+1,k}}{\Delta t}\Big) + \Big(\frac{w_h^{n,k+q} - w_h^{n,k}}{q\Delta t}\Big) + \frac{1}{12\mu_f}\overline{\nabla}\cdot\boldsymbol{\zeta}_h^{n+1,1+k} = \\
&\qquad \gamma_c\Big(\frac{{p_f}_h^{n,1+k} - {p_f}_h^{n,k}}{\Delta t}\Big) + \tilde{q}_{W_h} - \tilde{q_L}_h^{n+1,1+k} \ \text{ in } \mathcal{C}
\end{aligned}
$$

    if *mod(n,2) = 1* **then** /* coupling iteration index (n) is odd */

      for $m = 2, .., q$ **do** /* flow finer time steps iteration index */

        Solve for $p_h^{n+1,m+k}, \boldsymbol{z}_h^{n+1,m+k}, {p_f}_h^{n+1,m+k}$, *and* $\boldsymbol{\zeta}_h^{n+1,m+k}$ *satisfying:*

$$
\begin{aligned}
&(\frac{1}{M} + c_f\varphi_0 + \frac{\alpha^2}{\lambda})\Big(\frac{p_h^{n+1,m+k} - p_h^{n+1,m-1+k}}{\Delta t}\Big) + \frac{1}{\mu_f}\nabla\cdot\boldsymbol{z}_h^{n+1,m+k} = \\
&\frac{\alpha^2}{\lambda}\Big(\frac{p_h^{n,m+k} - p_h^{m-1+k}}{\Delta t}\Big) - \alpha\nabla\cdot\Big(\frac{\boldsymbol{u}_h^{n,k+q} - \boldsymbol{u}_h^{n,k}}{q\Delta t}\Big) + \tilde{q}_h \ \text{ in } \Omega\setminus\mathcal{C}, \\
&(\gamma_c + c_{fc})\Big(\frac{{p_f}_h^{n+1,m+k} - {p_f}_h^{n+1,m-1+k}}{\Delta t}\Big) + \Big(\frac{w_h^{n,k+q} - w_h^{n,k}}{q\Delta t}\Big) \\
&+ \frac{1}{12\mu_f}\overline{\nabla}\cdot\boldsymbol{\zeta}_h^{n+1,m+k} = \gamma_c\Big(\frac{{p_f}_h^{n,m+k} - {p_f}_h^{n,m-1+k}}{\Delta t}\Big) + \tilde{q}_{W_h} - \tilde{q_L}_h^{n+1,m+k} \ \text{ in } \mathcal{C}
\end{aligned}
$$

    else /* coupling iteration index (n) is even */

      for $m = 2, .., q$ **do** /* flow finer time steps iteration index */

        Solve for $p_h^{n+1,m+k}, \boldsymbol{z}_h^{n+1,m+k}, {p_f}_h^{n+1,m+k}$, *and* $\boldsymbol{\zeta}_h^{n+1,m+k}$ *satisfying:*

$$
\begin{aligned}
&(\frac{1}{M} + c_f\varphi_0 + \frac{\alpha^2}{\lambda})\Big(\frac{p_h^{n+1,m+k} - p_h^{n+1,m-1+k}}{\Delta t}\Big) + \frac{1}{\mu_f}\nabla\cdot\boldsymbol{z}_h^{n+1,m+k} - \frac{1}{\mu_f}\nabla\cdot\boldsymbol{z}_h^{n+1,m-1+k} \\
&= \frac{\alpha^2}{\lambda}\Big(\frac{p_h^{n,m+k} - p_h^{m-1+k}}{\Delta t}\Big) - \alpha\nabla\cdot\Big(\frac{\boldsymbol{u}_h^{n,k+q} - \boldsymbol{u}_h^{n,k}}{q\Delta t}\Big) + \tilde{q}_h - \frac{1}{\mu_f}\nabla\cdot\boldsymbol{z}_h^{n,m-1+k} \ \text{ in } \Omega\setminus\mathcal{C}, \qquad (6.6.115) \\
&(\gamma_c + c_{fc})\Big(\frac{{p_f}_h^{n+1,m+k} - {p_f}_h^{n+1,m-1+k}}{\Delta t}\Big) + \Big(\frac{w_h^{n,k+q} - w_h^{n,k}}{q\Delta t}\Big) \\
&+ \frac{1}{12\mu_f}\overline{\nabla}\cdot\boldsymbol{\zeta}_h^{n+1,m+k} - \frac{1}{12\mu_f}\overline{\nabla}\cdot\boldsymbol{\zeta}_h^{n+1,m-1+k} - \tilde{q_L}_h^{n+1,m-1+k} = \tilde{q}_{W_h} - \tilde{q_L}_h^{n+1,m+k} \\
&+ \gamma_c\Big(\frac{{p_f}_h^{n,m+k} - {p_f}_h^{n,m-1+k}}{\Delta t}\Big) - \frac{1}{12\mu_f}\overline{\nabla}\cdot\boldsymbol{\zeta}_h^{n,m-1+k} - \tilde{q_L}_h^{n,m-1+k} \ \text{ on } \mathcal{C} \qquad (6.6.116)
\end{aligned}
$$

    Second Step: Mechanics equations

    Given $p_h^{n+1,k+q}, \boldsymbol{z}_h^{n+1,k+q}, {p_f}_h^{n+1,k+q}$, *and* $\boldsymbol{\zeta}_h^{n+1,k+q}$, *solve for* $\boldsymbol{u}_h^{n+1,k+q}$ *satisfying:*

$$
-\operatorname{div}\boldsymbol{\sigma}^{\mathrm{por}}(\boldsymbol{u}_h^{n+1,k+q}, p_h^{n+1,k+q}) = \boldsymbol{f} \qquad (6.6.117)
$$

6.6.2 Proof of Contraction

We define the volumetric mean total stress, representing the quantity of contraction in the reservoir matrix, as:

$$\sigma_v^{n,m+k} = \sigma_v^{n,k} + \lambda\nabla\cdot\boldsymbol{u}_h^{n,k} - \alpha(p_h^{n,m+k} - p_h^{n,k}) \qquad \text{for } 1 \le m \le q-1, \tag{6.6.118}$$

$$\sigma_v^{n,k+q} = \sigma_v^{n,k} + \lambda\nabla\cdot\boldsymbol{u}_h^{n,k+q} - \alpha(p_h^{n,k+q} - p_h) \qquad \text{for } m = q. \tag{6.6.119}$$

In terms of the differences between two iterative coupling iterations, we can write:

$$\delta\sigma_v^{n+1,m+k} = \sigma_v^{n+1,m+k} - \sigma_v^{n,m+k} = -\alpha\delta p_h^{n+1,m+k} \qquad \text{for } 1 \le m \le q-1, \tag{6.6.120}$$

$$\delta\sigma_v^{n+1,k+q} = \lambda\nabla\cdot\delta\boldsymbol{u}_h^{n+1,k+q} - \alpha\delta p_h^{n+1,k+q} \qquad \text{for } m = q. \tag{6.6.121}$$

In a similar way, following (6.4.41), we define the quantity of contraction in the fracture as:

$$\chi\delta\sigma_f^{n+1,m+k} = \chi\sigma_f^{n+1,m+k} - \chi\sigma_f^{n,m+k} = \gamma_c\delta {p_f}_h^{n+1,m+k} \qquad \text{for } 1 \le m \le q-1, \tag{6.6.122}$$

$$\chi\delta\sigma_f^{n+1,k+q} = \gamma_c\delta {p_f}_h^{n+1,k+q} - \delta w_h^{n+1,k+q} \qquad \text{for } m = q. \tag{6.6.123}$$

In order to obtain the single rate weak formulation, we sum up local flow iterations in one coarse mechanics time step. Since we solve different mass balance equations in even versus odd coupling iterations, we consider each case separately:

- **Coupling iteration index, n, is odd:**

$$\begin{aligned}
&(\frac{1}{M} + c_f\varphi_0 + \frac{\alpha^2}{\lambda})\frac{1}{\Delta t}\sum_{m=1}^{q}\Big(p_h^{n+1,m+k} - p_h^{n+1,m-1+k}\Big) + \frac{1}{\mu_f}\nabla\cdot\sum_{m=1}^{q}\boldsymbol{z}_h^{n+1,m+k} \\
&= -\frac{\alpha}{\lambda\Delta t}\Big(-\alpha\sum_{m=1}^{q}\Big(p_h^{n,m+k} - p_h^{m-1+k}\Big) + \frac{\lambda}{q}\nabla\cdot\sum_{m=1}^{q}\Big(\boldsymbol{u}_h^{n,k+q} - \boldsymbol{u}_h^{n,k}\Big)\Big) + q\tilde{q}_h
\end{aligned} \tag{6.6.124}$$

$$\sum_{m=1}^{q}\boldsymbol{z}_h^{n+1,m+k} = -\boldsymbol{K}\nabla\Big(\sum_{m=1}^{q}p_h^{n+1,m+k}\Big) + \boldsymbol{K}q\rho_{f,r}g\nabla\eta \tag{6.6.125}$$

$$\begin{aligned}
&\frac{(\gamma_c + c_{fc})}{\Delta t}\sum_{m=1}^{q}\Big({p_f}_h^{n+1,m+k} - {p_f}_h^{n+1,m-1+k}\Big) + \frac{1}{12\mu_f}\overline{\nabla}\cdot\sum_{m=1}^{q}\boldsymbol{\zeta}_h^{n+1,m+k} \\
&- \frac{1}{\mu_f}\Big[\sum_{m=1}^{q}\boldsymbol{z}_h^{n+1,m+k}\Big]_{\mathcal{C}}\cdot n^+ = \frac{\gamma_c}{\Delta t}\sum_{m=1}^{q}\Big({p_f}_h^{n,m+k} - {p_f}_h^{n,m-1+k}\Big) \\
&+ \frac{1}{\Delta t}\Big([\boldsymbol{u}_h^{n,k+q}]_{\mathcal{C}}\cdot\boldsymbol{n}^+ - [\boldsymbol{u}_h^{n,k}]_{\mathcal{C}}\cdot\boldsymbol{n}^+\Big) + q\tilde{q}_{W_h}
\end{aligned} \tag{6.6.126}$$

$$\sum_{m=1}^{q} \boldsymbol{\zeta}_h^{n+1,m+k} = -K_{\mathcal{C}} \overline{\nabla} \sum_{m=1}^{q} \left({p_f}_h^{n+1,m+k} \right) + K_{\mathcal{C}} q \rho_{f,r} g \overline{\nabla}\, \eta, \tag{6.6.127}$$

$$w_h^{n,k+q} = -[\boldsymbol{u}_h^{n,k+q}]_{\mathcal{C}} \cdot \boldsymbol{n}^+. \tag{6.6.128}$$

(6.6.128) remains unchanged. We do not sum up mechanics equations since we solve them only once during every coupling iteration.

- **Coupling iteration index, n, is even:**

  Equations (6.6.125) and (6.6.127) remain unchanged.

$$\begin{aligned}
&(\frac{1}{M} + c_f \varphi_0 + \frac{\alpha^2}{\lambda}) \frac{1}{\Delta t} \sum_{m=1}^{q} \left(p_h^{n+1,m+k} - p_h^{n+1,m-1+k} \right) + \frac{1}{\mu_f} \nabla \cdot \sum_{m=1}^{q} \boldsymbol{z}_h^{n+1,m+k} \\
&- \frac{1}{\mu_f} \nabla \cdot \sum_{w=1}^{q-1} \boldsymbol{z}_h^{n+1,w+k} = -\frac{\alpha}{\lambda \Delta t} \Big(- \alpha \sum_{m=1}^{q} \left(p_h^{n,m+k} - p_h^{m-1+k} \right) \\
&+ \frac{\lambda}{q} \nabla \cdot \sum_{m=1}^{q} \left(\boldsymbol{u}_h^{n,k+q} - \boldsymbol{u}_h^{n,k} \right) \Big) + q \tilde{q}_h - \frac{1}{\mu_f} \nabla \cdot \sum_{w=1}^{q-1} \boldsymbol{z}_h^{n,w+k} \text{ in } \Omega \setminus \mathcal{C},
\end{aligned} \tag{6.6.129}$$

$$\begin{aligned}
&\frac{(\gamma_c + c_{fc})}{\Delta t} \sum_{m=1}^{q} \left({p_f}_h^{n+1,m+k} - {p_f}_h^{n+1,m-1+k} \right) + \frac{1}{12\mu_f} \overline{\nabla} \cdot \sum_{m=1}^{q} \boldsymbol{\zeta}_h^{n+1,m+k} \\
&- \frac{1}{\mu_f} \Big[\sum_{m=1}^{q} \boldsymbol{z}_h^{n+1,m+k} \Big]_{\mathcal{C}} \cdot n^+ - \frac{1}{12\mu_f} \overline{\nabla} \cdot \sum_{m=1}^{q-1} \boldsymbol{\zeta}_h^{n+1,m+k} + \frac{1}{\mu_f} \Big[\sum_{m=1}^{q-1} \boldsymbol{z}_h^{n+1,m+k} \Big]_{\mathcal{C}} \cdot n^+ \\
&= \frac{\gamma_c}{\Delta t} \sum_{m=1}^{q} \left({p_f}_h^{n,m+k} - {p_f}_h^{n,m-1+k} \right) + q \tilde{q}_{W_h} - \frac{1}{12\mu_f} \overline{\nabla} \cdot \sum_{w=1}^{q-1} \boldsymbol{\zeta}_h^{n+1,w+k} \\
&+ \frac{1}{\mu_f} \Big[\sum_{w=1}^{q-1} \boldsymbol{z}_h^{n+1,w+k} \Big]_{\mathcal{C}} \cdot n^+ + \frac{1}{\Delta t} \Big([\boldsymbol{u}_h^{n,k+q}]_{\mathcal{C}} \cdot \boldsymbol{n}^+ - [\boldsymbol{u}_h^{n,k}]_{\mathcal{C}} \cdot \boldsymbol{n}^+ \Big) \text{ in } \mathcal{C},
\end{aligned} \tag{6.6.130}$$

Now, we take the difference between an even and odd coupling iterations. Assuming, without loss of generality, that the coupling iteration index "$n+1$" represents an even coupling iteration, and "n" represents an odd coupling iteration, subtracting (6.6.124) from (6.6.129) yields (with appropriate cancellations):

$$\begin{aligned}
&(\frac{1}{M} + c_f \varphi_0 + \frac{\alpha^2}{\lambda}) \frac{1}{\Delta t} \delta p_h^{n+1,k+q} + \frac{1}{\mu_f} \nabla \cdot \sum_{m=1}^{q} \delta \boldsymbol{z}_h^{n+1,m+k} - \frac{1}{\mu_f} \nabla \cdot \sum_{w=1}^{q-1} \delta \boldsymbol{z}_h^{n+1,w+k} \\
&= -\frac{\alpha}{\lambda \Delta t} \delta \sigma_v^{n,k+q},
\end{aligned}$$

which can be written as

$$(\frac{1}{M}+c_f\varphi_0+\frac{\alpha^2}{\lambda})\frac{1}{\Delta t}\delta p_h^{n+1,k+q}+\frac{1}{\mu_f}\nabla\cdot\delta\boldsymbol{z}_h^{n+1,q+k}=-\frac{\alpha}{\lambda\Delta t}\delta\sigma_v^{n,k+q}. \tag{6.6.131}$$

Similarly, subtracting (6.6.126) from (6.6.130) yields (with appropriate cancellations):

$$\begin{aligned}&\frac{(\gamma_c+c_{fc})}{\Delta t}\delta {p_f}_h^{n+1,q+k}+\frac{1}{12\mu_f}\overline{\nabla}\cdot\sum_{m=1}^{q}\boldsymbol{\zeta}_h^{n+1,m+k}-\frac{1}{\mu_f}\Big[\sum_{m=1}^{q}\boldsymbol{z}_h^{n+1,m+k}\Big]_{\mathcal{C}}\cdot n^+\\&-\frac{1}{12\mu_f}\overline{\nabla}\cdot\sum_{w=1}^{q-1}\boldsymbol{\zeta}_h^{n+1,w+k}+\frac{1}{\mu_f}\Big[\sum_{w=1}^{q-1}\boldsymbol{z}_h^{n+1,w+k}\Big]_{\mathcal{C}}\cdot n^+=\frac{\gamma_c}{\Delta t}\delta {p_f}_h^{n,q+k}\\&+\frac{1}{\Delta t}[\boldsymbol{u}_h^{n,k+q}]_{\mathcal{C}}\cdot\boldsymbol{n}^+\ \text{ in } \mathcal{C}.\end{aligned}$$

This gives

$$\begin{aligned}&\frac{(\gamma_c+c_{fc})}{\Delta t}\delta {p_f}_h^{n+1,q+k}+\frac{1}{12\mu_f}\overline{\nabla}\cdot\boldsymbol{\zeta}_h^{n+1,q+k}-\frac{1}{\mu_f}\Big[\boldsymbol{z}_h^{n+1,q+k}\Big]_{\mathcal{C}}\cdot n^+\\&\qquad=\frac{\gamma_c}{\Delta t}\delta {p_f}_h^{n,q+k}+\frac{1}{\Delta t}[\boldsymbol{u}_h^{n,k+q}]_{\mathcal{C}}\cdot\boldsymbol{n}^+\ \text{ in } \mathcal{C}.\end{aligned} \tag{6.6.132}$$

We can also write for the last finer time step (within one multirate iterative coupling iteration):

$$\delta\boldsymbol{z}_h^{n+1,q+k}=-\boldsymbol{K}\nabla\delta p_h^{n+1,q+k} \tag{6.6.133}$$

$$\delta\boldsymbol{\zeta}_h^{n+1,q+k}=-K_{\mathcal{C}}\overline{\nabla}\,\delta {p_f}_h^{n+1,q+k} \tag{6.6.134}$$

Now, equations (6.6.131), (6.6.132), (6.6.133), and (6.6.134) involve only coarse time step variables. Considering the modified multirate iterative coupling scheme as a single rate scheme, in which both the flow and mechanics problems share the coarse time step, the weak formulation of the differences between coupling iterates reads:

$$\begin{aligned}\forall\theta_h\in Q_h\,,\ \Big(\frac{1}{\Delta t}(\frac{1}{M}+c_f\varphi_0+\frac{\alpha^2}{\lambda})\delta p_h^{n+1,k+q},\theta_h\Big)+\frac{1}{\mu_f}(\nabla\cdot\delta\boldsymbol{z}_h^{n+1,k+q},\theta_h)=\\\Big(-\frac{\alpha}{\lambda\Delta t}\delta\sigma_v^{n,k+q},\theta_h\Big)\end{aligned} \tag{6.6.135}$$

$$\begin{aligned}&\forall\theta_{c_h}\in Q_{c_h}\,,\ \Big(\frac{1}{\Delta t}(c_{fc}+\gamma_c)\delta {p_f}_h^{n+1,k+q},\theta_{c_h}\Big)+\frac{1}{12\mu_f}(\overline{\nabla}\cdot(\delta\boldsymbol{\zeta}_h^{n+1,k+q}),\theta_{c_h})_{\mathcal{C}}\\&-\frac{1}{\mu_f}([\delta\boldsymbol{z}_h^{n+1,k+q}]_{\mathcal{C}}\cdot\boldsymbol{n}^+,\theta_{c_h})_{\mathcal{C}}=\Big(\frac{\gamma_c}{\Delta t}\delta {p_f}_h^{n,k+q},\theta_{c_h}\Big)+(\frac{1}{\Delta t}[\delta\boldsymbol{u}_h^{n,k+q}]_{\mathcal{C}}\cdot\boldsymbol{n}^+,\theta_{c_h})_{\mathcal{C}}\end{aligned} \tag{6.6.136}$$

$$\forall \boldsymbol{q}_h \in \boldsymbol{Z}_h\,,\, (\boldsymbol{K}^{-1}\delta \boldsymbol{z}_h^{n+1,k+q}, \boldsymbol{q}_h) = (\delta p_h^{n+1,k+q}, \nabla\cdot \boldsymbol{q}_h) - (\delta p_{f_h}^{n+1,k+q}, [\boldsymbol{q}_h]_{\mathcal{E}}\cdot \boldsymbol{n}^+)_{\mathcal{E}} \quad (6.6.137)$$

$$\forall \boldsymbol{\mu}_{f_h} \in \boldsymbol{Z}_{\mathcal{E}h}\,,\, (K_{\mathcal{E}}^{-1}\delta \boldsymbol{\zeta}_h^{n+1,k+q}, \boldsymbol{\mu}_{f_h})_{\mathcal{E}} = (\delta p_{f_h}^{n+1,k+q}, \overline{\nabla}\cdot(\boldsymbol{\mu}_{f_h}))_{\mathcal{E}} \quad (6.6.138)$$

$$\begin{aligned}\forall \boldsymbol{v}_h \in V_h\,, 2G(\boldsymbol{\varepsilon}(\delta \boldsymbol{u}_h^{n+1,k+q}), \boldsymbol{\varepsilon}(\boldsymbol{v}_h)) + \lambda(\nabla\cdot\delta \boldsymbol{u}_h^{n+1,k+q}, \nabla\cdot\boldsymbol{v}_h)\\ - \alpha(\delta p_h^{n+1,k+q}, \nabla\cdot\boldsymbol{v}_h) + (\delta p_{f_h}^{n+1,k+q}, [\boldsymbol{v}_h]_{\mathcal{E}}\cdot\boldsymbol{n}^+)_{\mathcal{E}} = 0 \quad (6.6.139)\end{aligned}$$

Comparing (6.6.135), (6.6.136), (6.6.137), (6.6.138), and (6.6.139) to (6.4.43), (6.4.44), (6.4.45), (6.4.46), and (6.4.47), we conclude that the proof follows exactly in the same way as in the fully discrete single rate case considered earlier. Therefore, we have the following theorem:

Theorem 6.6.1. *The modified multirate iterative scheme is a contraction given by*

$$\begin{aligned}&\|\delta\sigma_v^{n+1,k+q}\|_{\Omega^+\cup\Omega^-} + \lambda^2\|\nabla\cdot\delta\boldsymbol{u}_h^{n+1,k+q}\|_{\Omega^+\cup\Omega^-} + \tfrac{2\Delta t}{\beta\mu_f}\|K^{-1/2}\delta\boldsymbol{z}_h^{n+1,k+q}\|_{\Omega^+\cup\Omega^-}\\ &+\tfrac{\Delta t}{6\mu_f\beta}\|K_{\mathcal{E}}^{-1/2}\delta\boldsymbol{\zeta}_h^{n+1,k+q}\|_{\mathcal{E}} + \|\delta\sigma_f^{n+1,k+q}\|_{\mathcal{E}} + (4G\lambda C^* - \tfrac{1}{\chi^2})\|\delta w_h^{n+1,k+q}\|_{\mathcal{E}}\\ &\qquad\le \max\left\{\frac{1/\lambda^2}{\left(\frac{1}{M\alpha^2}+\frac{c_f}{\alpha^2}\varphi_0+\frac{1}{\lambda}\right)^2}\,,\,\frac{\gamma_c}{(c_{fc}+\gamma_c)\lambda\left(\frac{1}{M\alpha^2}+\frac{c_f}{\alpha^2}\varphi_0+\frac{1}{\lambda}\right)}\right\}\left(\left\|\delta\sigma_v^{n,k+q}\right\|_{\Omega^+\cup\Omega^-} + \|\delta\sigma_f^{n,k+q}\|_{\mathcal{E}}\right).\end{aligned}$$

Furthermore, the sequences defined by this scheme converge to the unique solution of the weak formulation (6.4.18) - (6.4.22).

6.7 Conclusions and Discussion

In this chapter, we carried out a rigorous mathematical analysis of the single rate and multirate fixed-stress split iterative coupling schemes in fractured poro-elastic media. The analysis of the fully discrete single rate scheme follows a similar approach as the one presented in [43] for the continuous case. The analysis of the proposed multirate schemes is more involved. In both cases, the iterative coupling scheme is shown to be contractive, with a contraction coefficient strictly less than one. As a future work, the proposed multirate iterative coupling schemes will be implemented numerically, and the derived mathematical conditions will be validated as well.

Chapter 7

Explicit Coupling Schemes for Fractured Poroelastic Media

In this chapter, we consider explicit coupling schemes for coupling flow with geomechanics in fractured poro-elastic media. In practice, quite commonly explicit coupling schemes are more popular than iterative coupling scheme. However, they are only conditionally stable under certain conditions on the parameters. We recall that an explicit coupling scheme is a sequential procedure in which flow or mechanics is solved first followed by the other. In this chapter, we consider solving the flow problem followed by the mechanics problem. There is no coupling iteration between the two problems. This simply means that the algorithm keeps marching in time, advancing time steps, and solving exactly one (or possibly many with a fine time step) flow problems and one (with a possibly coarse time step) mechanics problem in a sequential manner. In this chapter, we will analyze the stability of both single rate and multirate explicit coupling schemes for fractured poro-elastic media. The stability analysis reveals the corresponding stability conditions for each case. We recall that in the single rate scheme (figure 7.1a), the flow and mechanics problems share the exact same time step. In contrast, in the multirate shceme (figure 7.1b), the flow problem takes several finer local time steps within one coarser mechanics time step. It should be noted that in explicit coupling algorithms, the fixed-stress split scheme does not apply as there is no coupling iteration between the two problems. In other words, the usual fixed-stress split regularization terms can not be added in this case.

7.1 Model Equations and Discretization

We adopt the same model as the one presented in Chapter 6 (for the iterative coupling case). For completeness, we briefly list the equations involved. The continuos in time for-

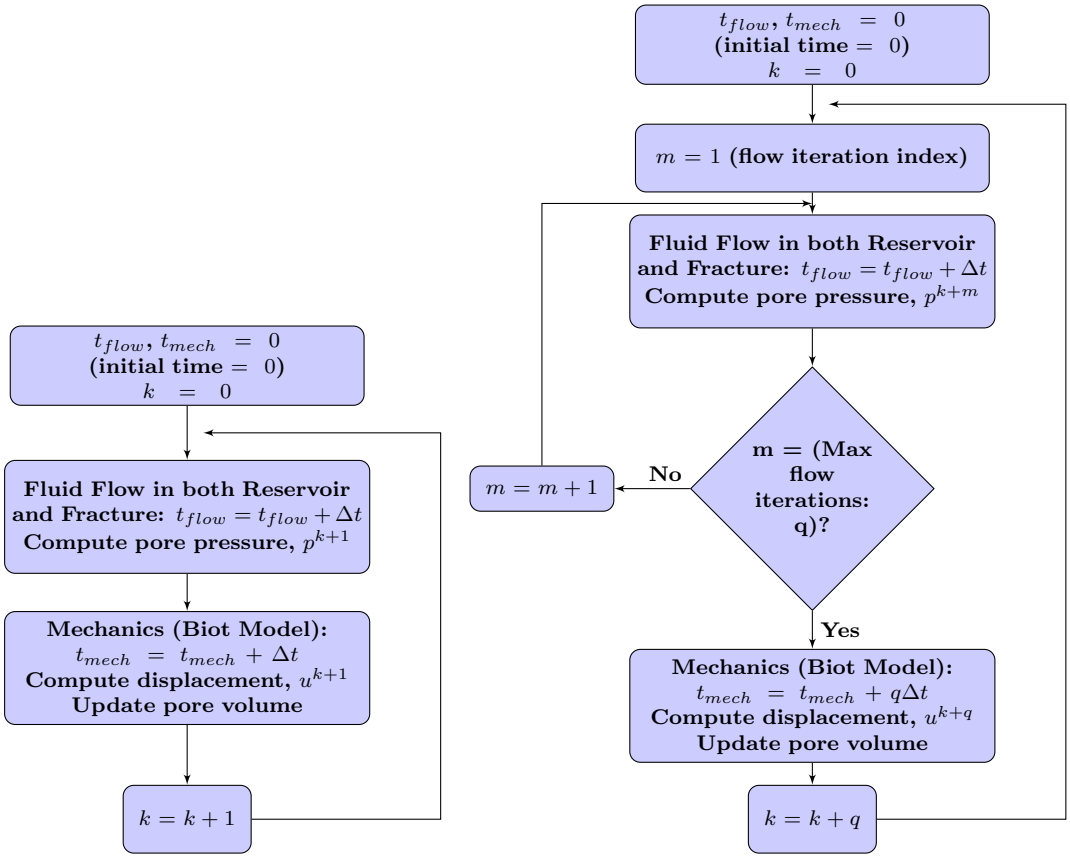

(a) Single Rate (b) Multirate

Figure 7.1: Flowchart for the explicit single rate and multirate time steppings for coupled geomechanics and flow problems in fractured poro-elastic media

mulation reads: Find $\boldsymbol{u}$, p, and $\tilde{q}_L$ satisfying the equations below for all time $t \in]0, T[$:

$$
\begin{aligned}
-\mathrm{div}\,\boldsymbol{\sigma}^{\mathrm{por}}(\boldsymbol{u},p) &= \boldsymbol{f} \ \text{ in } \Omega\setminus\mathcal{C},\\
\boldsymbol{\sigma}^{\mathrm{por}}(\boldsymbol{u},p) &= \boldsymbol{\sigma}(\boldsymbol{u}) - \alpha\, p\, \boldsymbol{I} \ \text{ in } \Omega\setminus\mathcal{C},\\
\tfrac{\partial}{\partial t}\Big((\tfrac{1}{M}+c_f\varphi_0)p + \alpha\nabla\cdot\boldsymbol{u}\Big) - \nabla\cdot\Big(\tfrac{1}{\mu_f}\boldsymbol{K}(\nabla p - \rho_{f,r}g\nabla\eta)\Big) &= \tilde{q} \ \text{ in } \Omega\setminus\mathcal{C},\\
c_f\tfrac{\partial p_f}{\partial t} + \tfrac{\partial}{\partial t}w - \overline{\nabla}\cdot(\tfrac{K_{\mathcal{C}}}{12\mu_f}(\overline{\nabla}\, p_f - \rho_{f,r}g\overline{\nabla}\,\eta)) &= \tilde{q}_W - \tilde{q}_L \ \text{ in } \mathcal{C},\\
(\boldsymbol{\sigma}^{\mathrm{por}}(\boldsymbol{u},p))^{\star}\boldsymbol{n}^{\star} &= -p|_{\mathcal{C}}\boldsymbol{n}^{\star}\ ,\ \star = +,- \ \text{ on } \mathcal{C},\\
\tfrac{1}{\mu_f}[\boldsymbol{K}(\nabla p - \rho_{f,r}g\nabla\eta)]_{\mathcal{C}}\cdot\boldsymbol{n}^{+} &= \tilde{q}_L \ \text{ on } \mathcal{C},\\
\text{where} \quad w &= -[\boldsymbol{u}]_{\mathcal{C}}\cdot\boldsymbol{n}^{+},\\
\text{Boundary Conditions: } \boldsymbol{u} = \boldsymbol{0}\ ,\ \boldsymbol{K}(\nabla p - \rho_{f,r}g\nabla\eta)\cdot\boldsymbol{n} &= 0 \ \text{ on } \partial\Omega,\\
\text{Initial Condition } \ (t=0): \ \Big((\tfrac{1}{M}+c_f\varphi_0)p + \alpha\nabla\cdot\boldsymbol{u}\Big)(0) &=\\
(\tfrac{1}{M}+c_f\varphi_0)p_0 + \alpha\nabla\cdot\boldsymbol{u}_0.&
\end{aligned}
$$

We use the same space and time discretizations as described in the previous chapter (Chapter 6).

7.1.1 Assumptions

We briefly recall the assumptions from the previous chapter. The reservoir is assumed to be homogeneous, isotropic and saturated poro-elastic medium. The fluid is assumed to be slightly compressible. Its density is a linear function of pressure, with a constant viscosity $\mu_f > 0$. The reference density of the fluid $\rho_f > 0$, the Lamé coefficients $\lambda > 0$ and $G > 0$, the dimensionless Biot coefficient α, and the pore volume φ^* are all positive. The absolute permeability tensors in the matrix and the fracture ($\boldsymbol{K}$ and $\boldsymbol{K}_c$), are assumed to be symmetric, bounded, uniformly positive definite in space and constant in time.
More assumptions (i.e. stability conditions) on the flow and mechanics parameters will be derived mathematically for both the single rate and multirate schemes.

Remark 7.1.1. Notation: *We recall the notation adopted in the previous chapters: k denotes the coarser mechanics time step index, m denotes the finer flow time step index, Δt stands for the unit (finer) time step, and q is the "fixed" number of fine flow time steps per one coarse mechanics time step.*

7.2 Single Rate Explicit Coupling Formulation and Analysis

7.2.1 Fully Discrete Scheme for Single Rate

Using the mixed finite element method in space for flow, continuous Galerkin for mechanics, and the backward Euler finite difference method in time, the weak formulation of the single rate explicit coupling scheme in fractured poro-elastic media reads as follows.

Definition 7.2.1. *(**flow equation**) Find* $p_h^{k+1} \in Q_h$, $p_{f_h}^{k+1} \in Q_{c_h}$, $\boldsymbol{z}_h^{k+1} \in \boldsymbol{Z}_h$, *and* $\boldsymbol{\zeta}_h^{k+1} \in \boldsymbol{Z}_{\mathcal{E}h}$ *such that,*

$$\forall \theta_h \in Q_h\,,\ \frac{\beta}{\Delta t}\Big(p_h^{k+1} - p_h^k, \theta_h\Big) + \frac{1}{\mu_f}(\nabla \cdot \boldsymbol{z}_h^{k+1}, \theta_h) = -\frac{\alpha}{\Delta t}\Big(\nabla \cdot (\boldsymbol{u}_h^k - \boldsymbol{u}_h^{k-1}), \theta_h\Big) + (\tilde{q}_h^{k+1}, \theta_h) \tag{7.2.1}$$

$$\begin{aligned}\forall \theta_{c_h} \in Q_{c_h}\,,\ \frac{c_{f_c}}{\Delta t}\Big(p_{f_h}^{k+1} - p_{f_h}^k, \theta_{c_h}\Big)_{\mathcal{E}} + \frac{1}{12\mu_f}(\overline{\nabla} \cdot (\boldsymbol{\zeta}_h^{k+1}), \theta_{c_h})_{\mathcal{E}} - \frac{1}{\mu_f}([\boldsymbol{z}_h^{k+1}]_{\mathcal{E}} \cdot \boldsymbol{n}^+, \theta_{c_h})_{\mathcal{E}} \\ = -\frac{1}{\Delta t}(w_h^k - w_h^{k-1}, \theta_{c_h})_{\mathcal{E}} + (\tilde{q}_{W_h}^{k+1}, \theta_{c_h})_{\mathcal{E}}\end{aligned} \tag{7.2.2}$$

$$\forall \boldsymbol{q}_h \in \boldsymbol{Z}_h\,,\ (\boldsymbol{K}^{-1}\boldsymbol{z}_h^{k+1}, \boldsymbol{q}_h) = (p_h^{k+1}, \nabla \cdot \boldsymbol{q}_h) - (p_{f_h}^{k+1}, [\boldsymbol{q}_h]_{\mathcal{E}} \cdot \boldsymbol{n}^+)_{\mathcal{E}} + (\nabla(\rho_{f,r} g \eta), \boldsymbol{q}_h) \tag{7.2.3}$$

$$\forall \boldsymbol{\mu}_{f_h} \in \boldsymbol{Z}_{\mathcal{E}h}\,,\ (K_{\mathcal{E}}^{-1}\boldsymbol{\zeta}_h^{k+1}, \boldsymbol{\mu}_{f_h})_{\mathcal{E}} = (p_{f_h}^{k+1}, \overline{\nabla} \cdot (\boldsymbol{\mu}_{f_h}))_{\mathcal{E}} + (\overline{\nabla}(\rho_{f,r} g \eta), \boldsymbol{\mu}_{f_h})_{\mathcal{E}}. \tag{7.2.4}$$

Definition 7.2.2. *(**mechanics equation**) Given* $p_h^{k+1}, \boldsymbol{z}_h^{k+1}, p_{f_h}^{k+1}, \boldsymbol{\zeta}_h^{k+1}$, *find* $\boldsymbol{u}_h^{k+1} \in \boldsymbol{V}_h$ *such that,*

$$\begin{aligned}\forall \boldsymbol{v}_h \in V_h\,,\ 2G(\boldsymbol{\varepsilon}(\boldsymbol{u}_h^{k+1}), \boldsymbol{\varepsilon}(\boldsymbol{v}_h)) + \lambda(\nabla \cdot \boldsymbol{u}_h^{k+1}, \nabla \cdot \boldsymbol{v}_h) - \alpha(p_h^{k+1}, \nabla \cdot \boldsymbol{v}_h) \\ + (p_{f_h}^{k+1}, [\boldsymbol{v}_h]_{\mathcal{E}} \cdot \boldsymbol{n}^+)_{\mathcal{E}} = (\boldsymbol{f}_h^{k+1}, \boldsymbol{v}_h)\end{aligned} \tag{7.2.5}$$

7.2.2 Single Rate Explicit Coupling Algorithm

We start by analyzing the single-rate explicit coupling algorithm, in which both flow and mechanics share the same time step. The algorithm is given as follows:

Algorithm 11: Single Rate Explicit Coupling Algorithm

Given initial conditions $\boldsymbol{u}_h^0$, p_h^0, $p_{f_h}^0 = p_h^0|_{\mathcal{C}}$ *solve fully implicitly for* $p_h^1, p_{f_h}^1, \boldsymbol{z}_h^1, \boldsymbol{\zeta}_h^1$, *and* $\boldsymbol{u}_h^1$ *satisfying the fractured Biot model*

for $k = 1, 2, \ldots$ **do** `/* time step index */`

  First Step: Flow equations

  Given $\boldsymbol{u}_h^k$ *and* $\boldsymbol{u}_h^{k-1}$*:*

    Solve for p_h^{k+1}, $p_{f_h}^{k+1}$, $\boldsymbol{z}_h^{k+1}$, *and* $\boldsymbol{\zeta}_h^{k+1}$ *satisfying definition 7.2.1*

  Second Step: Mechanics equations

  Given p_h^{k+1}, $p_{f_h}^{k+1}$, $\boldsymbol{z}_h^{k+1}$, *and* $\boldsymbol{\zeta}_h^{k+1}$*:*

    Solve for $\boldsymbol{u}_h^{k+1}$ *satisfying definition 7.2.2*

Note that we begin with $k = 1$ and we require both $\boldsymbol{u}_h^1$ and $\boldsymbol{u}_h^0$ for obtaining p_h^2, $p_{f_h}^2$, $\boldsymbol{z}_h^2$, and $\boldsymbol{\zeta}_h^2$. In the first step, we use a fully implicit method to solve for p_h^1, $p_{f_h}^1$, $\boldsymbol{z}_h^1$, and $\boldsymbol{\zeta}_h^1$, and $\boldsymbol{u}_h^1$. Alternatively, to keep the problem decoupled, we can use iterative techniques such as fixed stress splitting or undrained splitting [43, 64].

7.2.2.1 Assumptions

For notational convenience, we define

$$\beta = (\frac{1}{M} + c_f \varphi_0).$$

For stability to hold, we assume the following:

$$(\mathbf{A_1}) \quad \beta > \tfrac{\alpha^2}{\lambda} \qquad \& \qquad c_{f_c} > \tfrac{1}{GC^*}$$

where C^* is a product of optimal constants in Korn's, Poincare's, and trace inequalities, defined in (6.4.55).

7.2.2.2 Result

Our results make explicit the dependence of the stability on the difference of the above quantities. we have the following stability result.

Theorem 7.2.1. *[Single rate] Under the Assumption* $\mathbf{A_1}$ *above, the following stability result holds for the single rate explicit coupling scheme (in the fractured poro-elastic media) for*

time steps $t_0 \le t_k \le t_J$*:*

$$\frac{\Delta t}{2\mu_f}\Big[\Big\|\boldsymbol{K}^{-1/2}\boldsymbol{z}_h^{J+1}\Big\|^2+\sum_{k=1}^{J}\Big\|\boldsymbol{K}^{-1/2}(\boldsymbol{z}_h^{k+1}-\boldsymbol{z}_h^{k})\Big\|^2\Big]+\frac{\Delta t}{24\mu_f}\Big[\Big\|K_{\mathfrak{C}}^{-1/2}\boldsymbol{\zeta}_h^{J+1}\Big\|_{\mathfrak{C}}^2$$
$$+\sum_{k=1}^{J}\Big\|K_{\mathfrak{C}}^{-1/2}(\boldsymbol{\zeta}_h^{k+1}-\boldsymbol{\zeta}_h^{k})\Big\|_{\mathfrak{C}}^2\Big]+\frac{G}{2}\sum_{k=1}^{J}\Big\|\boldsymbol{\varepsilon}(\boldsymbol{u}_h^{k+1}-\boldsymbol{u}_h^{k})\Big\|^2+\frac{GC^*}{2}\Big\|w_h^{J+1}-w_h^{J}\Big\|_{\mathfrak{C}}^2$$
$$+\frac{\lambda}{2}\Big\|\nabla\cdot(\boldsymbol{u}_h^{J+1}-\boldsymbol{u}_h^{J})\Big\|^2\le C\Delta t+\frac{\Delta t^2}{4(\beta-\frac{\alpha^2}{\lambda})}\sum_{k=1}^{J}\Big\|\tilde{q}_h^{k+1}\Big\|^2+\frac{\Delta t^2}{4(c_{f_c}-\frac{1}{GC^*})}\sum_{k=1}^{J}\Big\|\tilde{q}_{W_h}^{k+1}\Big\|_{\mathfrak{C}}^2$$
$$+\frac{\mathcal{P}_\Omega^2 C_\kappa^2}{2G}\sum_{k=1}^{J}\Big\|\boldsymbol{f}_h^{k+1}-\boldsymbol{f}_h^{k}\Big\|^2$$

for a generic constant $C>0$*.*

7.2.3 Stability Analysis

- **Step 1: Flow equations**

  Consider (7.2.3) for two consecutive time steps: $t=t_k$ and $t=t_{k+1}$, and test both with $\boldsymbol{q}_h=\boldsymbol{z}_h^{k+1}$ to get:

$$(\boldsymbol{K}^{-1}\boldsymbol{z}_h^{k+1},\boldsymbol{z}_h^{k+1})=(p_h^{k+1},\nabla\cdot\boldsymbol{z}_h^{k+1})-(p_{f_h}^{k+1},[\boldsymbol{z}_h^{k+1}]_{\mathfrak{C}}\cdot\boldsymbol{n}^+)_{\mathfrak{C}}+(\nabla(\rho_{f,r}g\eta),\boldsymbol{z}_h^{k+1}),\tag{7.2.6}$$
$$(\boldsymbol{K}^{-1}\boldsymbol{z}_h^{k},\boldsymbol{z}_h^{k+1})=(p_h^{k},\nabla\cdot\boldsymbol{z}_h^{k+1})-(p_{f_h}^{k},[\boldsymbol{z}_h^{k+1}]_{\mathfrak{C}}\cdot\boldsymbol{n}^+)_{\mathfrak{C}}+(\nabla(\rho_{f,r}g\eta),\boldsymbol{z}_h^{k+1}).\tag{7.2.7}$$

  Taking the difference of the above two equations and rearranging terms, we obtain:

$$(p_h^{k+1}-p_h^{k},\nabla\cdot\boldsymbol{z}_h^{k+1})=(\boldsymbol{K}^{-1}(\boldsymbol{z}_h^{k+1}-\boldsymbol{z}_h^{k}),\boldsymbol{z}_h^{k+1})+(p_{f_h}^{k+1}-p_{f_h}^{k},[\boldsymbol{z}_h^{k+1}]_{\mathfrak{C}}\cdot\boldsymbol{n}^+)_{\mathfrak{C}}.\tag{7.2.8}$$

  Consider (7.2.1) and test with $\theta_h=p_h^{k+1}-p_h^{k}$ to obtain:

$$\frac{\beta}{\Delta t}\Big\|p_h^{k+1}-p_h^{k}\Big\|^2+\frac{\alpha}{\Delta t}\Big(\nabla\cdot(\boldsymbol{u}_h^{k}-\boldsymbol{u}_h^{k-1}),p_h^{k+1}-p_h^{k}\Big)+\frac{1}{\mu_f}(\nabla\cdot\boldsymbol{z}_h^{k+1},p_h^{k+1}-p_h^{k})$$
$$=(\tilde{q}_h^{k+1},p_h^{k+1}-p_h^{k}).\tag{7.2.9}$$

  Substitute (7.2.8) into (7.2.9) to derive:

$$\frac{\beta}{\Delta t}\Big\|p_h^{k+1}-p_h^{k}\Big\|^2+\frac{\alpha}{\Delta t}\Big(\nabla\cdot(\boldsymbol{u}_h^{k}-\boldsymbol{u}_h^{k-1}),p_h^{k+1}-p_h^{k}\Big)+\frac{1}{\mu_f}\Big[(\boldsymbol{K}^{-1}(\boldsymbol{z}_h^{k+1}-\boldsymbol{z}_h^{k}),\boldsymbol{z}_h^{k+1})$$
$$(p_{f_h}^{k+1}-p_{f_h}^{k},[\boldsymbol{z}_h^{k+1}]_{\mathfrak{C}}\cdot\boldsymbol{n}^+)_{\mathfrak{C}}\Big]=(\tilde{q}_h^{k+1},p_h^{k+1}-p_h^{k}).$$

With further simplifications, we obtain:

$$\frac{\beta}{\Delta t}\left\|p_h^{k+1}-p_h^k\right\|^2+\frac{1}{2\mu_f}\left[\left\|\boldsymbol{K}^{-1/2}\boldsymbol{z}_h^{k+1}\right\|^2-\left\|\boldsymbol{K}^{-1/2}\boldsymbol{z}_h^{k}\right\|^2+\left\|\boldsymbol{K}^{-1/2}(\boldsymbol{z}_h^{k+1}-\boldsymbol{z}_h^{k})\right\|^2\right]$$
$$+\frac{1}{\mu_f}(p_{f_h}^{k+1}-p_{f_h}^k,[\boldsymbol{z}_h^{k+1}]_{\mathfrak{e}}\cdot\boldsymbol{n}^+)_{\mathfrak{e}}=-\frac{\alpha}{\Delta t}\Big(\nabla\cdot(\boldsymbol{u}_h^k-\boldsymbol{u}_h^{k-1}),p_h^{k+1}-p_h^k\Big)+(\tilde{q}_h,p_h^{k+1}-p_h^k). \tag{7.2.10}$$

Consider now the flow in the fracture equation (7.2.4) for the difference of two consecutive time steps $t=t_k$, and $t=t_{k+1}$, and test with $\boldsymbol{\mu}_{f_h}=\boldsymbol{\zeta}_h^{k+1}$ to obtain:

$$(K_{\mathfrak{e}}^{-1}(\boldsymbol{\zeta}_h^{k+1}-\boldsymbol{\zeta}_h^k),\boldsymbol{\zeta}_h^{k+1})_{\mathfrak{e}}=(p_{f_h}^{k+1}-p_{f_h}^k,\overline{\nabla}\cdot\boldsymbol{\zeta}_h^{k+1})_{\mathfrak{e}}. \tag{7.2.11}$$

Testing (7.2.2) with $\theta_{c_h}=p_{f_h}^{k+1}-p_{f_h}^k$ yields:

$$\frac{c_{f_c}}{\Delta t}\left\|p_{f_h}^{k+1}-p_{f_h}^k\right\|_{\mathfrak{e}}^2+\frac{1}{12\mu_f}(\overline{\nabla}\cdot(\boldsymbol{\zeta}_h^{k+1}),p_{f_h}^{k+1}-p_{f_h}^k)_{\mathfrak{e}}-\frac{1}{\mu_f}([\boldsymbol{z}_h^{k+1}]_{\mathfrak{e}}\cdot\boldsymbol{n}^+,p_{f_h}^{k+1}-p_{f_h}^k)_{\mathfrak{e}}$$
$$+\frac{1}{\Delta t}(w_h^k-w_h^{k-1},p_{f_h}^{k+1}-p_{f_h}^k)_{\mathfrak{e}}=(\tilde{q}_{W_h}^{k+1},p_{f_h}^{k+1}-p_{f_h}^k)_{\mathfrak{e}}. \tag{7.2.12}$$

Now, substitute (7.2.11) into (7.2.12) to obtain:

$$\frac{c_{f_c}}{\Delta t}\left\|p_{f_h}^{k+1}-p_{f_h}^k\right\|_{\mathfrak{e}}^2+\frac{1}{12\mu_f}(K_{\mathfrak{e}}^{-1}(\boldsymbol{\zeta}_h^{k+1}-\boldsymbol{\zeta}_h^k),\boldsymbol{\zeta}_h^{k+1})_{\mathfrak{e}}-\frac{1}{\mu_f}([\boldsymbol{z}_h^{k+1}]_{\mathfrak{e}}\cdot\boldsymbol{n}^+,p_{f_h}^{k+1}-p_{f_h}^k)_{\mathfrak{e}}$$
$$+\frac{1}{\Delta t}(w_h^k-w_h^{k-1},p_{f_h}^{k+1}-p_{f_h}^k)_{\mathfrak{e}}=(\tilde{q}_{W_h}^{k+1},p_{f_h}^{k+1}-p_{f_h}^k)_{\mathfrak{e}}. \tag{7.2.13}$$

Next, add (7.2.10) to (7.2.13) to obtain with further simplifications:

$$\frac{\beta}{\Delta t}\left\|p_h^{k+1}-p_h^k\right\|^2+\frac{1}{2\mu_f}\left[\left\|\boldsymbol{K}^{-1/2}\boldsymbol{z}_h^{k+1}\right\|^2-\left\|\boldsymbol{K}^{-1/2}\boldsymbol{z}_h^{k}\right\|^2+\left\|\boldsymbol{K}^{-1/2}(\boldsymbol{z}_h^{k+1}-\boldsymbol{z}_h^{k})\right\|^2\right]$$
$$+\frac{c_{f_c}}{\Delta t}\left\|p_{f_h}^{k+1}-p_{f_h}^k\right\|_{\mathfrak{e}}^2+\frac{1}{24\mu_f}\left[\left\|K_{\mathfrak{e}}^{-1/2}\boldsymbol{\zeta}_h^{k+1}\right\|_{\mathfrak{e}}^2-\left\|K_{\mathfrak{e}}^{-1/2}\boldsymbol{\zeta}_h^{k}\right\|_{\mathfrak{e}}^2+\left\|K_{\mathfrak{e}}^{-1/2}(\boldsymbol{\zeta}_h^{k+1}-\boldsymbol{\zeta}_h^{k})\right\|_{\mathfrak{e}}^2\right]$$
$$=-\frac{\alpha}{\Delta t}\Big(\nabla\cdot(\boldsymbol{u}_h^k-\boldsymbol{u}_h^{k-1}),p_h^{k+1}-p_h^k\Big)-\frac{1}{\Delta t}(w_h^k-w_h^{k-1},p_{f_h}^{k+1}-p_{f_h}^k)_{\mathfrak{e}}$$
$$+(\tilde{q}_h^{k+1},p_h^{k+1}-p_h^k)+(\tilde{q}_{W_h}^{k+1},p_{f_h}^{k+1}-p_{f_h}^k)_{\mathfrak{e}}. \tag{7.2.14}$$

- **Step 2: Elasticity equation**

  Consider equation (7.2.5) for two consecutive time steps: $t = t_k$ and $t = t_{k+1}$, take the difference between the two, and test with $\boldsymbol{v}_h = \frac{\boldsymbol{u}_h^{k+1} - \boldsymbol{u}_h^k}{\Delta t}$ to obtain:

$$\frac{2G}{\Delta t}\left\|\boldsymbol{\varepsilon}(\boldsymbol{u}_h^{k+1} - \boldsymbol{u}_h^k)\right\|^2 + \frac{\lambda}{\Delta t}\left\|\nabla\cdot(\boldsymbol{u}_h^{k+1} - \boldsymbol{u}_h^k)\right\|^2 - \frac{\alpha}{\Delta t}(p_h^{k+1} - p_h^k, \nabla\cdot(\boldsymbol{u}_h^{k+1} - \boldsymbol{u}_h^k)) \\ -\frac{1}{\Delta t}(p_{f_h}^{k+1} - p_{f_h}^k, w_h^{k+1} - w_h^k)_{\mathfrak{C}} = \frac{1}{\Delta t}\Big(\boldsymbol{f}_h^{k+1} - \boldsymbol{f}_h^k, \boldsymbol{u}_h^{k+1} - \boldsymbol{u}_h^k\Big). \tag{7.2.15}$$

- **Step 3: Combining flow and elasticity equations**

  Adding (7.2.14) to (7.2.15) and bounding the term $\frac{G}{\Delta t}\left\|\boldsymbol{\varepsilon}(\boldsymbol{u}_h^{k+1} - \boldsymbol{u}_h^k)\right\|^2$ on the left hand side of (7.2.15) from below by (6.4.55), we obtain

$$\frac{\beta}{\Delta t}\left\|p_h^{k+1} - p_h^k\right\|^2 + \frac{1}{2\mu_f}\left[\left\|\boldsymbol{K}^{-1/2}\boldsymbol{z}_h^{k+1}\right\|^2 - \left\|\boldsymbol{K}^{-1/2}\boldsymbol{z}_h^k\right\|^2 + \left\|\boldsymbol{K}^{-1/2}(\boldsymbol{z}_h^{k+1} - \boldsymbol{z}_h^k)\right\|^2\right] \\ + \frac{c_{f_c}}{\Delta t}\left\|p_{f_h}^{k+1} - p_{f_h}^k\right\|_{\mathfrak{C}}^2 + \frac{1}{24\mu_f}\left[\left\|K_{\mathfrak{C}}^{-1/2}\boldsymbol{\zeta}_h^{k+1}\right\|_{\mathfrak{C}}^2 - \left\|K_{\mathfrak{C}}^{-1/2}\boldsymbol{\zeta}_h^k\right\|_{\mathfrak{C}}^2 + \left\|K_{\mathfrak{C}}^{-1/2}(\boldsymbol{\zeta}_h^{k+1} - \boldsymbol{\zeta}_h^k)\right\|_{\mathfrak{C}}^2\right] \\ + \frac{G}{\Delta t}\left\|\boldsymbol{\varepsilon}(\boldsymbol{u}_h^{k+1} - \boldsymbol{u}_h^k)\right\|^2 + \frac{GC^*}{\Delta t}\left\|w_h^{k+1} - w_h^k\right\|_{\mathfrak{C}}^2 + \frac{\lambda}{\Delta t}\left\|\nabla\cdot(\boldsymbol{u}_h^{k+1} - \boldsymbol{u}_h^k)\right\|^2 \\ \leq \underbrace{-\frac{\alpha}{\Delta t}\Big(\nabla\cdot(\boldsymbol{u}_h^k - \boldsymbol{u}_h^{k-1}), p_h^{k+1} - p_h^k\Big)}_{R_1} \underbrace{-\frac{1}{\Delta t}(w_h^k - w_h^{k-1}, p_{f_h}^{k+1} - p_{f_h}^k)_{\mathfrak{C}}}_{R_6} \\ \underbrace{+(\tilde{q}_h^{k+1}, p_h^{k+1} - p_h^k)}_{R_3} \underbrace{+(\tilde{q}_{W_h}^{k+1}, p_{f_h}^{k+1} - p_{f_h}^k)_{\mathfrak{C}}}_{R_4} \underbrace{+\frac{\alpha}{\Delta t}(p_h^{k+1} - p_h^k, \nabla\cdot(\boldsymbol{u}_h^{k+1} - \boldsymbol{u}_h^k))}_{R_2} \\ \underbrace{+\frac{1}{\Delta t}(p_{f_h}^{k+1} - p_{f_h}^k, w_h^{k+1} - w_h^k)_{\mathfrak{C}}}_{R_5} \underbrace{+\frac{1}{\Delta t}\Big(\boldsymbol{f}_h^{k+1} - \boldsymbol{f}_h^k, \boldsymbol{u}_h^{k+1} - \boldsymbol{u}_h^k\Big)}_{R_7}. \tag{7.2.16}$$

  Denoting by $R_1, R_2, R_3, R_4, R_5, R_6$ and R_7 the terms on the right hand side, together

with Poincaré's, Korn's, and Young's inequalities, we estimate

$$
\begin{aligned}
|R_1| &\leq \frac{\alpha}{\Delta t}\Big(\frac{1}{2\epsilon_1}\Big\|\nabla\cdot(\boldsymbol{u}_h^k-\boldsymbol{u}_h^{k-1})\Big\|^2+\frac{\epsilon_1}{2}\Big\|p_h^{k+1}-p_h^k\Big\|^2\Big),\\
|R_2| &\leq \frac{\alpha}{\Delta t}\Big(\frac{1}{2\epsilon_2}\Big\|p_h^{k+1}-p_h^k\Big\|^2+\frac{\epsilon_2}{2}\Big\|\nabla\cdot(\boldsymbol{u}_h^{k+1}-\boldsymbol{u}_h^k)\Big\|^2\Big),\\
|R_3| &\leq \frac{1}{2\epsilon_3}\Big\|\tilde{q}_h^{k+1}\Big\|^2+\frac{\epsilon_3}{2}\Big\|p_h^{k+1}-p_h^k\Big\|^2,\\
|R_4| &\leq \frac{1}{2\epsilon_4}\Big\|\tilde{q}_{W_h}^{k+1}\Big\|^2+\frac{\epsilon_4}{2}\Big\|{p_f}_h^{k+1}-{p_f}_h^k\Big\|_{\mathfrak{C}}^2,\\
|R_5| &\leq \frac{1}{\Delta t}\Big(\frac{1}{2\epsilon_5}\Big\|{p_f}_h^{k+1}-{p_f}_h^k\Big\|_{\mathfrak{C}}^2+\frac{\epsilon_5}{2}\Big\|w_h^{k+1}-w_h^k\Big\|_{\mathfrak{C}}^2\Big),\\
|R_6| &\leq \frac{1}{\Delta t}\Big(\frac{1}{2\epsilon_6}\Big\|w_h^k-w_h^{k-1}\Big\|_{\mathfrak{C}}^2+\frac{\epsilon_6}{2}\Big\|{p_f}_h^{k+1}-{p_f}_h^k\Big\|_{\mathfrak{C}}^2\Big),\\
|R_7| &\leq \frac{1}{2\Delta t\epsilon_7}\Big\|\boldsymbol{f}_h^{k+1}-\boldsymbol{f}_h^k\Big\|^2+\frac{\epsilon_7}{2\Delta t}\Big\|\boldsymbol{u}_h^{k+1}-\boldsymbol{u}_h^k\Big\|^2\\
&\leq \frac{1}{2\Delta t\epsilon_7}\Big\|\boldsymbol{f}_h^{k+1}-\boldsymbol{f}_h^k\Big\|^2+\frac{\epsilon_7\mathcal{P}_\Omega^2C_\kappa^2}{2\Delta t}\|\boldsymbol{\varepsilon}(\boldsymbol{u}_h^{k+1}-\boldsymbol{u}_h^k)\|^2,
\end{aligned}
$$

for $\epsilon_1,\epsilon_2,\epsilon_3,\epsilon_4,\epsilon_5,\epsilon_6,$ and $\epsilon_7>0$. Choosing $\epsilon_1=\frac{\alpha}{\lambda}$, $\epsilon_2=\frac{\lambda}{\alpha}$, $\epsilon_3=\frac{2}{\Delta t}\Big(\beta-\frac{\alpha^2}{\lambda}\Big)$, $\epsilon_4=\frac{2}{\Delta t}\Big(c_{f_c}-\frac{1}{GC^*}\Big)$, $\epsilon_5=GC^*$, $\epsilon_6=\frac{1}{GC^*}$, $\epsilon_7=\frac{G}{\mathcal{P}_\Omega^2C_\kappa^2}$, and multiplying (7.2.16) by Δt, we derive:

$$
\begin{aligned}
&\frac{\Delta t}{2\mu_f}\Big[\Big\|\boldsymbol{K}^{-1/2}\boldsymbol{z}_h^{k+1}\Big\|^2-\Big\|\boldsymbol{K}^{-1/2}\boldsymbol{z}_h^k\Big\|^2+\Big\|\boldsymbol{K}^{-1/2}(\boldsymbol{z}_h^{k+1}-\boldsymbol{z}_h^k)\Big\|^2\Big]\\
&+\frac{\Delta t}{24\mu_f}\Big[\Big\|K_{\mathfrak{C}}^{-1/2}\boldsymbol{\zeta}_h^{k+1}\Big\|_{\mathfrak{C}}^2-\Big\|K_{\mathfrak{C}}^{-1/2}\boldsymbol{\zeta}_h^k\Big\|_{\mathfrak{C}}^2+\Big\|K_{\mathfrak{C}}^{-1/2}(\boldsymbol{\zeta}_h^{k+1}-\boldsymbol{\zeta}_h^k)\Big\|_{\mathfrak{C}}^2\Big]\\
&+\frac{G}{2}\Big\|\boldsymbol{\varepsilon}(\boldsymbol{u}_h^{k+1}-\boldsymbol{u}_h^k)\Big\|^2+\frac{GC^*}{2}\Big\|w_h^{k+1}-w_h^k\Big\|_{\mathfrak{C}}^2+\frac{\lambda}{2}\Big\|\nabla\cdot(\boldsymbol{u}_h^{k+1}-\boldsymbol{u}_h^k)\Big\|^2\\
&\leq\frac{\lambda}{2}\Big\|\nabla\cdot(\boldsymbol{u}_h^k-\boldsymbol{u}_h^{k-1})\Big\|^2+\frac{GC^*}{2}\Big\|w_h^k-w_h^{k-1}\Big\|_{\mathfrak{C}}^2\\
&+\frac{\Delta t^2}{4\Big(\beta-\frac{\alpha^2}{\lambda}\Big)}\Big\|\tilde{q}_h^{k+1}\Big\|^2+\frac{\Delta t^2}{4\Big(c_{f_c}-\frac{1}{GC^*}\Big)}\Big\|\tilde{q}_{W_h}^{k+1}\Big\|_{\mathfrak{C}}^2+\frac{\mathcal{P}_\Omega^2C_\kappa^2}{2G}\Big\|\boldsymbol{f}_h^{k+1}-\boldsymbol{f}_h^k\Big\|^2. \qquad (7.2.17)
\end{aligned}
$$

Summing up (7.2.17) for $1\leq k\leq J$, for J time steps, with telescopic cancellations,

we obtain:

$$\frac{\Delta t}{2\mu_f}\Big[\Big\|\boldsymbol{K}^{-1/2}\boldsymbol{z}_h^{J+1}\Big\|^2+\sum_{k=1}^{J}\Big\|\boldsymbol{K}^{-1/2}(\boldsymbol{z}_h^{k+1}-\boldsymbol{z}_h^{k})\Big\|^2\Big]+\frac{\Delta t}{24\mu_f}\Big[\Big\|K_{\mathfrak{C}}^{-1/2}\boldsymbol{\zeta}_h^{J+1}\Big\|_{\mathfrak{C}}^2$$
$$+\sum_{k=1}^{J}\Big\|K_{\mathfrak{C}}^{-1/2}(\boldsymbol{\zeta}_h^{k+1}-\boldsymbol{\zeta}_h^{k})\Big\|_{\mathfrak{C}}^2\Big]+\frac{G}{2}\sum_{k=1}^{J}\Big\|\boldsymbol{\varepsilon}(\boldsymbol{u}_h^{k+1}-\boldsymbol{u}_h^{k})\Big\|^2+\frac{GC^*}{2}\Big\|w_h^{J+1}-w_h^{J}\Big\|_{\mathfrak{C}}^2$$
$$+\frac{\lambda}{2}\Big\|\nabla\cdot(\boldsymbol{u}_h^{J+1}-\boldsymbol{u}_h^{J})\Big\|^2\leq\frac{\Delta t}{2\mu_f}\Big\|\boldsymbol{K}^{-1/2}\boldsymbol{z}_h^{1}\Big\|^2+\frac{\Delta t}{24\mu_f}\Big\|K_{\mathfrak{C}}^{-1/2}\boldsymbol{\zeta}_h^{1}\Big\|_{\mathfrak{C}}^2$$
$$+\frac{\lambda}{2}\Big\|\nabla\cdot(\boldsymbol{u}_h^{1}-\boldsymbol{u}_h^{0})\Big\|^2+\frac{GC^*}{2}\Big\|w_h^{1}-w_h^{0}\Big\|_{\mathfrak{C}}^2+\frac{\Delta t^2}{4(\beta-\frac{\alpha^2}{\lambda})}\sum_{k=1}^{J}\Big\|\tilde{q}_h^{k+1}\Big\|^2$$
$$+\frac{\Delta t^2}{4(c_{f_c}-\frac{1}{GC^*})}\sum_{k=1}^{J}\Big\|\tilde{q}_{W_h}^{k+1}\Big\|_{\mathfrak{C}}^2+\frac{\mathcal{P}_\Omega^2C_\kappa^2}{2G}\sum_{k=1}^{J}\Big\|\boldsymbol{f}_h^{k+1}-\boldsymbol{f}_h^{k}\Big\|^2. \tag{7.2.18}$$

We recall that $\boldsymbol{u}_h^1,\boldsymbol{z}_h^1$, and $\boldsymbol{\zeta}_h^1$ have been computed using the fully implicit time discretization. Using standard a priori estimates for the fractured coupled Biot model (a very similar approach to the one used in equations (3.3.29) and (3.3.31)), we conclude that $\|\nabla\cdot\boldsymbol{u}_h^1-\nabla\cdot\boldsymbol{u}_h^0\|^2\leq C\Delta t$, $\Big\|w_h^1-w_h^0\Big\|_{\mathfrak{C}}^2\leq C\Delta t$, $\Big\|K_{\mathfrak{C}}^{-1/2}\boldsymbol{\zeta}_h^1\Big\|_{\mathfrak{C}}^2<C$, and $\Big\|K^{-1/2}\boldsymbol{z}_h^1\Big\|^2\leq C$ for a generic constant $C>0$. This completes the derivation.

Remark 7.2.1. The above proof also provides a way to devise an explicitly coupled algorithm that is unconditionally stable. For the single rate algorithm, we replace (7.2.1) and (7.2.2) by:

$$\forall\theta_h\in Q_h\,,\ \frac{\beta+\frac{\alpha^2}{\lambda}}{\Delta t}\Big(p_h^{k+1}-p_h^{k},\theta_h\Big)+\frac{1}{\mu_f}(\nabla\cdot\boldsymbol{z}_h^{k+1},\theta_h)=-\frac{\alpha}{\Delta t}\Big(\nabla\cdot(\boldsymbol{u}_h^{k}-\boldsymbol{u}_h^{k-1}),\theta_h\Big)$$
$$+(\tilde{q}_h^{k+1},\theta_h) \tag{7.2.19}$$

$$\forall\theta_{c_h}\in Q_{c_h}\,,\ \frac{c_{f_c}+\frac{1}{GC^*}}{\Delta t}\Big(p_{f_h}^{k+1}-p_{f_h}^{k},\theta_{c_h}\Big)_{\mathfrak{C}}+\frac{1}{12\mu_f}(\overline{\nabla}\cdot(\boldsymbol{\zeta}_h^{k+1}),\theta_{c_h})_{\mathfrak{C}}-\frac{1}{\mu_f}([\boldsymbol{z}_h^{k+1}]_{\mathfrak{C}}\cdot\boldsymbol{n}^+,\theta_{c_h})_{\mathfrak{C}}$$
$$=-\frac{1}{\Delta t}(w_h^{k}-w_h^{k-1},\theta_{c_h})_{\mathfrak{C}}+(\tilde{q}_{W_h}^{k+1},\theta_{c_h})_{\mathfrak{C}} \tag{7.2.20}$$

Note that the stabilisation terms $\frac{\alpha^2}{\lambda\Delta t}(p_h^{k+1}-p_h^{k})$ and $\frac{1}{GC^*\Delta t}(p_{f_h}^{k+1}-p_{f_h}^{k})$ have been added above in contrast to (7.2.1) and (7.2.2) respectively. The stability result is then obtained

with the assumption ($\mathbf{A_1}$) relaxed. The proof for the unconditional stability follows exactly the same ideas presented above and is skipped here. Similar to the derivation shown in [46], the consistence error is expected to be of the order of $O(\Delta t)$.

7.3 Multirate Explicit Coupling Formulation and Analysis

Recall that in the multirate explicit coupling approach, the flow problem is solved q times (with a finer time step) within one coarse mechanics time step.

7.3.1 Fully Discrete Scheme for Multirate

Using the mixed finite element method in space for flow, continuous Galerkin for mechanics, and the backward Euler finite difference method in time, the weak formulation of the multirate explicit coupling scheme for fractured poro-elastic media reads as follows.

Definition 7.3.1. *(**flow equations**) For $1 \leq m \leq q$, find $p_h^{m+k} \in Q_h$, $p_{f_h}^{m+k} \in Q_{c_h}$, $\boldsymbol{z}_h^{m+k} \in \boldsymbol{Z}_h$, and $\boldsymbol{\zeta}_h^{m+k} \in \boldsymbol{Z}_{\mathcal{E}h}$ such that,*

$$\forall \theta_h \in Q_h\,, \frac{1}{\Delta t}(\frac{1}{M} + c_f\varphi_0)\Big(p_h^{m+k} - p_h^{m-1+k}, \theta_h\Big) + \frac{1}{\mu_f}(\nabla \cdot \boldsymbol{z}_h^{m+k}, \theta_h) = -\frac{\alpha}{q\Delta t}\Big(\nabla \cdot (\boldsymbol{u}_h^k - \boldsymbol{u}_h^{k-q}), \theta_h\Big) + (\tilde{q}_h^{m+k}, \theta_h) \tag{7.3.21}$$

$$\forall \theta_{c_h} \in Q_{c_h}\,, \frac{c_{f_c}}{\Delta t}\Big({p_{f}}_h^{m+k} - {p_{f}}_h^{m-1+k}, \theta_{c_h}\Big)_{\mathcal{E}} + \frac{1}{12\mu_f}(\overline{\nabla} \cdot (\boldsymbol{\zeta}_h^{m+k}), \theta_{c_h})_{\mathcal{E}} - \frac{1}{\mu_f}([\boldsymbol{z}_h^{m+k}]_{\mathcal{E}} \cdot \boldsymbol{n}^+, \theta_{c_h})_{\mathcal{E}} + \frac{1}{q\Delta t}(w_h^k - w_h^{k-q}, \theta_{c_h})_{\mathcal{E}} = (\tilde{q}_{W_h}^{m+k}, \theta_{c_h})_{\mathcal{E}} \tag{7.3.22}$$

$$\forall \boldsymbol{q}_h \in \boldsymbol{Z}_h\,, (\boldsymbol{K}^{-1}\boldsymbol{z}_h^{m+k}, \boldsymbol{q}_h) = (p_h^{m+k}, \nabla \cdot \boldsymbol{q}_h) - ({p_{f}}_h^{m+k}, [\boldsymbol{q}_h]_{\mathcal{E}} \cdot \boldsymbol{n}^+)_{\mathcal{E}} + (\nabla(\rho_{f,r} g\eta), \boldsymbol{q}_h) \tag{7.3.23}$$

$$\forall \boldsymbol{\mu}_{f_h} \in \boldsymbol{Z}_{\mathcal{E}h}\,, (K_{\mathcal{E}}^{-1}\boldsymbol{\zeta}_h^{m+k}, \boldsymbol{\mu}_{f_h})_{\mathcal{E}} = ({p_{f}}_h^{m+k}, \overline{\nabla} \cdot (\boldsymbol{\mu}_{f_h}))_{\mathcal{E}} + (\overline{\nabla}(\rho_{f,r} g\eta), \boldsymbol{\mu}_{f_h})_{\mathcal{E}}. \tag{7.3.24}$$

Definition 7.3.2. *(**mechanics equation**) Given $p_h^{k+q}, \boldsymbol{z}_h^{k+q}, {p_{f}}_h^{k+q}, \boldsymbol{\zeta}_h^{k+q}$, find $\boldsymbol{u}_h^{k+q} \in \boldsymbol{V}_h$ such that,*

$$\forall \boldsymbol{v}_h \in V_h\,, 2G(\boldsymbol{\varepsilon}(\boldsymbol{u}_h^{k+q}), \boldsymbol{\varepsilon}(\boldsymbol{v}_h)) + \lambda(\nabla \cdot \boldsymbol{u}_h^{k+q}, \nabla \cdot \boldsymbol{v}_h) - \alpha(p_h^{k+q}, \nabla \cdot \boldsymbol{v}_h) + ({p_{f}}_h^{k+q}, [\boldsymbol{v}_h]_{\mathcal{E}} \cdot \boldsymbol{n}^+)_{\mathcal{E}} = (\boldsymbol{f}^{k+q}, \boldsymbol{v}_h) \tag{7.3.25}$$

7.3.2 Multirate Explicit Coupling Algorithm

The multirate explicit coupling algorithm for fractured poroelastic media is given below:

Algorithm 12: Multirate Explicit Coupling Algorithm

Given initial conditions $\boldsymbol{u}_h^0$, p_h^0, *and* $p_{f_h}^0 = p_h^0|_{\mathcal{C}}$, *solve implicitly for* $\boldsymbol{u}_h^m, p_h^m, \boldsymbol{z}_h^m, p_{f_h}^m, \boldsymbol{\zeta}_h^m, m = 1, 2, \ldots, q$ *satisfying fully coupled fractured Biot model*

for $k = q, 2q, 3q, ..$ **do** `/* mechanics time step iteration index */`

  First Step: Flow equations

  Given $\boldsymbol{u}_h^k$

  for $m = 1, 2, .., q$ **do** `/* flow finer time steps iteration index */`

    Solve for p_h^{m+k}, $\boldsymbol{z}_h^{m+k}$, $p_{f_h}^{m+k}$, *and* $\boldsymbol{\zeta}_h^{m+k}$ *satisfying definition 7.3.1*

  Second Step: Mechanics equations

  Given p_h^{k+q}, $p_{f_h}^{k+q}$, $\boldsymbol{\zeta}_h^{k+q}$, *and* $\boldsymbol{z}_h^{k+q}$

    Solve for $\boldsymbol{u}_h^{k+q}$ *satisfying definition 7.3.2*

7.3.2.1 Assumptions

The stability assumption in the multirate case takes the form:

$$(\mathbf{A_q}) \quad \beta > \tfrac{1}{2}(\tfrac{1}{q} + q)\tfrac{\alpha^2}{\lambda} \qquad \& \qquad c_{f_c} > \tfrac{1}{2}(\tfrac{1}{q} + q)\tfrac{1}{GC^*} \qquad \text{for} \qquad q \geq 1,$$

where q is the number of flow finer time steps within one coarse mechanics time step.

As in the single rate case, we need to prepare the initial data for starting the time stepping. Accordingly, in the first step of the multirate algorithm (Algorithm 12), for $k = 0$, and $m = 1, 2, \ldots, q$, the initial conditions are computed by solving the coupled fractured Biot system with a fully implicit time discretization (with a time step of size Δt for the "q" coupled solves). Alternatively, decoupled iterative schemes [8, 11, 43] such as the fixed stress split iterative (single rate) scheme can be used to compute $\boldsymbol{u}_h^m, p_h^m, \boldsymbol{z}_h^m, p_{f_h}^m, \boldsymbol{\zeta}_h^m$, for $m = 1, 2, \ldots, q$. Note that if $q = 1$, the multirate condition $(\mathbf{A_q})$ is identical to the single rate condition $(\mathbf{A_1})$.

Our main result is the following stability estimate.

Theorem 7.3.1. *[Multirate] Under the assumption* $(\mathbf{A_q})$*, the following stability result holds for the multirate explicit coupling scheme in fractured poro-elastic media for mechanics time steps* $t_0 \leq t_k \leq t_J$*,* $k = q, 2q, ..$*:*

$$\begin{aligned}
&\frac{\Delta t}{2\mu_f}\Big[\Big\|\boldsymbol{K}^{-1/2}\boldsymbol{z}_h^{J+q}\Big\|^2 + \sum_{k=q}^{J}\sum_{m=1}^{q}\Big\|\boldsymbol{K}^{-1/2}(\boldsymbol{z}_h^{m+k} - \boldsymbol{z}_h^{m-1+k})\Big\|^2\Big] \\
&+ \frac{\Delta t}{24\mu_f}\Big[\Big\|K_{\mathfrak{C}}^{-1/2}\boldsymbol{\zeta}_h^{J+q}\Big\|_{\mathfrak{C}}^2 + \sum_{k=q}^{J}\sum_{m=1}^{q}\Big\|K_{\mathfrak{C}}^{-1/2}(\boldsymbol{\zeta}_h^{m+k} - \boldsymbol{\zeta}_h^{m-1+k})\Big\|_{\mathfrak{C}}^2\Big] \\
&+ \frac{G}{2}\sum_{k=q}^{J}\Big\|\boldsymbol{\varepsilon}(\boldsymbol{u}_h^{k+q} - \boldsymbol{u}_h^{k})\Big\|^2 + \frac{GC^*}{2}\Big\|w_h^{J+q} - w_h^{J}\Big\|_{\mathfrak{C}}^2 + \frac{\lambda}{2}\Big\|\nabla\cdot(\boldsymbol{u}_h^{J+q} - \boldsymbol{u}_h^{J})\Big\|^2 \\
&\leq C\Delta t + \frac{\Delta t^2}{4\Big(\beta - \frac{1}{2}(\frac{1}{q}+q)\frac{\alpha^2}{\lambda})\Big)}\sum_{k=q}^{J}\sum_{m=1}^{q}\Big\|\tilde{q}_h^{m+k}\Big\|^2 \\
&+ \frac{\Delta t^2}{4(c_{f_c} - \frac{1}{2}(\frac{1}{q}+q)\frac{1}{GC^*})}\sum_{k=q}^{J}\sum_{m=1}^{q}\Big\|\tilde{q}_{W_h}^{m+k}\Big\|_{\mathfrak{C}}^2 + \frac{\mathcal{P}_\Omega^2 C_\kappa^2}{2G}\sum_{k=q}^{J}\Big\|\boldsymbol{f}_h^{k+q} - \boldsymbol{f}_h^{k}\Big\|^2 \qquad (7.3.26)
\end{aligned}$$

for a generic constant $C > 0$*.*

7.3.3 Stability Analysis

- **Step 1: Flow equations**

  Consider (7.3.21) and test with $\theta_h = p_h^{m+k} - p_h^{m-1+k}$ to obtain:

$$\begin{aligned}
&\frac{\beta}{\Delta t}\Big\|p_h^{m+k} - p_h^{m-1+k}\Big\|^2 + \frac{\alpha}{q\Delta t}\Big(\nabla\cdot(\boldsymbol{u}_h^{k} - \boldsymbol{u}_h^{k-q}), p_h^{m+k} - p_h^{m-1+k}\Big) \\
&\qquad + \frac{1}{\mu_f}(\nabla\cdot\boldsymbol{z}_h^{m+k}, p_h^{m+k} - p_h^{m-1+k}) = (\tilde{q}_h^{m+k}, p_h^{m+k} - p_h^{m-1+k}). \qquad (7.3.27)
\end{aligned}$$

  Now, consider (7.3.23) for the difference of two consecutive flow finer time steps ($t = t_{m+k}$ and $t = t_{m-1+k}$), and test with $\boldsymbol{q}_h = \boldsymbol{z}_h^{m+k}$ to derive:

$$\begin{aligned}
(p_h^{m+k} - p_h^{m-1+k}, \nabla\cdot\boldsymbol{z}_h^{m+k}) &= (\boldsymbol{K}^{-1}(\boldsymbol{z}_h^{m+k} - \boldsymbol{z}_h^{m-1+k}), \boldsymbol{z}_h^{m+k}) \\
&\quad + (p_{f_h}^{m+k} - p_{f_h}^{m-1+k}, [\boldsymbol{z}_h^{m+k}]_{\mathfrak{C}}\cdot\boldsymbol{n}^+)_{\mathfrak{C}}. \qquad (7.3.28)
\end{aligned}$$

Substitute (7.3.28) into (7.3.27) to obtain:

$$\frac{\beta}{\Delta t}\left\|p_h^{m+k}-p_h^{m-1+k}\right\|^2+\frac{1}{\mu_f}\Big[(\boldsymbol{K}^{-1}(\boldsymbol{z}_h^{m+k}-\boldsymbol{z}_h^{m-1+k}),\boldsymbol{z}_h^{m+k})$$
$$+(p_{f_h}^{m+k}-p_{f_h}^{m-1+k},[\boldsymbol{z}_h^{m+k}]_{\mathfrak{e}}\cdot\boldsymbol{n}^+)_{\mathfrak{e}}\Big]\leq-\frac{\alpha}{q\Delta t}\Big(\nabla\cdot(\boldsymbol{u}_h^k-\boldsymbol{u}_h^{k-q}),p_h^{m+k}-p_h^{m-1+k}\Big)$$
$$+(\tilde{q}_h^{m+k},p_h^{m+k}-p_h^{m-1+k}). \tag{7.3.29}$$

Consider (7.3.22) and test with $\theta_{c_h}=p_{f_h}^{m+k}-p_{f_h}^{m-1+k}$ to obtain:

$$\frac{c_{f_c}}{\Delta t}\left\|p_{f_h}^{m+k}-p_{f_h}^{m-1+k}\right\|_{\mathfrak{e}}^2+\frac{1}{12\mu_f}(\overline{\nabla}\cdot(\boldsymbol{\zeta}_h^{m+k}),p_{f_h}^{m+k}-p_{f_h}^{m-1+k})_{\mathfrak{e}}$$
$$-\frac{1}{\mu_f}([\boldsymbol{z}_h^{m+k}]_{\mathfrak{e}}\cdot\boldsymbol{n}^+,p_{f_h}^{m+k}-p_{f_h}^{m-1+k})_{\mathfrak{e}}+\frac{1}{q\Delta t}(w_h^k-w_h^{k-q},p_{f_h}^{m+k}-p_{f_h}^{m-1+k})_{\mathfrak{e}}$$
$$=(\tilde{q}_{W_h}^{m+k},p_{f_h}^{m+k}-p_{f_h}^{m-1+k})_{\mathfrak{e}}. \tag{7.3.30}$$

Now, consider (7.3.24) for the difference of two consecutive flow finer time steps ($t=t_{m+k}$ and $t=t_{m-1+k}$), and test with $\boldsymbol{\mu}_{f_h}=\boldsymbol{\zeta}_h^{m+k}$ to get:

$$(K_{\mathfrak{e}}^{-1}(\boldsymbol{\zeta}_h^{m+k}-\boldsymbol{\zeta}_h^{m-1+k}),\boldsymbol{\zeta}_h^{m+k})_{\mathfrak{e}}=(p_{f_h}^{m+k}-p_{f_h}^{m-1+k},\overline{\nabla}\cdot(\boldsymbol{\zeta}_h^{m+k}))_{\mathfrak{e}}. \tag{7.3.31}$$

Now, substitute (7.3.31) into (7.3.30) to get:

$$\frac{c_{f_c}}{\Delta t}\left\|p_{f_h}^{m+k}-p_{f_h}^{m-1+k}\right\|_{\mathfrak{e}}^2+\frac{1}{12\mu_f}(K_{\mathfrak{e}}^{-1}(\boldsymbol{\zeta}_h^{m+k}-\boldsymbol{\zeta}_h^{m-1+k}),\boldsymbol{\zeta}_h^{m+k})_{\mathfrak{e}}$$
$$-\frac{1}{\mu_f}([\boldsymbol{z}_h^{m+k}]_{\mathfrak{e}}\cdot\boldsymbol{n}^+,p_{f_h}^{m+k}-p_{f_h}^{m-1+k})_{\mathfrak{e}}+\frac{1}{q\Delta t}(w_h^k-w_h^{k-q},p_{f_h}^{m+k}-p_{f_h}^{m-1+k})_{\mathfrak{e}}$$
$$=(\tilde{q}_{W_h}^{m+k},p_{f_h}^{m+k}-p_{f_h}^{m-1+k})_{\mathfrak{e}}. \tag{7.3.32}$$

Next, add (7.3.29) to (7.3.32) to obtain (note canceling terms from each equation):

$$\frac{\beta}{\Delta t}\left\|p_h^{m+k}-p_h^{m-1+k}\right\|^2+\frac{1}{\mu_f}(\boldsymbol{K}^{-1}(\boldsymbol{z}_h^{m+k}-\boldsymbol{z}_h^{m-1+k}),\boldsymbol{z}_h^{m+k})+\frac{c_{f_c}}{\Delta t}\left\|p_{f_h}^{m+k}-p_{f_h}^{m-1+k}\right\|_{\mathfrak{e}}^2$$
$$+\frac{1}{12\mu_f}(K_{\mathfrak{e}}^{-1}(\boldsymbol{\zeta}_h^{m+k}-\boldsymbol{\zeta}_h^{m-1+k}),\boldsymbol{\zeta}_h^{m+k})_{\mathfrak{e}}+\frac{1}{q\Delta t}(w_h^k-w_h^{k-q},p_{f_h}^{m+k}-p_{f_h}^{m-1+k})_{\mathfrak{e}}$$
$$\leq-\frac{\alpha}{q\Delta t}\Big(\nabla\cdot(\boldsymbol{u}_h^k-\boldsymbol{u}_h^{k-q}),p_h^{m+k}-p_h^{m-1+k}\Big)+(\tilde{q}_h^{m+k},p_h^{m+k}-p_h^{m-1+k})$$
$$+(\tilde{q}_{W_h}^{m+k},p_{f_h}^{m+k}-p_{f_h}^{m-1+k})_{\mathfrak{e}}. \tag{7.3.33}$$

Finally, multiply (7.3.33) by Δt and sum across flow finer time steps ($1 \le m \le q$) to get (use $a(a-b) = \frac{1}{2}(a^2 - b^2 + (a-b)^2)$ and the telescopic cancellations)

$$
\begin{aligned}
&\beta \sum_{m=1}^{q} \left\| p_h^{m+k} - p_h^{m-1+k} \right\|^2 + \frac{\Delta t}{2\mu_f} \Big[\left\| \boldsymbol{K}^{-1/2} \boldsymbol{z}_h^{k+q} \right\|^2 - \left\| \boldsymbol{K}^{-1/2} \boldsymbol{z}_h^{k} \right\|^2 \\
&+ \sum_{m=1}^{q} \left\| \boldsymbol{K}^{-1/2} (\boldsymbol{z}_h^{m+k} - \boldsymbol{z}_h^{m-1+k}) \right\|^2 \Big] + c_{f_c} \sum_{m=1}^{q} \left\| p_{f_h}^{m+k} - p_{f_h}^{m-1+k} \right\|_{\mathfrak{e}}^2 \\
&+ \frac{\Delta t}{24\mu_f} \Big[\left\| K_{\mathfrak{e}}^{-1/2} \boldsymbol{\zeta}_h^{k+q} \right\|_{\mathfrak{e}}^2 - \left\| K_{\mathfrak{e}}^{-1/2} \boldsymbol{\zeta}_h^{k} \right\|_{\mathfrak{e}}^2 + \sum_{m=1}^{q} \left\| K_{\mathfrak{e}}^{-1/2} (\boldsymbol{\zeta}_h^{m+k} - \boldsymbol{\zeta}_h^{m-1+k}) \right\|_{\mathfrak{e}}^2 \Big] \\
&\le -\frac{1}{q} \Big(w_h^k - w_h^{k-q}, \sum_{m=1}^{q} (p_{f_h}^{m+k} - p_{f_h}^{m-1+k}) \Big)_{\mathfrak{e}} \\
&\quad - \frac{\alpha}{q} \Big(\nabla \cdot (\boldsymbol{u}_h^k - \boldsymbol{u}_h^{k-q}), \sum_{m=1}^{q} (p_h^{m+k} - p_h^{m-1+k}) \Big) \\
&\quad + \Delta t \sum_{m=1}^{q} (\tilde{q}_h^{m+k}, p_h^{m+k} - p_h^{m-1+k}) + \Delta t \sum_{m=1}^{q} (\tilde{q}_{W_h}^{m+k}, p_{f_h}^{m+k} - p_{f_h}^{m-1+k})_{\mathfrak{e}}. \qquad (7.3.34)
\end{aligned}
$$

- **Step 2: Elasticity equation**

  Consider equation (7.3.25) for the difference of two consecutive mechanics (coarse) time steps: $t = t_k$ and $t = t_{k+q}$ (recall that $k = 0, q, 2q, ..$), and test with $\boldsymbol{v}_h = (\boldsymbol{u}_h^{k+q} - \boldsymbol{u}_h^k)$ to obtain:

$$
\begin{aligned}
2G \left\| \boldsymbol{\varepsilon}(\boldsymbol{u}_h^{k+q} - \boldsymbol{u}_h^k) \right\|^2 + \lambda \left\| \nabla \cdot (\boldsymbol{u}_h^{k+q} - \boldsymbol{u}_h^k) \right\|^2 - \alpha (p_h^{k+q} - p_h^k, \nabla \cdot (\boldsymbol{u}_h^{k+q} - \boldsymbol{u}_h^k)) \\
- (p_{f_h}^{k+q} - p_{f_h}^k, w_h^{k+q} - w_h^k)_{\mathfrak{e}} = \Big(\boldsymbol{f}_h^{k+q} - \boldsymbol{f}_h^k, \boldsymbol{u}_h^{k+q} - \boldsymbol{u}_h^k \Big). \qquad (7.3.35)
\end{aligned}
$$

- **Step 3: Combining flow and elasticity equations**

  Add (7.3.34) to (7.3.35), bound the term $G \left\| \boldsymbol{\varepsilon}(\boldsymbol{u}_h^{k+q} - \boldsymbol{u}_h^k) \right\|^2$ on the left hand side of

(7.3.35) from below by (6.4.55) to obtain:

$$
\begin{aligned}
&\beta\sum_{m=1}^{q}\left\|p_h^{m+k}-p_h^{m-1+k}\right\|^2+\frac{\Delta t}{2\mu_f}\Big[\left\|\boldsymbol{K}^{-1/2}\boldsymbol{z}_h^{k+q}\right\|^2-\left\|\boldsymbol{K}^{-1/2}\boldsymbol{z}_h^{k}\right\|^2\\
&+\sum_{m=1}^{q}\left\|\boldsymbol{K}^{-1/2}(\boldsymbol{z}_h^{m+k}-\boldsymbol{z}_h^{m-1+k})\right\|^2\Big]+c_{f_c}\sum_{m=1}^{q}\left\|p_{f_h}^{m+k}-p_{f_h}^{m-1+k}\right\|_{\mathfrak{C}}^2\\
&+\frac{\Delta t}{24\mu_f}\Big[\left\|K_{\mathfrak{C}}^{-1/2}\boldsymbol{\zeta}_h^{k+q}\right\|_{\mathfrak{C}}^2-\left\|K_{\mathfrak{C}}^{-1/2}\boldsymbol{\zeta}_h^{k}\right\|_{\mathfrak{C}}^2+\sum_{m=1}^{q}\left\|K_{\mathfrak{C}}^{-1/2}(\boldsymbol{\zeta}_h^{m+k}-\boldsymbol{\zeta}_h^{m-1+k})\right\|_{\mathfrak{C}}^2\Big]\\
&+G\left\|\boldsymbol{\varepsilon}(\boldsymbol{u}_h^{k+q}-\boldsymbol{u}_h^{k})\right\|^2+GC^*\left\|w_h^{k+q}-w_h^{k}\right\|^2+\lambda\left\|\nabla\cdot(\boldsymbol{u}_h^{k+q}-\boldsymbol{u}_h^{k})\right\|^2\\
&\leq\underbrace{-\frac{1}{q}\Big(w_h^{k}-w_h^{k-q},\sum_{m=1}^{q}(p_{f_h}^{m+k}-p_{f_h}^{m-1+k})\Big)_{\mathfrak{C}}}_{R_6}\\
&\underbrace{-\frac{\alpha}{q}\Big(\nabla\cdot(\boldsymbol{u}_h^{k}-\boldsymbol{u}_h^{k-q}),\sum_{m=1}^{q}(p_h^{m+k}-p_h^{m-1+k})\Big)}_{R_1}\\
&\underbrace{+\Delta t\sum_{m=1}^{q}(\tilde{q}_h^{m+k},p_h^{m+k}-p_h^{m-1+k})}_{R_3}\underbrace{+\Delta t\sum_{m=1}^{q}(\tilde{q}_{W_h}^{m+k},p_{f_h}^{m+k}-p_{f_h}^{m-1+k})_{\mathfrak{C}}}_{R_4}\\
&\underbrace{+\alpha(p_h^{k+q}-p_h^{k},\nabla\cdot(\boldsymbol{u}_h^{k+q}-\boldsymbol{u}_h^{k}))}_{R_2}\underbrace{+(p_{f_h}^{k+q}-p_{f_h}^{k},w_h^{k+q}-w_h^{k})_{\mathfrak{C}}}_{R_5}\\
&\underbrace{+\Big(\boldsymbol{f}_h^{k+q}-\boldsymbol{f}_h^{k},\boldsymbol{u}_h^{k+q}-\boldsymbol{u}_h^{k}\Big)}_{R_7}.
\end{aligned}
\tag{7.3.36}
$$

Denoting by $R_1, R_2, R_3, R_4, R_5, R_6$ and R_7 the terms on the right hand side, together with Poincaré's, Korn's, and Young's inequalities, and noticing that,

$$
(p_h^{k+q}-p_h^{k})=\sum_{m=1}^{q}(p_h^{m+k}-p_h^{m-1+k}) \tag{7.3.37}
$$

$$
(p_{f_h}^{k+q}-p_{f_h}^{k})=\sum_{m=1}^{q}(p_{f_h}^{m+k}-p_{f_h}^{m-1+k}) \tag{7.3.38}
$$

we estimate:

$$
\begin{aligned}
|R_1| &\le \frac{\alpha}{q}\Big(\frac{q}{2\epsilon_1}\Big\|\nabla\cdot(\boldsymbol{u}_h^k-\boldsymbol{u}_h^{k-q})\Big\|^2+\frac{\epsilon_1}{2}\sum_{m=1}^{q}\Big\|p_h^{m+k}-p_h^{m-1+k}\Big\|^2\Big),\\
|R_2| &= |\alpha(\sum_{m=1}^{q}(p_h^{m+k}-p_h^{m-1+k}),\nabla\cdot(\boldsymbol{u}_h^{k+q}-\boldsymbol{u}_h^k))|\\
&\le \alpha\Big(\frac{1}{2\epsilon_2}\sum_{m=1}^{q}\Big\|p_h^{m+k}-p_h^{m-1+k}\Big\|^2+\frac{q\epsilon_2}{2}\Big\|\nabla\cdot(\boldsymbol{u}_h^{k+q}-\boldsymbol{u}_h^k)\Big\|^2\Big),\\
|R_3| &\le \Delta t\Big(\frac{1}{2\epsilon_3}\sum_{m=1}^{q}\Big\|\tilde{q}_h^{m+k}\Big\|^2+\frac{\epsilon_3}{2}\sum_{m=1}^{q}\Big\|p_h^{m+k}-p_h^{m-1+k}\Big\|^2\Big),\\
|R_4| &\le \Delta t\Big(\frac{1}{2\epsilon_4}\sum_{m=1}^{q}\Big\|\tilde{q}_{W_h}^{m+k}\Big\|_{\mathcal{C}}^2+\frac{\epsilon_4}{2}\sum_{m=1}^{q}\Big\|p_{f_h}^{m+k}-p_{f_h}^{m-1+k}\Big\|_{\mathcal{C}}^2\Big),\\
|R_5| &= |(\sum_{m=1}^{q}(p_{f_h}^{m+k}-p_{f_h}^{m-1+k}),w_h^{k+q}-w_h^k)_{\mathcal{C}}|\\
&\le \frac{1}{2\epsilon_5}\sum_{m=1}^{q}\Big\|p_{f_h}^{m+k}-p_{f_h}^{m-1+k}\Big\|_{\mathcal{C}}^2+\frac{q\epsilon_5}{2}\Big\|w_h^{k+q}-w_h^k\Big\|_{\mathcal{C}}^2,\\
|R_6| &\le \frac{1}{q}\Big(\frac{q}{2\epsilon_6}\Big\|w_h^k-w_h^{k-q}\Big\|_{\mathcal{C}}^2+\frac{\epsilon_6}{2}\sum_{m=1}^{q}\Big\|p_{f_h}^{m+k}-p_{f_h}^{m-1+k}\Big\|_{\mathcal{C}}^2\Big),\\
|R_7| &\le \frac{1}{2\epsilon_7}\Big\|\boldsymbol{f}_h^{k+q}-\boldsymbol{f}_h^k\Big\|^2+\frac{\epsilon_7}{2}\Big\|\boldsymbol{u}_h^{k+q}-\boldsymbol{u}_h^k\Big\|^2\\
&\le \frac{1}{2\epsilon_7}\Big\|\boldsymbol{f}_h^{k+q}-\boldsymbol{f}_h^k\Big\|^2+\frac{\epsilon_7\mathcal{P}_\Omega^2C_\kappa^2}{2}\|\boldsymbol{\varepsilon}(\boldsymbol{u}_h^{k+q}-\boldsymbol{u}_h^k)\|^2,
\end{aligned}
$$

for $\epsilon_1,\epsilon_2,\epsilon_3,\epsilon_4,\epsilon_5,\epsilon_6,$ and $\epsilon_7>0$. Choosing $\epsilon_1=\frac{\alpha}{\lambda}$, $\epsilon_2=\frac{\lambda}{\alpha q}$, $\epsilon_3=\frac{2}{\Delta t}\Big(\beta-\frac{1}{2}(\frac{1}{q}+q)\frac{\alpha^2}{\lambda}\Big)$,

$\epsilon_4 = \frac{2}{\Delta t}\Big(c_{f_c} - \frac{1}{2}(\frac{1}{q}+q)\frac{1}{GC^*}\Big)$, $\epsilon_5 = \frac{GC^*}{q}$, $\epsilon_6 = \frac{1}{GC^*}$, $\epsilon_7 = \frac{G}{\mathcal{P}_\Omega^2 C_\kappa^2}$, we have:

$$\begin{aligned}
&\frac{\Delta t}{2\mu_f}\Big[\Big\|\boldsymbol{K}^{-1/2}\boldsymbol{z}_h^{k+q}\Big\|^2 - \Big\|\boldsymbol{K}^{-1/2}\boldsymbol{z}_h^{k}\Big\|^2 + \sum_{m=1}^{q}\Big\|\boldsymbol{K}^{-1/2}(\boldsymbol{z}_h^{m+k} - \boldsymbol{z}_h^{m-1+k})\Big\|^2\Big] \\
&+ \frac{\Delta t}{24\mu_f}\Big[\Big\|K_{\mathcal{C}}^{-1/2}\boldsymbol{\zeta}_h^{k+q}\Big\|_{\mathcal{C}}^2 - \Big\|K_{\mathcal{C}}^{-1/2}\boldsymbol{\zeta}_h^{k}\Big\|_{\mathcal{C}}^2 + \sum_{m=1}^{q}\Big\|K_{\mathcal{C}}^{-1/2}(\boldsymbol{\zeta}_h^{m+k} - \boldsymbol{\zeta}_h^{m-1+k})\Big\|_{\mathcal{C}}^2\Big] \\
&+ \frac{G}{2}\Big\|\boldsymbol{\varepsilon}(\boldsymbol{u}_h^{k+q} - \boldsymbol{u}_h^{k})\Big\|^2 + \frac{GC^*}{2}\Big\|w_h^{k+q} - w_h^{k}\Big\|^2 + \frac{\lambda}{2}\Big\|\nabla\cdot(\boldsymbol{u}_h^{k+q} - \boldsymbol{u}_h^{k})\Big\|^2 \\
&\leq \frac{GC^*}{2}\Big\|w_h^{k} - w_h^{k-q}\Big\|_{\mathcal{C}}^2 + \frac{\lambda}{2}\Big\|\nabla\cdot(\boldsymbol{u}_h^{k} - \boldsymbol{u}_h^{k-q})\Big\|^2 + \frac{\Delta t^2}{4\Big(\beta - \frac{1}{2}(\frac{1}{q}+q)\frac{\alpha^2}{\lambda})\Big)}\sum_{m=1}^{q}\Big\|\tilde{q}_h^{m+k}\Big\|^2 \\
&\qquad + \frac{\Delta t^2}{4(c_{f_c} - \frac{1}{2}(\frac{1}{q}+q)\frac{1}{GC^*})}\sum_{m=1}^{q}\Big\|\tilde{q}_{W_h}^{m+k}\Big\|_{\mathcal{C}}^2 + \frac{\mathcal{P}_\Omega^2 C_\kappa^2}{2G}\Big\|\boldsymbol{f}_h^{k+q} - \boldsymbol{f}_h^{k}\Big\|^2. \qquad (7.3.39)
\end{aligned}$$

We need to impose the following conditions: $\beta - \frac{1}{2}(\frac{1}{q}+q)\frac{\alpha^2}{\lambda} > 0$ and $c_{f_c} - \frac{1}{2}(\frac{1}{q}+q)\frac{1}{GC^*}$, which are nothing but the conditions listed in Assumption $\mathbf{A_q}$. Summing up equation (7.3.40) for $q \leq k \leq J$ (k is a multiple of q, that is, k = q, 2q, ..), we write:

$$\begin{aligned}
&\frac{\Delta t}{2\mu_f}\Big[\Big\|\boldsymbol{K}^{-1/2}\boldsymbol{z}_h^{J+q}\Big\|^2 + \sum_{k=q}^{J}\sum_{m=1}^{q}\Big\|\boldsymbol{K}^{-1/2}(\boldsymbol{z}_h^{m+k} - \boldsymbol{z}_h^{m-1+k})\Big\|^2\Big] \\
&+ \frac{\Delta t}{24\mu_f}\Big[\Big\|K_{\mathcal{C}}^{-1/2}\boldsymbol{\zeta}_h^{J+q}\Big\|_{\mathcal{C}}^2 + \sum_{k=q}^{J}\sum_{m=1}^{q}\Big\|K_{\mathcal{C}}^{-1/2}(\boldsymbol{\zeta}_h^{m+k} - \boldsymbol{\zeta}_h^{m-1+k})\Big\|_{\mathcal{C}}^2\Big] \\
&+ \frac{G}{2}\sum_{k=q}^{J}\Big\|\boldsymbol{\varepsilon}(\boldsymbol{u}_h^{k+q} - \boldsymbol{u}_h^{k})\Big\|^2 + \frac{GC^*}{2}\Big\|w_h^{J+q} - w_h^{J}\Big\|_{\mathcal{C}}^2 + \frac{\lambda}{2}\Big\|\nabla\cdot(\boldsymbol{u}_h^{J+q} - \boldsymbol{u}_h^{J})\Big\|^2 \\
&\leq \frac{\Delta t}{2\mu_f}\Big\|\boldsymbol{K}^{-1/2}\boldsymbol{z}_h^{q}\Big\|^2 + \frac{\Delta t}{24\mu_f}\Big\|K_{\mathcal{C}}^{-1/2}\boldsymbol{\zeta}_h^{q}\Big\|_{\mathcal{C}}^2 + \frac{GC^*}{2}\Big\|w_h^{q} - w_h^{0}\Big\|_{\mathcal{C}}^2 \\
&+ \frac{\lambda}{2}\Big\|\nabla\cdot(\boldsymbol{u}_h^{q} - \boldsymbol{u}_h^{0})\Big\|^2 + \frac{\Delta t^2}{4\Big(\beta - \frac{1}{2}(\frac{1}{q}+q)\frac{\alpha^2}{\lambda})\Big)}\sum_{k=q}^{J}\sum_{m=1}^{q}\Big\|\tilde{q}_h^{m+k}\Big\|^2 \\
&+ \frac{\Delta t^2}{4(c_{f_c} - \frac{1}{2}(\frac{1}{q}+q)\frac{1}{GC^*})}\sum_{k=q}^{J}\sum_{m=1}^{q}\Big\|\tilde{q}_{W_h}^{m+k}\Big\|_{\mathcal{C}}^2 + \frac{\mathcal{P}_\Omega^2 C_\kappa^2}{2G}\sum_{k=q}^{J}\Big\|\boldsymbol{f}_h^{k+q} - \boldsymbol{f}_h^{k}\Big\|^2. \qquad (7.3.40)
\end{aligned}$$

We recall that $\boldsymbol{u}_h^q, \boldsymbol{z}_h^q$, and $\boldsymbol{\zeta}_h^q$ have been computed using the fully implicit time discretization. In a similar way as shown in section 4.3.2, we conclude that $\Big\|w_h^q - w_h^0\Big\|_{\mathcal{C}}^2 \leq Cq\Delta t$, $\Big\|\nabla\cdot(\boldsymbol{u}_h^q - \boldsymbol{u}_h^0)\Big\|^2 < Cq\Delta t$, $\Big\|\boldsymbol{K}^{-1/2}\boldsymbol{z}_h^q\Big\|^2 < C$, and $\Big\|K_{\mathcal{C}}^{-1/2}\boldsymbol{\zeta}_h^q\Big\|_{\mathcal{C}}^2 < C$, for a generic constant C. This completes the derivation.

Remark 7.3.1. As in the single rate case in remark 7.2.1, the multirate case can also be made unconditionally stable by adding stabilisation terms. In the definition 7.3.1, we modify the flow equations (in both the matrix and the fracture: (7.3.21) and (7.3.22)) by adding stabilisation terms $\frac{\gamma\alpha^2}{\lambda\Delta t}(p_h^{m+k} - p_h^{m-1+k})$, and $\frac{\gamma}{GC^*\Delta t}(p_{f_h}^{m+k} - p_{f_h}^{m-1+k})$ respectively (where $\gamma = \frac{1}{2}(\frac{1}{q} + q)$). The modified equations reads: For $1 \leq m \leq q$, find $p_h^{m+k} \in Q_h$, $p_{f_h}^{m+k} \in Q_{c_h}$, $\boldsymbol{z}_h^{m+k} \in \boldsymbol{Z}_h$, and $\boldsymbol{\zeta}_h^{m+k} \in \boldsymbol{Z}_{\mathfrak{e}h}$ such that,

$$\begin{aligned}\forall\theta_h \in Q_h\,, \frac{1}{\Delta t}(\frac{1}{M} + c_f\varphi_0 + \frac{\gamma\alpha^2}{\lambda})\Big(p_h^{m+k} - p_h^{m-1+k}, \theta_h\Big) + \frac{1}{\mu_f}(\nabla\cdot\boldsymbol{z}_h^{m+k}, \theta_h)\\ = -\frac{\alpha}{q\Delta t}\Big(\nabla\cdot(\boldsymbol{u}_h^k - \boldsymbol{u}_h^{k-q}), \theta_h\Big) + (\tilde{q}_h^{m+k}, \theta_h)\end{aligned} \tag{7.3.41}$$

$$\begin{aligned}\forall\theta_{c_h} \in Q_{c_h}\,, \frac{c_{f_c} + \frac{\gamma}{GC^*}}{\Delta t}\Big(p_{f_h}^{m+k} - p_{f_h}^{m-1+k}, \theta_{c_h}\Big)_{\mathfrak{e}} + \frac{1}{12\mu_f}(\overline{\nabla}\cdot(\boldsymbol{\zeta}_h^{m+k}), \theta_{c_h})_{\mathfrak{e}}\\ - \frac{1}{\mu_f}([\boldsymbol{z}_h^{m+k}]_{\mathfrak{e}}\cdot\boldsymbol{n}^+, \theta_{c_h})_{\mathfrak{e}} + \frac{1}{q\Delta t}(w_h^k - w_h^{k-q}, \theta_{c_h})_{\mathfrak{e}} = (\tilde{q}_{W_h}^{m+k}, \theta_{c_h})_{\mathfrak{e}}\end{aligned} \tag{7.3.42}$$

The proof for the unconditional stability follows exactly the same ideas and is skipped here.

Remark 7.3.2. All our obtained results remain valid if the multipoint flux mixed finite element method (MFMFE) [88,90] is used for flow discretization. Indeed, for such a scheme, the stability results (7.3.40) translates to

$$\begin{aligned}&\frac{\Delta t}{2\mu_f}\Big[\Big(\boldsymbol{K}^{-1}\boldsymbol{z}_h^{J+q}, \boldsymbol{z}_h^{J+q}\Big)_Q + \sum_{k=q}^{J}\sum_{m=1}^{q}\Big(\boldsymbol{K}^{-1}(\boldsymbol{z}_h^{m+k} - \boldsymbol{z}_h^{m-1+k}), (\boldsymbol{z}_h^{m+k} - \boldsymbol{z}_h^{m-1+k})\Big)_Q\Big]\\
&+ \frac{\Delta t}{24\mu_f}\Big[\Big(K_{\mathfrak{e}}^{-1}\boldsymbol{\zeta}_h^{J+q}, \boldsymbol{\zeta}_h^{J+q}\Big)_Q + \sum_{k=q}^{J}\sum_{m=1}^{q}\Big(K_{\mathfrak{e}}^{-1}(\boldsymbol{\zeta}_h^{m+k} - \boldsymbol{\zeta}_h^{m-1+k}), (\boldsymbol{\zeta}_h^{m+k} - \boldsymbol{\zeta}_h^{m-1+k})\Big)_Q\Big]\\
&+ \frac{G}{2}\sum_{k=q}^{J}\Big\|\boldsymbol{\varepsilon}(\boldsymbol{u}_h^{k+q} - \boldsymbol{u}_h^k)\Big\|^2 + \frac{GC^*}{2}\Big\|w_h^{J+q} - w_h^J\Big\|_{\mathfrak{e}}^2 + \frac{\lambda}{2}\Big\|\nabla\cdot(\boldsymbol{u}_h^{J+q} - \boldsymbol{u}_h^J)\Big\|^2\\
&\leq \frac{\Delta t}{2\mu_f}\Big(\boldsymbol{K}^{-1}\boldsymbol{z}_h^q, \boldsymbol{z}_h^q\Big)_Q + \frac{\Delta t}{24\mu_f}\Big(K_{\mathfrak{e}}^{-1}\boldsymbol{\zeta}_h^q, \boldsymbol{\zeta}_h^q\Big)_Q + \frac{GC^*}{2}\Big\|w_h^q - w_h^0\Big\|_{\mathfrak{e}}^2\\
&+ \frac{\lambda}{2}\Big\|\nabla\cdot(\boldsymbol{u}_h^q - \boldsymbol{u}_h^0)\Big\|^2 + \frac{\Delta t^2}{4\Big(\beta - \frac{1}{2}(\frac{1}{q} + q)\frac{\alpha^2}{\lambda})\Big)}\sum_{k=q}^{J}\sum_{m=1}^{q}\Big\|\tilde{q}_h^{m+k}\Big\|^2\\
&+ \frac{\Delta t^2}{4(c_{f_c} - \frac{1}{2}(\frac{1}{q} + q)\frac{1}{GC^*})}\sum_{k=q}^{J}\sum_{m=1}^{q}\Big\|\tilde{q}_{W_h}^{m+k}\Big\|_{\mathfrak{e}}^2 + \frac{\mathcal{P}_\Omega^2 C_\kappa^2}{2G}\sum_{k=q}^{J}\Big\|\boldsymbol{f}_h^{k+q} - \boldsymbol{f}_h^k\Big\|^2,\end{aligned} \tag{7.3.43}$$

where $(K^{-1}.,.)_Q$ is the quadrature rule defined in [90] for the MFMFE corresponding spaces (in the corresponding domain of integration for both "flow in matrix" variables, and "flow in fracture" variables). It was shown by Wheeler and Yotov in [90], and then extended to distorted quadrilaterals and hexahedra in [88], that for any $\boldsymbol{z}_h \in \boldsymbol{Z}_h, C_1\|\boldsymbol{z}_h\|^2 \leq (K^{-1}\boldsymbol{z}_h, \boldsymbol{z}_h)_Q \leq C_2\|\boldsymbol{z}_h\|^2$, for a constant $C_1, C_2 > 0$. This immediately leads to a similar stability result. The same argument holds for single rate case and for the unconditionally stable schemes.

Chapter 8

The Global Inexact Newton Method as a Nonlinear Solver Framework for Flow in Iteratively Coupled Problems

8.1 Introduction

The motivation behind introducing the global inexact Newton method at this point is the fact that it is one of the efficient candidate strategies to solve the nonlinear "multi-phase" flow equations in iteratively coupled flow and geomechanics problems. It is also applicable for multirate iterative coupling algorithms, described earlier. The global inexact Newton method combined with the line search backtracking optimization technique can be efficiently employed in this context to optimize the underlying nonlinear solver for the different kinds of operators arising in such highly nonlinear iterative coupling settings.

Our ultimate objective in this chapter is to design an efficient iterative coupling algorithm which will reduce both the number of flow and mechanics linear iterations for the coupled problem. This will subsequently reduce the CPU run time for the coupled scheme, without affecting the accuracy of the obtained solution. We have seen in previous chapters that the multirate scheme reduces the number of mechanics linear iterations efficiently. The global inexact Newton method with line-search backtracking helps reducing the number of consumed flow linear iterations. Combined together, we obtain a scheme that fulfills our ultimate objective.

This research work (including IPARSv2.1 and IPARSv3.1 associated implementations) is done primarily by Tameem Almani, with helpful discussions, inputs, and suggestions by Drs. Kundan Kumar, Gergina Pencheva, and Gurpreet Singh, under the supervision of Prof. Mary Wheeler.

Computational gains as a result of incorporating the line-search backtracking strategy into the inexact Newton method are twofold: first, it reduces the linear solver running time by allowing for mild linear solver tolerance values, and second, it allows for larger time steps while global convergence is maintained by continuously enforcing the sufficient decrease condition at every nonlinear iteration. Both of these advantages play a critical role in reducing the overall running time for iteratively coupled flow and geomechanics problems. In the context of multirate iteratively coupled problems, in which the mechanics problem takes coarse time time steps, allowing for larger time steps for the flow problem problem as well combined with mild linear solver tolerances leads to huge savings in the number of flow and mechanics linear iterations, and in turn, the CPU running time. Incorporating the line-search backtracking strategy when solving the nonlinear flow problem in the context of iteratively coupled flow and geomechanics problems is a novel approach which has not been explored in the past.

8.2 The Global Inexact Newton Method and Linesearch Backtracking Algorithm

For the flow part, we are interested in solving the following nonlinear system of equations

$$F(u) = 0 \qquad \text{where } F : \mathbb{R}^n \to \mathbb{R}^n$$

where $F(u)$ represents the nonlinear residual or the right hand side resulting from discretizing single phase/multiphase flow equations, and the superscript "n" represents the total number of unknowns. For the two-phase (water and oil) flow problem, the variable u represents oil pressures and concentrations. By a simple Taylor expansion, the Inexact Newton method reads:

$$J(u^{(k)})s^{(k)} = -F(u^{(k)}) + r^{(k)} \tag{8.2.1}$$

The residual $r^{(k)}$, at the k^{th} Newton iteration, represents the amount by which the solution $s^{(k)}(= u^{k+1} - u^k)$, given by the underlying linear solver (GMRES with Line SOR as a preconditioner for SPE10 results - implemented in IPARS v2.1 - and GMRES with AMG as a preconditioner (Hypre-BoomerAMG) for iteratively coupled problems - implemented

in IPARS v3.1) fails to satisfy the exact Newton Method [31]:

$$J(u^{(k)})s^{(k)} = -F(u^{(k)})$$

8.2.1 Algorithm

The global inexact Newton method algorithm with forcing terms and line search backtracking is as follows [56]: In the above algorithm, the linear solution is accepted when:

Algorithm 13: Global Inexact Newton with Line-search Backtracking and Forcing Functions

Let $u^{(0)}$ *be an initial guess and* $t \in (0,1)$ *be a constant (We use* $t = 10^{-4}$*)*
for $k = 1, 2, ..$ *until convergence* **do** `/* Nonlinear iteration loop */`
  CHOOSE $\eta^{(k)} \in [0,1), t \in (0,1)$ HERE, T $= 0.0001$
  USING AN ITERATIVE LINEAR SOLVER METHOD, FIND $s^{(k)}$ SATISFYING

$$J(u^{(k)})s^{(k)} = -F(u^{(k)}) + r^{(k)} \qquad \text{with} \qquad \frac{\|r^{(k)}\|}{\|F(u^{(k)})\|} \leqslant \eta^{(k)}$$

  INITIALIZE THE LINESEARCH BACKTRACKING LOOP: $s^{k,0} = s^k$, $\eta^{k,0} = \eta^k$, $i = 0$
  while $\|F(u^{(k)} + s^{(k)})\| > (1 - t(1 - \eta^{(k)}))\|F(u^{(k)})\|$ **do** `/* line-search backtracking loop */`
    Choose a contraction factor $\theta^i \in [0.1, 0.5]$ *(We used* $\theta^0 = 0.5$*)*
    Reduce solution increment $s^{k,i+1} = \theta^i s^{k,i}$
    Update the forcing factor $\eta^{k,i+1} = 1 - \theta^i(1 - \eta^{k,i})$
    Increment the loop index $i = i + 1$
  UPDATE SOLUTION $u^{(k+1)} = u^{(k)} + s^{(k)}$

$$\|r^{(k)}\| = \|F(u^{(k)}) + J(u^{(k)})s^{(k)}\| \leqslant \eta^{(k)}\|F(u^{(k)})\| \tag{8.2.2}$$

where $\eta^{(k)}$ is referred to as the"forcing term" or "forcing function". The sufficient decrease condition requires that the actual reduction in the right hand side (or nonlinear residual) to be greater than or equal to some fraction (the factor t above) of the predicted reduction given by the local linear model:

$$\|F(u^{(k)})\| - \|F(u^{(k+1)})\| \geq t(\|F(u^{(k)})\| - \|F(u^{(k)}) + J(u^{(k)})s^{(k)}\|) \tag{8.2.3}$$

Combining (8.2.2) and (8.2.3), we reach at:

$$\|F(u^{(k)} + s^{(k)})\| \leq (1 - t(1 - \eta^{(k)}))\|F(u^{(k)})\|$$

which is the condition we check in the backtracking inner loop above [31]. By this algorithm, the tolerance of the linear solver is dictated by the residual of the nonlinear system of equations using forcing functions. This results in tightening the tolerance of the linear solver in a progressive manner, which in turn, optimizes the computational efforts.

The way the forcing term $\eta^{(k)}$ is updated in the algorithm above can be justified as follows: by induction, the base case is trivial, as $\|F(u^{(k)}) + J(u^{(k)})s^{(k,0)}\| \leq \eta^{(k,0)}\|F(u^{(k)})\|$. This follows directly by step (2.2) in the algorithm above. Now, we write:

$$\begin{aligned}
\|F(u^{(k)}) + J(u^{(k)})s^{(k,i+1)}\| &= \|F(u^{(k)}) + J(u^{(k)})\theta^i s^{(k,i)}\| \\
&= \|F(u^{(k)}) - \theta^i F(u^{(k)}) + \theta^i F(u^{(k)}) + \theta^i J(u^{(k)})s^{(k,i)}\| \\
&= \|(1 - \theta^i)F(u^{(k)}) + \theta^i(F(u^{(k)}) + J(u^{(k)})s^{(k,i)})\| \\
&\leq (1 - \theta^i)\|F(u^{(k)})\| + \theta^i\|F(u^{(k)}) + J(u^{(k)})s^{(k,i)}\| \\
&\leq (1 - \theta^i)\|F(u^{(k)})\| + \theta^i\eta^{(i,k)}\|F(u^{(k)})\| \\
&\leq [(1 - \theta^{(i)}) + \theta^{(i)}\eta^{(i,k)}]\|F(u^{(k)})\| \\
&\leq \Big(1 - \theta^i(1 - \eta^{(k,i)})\Big)\|F(u^{(k)})\| \\
&\leq \eta^{(k,i+1)}\|F(u^{(k)})\| \qquad (8.2.4)
\end{aligned}$$

which is the update given in line (9) in the algorithm above.

Remark 8.2.1. *A quick derivation based on* (8.2.4) *leads to:*

$$\eta^{(k,i+1)} = 1 - \prod_{j=1}^{i} \theta^j(1 - \eta^{(k,0)})$$

As $\theta^i < 1.0$ *for all* $i \in \mathbb{N}$*, the sequence of forcing terms, as we take more line-search backtracking iterations, given by* $\{\eta^{(k,i)}\}_{i=0}^{\infty}$*, is a monotonically increasing sequence. This*

is in fact expected and can be justified as follows:

$$\begin{aligned}\lim_{i\to\infty}\|F(u^{(k)})+J(u^{(k)})s^{(k,i+1)}\| &= \lim_{i\to\infty}\|F(u^{(k)})+\Big(\prod_{j=1}^{i}\theta^j\Big)J(u^{(k)})s^{(k)}\| \\ &\leq \|F(u^{(k)})\|+\|J(u^{(k)})s^{(k)}\|\Big(\lim_{i\to\infty}\prod_{j=1}^{i}\theta^j\Big) \\ &\leq \|F(u^{(k)})\| \qquad (8.2.5)\end{aligned}$$

as the second term on the right hand side vanishes. Comparing (8.2.4) *to* (8.2.5)*, we conclude that as we take more line-search backtracking iterations, the inexact Newton condition will be satisfied with looser forcing terms. If we take infinitely many line-search backtracking iterations, the inexact Newton condition will be satisfied with a forcing term of the value 1. It should be noted that the as we take more Newton iterations, the norm of the nonlinear residual* $\|F(u^{(k)})\|$ *starts approaching zero. This leads to tightening the linear solver tolerance in a progressive manner as more Newton iterations are performed. Forcing terms represents an upper bound of the ratio between the norm of the linear residual and the norm of the nonlinear residual. As more line-search backtracking steps are performed, this ratio increases, justifying the increasing behavior of the sequence* $\{\eta^{(k,i)}\}_{i=0}^{\infty}$.

8.2.2 Choice of Forcing Terms

Several forcing terms (functions) have been widely used in the literature ([31], [33], [32]). Those are based on heuristic choices of η and suitable safeguards to provide an efficient mechanism to avoid over-solving the linearized system of equations without affecting the convergence of the method. It has been observed that the two choices listed in Table 8.1 work well in practice. The first choice reflects the agreement between F and its linear model at the previous iteration. With this choice, the linear solver tolerance is larger when the Newton step is not that close to the solution and smaller when the step is more likely to lead to a good approximation. More discussion on this choice of η can be found in [31]. The second choice in Table 8.1 reflects the size of decrease between the function evaluated at the current iterate and the function at the previous iterate. Suitable choice of the parameters γ and α and the reasoning behind it are provided in [31] and [33]. In our implementation, i.e.

Choice 1:	Choice 2:
$\eta^k = \min\left\{\eta_{\max}, \max\left(\tilde{\eta}^k, \left(\eta^{k-1}\right)^2\right)\right\}$	$\eta^k = \max\left\{\tilde{\eta}^k, \gamma\left(\eta^{k-1}\right)^2\right\}$
$\tilde{\eta}^k = \dfrac{\left\lvert \left\|F(u^k)\right\| - \left\|F(u^{k-1}) + J(u^{k-1})s^{k-1}\right\| \right\rvert}{\|F(u^{k-1})\|}$	$\tilde{\eta}^k = \gamma\left(\dfrac{\left\|F(u^k)\right\|}{\|F(u^{k-1})\|}\right)^{\alpha}$
We used $\eta_{\max} = 0.9999$	where α and γ are parameters to be chosen. Typical values are ($\alpha = 2$, $\gamma = 0.9$) and ($\alpha = \frac{1+\sqrt{5}}{2}$, $\gamma = 1$)

Table 8.1: Different Choices of Forcing Terms

in IPARS, $\eta_{\max} = 0.9999$, $\eta_{\text{initial}} = 0.5$. It should be noted that the contraction factor θ is to be obtained by solving a minimization problem of the function $g(\theta) = \|F(u^{(k)} + \theta s^{(k)})\|^2$. An optimal value of θ is the one which minimizes $g(\theta)$. Different ways of choosing θ are discussed in the next section.

8.3 Contraction Factor Minimization Models

We next discuss the selection of the contraction factor θ in line (7) in the Algorithm 13. It is chosen such that θs^k is a decent direction of $f(u^{(k+1)}) = \frac{1}{2}F(u^{(k+1)})^T F(u^{(k+1)})$ (i.e. $\nabla f(u^{(k)})^T(\theta s^k) = F(u^{(k)})^T J(u^{(k)})(\theta s^k) < 0$) and satisfies the sufficient decrease condition (also known as the Armijo condition):

$$f(u^{(k)} + \theta s^k) \leq f(u^{(k)}) + t\nabla f(u^{(k)})^T(\theta s^k)$$

where t is a small fixed constant (in Algorithm 13, t = 0.0001). In practice, the contraction factor θ can be determined in a number of different ways. The optimal way is to solve a minimization problem for the function $g(\theta) = \|F(u^{(k)} + \theta s^{(k)})\|^2$. Since the additional computational cost associated with finding the exact minimum of $g(\theta)$ (more nonlinear residuals have to be calculated) might not always pay off, we also consider some simplifications. In our work, the value of θ can be determined by one of the following:

- Choose any fixed value $\theta \in [0.1, 0.5]$ for a contraction factor, typically $\theta = 0.5$
- Solve approximately the problem of minimizing $g(\theta)$

The second choice is realized by constructing an approximation of $g(\theta)$ using either a two or three point parabolic model. More details can be found in [31, 49]. We have implemented three different minimization algorithms for obtaining the optimal value of θ.

- **"Algorithm (1)":**

  This algorithm builds a second degree interpolating polynomial for interpolating $g(\theta)$ by using the values of g and g' at $\theta = 0$ [49]. The main steps can be described as follows:

Algorithm 14: Algorithm (1) - Optimal value of Contraction Factor θ

Try initial/current θ, call it θ_c
if *θ_c is rejected* **then**
  obtain the values of $g(0)$ and $g'(0)$ as follows:

$$g(0) = \|F(u^{(k)})\|^2$$
$$g'(0) = 2(J(u^{(k)})^T s^{(k)})^T F(u^{(k)}) = 2F(u^{(k)})^T J(u^{(k)}) s^{(k)}$$
$$= 2F(u^{(k)})^T(-F(u^{(k)}) + r^{(k)}) = -2F(u^{(k)})^T F(u^{(k)}) + 2F(u^{(k)})^T r^{(k)}$$

  if $g'(0) \geq 0$ **then**
    $\theta = 0.5$
  else
    Minimize the quadratic polynomial: $p(\theta) = g(0) + g'(0)\theta + c\theta^2$ where,
    $c = \frac{g(\theta_c) - g(0) - g'(0)\theta_c}{{\theta_c}^2}$
    $\theta = -\frac{g'(0)}{2c}$

- **"Algorithm (2)":**

  This algorithm also builds a three-point parabolic model but avoids the need to compute g'(0) [49]. The main steps are as follows:

Algorithm 15: Algorithm (2) - Optimal value of Contraction Factor θ

Try $\theta = 0.5$, then $\theta = 0.25$.
if *both values are rejected* **then**
    Let the last two rejected values of θ be θ_1 and θ_2. Perform a quadratic interpolation of $(0, g(0)), (\theta_1, g(\theta_1))$, and $(\theta_2, g(\theta_2))$:
    Set:

$$p(\theta) = g(0) + \frac{\theta}{\theta_2 - \theta_1}\Big(\frac{(\theta - \theta_1)(g(\theta_2) - g(0))}{\theta_2} + \frac{(\theta_2 - \theta)(g(\theta_1) - g(0))}{\theta_1}\Big)$$

$$p''(\theta) = \frac{2}{\theta_2\theta_1(\theta_2 - \theta_1)}(\theta_1(g(\theta_2) - g(0)) - \theta_2(g(\theta_1) - g(0)))$$

    if $p''(\theta) > 0$ **then**
        set $\theta = -\frac{p'(0)}{p''(0)}$
    else
        Set $\theta = 0.5$

- **"Algorithm (3)":**

  This algorithm is similar to the previous two as it builds a second degree interpolating polynomial but using a basic Lagrange quadratic model [50]. The main steps are as follows:

Algorithm 16: Algorithm (3) - Optimal value of Contraction Factor θ

Build a basic Lagrange quadratic polynomial model using the last three rejected values of θ. (Initially, we choose $\theta_0 = 1$, $\theta_1 = 0.5$, and $\theta_2 = 0.25$).
if *The second derivative is positive* **then**
    The model has a local minimum, and we set θ to be the minimizer of the model.
else
    Set $\theta = 0.5$

8.4 Implicit Two-phase Model Results

In this section, we illustrate the advantages of the global inexact Newton method with the linesearch backtracking for two-phase fully implicit flow model (in IPARSv2.1). Based on our obtained results and findings, we will extend this work to multirate iteratively coupled problems in the next section. The efficiencies of three different nonlinear solver strategies will be compared:

- **Method 1:** The global inexact Newton method with forcing function, globalized by linesearch backtracking. It corresponds to the curves labeled "Forcing and Backtracking" in the results.

- **Method 2:** Inexact Newton method with forcing function but without linesearch backtracking. In this method we avoid the cost of backtracking but might find a local instead of global minimum of $F(u^k)$. In order to provide more "global" convergence properties, we dampen the forcing function by a constant user-defined factor $df \in (0, 1]$. That is, in line (4) in Algorithm 13 we are finding s^k such that:

$$J(u^k)s^k = -F(u^k) + r^{(k)} \quad \text{with} \quad \frac{\left\|r^{(k)})\right\|}{\|F(u^k)\|} \leqslant df \times \eta^k$$

  The corresponding curves are labeled "Forcing and No Backtracking".

- **Method 3:** Traditional "Exact" Newton method: we emulate it by using forcing with a fixed very small value of the forcing term η^k for all iterations. For both our SPE10 tests and iteratively coupled problems, we use $\eta^k =$ 1.E-6 for all nonlinear flow iterations. This approach has the drawback of keeping the linear solver tolerance too tight and and thus, oversolving the linear system.

8.4.1 SPE10 First Layer Results

This test case models a two phase flow (oil and water) and uses the highly heterogeneous permeability field from the SPE10 benchmark problem [27]. The permeability varies over 15 orders of magnitude; the top 50 layers are fluvial and the bottom 35 layers are highly channelized. The original 3D domain has size $170 \times 1200 \times 2200$ ft at a depth of 12000

ft, with a uniform discretization into $85 \times 60 \times 220 = 1.112$ million elements. In this case we used only the top layer, with $60 \times 220 = 13,200$ elements. We used a constant porosity of 0.3. Other data includes fluid viscocities $\mu_w = 0.3$, $\mu_o = 3.0$ cP and fluid compressibilities $c_w =$ 3.1E-6, $c_o =$ 4.2E-5 psi^{-1}. The initial conditions are taken to be oil pressure $p_o(0) = 6000$ psi and water saturation $S_w = 0.201$. There is a five-spot well pattern for well configuration. All wells are vertical and fully perforated. Water is injected in the center of the reservoir with BHP of 10000 psi and each of the four oil producers in the corners operate at BHP of 4000 psi. All wells start operating at the beginning of the simulation and the total simulation time is 2000 days.
The solver-related parameters we used are as follows:

- Nonlinear solver tolerance = 1.E-4 with maximum number of Newton iterations = 200
- Linear solver tolerance (initial for Methods 2 and 3 that use forcing function) = 1.E-6 with maximum number of linear iterations = 1000
- Forcing choice 1:

$$\tilde{\eta}^k = \frac{\left| \left\| F(u^{(k)}) \right\| - \left\| F^(u^{(k-1)}) + J(u^{(k-1)}) s^{k-1} \right\| \right|}{\| F(u^{(k-1)}) \|} \quad \eta^k = \min \left\{ \eta_{\max}, \max \left(\tilde{\eta}^k, \left(\eta^{k-1} \right)^2 \right) \right\}$$

- Constant contraction factor $\theta = 0.5$: the simplest, s^k is shrunk in half on each backtracking iteration

With respect to time step sizes, we consider two cases:

- Case (1): Gradual increase in time steps (in days): $\Delta t = 0.0005$ for $t \in [0, 0.001]$, $\Delta t = 0.001$ for $t \in [0.001, 0.01]$, $\Delta t = 0.01$ for $t \in [0.01, 0.1]$, $\Delta t = 0.1$ for $t \in [0.1, 1.0]$, $\Delta t = 0.5$ for $t \in [1.0, 5.0]$, and $\Delta t = 1.0$ for $t \in [5.0, 500]$.
- Case (2): Aggressive time stepping, i.e. taking Δt as in the following sequence: $\Delta t = (1.0, 2.0, 4.0, 8.0, ..,)$ with a maximum value of 300 days.

For Case (1), the CPU running times versus the number of simulation days are shown in figure 8.1a. Figure 8.1b shows the accumulated number of nonlinear iterations versus the number of simulated days for the SPE10 first layer model. The global inexact Newton method (Method 1) requires more nonlinear iterations compared to the inexact Newton method with forcing functions (Method 2), as well as the inexact Newton method without the use of forcing function (Method 3). Figure 8.1c shows the accumulated number of linear iterations versus the number of simulated days for the SPE10 first layer model. It is clear from the graph that the global inexact Newton method (Method 1) requires fewer linear iterations compared to the case of the inexact Newton method (not globalized by line-search backtracking) when the forcing function is damped by a factor of 0.1 (Method 2, $df = 0.1$).

For Case (2), CPU runtimes vs. simulation time are shown in Figures 8.2a and 8.2b. It can be seen that all cases except the global inexact Newton method (Method 1) and the inexact Newton method with damped forcing (Method 2, $df = 0.1$ or 0.2) failed to provide physical solution past 30 days (we got out-of-bounds saturations). After 60 days, (Method 2, $df = 0.2$) also failed. From the two methods left, (Method 1) globalized by linesearch backtracking provides **10%** reduction in computational time when compared to (Method 2, $df = 0.1$).

Inexact Newton method with heuristic damping of the forcing term is inadequate in assuring global Newton convergence unless severe damping is performed. This provides a clear hint that for iteratively coupled problems, this strategy (Method 2) should be avoided.

8.4.2 SPE10 Full Model Results

In this case, we run the full SPE10 model case described in the previous example, with the same parameters, for the two-phase fully implicit problem combined with line search backtracking in IPARS. The run was carried out in parallel (on Bevo3, on 16 processors). The model size now is 1,122,000 grid elements - 3D ($85 \times 60 \times 220$), and total simulation time is 1000 days. The same solver parameters were used as in the previous case.

We followed a graduate time stepping approach as follows (unit is days):

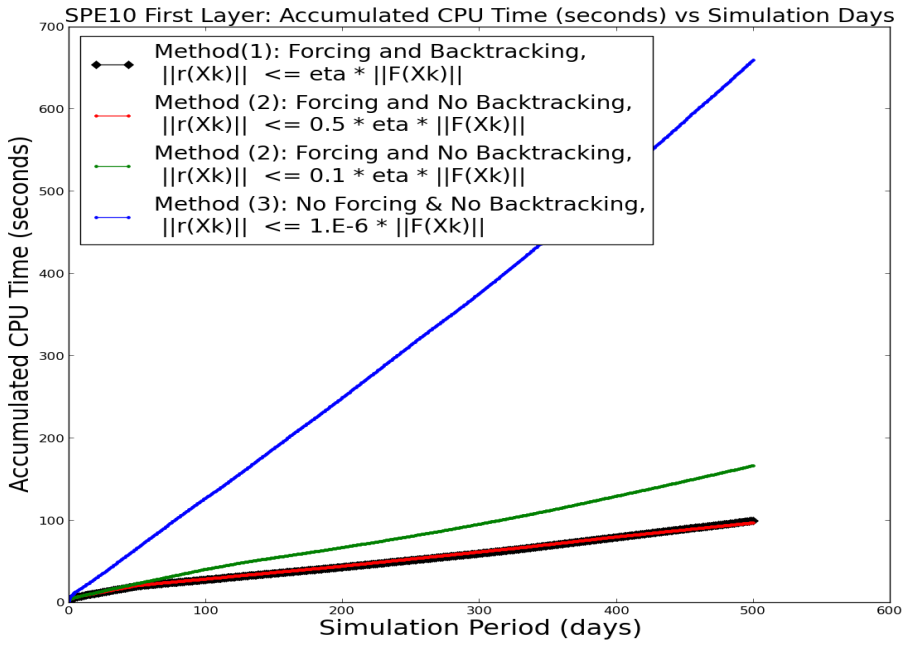

(a) Running Time vs Simulation Days, gradual increase in time steps, with a maximum value of 1.0 day. The global inexact Newton method (Method 1) and the inexact Newton method (Method 2, $df = 0.5$) have similar running times. However, in (Method 1), we are confident that the global solution is achieved, as the sufficient decrease condition is maintained in every Newton iteration.

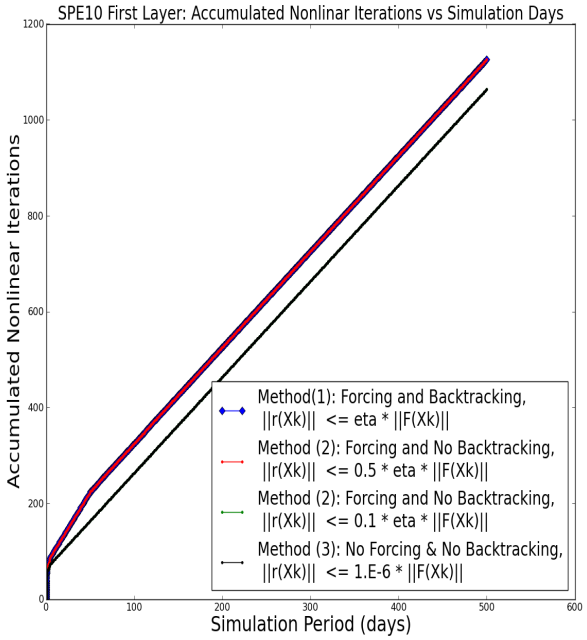

(b) Accumulated Number of Nonlinear Iterations vs Simulation Days (500 simulation days)

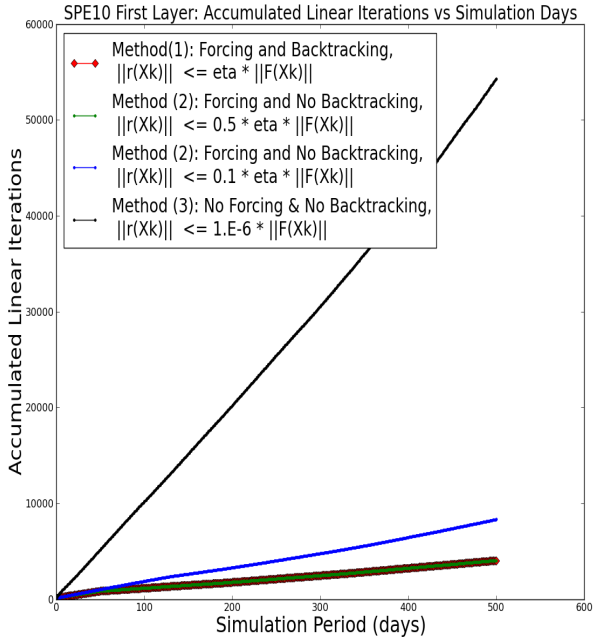

(c) Accumulated Number of Linear Iterations vs Sim--ulation Days (500 simulation days)

Figure 8.1: SPE10 First Layer Results

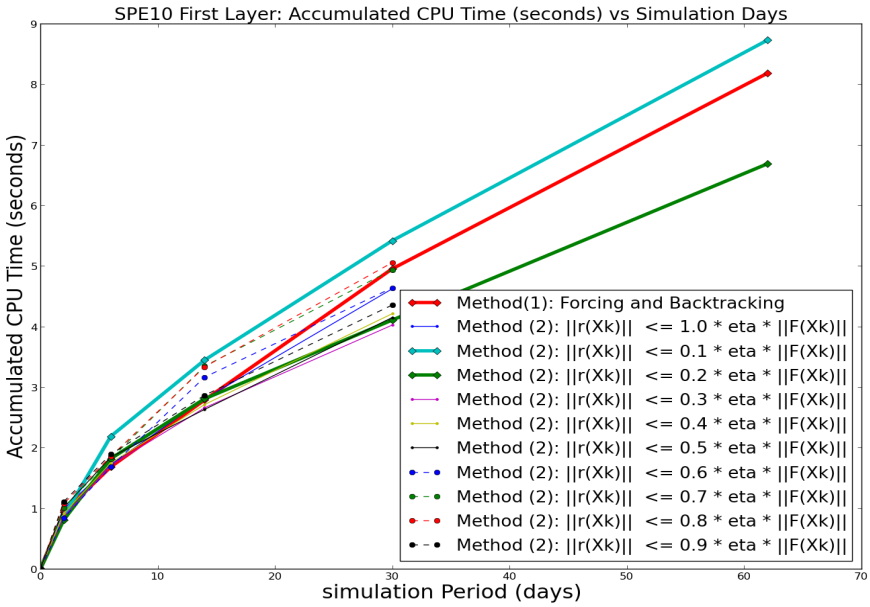

(a) Running time vs simulation days, aggressive time steps: $\Delta t = (1.0, 2.0, 4.0, 8.0, ..,)$ with a maximum value of 300 days (for the first 60 days). Only the global inexact Newton method (Method 1) and the inexact Newton method (Method 2, $df = 0.1$ and 0.2) made the run bevond 30 simulation davs.

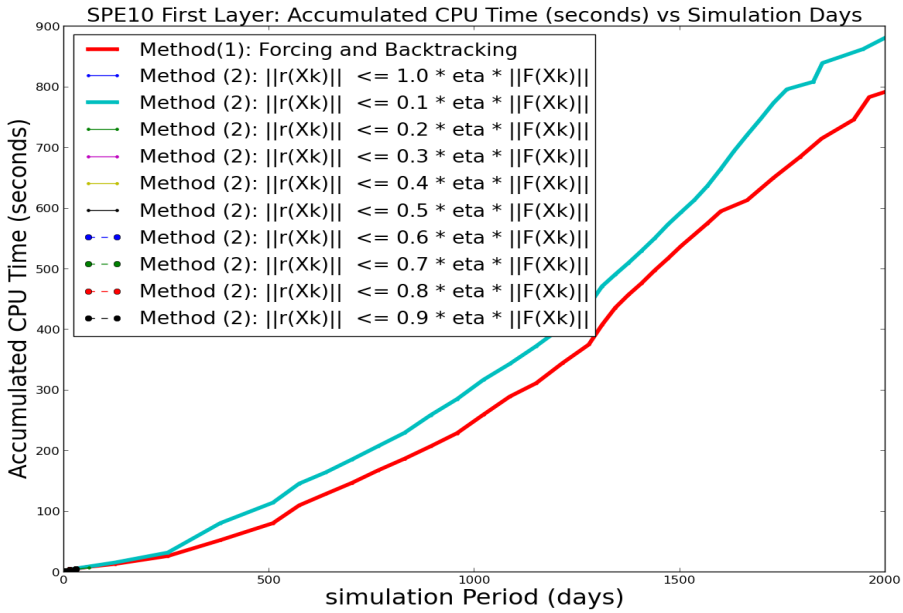

(b) Running time vs simulation days, aggressive time steps: $\Delta t = (1.0, 2.0, 4.0, 8.0, ..,)$ with a maximum value of 300 days (for 2000 days). Time step cutting (reduction by a factor of 0.5) is performed when convergence is not achieved. Only the global inexact Newton method (Method 1) and the inexact Newton Method (Method 2, $df = 0.1$) were able to proceed. (Method 1) results in **10%** reduction in computational time.

Figure 8.2: SPE10 First Layer Results (serial run): Running Times vs Simulation Days

- for $t \in [0, 0.001], \Delta t = 0.00007$ with a multiplier of 1.25, $\Delta t \in [0.00007, 0.001]$
- for $t \in [0.001, 0.1], \Delta t = 0.001$ with a multiplier of 1.01, $\Delta t \in [0.001, 0.1]$
- for $t \in [0.1, 1.0], \Delta t = 0.01$ with a multiplier of 1.01, $\Delta t \in [0.01, 0.1]$
- for $t \in [1.0, 5.0], \Delta t = 0.1$ with a multiplier of 1.01, $\Delta t \in [0.1, 0.5]$
- for $t \in [5.0, 10.0], \Delta t = 0.5$ with a multiplier of 1.01, $\Delta t \in [0.5, 1.0]$
- for $t \in [10.0, 1000.0], \Delta t = 1.0$ with a multiplier of 1.01, $\Delta t \in [1.0, 5.0]$

The CPU running times and numbers of nonlinear and linear iterations (all versus the number of simulation days) are shown in figures 8.3a, 8.4a, and 8.4b respectively. It is clear by figure 8.3a that for the full SPE10 model, running in parallel, the global inexact Newton method, globalized by line search backtracking (Method 1), results in 58% of computational time savings compared to the case when the forcing function is damped by a factor of 0.5 (Method 2, $df = 0.5$). In addition, (Method 1) results in 75% of computational time savings compared to the case when the forcing function is damped by a factor of 0.1 (Method 2, $df = 0.1$). Moreover, we observe that even though the number of nonlinear iterations for (Method 1) increases (as shown in figure 8.4a), the number of linear iterations is substantially smaller (as shown in figure 8.4b) and the overall result is a significant reduction in CPU runtime. This phenomena (i.e. the increase in the number of nonlinear iterations for (Method 1)) is due to incorporating the linesearch backtracking algorithm into the inexact Newton method nonlinear solver.

We note that for the full SPE10 model, (Method 3) resulted in the longest running time. The blue curve in figure 8.5 shows the CPU run time for (Method 3) for the full SPE10 model. The huge increase in CPU runtime is a consequence of oversolving the linear system. The simulation was stopped simulating 100 days.

The global inexact Newton method (globalized by line search backtracking) will be used to solve the nonlinear flow problem in the context of iteratively coupled flow and geomechanics single rate and multirate problems.

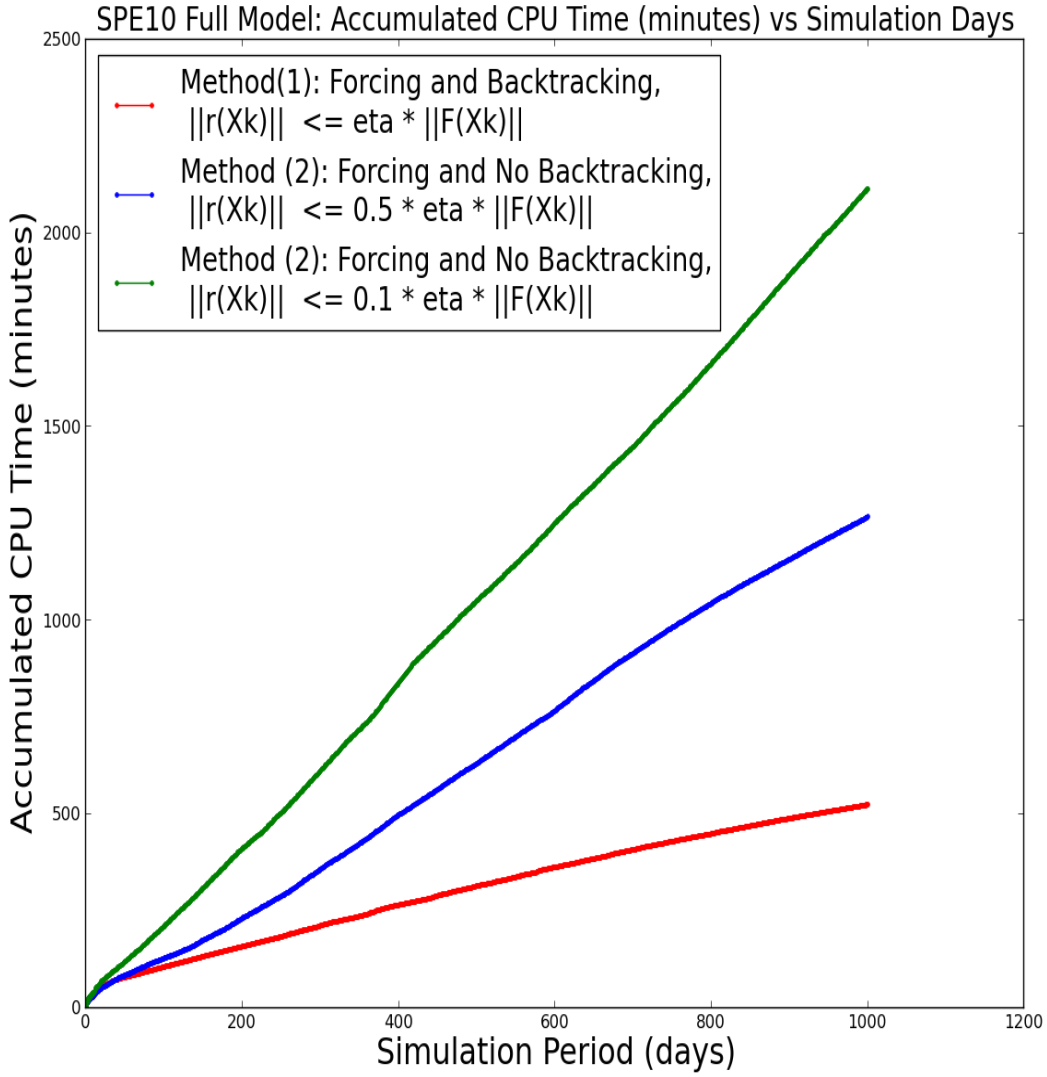

(a) Running time vs simulation days for the full SPE10 model (1000 simulation days). The global inexact Newton method (Method 1) results in **58%** of computational time savings compared to the case of the inexact Newton method (Method 2, $df = 0.5$). In addition, (Method 1) results in 75% of computational time savings compared to the case of (Method 2, $df = 0.1$).

Figure 8.3: Full SPE10 Model Runtime Results (parallel run on Bevo3 cluster, 16 processors).

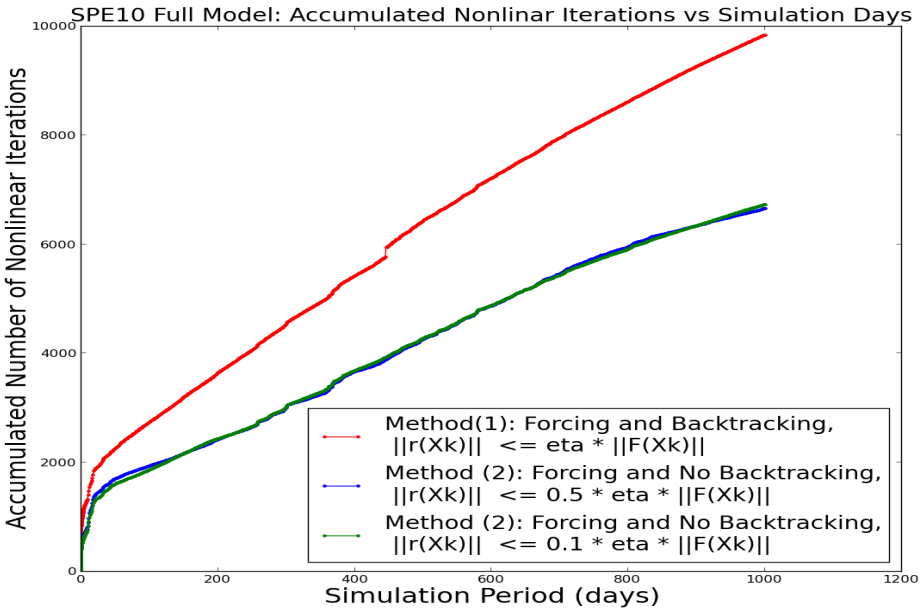

(a) Accumulated number of nonlinear iterations vs simulation days for the full SPE10 model (1000 simulation days). The global inexact Newton method (Method 1) results in a larger number of nonlinear iterations (increased by **32%**) compared to the inexact Newton method (Method 2, $df = 0.5$ and 0.1).

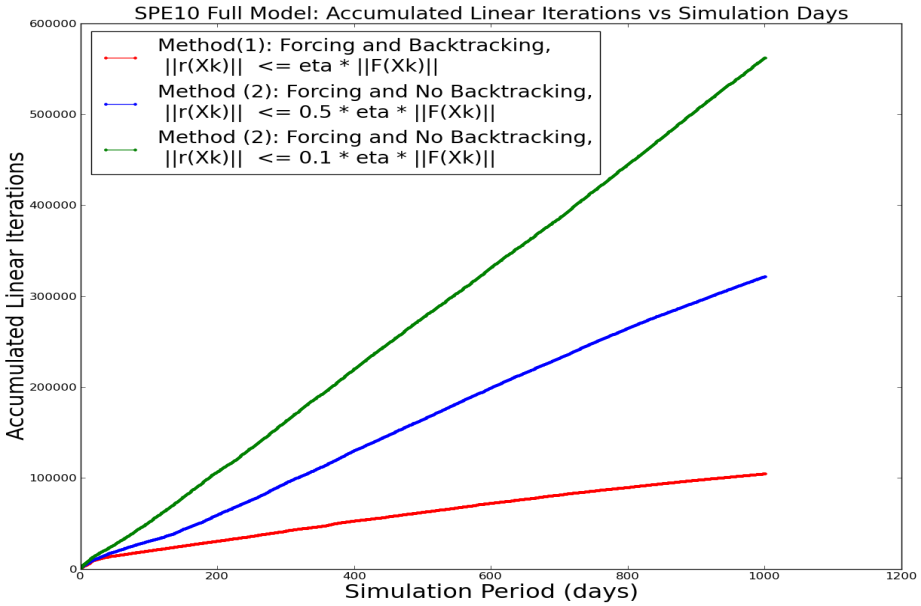

(b) Accumulated number of linear iterations vs simulation says for the full SPE10 model (1000 simulation days). The global inexact Newton method (Method 1) results in **68%** reduction in the number of linear iterations compared to the case of the inexact Newton method (Method 2, $df = 0.5$). In addition, it results in **82%** "linear iterations" reduction compared to the case of (Method 2, $df = 0.1$).

Figure 8.4: Full SPE10 Model Linear and Nonlinear Iterations Results (parallel run on Bevo3 cluster, on 16 processors).

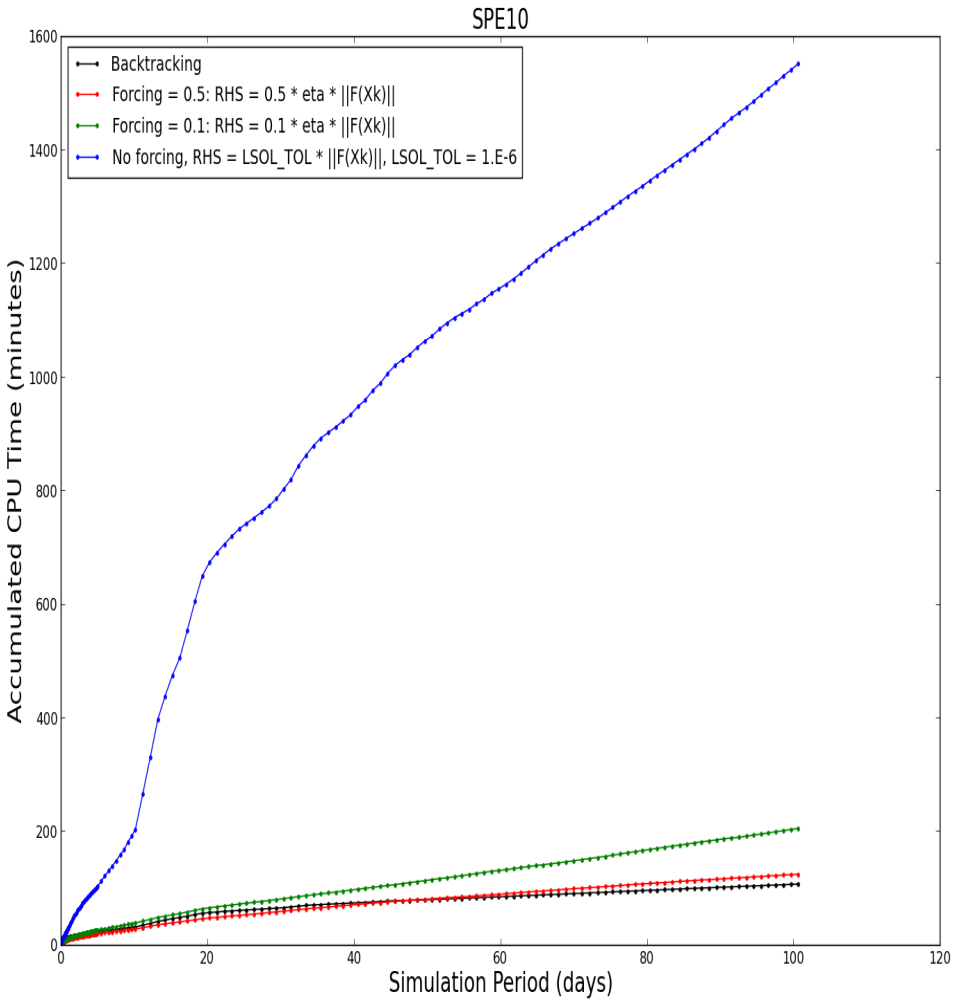

Figure 8.5: Running times vs simulation days for 100 days of simulation, (full SPE10 model, parallel run). The blue curve shows the run time for (Method 3). This result shows that for large and challenging reservoir models, as in the case of the full SPE10 model, the use of a small fixed linear solver tolerance value, as in (Method 3), can increase the run time dramatically. In contrast, (Method 2) reduces the run time but does not ensure global convergence. The global inexact Newton method, globalized by line search backtracking i.e. (Method 1), reduces the CPU run time efficiently, while ensuring global convergence. For multirate iteratively coupled problems, ensuring global convergence for the flow problem is of high importance as the accuracy of the obtained solution directly affects the number of flow-mechanics coupling iterations and hence the efficiency of the scheme. Therefore, we will be comparing the efficiency of (Method 1) versus (Method 3) for coupled flow and geomechanics problems in the next section.

8.4.3 Comparison Between Contraction Factor Optimization Algorithms

Figure (8.6) shows a comparison of the three different algorithms used to obtain the optimal value of the contraction factor "θ" used in the line search backtracking algorithm when applied to the SPE10 first layer model. From such preliminary results, "Algorithm (2)" is the most computationally efficient algorithm among the three. However, the efficiency of the minimization model implemented in "Algorithm (2)" is very comparable to the heuristic case in which the solution vector is shrinked by half in every backtracking iteration (contraction factor value of "$\theta = 0.5$" across all backtracking iterations). Therefore, for simplicity and ease of implementation, we will follow this approach when solving the nonlinear flow problem in iteratively coupled problems. Form our obtained results, we can draw the following conclusions:

- The line search backtracking globalization approach combined with forcing functions (Method 1) helps taking aggressive time steps while ensuring convergence. This results in 10% reduction of the overall CPU running time compared to the inexact Newton method (Method 2, $df = 0.1$) for the SPE10 first layer example.
- The line search backtracking globalization approach combined with forcing functions (Method 1) helps "loosening" the linear solver tolerance, while convergence is always ensured by continuously checking the sufficient decrease condition. For the full SPE10 model running in parallel, This approach results in 58% of computational time savings compared to the case when the forcing function is damped by a factor of 0.5 (Method 2, $df = 0.5$). In addition, it results in 75% of computational time savings when the forcing function is damped by a factor of 0.1 (Method 2, $df = 0.1$).
- The CPU computational time savings we obtained tend to increase as we increase the period of the simulation (number of simulated days). For instance, compare computational time savings of 75% (for the full SPE10 model simulating 1000 days) to 10% (for the first layer SPE10 model simulating 500 days). Running long simulations is typical in reservoir simulation, which makes this strategy (Method 1) very attractive. In the case of the full SPE10 model, this results in huge time savings (a factor of 58% compared to the case of (Method 2, $df = 0.5$).

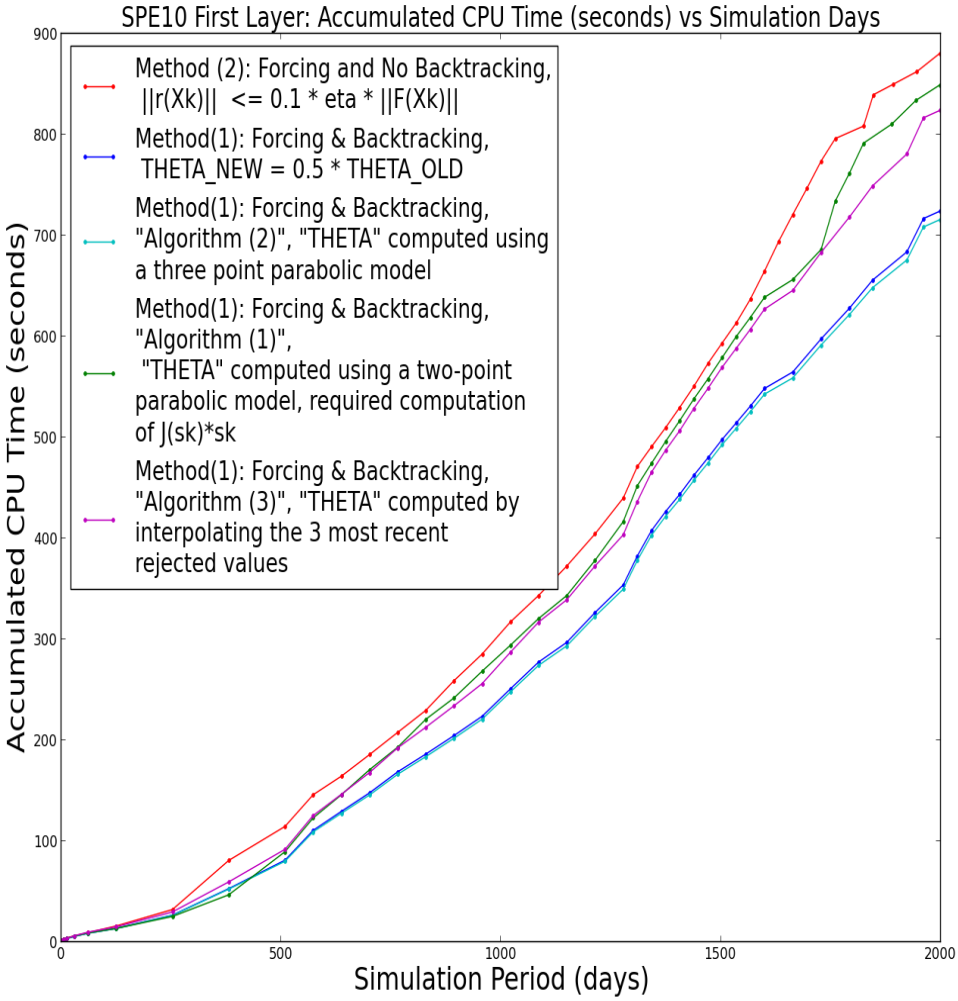

Figure 8.6: Comparison of different optimization algorithms for obtaining the value of θ for the SPE10 first layer model. We conclude that the efficiency of choosing $\theta = 0.5$ for all line-search backtracking iterations is comparable to the efficiency of the optimal algorithm (Algorithm (2): the three point parabolic model). Due to its simplicity and optimality, we will follow this approach ($\theta = 0.5$ for all line-search backtracking iterations) when solving the flow problem in multirate iteratively coupled problems.

- The results we obtained vary based on several input parameters (maximum number of Newton iterations, maximum number of linear iterations, and the sequence of timesteps specified)
- Overall, the line search backtracking computational time savings obtained by either taking aggressive time stepping or by loosening the linear solver tolerance overshadow the additional overhead of computing the right hand side at every Newton nonlinear iteration (to check the sufficient decrease condition).
- The inexact Newton method with a heuristic damping of the forcing term without incorporating the line-search backtracking algorithm (Method 2) does not necessarily ensure global convergence of the Newton iteration unless severe damping of the forcing term is enforced. For iteratively coupled problems (to be considered in the next section), we will abandon this strategy and compare the results of (Method 1) to (Method 3) when solving the nonlinear flow problem.
- Based on the comparison shown in figure 8.6, we will be using a contraction factor of the value of "$\theta = 0.5$" across all backtracking iterations in iteratively coupled problems (to be considered in the next section).

8.5 Iteratively Coupled Problems (Implicit Two-phase Flow Model Coupled with Geomechanics) Results

In this section, we provide an implementation of the global inexact Newton method as a nonlinear solver framework for the flow problem in iteratively coupled flow and mechanics problems. The global inexact Newton method, globalized by line-search backtracking, helps reducing the number of flow linear iterations, while ensuring that the sufficient decrease condition is satisfied at every Newton iteration. In contrast, the multirate coupling algorithm helps reducing the number of mechanics linear iterations, as illustrated earlier. Combining the two approaches (the multirate scheme for the coupled problem along with the global Inexact Newton method for flow) results in reducing both the number of flow and mechanics linear iteration, while maintaining an acceptable level of accuracy. The combined scheme is illustrated in figure 8.7.

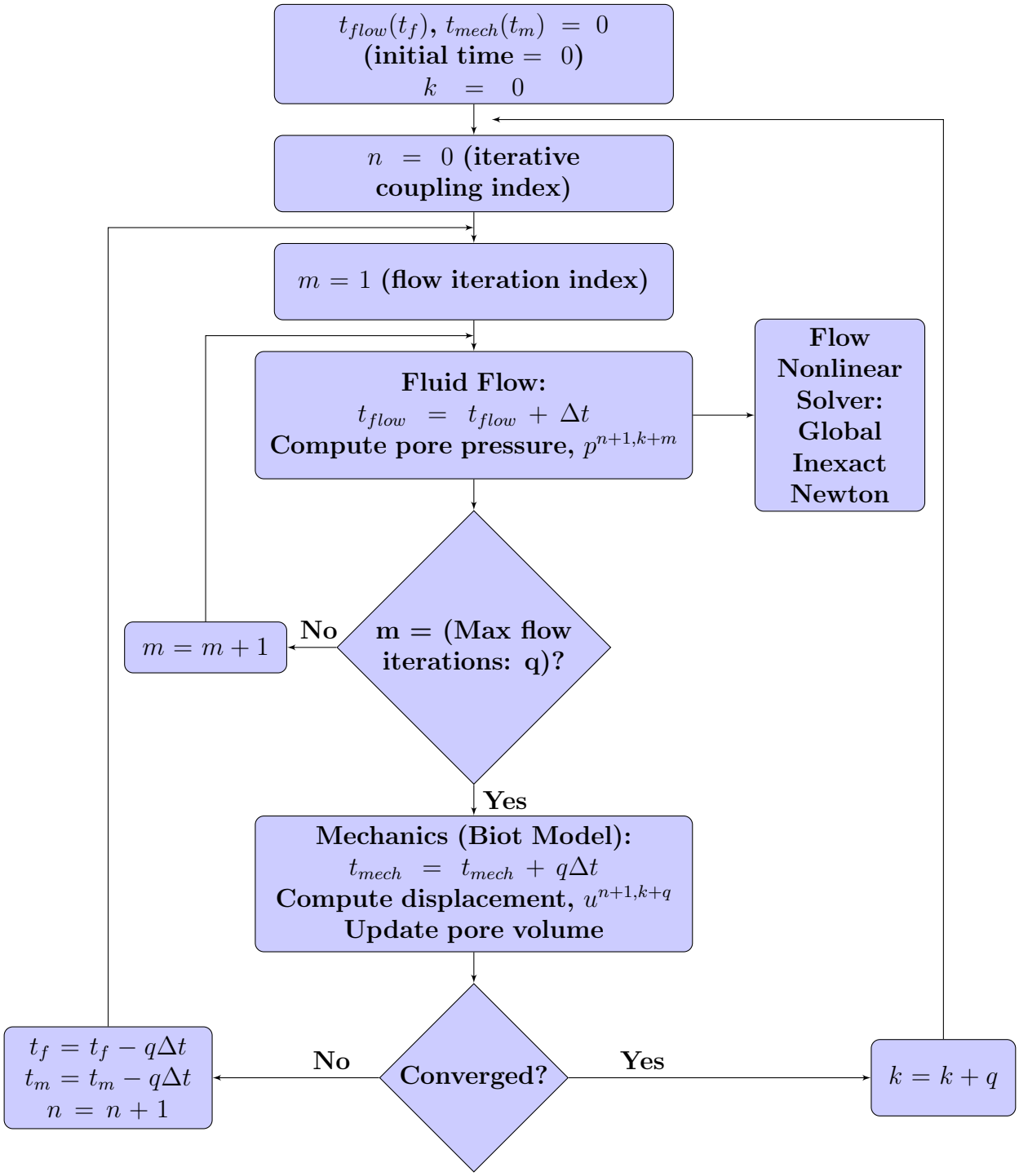

Figure 8.7: Multirate Iterative Flow and Mechanics Coupling Algorithm with The Global Inexact Newton Method as a Nonlinear Solver Framework.

8.5.1 Test Case: Frio Field Model

The scheme described in figure 8.7 is implemented in IPARS for the two-phase implicit MFMFE flow model coupled with linear elasticity. We consider the Frio field model (studied and described in Chapters 2 and 4). The model input specifications are shown in Table 8.2. The simulation is run for five different cases, as follows:

- Case (1): Single Rate Iterative Coupling ($q = 1$) with "Exact Newton" flow solve (Method 3: no forcing and no backtracking, $\eta^{(k)} = 1.E-6$, for all backtracking iterations, indexed by "k").
- Case (2): Multirate Iterative Coupling ($q = 2$) with "Global Inexact Newton" flow solve (Method 1: forcing and backtracking).
- Case (3): Multirate Iterative Coupling ($q = 4$) with "Global Inexact Newton" flow solve (Method 1: forcing and backtracking).
- Case (4): Multirate Iterative Coupling ($q = 8$) with "Global Inexact Newton" flow solve (Method 1: forcing and backtracking).
- Case (5): Multirate Iterative Coupling ($q = 16$) with "Global Inexact Newton" flow solve (Method 1: forcing and backtracking).

We expect the first case to result in the largest number of both flow and mechanics linear iterations. This overhead should lead to an increase in the CPU time as well.

8.5.2 Results

Figures 8.8 and 8.9 show the water pressure and saturation profiles after 48.0 days of simulation for the five different cases. In addition, figures 8.10, 8.11, and 8.12 show the displacements in the x, y, and z directions after 48.0 days of simulation. The five cases result in almost identical solutions, with minor mismatches near wells for higher values of q ($q > 4$) - nearly invisible -. This is primarily due to the multirate nature of the scheme (as expected), and is not a result of the global Inexact Newton method. In general, the five different cases result in similar pressure and saturation profiles.

Wells:	3 production wells, 6 injection well
Injection well (1):	Pressure specified, 4000.0 psi
Injection well (2):	Pressure specified, 3300.0 psi
Injection well (3):	Pressure specified, 4000.0 psi
Injection well (4):	Pressure specified, 4400.0 psi
Injection well (5):	Pressure specified, 3700.0 psi
Injection well (6):	Pressure specified, 4400.0 psi
Production well (1):	Pressure specified, 2000.0 psi
Production well (2):	Pressure specified, 2000.0 psi
Production well (3):	Pressure specified, 2000.0 psi
Total Simulation time:	56.0 days
Fine flow time step:	$\Delta t = 0.01$ for $t \in [0.0, 8.0]$ days $\Delta t = 0.02$ for $t \in [8.0, 16.0]$ days $\Delta t = 0.05$ for $t \in [16.0, 24.0]$ days $\Delta t = 0.1$ for $t \in [24.0, 32.0]$ days $\Delta t = 0.25$ for $t \in [32.0, 40.0]$ days $\Delta t = 0.50$ for $t \in [40.0, 56.0]$ days
Number of grid elements:	891 grids ($33 \times 9 \times 3$)
Absolute Permeabilities: k_{xx}, k_{yy}, k_{zz}	highly varying, range: (5.27E-10, 3.10E+3) md
Initial porosity, φ_0:	0.2
Water viscosity, μ_w:	1.0 cp
Oil viscosity, μ_o:	2.0 cp
Water compressibility c_w:	1.E-6 (1/psi)
Oil compressibility c_o:	1.E-4 (1/psi)
Rock compressibility:	1.E-6 (1/psi)
Rock density:	165.44 lb_m/ft^3
Initial water density, ρ_w:	62.34 lb_m/ft^3
Initial oil density, ρ_o:	56.0 lb_m/ft^3
Initial oil pressure, p_o:	400.0 psi
Initial water saturation, S_w:	0.2
Young's Modulus (E):	5.E5 psi
Possion Ratio, ν:	0.4
Biot's constant, α:	1.0
Biot Modulus, M:	1.0E8 psi
$\lambda = \frac{E\nu}{(1+\nu)(1-2\nu)}$:	714286.0 psi
Flow boundary bonditions:	no flow boundary condition on all 6 boundaries
Mechanics B.C.:	
"X+" boundary (EBCXX1()):	$\sigma_{xx} = \sigma \cdot n_x = 12,000psi$, (overburden pressure)
"X-" - boundary (EBCXXN1()):	$\boldsymbol{u} = 0$, zero displacement
"Y+" - boundary (EBCYY1()):	$\boldsymbol{u} = 0$, zero displacement
"Y-" - boundary (EBCYYN1()):	$\sigma_{yy} = \sigma \cdot n_y = 6000psi$
"Z+" - boundary (EBCZZ1()):	$\boldsymbol{u} = 0$, zero displacement
"Z-" - boundary (EBCZZN1()):	$\sigma_{zz} = \sigma \cdot n_z = 1000psi$

Table 8.2: Input Parameters for the Frio Field Model

Figure 8.13a shows the accumulated CPU runtime for the whole simulation run in the five different cases. We see a monotonically decreasing trend in CPU runtime up to $q = 8$, which corresponds to Case (4). However, the CPU runtime starts increasing again for $q = 16$, which corresponds to Case (5). This is due to the fact that for larger values of q, the algorithm requires more iterative coupling iterations to converge for each coarse mechanics time step, as shown in figure 8.13d. More iterative coupling iterations result in more flow and mechanics linear iterations which, in turn, increase the overall CPU runtime, as shown in figures 8.13b and 8.13c. Table 8.3 shows the computational time savings for Case (2), (3), (4), and (5) relative to Case (1).

From the above results, we can draw the following conclusions:

- The global Inexact Newton method (Method 1: forcing with backtracking) helps reducing the number of consumed flow linear iterations in the multirate iteratively coupled scheme compared to the single rate scheme with the exact Newton flow solve (Method 3). In general, subject to the value of the coupling iteration tolerance, the time step size, and other input parameters, the multirate iteratively coupled scheme might result in an increase in the number of flow linear iterations (if we do not incorporate the global inexact Newton method for the nonlinear flow solve, as in the case of figure 2.8c in Chapter 2). The obtained results suggest that this problem (i.e. the increase in the number of flow linear iterations in the multirate scheme) can be alleviated if the global inexact Newton method is used for the flow solve.

- Larger values of q result in more iterative flow-mechanics coupling iterations. This can increase the number flow and mechanics linear iterations, and hence spoil the computational time savings obtained by combining the multirate coupling algorithm with the global inexact Newton method for the flow solve (the case of $q = 16$).

- We conclude that for multirate iteratively coupled problems, (Method 1) is highly recommended for solving the nonlinear flow problem. Provided that the value of q is not very large, the combined scheme (multirate coupling with the global inexact

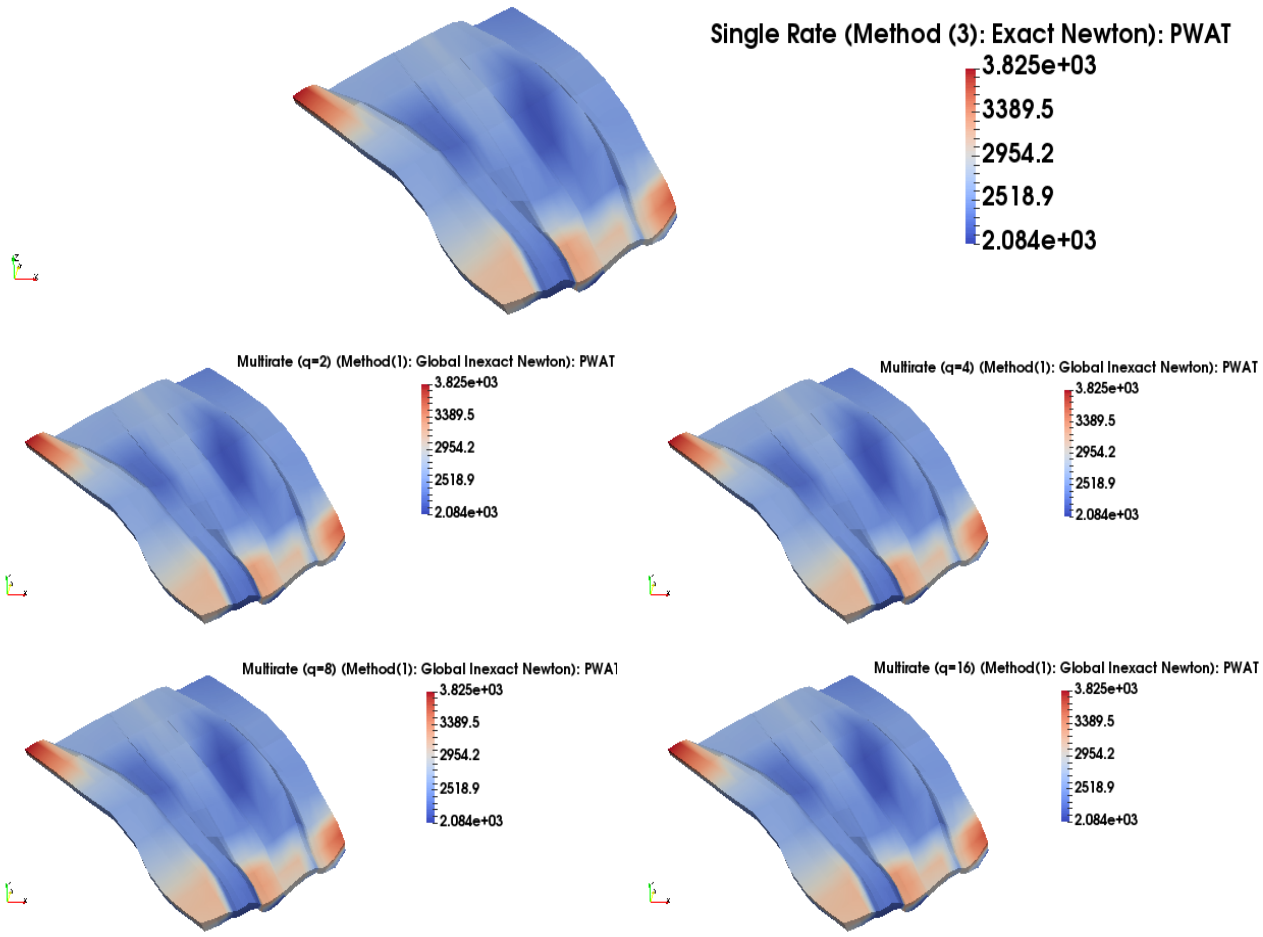

Figure 8.8: Water Pressure Profiles (psi) of the Frio Field Model after 48.0 Simulation Days for the Five Different Cases.

Newton method for the flow solve) efficiently reduce the number of flow and mechanics linear iterations, without affecting the accuracy of the solution. This leads to substantial CPU time savings.

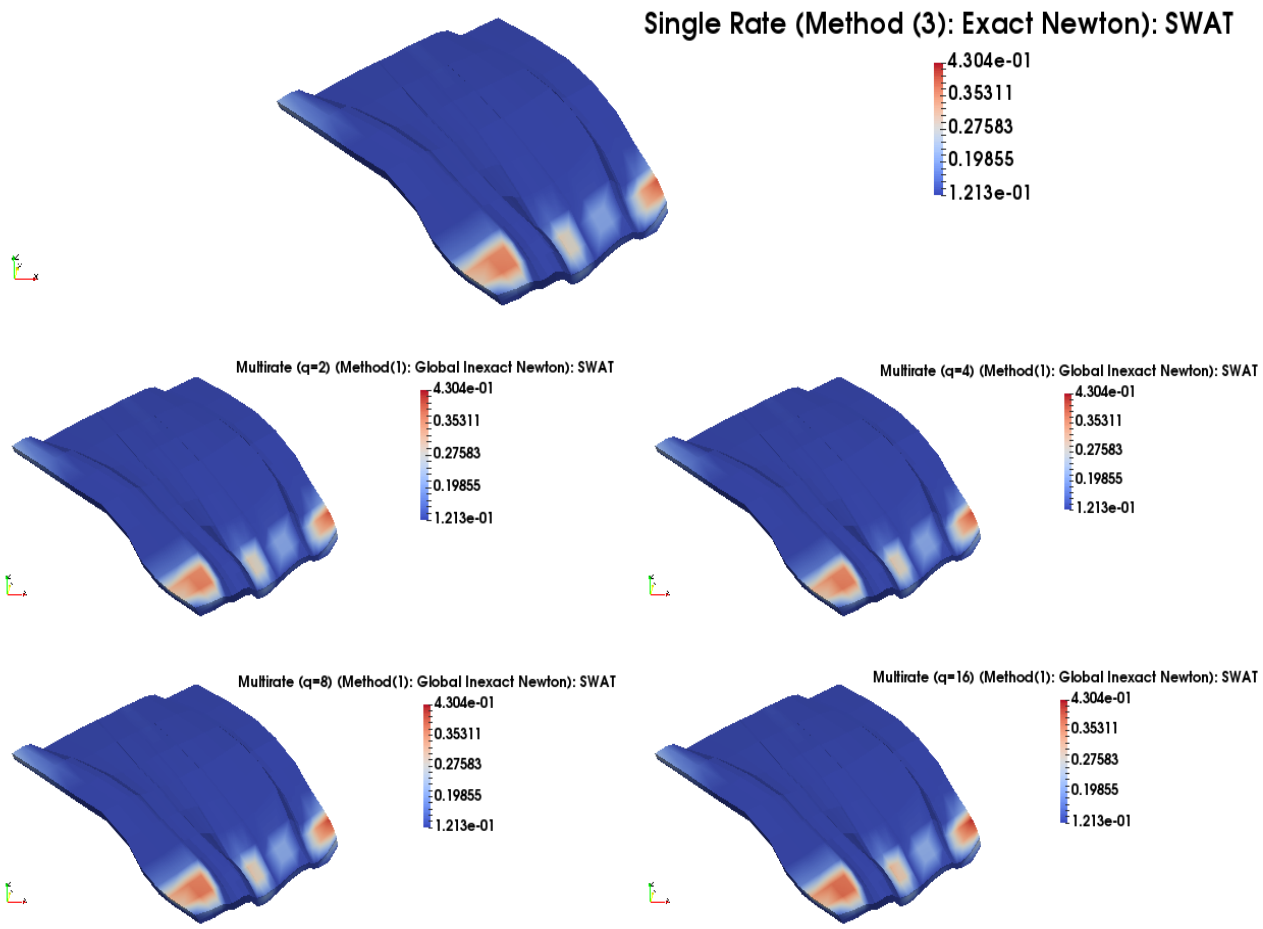

Figure 8.9: Water Saturation Profiles of the Frio Field Model after 48.0 Simulation Days for the Five Different Cases.

Computational Savings Relative to Case (1)	Case (2)	Case (3)	Case (4)	Case (5)
CPU run time	11.76%	21.59%	24.97%	10.70%
Number of flow linear iterations	37.96%	26.50%	21.24%	0.49%
Number of mechanics linear iterations	49.93%	74.12%	86.47%	91.71%

Table 8.3: Computational savings of "Case (2)", "Case (3)", "Case (4)", and "Case (5)" relative to "Case (1)" for the whole simulation run. We see that for $q = 16$, which corresponds to "Case (5)", the efficiency of the scheme is severely affected by the increase in the number of flow linear iterations, as a result of the increased number of flow-mechanics iterative coupling iterations shown in figure 8.13d.

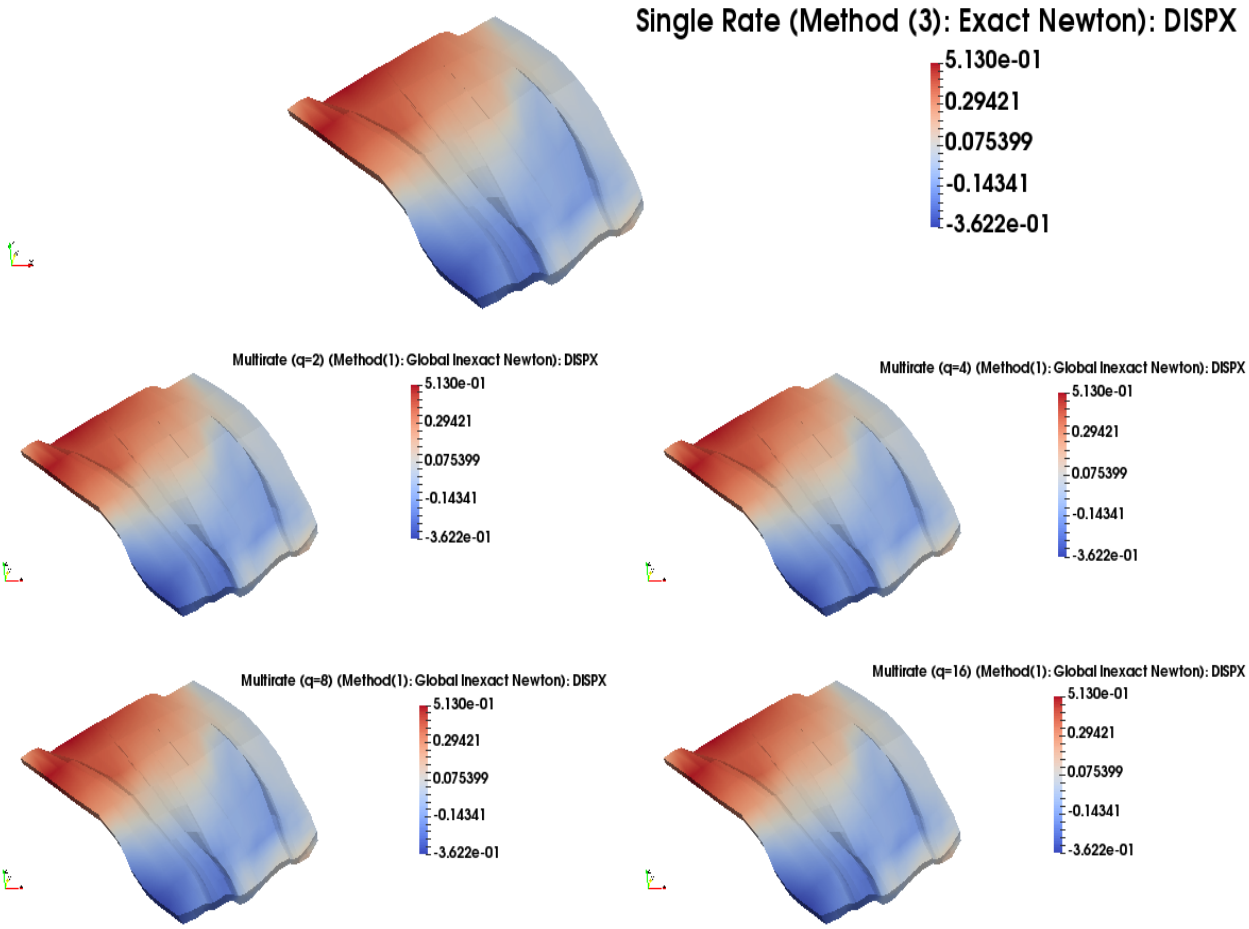

Figure 8.10: Displacement in (x) Direction (ft) for the Frio Field Model after 48.0 Simulation Days for the Five Different Cases.

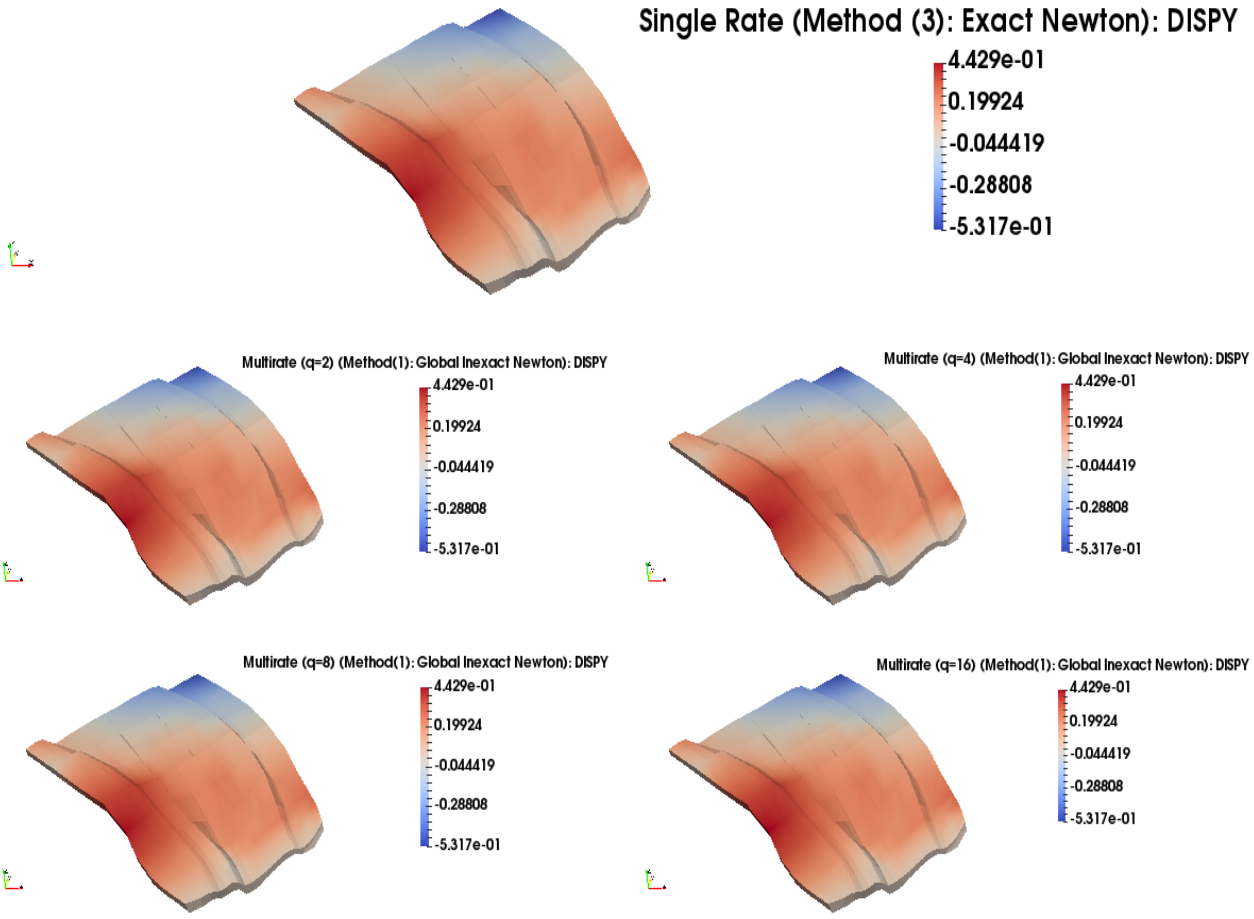

Figure 8.11: Displacement in (y) Direction (ft) for the Frio Field Model after 48.0 Simulation Days for the Five Different Cases.

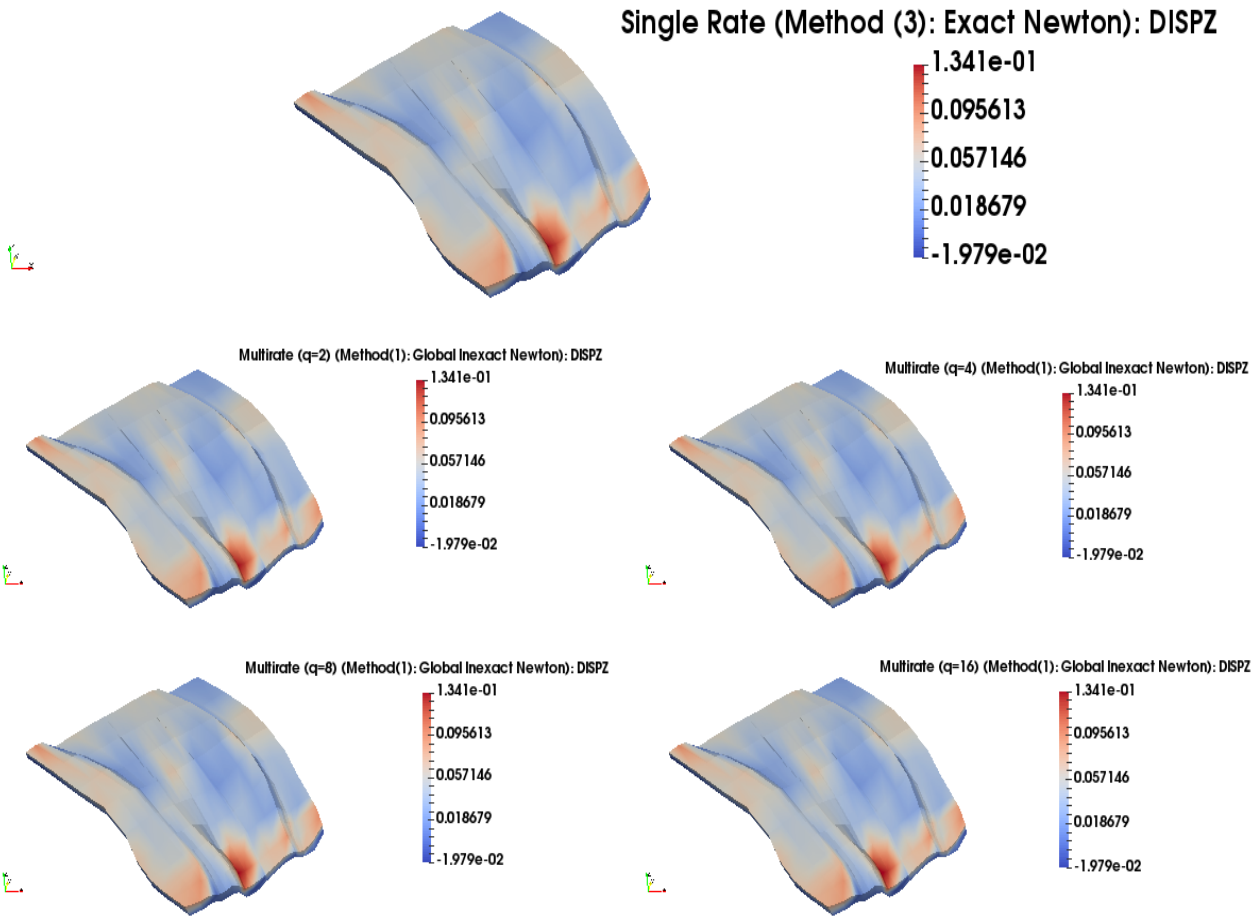

Figure 8.12: Displacement in (z) Direction (ft) for the Frio Field Model after 48.0 Simulation Days for the Five Different Cases.

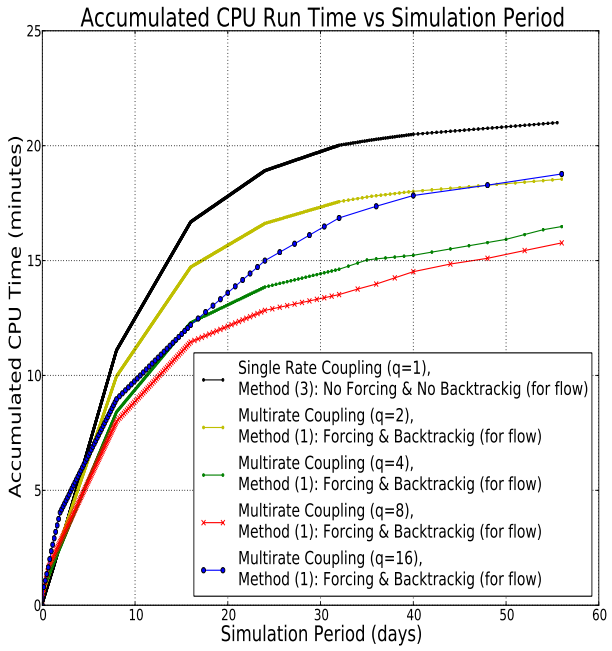

(a) CPU Run Time vs Simulation Days

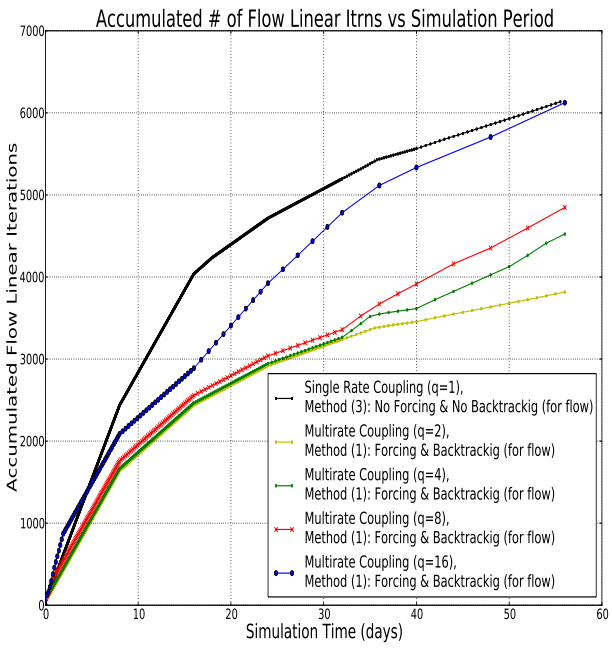

(b) Total Number of Flow Linear Iterations vs Simulation Days

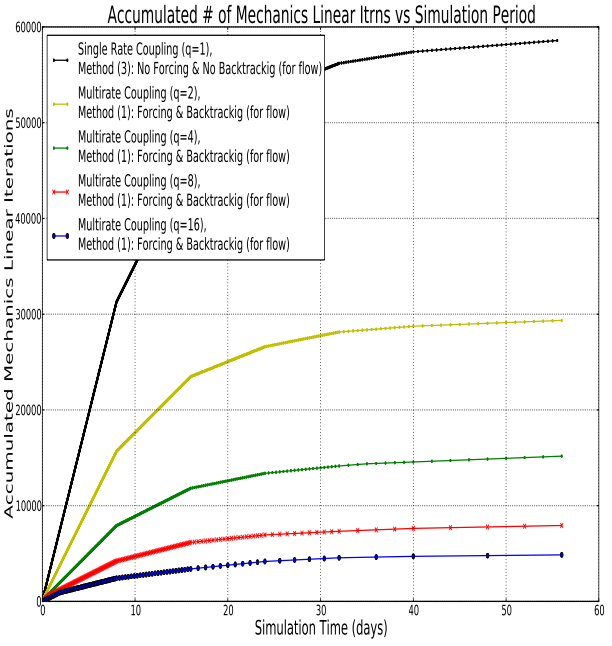

(c) Total Number of Mechanics Linear Iterations vs Simulation Days

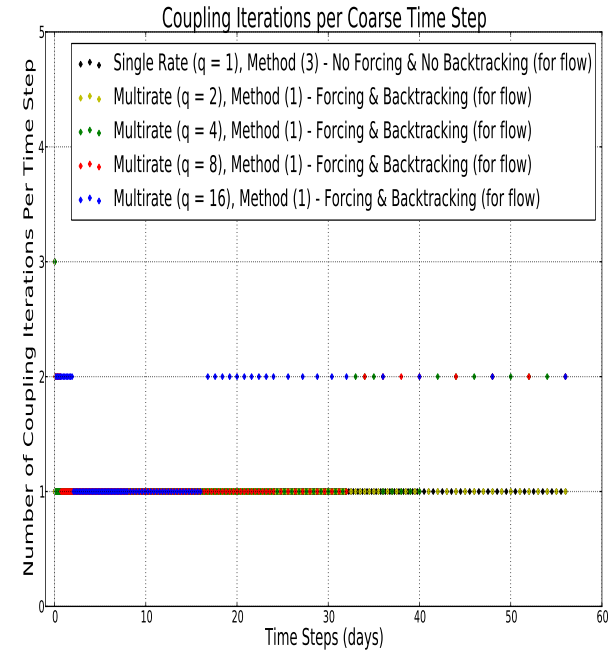

(d) Number of Iterative Coupling Iterations Per Coarser Time Step

Figure 8.13: Frio Field Model (Multirate/Global Inexact Newton) Numerical Results

Chapter 9

Conclusions

In this work, we considered different coupling schemes for coupling flow with linear elasticity (the quasi-static Biot Model). We rigorously formulated single rate and multirate iterative and explicit coupling schemes in both poro-elastic and fractured poro-elastic media. In the single rate case, the flow and mechanics problems share the same time step, while in the multirate case, the flow takes multiple finer time steps within each coarser mechanics time step. We thoroughly investigated the contracting behavior for all considered iterative coupling schemes, both theoretically and numerically (in IPARS). Moreover, we analyzed the stability of the proposed explicit coupling schemes, and showed that they are only conditionally stable, under certain conditions on the flow and mechanics parameters. Stability conditions have been derived for both poro-elastic and fractured poro-elastic media. The condition for the poro-elastic case was validated numerically against field-scale problems. This gives us a practical hint that for explicit coupling schemes to be numerically stable, sufficient level of compressibility should be maintained for both the fluid and the solid (i.e. the poro-elastic media). Unconditionally stable explicit coupling schemes have been proposed as well, by introducing theoretically derived stabilisation terms.

For both iterative and explicit coupling schemes, our numerical results highlight the efficiency of the multirate scheme in reducing the number of mechanics linear iterations, and subsequently, the CPU run time, while maintaining an acceptable level of accuracy compared to the results obtained by the single rate scheme. Moreover, subject to the value of the damping factor obtained in remark 2.3.3, by comparing our theoretical contraction estimates against numerical computations, we conclude that the theoretical estimates can predict the contracting behavior, and subsequently, the rate of convergence of the corresponding iterative scheme with high accuracy.

Our main contributions in this dissertation can be summarized as follows:

9.1 Contributions

- For multirate iterative coupling schemes, the main contributions are as follows:
  - For the quasi-static Biot model in poroelastic media, we established the contracting behavior leading to geometric speed of convergence for two iterative coupling schemes (the fixed-stress split and the undrained-split coupling schemes). Banach fixed-point contraction results were derived in both cases. In addition, both schemes were extended to the multirate settings, and Banach fixed-point contraction results were rigorously established for the both multirate schemes for the first time (to the best of our knowledge). (**Area A**)
  - For both schemes (fixed stress split and undrained split), the derived mathematical proofs provide the optimal values of the coefficients in the regularization terms used in both schemes. (**Area A**)
  - We proposed an alternative modified multirate scheme for the fixed-stress split coupling algorithm. Banach contraction was established for this scheme as well, and the quantity of contraction is independent of the number of flow fine time steps taken within one coarse mechanics time step (q). (**Areas A & B**)
  - For fractured poroelastic media, Banach contraction results were established for the fixed-stress split multirate iterative coupling scheme (extending the work of [43]). A modified multirate coupling scheme was proposed as well (in which the combined quantity of contraction is independent of q). Our proofs provide the optimal values of the coefficients of the regularization terms considered in this case as well. (**Area A**)
  - We derived a priori error estimates for the single rate fixed-stress split iterative coupling scheme. To the best of our knowledge, this is the first rigorous derivation of a priori error estimates for the fixed-stress split iterative coupling scheme for the quasi-static Biot model. The novelty of the approach used in deriving

our error estimates lies in its ability to utilize previously established results for the simultaneously coupled scheme. A similar result can be obtained for the undrained split coupling scheme, and is left for future work. (**Area A**)

- We established the "localized" contracting behavior (leading to geometric speed of convergence) for the fixed-stress split algorithm in (spatially and temporally) heterogeneous poro-elastic media. An upper bound on q was derived theoretically in this case. (**Area A**)
- We implemented and validated the efficiency of the proposed multirate iterative coupling scheme - Algorithm 2 - for different flow models in IPARS. This includes the single-phase MFMFE flow model, and the two-phase MFMFE (both IMPES and implicit schemes) flow models coupled with linear elasticity. The efficiency of the scheme was validated against two field-scale problems (the Frio field model, and the Brugge field model). (**Areas B & C**)
- We compared the values of the contraction estimates derived theoretically against numerically computed values for field-scale problems. This confirmed that theoretical contraction estimates provide an upper bound for numerically computed values. Moreover, the effect of the Lame parameters on the contracting behavior of the scheme was investigated both theoretically and numerically. As predicted in theory, for a fixed value of the poisson's ratio, theoretical contractions coefficients are sharper for larger Young's modulus values. (**Area C**)
- It was observed by numerical simulations that the multirate scheme can (sometimes) result in an increase in the number of flow-mechanics iterative coupling iterations. This leads to an increase in the number of flow linear iterations. The global Inexact Newton (combined with forcing functions and line-search backtracking) was incorporated in the multirate iteratively coupled algorithm to alleviate this effect. The combined algorithm (multirate coupling with the global Inexact Newton method for the flow solve) resulted in a robust, and efficient scheme (validated against the Frio field model). Incorporating the global inexact Newton method as a nonlinear solver framework for the flow problem in

multirate iteratively coupled problems is a novel idea that has not been explored in the past. (**Area B**)

- For multirate explicit coupling schemes, the main contributions are as follows:
  - For both poro-elastic and fractured poro-elastic media, we performed rigorous stability analysis of the single rate and multirate explicit coupling schemes. We also derived the conditions on reservoir and fracture parameters under which the corresponding explicit coupling scheme is stable. (**Areas A & C**)
  - For the explicit coupling scheme in poro-elastic media, the derived stability criterion was validated numerically against the Frio field model (in IPARS). (**Area C**)
  - The efficiency and computational time savings of multirate explicit coupling schemes versus multirate iterative coupling schemes were investigated numerically for a realistic field-scale problem (the Brugge field model). Our computational results suggest that if the considered parameters satisfy the derived stability conditions, explicit coupling schemes reduce the CPU run time efficiently compared to their counterpart iterative coupling schemes. (**Areas B & C**)

9.2 Future Work

This work can be extended in different directions. The list below provides possible extensions which will be considered for future work:

- Validating (numerically) our derived stability conditions for explicit coupling schemes in fractured-poroelastic media.
- Comparing the efficiency of the standard multirate iterative coupling scheme to the efficiency of the modified multirate iterative coupling scheme for both poroelastic and fractured poroelastic media.

- Deriving Banach contraction estimates for multirate iterative coupling schemes involving finer flow solves with varying time step sizes (i.e. Δt is not constant within one particular coarse mechanics solve).

- Deriving error estimates (a priori and a posteriori error estimates) for multirate iterative coupling schemes in both poro-elastic and fractured poroelastic reservoirs.

- Deriving error estimates (a priori and a posteriori error estimates) for multirate explicit coupling schemes in both poroelastic and fractured poroelastic reservoirs.

- Investigating nonlinear extensions of the considered algorithms, their analyses, and computational performance. This includes nonlinear flow models coupled with nonlinear mechanics models (e.g plasticity, thermoporoelasticity, thermoporoplasticity .. etc).

Appendices

Appendix A

The Multipoint Flux Mixed Finite Element Method

We provide a brief review of the finite element spaces used in the MFMFE scheme. It should be pointed out that the MFMFE scheme has been developed by Wheeler and Yotov [90] in 2006 for simplicial and quadrilateral grids. It was then extended to general hexahedral grids [47], and distorted quadrilaterals and hexahedra [87] in 2010, 2012 respectively.

We assume our elements to be quadrilatrs in 2D and hexahedra in 3D. We recall that $\mathfrak{T}_h$ represents the finite element partition of $\bar{\Omega}$, which is assumed to be shape-regular [39]. On a physical element E, the pressure and flux finite element spaces are defined through the transformations:

$$\text{Scalar Transformation:} \qquad w \leftrightarrow \hat{w} : w = \hat{w} \circ F_E^{-1} \tag{A.0.1}$$

$$\text{Piola Transformation:} \qquad \boldsymbol{z} \leftrightarrow \hat{\boldsymbol{z}} : \boldsymbol{z} = \frac{1}{J_E} \mathbb{DF}_E \hat{z} \circ F_E^{-1} \tag{A.0.2}$$

in which F_E is a mapping from the reference element $\hat{E}$ to the physical element E. The Jacobian of the mapping F_E is given by $\mathbb{DF}_E$, and $J_E = |det \mathbb{DF}_E|$. We note that the Piola transformation preserves the divergence and the normal components of the flux vectors on the faces (3D) and edges (2D) [39], which is need for $H(div;\Omega)$-conforming flux space. Thus, we have:

$$\Big(\nabla \cdot \boldsymbol{z}, w\Big)_E = \Big(\hat{\nabla} \cdot \hat{\boldsymbol{z}}, \hat{w}\Big)_{\hat{E}} \qquad \text{and} \qquad \langle \boldsymbol{z} \cdot \boldsymbol{n}, w \rangle_E = \langle \hat{\boldsymbol{z}} \cdot \hat{\boldsymbol{n}}, \hat{w} \rangle_{\hat{E}}$$

A.1 MFMFE Spaces

We recall that the infinite dimensional mixed finite element spaces for pressure and flux are given by:

$$Q = L^2(\Omega), \quad \text{and} \quad \boldsymbol{Z} = \{\boldsymbol{q} \in H(\text{div};\Omega)^d ; \boldsymbol{q} \cdot \boldsymbol{n} = 0 \text{ on } \partial\Omega\} \tag{A.1.3}$$

respectively. The finite dimensional discretized MFMFE spaces are given by:

$$Q_h = \{w \in Q\,; w|_E \leftrightarrow \hat{w}, \hat{w} \in \hat{Q}(\hat{E}), \forall E \in \mathfrak{T}_h\}$$
$$\boldsymbol{Z}_h = \{\boldsymbol{z} \in \boldsymbol{Z}\,; \boldsymbol{z}|_E \leftrightarrow \hat{\boldsymbol{z}}, \hat{\boldsymbol{z}} \in \hat{\boldsymbol{Z}}(\hat{E}), \forall E \in \mathfrak{T}_h\}$$

where $\hat{\boldsymbol{Z}}(\hat{E})$ and $\hat{Q}(\hat{E})$ are finite element spaces on the reference element $\hat{E}$. In what follows, we recall that P_k denotes the space of polynomials of degree k in two or three variables. Consider a hexahedral element in the reference domain (i.e. unit cube $\hat{E}$). Its vertices are given by $\hat{\boldsymbol{r}}_1 = (0,0,0)^T$, $\hat{\boldsymbol{r}}_2 = (1,0,0)^T$, $\hat{\boldsymbol{r}}_3 = (1,1,0)^T$, $\hat{\boldsymbol{r}}_4 = (0,1,0)^T$, $\hat{\boldsymbol{r}}_5 = (0,0,1)^T$, $\hat{\boldsymbol{r}}_6 = (1,0,1)^T$, $\hat{\boldsymbol{r}}_7 = (1,1,1)^T$, $\hat{\boldsymbol{r}}_8 = (0,1,1)^T$. The map F_E is defined as follows:

$$\begin{aligned} F_E =& \boldsymbol{r}_1(1-\hat{x})(1-\hat{y})(1-\hat{z}) + \boldsymbol{r}_2\hat{x}(1-\hat{y})(1-\hat{z}) + \boldsymbol{r}_3\hat{x}\hat{y}(1-\hat{z}) + \boldsymbol{r}_4(1-\hat{x})\hat{y}(1-\hat{z}) \\ &+ \boldsymbol{r}_5(1-\hat{x})(1-\hat{y})\hat{z} + \boldsymbol{r}_6\hat{x}(1-\hat{y})\hat{z} + \boldsymbol{r}_7\hat{x}\hat{y}\hat{z} + \boldsymbol{r}_8(1-\hat{x})\hat{y}\hat{z} \end{aligned}$$

The space $\hat{\boldsymbol{Z}}(\hat{E})$ is the enhanced $BDDF_1$ space, given as follows:

$$\begin{aligned} \hat{\boldsymbol{Z}}(\hat{E}) =& BDDF_1(\hat{E}) + s_2 curl(0,0,\hat{x}^2\hat{z})^T + s_3 curl(0,0,\hat{x}^2\hat{y}\hat{z})^T + t_2 curl(\hat{x}\hat{y}^2,0,0)^T \\ &+ t_3 curl(\hat{x}\hat{y}^2\hat{z},0,0)^T + r_2 curl(0,\hat{y}\hat{z}^2,0)^T + r_3 curl(0,\hat{x}\hat{y}\hat{z}^2,0)^T \\ =& BDDF_1(\hat{E}) + s_2(0,-2\hat{x}\hat{z},0)^T + s_3(\hat{x}^2\hat{z},-2\hat{x}\hat{y}\hat{z},0)^T + t_2(0,0,-2\hat{x}\hat{y})^T \\ &+ t_3(0,\hat{x}\hat{y}^2,-2\hat{x}\hat{y}\hat{z})^T + r_2(-2\hat{y}\hat{z},0,0)^2 + r_3(-2\hat{x}\hat{y}\hat{z},0,\hat{y}\hat{z}^2)^T \end{aligned}$$

where the space $BDDF_1$ is given as:

$$\begin{aligned} BDDF_1(\hat{E}) &= P_1(\hat{E})^3 + s_0 curl(0,0,\hat{x}\hat{y}\hat{z})^T + s_1 curl(0,0,\hat{x}\hat{y}^2)^T + t_0 curl(\hat{x}\hat{y}\hat{z},0,0)^T \\ &+ t_1 curl(\hat{y}\hat{z}^2,0,0)^T + r_0 curl(0,\hat{y}\hat{y}\hat{z},0)^T + r_1 curl(0,\hat{x}^2\hat{z},0)^T \\ &= P_1(\hat{E})^3 + s_0(\hat{x}\hat{z},-\hat{y}\hat{z},0)^T + s_1(2\hat{x}\hat{y},-\hat{y}^2,0)^T + t_0(0,\hat{x}\hat{y},-\hat{x}\hat{z})^2 + \\ &+ t_1(0,2\hat{y}\hat{z},-\hat{z}^2)^T + r_0(-\hat{x}\hat{y},0,\hat{y}\hat{z})^T + r_1(-\hat{x}^2,0,2\hat{x}\hat{z})^T \end{aligned} \tag{A.1.4}$$

where, s_i, t_i, and r_i for $i = 0, 1, 2$, and 3, are real constants. The space $\hat{Q}(\hat{E})$ is given as:

$$\hat{Q}(\hat{E}) = P_0(\hat{E})$$

We note that the flux degrees of freedom are chosen to be the normal components at the vertices for each edge (face). It should be noted that the original $BDDF_1$ spaces have only three degrees of freedom per square face. The enhanced $BDDF_1$ space has four degrees of freedom per square face, which is needed in the reduction of the discretized system to a cell-centered pressure stencil for pure Darcy flow problem [39].

A.2 Quadrature Rules

By mapping the physical element to the reference element (using Piola transformation for fluxes), the integration can be carried out over $\hat{E}$ using a quadrature rule. By the Piola transformation, we have:

$$\begin{aligned}\Big(\boldsymbol{K}^{-1}\boldsymbol{z},\boldsymbol{q}\Big)_E &= \Big(\frac{1}{J_E}\mathbb{DF}_E^T\boldsymbol{K}^{-1}(F_E(\hat{r}_i))\mathbb{DF}_E\hat{\boldsymbol{z}},\hat{\boldsymbol{q}}\Big)_{\hat{E}}\\ &= \Big(\mathcal{M}_E\hat{\boldsymbol{z}},\hat{\boldsymbol{q}}\Big)_{\hat{E}}\end{aligned}$$

where $\mathcal{M}_E = \frac{1}{J_E}\mathbb{DF}_E^T\boldsymbol{K}^{-1}(F_E(\hat{x}))\mathbb{DF}_E$, where $\hat{x}\in\hat{E}$. The trapezoidal rule on the reference element $\hat{E}$ is defined by: $\text{Trap}(\hat{\boldsymbol{z}},\hat{\boldsymbol{q}}) \equiv \frac{|\hat{E}|}{k}\sum_{i=1}^{k}\hat{\boldsymbol{z}}(\hat{r}_i)\cdot\hat{\boldsymbol{q}}(\hat{r}_i)$, where $\{\hat{r}_i\}$ denote the vertices of $\hat{E}$. Thus, we define the quadrature on the physical element E as:

$$\begin{aligned}\Big(\boldsymbol{K}^{-1}\boldsymbol{z},\boldsymbol{q}\Big)_{Q,E} &\equiv \text{Trap}(\hat{\boldsymbol{z}},\hat{\boldsymbol{q}})\\ &= \frac{|\hat{E}|}{k}\sum_{i=1}^{k}\mathcal{M}_E(\hat{\boldsymbol{r}}_i)\hat{\boldsymbol{z}}(\hat{r}_i)\cdot\hat{\boldsymbol{q}}(\hat{r}_i)\end{aligned}$$

Mapping back to a physical hexahedral element, we obtain:

Symmetric Quadrature Rule:

$$\Big(\boldsymbol{K}^{-1}\boldsymbol{z},\boldsymbol{q}\Big)_{Q,E} = \frac{1}{8}\sum_{i=1}^{8}J_E(\hat{r}_i)(\mathbb{DF}_E^{-1})^T(r_i)\mathbb{DF}_E{}^T(r_i)\boldsymbol{K}_E{}^{-1}(F_E(\hat{r}_i))\boldsymbol{z}(r_i)\cdot\boldsymbol{q}(r_i)$$

Non-Symmetric Quadrature Rule:

$$\Big(\boldsymbol{K}^{-1}\boldsymbol{z},\boldsymbol{q}\Big)_{Q,E} = \frac{1}{8}\sum_{i=1}^{8}J_E(\hat{r}_i)(\mathbb{DF}_E^{-1})^T(r_i)\mathbb{DF}_E{}^T(\hat{r}_{c,\hat{E}})\bar{\boldsymbol{K}}_E^{-1}\boldsymbol{z}(r_i)\cdot\boldsymbol{q}(r_i)$$

where $\hat{r}_{c,\hat{E}}$ is the center of mass of $\hat{E}$, and $\bar{K}_E$ is the mean of K on E [39, 47, 82, 87, 90].

Bibliography

[1] Y. Abousleiman, A. H. D. Cheng, L. Cui, E. Detournay, and J. C. Roegiers. Mandel's problem revisited. *Géotechnique*, 46(2):187–195, 1996.

[2] O. Al-Hinai, G. Singh, G. Pencheva, T. Almani, and M. F. Wheeler. Modeling multiphase flow with nonplanar fractures. In *The SPE Reservoir Simulation Symposium, The Woodlands, Texas*, Feb. 18-20, 2013.

[3] O. A. Al-Hinai. *Mimetic finite differences for porous media applications.* PhD thesis, The University of Texas at Austin, Austin, Texas, 2014.

[4] C. Alboin, J. Jaffre, J. E. Roberts, and C. Serres. Modeling fractures as interfaces for flow and transport in porous media. In *Z. Chen and R. E. Ewing, editors, Fluid flow and transport in porous media: mathematical and numerical treatment, Contemporary mathematics*, volume 295, pages 13–24. American Mathematical Society, 2002.

[5] D. R. Allen. Physical changes of reservoir properties caused by subsidence and repressurizing operations. Society of Petroleum Engineers, January 1968. SPE 1811.

[6] T. Almani, A. H. Dogru, K. Kumar, G. Singh, and M. F. Wheeler. Convergence of multirate iterative coupling of geomechanics with flow in a poroelastic medium. *Saudi Aramco Journal of Technology*, Spring 2016.

[7] T. Almani, K. Kumar, A. Dogru, G. Singh, and M. F. Wheeler. Convergence analysis of multirate fixed-stress split iterative schemes for coupling flow with geomechanics. *Computer Methods in Applied Mechanics and Engineering*, 311:180 – 207, 2016.

[8] T. Almani, K. Kumar, A. H. Dogru, G. Singh, and M. F. Wheeler. Convergence analysis of multirate fixed-stress split iterative schemes for coupling flow with geomechanics. ICES Report 16-07, Institute for Computational Engineering and Sciences, The University of Texas at Austin, Austin, Texas, 2016.

[9] T. Almani, K. Kumar, G. Singh, and M. F. Wheeler. Stability of multirate explicit coupling of geomechanics with flow in a poroelastic medium. ICES Report 16-12, Institute for Computational Engineering and Sciences, The University of Texas at Austin, Austin, Texas, 2016.

[10] T. Almani, K. Kumar, G. Singh, and M. F. Wheeler. Convergence and error analysis of fully discrete iterative coupling schemes for coupling flow with geomechanics. In *ECMOR XV*. 15th European Conference on the Mathematics of Oil Recovery, Aug. 29 - Sep. 1, 2016.

[11] T. Almani, K. Kumar, G. Singh, and M. F. Wheeler. Multirate undrained splitting for coupled flow and geomechanics in porous media. In *ENUMATH 2015 Proceedings*. European Conference on Numerical Mathematics and Advanced Applications, September 14-18, 2015. accepted.

[12] T. Almani, K. Kumar, and M. F. Wheeler. Convergence and error analysis of fully discrete iterative coupling schemes for coupling flow with geomechanics. ICES Report 16-24, The Institute for Computational Engineering and Sciences, The University of Texas at Austin, Austin, Texas, 2016.

[13] T. Almani, K. Kumar, and M. F. Wheeler. Multirate undrained splitting for coupled flow and geomechanics in porous media. ICES Report 16-13, Institute for Computational Engineering and Sciences, The University of Texas at Austin, Austin, Texas, 2016.

[14] M. A. Biot. General solutions of the equations of elasticity and consolidation for a porous material.

[15] M. A. Biot. Consolidation settlement under a rectangular load distribution. *Journal of Applied Physics*, 12(5):426–430, 1941.

[16] M. A. Biot. General theory of three-dimensional consolidation. *Journal of Applied Physics*, 12(2):155–164, 1941.

[17] M. A. Biot. Theory of elasticity and consolidation of a porous anisotropic solid. *Journal of Applied Physics*, 1955.

[18] M. A. Biot. Theory of deformation of a porous viscoelastic anisotropic solid. *Journal of Applied Physics*, 1956.

[19] M. A. Biot. Thermoelasticity and irreversible thermodynamics. *Journal of Applied Physics*, 1956.

[20] M. A. Biot. Mechanics of deformation and acoustic propagation in porous media. *Journal of Applied Physics*, 1962.

[21] S. C. Brenner and L. R. Scott. *The Mathematical Theory of Finite Element Methods*. Springer-Verlag, third edition, 2008.

[22] M. Bukac, I. Yotov, R. Zakerzadeh, and P. Zunino. Partitioning strategies for the interaction of a fluid with a poroelastic material on a Nitsche's coupling approach. Preprint submitted to Elsevier, 2014.

[23] N. Castelletto, J. A. White, and H. A. Tchelepi. Accuracy and convergence properties of the fixed-stress iterative solution of two-way coupled poromechanics. *International Journal for Numerical and Analytical Methods in Geomechanics*, 2015.

[24] N. Castelletto, J. A. White, and H. A. Tchelepi. A unified framework for fully-implicit and sequential-implicit schemes for coupled poroelasticity. In *ECMOR XIV*. 14th European Conference on the Mathematics of Oil Recovery, Sep. 8-11, 2014.

[25] L. Y. Chin, R. Raghaven, and L. K. Thomas. Fully-coupled geomechanics and fluid-flow analysis of wells with stress-dependent permeability. In *1998 SPE International Conference and Exhibition, Beijing, China*, Nov. 2-6, 1998.

[26] L. Y. Chin, L. K. Thomas, J. E. Sylte, and R. G. Pierson. Iterative coupled analysis of geomechanics and fluid flow for rock compaction in reservoir simulation. *Oil and Gas Science and Technology*, 57(5):485–497, 2002.

[27] M. A. Christie and M. J. Blunt. Tenth SPE comparative solution project: a comparison of upscaling techniques. *SPE Reservoir Evaluation & Engineering*, 4(4):308–317, 2001.

[28] O. Coussy. A general theory of thermoporoelastoplasticity for saturated porous materials. *Transport in Porous Media*, 4:281–293, June 1989.

[29] O. Coussy. *Mechanics of Porous Continua*. Wiley, West Sussex PO19 1UD, England, 1995.

[30] O. Coussy. *Poromechanics*. Wiley, West Sussex PO19 8SQ, England, 2004.

[31] C. N. Dawson, H. Klie, M. F. Wheeler, and Carol S. Woodward. A parallel, implicit, cell-centered method for two-phase flow with a preconditioned Newton-Krylov slover. *Computational Geosciences*, 1:215–249, 1997.

[32] S. C. Eisenstat and H. F. Walker. Globally convergent inexact Newton methods. *Siam Journal of Optimization*, 4:393–422, 1994.

[33] S. C. Eisenstat and H. F. Walker. Choosing the forcing terms in an inexact Newton method. *SIAM Journal of Scientific Computing*, 17:16–32, 1996.

[34] A. Ern and S. Meunier. A posteriori error analysis of Euler-Galerkin approximations to coupled elliptic-parabolic problems. *ESAIM: Mathematical Modelling and Numerical Analysis*, 43(2):353–375, 12 2008.

[35] L. S. K. Fung, L. Buchanan, and R. G. Wan. Coupled geomechanical-thermal simulation for deforming heavy-oil reservoirs. *Journal of Canadian Petroleum Technology*, 33(4), April 1994.

[36] X. Gai. *A coupled geomechanics and reservoir flow model on parallel computers*. PhD thesis, The University of Texas at Austin, Austin, Texas, 2004.

[37] X. Gai, R. H. Dean, M. F. Wheeler, and R. Liu. Coupled geomechanical and reservoir modeling on parallel computers. In *The SPE Reservoir Simulation Symposium, Houston, Texas*, Feb. 3-5, 2003.

[38] X. Gai, S. Sun, M. F. Wheeler, and H. Klie. A timestepping scheme for coupled reservoir flow and geomechanics on nonmatching grids. In *SPE Annual Technical Conference and Exhibition*, 2005. SPE97054.

[39] B. Ganis, V. Girault, M. E. Mear, G. Singh, and M. F. Wheeler. Modeling fractures in a poro-elastic medium. *Oil and Gas Science and Technology - Rev. IFP Energies nouvelles*, 69:515–528, 2014.

[40] F. J. Gaspar, F. J. Lisbona, and P. N. Vabishchevich. A finite difference analysis of Biot's consolidation model. *Applied Numerical Mathematics*, 44(4):487 – 506, 2003.

[41] J. Geertsma. Problems of rock mechanics in petroleum production engineering. In *Proceedings of First Congress International Society of Rock Mechanics, Lisbon*, pages 585–594, 1996.

[42] V. Girault, K. Kumar, and M. F. Wheeler. Convergence of iterative coupling of geomechanics with flow in a fractured poroelastic medium. ICES Report 15-05, Institute for Computational Engineering and Sciences, The University of Texas at Austin, Austin, Texas, 2015.

[43] V. Girault, K. Kumar, and M. F. Wheeler. Convergence of iterative coupling of geomechanics with flow in a fractured poroelastic medium. *Computational Geosciences*, pages 1–15, 2016.

[44] V. Girault, G. Pencheva, M. F. Wheeler, and T. Wildey. Domain decomposition for poroelasticity and elasticity with dg jumps and mortars. *Mathematical Models and Methods in Applied Sciences*, 21(1):169–213, 2011.

[45] V. Girault, M. F. Wheeler, B. Ganis, and M. Mear. A lubrication fracture model in a poro-elastic medium. ICES Report 13-32, The Institute for Computational Engineering and Sciences, The University of Texas at Austin, Austin, Texas, 2013.

[46] V. Girault, M. F. Wheeler, K. Kumar, and G. Singh. Mixed formulation of a linearized lubrication fracture model in a poro-elastic medium. ICES Report 16-06, Institute for

Computational Engineering and Sciences, The University of Texas at Austin, Austin, Texas, 2016.

[47] R. Ingram, M. F. Wheeler, and I. Yotov. A multipoint flux mixed finite element method on hexahedra. *SIAM Journal on Numerical Analysis*, 48:1281–1312, 2010.

[48] M. Juntunen and M. F. Wheeler. Two-phase flow in complicated geometries - Modeling the Frio data using improved computational meshes. *Computational Geosciences*, 17:239–247, 2013.

[49] C. T. Kelley. *Iterative Methods for Linear and Nonlinear Equations*. Frontiers of Applied Mathematics 16. Society for Industrial and Applied Mathematics, Philadelphia, 1995.

[50] C. T. Kelley. *Solving Nonlinear Equations with Newton's Method*. Fundamentals of Algorithms. Society for Industrial and Applied Mathematics, Philadelphia, 2003.

[51] J. Kim, H. A. Tchelepi, and R. Juanes. Stability and convergence of sequential methods for coupled flow and geomechanics: drained and undrained splits. *Computer Methods in Applied Mechanics and Engineering*, 200(23-24):2094–2116, 2011.

[52] J. Kim, H. A. Tchelepi, and R. Juanes. Stability and convergence of sequential methods for coupled flow and geomechanics: fixed-stress and fixed-strain splits. *Computer Methods in Applied Mechanics and Engineering*, 200(13-16):1591–1606, 2011.

[53] J. Kim, H. A. Tchelepi, and R. Juanes. Stability, accuracy, and efficiency of sequential methods for coupled flow and geomechanics. In *The SPE Reservoir Simulation Symposium, Houston, Texas*, February 2-4, 2009. SPE119084.

[54] R. A. Klausen, F. A. Radu, and G. T. Eigestad. Convergence of MPFA on triangulations and for Richard's equation. *International Journal for Numerical Methods in Fluids*, 58(12):1327–1351, 2008.

[55] R. A. Klausen and R. Winther. Convergence of multipoint flux approximations on quadrilateral grids. *Numerical Methods for Partial Differential Equations*, 22(6):1438–1454, 2006.

[56] H. Klie and M. F. Wheeler. Nonlinear Krylov-secant solvers. ICES Report, The Center for Subsurface Modeling (CSM), The Institute for Computational Engineering and Sciences (ICES), The University of Texas at Austin, Austin, Texas, 2006.

[57] S. Lacroix, Y. Vassilevski, J. Wheeler, and M. .F. Wheeler. Iterative solution methods for modeling multiphase flow in porous media fully implicitly. *SIAM Journal of Scientific Computing*, 25:905–926, 2003.

[58] S. Lacroix, Y. V. Vassilevski, and M. F. Wheeler. Decoupling preconditioners in the implicit parallel accurate reservoir simulator (IPARS). *Numerical Linear Algebra Applications*, 8:537–549, 2001.

[59] J. J. Lee. Robust error analysis of coupled mixed methods for Biot's consolidation model. *Journal of Scientific Computing*, pages 1–23, 2016.

[60] M. Mainguy and P. Longuemare. Coupling fluid flow and rock mechanics: formulations of the partial coupling between reservoir and geomechanics simulators. *Oil and Gas Science and Technology - Rev. IFP*, 57(4):355–367, 2002.

[61] J. Mandel. Consolidation des sols (Étude mathématique). *Géotechnique*, 3(7):287–299, 1953.

[62] V. Martin, J. Jaffré, and J.E. Roberts. Modeling fractures and barriers as interfaces for flow in porous media. *SIAM Journal on Scientific Computing*, 26(5):1667–1691, 2005.

[63] A. Mikelic, B. Wang, and M. F. Wheeler. Numerical convergence study of iterative coupling for coupled flow and geomechanics. *Computational Geosciences*, 18:325–341, 2014.

[64] A. Mikelic and M. F. Wheeler. Convergence of iterative coupling for coupled flow and geomechanics. *Computational Geosciences*, 17:455–461, 2013.

[65] A. Mikelić, M. F. Wheeler, and T. Wick. A phase-field approach to the fluid-filled fracture surrounded by a poro-elastic medium. ICES Report 13-15, Institute for

Computational Engineering and Sciences, The University of Texas at Austin, Austin, Texas, 2013.

[66] A. Mikelić, M. F. Wheeler, and T. Wick. A quasi-static phase-field approach to the fluid-filled fracture. ICES Report 13-22, Institute for Computational Engineering and Sciences, The University of Texas at Austin, Austin, Texas, 2013.

[67] F. Morales and R. E. Showalter. The narrow fracture approximation by channeled flow. *Journal of Mathematical Analysis and Applications*, 365(1):320–331, 2010.

[68] F. Morales and R. E. Showalter. Interface approximation of Darcy flow in a narrow channel. *Mathematical Methods in the Applied Sciences*, 35(2):182–195, 2012.

[69] M. A. Murad, V. Thomée, and A. F. D. Loula. Asymptotic behavior of semidiscrete finite-element approximations of Biot's consolidation problem. *SIAM Journal of Numerical Analysis*, 33:1065–1083, 1996.

[70] P. J. Phillips and M. F. Wheeler. A coupling of mixed and continuous Galerkin finite element methods for poroelasticity I: the continuous in time case. *Computational Geosciences*, 11(2):131–144, 2007.

[71] P. J. Phillips and M. F. Wheeler. A coupling of mixed and continuous Galerkin finite element methods for poroelasticity II: the discrete-in-time case. *Computational Geosciences*, 11(2):145–158, 2007.

[72] I. S. Pop, F. Radu, and P. Knabner. Mixed finite elements for the Richards' equation: Linearization procedure. *Journal of Computational and Applied Mathematics*, 168((1-2)):365–373, July 2004.

[73] F. A. Radu, J. M. Nordbotten, I. S. Pop, and K. Kumar. A robust linearization scheme for finite volume based discretizations for simulation of two-phase flow in porous media. *Journal of Computational and Applied Mathematics*, 289:134–141, 2015.

[74] J. R. Rice and M. P. Cleary. Some basic stress diffusion solutions for fluid-saturated elastic porous media with compressible constituents. *Reviews of Geophysics and Space Physics*, 1976.

[75] C. Rodrigo, F. J. Gaspar, X. Hu, and L. T. Zikatanov. Stability and monotonicity for some discretizations of the Biot's consolidation model. *Computer Methods in Applied Mechanics and Engineering*, 298:183 – 204, 2016.

[76] I. Ruddy, M. A. Andersen, P. D. Pattillo, M. Bishlawl, and N. Foged. Rock compressibility, compaction, and subsidence in a high-porosity chalk reservoir: A case study of Valhall field. Society of Petroleum Engineers, 1989. SPE 18278.

[77] P. Samier, A. Onaisi, and S. d. Gennaro. A practical iterative scheme for coupling geomechanics with reservoir simulation. *SPE Reservoir Evaluation and Engineering*, 11:892–901.

[78] A. Settari and F. Mourits. A coupled reservoir and geomechanical simulation system. *SPE Journal*, Sep. 1998.

[79] A. Settari and F. M. Mourits. Coupling of geomechanics and reservoir simulation models. In Siriwardane and Zema, editors, *Computer Methods and Advances in Geomechanics*, pages 2151–2158, Balkema, Rotterdam, 1994.

[80] L. Shan, H. Zheng, and W. J. Layton. A decoupling method with different subdomain time steps for the nonstationary Stokes-Darcy model. *Numerical Methods for Partial Differential Equations*, 29(2):549–583, 2013.

[81] R. E. Showalter. Diffusion in poro-elastic media. *Journal of Mathematical Analysis and Applications*, 251(1):310–340, 2000.

[82] G. Singh. *Coupled flow and geomechanics modeling for fractured poroelastic reservoirs.* PhD thesis, The University of Texas at Austin, Austin, Texas, 2014.

[83] J. C. Small, J. R. Booker, and E. H. Davis. Elasto-plastic consolidation of soil. *International Journal of Solids and Structures*, 12(6):431–448, 1976.

[84] K. V. Terzaghi. *Theoretical Soil Mechanics.* Wiley, New York, 1943.

[85] J. Wan. *Stabilized finite element methods for coupled geomechanics and multiphase flow.* PhD thesis, Stanford University, Stanford, California, 2003.

[86] B. Wang. *Parallel simulation of coupled flow and geomechanics in porous media*. PhD thesis, The University of Texas at Austin, Austin, Texas, 2014.

[87] M. F. Wheeler, G. Xue, and I. Yotov. A family of multipoint flux mixed finite element methods for elliptic problems on general grids. In *Procedia Computer Science*, volume 4, pages 918–927. International Conference on Computational Science, ICCS 2011, 2011.

[88] M. F. Wheeler, G. Xue, and I. Yotov. A multipoint flux mixed finite element method on distorted quadrilaterals and hexahedra. *Numerische Mathematik*, 121(1):165–204, 2012.

[89] M. F. Wheeler, G. Xue, and I. Yotov. Coupling multipoint flux mixed finite element methods with continuous Galerkin methods for poroelasticity. *Computational Geosciences*, 18(1):57–75, 2014.

[90] M. F. Wheeler and I. Yotov. A multipoint flux mixed finite element method. *SIAM Journal of Numerical Analysis*, 44:2082–2106, 2006.

[91] T. Wick, G. Singh, and M. F. Wheeler. Pressurized fracture propagation using a phase-field approach coupled to a reservoir simulator. In *SPE Hydraulic Fracturing Technology Conference, The Woodlands, Texas*. Society of Petroleum Engineers, 2014. SPE 168597-MS submitted.

[92] X. Xiong. Analysis of a multi-rate splitting method for uncoupling evolutionary groundwater-surfacewater flows. Technical report, University of Pittsburgh, Aug. 8, 2012.

Vita

Tameem Almani is an Aramco-sponsored PhD candidate in the Computational Sciences, Engineering, and Mathematics program at the University of Texas at Austin. He is working under the supervision of Prof. Mary F. Wheeler on the analysis and modeling of coupled multiphase flow and geomechanics problems in porous media, with emphasis on multi-rate couplings and linear and nonlinear solvers for the related discretized systems. Before joining the Univesity of Texas at Austin, Tameem completed his BS degree in Computer Scinece, with first honors, at King Fahd University of Petroleum and Minerals in 2007. Following his graduation, he joined the Computational Modelling Technology team at EXPEC ARC, as a Petroleuem Engineering System Analyst, participating in the development of GigaPOWERS. He obtained his first MS degree in Computational and Mathematical Engineering from Stanford University in 2011. He obtained his second MS degree in Computational Scineces, Engineering, and Mathematics from the University of Texas at Austin in 2014. In addition, he completed eight graduate level courses, as a part time student, in the Computer Engineering department at KFUPM, spanning the areas of parallel processing architectures, mobile and heterogenous computing, computer algorithms, and artificial intelligence. Tameem is the recipient of Prince Mohammad Al-Saud (former governor of the eastern province in Saudi Arabia) award for academic achievement at KFUPM in 2008. In addition, he was awarded by STC (Saudi Telecom Company) as one of the top ten graduate students at KFUPM in 2009.

Permanent address: tameemam@gmail.com

This dissertation was typeset with LaTeX[†] by the author.

[†]LaTeX is a document preparation system developed by Leslie Lamport as a special version of Donald Knuth's TeX Program.